N
36. H. 14

THE LIBRARY
UNIVERSITY OF NOTTINGHAM

Class Mark —

Book Number 165788

PRESENTED TO
THE UNIVERSITY OF NOTTINGHAM
BY
Science Museum Library
1958

PERIODICALS

Only staff and research students may borrow periodical volumes from the Library

DATE OF ISSUE

Any volume which you borrow remains your responsibllity until the loan slip is cancelled

Digitized by the Internet Archive
in 2026

https://archive.org/details/sciencereportsof0014vari

東北帝國大學

理科報告

(數學, 物理學, 化學)

第十四卷

THE

SCIENCE REPORTS

OF THE

TÔHOKU IMPERIAL UNIVERSITY

FIRST SERIES

(Mathematics, Physics, Chemistry)

SENDAI, JAPAN

Vol. XIV

On Sale by

MARUZEN COMPANY, LTD., TOKYO AND SENDAI.

1925.

27 MAY 1958

C

CONTENTS.

PAGE.

On the Reaction Products of Ruthenium Tetroxide and Hydrochloric Acid.
By S. Aoyama. 1

On the Equilibrium Diagram of the System Iron-Carbon-Titanium.
By K. Tamaru. 25

The X-ray Examination of Inner Structure of Various Calcium Carbonates.
By A. Ôsawa. 33

On the Atomic Structure of Palladium and Platin Black which absorb Gases.
By A. Ôsawa. 43

The Use of Liquid Amalgam in Volumetric Analysis. Part 1. Application of Zinc and Bismuth Amalgams.
By K. Someya. 47

Some Experiments on the Abrasion of Metals.
By K. Honda and R. Yamada.... 63

Uber die Convex geschlossenen Mannigfaltigkeiten im n-dimensionalen Raume.
Von T. Kubota. 85

On the Determination of Cyanides and the Use of Benzene as an Indicator in Iodimetry.
By N. Kanô.... 101

Application of Liquid Amalgams to Volumetric Analysis. Part. 1. Estimation of Molybdenum, Titanium and Iron.
By T. Nakazono.... 109

PAGE.

Relation between the Chemical Constitution and the Pungency. Synthesis of the Reduction Products of Zingerons and Di-4-hydroxy-3-methoxyphenylethyl Ketone.
By H. Nomura and S. Hotta. 119

The Condensation of Vanillin with Methyl Ethyl Ketone.
By J. Ichikawa. 127

Synthesis of the Homologues of Zingerone.
By H. Nomura and S. Hotta. 131

Preparation of Zingerone, 4-Hydroxy-3 methoxyphenylethylmethyl Ketone.
By H. Nomura. 143

Synthesis of a Homologue of Zingerone, 4-hydroxy-3 methoxyphenylethyl n-Phenyl Ketone.
By J. Murai 145

Synthesis of m-Hydroxyphenylethyl Methyl Ketone and 3-Hydroxy-4-methoxyphenylethyl Methyl Ketone (Iso-zingerone)
By J. Murai 149

Uber die (2, 2) deutigen quadratischen Verwandtschaften V.
By T. Kubota. 155

On the Formation of Martensite in Carbon Steels.
By K. Honda. 165

On the Equilibrium Diagram of the Iron-Carbon Nickel System.
By T. Kasé. 173

On the Law of Depression of Freezing Points in Metallic Alloys.
By K. Honda and T. Ishigaki.... 219

The use of Liquid Amalgams in Volumetric Analysis. Part II. Oxidimetric Estimation of Tungsten, etc. by Using Lead and Bismuth Amalgams.
By K. Someya. 235

PAGE.

The Vapor Pressures of Hydrogen Chloride on Aqueous Solutions. Part. 1.

By S. Mitsukuri and T. Rokkaku and T. Watase. 251

Bemerkungen zu den geodätischen Linien auf Böschungflächen.

By T. Takasu. 259

On the Relation between the Intrinsic Equations of Analytic Functions under Linear Transformations and Curves under Inversions.

By T. Takasu. 263

Geometry of Doubly Oriented Spheres in Non-Euclidean Space.

By T. Takasu. 279

The Influence of Metallic Elements on the Corrosion of Iron and Steel.

By Y. Utida and M. Saitô. 295

Some Experiments on the Contact Electric Layers.

By M. Satô. 313

On the Variation of Residual Charge and the Ratio of Electrical Conductivity to Capacity due to Temperature.

By H. Saegusa. 319

Further Studies on the Variation of Residual Charge and the Ratio of Electrical Conductivity to Capacity due to Temperature.

By H. Saegusa. 335

The Effect of Cold-Working and Annealing on some Physical Properties of Copper, Aluminium and their Alloys.

By T. Matsuda. 343

On the Influence of some Elements on the Spheroidization of Carbides in Steels.

By T. Ishihara. 377

PAGE.

Uber die Doppelsechs.
Von T. Kubota. 391

Uber die Eibereiche im n-dimensionalen Raume.
Von T. Kubota. 399

A Kinetic Theory of the Viscosity of Liquids.
By M. Satô. 403

Dielectric Constants of Liquids. Part. I. On the Method of Measuring Dielectric Constants of Liquids.
By Y. Matsuike. 445

On the Stractural Diagrames of some Special Steels.
By T. Kasé. 453

On the Relation between the Equilibrium Diagram and the Magnetic Susceptibility in Binary Alloys.
By H. Endô.... 479

Dilatometric Investigation of the A_3 and A_1 Transformations in Pure Iron.
By S. Satô. 513

On the Solidus Line in the Iron-Carbon System.
By S. Kaya. 529

On the Wismannstätten Structure in Iron-Carbon and Iron-Nickel Alloys and in Meteorites.
By T. Kasé. 537

On the Determination of the Heat of Precipitation of Cementite from α and β Martensites.
By M. Kawakami. 559

The Use of Liquid Amalgams in Volumetric Analysis. Part III. Determination of Phosphoric Acid by Using Lead Amalgam.
By K. Someya. 568

Ein Verfahren zur Bestimmung von Vanadium in Ferrovanadium.
By K. Someya. 577

On the Reaction Products of Ruthenium Tetroxide and Hydrochloric Acid.

By

Shin'ichi Aoyama.

(1) Tetrachlor-Oxyruthenic Acid ($H_2RuO_2Cl_4.3H_2O$)
(2) Ammonium Hexachlor-Ruthenate ($(NH_4)_2RuCl_6\,\frac{1}{2}H_2O$)
(3) Potassium Hexachlor-Ruthenate (K_2RuCl_6)
(4) γ-Potassium Pentachlor-Ruthenite (γ-K_2RuCl_5)

HISTORY.

U. Antony[1] obtained the crystals of K_2RuCl_6 by fusing ruthenium with caustic potash and potassium chlorate.

J. L. Howe[2] dissolved ruthenium tetroxide in cold hydrochloric acid, obtaining ruthenium trichloride and stated the velocity of the change to be proportional to the concentration of the acid. The same authority obtained the crystals of $Cs_2RuO_2Cl_4$ and $Rb_2RuO_2Cl_4$ by adding to ruthenium tetroxide a concentrated solution of the chloride of caesium or rubidium. He[3] also obtained the crystals of $M_2Ru(OH_2)Cl_5$ by adding alcohol to a weakly acid solution of M_2RuCl_5 (M, alkali metal) and boiling the mixture. The passage of chlorine gas into this concentrated solution resulted in M_2RuCl_6. On the other hand, he obtained K_2RuCl_5 by heating $M_2Ru(OH_2)Cl_5$, which was named dehydrated "aquo" chlorruthenate, and supposed it to be an isomer of the ordinary ruthenite.

(1) Gazz. Chem. Itali., **29**, II. 82.
(2) J. Amer. Chem. Soc., (1901), **25**, 775.
(3) J. Amer. Chem. Soc., (1904), **26**, 543.

Mylius & Mazzucchelli[1] made hydrochloric acid act upon the product of the distillation of ruthenium tetroxide, to which after dilution with water, was added a saturated solution of ammonium chloride, obtaining $(NH_4)_2RuCl_6$. But he also observed that if the product of decomposition by hydrochloric acid is evaporated or alcohol added to it, ruthenium trichloride is formed, and when chlorine is passed into it, it changes into a solution of ruthenium tetrachloride.

A. Gutbier[2] argued that the product obtained by Mylius and his co-worker was probably $(NH_4)_2RuCl_5.H_2O$.

H. Remy[3] stated that ruthenium tetrachloride is easily formed by the action of ruthenium tetroxide and hydrochloric acid.

A. Gutbier, F. Falco & Th. Vogt[4] obtained $M_2RuCl_5.H_2O$ by the action of ruthenious acid and alkali salt from the hydrochloric acid solution.

F. Kraus[5] made a large quantity of hydrochloric acid act upon ruthenium tetroxide. The product was diluted with water and 5 % alkali chloride was added, whereby $Cs_2RuCl_6.H_2O$ was obtained in a pure crystalline form, but he reported that in the cases of Rb_2RuCl_6 and K_2RuCl_6, they are mixed with ruthenious salts. And from the aqueous solution of caesium and rubidium, ruthenium could be completely precipitated by hydrogen sulphide, but $M_2Ru(OH_2)Cl_5$ and $M_2RuO_2Cl_4$ reported by Howe, could not be obtained.

THE OBJECT OF THE INVESTIGATION.

Summarizing the works of the foregoing authorities, we see that their arguments can be divided into two groups, one of which is to assert the formation of the double salts, such as M_2RuCl_5 or $M_2RuCl_5.H_2O$, etc., in the case of the action of ruthenium tetroxide with hydrochloric acid, as a result of the formation of ruthenium trichloride, and to deny

(1) Z. anorg. Chem., **89**, (1914), 1.
(2) Z. anorg. Chem., **109**, (1919), 187.
(3) J. prakt. Chem., ii, 101, (1920), 341.
(4) Z. anorg. Chem., **115**, (1921), 225.
(5) Z. anorg. Chem., **117**, (1921), 111.

the formation of M_2RuCl_6 derived from ruthenium tetrachloride, while the other insists upon the formation of ruthenium tetrachloride in the same case. All the authorities who adopt the former view, however, agree in stating that the rate of formation of ruthenium trichloride is very slow. The writer carried out the present investigation with the object of making these relations clear, which may possibly be a help in the separation of the platinum group elements.

NOTES ON THE MATERIAL AND EXPERIMENTS.

(1) The raw material of ruthenium 10 grs. as K_2RuCl_5, was one obtained from iridosmium from Hokkaidô, and frequently purified by Prof. Ogawa himself which was kindly given to the writer, who in turn reduced it in a stream of hydrogen, heated strongly in one of oxygen and again reduced, whereby it attained a state of very high purity.

(2) Ruthenium Tetroxide. On each occasion 0.5 gr. of the sample was taken and fused for 10 minutes in a round-bottomed nickel crucible with 1 gr. of caustic soda and 3 grs. of sodium peroxide. The melt was placed in a distillating apparatus, depicted in Fig. I, into which was passed chlorine gas to form the vapour of ruthenium tetroxide. The ruthenium tetroxide formed was first led into a calcium chloride chamber to remove a large part of the moisture.

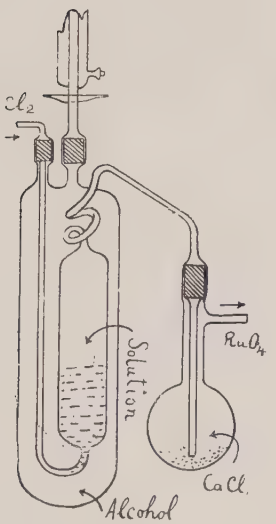

Fig. I.

(3) Hydrochloric Acid Gas. The gas evolved when sulphuric acid is dropped upon carefully dehydrated table salt, was dried by passing it through two sulphuric acid washing bottles and two calcium chloride U-tubes.

(4) Chlorine Gas. The gas formed by dropping concentrated hydrochloric acid on crystalline potassium permanganate was washed with water and dried by passing it through a

washer of concentrated sulphuric acid and 2 U-tubes containing pure phosphorus pentoxide.

But the chlorine used for the evolution of ruthenium tetroxide was washed with water only.

(5) The Drying Apparatus. A special drying tube was made as is shown in Fig. II. As a drying agent phosphorus pentoxide was introduced. It was made in such a way, that as the tube was turned a fresh part of the phosphorus pentoxide was always exposed on the surface. The reaction tube was put in or taken out by removing the ground stopper (a). The ground joints of stoppers (a) and (b) were made in such a way that the tube (c) was capped by the stoppers on both sides.

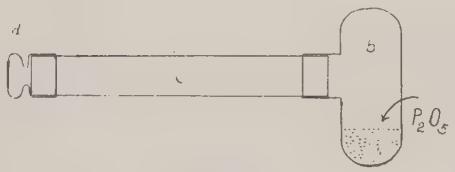

Fig. II.

(6) The other points to be noted in the following description are abbreviated since they are the same as those described by the writer in the article on the Quantitative Separation of Platinum and Iridium. (Sci. Rept. Tôhoku Imp. Univ., Vol. XII, No. 4, P. 368; Journal of the Japan Chemical Society, **44**, 5, P. 427).

EXPERIMENT A_1.

The Reaction between Ruthenium tetroxide and Hydrochloric Acid Gas.

The apparatus for the experiment is as shown in the figure.

First a mixture of dry chlorine and hydrochloric acid gas is made to effuse from the inner tube which corresponds to a spray jet, and ruthenium tetroxide is sent from the outer tube, whereby the reaction immediately ensues, causing a dark brown semifluid substance to adhere to the side of not only the chamber, but also of (b) and (c). The quantity of the substance deposited decreases the farther it recedes from the chamber, but the thickness increases gradually with the lapse of

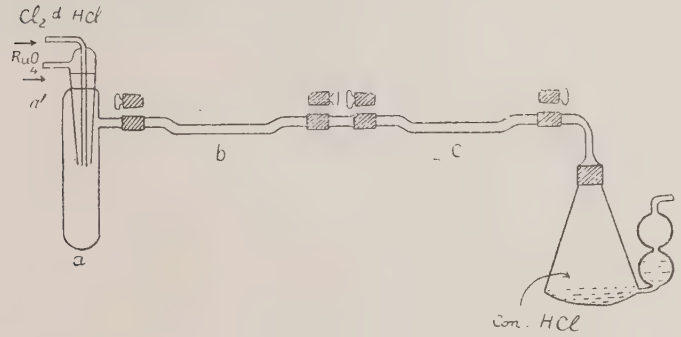

Fig. III.

time. In the absorption flask are arrested all the compounds which are to pass off. Except the liquid attaching to the lower part of the chamber, (a), all the parts of the semifluid form brown fibrous crystals in one or two hours.

Fig. IV,

Fig. IV is the photograph of the part a′ of the reaction chamber $\left(\text{magnification } \frac{15}{16}\right)$. The substance remaining at the lower part of the chamber (a) presented an appearance of some concentrated aqueous solution and did not crystallize easily. After allowing it to stand for 30 days in a phosphorus pentoxide desiccator, large, dark brown needle, like crystals having a strong lustre like that of potassium permanganate were obtained.

The weighing tubes (b) and (c) were weighed before and again after the reaction, obtaining 0.29453 and 0.14927 gr. respectively as the weights of the contents. These were put in the special drying spparatus

and the decrease of weight was measured, the result being as follows. The weighing was confined to the contents of tube (c).

Decrease of Weight	Time	Note
0.01017 gr.	36 hours	
0.01550	60	
0.01902	84	
0.02198	108	Emits the odour of hydrochloric acid gas
0.02492	132	,,
0.02839	163	,,
0.03254	204	,,
0.03429	228	,,
0.03577	252	The odour of hydrochloric acid gas not perceptible
0.03772	300	
0.03782	321	
0.03790	330	
0.03790	390	

If now the decrease of the weight is represented by the percentage, and taken as the ordinate, and the time taken as the abscissa, a curve in the Fig. V is obtained. As is clear from this curve, the decrease of the weight of the compound shows that the water adhering to the crystals is removed, and moreover that, even if the compound contains the water of crystallization, no change in

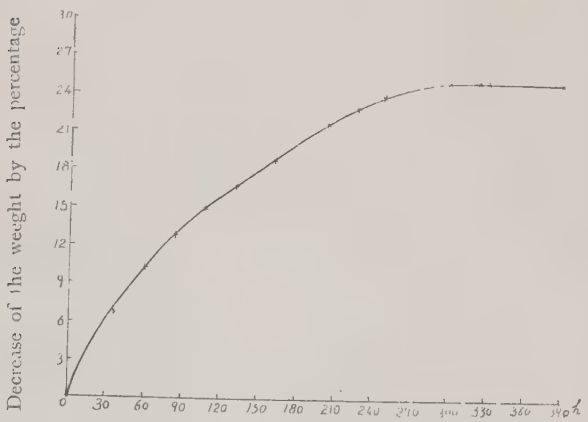

Time.

Fig. V.

this water of crystallization occurs at ordinary temperatures when it is placed in a phosphorus pentoxide desiccator.

THE ANALYSIS.

The tube (c) was heated in a combustion tube, a stream of oxygen being passed through it and the hydrochloric acid and chlorine was led over heated silver gauze and weighed as silver chloride. After heating for one hour, what remained was weighed as ruthenium dioxide. (p. 20). The result is shown in the Analysis Table I. In II, the sample was heated in an oxygen stream as was done in the tube (c), but the chlorine evolved was made to react with molecular silver according to the method of Denstedt, the water formed at the same time being absorbed in a calcium chloride tube. III was obtained by analysing a freshly made sample by the same method as that of II, while IV shows the result obtained when the metallic ruthenium obtained by reduction in a hydrogen stream was recalculated to ruthenium dioxide, the hydrochloric acid being absorbed in a silver nitrate solution. The "calculated number" means that calculated from $H_2RuO_2Cl_4.3H_2O$.

Analysis Table (I)

	Ruthenium Dioxide	Chlorine	Water
I.	40.20 %	42.15 %	——
II.	40.32	42.58	22.02
III.	40.18	42.50	22.87
IV.	40.30	42.10	——
Calculated number	40.31	42.63	21.73

The crystal is that of a new compound agreeing well with the molecular formula $H_2RuO_2Cl_4.3H_2O$ and will be named tetrachlordioxyruthenic acid. The mechanism of the formation of the substance will be

$$RuO_4 + 6HCl = H_2RuO_2Cl_4 + Cl_2 + 2H_2O.$$

The water of cyrstallization of the oxyruthenic acid perhaps came from the water formed in the reaction and the moisture contained in ruthenium tetroxide.

PROPERTIES.

The characteristic properties of tetrachlor-dioxyruthenic acid are as follows.

(1) Its hygroscopicity is extremely large. When taken out of the desiccator, it immediately changes into a reddish brown liquid, but on letting it stand in the desiccator it again forms the original needlelike crystals.

(2) It dissolves in water and alcohol with extreme ease. The aqueous solution presents an acid reaction, but the dilute solution hydrolyses very rapidly into a black colloidal liquid. The concentrated solution is stable as an aqueous or hydrochloric acid solution.

(3) When a concentrated ammonium chloride is added to its concentrated solution, a black crystalline precipitate immediately forms and the solution emits the odour of ruthenium tetroxide.

(4) When concentrated hydrochloric acid is added to this substance, it dissolves evolving chlorine gas at the same time and changes into a reddish brown solution.

(5) When ammonia is added to the aqueous solutisn, a white precipitate forms instantaneously, which however, immediately dissolves to form a reddish brown solution, and then a grayish green precipitate begins to form from the upper part, and finally turns black. This dissolves in an excess of ammonia turning grayish blue. When this is boiled, it becomes green and forms a beautiful deep violet solution as the ammonia gas escapes. When this solution is allowed to evaporate in a desiccator, violet amorphous powder is obtained. This contained ammonium chloride, which was dissolved away by 90 % alcohol and was analysed, the result agreeing quite well with the molecular formula $Ru(NH_3)_3.(H_2O)_2.Cl_2$, This is an ammine compound unrecorded in the

past literature, and the writer is now making an investigation of this substance.

(6) When heated in a stream of hydrogen, it loses the larger part of the water at 90–100°, and melts at about 120°, presenting a transparent thick reddish brown appearance. When the temperature is raised further, chlorine and hydrochloric acid gas is evolved, and it blackens and solidifies at about 140°. When kept at about 260°, it changes into ruthenium dioxide which has apparently a strong graphite-like lustre. If the compound is suddenly heated at the outset to attain a temperature of about 260°, a brown substance, though small in quantity adheres to the sides of the combustion tube. So when heating, it must be decomposed at first at low temperatures and very gradually.

EXPERIMENT A_2.

The Reaction between Tetrachlor-Dioxy-Ruthenic Acid and Concentrated Hydrochloric Acid.

As has been already mentioned, when concentrated hydrochloric acid is added to the oxyruthenic acid, chlorine is evolved, heat being generated at the same time. If a saturated ammonium chloride solution is added to it, it readily forms dark brown crystals. The composition of this substance varies with every synthesis, but from the results of the analysis, it was inferred that it is a mixture of $(NH_4)_2RuCl_6$ and $(NH_4)_2RuCl_5$. Consequently the formation of ruthenium trichloride and ruthenium tetrachloride is possible. The mechanism of the change may be as follows;

(1) $H_2RuO_2Cl_4 + 4HCl = H_2RuCl_6 + 2H_2O + Cl_2$

(2) $2H_2RuCl_6 \rightleftarrows 2H_2RuCl_5 + Cl_2$.

EXPERIMENT A_3.

The Reaction between Tetrachlor-Dioxy-Ruthenic Acid and the Solution of Ammonium Chloride.

The immediate black precipitate forms on the reaction of the two, but at the same time small bubbles are produced and the odour of

ruthenium tetroxide and chlorine is emitted. If the two reacting substances are well cooled before the synthesis, only a slight emission of gas bubbles is recognized, but no odour of ruthenium tetroxide. But as the solution comes to attain room temperature, the same phenomena as before occurs. The crystalline precipitate has no odour of ruthenium tetroxide. These compounds vary in composition at every time of its synthesis, but the sample, which was prepared very carefully, can be inferred on analysis to be a mixture of $2((NH_4)_2RuCl_6 \cdot \frac{1}{2}H_2O) + (NH_4)_2RuCl_5$.

Thus, $6H_2RuO_2Cl_4 + 12NH_4Cl$

$$= 4((NH_4)_2RuCl_6) + 2(NH_4)_2RuCl_5 + Cl_2 + 6H_2O + 2O_3.$$

The chlorine and ozone formed here are supposed to act on the mother liquor to form ruthenium tetroxide.

The writer inferred from the study of Howe (1901) that he might be able to obtain $(NH_4)_2RuO_2Cl_4$, and carried out the above described experiments, but they finally proved to be a failure. Kraus (1921) also reported that he could not obtain $M_2(RuO_2Cl_4)$.

EXPERIMENT B_1.

The Reaction between Ruthenium Tetroxide and Concentrated Hydrochloric Acid, and the Method of Preparation of $(NH_4)_2RuCl_6 \cdot \frac{1}{2}H_2O$.

When the ruthenium tetroxide was obtained from 1 gr. of metallic ruthenium added to concentrated hydrochloric acid, it rapidly dissolved forming a reddish brown liquid, chlorine being evolved at the same time. Into this liquid was passed the mixed gas of chlorine and hydrogen chloride with constant heating at the same time, the heating being stopped after 5 hours, and the chlorine gas was made to saturate until the liquid quite cooled down. Separately, chlorine gas was made to saturate 400 cc. of concentrated hydrochloric acid and 4.5 grams of ammonium chloride were dissolved in the above mixture. When cooling the two solutions in ice the former is slowly dropped on to the latter, crystals as shown in the Fig. VI_1 and VI_2 were formed, whose colour was dull grayish brown. They were filtered, using asbestos, washed five times with a solution of concentrated hydrochloric acid saturated with chlorine, and

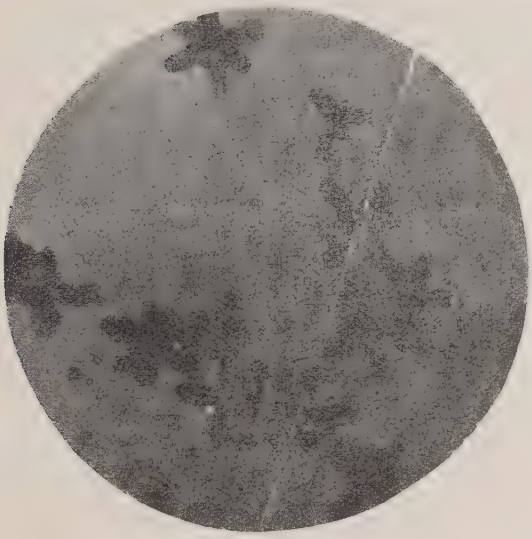

Fig. VI_1.

then three times with anhydrous alcohol. A part of the crystals was dried in a sulphuric acid desiccator, the other in a steam bath, the result however, being the same in both cases. Accordingly the method of drying by a steam bath was adopted in subsequent experiments.

The yield was 94 %. The mother liquor contained 0.005 gr. of ruthenium per 100 cc. the washing solution 0.0087 gr. for the same quantity.

The explanation of the Fig. VI_1 and VI_2.

The crystal belongs to the regular system, and the appearance is like an octahedron, but the vertical angles are not acute, and a large number of crystals are heaped up together like a tower, and radiate in six directions. When a microscope is focussed at a certain point, the 3 rays become distinct while the other three become vague.

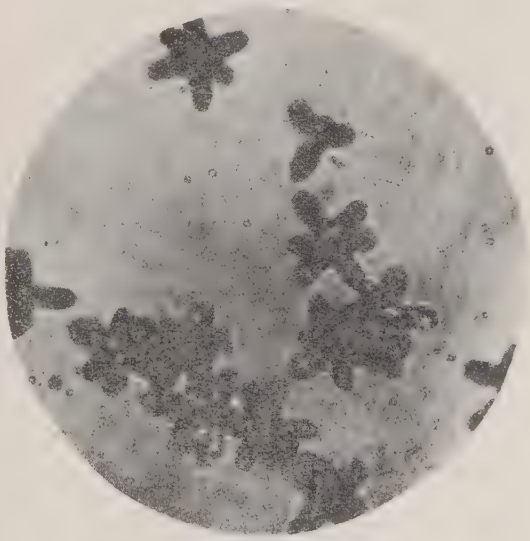

Fig. VI_2.

If it is focussed at a little lower or higher points, the rays which were vague become clear and those which were distinct before become vague. The two pictures, Fig. VI_1 and VI_2 were taken from one and the same preparation and show the above mentioned relation.

ANALYSIS TABLE (II.)

	Ruthenium	Chlorine	Ammonia	Water
I.	28 28	58.56	8.87	.....
II.	28.33	58.83	8 99	.....
III.	28.20	.....	9 07	.....
IV.	28.30	.....	.....	2.37
V.	28.19	59 38	8.98	.....
Calculated number	28.21	59 17	9.35	2 50

The "calculated number" means the one which was calculated from $(NH_4)_2RuCl_6.\frac{1}{2}H_2O$, and shows satisfactory agreement with the result of the analysis. I and II were treated in a hydrogen stream, III in an oxygen stream, and all of them weighed in the form of metallic ruthenium. IV shows the decrease in the weight when the sample was heated to 180–190° in a stream of hydrogen chloride gas, and almost no decrease was recognized when the temperature was raised to 240°. The decrease was inferred to have been due to water, because in the cases of I, II and III, the condensation of a considerable quantity of water was clearly recognized. V represents the weight of the product which resulted by reducing in a hydrogen stream the precipitate, which formed when the aqueous solution of the sample was boiled with a solution of concentrated sodium hydroxide to determine ammonia. In this case ruthenium is completely deposited. The ammonia was determined volumetrically in the usual way, after causing it to be absorbed in a normal sulphuric acid solution.

The chief properties of $(NH_4)_2RuCl_6\,\frac{1}{2}H_2O$ are as follows.

(1) It easily dissolves in water to become reddish brown. Its solubility differs from that of the compound obtained by Mylius and Mazzuchelli and resembles that of the compound obtained by Howe. When it is diluted, it becomes yellow, and gradually hydrolyses to become black and finally forms a precipitate. In the presence of hydrochloric acid, this change is not observed.

(2) It is only with great difficulty soluble in anhydrous alcohol and concentrated hydrochloric acid, and it is to be noted that a sample

once dried is not dissolved at all by these solvents.

(3) When ammonia or caustic soda is added to its aqueous solution, the solution becomes colourless and forms a black precipitate on boiling.

(4) The violet colour reaction (Howe) is distinct but not so sensitive as in the case of K_2RuCl_6.

(5) No change occurs with bromine water.

(6) The action towards hydrogen sulphide is entirely different from the behaviour of the aqueous solution of tervalent ruthenium. It was long recognized as a sensitive and characteristic reaction of ruthenium that when hydrogen sulphide is passed into an aqueous solution of tervalent ruthenium salts for a long time, the solution turns azure blue and black precipitate forms locally (J. N. Friend :— Text Book of Inorganic Chemistry, Vol. IX, Part I, P. 331 ; Treadwell :— Analytical Chemistry Vol. I, P. 511.). But when the aqueous solution of ammonium salts of the tetravalent ruthenium obtained by the writer is made acid by hydrochloric acid and hydrogen sulphide is passed into it, the colour first fades and then gradually turns brown, finally forming a violet black precipitate which can not be filtered. When filtered after being allowed to stand for 24 hours, the reaction of ruthenium with sodium thiosulphate is no longer recognized in the filtrate. If hydrogen sulphide is passed into the neutral solution a similar change occurs as before, but no precipitate is formed, but the mixture only has an appearance of a dark brown colloidal solution. When, however, this is boiled, a precipitate forms locally, but the solution is coloured deep brown. In the latter case no azure blue colour is presented however long the hydrogen sulphide be passed. If the solution is acid, the reaction does show, but is not sensitive.

(7) The change taking place when the crystal is heated in a hydrogen stream is as follows :

No change is recognized till 130°, but from about 140° the evolution of water vapour is distinctly recognizable, which stops at about 160°. From above 155°, hydrogen chloride is evolved which becomes most remarkable at about 200°. From about 170°, the volatilization of

ammonium chloride is perceptible. At about 360°, the whole seems to be reduced to metallic ruthenium, but to attain constancy of weight rapidly; the sample was always heated above 400° in the experiments.

EXPERIMENT B_2.

The Preparation of $(NH_4)_2RuCl_6.\frac{1}{2}H_2O$ from the Reaction Product of $H_2RuO_2Cl_4.3H_2O$ and Hydrochloric Acid. As was mentioned in A_2, the writer expected the formation of H_2RuCl_6 in the presence of the excess of chlorine from the reaction products of the two, and the complex salt of the resulting substance with ammonium chloride was found to coincide entirely with $(NH_4)_2RuCl_6.\frac{1}{2}H_2O$ in colour, form and properties of the crystal and also in the results of the analysis. So it can be inferred that the reaction product of ruthenium tetroxide and concentrated hydrochloric acid and that of $H_2RuO_2Cl_4.3H_2O$ with concentrated hydrochloric acid are quite identical. Hence $H_2RuO_2Cl_4+4HCl = H_2RuCl_6+Cl_2+2H_2O$.

EXPERIMENT C_1.

The Preparotion of K_2RuCl_6. Chlorine gas is passed into the reaction product of ruthenium tetroxide and hydrochloric acid obtained, in exactly the same way as in B_1 for four to five hours with constant heating on a water bath and a saturated hot solution of potassium chloride is slowly added, and then further heating is continued for five hours. The crystals which separated were filtered before the solution cooled down. The precipitate was washed 4 times with chlorine saturated hydrochloric acid and 3 times with alcohol and then dried in a steam bath. The crystals were of strong lustre and dark brown in colour the form resembled the complex salt of ammonium chloride well, but were very much greater. Several crystals form an irregular aggregate, but each crystal seems to form a regular octahedron.

In analysis I, the crystals were heated for about an hour in a hydrogen stream at a temperature below 150° (to prevent the spattering of the crystal) and then heated to 550°. The hydrogen chloride which came out was absorbed in a silver nitrate solution, and the residue in

the boat was weighed as $Ru+KCl$, and after lixiviating this with water, ruthenium was determined which was in the reduced metallic condition, and potassium chloride as the double chloride of potassium, hexachlor platinate. In II, the sample was heated in the same order, and the operations were the same as were performed in I except that the chlorine gas was weighed by making it act upon molecular silver. I and II represent, however, the samples prepared on different days.

Analysis Table III.

	Ruthenium	Chlorine (Combined with ruthenium)	Potassium Chloride
I.	25.27	35.54	37.07
II.	25.57	36.03	37.83
Calcutated number	25.90	36.11	37.97

The "calculated number" is the one calculated from K_2RuCl_6. which agrees quite well with the results of the experiments.

The characteristic properites of K_2RuCl_6 are as follows:—

(1) It is very easily soluble in water. In this respect it differs from the compound obtained by Antony and closely resembles that obtained by Howe. The dilute solution is yellow, and the solution hydrolyses, its colour turning black, and the greater the dilution, the faster the hydrolysis.

(2) The action towards concentrated hydrochloric acid and alcohol is nearly similar to that of $(NH_4)_2RuCl_6.\frac{1}{2}H_2O$.

(3) If the crystals are dissolved to make a dilute solution and the solution is immediately boiled, it presents a light violet brown colour. If then a drop of concentrated hydrochloric acid is added, it is temporarily coloured deep violet but it slowly fades to become yellow. This is in quite satisfactory agreement with the violet colour reaction of Howe.

(4) Bromine water is only capable of making the colour a little thicker.

(5) Ammonia makes the colour of the solution fade a little and a dirty white precipitate is formed in a short time.

(6) A caustic soda solution makes the solution yellow and finally forms a dirty green colloidal solution. When this is boiled the compound is completely deposited as a black precipitate. The precipitate is insoluble in dilute alkali and has approximately the composition $Ru(OH)_4 H_2O$.

(7) The behaviour towards hydrogen sulphide not only closely resembles that of the ammonium complex salt, but in a cold acid solution is more remarkable, and the most noteworthy facts are that it presents a slightly azure-blue colour and that it is completely precipitated as a sulphide.

(8) When the K_2RuCl_6 is heated in a dry hydrochloric acid gas at 540°–550° it loses one atom of chlorine to form K_2RuCl_5. A special article will be devoted to the study of it.

EXPERIMENT C_2.

The Preparation of K_2RuCl_6 from a Cold Solution.

A solution obtained in Exactly the same way as in C_1, is saturated with chlorine. Separately a solution saturated with potassium chloride and chlorine is made. When the former is dropped upon the latter with constant cooling in ice, a dark brown precipitate immediately forms. The crystalline form resembles that of C_1, but is of a dull colour. The properties and the compositon are also the same. The writer carried out this experiment thinking that it might be possible to obtain by this method, potassium hexachlor-ruthenate with the water of crystallization, but the attempt finally proved to be a failure.

EXPERIMENT D.

The Preparation of Potassium Pentachlor-Ruthenite from Potassium Hexachlor-Ruthenate.

When potassium hexachlor-ruthenate is heated in a dry hydrochloric acid gas, no change is observed till 500°, but above this temperature, chlorine is gradually evolved and the weight becomes once constant

at about 540°–560°, and when further heated for 3 to 4 hours at 600°, it again shows a constant weight and no further change occurs. But at such a temperature there is a danger of a small quantity of potassium chloride being sublimated and lost.

The aspects of these changes are shown in the Table IV.

TABLE IV.

Time of heating (h)	1	2	1	3	2	2	2
Temp. of heating (c°)	0°–500°	500°–510°	510°–520°	520°–530°	530°–540°	540°–550°	550°–560°
Decrease in weit. (%)	00	7.44	7.80	8.34	9.00	9.09	9.19

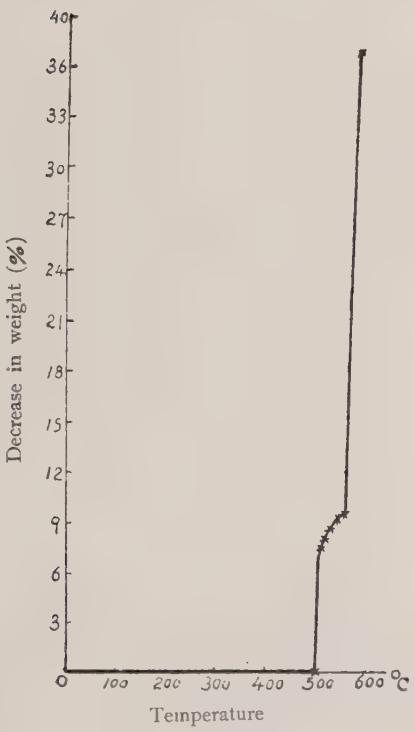

Fig. VII.

The relationship is shown in Fig. VII. The ordinate represents the percentage decrease and the abscissa the temperature. The decomposition begins at 500° and stops for a while at 560°, and then the 2nd decomposision occurs, which is clearly shown in the figure.

THE ANALYSIS.

The analysis was made in (Exactly) the same manner as that of K_2RuCl_6, and the calculated number was the one calculated from K_2RuCl_5. The results of the analysis agree qnite well with those of potassium pentachlor-ruthenite.

Analysis Table V shows these relationships.

ANALYSIS TABLE V.

Ruthenium		Chlorine (combined with Ru)	Potassium chloride
I.	28.60	19.02	51.83
II.	28.58	18.97	51.99
Cal.	28.47	19.85	51.67

Let us name the compound obtained γ-potassium pentachlor-ruthenite, that obtained by Howe provisionally β-potassium pentachlor-ruthenite, and the one obtained by ordinary methods α-potassium pentachlro-ruthenite, and compare their properties. (All the reactions were carried out at ordinary temperatures, except the violet colour reaction).

Reagents	γ	β	α
water	Extremely soluble.	Easily soluble.	Difficultly soluble.
The colour of the aqueous sol. when concentrated.	Yellowish.	Rose colour.	Reddish brown.
Dilute aqueous solution.	Bright yellow colour. No change for a few days.	Yellow. Immediately becomes a black colloidal solution.	Yellow. Immediately becomes a colloidal solution.
Violet clour Reaction.	None.	None.	None.
Bromine water	Immediately forms a black precipitate.	Immediately forms a black precipitate.	Only deepens the colour.
Ammonia water	Immediately a fine fugitive green colour which gradually turns brown.	The colour fades, forming a black precipitate.	At first the solution becomes dirty green. Then a brown precipitate gradually forms.
Aqueous caustic soda solution.	At first a deep blue colour. Then becomes greenish yellow, then a dirty green colloidal solution and finnally forms a black precipitate.	Immediately forms a dirty white precipitate, and then a black precipitate.	Immediately fades and presents a dirty green colour.
Hydrogen sulphide passed into its acid solution.	The solution is coloured a beautiful green very slowly, then gradually azure-blue, and finally forms a black precipitate. The azure-blue solution faded on being allowed to stand for 3 days.	The colour gradually fades and becomes colourless at one time. Then turns yellowish brown, and gradually forms a precipitate and a very slight azure-blue colour is recognized.	The solution gradually fades and is colourless at one time. Again becomes brown, and shows the characteristic azure-blue colour very slowly, and at the same time a precipitate is formed. The colour of the solution fades on being allowed to stand for 2 days.

The above table shows that the properties differ markedly, but the composition agrees quite well with K_2RuCl_5, so that these must be regarded as three isomers. Howe postulated the existence of two isomers, but the writer withes to make an addition of one isomer, and he believes that the existence of these three isomers should not be overlooked in attempting a stereochemical explanation of the complex salts (e. g. M_2RuX_5) formed by tervalent elements.

EXPERIMENT E.

The Precipitation of Potassium or Ammonium Hexachlor-Ruthenate Solution by Hydrogen Sulphide.

A solution of potassium hexachlor-ruthenate was made which contained 0.1 mg. per 1 cc. as metal. 4 cc. of concentrated hydrochloric acid (1.19) was added to every 100 cc. of the solution. On each occasion 500 cc. of the solution was taken in an Erlemmeyer flask as a sample, and hydrogen sulphide was passed into it. The solution is coloured a deep brown. When hydrogen sulphide was passed, the colour gradually faded and a slight turbidity was formed by the separation of sulphur. When the passing of hydrogen sulphide was continued further, the solution became gradually brownish and finally formed a black precipitate. In one hour, the introduction of hydrogen sulphide was stopped and the solution was allowed to stand for 24 hours. The colour seems to have becoms blue within these hours, but the reaction is not sensitive.

If the solution is sufficiently boiled, the filtration is very easy and there is no danger of the precipitate passing through the filter. The precipitate was washed with hot water five times and after drying partially, it was carefully ignited together with the filter and reduced in a stream of hydrogen. After treating the filtrate with aqua regia, the sodium thiosulphate reaction was tried, but did not respond. The sample contained 0.0503 gr., and from the hydrogen sulphide precipitate there were obtained (1) 0.0501, (2) 0.0501 and (3) 0.0500 gr.

Nearly the same result was obtained with an aqueous solution of the ammonium salt.

The writer believes that these facts claim careful consideration in his future work on the separation of the platinum group elements.

EXPERIMENT F.

A Method of Preparation of Ruthenium Dioxide.

Ruthenium dioxide has already been described by Claus.[1] Devill & Rausohoff,[2] Gutbier & Rausohoff,[3] etc., obtained it as a sublimate by igniting metallic ruthenium in a stream of oxygen. Also the former obtained crystals of an octahedral pyramid by roasting ruthenium sulphate or ruthenium disulphide. Gutbier & Leuchs[4] reported that the oxidation of ruthenium occurs at 600° and proceeds rapidly with the rise of temperature and that if the metallic ruthenium is ignited in a hydrogen stream beforehand, the velocity of oxidation is considerably slackened.

The writer heated $H_2RuO_2Cl_4.3H_2O$ in a stream of oxygen at a temperature below 140° at first, and then finally at 400°, and obtained thin flakes of an oxidation product with a strong graphitoid lustre. It was ascertained that the oxidation product was no other than RuO_2 as rsults of reduction in a stream of hydrogen.

Analysis Table VI.

		Ruthenium
Ex.	I.	76.00 %
	II.	76.02
	Cal.	76.06

The calculated number is the value reduced to metallic ruthenium from ruthenium dioxide.

Also $(NH_4)_2RuCl_6.\frac{1}{2}H_2O$ was strongly heated at 540° in a stream of oxygen, obtaining lustrous bluish black crystals. These were reduced in a stream of hydrogen obtaining 76.04 %, which, too, agrees with the calcualted number.

Also the crystals of K_2RuCl_6 were strongly heated in air, over the

(1) Annalen **56**, (1845), 257.
(2) Ann. Chim. Phys, **56**. (1905), 385.
(3) Z. anorg. Chem., **45**, (1905), 243.
(4) Z. anorg. Chem. **96**, (1916,) 182.

blast lamp dark brown lustrous crystals remained. When this was reduced in a stream of hydrogen, 76.07 % of Ruthenum was obtained.

From the above results, it was ascertained that ruthenium dioxide can always be obtained at a comparatively low temperature by heating any of $H_2RuO_2Cl_4.3H_2O$, $(NH_4)_2RuCl_6.\frac{1}{2}H_2O$ and K_2RuCl_6 in a good supply of oxygen, and the temperature need not be higher than 540°. But it was made clear that when the metal which has been reduced in a stream of hydrogen is heated to 540° in a stream of oxygen, the metal is oxidized with the lapse of time, but it does not readily become a dioxide. In the following table are tabulated the time of ignition and the increase in weight expressed in percentage. The material used in this experiment was the ruthenium obtained from $(NH_4)_2RuCl_6.\frac{1}{2}H_2O$.

$$(NH_4)_2RuCl_6.\tfrac{1}{2}H_2O \rightarrow RuO_2 \rightarrow Ru).$$

The Analysis Table VII.

Time (hours)	Increase in weight.
1.	10.43 %
2.5	11 80
4.5	13 11
6.	14.37
8.5	15.20
11.	16.02
13.	16.40
14.5	16.56
17.5	17.5
20.5	18.17
23.5	18.67
28.5	18.93
30.	19.30
31.5	19.50
34 5	20.45
36.5	20.48
38.5	20.88
42.5	21.22
45.5	21.79
47.5	21.96
50.	22.20

The result is shown in the accompanying figure taking the percentage increase in weight as the ordinate and the time as the abscissa. It clearly shows that the preparation of rutheinum dioxide by heating at such a low temperature as 540°, a metal which has been once reduced in a stream of hydrogen is well-nigh impossible and as is seen from the direction of the curve, Ru_2O_3 will probably be obtained as the highest oxide. The curve shows also some breaks at points which nearly correspond to RuO and $3RuO.Ru_2O_3$, but it seems to be extremely doubtful whether such definite compounds are formed or not.

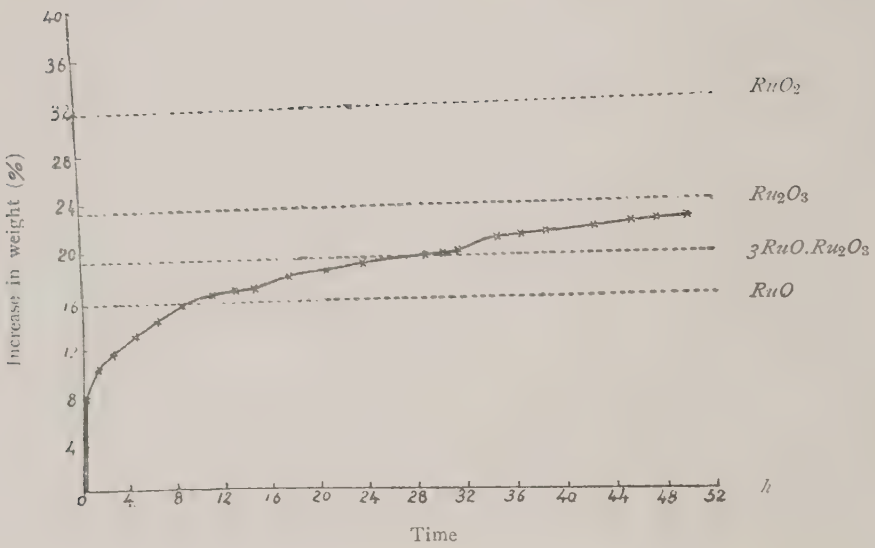

Fig. VIII.

SUMMARY.

(1) A new compound tetrachlor-oxyruthenic acid ($H_2RuO_2Cl_4.3H_2O$) was obtained in the form of reddish brown needles, by the interaction of hydrochloric acid gas and ruthenium tetroxide. The characteristic properties consist in its extreme hygroscopicity and the change of colour of its solution towards ammonia water. From it a new ammine compound ($Ru(NH_3)_3(OH_2)_2Cl_2$) was obtained.

(2) Tetrachlor-oxyruthenic acid or ruthenium tetroxide was made to react upon concentrated hydrochloric acid. The product was heated on a water bath, into which was passed chlorine gas and hydrochloric acid gas for 4–5 hours and cooled. The solution obtained was dropped into a concentrated hydrochloric acid saturated with chlorine and further with ammonium or potassium chloride, obtaining $(NH_4)_2RuCl_6\,\frac{1}{2}H_2O$, and K_2RuCl_6 respectively. The latter was also obtained from the hot solution in a similar way.

As characteristic of these hexachlor-ruthenic acid salts, besides that they present the violet colour reaction of Howe, is especially noticable

the fact that they are completely precipitated by hydrogen sulphide. The azure-blue coloration reaction is in this case insensitive.

(3) The writer infers that the reaction hetween ruthenium tetroxide and hydrochloric acid will proceed according to the following mechanism, from his study of the results obtained when the hydrochloric acid was substituted by hydrochloric acid gas.

(1) $RuO_4+6HCl_{gas} = H_2RuO_2Cl_4+Cl_2+2H_2O.$

(2) $H_2RuO_2Cl_4+4HCl_{solut.} = H_2RuCl_6+Cl_2+2H_2O,$

(3) $2H_2RuCl_6 \rightleftarrows 2H_2RuCl_5+Cl_2.$

If we assume that the reaction takes place in these three stages, we can readily explain the difficulty of obtaining hexachlor-ruthenic acid, and its salts pure, and that some time and some special device are necessary to prepare ruthenium trichloride also in a pure condition. The writer carried out his experiments taking these into consideration and succeeded in preparing two compounds which irrefutably proved to be $(NH_4)_2RuCl_6\,\frac{1}{2}H_2O$ and K_2RuCl_6.

(4) By heating K_2RuCl_6 at 530–540° in a stream of hydrochloric acid gas, K_2RuCl_5, less by one chlorine atom, was obtained, and was named γ-potassium pentachlor-ruthenite. The characteristic property of this substance is that its dilute solution is yellow and suffers no change when allowed to stand for several days, and that it is coloured green by ammonia water, and intense blue by caustic soda. The reaction towards hydrogen sulphide is more remarkable than that of ordinary ruthenium salts.

We must recognize the existence of the three isomers of K_2RuCl_5, one prepared by the ordinary methods, another obtained by Howe, and still another, that obtained by the writer. These will be called α–, β– and γ–potassium pentachlor-ruthenite respectively.

(5) The fact that the aqueous solution of potassium hexachlor-ruthenate or the ammonium salt is completely precipitated by hydrogen sulphide will be of some use in the separation of platinum group elements from each other or from elements other than platinum group elements.

(6) Ruthenium dioxide was obtained by heating tetrachlor-oxyruthenic acid or hexachlor-ruthenic acid salts at the low temperature of 540°. But after it is once reduced in a stream of hydrogen, it is difficult to obtain ruthenium dioxide. After prolonged heating the weight corresponding to Ru_2O_3 was attained.

(7) The material used in the present experiment is one which had been purified by Prof. Ogawa himself with years of labour. This to a great extent spared the writer the trouble of purification. Moreover, he feels deeply indebted for Prof. Ogawa's constant interest and useful suggestions for the investigation. Finally he also wishes to extend his thanks to Mr. Shigeo Saegusa for his trouble in the preparation of K_2RuCl_6 and γ-K_2RuCl_5.

July 1923. Laboratory of Inorganic Chemistry,
Chemical Institute, Science College,
Tôhoku Imperial University, Sendai, Japan.

On the Equilibrium Diagram of the System Iron-Carbon-Titanium.[1]

By

Kanzi Tamaru.

§ 1. INTRODUCTION.

A great deal of iron sand has been found in many localities in the world, such as New Zealand, Canada and the U. S. A. A deposit in New Zealand is said to extend for over 300 miles and to be more than 50 ft. deep: that of the St. Lawrence river in Canada is well known. In our country, also, many deposits of iron sand have been found on the northeastern coast as well as on the western; one of the northeastern deposits is reported to contain 200,000,000 tons. Thus the total amount of this sand in the world is very large.

Iron sand always contains more or less titanium and it reaches 7 percent in one of our deposits, It was formerly believed that the main constituent of iron sand was magnetic iron. According to the recent investigation by K. Inouye,[2] Assist. Prof. of Tokyo Univ., however, it principally consists of titaniferous magnetic oxide, i.e. a solid solution of ilumenite, ferric and ferrous oxides, the pure magnetic oxide being only about 10 percent.

Unfortunately this iron sand cannot as yet be used for blast furnaces. The reason is twofold; first as the sand is in a fine state, it is necessary to utilise it in briquets for the blast furnace; secondly, in virture of the

(1) The ninety eighth report from the Research Institute for Iron, Steel and Other Mitals.
(2) Tetu to Hagane, **8**, (1922).

presence of titanium, it is very difficult to run the furnace smoothly. Thus repeated experimental blowings in many distlicts in the world, especially in New Zealand, were carried out without success. But it is considered that, in the future it will be one of the raw materials for the manufacture of iron and steel. Hence it is very desirable to study the properties of steels containing titanium, and as a preliminary the ternary diagram of iron-carbon-titanium.

§ 2. SOME PROPERTIES OF TITANIUM.

Both titanium and silicon belong to the fourth group of the periodic system and hence their properties are very similar to each other. Like silicon, titanium has a strong affinity for oxygen, and easily combines with nitrogen. According to Comstock,[1] a steel treated with 0.1 percent of titanium contains 0.0035 percent of nitrogen, while one not so treated 0.0046 percent. Thus ferrotitanium is frequently used for the purpose of removing nitrogen and oxygen in molten iron and steel.

The melting point of titanium is not certain; according to Kaye's table it is 1800°C.

The density of titanium has not been accurately determined; Moissan gives 4.87 with a sample containing 2 percent of carbon.

§ 3. IRON-TITANIUM DIAGRAM.

Fig. 1 shows a diagram of the iron-titanium system obtained by Lamort.[2] As shown in the figure, the saturation point of titanium in iron is 6 percent and an indeterminate compound (Fe_3Ti?) lies at concentration of 22.31 per-

Fig. 1.

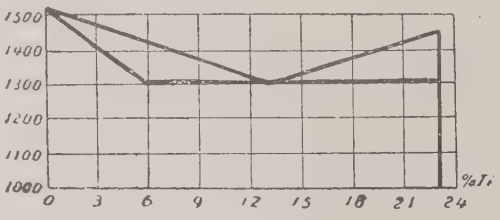

Fe-Ti Diagrrm.

(1) Chem. Met. Eng., **22**, (1920) 400.
(2) Ferrum 1914, p. 225.

cent of titanium. These two constituents form a eutectic consisting of 13.2 percent of titatium at 1298° C.

Titanium has not only a high melting point, but also a great viscosity in the liquid state; hence with an increase of titanium content, it is very difficult to obtain a homogeneous melt. Therefore Lamort prepared the samples by the thermit process.

§ 4. THERMAL ANALYSIS.

The ferrotitanium used in the present investigation is that from the Metal and Thermit Corporation in America. The analysis is as follows :—

$Ti = 24.69\ \%$, $Al = 4.12\ \%$, $Si = 2.00\ \%$, $Fe =$ remainder.

At the outset of the present investigation, wrought iron was melted, then fine grains of the ferrotitanium were added, and the mixture heated to 1700° C with the expectation of obtaining a homogeneous liquid. The ferrotitanium, however, hardly diffuses at all and the mixture resulting in a heterogeneous solid mass, since the melting point of this ferrotitanium (containing 24.69 percent of titanuim) is below 1500° C in Lamort's diagram.

After many unsuccessful attempts to prepare a homogeneous alloy, the following method was used.

Required amounts of finely powdered ferrotitanium, reduced iron and graphite were completely mixed together, pasted together with gum arabic and then briquetted by pressing the mixture into a mould. This briquet weighted 20 grams after being sufficiently dried.

A magnesia crucible was heated to about 1700° C, and hydrogen introduced to replace the air in the crucible. Then the dried briquet was placed in the crucible, hydrogen being continually introduced. When the briquet melted, a graphite rod was inserted into the molten mass to increase the carbon content, because the greater part of the graphite mixed in the briquet was burned off before it melted. During cooling from the melt the cooling curve was taken by means of a platinum platinum-rhodium thermocouple from 1500° C. In alloys containing more

than 4 percent of titanium a considerable amount of oxide, nitride and probably cyanide was found, notwithstanding that hydrogen gas was continually passed, so that the present investigation was carried out on specimens containing less than 4 percent of titanium.

The results of the thermal analysis are given below :—

Specimen No.	Analysis		Liquidus	Eutectic
	Ti (%)	C (%)		
1	1.80	4.35	1233°C	1143°C
2	2.28	4.05	1183	1146
3	2.67	4.32	1183	1145
4	3.76	3.70	1220	1150
5	1.60	3.61	1226	1142
6	2.29	3.49	1234	1145
7	4.45	3.21	1278	1157
8	3.00	3.16	1281	1146
9	3.77	3.18	1322	1151
10	0.84	2.78	1344	1137
11	1.23	2.26	1355	1139
12	4.31	2.64	1378	1158
13	4.37	2.23	1385	1156
14	2.00	1.82	1405	1148
15	2.75	1.75	1429	1146
16	2.12	1.19	1411	—
17	2.37	1.40	1425	—
18	3.18	1.39	—	—
19	0.50	0.91	—	—
20	1.74	1.01	—	—
21	2.50	1.02	—	—
22	1.40	0.72	—	—
23	1.95	0.73	—	—
24	2.38	0.94	—	—

The specimens from No. 1 to 15 have two breaks, owing to the primary crystallisation and eutectic separation, except specimen No. 2 which has the latter change only.

Specimens Nos. 16, 17 and 18 have only one break, showing that the whole mass solidifies as a solid solution. Specimens Nos. 19 to 24 were used for determining eutectoid point under the microscope.

Some of the cooling curves are shown in Fig. 2; curve *a* is for

Fig. 2.

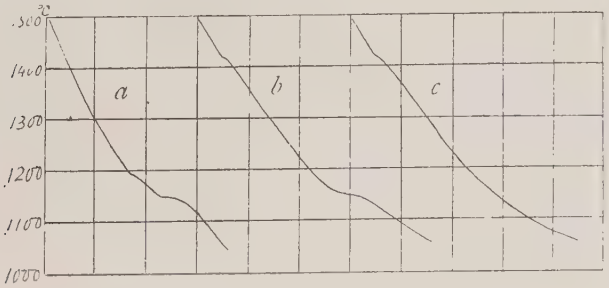

Cooling curve.

specimen No. 4 having a composition close to the eutectic point, *b* is for specimen No. 15 and *c* for No. 17.

Fig. 3.

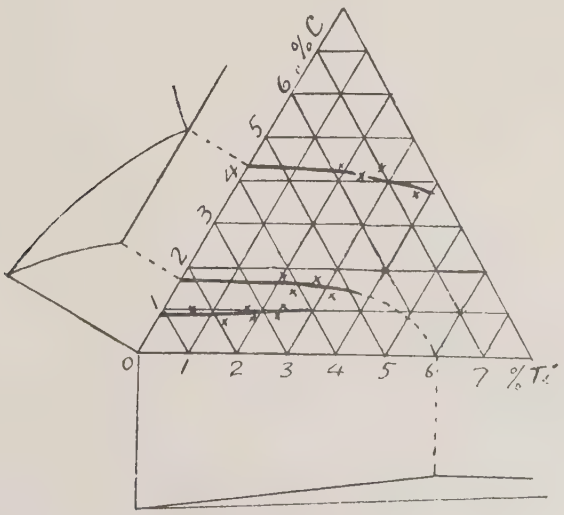

Structural diagram.

Fig. 3 shows the structural diagram of the system obtained by the result of the thermal analysis, from which the following conclusions may be drawn :—

(1) With an increase of titanium, the eutectic point consisting of austenite and carbide gradually decreases in carbon content and the temperature rises. That is, the eutectic point in alloys containing 4 percent of titanium is 1180° C with 3.8 percent of carbon, while in the case of the iron-carbon system, it is 1130° with 4.3 percent of carbon.

(2) By the addition of titanium, the saturation point of carbon in austenite decreases, though the eutectic temperature at which the austenite has a maximum solublity rises. That is, in alloys containing 3.5 percent of titanium, 1.5 percent of carbon is dissolved at 1150° C, while in the pure iron-carbon system, the austenite dissolves up to 1.7 percent of carbon at 1130° C.

(3) With an increase of titanium, the eutectoid point increases in carbon up to 1 percent in an alloy containing 3 percent of titanium. This is determined by microscopic observation; further investigation of this change is in progress in our institute.

From these results the saturation point of titanium in austenite or end point of the eutectic will be shown by a dotted line in Fig. 3.

Though the equilibrium diagram of titanium and carbon is not yet known, it is very probable that the ternary eutectic curve runs from the iron-carbon side down to that of the iron-titanium; because with an increase of titanium, the eutectic temperature of the iron-carbon system rises and tends to that of the iron titanium system, that is to say, the ternary eutectic is not present.

Fig. 4 shows the isothermals on the surface of crystallisation; that of 1150° C meets the eutectic curve at 2.25 percent of titanium, while those of 1200° C. 1250° C. do not meet the curve, provided the titanium is less than 4 percent.

Fig. 4.

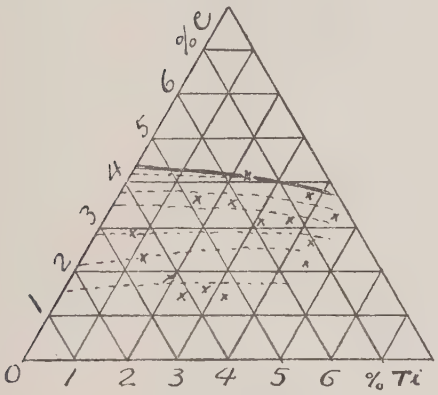

Fig. 5.

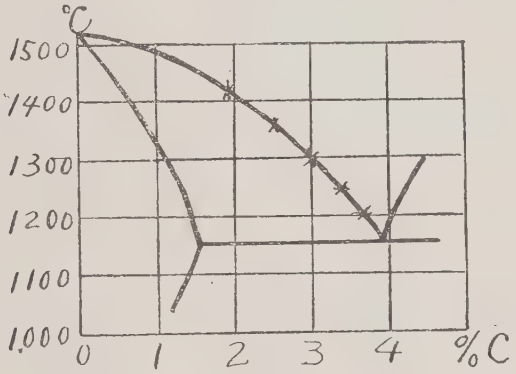

Fig. 5 shows the sectional diagram at 3.5 percent of titanium. The eutectic point lies at 3.9 percent of carbon consisting of carbide and austenite containing 1.5 percent of carbon.

§ 5. MICROSCOPIC INVESTIGATION.

The iron-carbon-titanium alloys containing less than 4 percent of titanium observed in the present investigation shows no special phase.

In the specimens subjected to thermal analysis, we see the graphite flakes in the matrix of pearlite as shown in Figs. 6 and 7.

Fig. 6 shows the structure of a hypereutectic alloys in which large and small graphite flakes are observable, the former being a decomposition product of the primary carbide and the latter that of the eutectic. The graphite in Fig. 7 showing the structure of a hypoeutectic alloys is that formed by the decomposition of the eutectic carbide. We can observe a pearlitic matrix changed from the primary austenite. In specimens corresponding to the hypoeutectoid composition, ferrite separated from austenite is seen.

The effect of titanium on graphitisation is similar to that of silicon. Specimens cooled slowly in the furnace are shown in Figs 8 and 9.

Fig. 8 shows the structure of a specimen containing no titanium and 3.32 percent of carbon in which we see the primary austenite and

undecomposed cementite. In a specimen containing 2.49 percent of titanium and 4.08 percent of carbon the eutectic cementite is all decomposed as shown in Fig. 9, the matrix being pearlitic.

Figs. 10, 11 and 12 illustrate the effect of annealing on cast specimens. Fig. 10 shows the structure of a cast specimen containing 3.01 percent of titanium and 3.55 percent of carbon. Fig. 11 shows the structure of the same specimen annealed for one hour at 1000° C. Undecomposed cementite appears as fine globules and graphite as minute spots. Fig. 12 shows the structure of a specimen containing 2.35 percent of titauium and 4.02 percent of carbon annealed for two hours at 1000° C. Well developed graphite is seen, the matrix being pearlitic.

§ 6. SUMMARY

(1) In the ternary alloys of iron-carbon-titanium containing less than 4 percent of titanium, no particular phase is found, titanium being contained in ferrite as a solid solutihn, i.e. titanoferrite.

(2) With an increase of titanium, the content of carbon in the eutectic point decreases and the temperature rises, consequently the ternary eutectic curve probably runs from the binary eutectic of the iron-carbon system to that of iron-titanium.

(3) As the titanium increases, the solubility of the carbon in austenite decreases and probably tends to zero on the iron-titanium side.

(4) Titanium accelerates the graphitisation of carbide in the alloys, the mechanism being probably similar to that in the case of iron-carbon-silicon alloys.

In conclusion, the present writer expresses his cordial thanks to Professor K. Honda, under whose direction the present work was carried out.

Plate I.

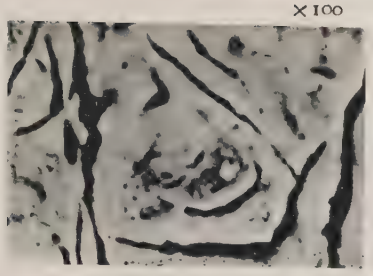

Fig. 6. Specimen No. 1
Ti 1·80 %, C 4·35 %

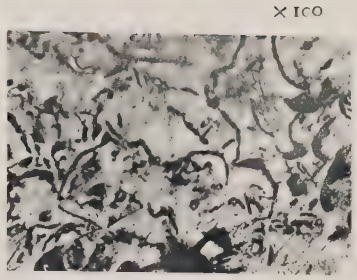

Fig. 7. Specimen No. 4
Ti 3·76 %, C 3·70 %

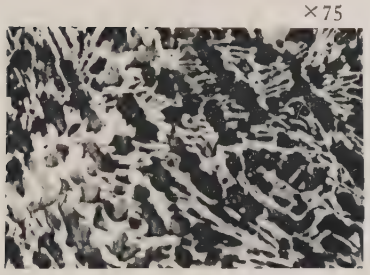

Fig. 8. *Ti* 0 %, C 3·32 %

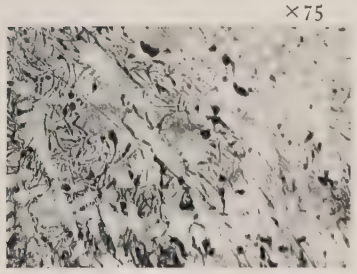

Fig. 9. *Ti* 2·49 %, C 4·08 %

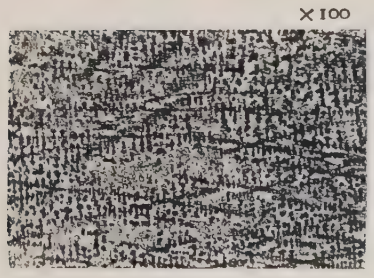

Fig. 10. *Ti* 3·01 %, C 3·55 %
Cast

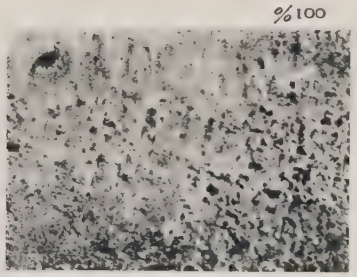

Fig. 11. *Ti* 3·01 %, C 3.55 %
Annealed for 1 h.

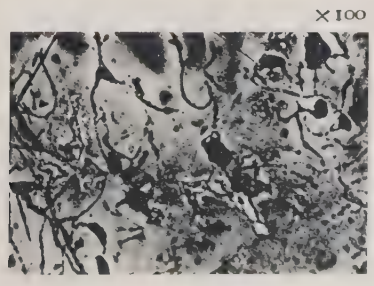

Fig. 12. *Ti* 2 45 %, C 4.02 %
annealed for 2 hs.

The X-ray Examination of Inner Structure of Various Calcium Carbonates.[1]

By

Atomi Ôsawa.

§ 1. Calcium carbonate, which is widely distributed in the earth-crust, appears naturally in various forms, that is, in crystalline forms:—calcite, aragonite, the nail-head-spar, the dog-tooth-spar, etc., in the so called amorphous forms:—chalk, lithographic lime stone etc., and finally as a hot spring:—calcsinter. Of these various forms, the nail-head-spar and the dog-tooth-spar belong to the same modification as calcite, differing only in their external shape. But the aragonite is a modification which is entirely different from calcite, having a different atomic arrangment from that of calcite.[2]

The occurrence of calcium carbonate is not confined to the mineral domain. In the botanical domain, it is found in the cells of phanerogams, that is, in the sago-palm (*cycus revoluta*), prickly-pear (*cactus*), and the leaves of the costus. In the zoological domain, we know that the egg shells of birds, corals, the shells of crustacea and mollusca are chiefly formed of calcium carbonate. But to what modification of calcium carbonate they belong, we do not know. Their forms depend on the conditions of their production.

The calcite being the form of the most frequent occurrence, will probably be the most stable form of all.

(1) The ninety-ninth report of the Research Institute for Iron, Steel and Other Metals.

(2) Haga and Jäger, Proc. Acad. Amsterdum, **18**, (1915), 545, 559.

Hence it is probable that the calcium carbonates in the zoological domain will have the atomic arrangement of calcite. Thus it is very interesting to study the atomic distribution in various kinds of calcium carbonates by x-ray analysis.

§ 2. The arrangement of the experiment is shown in Fig. 1. B is a Coolidge tube with a molybdenum anticathode, S_1, S_2 are two slits 1×4 mm in dimension, Z is a zirconium filter for absorbing $K\beta$-ray, H a specimen holder, R a circular frame 3.76 cm in radius, holding an

Fig. 1.

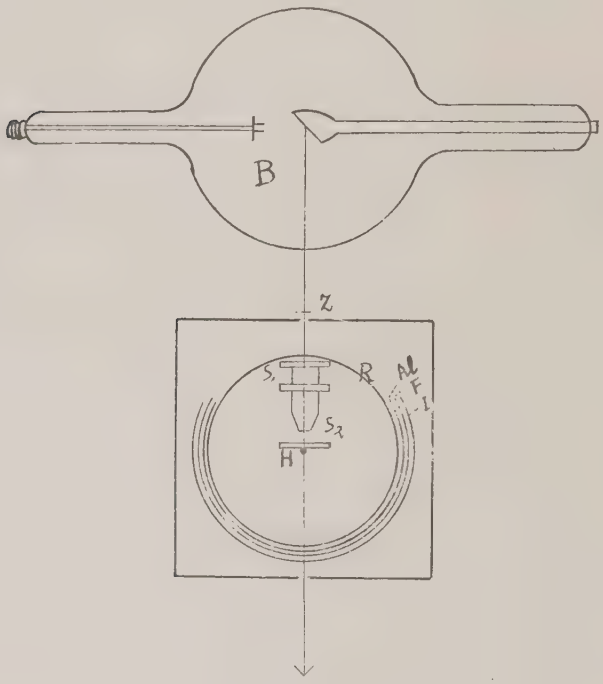

Al.....aluminium filter.
F .....photograhic film.
I .....intensifying screen.

aluminium filter of a thickness of 0.25 mm to absorb diffused radiation from the specimen, a photographic film and an intensifying screen, in position. The Coolidge tube is operated by a high tension transformer, the applied voltage being always 30 K. V. and the current 5 to 6 M. A. The exposure is about 15 hours.

The calcium carbonates examined were as follows:—

1. coral trees, red and white,
2. sea-ear,
3. pearl-oyster,
4. oyster,
5. pecten,
6. trubo cornutus,
7. strombus luhuanus,
8. septifer bilocularis,
9. an acropora,
10. a favia,
11. shield of a sea-urchin.
12. shield of a crab-fish,
13. shell of fowl's egg,
14. calcite crystal,
15. aragonite I, II, III (an unknown substance in Japan),
16. a supposed aragonite (Shinano, Tahira-Mura product),
17. marble,
18. shell of ostrich's egg,
19. lime stone, amorphous, russet colour,
20. $CaCO_3$, chemically deposited.

Aragonite I obtained from Herrland in Hungary, is a transparent crystal having a well defined crystal form. Aragonite II was one from Eisenerz in Steinmark, having an irregular form, and was not transparent. Aragonite III was an aggregate of small crystals, but its modification was clearly distinguished from calcite by means of chemical reaction, optical method, and the measurement of its density. Sample 16 was a supposed aragonite, the shape of which was a small pentagonal dodecahedron, and was not transparent.

At first it is necessary to confirm Haga and Jäger's experimental result[1] by the powder method with well defined mineral crystals. The results thus obtained are shown in an annexed plate by the two Röntgenograms obtained from calcite and aragonite powders: they are entirely different from each other.

It was ascertained that sample 16 was not an aragonite crystal, but really a calcite, and sample 18 was also composed of very minute calcite crystals. The samples we examined were all crushed into fine powders and then made into a rod, 1 mm in diameter, a small quantity of starch being used as a cementing material.

(1) loc. cit.

According to the study of röntgenograms, the calcium carbonates examined may be classified as follows :—

1. Calcite Modification :
   calcite crystal,
   lime stone,
   marble,
   a supposed aragonite,
   coral trees, red and white,
   pearl-oyster,
   oyster,
   sea-ear,
   shield of a sea-urchin,
   shield of a crab-fish,
   shell of a fowl's egg,
   shall of an ostrich's egg,
2. Aragonite Modification :
   aragonite crystal, I, II, and III,
   trubo cornutus,
   septifer bilocularis,
   an acropora,
   a favia.

§ 3. CALCITE MODIFICATION :

The following table shows the distances of the spectral lines from the center, for the röntgenograms obtained from specimens belonging to the calcite modification.

TABLE I.

Calcite crystal	lime stone	oyster	seaurchin	egg shell	coral	marble	indices
0.84cm	0.85cm	0.85cm	0.85cm	0.84cm	0.83cm	0.86cm	(100)
1.04	1.00	0.96	0.99	0.98	0.95	0.96	(110)
1.36	1.35	1.36	1.35	1.37	1.38	1.39	(110)
1.74	1.73	1.76	1.75	1.77	1.77	1.78	$(100)^2$
1.84	1.85	1.84	1.85	1.82	1.84	1.86	$(211)^2$
2.26	2.25	2.25	2.25	2.28	2.26	2.26	$(110)^3$
2.54	2.53	2.54	2.55	2.56	2.54	2.55	$(100)^2$
2.72	2.74	2.75	2.75	2.75	2.74	2.73	(110)

As seen from the above table and the röntgenograms, the position of the spectral lines for these samples almost coincides with that of calcite and the blackness of the lines are also the same for all specimens. Photograph 1 is the röntgenogram of the natural sea-ear, taking the specimen from its inner side. Photographs 2 and 3 are these of the natural red and white corals. Photograph 4 is a röntgenogram of a natural marble, the specimen being in the form of a thin plate, 0.5 mm thick, which shows that the marble is an aggregation of fine crystals. Notwithstanding that all these specimens show the spectral lines, the egg shell and the shield of the sea-urchin show the Laue-spot, so that the egg shell of a fowl and the shield of a sea-urchin are composed of relatively large crystals. The Laue photograph for these substances obtained by using the white ray from tungsten anticathode, are shown in photograph 20 and 21 in the annexed plate. As seen from these figures, the grain size of the fine crystals of the egg shell is smaller than that of the sea-urchin's shield, for the latter shows almost perfect Laue-spots, while the former shows a flaky interference figure under the same condition. It is also ascertained that a large number of organic substances, namely, gelatine, cellulose, etc. contained in the shield of the crab-fish and the egg shell of a fowl give no interference figure on the röntgenograms. Hence they seem like a cementing material of an amorphous nature.

§ 4. ARAGONITE MODIFICATION:

All the röntgenograms obtained by these specimens belonging to the aragonite modification are in good agreement with that for an aragonite, which is well defined by Mineralogists. They are given in the annexed plate. The distances from the center to each line in the röntgenograms for some samples are tabulated below:—

TABLE 2.

aragonite (I)	aragonite (II)	turbo cornutus	little basket	zoatheria
cm	cm	cm	cm	cm
0.77	0.77	0.77	0.76	0.76
0.95	0.95	0.95	0.88	0.95
1.08	1.08	1.10	1.06	1.09
1.16	1.18	1.19	1.18	1.16
1.29	1.30	1.31	1.30	1.28
1.39	1.39	1.39	1.36	
1.57	1.58	1.53	1.54	1.51
1.82	1.80			1.81
2.09	2.10			2.07
2.22	2.21			2.12

As seen from the above table, the position of the lines for various aragonites coincide satisfactorily with each other.

If we cut the shell of a trubo cornutus into two portions, we find two distinct layers in the section. According to x-ray analysis, these layers are the same atomic arrangement and both belong to the aragonite modification, differing only in the grain size of the crystal; the grain in the outer layer seems to be smaller than that in the inner.

It is well known that aragonite. when heated to a temperature of about 400°C, changes its atomic arrangement and is transformed into calcite. This transformation takes place in the range of 350°C—450°C. The present writer also made the following experiments:—a well defined transparent crystal was cut into three portions, and each portion was heated up to 330°C, 400°C, and 480°C respectively, for five hours, and then quenched in mercury. As result of this process, the first specimen did not change its transparency or its atomic arrangement, but the second and the third lost their transparency, becoming amorphous-like substances and their atomic arrangement being changed into that of calcite. Hence it is concluded that the transformation takes place between 330°C and 400°C.

The atomic arragement of the aragonite is not yet clearly known.

The present writer has also endeavoured to determine this arrangement by x-ray analysis and obtained the following result: According to the carystallographical data, aragonite belong to the rhombic system and has an axial ratio of

$$a : b : c = 0.6228 : 1 : 0.7204,$$

its density being 2.926 to 2.933. From the röntgenogram obtained of the powder of a transparent aragonite crystal, we calculated the spacing distances of the atomic layers in the crystal as shown in the fourth column in table 3.

TABLE 3.

Didtance from the spectral line	intensity in arbitary unit	reflected angle θ	spacing of net plane of atom	calculated value from Bragg's model		calculated value from Huggin's model	
				$d \times 10^{-8}$ cm	indices	$d \times 10^{-8}$ cm	indices
cm							
0.77	10	6° 1′	3.390	3.390	(222)	3.340	(220)
0.95	6	7° 24′	2.750	2.688	(024)	2.680	(222)
1.08	9	8° 25′	2.475	2.470	(100)	2.460	(400)
1.18	3	9° 11′	2.225	2.220	(402)	2.272	(001)
1.30	8	10° 13′	2.005	1.985	$(010)^2$	1.965	(100)
1.39	4	10° 50′	1.860	1.872	(101)	1.740	(011)
1.58	7	12° 19′	1.665	1.665	(117)	1.670	(110)
1.80	2	14° 0′	1.465	1.430	$(001)^2$	1.485	(101)
2.10	2	16° 23′	1.360	1.344	(012)	1.340	(111)
2.21	5	17° 9′	1.253	1.255	$(100)^2$	1.232	$(001)^2$

In the above table, the calculated spacing and indices are obtained under the assumption that the aragonite model proposed by M. L. Huggins[1] and the one, which is recentry determined by W. L. Bragg[2] by means of the ionization method, are correct. Hunggins' model is based on considerations of the electrons in the light element and the nature of the valency electron,[3] and illustrated in figs. 2 and 3. He

(1) Phys. Rev. (2) 19, (1922), 354.
(2) Proc. Royal Soc. of London, No. A. 729. (1923). 105.
(3) Journ. Phys. Chem. (1922), 601.

calculated the spacing distances of aragonite which is intimately related to calcite, but he did not carry out any measurement.

Fig. 2

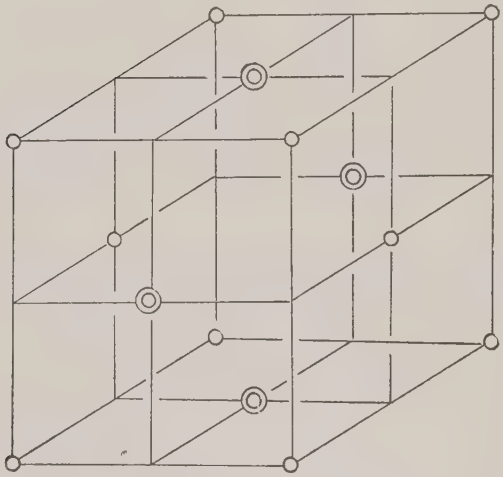

unit shell containing *C* and *Ca* atoms only

Fig. 3.

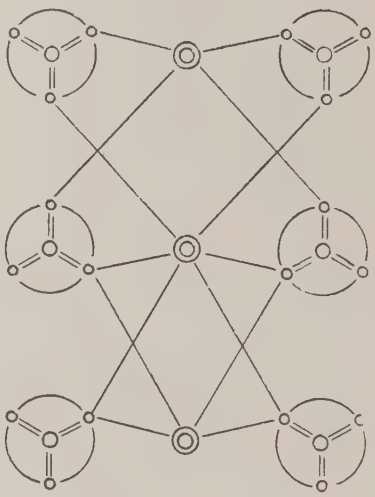

(011)—plane

Fig. 4.

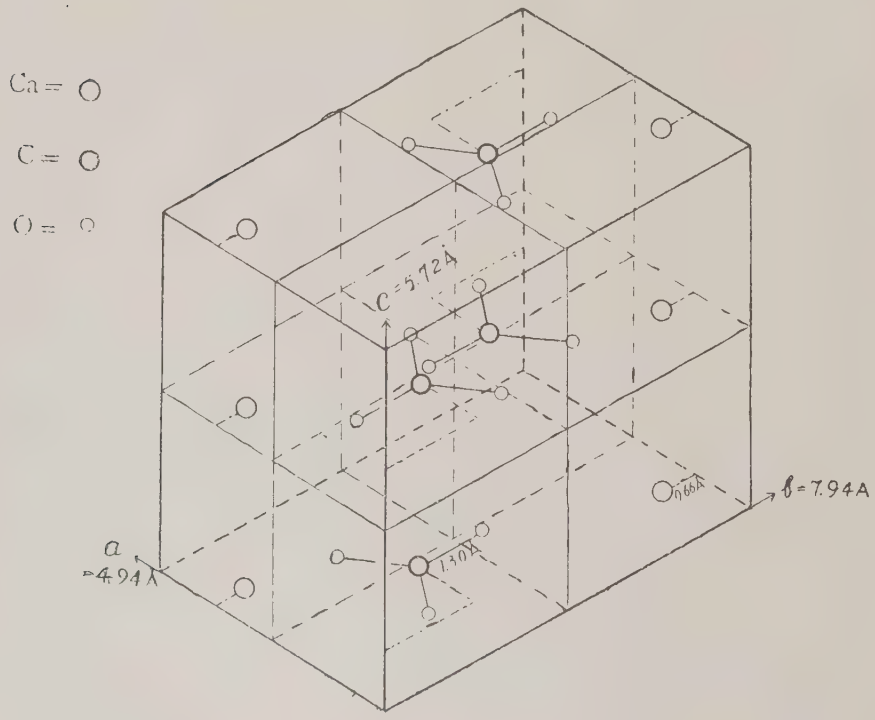

Fig. 2. shows the Huggins' aragonite model containing two molecules of $CaCO_3$. Recentry Bragg has determined the aragonite model, as shown Fig 4, from his experimental results. Four molecules of $CaCO_3$ are bore in it.

As seen from Table 3, our observed values are relatively good agreement with the values calculated from the Bragg's model than Huggins' one.

Hence Bragg's aragonite model is correct in our experiment.

In conclusion the present writer wishes to express his cordial thanks to Professors K. Honda and M. Yamada for their kind guidance and also to Messrs K. Hattori and M. Higuchi, for their valuable suggestions, during the course of the present investigation He is also much indebted to Professor S. Kozu who has given him many valuable specimens.

Photographic Plate I.

1. Natural sea-ear for $K^{-}_{\alpha\beta}$—rays

2. Natural red coral for $K^{-}_{\alpha\beta}$—rays

3. Natural white coral for $K^{-}_{\alpha\beta}$—rays

4. Natural marble for $K^{-}_{\alpha\beta}$—rays

5. Marble for $K^{-}_{\alpha\beta}$—rays (powder)

6. Marble powder for K^{-}_{α}—ray

7. White coral for K^{-}_{α}—ray (powder)

8. Red coral for K^{-}_{α}—ray (powder)

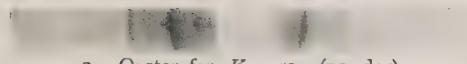

9. Oyster for K^{-}_{α}—ray (powder)

10. Pecten for K^{-}_{α}—ray (powder)

11. Pearl oyster for $K^{-}_{\alpha\beta}$—rays (natural)

Photographic Plate II.

12. Calcite crystat (powder)

13. Shell of fowl's egg (powder)

14. Scallap (powder)

15. Shield of sea-urchin (powder)

16. Aragonite crystal (powder)

17. Horned top

18. Septifer bilocularis

19. An acropora

20. Lune photograph of the egg shell of hen (natural)

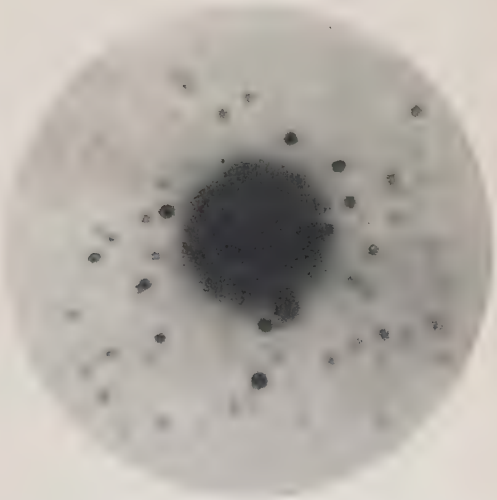

21. Lune photograph of the shield of sea-urchin

On the Atomic Structure of Palladium and Platin Black which absorb Gases.[1]

By

Atomi Osawa.

§ 1. The platinum and palladium blacks, which consist of fine black powders, are obtained by the reduction of their salts, or by the electrolysis of the water solution of their chloride. The atomic structure had not been examined, until recently F. Kirchner[2] obtained platinum black deposited on a very thin copper plate and took its röntgenogram. He could find no platinum lines, while the photographic film was uniformly blackened. Hence he concluded that platinum black is in an amorphous state, the blackening being due to the irregular radiation of it. If Kirchner's conclusion be correct, it is very important to examine, whether platinum blacks obtained by other methods are also amorphous. With this object, the following x-ray analysis was carried out. The method used is that of Debye and Scherrer.[3]

§ 2. Several specimens were obtained by the electrolysis and chemical decomposition. In the case of the former method, a platinum wire was placed in a dilute solution of chloroplatinate as the anode and a copper wire, 0.2 mm thick, was used as the cathode. The voltage applied was 6 volts and a current of 20 miliampères supplied for 10 hours. In the case of latter method, a specimen was prepared by

(1) The hundredth report of the Research Institute for Iron, Steel and Other Metals.

(2) Ann. d. Phys. **69**, (1922), Nr. 17.

(3) The apparatus is the same as that used by Prof. M. Yamada, as described in the Phil Mag. **14**, (Jan., 1923).

heating the alcohole solution of chloroplatinate, and two other specimens were prepared by the decompoition of sold chloroplatinate, by heating them with a Bunsen burner. From the powders obtained by these methods, several rods, each 0.2 mm thick, were made, using fine glass rods as the core and a small quantity of starch as the binding material.

The röntgenograms thus obtained are shown in the annexed plates. Contrary to the Kirchner's result, all specimens showed several lines belonging to platinum or palladium. Hence we can conclude that platinum and palladium blacks have also the same crystalline structure as those of the respective metals.

§ 3. It is well known that platinum and palladium blacks absorb a large quantity of gases. That is, platinum black absorbs carbon monoxide, oxygen and hydrogen by 60, 100, and 100 times the volumes respectively, while palladium black absorbs more than 600 times its volume of hydrogen gas. But the mechanism of the gas absorption is not yet clear. Some investigators assert that the absorbed gas forms a mechanical compound with metal, but all efforts to isolate such a sustance have failed. Others consider the absorbed gas to be in a solid solution.

Professor M. Yamada[1] investigated metallic palladium absorbing a large quantity of hydrogen by means of the X-ray analysis, and concluded that the absorbed gas is contained as a solid solution, hydrogen atoms entering into the interspace of the atomic lattice in palladium. Recently L. W. Mckeenhan[2] has attacked the same problem.

He also found a uniform expansion of the lattice of the palladium metal due to the absorption of hydrogen gas. The lattice constant of the palladium saturated with hydrogen varied from 4.000 to 4.039 10^{-8} cm, while that of the pure metallic palladium is 3.900 10^{-8} cm, the value 4.039×10^{-8} cm, according to him, probably corresponding to a compound Pd_2H, with a desity of 10.76 gm/cm^3.

The present writer also made a similar experiment with platinum

(1) Phil. Mag. **14**, (Jan. 1923).
(2) Phys. Rev. **21**, (March, 1923).

black absorbing hydrogen, oxygen, and carbon monoxide gases, and also palladium black absorbing hydrogen gas. The röntgenograms were the same as those of the metallic element in every cases, the only difference being a slight diminution in the diffraction angles of the spectral lines. This diminution indicates an uniform expansion of the space lattice in these metals. Hence we may at least conclude that the atomic arrangement in palladium and platinum is not changed by the absorption of gases. It is a noteworthy fact that the palladium black absorbing hydrogen gas was exactly the same as that of the metallic palladium saturated with hydrogen examined by Prof. Yamada, the linear expansion of the lattice being 2.8 percent in both cases. In the case of platinum black, the linear expansion of the lattice was for hydrogen, oxygen and carbon monoxide 2.4, 2.9 and 2.8 percent respectively. Since the space lattice of platinum and palladium only uniformly expands on the absorption of the gases, it is highly probable that these gases enter into the space lattice of these metals. Thus the absorbed gases are contained in these metals as a solid solution, this being in agreement with Mr. M. Yamada's view. But as the molecular dimensions of oxygen and carbon monoxide are large compared with those of hydrogen, it is very difficalt to conceive the mechanism of the diffusion of these gases in the metals.

In conclution the present writer expresses his hearty thanks to Prof. Dr. K. Honda and Prof. M. Yamada under whose kind guidance this experiment has been carried out.

Photographic Plate I.

Powdered platinum metal.

Platinum black obtained by electrolysis: hydrogen absorbed.

Platinum black from alcoholic solution of chloroplatinate: carbon monoxide absorbed.

Powdered palladium metal.

Palladium black from alcoholic solution of palladium chloride absorbed hydrogen.

The Use of Liquid Amalgam in Volumetric Analysis, Part I. Application of Zinc and Bismuth Amalgams.[1]

By

Kinichi Someya.

I. INTRODUCTION.

The use of liquid zinc amalgam was first introduced into the field of analytical chemistry by Nakazono.[2] He devised a simple and convenient reductor and succeeded in getting an accurate volumetric determination of iron, molybdenum, vanadium, uranium and titanium by reducing these elements by means of zinc amalgam and oxidizing them back with potassium permanganate. He showed that the method possesses special advantages in that (1) the time required for complete reduction is only a few minutes; (2) no blank correction is necessary as is the case with the Jones reductor; (3) the method furnishes very accurate results; (4) the zinc amalgam permits of repeated uses.

Kikuchi[3] applied the method to the estimation of iodic, bromic and chloric acids, and also of methylene blue.[3] Kano[4] investigated the applicability of cadmium amalgam. The same investigator successfully applied the amalgam method to the electrometric titration of iron,

(1) The one hundred and first report from the Research Insitute for Iron, Steel and Other Metals.

(2) Nakazono, Journ. Jap. Chem. Soc. **42**, (1921), 526; Ibid. 761; Chem. Abstr. **16**, (1922), 1543.

(3) Kikuchi, Journ. Jap. Chem. Soc. **43**, (1922), 173; Chem. Abstr. **16**, (1922), 1716.

(4) Kano, Journ. Jap. Chem. Soc. **43**, (1922), 333; Chem. Abstr. **16**, (1920), 1818.

molybdenum, uranium, vanadium and titanium.[1] Hakomori[2] estimated phosphoric acid by its application on the phosphomolybdate precipitate. The differential titration of titanium and uranium, of titanium and iron, as well as that of uranium and iron was also accomplished by Kikuchi.[3] Kano[4] also estimated iron and chromium by making use of zinc amalgam. The amalgam method saw one more case of application in a somewhat different direction; i.e., Wada and Nakazono[5] used the zinc amalgam in the preparation of titanous sulphate, which was utilized in the qualitative separation of platinum and iridium. The writer, being connected with the work of steel analysis, saw that this method finds extensive application in his daily work, and attempted, if possible, to make some extension of it. Finding that, besides zinc and cadmium amalgam, bismuth amalgam also possesses some properties which could be utilized in volumetric analysis with advantage, he could make successful titration of iron, titanium, vanadium and molybdenum, as well as the combination of the last two elements with iron, which occurs very frequently in the analysis of special steels.

It is also frequently desirable to work with solutions containing a chloride ion. All the above-mentioned workers worked with sulphate solutions containing free sulphuric acid. Several cases were investigated and suitable conditions were determined for each of them, to be described in the Experimental Part.

EXPERIMENTAL PART.

Apparatus and Methods: Essentially the same as that described by Nakazono.

(i) Preparation of Zinc Amalgam.—About 3 g. of pure zinc (granulated or stick) are heated on a water-bath with about 100 g. of mercury

(1) Kano, Journ. Jap. Chem. Soc. **43**, (1922), 550; Chem. Abstr. **17**, (1924), 247.
(2) Hakomori, Journ. Jap. Chem. Soc. **43**, (1922), 734; Chem. Abstr. **17**, (1923), 1930.
(3) Kikuchi, Journ. Jap. Chem. Soc. **43**, (1422), 544; Chem. Abstr. **17**, (1923), 247.
(4) Kano, Journ. Jap. Chem. Soc. **44**, (1923), 37; Chem. Abstr. **17**, (1423), 2848.
(5) Wada & Nakazono, Sc. Pap. Inst. Phy. Chem. Res. **1**, (1923), 139–54.

and a small quantity of dilute sulphuric acid and cooled. The amalgam is washed thoroughly with water and separated from any solid substance by making use of a separating funnel. Since it reacts only very slowly with diluted sulphuric acid, it permits of repeated uses and long preservation. The solid conglomerate of zinc and mercury is preserved for further use, which is added to the amalgam that has repeatedly been used and whose zinc content has become small.

(ii) Preparation of Bismuth Amalgam.—In the above zinc is substituted by bismuth and sulphuric acid by hydrochloric acid.

(iii) Apparatus for Reduction.—(A) is a kind of a separating funnel, ca. 10 cc. capacity, and is provided with a stop-cock (a). The lower part (B) is a larger one of 150–200 cc. capacity. It has a gas-delivery tube (D) with a stop-cock (b). (C) is a kind of a small bottle, ca. 15–20 cc. capacity and is connected with the tube of the separating funnel (B) by means of a rubber tubing (E). A pinck-cock (e) is used to prevent the rubber tubing getting out of the tube.

Fig. 1.

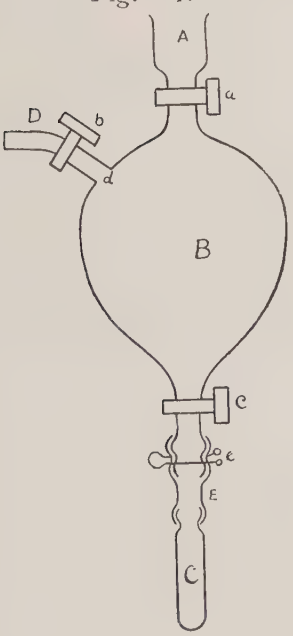

(iv) Reduction of the Solution to be Analysed and the Titration of the Reduced Solution.—The bottle (C) and the rubber tubing (E) are filled with freshly boiled water and about 1 cc. of water is put in the separating funnel (B). The stop-cock (c) and the pinch-cock (e) are closed after air-bubbles in (E) and (C) are completely expelled by pressing the rubber tubing. 100–200 g. of zinc or bismuth amalgam and the solution to be analysed are introduced into (B) through the funnel (A). When necessary the air in (B) is completely replaced by carbon dioxide introduced through (D), (b) and (d), and after closing the stop-cocks, the mixture is thoroughly shaken. The characteristic color of the solution easily tells

when the reduction is complete. On opening the stopcock (C) and pressing the rubber tubing at (E), the amalgam comes down into the tubing and the water in it takes its place, washing the amalgam on its way up. In this way all the amalgam can be separated from the solution without losing any of the latter. The solution in (B) is titrated by introducing some suitable standard solution into (B) through (A). When the solution is sensitive to atmospheric oxygen and carbon dioxide is used, the latter remains dissolved and reduces the pressure within the reductor, so that there is usually no difficulty in introducing the standard solution through (A). A similar phenomenon takes place even with air, though somewhat to a smaller degree. When this does not occur, the solution can be introduced by exerting a slight pressure upon the cock (a) by stopping (A) with a flat hand.

1. Reduction of Vanadium and Iron with Bismuth Amalgam.

Material:—Vanadium Pentoxide Solution. Pure vanadium pentoxide (Kahlbaum, zur Analyse) was taken and was dissolved in sulphuric acid and was diluted to 1000 cc. The solution was standardized by reduction to the divalent condition by means of zinc amalgam and then titrating with a decinormal potassium permanganate solution standardized against pure oxalic acid.[1]

Ferric Salt Solution:—This was made by dissolving 1/20 mol of Merck's c.p. ferric ammonium alum in dilute sulphuric acid. This was also standardized in the same way by means of zinc amalgam and potassium permanganate.

As it has already been shown by Nakazono[2] that these methods are accurate enough for standardization, no other methods were tried for this purpose.

First, experiments were made to determine the nature of the reducing action of the bismuth amalgam. Bismuth amalgam was carefully

(1) Nakazono, Journ. Jap. Chem. Soc. **42**, (1921), 526.
(2) Nakazono, l.c.

washed with distilled water and was introduced into the above-mentioned reductor followed by some definite quantities of the vanadium or iron solution. The solutions were naturally acid with the sulphuric acid present in then. The reduction went smoothly when the acidity of the solution was made stronger by adding 5–10 cc. of sulphuric acid (1 : 1) or 5 cc. of concentrated hydrochloric acid. Moderate excess of the acid did no harm. After drawing out the bismuth amalgam 20 cc. of the Zimmermann-Reinhardt mixture was added. In the absence of hydrochloric acid, a white turbidity due to the formation of bismuth phosphate appeared, which was made to vanish by adding a small quantity of concentrated hydrochloric acid. The reduced iron solution was colorless and the vanadium solution beautiful light blue characteristic of the quadrivalent vanadium. The former was titrated cold with potassium permanganate, and the latter warm (80°) near the end point, whereby the contents of the reductor were washed into a conical beaker and were heated. The results are shown in the following table.

TABLE I. Reduction of Vanadium with Bismuth Amalgam.

V_2O_5 sol. taken, 20 cc. Titrated with 0.10099 N $KMnO_4$ sol.

Exp.	KMn_4O req. (cc.) (Zn amalg.)	V_2O_5 standardized, (g.)	Z.R. Mixfure, (cc.)	Atmasphere.	$KMnO_4$ req., (cc.) (Bi amalg.)	V_2O_5 found, (g.)	V_2O_5 error, (g.)
1.	40.26	0.12361	20	CO_2	13.41	0.12352	0.00009
2.	40.26	0.12361	—a	air	13.42	0.12361	0.00000
3.	39.61	0.12161	20	CO_2	13.18	0.12139	0.00022
4.	39.61	0.12161	20	CO_2	13.20	0.12161	0.00000
5.	39.61	0.12161	20	air	13.13	0.12093	0.00068
6.	39.61	0.12161	20	air	13.18	0.12139	0.00022

a. When enough sulphuric acid was added to the solution, the hydrolysis of bismuth could be prevented and consequently no addition of hydrochloric acid and the Zimmermann-Reinhardt mixture was necessary. However, with a dilute sulphuric acid solution the hydrolysis always

occurred, and it seemed more convenient to dissolve the separated bismuth with hydrochloric acid and titrate the solution in the presence of 20 cc. of the Zimmermann-Reinhardt mixture.[1]

TABLE II.

Reduction of Iron with Bismuth Amalgam.

Ferric alum sol. taken 20 cc. Titrated with 0.08987 $N\,KMnO_4$ sol.

Exp.	Fe_2O_3 taken (g.)	$KMnO_4$ req. (cc.) (Zn amalg.)	$KMnO_4$ req., (cc.) (Bi amalg.)	Atmosphere	Z.R. Mixture, (cc.)	Fe_2O_2 found, (g.)	Fe_2O_2 error, (g.)
1.	0.14702 a	20.49 a	—	CO_2	—	—	—
2.	0.14702	20.49	20.52	CO_2 b	20	0.14724	0.00022
3	0.14702	20.49	20.49	CO_2 b	20	0.14702	0.00000

a. Mean of 3 determinations. b. In the case of iron, using *KSCN* as an indicator, and also by actual titration, it was shown that the reduction is never complete in air, even after prolonged shaking. See also Art. 4, of the differential titration of molybdenum and iron.

The results shown in Tables I and II prove that bismuth amalgam reduces ferric iron quantitatively to the ferrous condition in the atmosphere of carbon dioxide, and pentavalent vanadium to the quadrivalent one either in air or in carbon dioxide. The titration of vanadium in hydrochloric acid solution has already been studied by Erich Müller and Otto Diefenthäler.[2]

2. Differential Titration of an Iron and Vanadium Mixture.

Several successful attempts have already been made of the differential titration of a vanadium and iron mixture by making use of the

(1) Treadwell, Lehrbuch d. anal. Chem. II, 5 Aufl., S. 506.

(2) Erich Müller & Otto Diefenthäler, Zeit. anorg. Chem., **71**, (1911), 243–249.

reducing action of sulphurous acid,[1] hydrogen iodide,[2] hydrogen sulphide,[3] ferrous sulphate,[4] etc. The new method here proposed is believed to have some advantage in that it is free from the inaccuracies due to often experienced incompleteness of the reduction,[5] and also from the inconvenience of having recourse to the spot test.

The method of procedure was as follows:—The solution of ferric ammonium alum and vanadic acid is divided into two portions. (I) One portion is reduced with bismuth amalgam and titrated with potassium permanganate usually with hydrochloric acid and 20 cc. of the Zimmermann-Reinhardt mixture. (2) The second portion is then reduced with zinc amalgam and titrated with potassium permanganate. In both cases the solution was taken out of the reductor near the end point, and was titrated hot to the characteristic tint. The reduction was always rapid and complete. The results are shown in the following table.

TABLE III. Differential Titration of Vanadium and Iron.

Exp.	V_2O_5 taken, (g.)	V_2O_5 found, (g.)	V_2O_5 error, (g.)	Fe_2O_3 taken, (g.)	Fe_2O_3 found, (g.)	Fe_2O_3 error, (g.)	(I) $\frac{N}{10}$ $KMnO_4$, (cc.)	(II) $\frac{N}{10}$ $KMnO_4$, (cc.)
1.	0.12224	0.12218	0.00006	0.16136	0.16056	0.00080	33.35	60.02
2.	0.12224	0.12208	0.00016	0.16136	0.16122	0.00014	33.40	60.05
3.	0.12224	0.12218	0.00006	0.16136	0.16122	0.00014	33.39	60.04
4.	0.12208	0.12208	0.00000	0.16136	0.16144	0.00008	39.43	60.05
5.	0.06101	0.06107	0.00006	0.15798	0.15785	0.00013	26.47	39.86
6.	0.06101	0.06107	0.00006	0.15798	0.15798	0.00000	26.48	39.87
7.	0.06101	0.06111	0.00010	0.15798	0.15781	0.00017	26.47	39.87

(1) Griffin, Mining Eng. World, **37**, 247–8; Woldemar Trautmenn, Zeit. anal. Chem. **55**, 371–2; A.A. Blair, Journ. Amer. Chem. Soc. **30**, (1908), 1229–33; Classen, Handbuch d. quantitativen Anal. (1920), 7 Aufl. S. 352; Vicent Garcia Rodeja, Anales Soc. cspañ fis quim, **12**, 378–82; E.P. Alvarez, Rev. real. acad. cien. Madrid **8**, 160–2; A. Heinzelmann, Chem. Ztg. **39**, (1915), 285–7; Gustav Wegelin, Zeit. anal. Chem. **53**, (1914), 81–99; E. Müller & O. Diefenthäler, Zeit. anorg. Chem. **71**, (1911), 243–9.

(2) C. C. Perkins, Amer. Journ. Sc. **29**, 540–2; G. Edgar, Journ. Amer. Chem. Soc. **38**, (1916), 2369–77; G. Edgar, Amer. Sc. **26**, (1908), 333–8.

(3) E. D. Campbell & E. L. Woodhams, Journ. Amer. Chem. Soc. **30**, (1908), 1233–36.

(4) D. J. Demorest, J. Ind. Eng. Chem. **4**, 895; W.W. Clark, Met. Chem. Eng. **11**, 195–7; H. H. Willard & F. Fenwick, Journ. Amer. Chem. Soc. **45**, (1923), 83.

(5) The writer tried the sulphurous acid solution for reduction, finding that only one boiling with the acid always failed to bring the reduction to completion. See also Classen; Handbuch der quantitativen Analyse, 7 Auflage, (1920), S. 352.

Normality of $KMnO_4$ 0.10005 N.

Separate titrations :—20 cc. of V_2O_5 sol. required 39.92 cc. on the average.

Separate titrations :—20 cc. of Fe_2O_3 sol. required 20.11 cc. on the average.

A trial analysis of a sample of ferro-vanadium was made by applying this method. The powdered sample ca. 2 g. were dissolved in a mixture of sulphuric acid and a small quantity of nitric acid, and after evaporated to fuming, filtered from the silica residue, and the resulting solution was diluted to 250 cc. of the solution. 20 cc. was taken for separate titration.

TABLE IV. Analysis of Ferro-vanadium.

Zn amalgam	Bi amalgam	% of vanadium found.
Sample taken 2.0000 g. Normality of $KMnO_4$ 0.10177 N. $KMnO_4$ required, cc.		
50.89	28.42	
50.94	28.46	
50.91	28.44	36.35
Sample taken 1.9392 g. Normality of $KMnO_4$ 0.09960 N.		
50.30	27.97	
50.26	28.00	
50.24	27.98	36.60

3. Reduction of Molybdenum with Bismuth Amalgam.

The molybdenum solution here used was made by dissolving pure commercial ammonium molybdate (Kahlbaum, for analysis) crystals in water. The standardization was made by means of zinc amalgam according to the method of Nakazono.[1] The reduction by means of bismuth amalgam was done in the presence of 5–10 cc. of concentrated hydrochloric acid per 20–50 cc. of the solution to be reduced, and the

(1) Nakazono, l.c.

titration of the reduced solution was made after adding 20 cc. of the Zimmermann-Reinhardt mixture. The results are shown in the following table.

TABLE V. Reduction of Molybdenum with Bismuth Amalgam.

Exp.	MoO_3 taken, (g.)	$KMnO_4$ req., (cc.) (Zn amalg.)	$KMnO_4$ req., (cc.) (Bi amalg.)	Atmosphere	Z.R. Mixture	MoO_3 found, from Bi amalg. red.	MoO_3 error, (g.)
1.	0.19482	40.60	13.53	air	20	0.19487	0.00005
2.	0.19482	40.60	13.51	air	20	0.19458	0.00024
3.	0.24472	50.98	17.00	air	20	0.24486	0.00014
4.	0.24472	50.98	16.99	air	20	0.24472	0.00000
5.	0.19735	41.12	16.00	CO_2	20	0.23033	0.03298
6.	0.19745	41.14	15.99	CO_2	20	0.23081	0.03336
7.	0.19735	41.12	15.47	CO_2	20	0.22278	0.02543

MoO_3 taken 20 cc. Titrated with ca. 0.1 N. $KMnO_4$.

The table shows that the bismuth amalgam reduces molybdenum quantitatively to the pentavalent condition in presence of air, but in carbon dioxide, the reduction goes too far.

4. Differential Titration of Molybdenum and Iron.

It has already been proved by Nakazono[1] that the reduction of molybdenum by means of zinc amalgam in the carbon dioxide atmosphere carries it as far as to the tervalent condition, and also that ferric salt under the same condition to the ferrous condition. Now it has been shown by the writer that bismuth amalgam reduces ferric iron to the ferrous condition and molybdenum to the pentavalent condition in presence of air. Hence it was thought that it might be possible to work out a method for the differential titration of molybdenum and iron by carrying out two reductions by means of zinc and bismuth amalgam. As was shown in Art. 3, ferric salt cannot, in presence of air, be completely

(1) Kano, Journ. Jap. Chem. Soc. **44**, (1923), 44.

reduced to the ferrous condition. On the other hand, it has been shown by Kano[1] that the stability of ferrous iron in presence of sulphuric acid is so great that even on 15 minutes' shaking with air the permanganate titer is not appreciably different. It was therefore tried to bring back the molybdenum solution, over-reduced beyond the pentavalent condition by shaking with air, leaving the ferrous iron mixed in the solution unaffected. But even shaking for 15 minutes failed to produce the desired result. As an alternative, the reduction of iron in air under various conditions was tried, finding that with suitable regulation of the conditions, the amount of iron left unreduced was always nearly constant as is shown below.

TABLE VI. Reduction of Iron by Bismuth Amalgam in Presence of Air.

$\frac{N}{10}$ *Fe* sol. Taken, (cc.)	$KMnO_4$ reg., (cc.) theory from *Zn* amal. red. in CO_2	*HCl* added, (cc.)	Time of shaking. (m.)	Total vol. (cc.)	$\frac{N}{10}$ $KMnO_4$ after shaking in air, (cc.)	Error, (cc.)
10	10.25	5	5	15	10.08	−0.17
10	10.25	5	10	35	10.08	−0.17
10	10.25	5	5	50	10.07	−0.18
20	20.51	5	5	35	20.30	−0.21
20	20.51	5	10	35	20.30	−0.21
20	20.51	5	5	50	20.33	−0.18
20	20.51	5	10	50	20.33	−0.18
20	20.51	5	10	100	20.28	−0.23
20	20.51	10	10	100	20.30	−0.21
50	51.64	5	5	65	51.45	−0.19
50	51.64	10	10	65	51.45	−0.19
50	51.64	5	5	100	51.04	−0.60 a
50	51.64	10	10	100	51.50	−0.14

a. The solution showed visible hydrolysis of the bismuth salt present in it.

(1) Kano, Journ. Jap. Chem. Soc., **44**, (923), 44.

The result shows that with suitable regulation of the condition, the errer may be made nearly constant, the mean error under suitable conditions being 0.2 cc.

Supposing that it was very probable that with suitable control of the conditions, the reduction of the mixture of iron and molybdenum solutions by means of zinc amalgam (in carbon dioxide atmosphere), and by means of bismuth amalgam (in presence of air) would go on additively, the permanganated titrations of the reduced solutions were made. The former of these suppositions proved true, but in the latter case, it was found, contrary to what had been expected, the presence of molybdenum, whether small or large in quantity, act catalytically to make the bismuth amalgam reduction of the ferric salt in presence of air complete, while molybdenum itself is reduced quantitatively to the pentavalent condition. Large number of differential titrations were made in a manner similar to the case of the vanadium-iron mixture, with varying proportions of iron and molybdenum, which convinced the writer that the reaction goes on in every case as was above described, and that consequently the method is accurate and satisfactory. There was at first some difficulty in determining the end point, which could be overcome by a little practice. The reduction could be made either in sulphuric acid solution or with the mixture of sulphuric and hydrochloric acid. When hydrochloric acid was added to the solution, the Zimmermann-Reinhardt mixture was used in the titration. Table VII shows the result.

TABLE VII. Differential Titration of Molybdenum and Iron.

Exp.	MoO_3 taken, (g.)	MoO_3 found, (g.)	MoO_3 error, (g.)	Fe_2O_3 taken, (g.)	Fe_2O_3 found, (g.)	Fe_2O_3 error, (g.)	(I) $\frac{N}{10}$ $KMnO_4$, (cc.)	(II) $\frac{N}{10}$ $KMnO_4$, (cc.)
1.	0.21651	0.21649	0.00002	0.15927	0.15927	0.00000	34.96	64.98
2.	0.21651	0.21666	0.00015	0.15927	0.15916	0.00011	34.95	64.98
3.	0.21651	0.21642	0.00009	0.15927	0.15939	0.00012	34.95	64.98
4.	0.21617	0.21613	0.00004	0.15927	0.15943	0.00016	34.98	65.00
5.	0.21617	0.21613	0.00004	0.15927	0.15927	0.00000	34.66	64.98
6.	0.21617	0.21606	0.00011	0.15927	0.15939	0.00012	34.97	64.98
7.	0.10808	0.10813	0.00005	0.15884	0.15888	0.00004	27.40	42.43
8.	0.10808	0.10805	0.00003	0.15884	0.15908	0.00024	27.43	42.44
9.	0.10808	0.10798	0.00010	0.15884	0.15904	0.00020	27.44	42.44
10.	0.05420	0.05421	0.00001	0.15884	0.15864	0.00020	23.64	31.16
11.	0.05420	0.05414	0.00006	0.15884	0.15905	0.00021	23.64	31.15
12.	0.05420	0.05394	0.00026	0.15884	0.15872	0.00012	23.64	31.14
13.	0.21617	0.21613	0.00004	0.03982	0.04008	0.00026	20.03	50.04
14.	0.21617	0.21606	0.00011	0.03982	0.04008	0.00026	20.03	50.04
15.	0.21617	0.21584	0.00033	0.03982	0.04008	0.00026	20.02	49.99
16.	0.02116	0.02159	0.00043	0.15928	0.15936	0.00008	21.46	24.46
17.	0.02116	0.02159	0.00043	0.15928	0.15943	0.00015	21.47	24.47
18.	0.02116	0.02159	0.00043	0.15928	0.15951	0.00023	21.48	24.48
19	0.01058	0.01070	0.00013	0.15928	0.15920	0.00008	20.66	22.15
20	0.01058	0.01064	0.00006	0.19528	0.15948	0.00020	20.69	22.16
21.	0.01058	0.01064	0.00006	0.15928	0.15849	0.00079	20.68	22.15

5. Amalgam Reduction of a Ferric Chloride Solution.

It may sometimes be desirable to titrate directly a ferrous chloride solution. Previous workers on the amalgam method only tried the reduction of ferric sulphate with respect to the reduction of iron, so that it seemed worth while to try to show that this method also applies well to the chloride solution.

An approximately 0.13 N solution of a ferric chloride solution was made by dissolving it in concetrated hydrochloric acid and evaporating to fuming to expel traces of chlorine which might have been present and then dissolving it in hydrochloric acid and diluting to 1 litre. A suitable quantity of hydrochloric acid (here 50 cc. per litre) was used to prevent hydrolysis.

Of the solution 20 cc. was taken and standardized by reducing with zinc amalgam and titrating with a decinormal potassium permanganate solution after converting it into a sulphate by adding 10 cc. of sulphuric acid (1 : 1) and evaporating to fuming. It could next be shown, by taking the same quantity of the solution and reducing with bismuth[1] or zinc amalgam and titrating in the presence of 20 cc. of the Zimmermann-Reinhardt mixture, that the permaganate titer agrees perfectly well with the former values within an experimental error. The following table shows the results.

TABLE VIII. Reduction of a Ferric Chloride Solution.

$FeCl_3$ taken (cc.)	Bi amalgam	Zn amalgam	$FeCl_3$ taken (cc.)	$\rightarrow Fe_2(SO_4)_3$
	$KMnO_4$ (cc.)			
20	27.27		20	27.27
20	27.27		20	27.29
20	27.27		20	27.27
20	27.28		20	27.27
20		27.28	20	27.27
20		27.28		27.31

6. Reduction of Titanium by Bismuth Amalgam.

A few trial experiments on the reduction of titanic sulphate prepared by fusing pure commercial titanic sulphate with potassium bisulphate and

(1) When bismuth amalgam was used for reduction, 5 cc. of concentrated hydrochloric acid was used.

dissolving the melt in cold 10 % sulphuric acid, showed that the salt is reduced at ordinary temperatures, producing the characteristic colour, when it is shaken with bismuth amalgam in the atmosphere of carbon dioxide, but even prolonged shaking did not bring the reduction to completion. On adding 10 cc. of concentrated hydrochloric acid for about 20 cc. of the solution (total volume becoming ca. 35 cc. with the water to wash in any small part which had been retained at (A) and shaking for 15 minutes with constant heating of the side of the reductor (B) over wire gauze at 60–70° made the reduction complete, and the permanganate titer showed a good agreement with the case where zinc amalgam was used and titanic solution was reduced cold, in which case, as has already been shown by Nakazono, the reduction to titanous condition is complete. The following table shows the results.

TABLE IX. Reduction of Titanic Sulphate by Bismuth Amalgam.

$Ti(SO_4)_2$ sol. taken 20 cc. Normality of $KMnO_4$ 0.10045 N. $KMnO_4$ required, cc.

Zn amalgam	Bi amalgam
25.31	25.31
25.30	25.30

All the above-mentioned reductions were, expcept in the case of titanium, made at ordinary temperatures. The writer noticed in the course of his experiments, that the reduction of molybdenum and vanadium by bismuth amalgam proceeded much further than the pentavalent and quadrivalent condition respectively, when the reduction was made at 60–70° as was done in the case of titanium, but it failed to stop at any definite stage of oxidation. In both cases prolonged shaking brought the reduction stage near, but not exactly to, trivalent and divalent condition. These phenomena will be the subject of his further investigation.

SUMMARY.

1. Liquid bismuth amalgam reduces vanadic acid to the tetravalent,

ferric to ferrous, and titanic acid to the titanous condtion, and molybdic acid to pentavalent molybdenum under suitable conditions.

2. Methods of differential titration of the combinations vanadium and iron, and molybdenum and iron were worked out, by making use of the reducing action of bismuth and zinc amalgam.

3. It was experimentally shown that hexavalent molybdenum, when present with iron and the mixture is shaken with liquid bismuth amalgam, in presence of air, act catalytically to bring the reduction of iron to completion, while the molybdenum itself is reduced to the pentavalent condition.

4. Suitable conditions for reduction and titration of the solution of molybdenum, vanadium, titanium and iron containing a chloride ion were studied.

In conclusion the writer wishes to express his heartfelt thanks to Prof. Kobayashi for his useful suggestions and also to Mr. T. Kato for his zealous assistance during the course of his work.

Some Experiments on the Abrasion of Metals.[1]

By

Kôtarô Honda and Ryônoské Yamada.

§ 1. INTRODUCTION.

The abrasion of metals is an important subject for investigation both from the engineering and scientific point of view, but as yet we have no experiments[2] which are comparable with each other, these being affected by various factors. For, in the abrasion experiment, the most important factor is the condition of abrasing surfaces, which can be, however, defined by the coefficient of friction between them. Hence in comparing the wears of different metals against a standard surface, it is first of all necessary to conduct the experiments under the same coefficient of friction; in all previous experiments, however, this was not the case. Hence the present writers have carried a new experiment with an apparatus similar to that used by F. Robin to investigate the abrasion in the first place of soft metals, such as copper, cadmium, lead, magnesium, tin, antimony, zinc and bismuth by cast iron plates, and in the second place, of carbon steels by emery discs.

(1) The one hundred and second report from the Research Institute of Iron, Steel and Other Metals.

(2) E. H. Saniter: Journ. of Iron and Steel Inst., No. 3, (1908), 73.
F. Robin: ditto, Carn. Schol. Mem., **2**, (1910), 1.
Report of the Hardness Test Research Comm.: Inst. of Mech. Eng., (1916), 677.
Stanton and Batson: Bulletin of National Physical Labolatory No. 1, (1920).
H. Meyer and F. Nehl: Stahl u. Eisen Heft 17, (1924), 457.

§ 2. APPARATUS.

The apparatus used is shown in Fig. 1. The disc *A* is made of cast iron or emery, its diameter being 15 cm., and it is made to rotate at a rate of about 60 revolutions per minute by a motor through gear

Fig. 1.

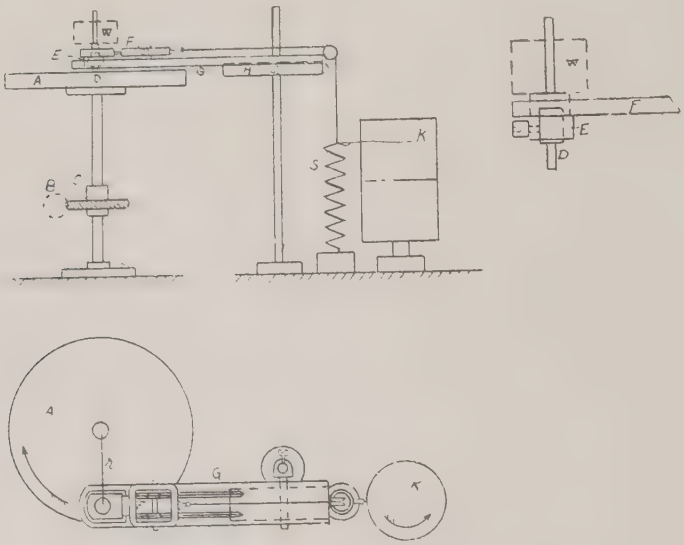

wheels *B* and *C*. The test- piece *D* is fixed by means of a set screw in a hole at *E*, which is again fitted into a hole in a small table F. This table is supported horizontally by the test-piece and two rollers which move in two grooves on a horizontal table *G*, the position of which can be suitably adjusted by means of an adjustable stand *H*. A string connects *F* and the vertical spring *S* through a roller at the right hand end of the stand *H*. *K* is a drum which is rotated about a vertical axis by clock-work. When a weight *W* is applied to *E* and the disc *A* is rotated in the direction as shown by the arrow, the test-piece is pulled forward by the frictional force between it and the disc and this causes an elongation of the spring, till the force of the spring and the frictional force are in equilibrium. It is also necessary that the position of *G* and *H* should be so adjusted that the direction of the string passes

through the centre of the test-piece and is at right angles to the radius of the disc. The elongation of the spring is continuously traced by a pen on paper attached to the drum, the relation between the elongation of the spring and the corresponding force having been previously measured.

If we neglect the very small friction at the rollers attached to F and G, the frictional force between the disc and the test-piece is equal to the tension of the spring.

Now, if we use the following notations:—

n=number of revolutions per second of the disc,

r=distance of the test-piece from the centre of the disc in cm,

F=the frictional force in grams,

H=frictional horse power,

μ=coefficient of friction,

w=weight of test-piece worn out due to the friction in milligrams,

then we have

$$H = \frac{2\pi r F n}{75 \times 10^5}$$

If W' be the total weight applied to the test-piece, that is, the sum of the weights W, the test-piece and a part of E and F, then

$$\mu W' = F$$

$$\therefore \quad \mu = \frac{F}{W'}$$

Thus the coefficient of friction can be calculated.

§ 3. ABRASION OF SOFT METALS.

The specimens of soft metals were prepared by casting them in the form of cylinder of double diameters, the thiner portion of the cylinder being 5 mm. in diameter.

The cast iron disc was polished with emery sand to produce a uniform roughness all over the surface and the position of the test-piece was changed at each measurement in order to maintain a constant coefficient of friction in the course of the same series of experiments.

For each metal, the relation between frictional horse powers obtained by changing the weight W and the corresponding amounts of wear of the test-piece during a definite number of revolutions of the disc was first measured. The duration of the test was restricted to the time during which the elongation of the spring, that is, the frictional force, could be maintained constant, and this time was one minute in each experiment. The change in the frictional force is due to the abrasion of the rough surface of the cast iron and the filling up of the minute depressions by fine praticles of the worn metal. The results of observations are given in Table I.

TABLE I.

Zn		
w	H	μ
0.7 mg.	5.06×10^{-4}	0.214
1.1	8.12	0.218
1.3	8.9	0.218
1.4	10.6	0.206
1.6	10.75	0.205

Pb		
w	H	μ
0.9 mg.	2.98×10^{-4}	0.43
1.6	4.90	0.428
1.7	5.73	0.420
3.3	9.00	0.441
5.5	15.20	0.430

Mg		
w	H	μ
0.4 mg.	6.00×10^{-4}	0.258
0.5	8.11	0.254
0.5	8.25	0.242
0.9	11.00	0.250
0.9	12.2	0.250

Cd		
w	H	μ
0.3 mg.	3.34×10^{-4}	0.263
0.3	3.4	0.264
0.7	7.52	0.280
0.8	7.85	0.286
0.9	11.25	0.272

Cu		
w	H	μ
0.2 mg.	3.3×10^{-4}	0.285
0.3	6.2	0.290
0.5	9.5	0.288
0.7	14.0	0.293

Sn		
w	H	μ
0.6 mg.	3.2×10^{-4}	0.312
1.1	5.8	0.328
2.4	10.7	0.33
3.0	14.5	0.328
3.3	15.8	0.325

Sb		
w	H	μ
0.9 mg.	3.37×10^{-4}	0.297
1.6	5.8	0.3
1.6	6.5	7.29
2.1	8.0	0.287
3.4	11.5	0.302

Bi		
w	H	μ
4.6 mg.	2.92×10^{-4}	0.287
4.7	4.46	0.282
7.2	6.5	0.283
13.5	11.0	0.29
14.1	12.85	0.290

The results in the above table are also shown in Fig. 2, in which curves are drawn one upon another to avoid overlapping.

From these results, we see that the amount of wear is proportional to the frictional horse power, provided that the coefficient of friction is constant. These results agree with those of F. Robin; because he found that in some steels, the amount of wear is proportional to the pressure applied. That proportional constant between the amount of wear and the frictional horse power is a quantity depending on the nature of the materials and the condition of the two abrasing surfaces.

The relation between the amount of abrasion and the frictional horse power being thus established, it is then necessary to measure the amount of abrasion under varying coefficients of friction. The present writers, therefore, carried out their experiments in the same way as above mentioned by varying the coefficient of friction as widely as possible, this being effected by polishing the surface of the disc with a suitably chosen emery sand. For each experiment, the frictional horse power was reduced from the actually used to 15×10^{-4} and the corresponding amount of wear was calculated, the relation of this amount of wear to the coefficient of friction being thus found. The results are given in Table II, in which w' is the reduced amount of wear. The duration of each observation was taken as one minute.

Fig. 2.

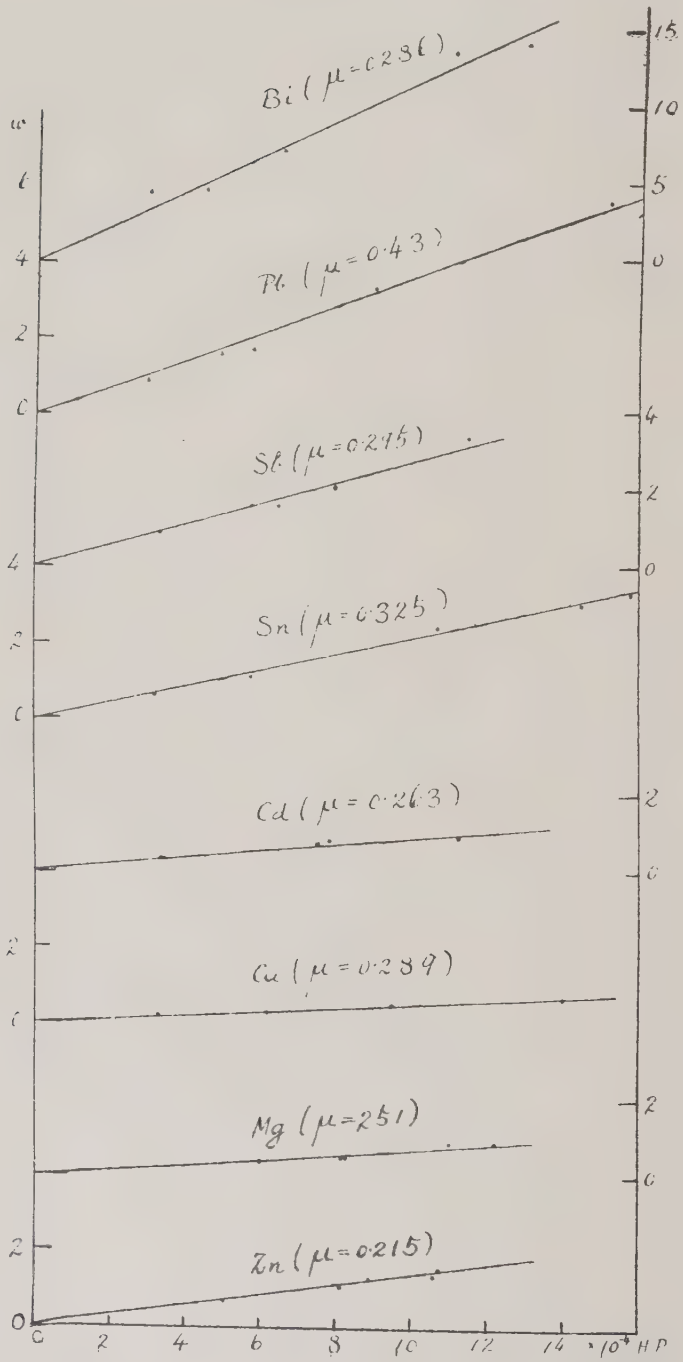
Bi (μ=0.286)
Pt (μ=0.43)
Sb (μ=0.245)
Sn (μ=0.325)
Cd (μ=0.263)
Cu (μ=0.289)
Mg (μ=251)
Zn (μ=0.215)
0
2
4
6
8
10
12
14
×10⁴ H P
15
10
5

TABLE II.

Zn

μ	H	w	w'
0.146	5.70×10^{-4}	0.35 mg.	0.9 mg
0.205	10.75	1.6	2.22
0.206	10.60	1.4	1.98
0.214	5.06	0.7	2.1
0.218	8.12	1.1	2.0
0.218	8.9	1.3	2.18
0.27	10.0	2.0	3.0
0.28	14.15	4.2	4.5
0.326	5.08	2.5	7.5
0.352	5.00	2.7	8.1

Pb

μ	H	w	w'
0.252	4.50×10^{-4}	0.5 mg.	1.2 mg
0.260	4.95	0.4	1.5
0.351	9.8	1.5	2.3
0.370	12.2	2.5	2.5
0.375	13.0	3.5	4.0
0.420	5.73	1.7	4.5
0.428	4.9	1.6	4.8
0.430	2.98	0.9	4.5
0.441	9.00	3.3	5.5
0.481	15.20	5.5	5.41

Mg

μ	H	w	w'
0.242	8.28×10^{-4}	0.5 mg	0.91 mg
0.250	11.0	0.9	1.24
0.250	12.2	0.9	1.10
0.254	8.11	0.5	0.93
0.258	6.00	0.4	1.0
0.271	6.30	0.5	1.19
0.275	4.44	0.4	1.33
0.280	4.56	0.5	1.6

Cd

μ	H	w	w'
0.176	7.85×10^{-4}	0.3 mg.	0.58 mg
0.20	9.85	0.3	0.45
0.24	5.5	0.3	0.8
0.263	3.34	0.3	1.35
0.264	3.4	0.3	1.3
0.272	11.25	0.9	1.2
0.280	7.52	0.7	1.4
0.286	7.85	0.8	1.5
0.320	10.5	2.0	1.9

Cu

μ	H	w	w'
0.26	11.0×10^{-4}	0.4 mg.	0.5 mg
0.285	3.3	0.2	0.91
0.288	9.5	0.5	0.79
0.290	6.2	0.3	0.73
0.330	8.5	0.8	1.5
0.34	8.6	0.9	1.8
0.37	9.1	1.3	2.1

Sn

μ	H	w	w'
0.255	9.44×10^{-4}	0.6 mg.	0.95 mg
0.256	9.5	0.7	1.11
0.312	3.2	0.6	2.82
0.325	15.8	3.3	3.12
0.328	5.8	1.1	2.85
0.328	14.5	3.0	3.10
0.33	10.7	2.4	3.37
0.362	4.55	1.0	3.3
0.374	5.6	1.5	4.0

Bi

μ	H	w	w'
0.245	3.25×10^{-4}	1.6 mg	7.4 mg
0.264	2.42	2.6	16.2
0.265	9.5	9.8	15.4
0.282	4.46	4.7	16.0
0.293	6.5	7.2	16.6
0.287	2.92	4.6	23.6
0.290	11.0	13.5	18.4
0.290	14.1	12.85	13.6
0.318	12.0	17.0	21.0

Sb

μ	H	w	w'
0.287	8.0×10^{-4}	2.1 mg.	3.9 mg
0.290	6.5	1.5	3.46
0.297	3.37	0.9	4.0
0.30	5.8	1.6	3.88
0.302	11.5	3.4	4.44
0.360	3.25	2.2	10.3
0.403	8.50	12.8	22.5
0.425	4.81	7.5	23.4

Fig. 3.

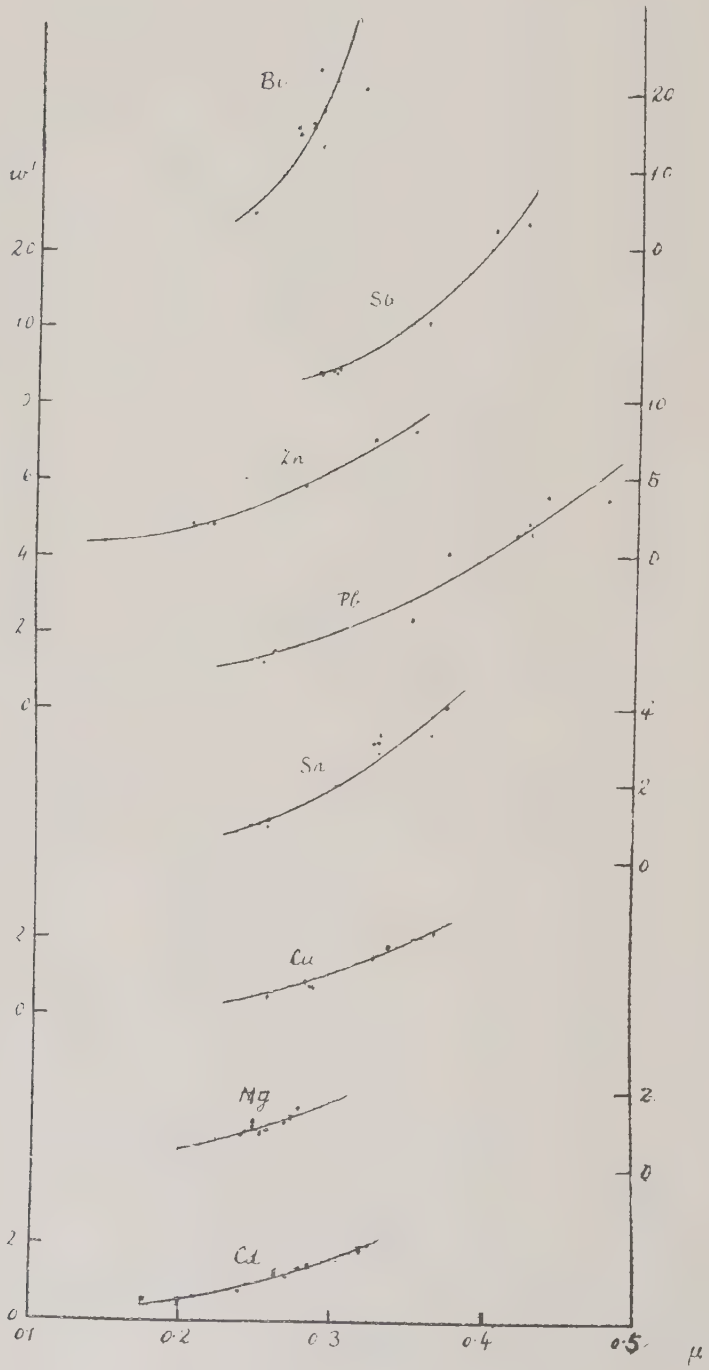

These results given above are shown in Fig. 3. Thus the wear under a constant horse power always increases with the coefficient of friction. Hence in comparing the relative coefficient of abrasion of metals, we must calculate the wear under a constant coefficient of friction; taking the coefficient of friction to be 0.3, we get Table III.

TABLE III.

	Density	Relative Coeff. of Abrasion
Cu	8.93	$0.67\left(\frac{gr}{H.P.}\right)$
Cd	8.64	1.10
Mg	1.74	1.27
Pb	6.62	1.27
Sn	7.29	1.33
Sb	11.37	2.93
Zn	7.1	3.40
Bi	9.8	14.73

The magnitude of the relative coefficient of abrasion given above corresponds generally to the degree of the brittleness of these metals.

§ 4. ABRASION OF CARBON STEELS.

The experiments on carbon steels were carried out with emery discs. Swedish steels were used; they had the following constituents:—

Carbon percent	Silicon percent	Sulphur percent	Phosphorus percent	Manganese percent
0.09	trance	0.021	0.021	0.38
0.28	0.3	0.010	0.012	0.44
0.49	0.27	0.029	0.029	0.41
0.69	0.27	0.029	0.023	0.21
0.88	0.34	0.028	0.015	0.19
1.11	0.27	0.029	0.020	0.23

These steels were tested in different conditions, i.e. the normalised,

martensitic, troostitic and sorbitic structures. In the first place, it was tested, in both the normal and martensitic conditions, to see whether the proportionality between the amount of wear and the frictional horse power holds good as in the case of former metals, the coefficient of friction being kept constant. The results of experiments are given in Table IV.

TABLE IV.

Normal Structure

0.1% C		
w	H	μ
1.6 mg.	3.76×10^{-4}	0.306
2.7	6.7	0.303
4.7	11.4	0.3
4.6	12.0	0.318
6.1	14.6	0.296

0.3% C		
w	H	μ
1.2 mg.	3.23×10^{-4}	0.276
2.6	7.61	0.274
3.8	10.2	0.292
4.5	12.8	0.274
5.0	13.4	0.280

0.5% C		
w	H	μ
1.4 mg.	3.57×10^{-4}	0.297
2.4	6.36	0.292
3.4	8.8	0.3
4.5	11.15	0.3
5.7	14.42	0.3

0.7% C		
w	H	μ
1.9 mg.	6.15×10^{-4}	0.292
2.5	7.32	0.320
3.0	9.05	0.320
3.9	11.05	0.296
5.3	14.30	0.286

0.9% C		
w	H	μ
0.7 mg.	3.06×10^{-4}	0.285
1.9	6.41	0.276
2.9	10.45	0.275
3.9	14.3	0.286
4.3	15.3	0.305

1.1% C		
w	H	μ
0.8 mg.	3.41×10^{-4}	0.276
1.8	6.46	0.297
2.8	10.8	0.30
3.1	11.0	0.294
3.8	13.65	0.286

TABLE IV.

Martensitic Structure

0.1% C		
w	H	μ
0.9 mg.	4.11×10^{-4}	0.332
1.8	7.95	0.352
1.9	8.45	0.361
2.4	10.65	0.350
3.2	14.30	0.362

0.3% C		
w	H	μ
0.7 mg.	6.35×10^{-4}	0.275
1.3	7.12	0.318
1.2	9.01	0.294
1.4	9.8	0.328
1.4	10.8	0.278

0.5% C		
w	H	μ
1.4 mg.	5.5×10^{-4}	0.350
2.0	8.35	0.333
2.3	8.5	0.345
3.5	12.8	0.392
4.1	15.1	0.367

0.7% C		
w	H	μ
2.1 mg.	7.44×10^{-4}	0.372
2.9	8.85	0.380
3.5	12.1	0.380
4.7	14.6	0.351
4.7	15.0	0.367

0.9% C		
w	H	μ
1.2 mg.	4.8×10^{-4}	0.318
2.2	9.12	0.292
2.3	9.35	0.302
3.2	12.1	0.306
3.9	14.5	0.306

1.1% C		
w	H	μ
0.9 mg.	3.32×10^{-4}	0.272
2.0	7.9	0.284
2.4	8.3	0.284
3.4	11.7	0.287
3.7	13.8	0.287

The results given above are shown in Figs. 4 and 5.

Thus we see that the amount of wear is proportional to the frictional horse power, that is, the relative coefficient of abrasion is constant, provided that the coefficient of friction remained constant.

Next the change in the amount of wear due to varying coefficient of friction was investigated by using emery wheels varying in roughness. As in the case of former metals, the frictional horse power was reduced to 15×10^{-4}; the results of experiments are given in Table V.

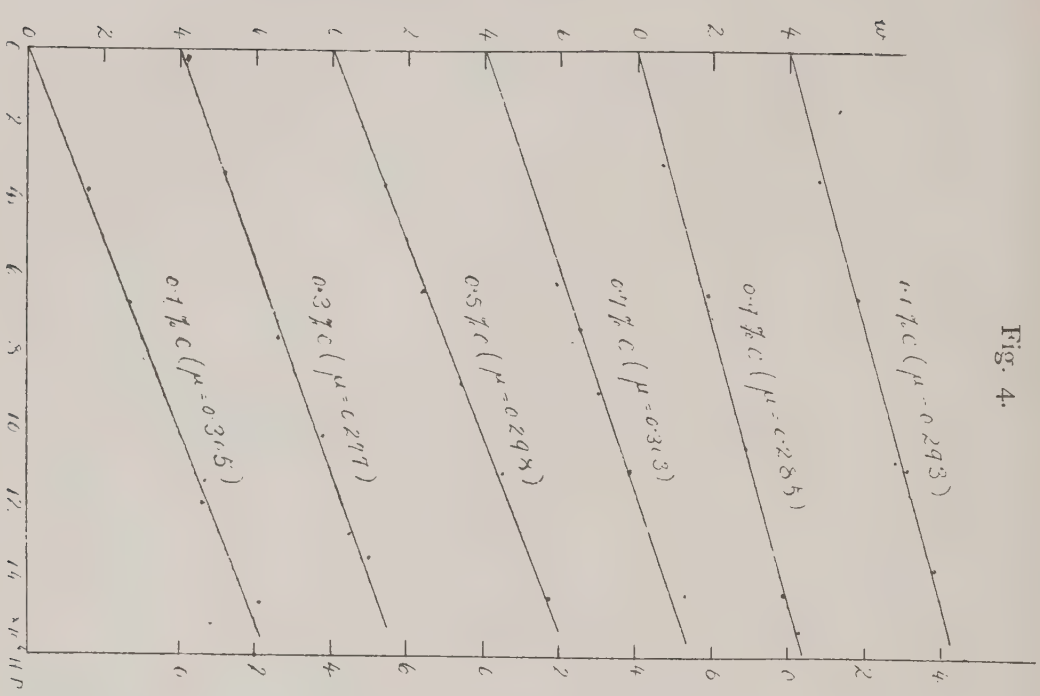
1·1 % C (μ = 0·293)
0·9 % C (μ = 0·285)
0·7 % C (μ = 0·313)
0·5 % C (μ = 0·298)
0·3 % C (μ = 0·277)
0·1 % C (μ = 0·315)
H

Fig. 4.

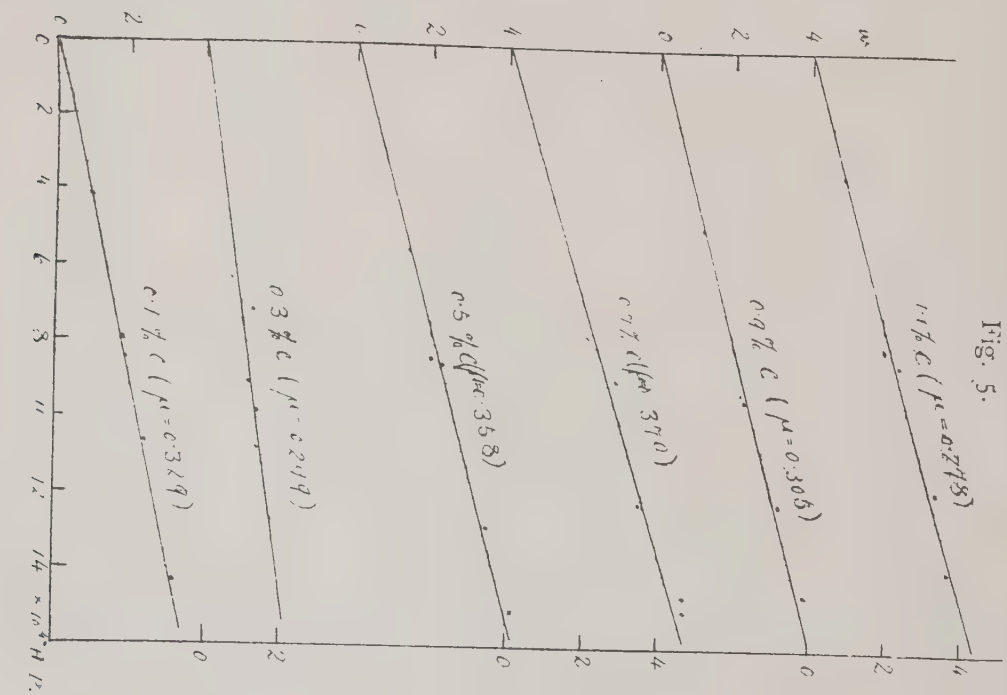
1·1 % C (μ = 0·278)
0·9 % C (μ = 0·305)
0·7 % C (μ = 0·370)
0·5 % C (μ = 0·358)
0·3 % C (μ = 0·249)
0·1 % C (μ = 0·324)
H

Fig. 5.

TABLE V.

Normal Structure.

0.1% C			
μ	H	w	w'
0.296	14.6×10^{-4}	6.1 mg.	6.27 mg
0.3	11.4	4.7	6.2
0.303	6.7	2.7	6.05
0.306	3.76	1.5	6.0
0.318	12.0	4.6	5.75
0.483	10.4	6.8	9.85
0.505	11.6	8.0	10.35
0.51	11.5	7.6	9.92

0.3% C			
μ	H	w	w'
0.274	7.61×10^{-4}	2.6 mg.	5.1 mg.
0.274	12.80	4.5	5.3
0.276	3.23	1.2	5.6
0.280	13.40	5.0	5.5
0.292	10.2	3.8	5.5
0.448	10.0	5.4	8.25
0.46	10.4	5.6	9.1
0.47	10.5	5.7	8.9
0.475	10.55	5.9	9.0

0.5% C			
μ	H	w	w'
0.292	6.36×10^{-4}	2.4 mg.	5.55 mg.
0.297	3.57	1.4	5.9
0.3	8.8	3.4	5.8
0.3	11.15	4.5	6.05
0.3	14.42	5.7	5.9
0.414	9.48	4.7	7.0
0.44	10.00	5.1	7.7
0.455	10.4	5.3	7.72
0.5	11.45	7.1	9.3

0.7% C			
μ	H	w	w'
0.286	14.3×10^{-4}	5.3 mg	5.4 mg
0.296	11.05	3.9	5.3
0.32	7.32	2.5	5.13
0.32	7.32	2.5	5.13
0.32	9.05	3.0	5.00
0.396	9.80	3.0	6.5
0.44	10.0	4.4	7.0
0.455	10.2	4.9	7.2
0.46	10.1	4.9	7.0

0.9% C			
μ	H	w	w'
0.255	3.06×10^{-4}	0.7 mg.	3.44 mg.
0.275	10.45	2.9	4.16
0.276	6.41	1.9	4.45
0.286	14.3	3.9	4.08
0.305	15.3	4.3	4.2
0.448	9.65	5.2	8.1
0.483	10.6	6.0	8.5
0.486	10.4	5.8	8.38

1.1% C			
μ	H	w	w'
0.276	3.41×10^{-4}	0.8 mg.	3.5 mg.
0.286	13.65	3.8	4.2
0.294	11.0	3.1	4.23
0.297	6.46	1.8	4.19
0.300	10.8	2.8	3.9
0.396	9.8	4.4	6.65
0.43	10.16	5.1	6.95
0.455	10.55	5.6	8.00

TABLE V.

Sorbitic Structure.

0.1% C			
μ	H	w	w'
0.268	6.1×10^{-4}	1.7 mg.	4.2 mg.
0.292	6.05	2.0	4.3
0.292	6.05	2.1	4.55
0.345	8.02	2.6	4.86
0.483	10.7	5.7	8.0
0.483	10.88	5.7	7.8
0.498	11.4	6.0	7.8
0.532	12.2	6.5	8.0

0.3% C			
μ	H	w	w'
0.275	5.7×10^{-4}	1.5 mg.	3.05 mg.
0.296	6.2	1.5	3.67
0.303	6.48	1.8	4.17
0.319	6.85	1.9	4.17
0.487	11.7	4.7	6.4
0.487	11.4	4.9	6.45
0.498	9.85	4.2	6.4
0.518	11.7	5.6	7.2

0.5% C			
μ	H	w	w'
0.292	6.25×10^{-4}	1.5 mg.	3.61 mg.
0.303	6.85	1.6	3.5
0.313	7.2	2.0	4.17
0.345	8.35	2.0	3.6
0.43	9.85	3.4	5.17
0.43	9.85	3.4	5.17
0.43	10.2	3.6	5.44
0.475	10.35	4.0	5.8

0.7% C			
μ	H	w	w'
0.296	6.59×10^{-4}	1.5 mg.	3.41 mg.
0.303	6.63	1.3	2.93
0.319	7.6	1.7	3.35
0.326	7.22	1.6	3.33
0.425	10.3	3.2	4.65
0.441	10.2	3.5	5.14
0.46	10.6	3.9	5.50

0.9% C			
μ	H	w	w'
0.282	6.25×10^{-4}	1.4 mg	3.36 mg.
0.282	6.25	1.4	3.36
0.282	6.35	1.2	2.84
0.428	9.8	3.5	5.35
0.448	10.3	3.6	5.25
0.483	11.22	4.1	5.48

1.1% C			
μ	H	w	w'
0.272	5.9×10^{-4}	1.2 mg	3.05 mg.
0.275	6.15	1.4	3.42
0.292	6.3	1.5	3.57
0.386	9.15	2.6	4.26
0.414	9.05	3.1	4.8
0.442	10.45	3.4	4.88

TABLE V.

Troostitic Structure.

0.1% C			
μ	H	w	w'
0.338	7.65×10^{-4}	2.0 mg.	3.92 mg.
0.338	7.65	1.9	3.73
0.338	7.65	1.9	3.73
0.382	8.6	2.6	4.53
0.402	9.8	3.3	5.02
0.430	10.4	3.8	5.5

0.3% C			
μ	H	w	w'
0.318	7.62×10^{-4}	1.8 mg.	3.54 mg
0.318	7.5	1.7	3.4
0.318	7.3	1.8	3.7
0.418	10.06	3.5	5.22
0.43	10.25	3.4	5.00

0.5% C			
μ	H	w	w'
0.283	6.48×10^{-4}	1.0 mg.	2.32 mg
0.318	7.5	1.7	3.4
0.318	7.4	1.4	2.85
0.330	7.85	1.6	3.06
0.406	9.8	3.3	5.06
0.414	10.1	3.4	5.20

0.7% C			
μ	H	w	w'
0.33	8.1×10^{-4}	1.6 mg.	2.96 mg.
0.352	8.7	2.0	3.44
0.352	8.55	1.8	3.15
0.39	9.7	3.0	4.62
0.402	9.7	2.9	4.5

0.9% C			
μ	H	w	w'
0.35	8.35×10^{-4}	1.7 mg.	3.05 mg.
0.382	9.15	2.2	3.6
0.392	9.3	2.4	3.87
0.402	9.95	3.0	4.5

1.1% C			
μ	H	w	w'
0.31	7.36×10^{-4}	1.1 mg.	2.24 mg.
0.318	7.3	1.4	2.87
0.372	9.38	2.2	3.52
0.43	10.2	3.8	5.6
0.441	11.2	4.4	5.9
0.45	10.5	4.5	6.4

TABLE V.

Martensitic Structure

0.1% C			
μ	H	w	w'
0.332	4.11×10^{-4}	0.9 mg.	3.29 mg.
0.350	10.65	2.4	3.37
0.352	7.05	1.8	3.4
0.361	8.45	1.9	3.38
0.302	14.3	3.2	3.30
0.50	11.9	5.3	0.05
0.51	0.75	2.8	6.2
0.51	12.1	5.6	0.9
0.512	16.5	7.7	7.0
0.53	12.7	5.3	0.25

0.3% C			
μ	H	w	w'
0.275	6.35×10^{-4}	0.7 mg	1.65 mg
0.278	10.8	1.4	1.8
0.204	9.01	1.2	2.0
0.318	7.12	1.3	2.73
0.328	0.8	1.4	2.14
0.40	11.2	3.8	5.1
0.402	14.5	5.1	5.3
0.484	11.4	4.4	5.8
0.484	11.7	3.7	4.75
0.485	0.0	2.6	5.0

0.5% C			
μ	H	w	w'
0.281	0.3×10^{-4}	1.1 mg.	2.6 mg.
0.333	8.35	2.0	3.0
0.345	8.5	2.3	4.05
0.350	5.5	1.4	3.8
0.367	15.1	3.6	3.57
0.302	12.8	3.5	4.1
0.302	12.8	4.1	4.7
0.45	7.5	2.8	5.0

0.7% C			
μ	H	w	w'
0.200	6.00×10^{-4}	1.1 mg	2.73 mg.
0.282	7.2	1.4	2.92
0.351	14.0	4.7	4.84
0.307	15.0	4.7	4.7
0.372	7.44	2.1	4.24
0.380	8.85	2.9	4.9
0.380	12.1	3.5	4.34

0.9% C			
μ	H	w	w'
0.240	5.0×10^{-4}	1.0 mg	2.54 mg.
0.265	0.32	1.3	3.1
0.202	0.12	2.2	3.02
0.302	0.35	2.9	3.7
0.300	12.1	3.2	3.05
0.300	0.35	2.3	3.70
0.315	4.8	1.2	3.75

1.1% C			
μ	H	w	w'
0.246	5.55×10^{-4}	1.2 mg.	3.25 mg.
0.257	6.00	1.3	3.25
0.273	3.32	0.9	4.07
0.284	8.3	2.4	4.34
0.284	7.0	2.0	3.8
0.287	11.7	3.4	4.36
0.287	13.8	3.7	4.03

The results given above are shown in Figs. 6, 7, 8, and 9.

Next the relation between the coefficient of abrasion and the carbon content under a constant coefficient of friction, say 0.32, is given in Fig. 10. In the normalized condition, the amount of wear decreases steadily from 0.1 to 1.1 percent of carbon, in the sorbitic structure, it decreases

Fig. 6.

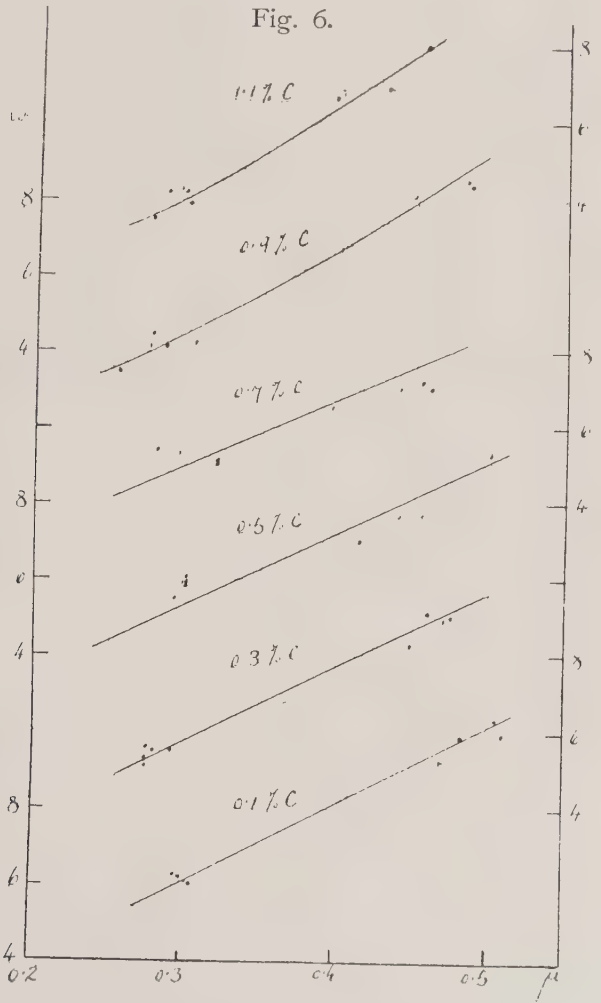

gradually up to 0.7 percent of carbon content, and then increases again in the case of a higher percentage of carbon. In the troostitic structure the amount of wear is least in a 0.9 percent carbon steel, but in the case of the martensitic structure it decreases from 0.1 to 0.3 percent of carbon

Fig. 7.

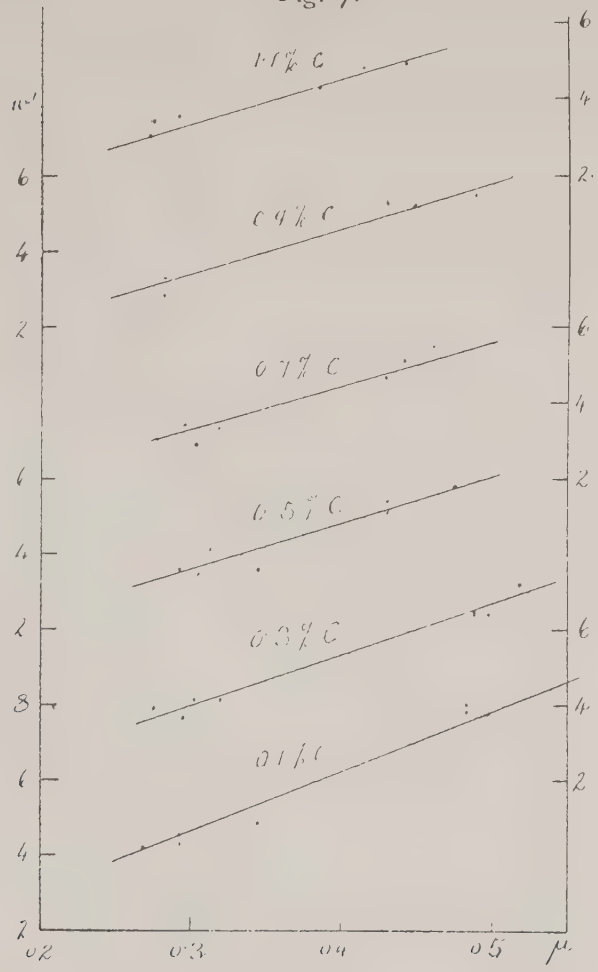
1.1% C
0.9% C
0.7% C
0.5% C
0.3% C
0.1% C
w'
μ
0.2
0.3
0.4
0.5

Fig. 8.

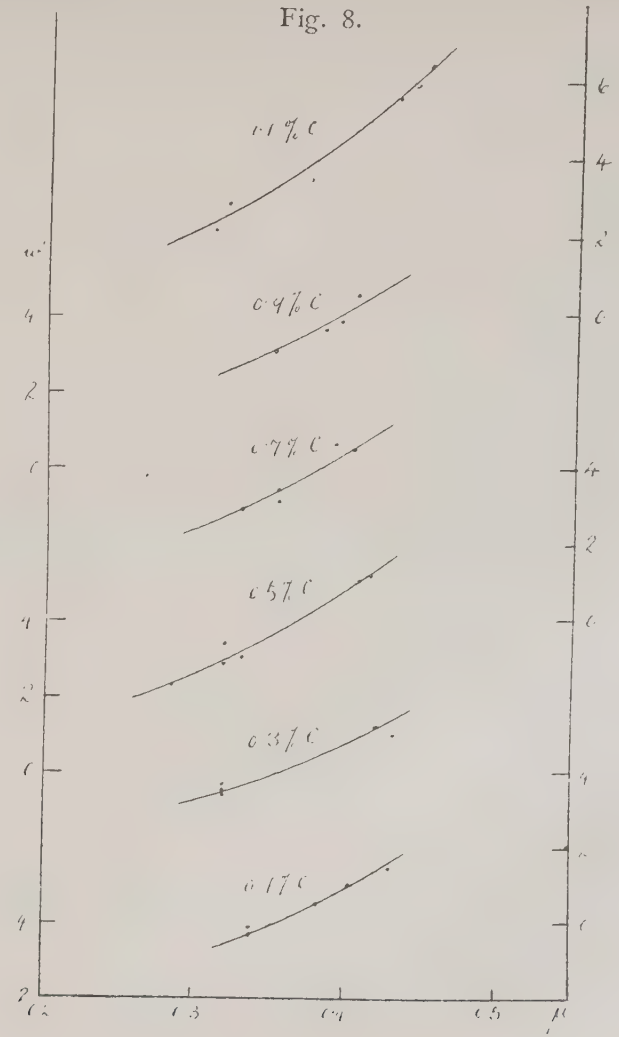
1.1% C
0.9% C
0.7% C
0.5% C
0.3% C
0.1% C
w'
μ
0.2
0.3
0.4
0.5

and then increases gradually up to 1.1 percent of carbon content. Comparing the amounts of wear in each case, we see that the wear of steels is greatest under the normalised condition and becomes less in the sorbitic, troositic and martensitic structure; but in high carbon steels, the wear of martensite increases beyond that of troostite or sorbite.

Fig. 9.

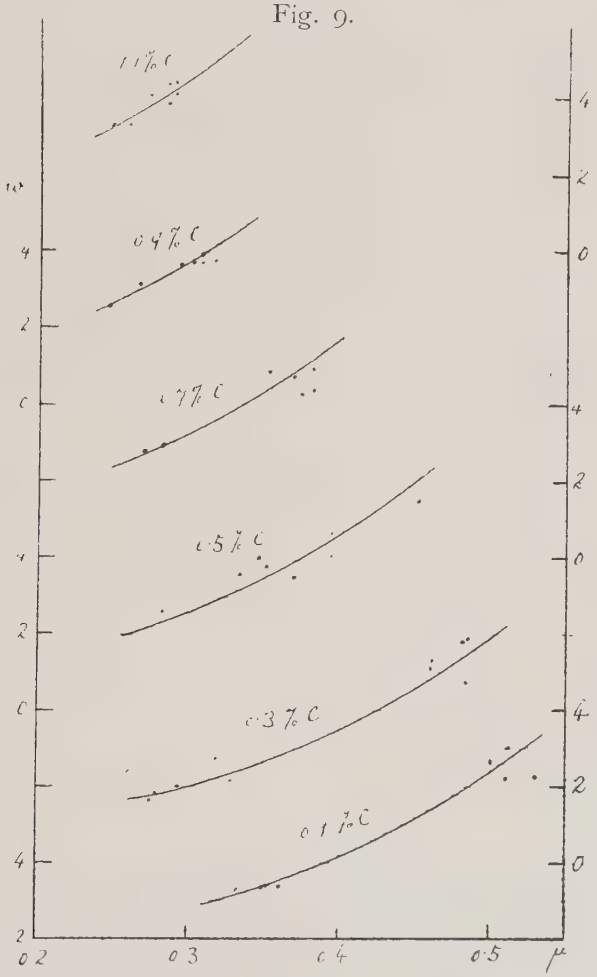

§ 5. INFLUENCE OF THE VELOCITY ON THE ABRASION OF METALS.

As regard to the results so far obtained, it was thought necessary to study the effect of the velocity of abrasion under varying velocities of

the abrasing disc. For this purpose, both the number of revolutions per minute of the emery disc and the distance of the test-piece from the centre of the disc were varied as widely as possible, so that the linear velocity was changed from fifteen to forty metres per minute. In the first place, the relation between the coefficient of friction and the amount of wear in one minute reduced to 15×10^{-4} horse power was measured for 0.3 percent carbon steel of sorbitic structure. Results of experiments are given in Table VI, and also shown in Fig. 11, the result shown in Fig. 5 being also here included.

Fig. 10.

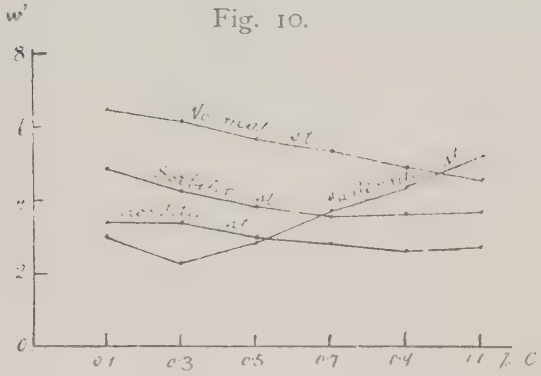

Fig. 11.

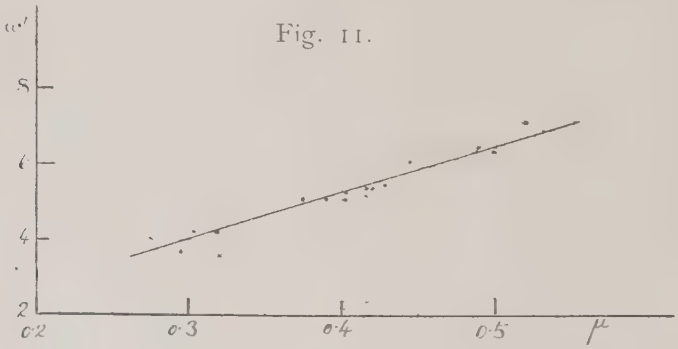

TABLE VI.

μ	v	w'	w''	μ	v	w'	w''
0.416	15.3 $\frac{\text{metre}}{\text{min.}}$	5.4 mg.	5.2 mg.	0.416	22.6 $\frac{\text{metre}}{\text{min.}}$	5.2 mg.	5.4 mg.
0.402	15.4	5.3	5.2	0.444	23.0	6.1	5.5
0.402	15.5	5.1	5.1	0.427	23.0	5.5	5.2
0.498	20.4	6.4	5.1	0.375	23.4	5.1	5.4
0.275	21.3	4.0	5.8	0.42	23.4	5.4	5.2
0.296	21.8	3.7	5.0	0.487	39.5	6.4	5.3
0.303	22.1	4.2	5.5	0.518	39.5	7.2	5.6
0.319	22.2	4.2	5.2	0.487	40.7	6.5	5.3
0.390	22.25	5.1	5.2				

From this we notice that the relation between the coefficient of friction and the amount of wear referred to in the above holds good how the velocity of abrasion may change in the said range. In other words, the amount of wear under a constant coefficient of friction is constant for varying velocity from fifteen to forty metres per minute. Taking the coefficient of friction to be 0.4, we get the reduced amount of wear w'' given in the last column in the above Table. Fig. 12 shows the relation between this wear and the velocity of abrasion. From this curve, we see that the change of the reduced amount of wear for varying velocity is so slight that it may be neglected within the limits of the range investigated.

Fig. 12.

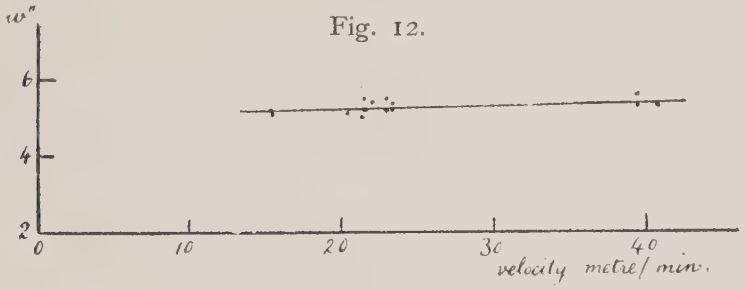

§ 6. SUMMARY.

1. The amount of wear under different frictional horse power and under different coefficients of friction was measured with respect to soft metals and carbon steels.

2. In these metals, the amount of wear is proportional to the frictional horse power, provided that the coefficient of friction is constant.

3. The amount of wear of these metals and steels under a constant frictional horse power increases with the coefficient of friction.

4. The effect of the velocity of abrasion on the amount of wear is negligibly small in the range of velocity investigated.

Über die konvex-geschlossenen Mannigfaltigkeiten im n-dimensionalen Raume.[1]

Von

Tadahiko Kubota.

In diesen „Reports" Bd. 12, S. 45–65 habe ich einige Ungleichheiten für die Eilinien und Eiflächen behandelt. Hier möchte ich gewisse Resultate darunter auf die konvex-geschlossene Mannigfaltigkeit im n-dimensionalen Raume übertragen.

1. HYPERKUGELFUNKTIONEN IM N-DIMENSIONALEN RAUME.

Bezeichnet man die rechtwinkligen Koordinaten im n-dimensionalen Raume mit $x_1, x_2 \ldots\ldots x_n$ und den Differentialausdruck

$$\frac{\partial^2}{\partial x_1^2}+\frac{\partial^2}{\partial x_2^2}+\ldots\ldots+\frac{\partial^2}{\partial x_n^2}$$

mit ∇^2 und ferner

$$\sqrt{x_1^2+x_2^2+\ldots\ldots+x_n^2}$$

mit r, dann gilt bekanntlich nach Mehler[2]

$$\nabla^2 (r^{2-n}) = 0.$$

Entwickelt man die Funktion

(1) Diese Arbeit ist durch Anregung des Herrn Dr. W. Süss entstanden. Er hat mich durch Fragestellung angeregt, ob meine Untersuchung über Eilinien und Eiflächen sich auf den n dimensionalen Raum verallgemeinern lasse.

(2) Mehler, Crelle's Journal 66.

$$(1-2z\cos\gamma+z^2)^{-\frac{n-2}{2}}$$

für $|z|<1$ in die Reihe

$$1+L_1(\cos\gamma)\,z+L_2(\cos\gamma)\,z^2+\ldots\ldots+L_n(\cos\gamma)\,z^n+\ldots\ldots(1)$$

so sind $L_n(\cos\gamma)$ ganze rationale Funktionen von $\cos\gamma$.

Betrachtet man zwei Punkte $P(x_1\,x_2\ldots\ldots x_n)$ $P'(x_1'\,x_2'\ldots\ldots x_n')$ im Raume und setzt man

$$r=\sqrt{x_1^2+x_2^2+\ldots\ldots+x_n^2},$$

$$r'=\sqrt{x_1'^2+x_2'^2+\ldots\ldots+x_n'^2},$$

$$r\,r'\cos\gamma=x_1\,x_1'+x_2\,x_2'+\ldots\ldots+x_n\,x_n',$$

dann ist

$$PP'^{2-n}=(r^2-2r\,r'\cos\gamma+r'^2)^{-\frac{n-2}{2}}$$

$$=\frac{1}{r'^{n-2}}\left[1+L_1(\cos\gamma)\,\frac{r}{r'}+L_2(\cos\gamma)\,\frac{r^2}{r'^2}+\ldots\ldots\right.$$

$$\left.+L_m(\cos\gamma)\,\frac{r^m}{r'^m}+\ldots\ldots\right. \qquad (2)$$

Da aber PP'^{2-n} die Laplacesche Differentialgleichung

$$\nabla^2 u=0$$

erfüllt, so müssen

$$r\,L_1(\cos\gamma),\ r^2\,L_2(\cos\gamma),\ldots\ldots r^m\,L_m(\cos\gamma)\ldots\ldots$$

auch die Laplacesche Gleichung erfüllen.

Die ganze rationale homogene Funktion X_m mten Grades von $x_1\,x_2$ $\ldots\ldots x_n$, welche der Relation

$$\nabla^2 X_m=0$$

genügt, heisst die Hyperkugelfunktion m ten Grades.

Bezeichnet man das Hyperflächenelement der Kugel

$$x_1^2+x_2^2+\ldots\ldots+x_n^2=1$$

mit $d\omega$ und sind X_m, $X_{m'}$ zwei Hyperkugelfunktionen verschiedenen Grades m und m' dann

$$\iint \ldots\ldots \int X_m X_{m'} \, d\omega = 0,$$

wobei die Integration auf die ganze Mannigfaltigkeit

$$x_1^2 + x_2^2 + \ldots\ldots + x_n^2 = 1$$

zu erstrecken ist. Dies ist ganz in derselben Weise wie im dreidimensionalen Falle beweisbar. Aus (1) erhält man durch Differentiation

$$\frac{2\cos\gamma - 2z}{(1 - 2\cos\gamma z + z^2)^{\frac{n}{2}}} = \frac{2}{n-2}\Big[L_1(\cos\gamma) + 2L_2(\cos\gamma)\, z$$

$$+ 3\, L_3(\cos\gamma)\, z^2 + \ldots\ldots + m\, L_m(\cos\gamma)\, z^{m-1} + \ldots\ldots\Big] \qquad (3)$$

Durch Addieren von (1) und (3)

$$\frac{1 - z^2}{(1 - 2z\cos\gamma + z^2)^{\frac{n}{2}}} = 1 + \frac{n}{n-2} L_1(\cos\gamma)\, z$$

$$+ \frac{n+2}{n-2} L_2(\cos\gamma)\, z^2 + \ldots\ldots$$

$$+ \frac{n+2\,m-2}{n-2} L_m(\cos\gamma)\, z^m + \ldots\ldots \qquad (4)$$

Satz 1. *Es sei* $f(\theta_1, \theta_2, \ldots\ldots \theta_{n-1})$ *eine eindeutige und stetige Funktion des Punktes auf der Hyperkugelfläche*

$$x_1^2 + x_2^2 + \ldots\ldots + x_n^2 = 1,$$

wobei $\theta_1, \theta_2 \ldots\ldots \theta_{n-1}$ *Polarkoordinaten im n-dimensionalen Raume bedeuten. Bezeichnet man den Winkel der Geraden, welche den Anfangspunkt mit den Punkten* $(x_1, x_2, \ldots\ldots x_n;\ \theta_1\, \theta_2 \ldots\ldots \theta_{n-1})$ $(x_1'\, x_2' \ldots\ldots x_n';\ \theta_1', \theta_2' \ldots\ldots \theta'_{n-1})$ *verbinden, mit* γ, *dann ist*

$$\frac{\Gamma\left(1 + \frac{n}{2}\right)}{n\pi^{\frac{n}{2}}} \sum_{m=0}^{\infty} \frac{n+2\,m-2}{n-2} \iint \ldots\ldots \int L_m(\cos\gamma)\, f(\theta_1\, \theta_2 \ldots\ldots \theta_{n-1})\, d\omega$$

im Abel'schen Sinne gleichmässig summierbar und stellt die Funktion $f(\theta_1' \theta_2' \ldots\ldots \theta'_{n-1})$ *dar.*

Der Beweis ist ganz derselbe wie im dreidimensionalen Falle. Teilt man nun die Hyperkugelfläche K

$$x_1^2 + x_2^2 + \ldots\ldots + x_n^2 = 1$$

in zwei Teile K_1 und K_2 derartig, dass K_1 eine Punktmenge von Punkten der Hyperkugelfläche bilden, deren sphärischer Abstand vom Punkte $(1\ \theta_1' \theta_2' \ldots\ldots \theta'_{n-1}) \leqq \varepsilon$ ist und K_2 den übrigen Teil der Hyperkugel bedeutet.

Für die Punktmenge K_2 konvergiert das Integral

$$\iint\ldots\ldots\int_{K_2} \frac{1-z^2}{(1-2z\cos\gamma+z^2)^{\frac{n}{2}}} f(\theta_1 \theta_2 \ldots\ldots \theta_{n-1})\, d\omega$$

gleichmässig gegen Null, wenn z sich gegen 1 nähert.

Wenn ε hinreichend klein angenommen ist, so gilt für die Punktmenge K_1

$$| f(\theta_1 \theta_2 \ldots\ldots \theta_{n-1}) - f(\theta_1' \theta_2' \ldots\ldots \theta'_{n-1}) | < \varepsilon'.$$

Folglich

$$\iint\ldots\ldots\int_{K_1} \frac{1-z^2}{(1-2z\cos\gamma+z^2)^{\frac{n}{2}}} f(\theta_1, \theta_2, \ldots\ldots \theta_{n-1})\, d\omega$$

$$= [f(\theta_1', \theta_2', \ldots\ldots \theta'_{n-1}) + \eta] \iint\ldots\ldots\int_{K_1} \frac{1-z^2}{(1-2z\cos\gamma+z^2)^{\frac{n}{2}}}\, d\omega$$

wobei

$$|\eta| < \varepsilon'.$$

Anderseits ist

$$\lim_{z\to 1} \iint\ldots\ldots\int_{K_1} \frac{1-z^2}{(1-2z\cos\gamma+z^2)^{\frac{n}{2}}}\, d\omega,$$

$$= \lim_{z\to 1} \iint\ldots\ldots\int_{K} \frac{1-z^2}{(1-2z\cos\gamma+z^2)^{\frac{n}{2}}}\, d\omega$$

$$= \lim_{z\to 1}\iint\limits_{K}\cdots\int\left[1+\frac{n}{2}L_1(\cos\gamma)\,z+\frac{n+2}{n-2}L_2(\cos\gamma)\,z^2+\cdots\cdots\right.$$

$$\left.+\frac{n+2\,m-2}{n-2}L_m(\cos\gamma)\,z^m+\cdots\cdots\right]d\omega=\frac{n\pi^{\frac{n}{2}}}{\Gamma(1+\frac{n}{2})}.$$

Folglich gilt gleichmässig

$$\lim_{z\to 1}\iint\limits_{K}\cdots\int\frac{1-z^2}{(1-2z\cos\gamma+z^2)^{\frac{n}{2}}}f(\theta_1\,\theta_2\cdots\cdots\theta_{n-1})\,d\omega$$

$$=\frac{n\pi^{\frac{n}{2}}}{\Gamma(1+\frac{n}{2})}f(\theta_1'\,\theta_2'\cdots\cdots\theta'_{n-1}),$$

d. h.

$$f(\theta_1',\,\theta_2'\cdots\cdots\theta'_{n-1})$$

$$\sim\frac{\Gamma(1+\frac{n}{2})}{n\pi^{\frac{n}{2}}}\sum_{m=0}^{\infty}\frac{n-2\,m-2}{n-2}\iint\cdots\int L_m(\cos\gamma)f(\theta_1,\,\theta_2,\cdots\cdots\theta_{n-1})\,d\omega.$$

und diese Reihe ist im Abelschen Sinne gleichmässig summierbar und stellt die gegebene Funktion dar.

Daraus ergibt sich der folgende verallgemeinerte Hurwitzsche Satz.

Satz 2. *Wenn die beiden Funktionen* $f(\theta_1\,\theta_2\cdots\cdots\theta_{n-1})$ $\varphi(\theta_1\,\theta_2\cdots\cdots\theta_{n-1})$ *eindeutig und stetig auf der Einheitshyperkugelfläche sind und ihre Entwickelungen in die Reihen der Hyperkugelfunktionen seien*

$$f(\theta_1\,\theta_2\cdots\cdots\theta_{n-1})\sim X_0+X_1+X_2+\cdots\cdots+X_m+\cdots\cdots,$$

$$\varphi(\theta_1\,\theta_2\cdots\cdots\theta_{n-1})\sim Y_0+Y_1+Y_2+\cdots\cdots+Y_m+\cdots\cdots,$$

dann gilt

$$\iint\limits_{K}\cdots\int f(\theta_1\,\theta_2\cdots\cdots\theta_{n-1})\,\varphi(\theta_1\,\theta_2\cdots\cdots\theta_{n-1})\,d\omega$$

$$=\sum_{m=0}^{\infty}\iint\limits_{K}\cdots\int X_m\,Y_m\,d\omega.$$

2. DIE VERALLGEMEINERTEN MINKOWSKISCHEN MITTLEREN HYPERFLÄCHENINHALTE DER KONVEX GESCHLOSSENEN MANNIGFALTIGKEIT.

Bezeichnet man das Volumen der Parallelhyperfläche der gegebenen konvex-geschlossenen Mannigfaltigkeit mit dem Abstande h durch $V(h)$, dann gilt

$$V(h) = V + V_1 h + V_2 h^2 + \cdots\cdots + V_{n-1} h^{n-1} + V_n h^n,$$

wobei

$$V_n = \frac{\pi^{\frac{n}{2}}}{\Gamma(1+\frac{n}{2})},$$

und V das Volumen der gegebenen konvex-geschlossenen Mannigfaltigkeit bedeutet.

Wir wollen nach Minkowski $V_2, V_3 \cdots\cdots V_{n-1}$ die mittleren Hyperflächeninhalte nennen. V_1 bedeutet den Hyperflächeninhalt der Mannigfaltigkeit.

Bezeichnet man nun die Stützhyperebenenfunktion mit H und die Hauptkrümmungsradien mit $R_1, R_2 \cdots\cdots R_{n-1}$, dann ist

$$V(h) = \frac{1}{n}\int\int\cdots\cdots\int (H+h)(R_1+h)(R_2+h)\cdots\cdots(R_{n-1}+h)\, d\omega,$$

wobei $d\omega$ das Hyperflächenelement der Einheitshyperkugel bedeutet. Daraus folgt

$$V = \frac{1}{n}\int\int\cdots\cdots\int H R_1 R_2 \cdots\cdots R_{n-1}\, d\omega,$$

$$V_1 = \frac{1}{n}\int\int\cdots\cdots\int H R_1 R_2 \cdots\cdots R_{n-1}\left(\frac{1}{R_1}+\frac{1}{R_2}+\cdots\cdots+\frac{1}{R_{n-1}}\right) d\omega$$

$$+\frac{1}{n}\int\int\cdots\cdots\int R_1 R_2 \cdots\cdots R_{n-1}\, d\omega, \cdots\cdots$$

$$\cdots\cdots\cdots\cdots\cdots\cdots$$

$$V_{n-2} = \frac{1}{n}\int\int\cdots\cdots\int H(R_1+R_2+\cdots\cdots R_{n-1})\, d\omega,$$

$$+\frac{1}{n}\int\int\cdots\cdots\int (R_1 R_2 + R_1 R_3 + \cdots\cdots + R_{n-1} R_{n-2})\, d\omega,$$

$$V_{n-1} = \frac{1}{n}\iint\ldots\ldots\int H\,d\omega + \frac{1}{n}\iint\ldots\ldots\int (R_1 + R_2 + \ldots\ldots + R_{n-1})\,d\omega.$$

Bezeichnet man anderseits den Hyperflächeninhalt der Parallelhyperfläche mit $V_1(h)$, dann ist

$$V_1(h) = \frac{d\,V(h)}{dh},$$

d. h.

$$V_1(h) = V_1 + 2\,V_2\,h + 3\,V_3\,h^2 + \ldots\ldots + n\,V_n\,h^{n-1}$$

$$= \iint\ldots\ldots\int (R_1 + h)\,(R_2 + h)\ldots\ldots(R_{n-1} + h)\,d\omega.$$

Also ist

$$V_1 = \iint\ldots\ldots\int R_1\,R_2\ldots\ldots R_{n-1}\,d\omega,$$

$$= \frac{1}{n-1}\iint\ldots\ldots\int H\,R_1\,R_2\ldots\ldots R_{n-1}\left(\frac{1}{R_1} + \frac{1}{R_2} + \ldots\ldots + \frac{1}{R_{n-1}}\right)d\omega,\ldots\ldots$$

$$V_{n-2} = \frac{1}{2}\iint\ldots\ldots\int H\,(R_1 + R_3 + \ldots\ldots R_{n-1})\,d\omega$$

$$= \frac{1}{n-2}\iint\ldots\ldots\int (R_1\,R_2 + R_1\,R_2 + \ldots\ldots + R_{n-2}\,R_{n-1})\,d\omega,$$

$$V_{n-1} = \iint\ldots\ldots\int H\,d\omega = \frac{1}{n-1}\iint\ldots\ldots\int (R_1 + R_2 + \ldots\ldots + R_{n-1})\,d\omega,$$

$$V_n = \frac{\pi^{\frac{n}{2}}}{\Gamma\left(1 + \frac{n}{2}\right)}.$$

3. ERWEITERUNG DER CHRISTOFFEL'SCHEN FORMEL.

Bezeichnet man die Stützhyperebenenfunktion mit $H(\alpha_1\,\alpha_2\ldots\ldots\alpha_n)$ wobei $\alpha_1^2 + \alpha_2^2 + \ldots\ldots + \alpha_n^2 = 1$ ist und entwickelt man H in die Reihe der Hyperkugelfunktionen

$$H(\alpha_1\,\alpha_2\ldots\ldots\alpha_n) \sim X_0 + X_1 + X_2 + \ldots\ldots + X_m + \ldots\ldots,$$

und wenn H so angenommen ist, dass

$$H(\lambda a_1, \lambda a_2 \ldots\ldots \lambda a_n) = \lambda H(a_1 a_2 \ldots\ldots a_n) \text{ für } \lambda > 0,$$

dann kann man in genau derselben Weise wie im drei-dimensionalen Falle beweisen, dass

$$\frac{\partial^2 H}{\partial a_1^2} + \frac{\partial^2 H}{\partial a_2^2} + \ldots\ldots + \frac{\partial^2 H}{\partial a_n^2} = R_1 + R_2 + \ldots\ldots R_{n-1}.$$

Setzt man nun

$$r = \sqrt{a_1^2 + a_2^2 + \ldots\ldots + a_n^2},$$

dann ist

$$H(a_1 a_2 \ldots\ldots a_n) \sim \sum_{m=0}^{\infty} \frac{X_m}{r^{m-1}}.$$

$$\sum \frac{\partial^2}{\partial a_i^2} \frac{X_m}{r^{m-1}} = \frac{1}{r^{m-1}} \sum \frac{\partial^2 X_m}{\partial a_i^2} + 2 \sum \frac{\partial X_m}{\partial a_i} \frac{\partial}{\partial a_i} \left(\frac{1}{r^{m-1}} \right)$$

$$+ X_m \sum \frac{\partial^2 m}{\partial a_i^2} \left(\frac{1}{r^{m-1}} \right)$$

$$\sum \frac{\partial X_m}{\partial a_i} \frac{\partial}{\partial a_i} \left(\frac{1}{r^{m-1}} \right) = - \frac{m(m-1)}{r^{m+1}} X_m,$$

$$\sum \frac{\partial^2}{\partial a_i^2} \left(\frac{1}{r^{m-1}} \right) = \frac{(m-1)(m-n+1)}{r^{m+1}}.$$

Folglich

$$\sum \frac{\partial^2}{\partial a_i^2} \left(\frac{X_m}{r^{m-1}} \right) = - \frac{(m-1)(m+n-1)}{r^{m+1}} X_m.$$

Somit erhält man die verallgemeinerte Christoffelsche Formel:

$$R_1 + R_2 + \ldots\ldots + R_{n-1} = - \sum_{m=0}^{\infty} (m-1)(m+n-1) X_m.$$

Daraus ergibt sich

$$V_{n-2} = \frac{1}{2} \iint \ldots\ldots \int H(R_1 + R_2 + \ldots\ldots + R_{n-1}) \, d\omega.$$

$$= - \frac{1}{2} \sum_{m=0}^{\infty} (m-1)(m+n-1) \iint \ldots\ldots \int X_m^2 \, d\omega.$$

Für V_{n-1} gilt

$$V_{n-1} = \iint \cdots \int H \, d\omega$$

$$= X_0 \iint \cdots \int d\omega = \frac{n\pi^{\frac{n}{2}}}{\Gamma(1+\frac{n}{2})} X_0$$

Anderseits

$$V_{n-2} \leqq \frac{n-1}{2} X_0^2 \frac{n\pi^{\frac{n}{2}}}{\Gamma(1+\frac{n}{2})}.$$

Folglich erhält man den verallgemeinerten Minkowskischen Satz:

Satz 3. *Zwischen V_{n-1}, V_{n-2} einer konvex-geschlossenen Mannigfaltigkeit besteht die Ungleichheit*

$$\frac{n\pi^{\frac{n}{2}}}{\Gamma(1+\frac{n}{2})} V_{n-2} \leqq \frac{n-1}{2} V_{n-1}^2,$$

wobei die Gleichheit dann und nur dann gilt wenn die Mannigfaltigkeit eine Hyperkugel ist.

4. DIE VERALLGEMEINERUNG DES CAUCHYSCHEN SATZES ÜBER EIFLÄCHEN AUF DEN N-DIMENSIONALEN RAUM.

Nachdem ich einen Beweis des Cauchyschen Satzes durch Übertragung der Minkowskischen Methode veröffentlicht hatte,[1] hat Herr Prof. W. Blaschke mir freundlichst einen einfachen Beweis mitgeteilt. Sein Beweis erlaubt sich den Cauchyschen Satz auf den n-dimensionalen Raum zu verallgemeinern:

Satz. 4. *Man bilde die stützzylindrische Mannigfaltigkeit einer gegebenen konvex-geschlossenen Mannigfaltigkeit im n-dimensionalen Raume. Bezeichnet man das Hypervolumen, den Oberflächeninhalt uud die mittleren Flächeninhalte der Normalschnitte der stützzylendrischen Mannigfaltigfaltigkeit mit V', V_1', V_2' $\cdots\cdots$ V'_{n-2}, welche Funktionen der Richtung der Erzeugenden sind, bedeuten, dann*

(1) Tôhoku Mathematical Journal 21.

$$V_1 = \frac{\Gamma(\frac{n+1}{2})}{\pi^{\frac{n-1}{2}}} \iint \cdots\cdots \int V' \, d\omega,$$

$$V_2 = \frac{\Gamma(\frac{n+1}{2})}{2\pi^{\frac{n-1}{2}}} \iint \cdots\cdots \int V_1' \, d\omega,$$

$$\cdots\cdots\cdots\cdots\cdots\cdots$$

$$V_{n-1} = \frac{\Gamma(\frac{n+1}{2})}{(n-1)\,\pi^{\frac{n-1}{2}}} \iint \cdots\cdots \int V'_{n-2} \, d\omega.$$

Man nehme ein konvexes Polytop in einer (n-1-dimensionalen) Hyperebene und projiziere es orthogonal auf eine durch den Anfangspunkt gehende Hyperebene. Dann ist das Volumen der Projektion gleich dem ursprünglichen Volumen multipliziert durch den Kosinus des Winkels zweier Hyperebenen. Dreht man diese Hyperebene um den Anfangspunkt und bezeichnet man das Volumen des Polytops mit V dann ist

$$2V = \frac{\Gamma(\frac{n+1}{2})}{\pi^{\frac{n-1}{2}}} V' \iint \cdots\cdots \int \cos\theta \, d\omega.$$

Denn

$$\iint \cdots\cdots \int \cos\theta \, d\omega$$

$$= 2\int_0^{\frac{\pi}{2}} \cos\theta \, \frac{(n-1)\,\pi^{\frac{n-1}{2}}}{\Gamma(1+\frac{n-1}{2})} \sin^{n-2}\theta \, d\theta$$

$$= \frac{2\pi^{\frac{n-1}{2}}}{\Gamma(\frac{n+1}{2})}.$$

Damit ist der erste Teil des Satzes für das doppeltgezählte Polytop in einer (n-1-dimensionalen) Hyperebene bewiesen.

Dass das Polytop im n-dimensionalen Raume durch die Polytope in den Hyperebenen begrenzt wird so kann man aus dem obigen die allgemeine Gültigkeit des ersten Teils des Satzes behaupten.

Da diese Tatsache für Parallelhyperfläche gilt

$$V_1(h) = \frac{\Gamma(\frac{n+1}{2})}{\pi^{\frac{n-1}{2}}} \iint \ldots\ldots \int V'(h)\, d\omega,$$

wobei

$$V'(h) = V' + V_1' h + V_2' h^2 + \ldots\ldots V'_{n-1} h^{n-1},$$

$$V_1(h) = V_1 + 2h V_2 + 3h^2 V_3 + \ldots\ldots + nh^{n-1} V_n,$$

Daraus ergibt sich

$$2 V_2 = \frac{\Gamma(\frac{n+1}{2})}{\pi^{\frac{n-1}{2}}} \iint \ldots\ldots \int V_1'\, d\omega,$$

$$3 V_3 = \frac{\Gamma(\frac{n+1}{2})}{\pi^{\frac{n-1}{2}}} \iint \ldots\ldots \int V_2'\, d\omega,$$

$$\ldots\ldots\ldots\ldots$$

$$(n-1) V_{n-1} = \frac{\Gamma(\frac{n+1}{2})}{\pi^{\frac{n-1}{2}}} \iint \ldots\ldots \int V'_{n-2}\, d\omega,$$

w. z. b. w.

5. ZENTRALE SYMMETRISIERUNG.

Es sei $H(a_1 a_2 \ldots\ldots a_n)$ die Stützhyperebenenfunktion der gegebenen konvex-geschlossenen Mannigfaltigkeit. Daraus bilde man eine neue konvex-geschlossene Mannigfaltigkeit mit der Stützhyperebenenfunktion

$$\frac{H(a_1 a_2 \ldots\ldots a_n) + H(-a_1, -a_2, \ldots\ldots -a_n)}{2}.$$

Diese neue konvex-geschlossene Mannlgfaltigkeit nennt man die Zentralsymmetrisierte von der gegebenen konvex-geschlossenen Mannigfaltigkeit.

Dies stimmt mit dem ursprünglichen dann und nur dann überein, wenn die gegebene zentral ist. Dann gilt der folgende fundamentale Hilfssatz :

Satz 5. *Die Grössen* V, V_1, V_2,.....V_{n-2} *einer nichtzentralen konvexgeschlossenen Mannigfaltigkeit werden durch Zentralsymmetrisierung vergrössert, während* V_{n-1} *ungeändert bleibt.*

Für V ist der obige Satz durch den folgenden verallgemeinerten Minkowskischen Satz leicht beweisbar.

Es seien zwei konvex-geschlossene Mannigfaltigkeiten mit den Stützhyperebenenfunktionen H_1 und H_2. Bezeichnet man nun das Volumen der mittleren konvex-geschlossenen Mannigfaltigkeit mit der Stützhyperebenenfunktion $H = H_1(1-\vartheta)+H_2\vartheta$ durch $V(\vartheta)$, dann ist die Funktion $\sqrt[n]{V(\vartheta)}$ konvexe oder lineare Funktion von ϑ und sie ist dann und nur dann linear, wenn die beiden Mannigfaltigkeiten ähnlich und ähnlich gelegen sind.[1]

Betrachtet man den Spezialfall des Satzes für

$$H_2(\alpha_1\,\alpha_2.....\alpha_n) = H_1(-\alpha_1, -\alpha_2,.....-\alpha_n),$$

dann ist unser Haupthilfssatz für das Volumen leicht ersichtlich.

Zum Beweis des Satzes für die anderen Fälle setze man voraus, dass der Satz für $n-1$—dimensionalen Raum giltig sei. Nun seien $V_1^{(n)}$, $V_2^{(n)}$.....$V_{n-1}^{(n)}$ der Oberflächeninhalt und die mittleren Flächeninhalte der gegebenen konvex-geschlossenen Mannigfaltigkeit und $\overline{V}_1^{(n)}$ $\overline{V}_2^{(n)}$..... $\overline{V}_{n-1}^{(n)}$ seien die entsprechenden Grössen für die Zentralsymmetrisierte. Nun seien $V^{(n-1)}$ $V_1^{(n-1)}$.....$V_{n-2}^{(n-1)}$ das Volumen, der Oberflächeninhalt und die mittleren Flächenenhalte des Normalschnittes des Stützzylinders und $\overline{V}^{(n-1)}$ $\overline{V}_1^{(n-1)}$.....$\overline{V}_{n-2}^{(n-1)}$ seien die entsprechenden Grössen für die Zentralsymmetrisierte, dann ist nach dem obenbewiesenen

$$V^{(n-1)} \leqq \overline{V}^{(n-1)}$$

und nach der Voraussetzung

$$V_i^{(n-1)} \leqq \overline{V}_i^{(n-1)} \quad (i = 1, 2, 3.....n-2)$$

Wenn man

$$V_0^{(n)} = V^{(n)}$$

setzt, so kann man schreiben

(1) Minkowski, Geometrie der Zahlen, S. 209.

$$V_i^{(n-1)} \leqq \overline{V}_i^{(n-1)} \quad (i = 0, 1\ 2\ 3 \ldots\ldots n-2).$$

Nach dem erweiterten Cauchyschen Satze

$$V_i^{(n)} = \frac{\Gamma\left(\frac{n+1}{2}\right)}{i\pi^{\frac{n-1}{2}}} \iint \ldots\ldots \int V_{i-1}^{(n-1)}\, d\omega,$$

$$\overline{V}_i^{(n)} = \frac{\Gamma\left(\frac{n+1}{2}\right)}{i\pi^{\frac{n-1}{2}}} \iint \ldots\ldots \int \overline{V}_{i-1}^{(n-1)}\, d\omega,$$

Daraus folgt dass

$$V_i^{(n)} \leqq \overline{V}_i^{(n)} \quad (i = 1, 2\ 3 \ldots\ldots n-2).$$

Es ist leicht beweisbar, dass

$$V_{n-1}^{(n)} = \overline{V}_{n-1}^{(n)}.$$

In $V_i^{(n)} \leqq \overline{V}_i^{(n)}$ gilt die Gleichheit dann und nur dann, wenn die gegebene konvex-geschlossene Mannigfaltigkeit zentral ist.

Damit ist der Hauptsatz durch vollständige Induktion bewiesen.

In Beziehung zum obigen Satze kann man den nachstehenden Satz beweisen.

Wenn eine konvex-geschlossene Mannigfaltigkeit in einer anderen konvex-geschlossenen Mannigfaltigkeit vollständig enthalten ist, so sind V, V_1 $V_2 \ldots\ldots V_{n-1}$ *der ersten Mannigfaltigkeit kleiner als die entsprechenden Grössen der zweiten Mannigfaltigkeit.* Dieser Satz gilt selbstverständlich für V und V_{n-1}.

Diesen Satz beweisen wir wieder durch vollständige Induktion. Man setze voraus, dass dieser Satz im $n-1$-dimensionalen Raum giltig sei.

$V_i^{(n)}$ $V_2^{(n)} \ldots\ldots V_{n-1}^{(n)}$ seien die Grössen für die erste Mannigfaltigkeit und $V_1^{(n)}$ $V_2^{(n)} \ldots\ldots V_{n-1}^{(n)}$ seien die Grössen für die zweite. Ferner seien die zu den obigen entsprechenden Grössen für die Normalschnitte des Stützzylinders bzw. mit $V^{(n-1)}$ $V_1^{(n-1)}$ $V_2^{(n-1)} \ldots\ldots V_{n-2}^{(n-1)}$ und $\overline{V}^{(n-1)}$ $\overline{V}_1^{(n-1)}$ $\overline{V}_2^{(n-1)} \ldots\ldots \overline{V}_{n-2}^{(n-1)}$ bezeichnet. Dann

$$V_i^{(n)} = \frac{\Gamma\left(\frac{n+1}{2}\right)}{i\pi^{\frac{n-1}{2}}} \iint \cdots\cdots \int V_{i-1}^{(n-1)}\, d\omega,$$

$$\overline{V}_i^{(n)} = \frac{\Gamma\left(\frac{n+1}{2}\right)}{i\pi^{\frac{n-1}{2}}} \iint \cdots\cdots \int \overline{V}_{i-1}^{(n-1)}\, d\omega,$$

wobei nach der Voraussetzung

$$V_{i-1}^{(n-1)} < \overline{V}_{i-1}^{(n-1)} \quad i = 1, 2, 3 \cdots\cdots n-2.$$

Folglich

$$V_i^{(n)} < \overline{V}_i^{(n)} \qquad i = 1, 2, 3 \cdots\cdots n-2.$$

Somit ist der Satz bewiesen.

6. SCHLUSSFOLGERUNG.

Nach den obigen Vorbereitungen können wir genau in derselben Weise wie im drei dimensionalen Falle[1] verfahren und gelangen wir zum Resultat.

Wir bezeichnen die konvex geschlossene Mannigfaltigkeit, welche durch die Kugel

$$x_1^2 + x_2^2 + \cdots\cdots + x_{n2} = \frac{D^2}{4},$$

und die Hyperebenen

$$x_n = \frac{\Delta}{2}, \qquad x_n = -\frac{\Delta}{2},$$

begrenzt wird, mit E bezeichnet.

Wenn der Durchmesser D und die Dicke Δ einer konvex geschlossenen Mannigfaltigkeit gegeben sind, so werden V, V_1, V_2.....V_{n-2} dann und nur dann maximum wenn die Mannigfaltigkeit von der Form E ist.

Wir bezeichnen die konvex-geschlossene Mannigfaltigkeit, welche durch die Kugel

(1) Diese „Reports," Bd. 12. S. 45–65.

$$x_1^2+x_2^2+\ldots\ldots+x_n^2=\frac{\Delta^2}{4}.$$

und durch die umhüllenden Kegel aus den Mittelpunkten $\left(0,\ 0,\ 0\ldots\ldots\frac{D}{2}\right)$ $\left(0,\ 0,\ 0\ldots\ldots-\frac{D}{2}\right)$ *begrenzt wird, mit* E'.

Wenn der Durchmesser D *und die Dicke* Δ *der konvex-geschlossenen Mannigfaltigkeit gegeben sind, so wird* V_{n-1} *dann und nur dann maximum wenn die Mannigfaltigkeit von solcher Art ist, dass sie durch Zentralsymmetrisieneng zur Mannigfaltigkeit von der Form* E *übergeht; und* V_{n-1} *wird dann und nur dann minimum, wenn die Mannigfaltigkeit von solcher Art ist dass sie durch Zentralsymmetrisierung zur Mannigfaltigkeit von der Form* E' *übergeht.*

7. ANDERER BEWEIS FÜR DEN FUNDAMENTALEN HILFSSATZ.

Den Satz 5 für V_{n-2} kann man durch die verallgemeinerte Christoffelsche Formel beweisen.

Wenn

$$H\sim X_0+X_1+X_2+\ldots\ldots+X_m+\ldots\ldots$$

$$V_{n-2}=-\frac{1}{2}\sum_{m=0}^{\infty}(m-1)(m+n-1)\iint\ldots\ldots\int X_m^2\,d\omega.$$

Für die Zentralsymmetrisierte ist die Stützhyperebenenfunktion $\overline{H}$, wobei

$$H\sim X_0+X_2+X_4+\ldots\ldots+X_{2m}+\ldots\ldots$$

ist, dann

$$\overline{V}_{n-2}=-\frac{1}{2}\sum_{k=0}^{\infty}(2k-1)(2k+n-1)\iint\ldots\ldots\int X_{2k}^2\,d\omega$$

woraus sich ergibt

$$V_{n-2}<\overline{V}_{n-2},$$

wenn die ursprüngliche Mannigfaltigkeit nicht zentral ist.

On the Determination of Cyanides and the Use of Benzene as an Indicator in Iodimetry.[1]

By

Naotsuna Kanô.

A few investigations on the determination of cyanides have appeared since Fordos and Gélis.[2] All of these utilize the reaction $KCN+I_2 = KI+ICN$, and agree in that use is made of a supersaturated solution of carbonic acid (Drinking soda water as "Selterswasser" etc.) or sodium bicarbonate to make the sample nearly neutral, and in that the use of starch is considered objectionable on account of its action upon cyanogen iodide. But the use of ordinary soda water is very inconvenient, and the determination of the end point only from the colour of the excess of iodine without an indicator causes frequent trouble, especially when the sample solution is colored. In order to improve this method of determination by substituting a simpler and more exact one, the author searched for a suitable condition which would save the trouble of using carbonic acid water (Soda water) and at the same time permit the use of an indicator.

1. POTASSIUM CYANIDE.

Sample. A solution of potassium cyanide was made from a Kahlbaum reagent ("zur Analyse"), and was standardized with a known quantity of silver nitrate. The iodine solution was standardized with oxalic

(1) Published in the Journal of the Chemical Society of Japan, **42**, 454, (1921).

(2) Fordos & Gélis: J. Pharm. Chim., **23**, 48, (1853); Robertson: Jahresber., 681, (1853) Tipp: Jahresber., **817**, (1855); Rupp & Schiedt: Arch. Pharm., **244**, 328, (1903).

acid from Kahlbaum ("zur Analyse") as the basis of its standardization, and in the order: potassium permanganate, sodium thiosulphate and iodine.

Indicator. To find which of the following, starch, carbon disulphide and benzene, was best fitted for an indicator, definite quantities of a potassium cyanide solution were titrated with iodine solution (0.0998 *N*) using each of the three reagents in order to examine which gave the value nearest to that standardized by the silver nitrate (0.0968 *N*).

Indicator	None	Starch	Carbon disulphide	Benzene
Normality of Potassium Cyanide	0.0945	0.0933	0.0962	0.0967
	0.0949	0.0934	0.0967	0.0966
	0.0962	0.0935	0.0960	0.0965
Mean	0.0952	0.0934	0.0963	0.0966

When using carbon disulphide or benzene, the procedure adopted was to add about 20 cc. to the solution and shake the solution in a 250 cc. reagent bottle. The above figures show that benzene was the fittest, and this was accordingly used for further experiments.

The Use of Cabonic Acid, Boric Acid and their Salts. Ordinarily use is made of drinking carbonic acid water in the determination of cyanides to convert the caustic alkali or alkali canonate into the form of bicarbonate. The trial with "Hiranosui"[3] gave the following results:—

Potassium cyanide (cc)	Iodine (cc)	Carbonic acid water (cc)	Normality of potassium cyanide
12.78	20.30	20	0.0793
10.08	16.64	20	0.0823

(3) A kind of natural soda water sold widely.

This clearly shows that cyanogen iodide is sensitive to the indicator even in the presence of supersaturated cabonic acid water, and premature and irregular end points are obtained, proving that the methods hitherto adopted have been greatly at fault.

Hereupon it suggested itself to the author that since boric acid is a very weak acid and small in solubility, a very convenient substitute could be found in it for making the sample weakly acid, or in borax when it is acid, and it would permit the use of an indicator. Experiments were made with mixtures of boric acid and borax in varying proportions, to determine the range of applicability of this method, as can be seen in the following table. (The boric acid solution was 1%, the borax solution 1%).

Potassium cyanide (cc)	Iodine (cc)	Boric acid (cc)	Borax (cc)	Normality of potassium cyanide
9.97	19.34	0	100	0.0968
10.05	19.49	50	50	0.0968
9.61	18.58	60	40	0.0965
9.68	18.59	70	30	0.0958
10.08	19.28	80	20	0.0952
10.31	19.50	90	10	0.0944

The above results show that an exact determination could be made by first adding a dilute boric acid solution and then the same quantity of borax solution.

Next experiments were made with mixtures of sodium bicarbonate and hydrochloric acid. Thus, first Kahlbaum sodium bicarbonate solution (containing 8.41 grs. in 1 litre) was made, to this was added the equivalent quantity of hydrochloric acid (2 N). The supersaturated carbonic acid water obtained in this way was used in the cyanide determination, which showed that the influence of the acid was quite marked, as in the following table.

Potassium cyanide (cc)	Iodine (cc)	$NaHCO_3 + HCl$ (cc)	Normality of potassium cyanide
10.22	18.92	20	0.0924
11.25	20.72	20	0.0919
9.82	18.27	20	0.0928

Accordingly experiments were made with hydrochloric acid decreased to 1/3 of the equivalent amount, but still a slight decomposition of cyanogen iodide was recognized.

Potassium cyanide (cc)	Iodine (cc)	$NaHCO_3 + \frac{1}{3}HCl$ (cc)	Normality of potassium cyanide
10.03	19.17	20	0.0954
9.66	19.00	20	0.0952
10.02	19.24	20	0.0958

When no hydrochloric acid was added, the following result was obtained, showing that when the sample contains no caustic alkali or alkali carbonate, a good result can be obtained by adding sodium bicarbonate only and with benzene as an indicator. But the above-mentioned impurities are usually present, so that their preliminary neutralization will be necessary.

Potassium cyanide (cc)	Iodine (cc)	$NaHCO_3$ (cc)	Normality of potassium cyanide
9.90	19.33	20	0.0972
10.06	19.56	20	0.0970
10.11	19.63	20	0.0969
10.24	19.96	20	0.0971

From the foregoing results we see that the decomposition of cyanogen iodide can be prevented and an exact determination can be made if we first titrate with a supersaturated carbonic acid solution obtained by adding to sodium bicarbonate the equivalent amount of hydrochloric acid in order

to neutralize the impurities in the sample, and then add a further quantity of sodium bicarbonate when the benzene is coloured, the titration being continued until the end point is reached.

Potassium cyanide (cc)	Iodine (cc)	$NaHCO_3 + HCl$ (cc)	$NaHCO_3$ (cc)	Normality of potassium cyanide
10.16	19.63	20	40	0.0964
10.06	19.54	40	20	0.0969
10.20	19.69	20	60	0.0963
10.04	19.51	20	70	0.0970

The above experiments determined the conditions under which an indicator can be used in the determination of cyanides, and the method is superior to any of the previous ones in that the titration can be made even when the solution is turbid or coloured.

2. POTASSIUM CHROMATE AND POTASSIUM FERRICYANIDE.

Benzene forms the upper layer of a solution, which fact makes it very convenient in recognizing a colour, so that it is frequently expedient to employ this reagent when the sample is strongly coloured or when it contains a precipitate.

Potassium Chromate. Though iodimetric determination of a chromate is suitable for the standardization of sodium thiosulphate, the colour of the solution becomes greenish blue owing to the formation of tervalent chromium compound, as shown in the following equation,

$$K_2CrO_4 + 3\,KI + 8\,HCl = 5KCl + CrCl_3 + 4H_2O + 3I,$$

making it exceedingly difficult to distinguish the colour of the end points when starch is employed. But the use of benzene enables us to recognize this colour easily. The sample solution (0.0758 *N*) was made from Kahlbaum potassium chromate ("zur Analyse"). The results of the experiment are as follows. (The solution of sodium thiosulphate 0.0958 *N*).

Potassium chromate (cc)	Sodium thiosulphate (cc)	Normality of potassium chromate
10.09	7.95	0.0755
10.12	8.00	0.0758

Potassium Ferricyande.

To complete the reaction of ferricyanides with potassium iodide $2K_3Fe(CN)_6 + 2KI \rightleftarrows 2K_4Fe(CN)_6 + I_2$ quickly, it is necessary to remove the ferrocyanide ion by adding zinc sulphate. But ordinary zinc sulphate, even so-called pure, often contains a small quantity of iron which forms iron ferrocyanide, of the colour indistinguishable from that of iodo-starch, and vitiates the analysis. The use of benzene has the advantage that it not only forms the upper layer and the end point colour can be recognized even when there is some coloration due to iron ferrocyanide, but also it extracts from the aqueous solution a large part of the iodine which causes the reversible reaction.

The following table shows well concordant results obtained when the solution of Kahlbaum potassium ferricyanide (0.0447 *N*) was determined. (Zinc sulphate, Kahlbaum, " zur Analyse ")

Potassium ferricyanide (cc)	Sodium thiosulphate (cc)	Normality of potassium ferricyanide
21.13	9.90	0.0447
21.41	10.02	0.0447
20.95	9.76	0.0446
21.03	9.82	0.0447
21.07	9.82	0.0446

SUMMARY.

1. The condition was determined under which cyanides could be accurately determined by iodimetry with benzene as an indicator.

2. The method gave the advantage of enabling us to determine even in a coloured or turbid solution.

3. It was shown that the use of benzene as an indicator is also more advantageous than the use of starch when the solution is coloured or contains a precipitate.

In conclusion the author wishes to express his heartiest thanks to Prof. M. Kobayashi for his kind guidance.

Application of Liquid Amalgams to Volumetric Analysis. Part 1. Estimation of Molybdenum, Titanium and Iron,[1]

By

Tamaki Nakazono.

To convert various metallic oxides in a higher state of oxidation to those in a lower one and then to estimate this volumetrically by reoxidizing them with some standard solution, is a method frequently employed. Among the commonest ones are, (1) the reduction by means of zinc with the exclusion of the influence of air, not only involves the elevation of temperature, the use of a large quantity of zinc, and the reduction of blank, but also needs a long time for its complete dissolution, and even then the presence of traces of zinc or its impurity remaining in the solution give rise to considerable error. (2) When using the Jones reductor, we must pay constant attention to the pouring of the solution and the action of a suction pump to adjust the velocity of the outflow of the solution properly. Moreover it has the disadvantage that the total quantity of the solution easily tends to become too large, with the consequent increase of blank, and the path of the reductor frequently stops, so that many experiments cannot be carried out continuously.

To eliminate all these disadvantages, the author tried a method of using liquid zinc amalgam, and shaking the solution of a metallic salt in a kind of a separating funnel, taking out the amalgam and then titrating

1) Published in the Journal of the Chemical Society of Japan, **42**, 526, (1921).

with a standard solution. Applying this method to molybdenum, titanium and iron, it was found that no raising of temperature was necessary, the time required for the reduction being only from half to one minute, and the object could be attained at a very little expense of the reducing agent. He also found that the amalgam once used in this way shows no decrease of the velocity of reduction after being further used dozens of times, and that there was no disadvantage of making the volume too large, and an exact determination could be made by a simple procedure which excludes the influence of air. Further he confirmed that even with amalgam made from impure zinc, little care for the blank is necessary, and all the disadvantages enumerated above which cling to other methods could be eliminated.

1. MOLYBDENUM.

The reduction of molybdenum with zinc has been studied by a number of investigators. Wernke[1] was able to reduce to the stage of approximately $Mo_{12}O_{19}$, Dudley[2] obtained a result slightly differing from this, using a Jones reductor. Jones & Doolittle[3] and Eavenson[4] attained the value approximating to that of Wernke. Blair & Whitfield[5] and Miller & Frank[6] to approximately $Mo_{24}O_{37}$. Noyes & Frohman[7] and Rundall[8] stated to have been able to reduce to Mo_2O_3. Recently Scott[9] reduced to Mo_2O_3 by rotating a zinc cylinder in a solution, and claims that the method is a convenient substitute for a Jones reductor, but said that proper caution is necessary for the dropping of small fragments of zinc and its being subject to the influence of air. The author himself has often tried to reduce molybdic acid with zinc and

(1) Z. anal. Ch., **14**, 1, (1875).
(2) J. Amer. Chem. Soc., **15**, 519, (1893).
(3) Amer. Inst. Min. Eng., **18**, 705, (1889).
(4) J. Amer. Chem. Soc., **16**, 234, (1894).
(5) Ibid., **17**, 747, (1895).
(6) Ibid., **25**, 919, (1903).
(7) Ibid., **16**, 553, (1894).
(8) Am. J. Sc., 4, **24**, 313, (1907).
(9) J. In. Eng. Chem., **12**, 578, (1920).

sulphuric acid or hydrochloric acid, and then titrate, but recognized that on account of the above-mentioned faults, it was not easy to obtain quantitaive results.

The Preparation of Amalgam.

3 to 4 grams of zinc granules were well washed with dilute sulphuric acid and heated on a water-bath for about an hour with about 100 grs. of mercury and some dilute sulphuric acid. The complete dissolution of zinc in the mercury took place. If zinc shavings are used, a few minutes will suffice. It was washed several times with water containing sulphuric acid and after cooling, separated from the solid part in a separating funnel. The liquid amalgam obtained in this way reacts only with extreme sluggishness with dilute sulphuric acid and can be kept for a long time.

The Reduction by Means of the Amalgam. When the mixture of dilute sulphuric acid and ammonium molybdate is added and is allowed to stand, only the boundary surface changes from blue to brown, and it never happens that all of the solution is subject to complete reduction. When this is stirred (1) with a glass rod using a water turbine, or (2) the whole vessel rotated several hundred times a minute, the velocity of reduction is not yet large, but (3) when put in a tightly closed vessel and shaken vigorously, it very rapidly attains the state of tervalent molybdenum, as can be seen clearly from the requisite potassium permanganate titre shown in the first table. The zinc, ammonium molybdate and the oxalic acid used in the experiments were all Kahlbaum made (zur Analyse). (The ammonium molybdate contained 81.35 % of MoO_3).

TABLE I.

(The solution of potassium permanganate, 0.01243 *N*).

Molybdic acid (gr.) MoO_3	Potassium permanganate (cc.)	Time of reduction (sec.)	Method.
0.1627	14.55	300	(1)
0.1627	27.10	600	(2)

TABLE I. *Continued.*

Molybdic acid (gr.) MoO_3	Potassium permanganate (cc.)	Time of reduction (sec.)	Method.
0.1627	26.95	20	(3)
0.1627	27.20	30	(3)
0.1627	27.22	180	(3)
Theoretical number. ...	27.18	—	—

(On reduction, the solution changed to dark green, through indigo, blue and brown).

Apparatus. Founded upon the above result, a kind of separating funnel, shown in the figure was devised. First freshly boiled distilled water was filled in the glass tube *E* and the rubber tubing *G*, and also about 10 cc. to *D*. *C* was closed after driving out the small air bubbles which had entered into *E* and *G*. About 100–200 grs. of amalgam and 10 cc. of sulphuric acid (2 *N*) were introduced through *F*, then a molybdic acid solution (containing about 0.1 gr. as MoO_3) was added, the part *F* was washed. The rubber tubing *H* was connected with a Kipp apparatus and a washing bottle. After passing carbon dioxide gas for two or three minutes, all the stop-cocks were closed, and the vessel was shaken vigorously for one minute. When *C* was opened and *G* pressed with a finger, the amalgam fell to *G*, being simultaneously washed with the rising water. When *P* was opened, it changed place with the water in *E*. When the whole of the amalgam had passed through *C*, we were able to separate the amalgam without any loss of the solution. After this a solution of potassium permanganate was added in a suitable quantity and A opened a little,

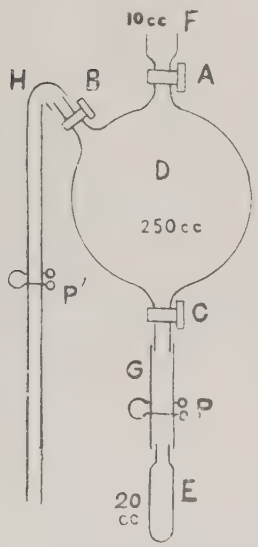

whereby owing to the reduced pressure prevailing in *D*, it entered gradually into it, and we were able to add the standard solution without giving air any chance to enter *D* till the state of oxidation insensitive to atmospheric oxygen was reached. Hereupon 10 cc. of sulphuric acid (1 : 1) were added and the end point of the titration was carefully determined. The rusults of the determination carried out in this way are good as seen in the second table. With 100 grams of amalgam, it took more than 50 seconds, but with 200 grams, the reduction was completed in only 30 seconds. It is considered that though in reality the reduction is made more rapidly, the trace of oxygen found in *D* affects tervalent molybdenum, and 30 seconds are required in the latter case to eliminate even that trace ; this is clear from the fact that when shaken vigorously for more than that length of time, the requisite titre does not change even on long standing.

TABLE II.

Molybdic acid. MoO_3 taken. (gr.)	Molybdic acid. MoO_3 found. (gr.)	Error. (gr.)	Time of reduction. (sec.)	Amalgam. (gr.)
0.1224	0.1209	−0.0015	40	100
0.1223	0.1221	−0.0002	40	100
0.1224	0.1218	−0.0006	50	100
0.1224	0.1224	0.0000	50	100
0.1224	0.1224	0.0000	60	100
0.1224	0.1228	+0.0004	60	100
0.1223	0.1225	+0.0002	120	100
0.1224	0.1226	+0.0002	180	100
0.1224	0.1226	+0.0002	300	100
0.1224	0.1200	−0.0024	20	200
0.1224	0.1212	−0.0012	20	200
0.1224	0.1225	+0.0001	30	200
0.1224	0.1224	0.0000	30	200
0.1224	0.1225	+0.0001	30	200

The Use and Preservation of the Amalgam. The amalgam can be used for further dozens of experiments without adding more zinc, and as it shows no decrease of the reduction velocity after a number of experiments, we learn that all the zinc in it is effectively used and its concentration in the amalgam is almost indedendent of the velocity. If an amalgam containing too much zinc and too large a quantity of sulphuric acid is used, there is a danger of the small particles of the amalgam floating with the hydrogen bubbles, making the separation from the solution difficult. But it is always necessary to add a small quantity of sulphuric acid before the molybdic acid solution and the amalgam are brought into contact; or else a dark brown lower oxide is formed on the surface of the amalgam, making the reduction and the titration uncertain. Also the examination of the amalgam which has been allowed to stand for several days in contact with dilute sulphuric acid shows no difference in its reducing power. From the foregoing results we see that the amalgam is very convenient for preservation and continual use.

The Influence of Contaminating Impurities. Experimented with impure zinc for hydrogen evolution, the titre shows a slight tendency to increase, but in ordinary cases almost no blank is necessary, as shown in the Table III. When the impurities in the zinc used in this experiment were measured in the usual way, 10 grs. of it tequired 0.74 cc. of the potassium permanganate solution.

TABLE III.

Molybdic acid. MoO_3 taken. (gr.)	Molybdic acid. MoO_3 found. (gr.)	Error. (gr.)	Time of reduction. (sec.)	Amalgam. (gr.)
0.1223	0.1231	+0.0008	60	100
0.1223	0.1226	+0.0003	60	100
0.1223	0.1225	+0.0002	60	100
0.1223	0.1228	+0.0005	60	100
0.1223	0.1226	+0.0003	300	100

Comparison with Jones Reductor. The comparison of the Jones reductor method and the amalgam method was made with the same impure zinc, the result of which experiment is shown in the Table IV. The former requires a very long time and is very troublesome and is frequently attended with a large error, the total volume reaching 500 cc. and the blank potassium permanganate solution often become even as large as 1 cc. While the latter has the advantage of giving an exact value with a simple operation and with one minute's reduction, the total volume being less than 100 cc., and moreover requiring no blanks. The zinc used required 1.20 cc. of the potassium permanganate solution per 10 grs.

TABLE IV.

Molybdic acid, MoO_3 taken. (gr.)	Molybdic acid, MoO_3 found. (gr.)	Error. (gr.)	Method.
0.1627	0.1587	−0.0040	Jones reductor method.
0.1627	0.1549	−0.0078	
0.1223	0.1225	+0.0002	Amalgam method.
0.1123	0.1225	+0.0002	

2. TITANIUM.

In old literature titanium is described as being reduced by zinc to Ti_3O_5. Knecht,[1] however, obtained a solution of titanium trichloride by reducing a solution of titanium tetrachloride with zinc and hydrochloric acid. Stähler[2] and others prepared from this the sulphate of tervalent titanium and proved that the state of Ti_2O_3 is attained.

The author used the sample made by heating Kahlbaum hydrated titanic acid with concentrated sulphuric acid and dissolving it in cold water and tried the permanganate titration after applying the amalgam

(1) Ber., **36**, 166, (1903).
(2) Ber., **37**, 4405, (1904).

method, and saw that the reduction was completed in 1 minute, as seen in the Table V.

TABLE V.

Titanium dioxide. TiO_2 taken. (gr.)	Titanium dioxide. TiO_2 found. (gr.)	Error. (gr.)	Time of reduction. (sec.)
0.1165	0.1146	−0.0019	30
0.1165	0.1149	−0.0016	30
0.1165	0.1160	−0.0005	60
0.1165	0.1160	−0.0005	60
0.1165	0.1159	−0.0006	60
0.1165	0.1158	−0.0007	60
0.1165	0.1159	−0.0006	120
0.1165	0.1157	−0.0008	180

(On reduction the colour of the solution changed from colourless to violet through reddish brown).

By way of trial the experiment was made in the presence of air, obtaining 0.1148 gr. as the experimental value, which shows that the replacement of air with carbonic acid is necessary.

The theoretical value in the above table was calculated from the result of the weighing after ignition of the precipitate produced by adding ammonia to the sample solution, and the smaller experimental value was considered to be attributable to a small impurity in the sample.

3. IRON.

It is generally known that iron is reduced with zinc and sulphuric acid from the tervalent condition to the bivalent one. The author applied the amalgam method to a solution of Kahlbaum iron alum, and carried out the permanganate titration, and obtained the results shown in the Table VI. It is seen that 30 seconds suffice for the reduction.

TABLE VI.

Ferric oxide. Fe_2O_3 taken. (gr.)	Ferric oxide. Fe_2O_3 found. (gr.)	Error. (gr.)	Time of reduction. (sec.)
0.0837	0.0841	+0.0004	30
0.0837	0.0842	+0.0005	30
0.0836	0.0842	+0.0006	60
0.0837	0.0841	+0.0004	60
0.0837	0.0841	+0.0004	300

(On reduction, the colour of the solution rapidly changed from yellow to colourless).

The theoretical value was calculated from that obtained by weighing after ignition of the precipitate which resulted on adding ammonia to the test solution. But the application of the amalgam method to the filtrate expended potassium permanganate corresponding to 0.0005 gr. of iron, so that the error was inferred to have been due to the impurities admixed in the sample.

When a small quantity of potassium thiocyanate was previously added to the sample and then reduction carried out in air, the red colour rapidly became fainter, but did not completely decolorize even after long shaking, but on the contrary, when the air was replaced by carbonic acid gas, the colour was very easily seen to fade.

SUMMARY.

1. A new method of volumetric analysis was found in the use of a liquid amalgam.

2. The method was applied to the estimation of molybdenum, titanium and iron, and cleared away many of the faults attending the previous methods. Further the method finds many other applications.

In conclusion the author wishes to express his heartiest thanks to Prof. M. Kobayashi for his kind directions during the work.

Relation between the Chemical Constitution and the Pungency. Synthesis of the Reduction Products of Zingerone and Di-4-hydroxy-3-methoxyphenylethyl Ketone.

By

Hiroshi Nomura and Seinosuke Hotta.

In the previous communication,[1] one of the authors discussed the relationship between the constitution of some phenolic ketones and their pungent taste. In the present communication, we have examined, first, the effect of the carbonyl group in the side chain $CH_2CH_2COCH_3$ and, secondly, the double effect of a 4-hydroxy-3-methoxyphenylethyl group, $C_6H_3(OH)(OCH_3)CH_2CH_2$, of zingerone (I) on the pungency.

For the first purpose, we synthesised 4-hydroxy-3-methoxyphenylethyl methyl carbinol, $C_6H_3(OH)(OCH_3)CH_2CH_2CH(OH)CH_3$, and 4-hydroxy-3-methoxyphenylbutane, $C_6H_3(OH)(OCH_3)CH_2CH_2CH_2CH_3$, by the reduction of the zingerone. 4-Hydroxy-3-methoxyphenylbutane was readily synthesised by Clemmensen's method,[2] but some difficulty was experienced in preparing 4-hydroxy-3-methoxyphenylethyl methyl carbinol. Harries and his collaborator[3] found that the ketone of the type (II) is stable towards an alkaline reducing agent, but readily reduced by zinc dust and alcoholic hydrochloric acid with the formation of the derivative of chroman (III) according to the following scheme:

(1) Sci. Rep., **7**, (1918), 79.
(2) Ber., **46**, (1913), 1837.
(3) Ber., **28**, (1895), 503; **29**, (1896), 375.

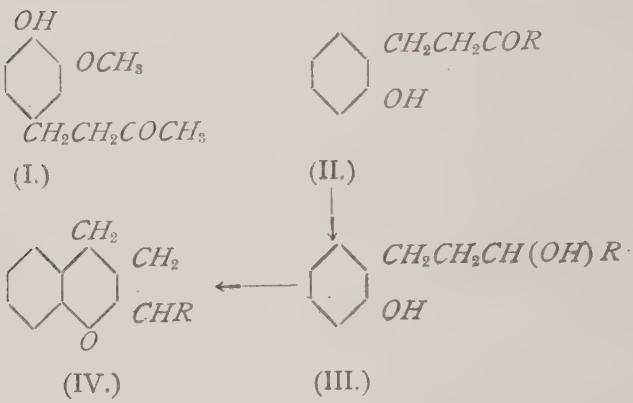

It was thought possible that, in the case of a p-hydroxy-compound, as zingerone, the reduction product might be the corresponding alcohol, $C_6H_3(OH)(OCH_3)CH_2CH_2CH(OH)CH_3$, the interaction between phenolic hydroxyl and alcoholic hydroxyl not being possible. With this point in view, an attempt was made to reduce zingerone to the corresponding alcohol by Harries' method, namely, by zinc dust and alcoholic hydrochloric acid, but the result was unsatisfactory. Since Vavon[1] synthesised phenylethyl methyl carbinol, $C_6H_5CH_2CH_2CH(OH)CH_3$, by the catalytic reduction of benzylidene acetone, $C_6H_5CH:CHCOCH_3$, the authors attempted to reduce zingerone catalytically with hydrogen in the presence of platinum black for the preparation of the alcohol. On failing again in this method of reduction, 4-hydroxy-3-methoxyphenylethyl methyl carbinol was finally synthesised by reducing with metallic sodium and absolute alcohol.

For the second purpose, di-4-hydroxy-3-methoxyphenylethyl ketone was synthesised by condensing vanillin and acetone in the presence of concentrated hydrochloric acid and reducing the product either catalytically with hydrogen or with sodium amalgam and water.

Comparing the taste of the three above-mentioned substances, the first two substances, 4-hydroxy-3-methoxyphenylethyl methyl carbinol and 4-hydroxy-3-methoxyphenylbutane had a pungent taste similar to

(1) Ann. de chim., 9e Série. 1, (1914), 191.

that of zingerone. The taste was, however, not so agreeable as that of zingerone. Di-4-hydroxy-3-methoxyphenylethyl ketone was almost tasteless in the solid state, but a little pungent in an alcoholic solution. From this, it appears that the presence of the carbonyl group in the side chain of zingerone is not essential to its pungency, although it has some effect.

EXPERIMENTAL.

4-Hydroxy-3-methoxyphenylethyl Methyl Carbinol, $C_6H_3(OH)(OCH_3)CH_2CH_2CH(OH)CH_3$.

To six grams of metallic sodium placed in a round bottomed flask, a solution of 18 grams of zingerone in 90 c.c. of absolute alcohol was gradually added and heated on a water-bath under a reflux condenser until the whole of the sodium disappeared. After the removal of most of the alcohol, the product was acidified with 200 c.c. of dilute hydrochloric acid and extracted with ether. The ethereal solution was washed with water and shaken with a concentrated solution of sodium bisulphite, in order to remove the unchanged zingerone. As, however, the bisulphite compound did not separate even after shaking for two hours, the ethereal layer was separated and washed successively with water, a solution of sodium carbonate and with water until free from alkali. The dried ethereal solution was evaporated and the residual oil was purified by distillation under a diminished pressure of 17 mm., when a colourless viscid oil passed over at 196–197°. The yield was 6.5 grams:

0.1117 gave 0.2734 CO_2 and 0.0797 H_2O. $C = 66.77$; $H = 7.98$ per cent.

$C_{11}H_{16}O_3$ requires $C = 67.31$; $H = 8.03$ per cent.

The Diacetyl Derivative, $C_6H_3(OCOCH_3)(OCH_3)CH_2CH_2CH(OCOCH_3)CH_3$ ——— Four and a half grams of 4-hydroxy-3-methoxyphenylethyl methyl carbinol were boiled for one hour with 4.5 grams of fused sodium acetate and 15 grams of acetic anhydride. After the removal of the excess of acetic anhydride under diminished pressure, the product was extracted with ether and the ethereal solution washed with a dilute

solution of sodium bicarbonate and, then, thoroughly with water. The dried ethereal solution was evaporated and the residual oil subjected to fractional distillation under diminished pressure. During the first distillation, almost the whole quantity passed over at 212–213°/18 mm. The yield was 5.2 grams. On repeating the distillation, a colourless oil boiling at 209.5—210.5°/15.5 mm. was obtained:

0.1256 gave 0.2971 CO_2 and 0.0824 H_2O. $C = 64.53$; $H = 7.34$ per cent.

$C_{15}H_{20}O_5$ requires $C = 64.26$; $H = 7.20$ per cent.

4-Hydroxy-3-methoxyphenylbutane, $C_6H_3(OH)(OCH_3)CH_2CH_2CH_2CH_3$.

To 35 grams of granulated zinc, 100 c.c. of a 5 per cent. solution of mercuric chloride were added, and, after standing for an hour, the supernatant liquid was poured off. 10 grams of zingerone and dilute hydrochloric acid (1 : 1) sufficient to cover the amalgamated zinc were then added and heated to boiling in a sand-bath for five hours under a reflux condenser, further quantities of hydrochloric acid of the same strength being frequently added, in order to keep up a lively evolution of hydrogen. The product was distilled in steam, and the distillate extracted with ether. The ethereal solution was well washed with water, dried over anhydrous sodium sulphate and evaporated. The residual oil was then distilled under diminished pressure, when 4 grams of a colourless oil boiling at 140.5–145.5°/14.5–15 mm. (principally 142.5–143.5°) were obtained. On repeating the operation, the oil distilled at 141–142°/13.5 mm.:

0.1017 gave 0.2717 CO_2 and 0.0785 H_2O. $C = 72.86$; $H = 8.63$ per cent.

$C_{11}H_{16}O_2$ requires $C = 73.28$; $H = 8.95$ per cent.

The Benzoyl Derivative, $C_6H_3(OCOC_6H_5)(OCH_3)C_4H_9$. ——— This substance (0.7 gram) was shaken with 2.5 c.c. of benzoyl chloride and 25 c.c. of a 10 per cent. solution of sodium hydroxide for two hours, when colourless crystals separated, which were collected, washed with

water and dried. They melted at 92.5–93° after two crystallisations from absolute alcohol and analysed with the following results:

0.1166 gave 0.3219 CO_2 and 0.0732 H_2O. $C = 75.32$; $H = 7.03$ per cent.

$C_{18}H_{20}O_3$ requires $C = 76.02$; $H = 7.09$ per cent.

Synthesis of Di-4-hydroxy-3-methoxyphenylethyl Ketone.

Di-4-hydroxy-3-methoxystyryl ketone, $C_6H_3(OH)(OCH_3)CH:CH\,CO\,CH:CH\,C_6H_3(OH)(OCH_3)$.——— To a mixture of vanillin (15 grams) and acetone (4 c.c.), 30 c.c. of concentrated hydrochloric acid (D 1.18) were added, when a reddish violet solution was obtained, which passed gradually into a dark violet mass. After being left for six days, the product was diluted with 200 c.c. of water and a dark green precipitate collected. As the precipitate was difficult to filter, it was dissolved in a 2 per cent. solution of sodium hydroxide and acidified with dilute hydrochloric acid. The yellowish brown precipitate thus obtained was readily washed with water and recrystallised from dilute alcohol. The yield was 12.7 grams after one crystallisation. It separated in brick-red crystals and melted indefinitely between 115.5° and 119.5° after being dried in the air. When heated at about 78° under a diminished pressure of 10.5–12 mm., it lost 4.68 per cent. in weight and melted sharply at 141.5–142.5°, whilst the theoretical loss for $C_{19}H_{18}O_5.\ H_2O$ is 5.23. The anhydrous substance was yellow and analysed with the following results:

0.2058 gave 0.5241 CO_2 and 0.1023 H_2O. $C = 69.45$; $H = 5.56$ per cent.

$C_{19}H_{18}O_5$ reqiures $C = 69.91$; $H = 5.56$ per cent.

It is readily soluble in a 2 per cent. solution of sodium hydroxide with a deep red colour. On rubbing the wall of a test tube containing a yellow alcoholic solution of the substance with a glass rod, a red colour was developed. It is possible that this property may be used as an indicator.

Di-4-hydroxy-3-methoxyphenylethyl ketone, $C_6H_3(OH)(OCH_3)CH_2$

$CH_2CO\,CH_2CH_2C_6H_3(OH)(OCH_3)$, was prepared in the following two ways.

(A) Catalytic Reduction of Di-4-hydroxy-3-methoxystyryl Ketone. ——— Three grams of the ketone were suspended in 50 c.c. of absolute ether and reduced by hydrogen in the presence of platinum black. The hydrogen absorbed was 600 c.c. for twenty seven and a half hours (at 24.5–27° and 751–754 mm.). After filtering the platinum black, the filtrate and ethereal washings were combined and evaporated, and the residual oil solidified to a somewhat brown mass on being kept over calcium chloride and paraffin in a desiccator (yield 2.8 grams). The precipitate was collected, washed with the least possible quantity of ether and recrystallised from dilute methyl alcohol with the addition of animal charcoal, when colourless crystals melting at 89.5–90.5° were obtained:

0.1217 gave 0.3102 CO_2 and 0.0770 H_2O. $C = 69.54$; $H = 7.08$ per cent.

$C_{19}H_{22}O_5$ requires $C = 69.05$; $H = 6.71$ per cent.

(B) Reduction of Di-4-hydroxy-3-methoxystyryl Ketone with Sodium Amalgam and Water. ——— Twenty five grams of di-4-hydroxy-3-methoxystyryl ketone were suspended in 500 c.c. of water and reduced with 280 grams of sodium amalgam (3 %). After acidification with hydrochloric acid, the product was extracted with ether, and the ethereal solution washed well with water, dried and evaporated. The crystals (18.7 grams) thus obtained were recrystallised from dilute alcohol, when they melted at 89–90°.

The Dibenzoyl Derivative. ——— Benzoyl chloride (0.9 gram) was added to a solution of one gram of di-4-hydroxy-3-methoxyphenylethyl ketone in 5 grams of pyridine and the mixture allowed to stand for two days. In order to remove the pyridine, the product was treated with dilute sulphuric acid, when a deep-red oily substance was deposited, which solidified after standing for three days. The precipitate was collected, washed with water and dried. On recrystallisation from

methyl or ethyl alcohol with the addition of animal charcoal, it separated in colourless crystals melting at 129–130°.

0.1030 gave 0.2762 CO_2 and 0.0492 H_2O. $C = 73.16$; $H = 5.35$ per cent.

$C_{33}H_{30}O_7$ requires $C = 73.58$; $H = 5.62$ per cent.

Di-3 : 4-dimethoxyphenylethyl ketone, $C_6H_3(OCH_3)_2\,CH_2CH_2CO\,CH_2\,CH_2C_6H_3(OCH_3)_2$.

A mixture of di-4-hydroxy-3-methoxyphenylethyl ketone (10.7 grams) and a 10 per cent. solution of sodium hydroxide (80 grams) was shaken with 8 grams of methyl sulphate for two hours, when faint yellow crystals were obtained. The crystals were collected, washed well with water, and recrystallised three times from dilute alcohol. The yield was 6 grams after once crystallising. The colourless crystals thus purified melted at 83.5–84.5° and analysed with the following results:

0.1127 gave 0.2901 CO_2 and 0.0746 H_2O. $C = 70.22$; $H = 7.41$ per cent.

$C_{21}H_{26}O_5$ requires $C = 70.35$; $H = 7.32$ per cent.

The Oxime.——— To a mixture of the ketone (3.5 grams), hydroxylamine hydrochloride (0.7 gram) and sodium acetate (1.4 grams), 37 c.c. of dilute alcohol were added and heated on a water-bath for two hours. After evaporating the greater part of the alcohol, colourless crystals separated, which were collected, washed with water and recrystallised three times from dilute alcohol. The crystals thus purified melted at 138.5–139.5°:

0.2954 gave 9.20 c.c. N_2 at 10° and 765.5 mm. $N = 3.74$ per cent.

$C_{21}H_{27}O_5N$ requires $N = 3.75$ per cent.

[June 16th, 1924].

The Condensation of Vanillin with Methyl Ethyl Ketone.

By

Johei Ichikawa.

Harries and Müller[1] showed that methyl ethyl ketone condenses with benzaldehyde in the presence of an alkali to form the α-benzylidene derivative, $C_6H_5CH:CH\,CO\,C_2H_5$, and in the presence of hydrochloric acid to form the γ-benzylidene derivative, $C_6H_5CH:C(CH_3)\,CO\,CH_3$. Vanillin was condensed with methyl ethyl ketone in the hope of obtaining 4-hydroxy-3-methoxystyryl ethyl ketone, $C_6H_3(OH)(OCH_3)\,CH:CH\,CO\,CH_2CH_3$, and α-methylvanillalacetone, $C_6H_3(OH)(OCH_3)\,CH:C(CH_3)\,CO\,CH_3$, either caustic soda or hydrochloric acid being used as a condensing agent, and comparing the taste of their reduction products. In the former case, the condensation of vanillin with methyl ethyl ketone proceeded normally and resulted in the formation of 4-hydroxy-3-methoxystyryl ethyl ketone, but, in the latter, the condensation product was $\alpha\alpha'$-divanillalmethylethyl ketone arising from the interaction of two molecules of vanillin and one molecule of methyl ethyl ketone, in place of the expected α-methylvanillalacetone. 4-Hydroxy-3-methoxystyryl ethyl ketone was reduced with hydrogen in the presence of platinum black, and the resulting substance, 4-hydroxy-3-methoxyphenylethyl ethyl ketone was pungent as the lower homologue, zingerone.

(1) Ber., **35**, (1902), 968.

EXPERIMENTAL.

Condensation of Vanillin with Methyl Ethyl Ketone in the Presence of Caustic Soda.

4-Hydroxy-3-methoxystyryl Ethyl Ketone, $C_6H_3(OH)(OCH_3)CH:CH\,CO\,C_2H_5$.——— To a mixture of vanillin (21 grams) and methyl ethyl ketone (10 grams), 41 c.c. of water and 58 c.c. of a 10 per cent. solution of caustic soda were added. After being allowed to remain for six days, the deep red solution was acidified with dilute hydrochloric acid, when a brown oil, which gradually solidified, separated. It was collected, washed well with water and recrystallised twice from dilute alcohol. The yield was 3.7 grams. The crystals thus purified were faintly yellow and melted at 91–92°:

0.1132 gave 0.2882 CO_2 and 0.0687 H_2O. $C = 69.43$; $H = 6.79$ per cent.

$C_{12}H_{14}O_3$ requires $C = 69.87$; $H = 6.85$ per cent.

4-Hydroxy-3-methoxyphenylethyl Ethyl Ketone, $C_6H_3(OH)(OCH_3)CH_2CH_2CO\,C_2H_5$.——— 4-Hydroxy-3-methoxystyryl ethyl ketone (4.4 grams) was suspended in 40 c.c. of absolute ether and reduced with hydrogen in the presence of platinum black. The hydrogen absorbed was about 730 c.c. (at 17.5–18.5° and 753–754 mm.) for eight hours. After filtering off the platinum black, the filtrate and ethereal washings of the platinum black were evaporated and the residual oil, on distillation under 12.5 mm., distilled at 189.5–190.5°. The yield was 3.1 grams. On repeating the distillation, a colourless oil boiling at 187–188° under 11.5 mm. was obtained:

0.1250 gave 0.3140 CO_2 and 0.0877 H_2O. $C = 68.51$; $H = 7.85$ per cent.

$C_{12}H_{16}O_3$ requires $C = 69.23$; $H = 7.75$ per cent.

This substance has a pungent taste like zingerone.

Condensation of Vanillin with Methyl Ethyl Ketone in the Presence of Hydrochloric Acid.

A well-cooled mixture of vanillin (5 grams) and methyl ethyl ketone (3 grams) was saturated with dry hydrogen chloride, when a blue mass was obtained. After standing overnight, the mass was ground with water in a mortar, collected, washed thoroughly with water and dried. The yield was 4.2 grams. It was dissolved in benzene, boiled with the addition of animal charcoal, and, after filtering, precipitated with petroleum ether. On repeating this process, a brick red precipitate was obtained and analysed with the following results:

0.1461 gave 0.3780 CO_2 and 0.0656 H_2O. $C = 70.56$; $H = 5.02$ per cent.

$C_{20}H_{20}O_5$ requires $C = 70.56$; $H = 5.93$ per cent.

This substance begins to discolour at about 223° and darkens at about 255°. It is readily soluble in alcohol or chloroform; rather less so in benzene and sparingly soluble in other ordinary organic solvents.

[June 16th, 1924.]

Synthesis of the Homologues of Zingerone.

By

Hiroshi Nomura and Seinosuke Hotta.

Lapworth and his collaborators[1] have stated that gingerol, the pungent principle of ginger, is essentially a mixture of optically active saturated phenolic compounds derived from a residue of zingerone associated with a molecular proportion of the residue of a saturated aliphatic aldehyde which, in the main constituent, is n-heptaldehyde, and that the constituents are probably "aldols" (β-hydroxy-ketones) of the general formula:

$C_6H_3(OH)(OCH_3)\,CH_2CH_2CO\,CH_2CH(OH)(CH_2)_nCH_3$, where n in the principal constituent is 5, and 4, or possibly 3, in the main secondary constituent.

If this view of the constitution of gingerol is correct, it would be possible to produce unsaturated ketones by the distillation of gingerol as in the case of the formation of crotonic aldehyde, $CH_3CH:CH\,CHO$, from aldol, $CH_3CH(OH)\,CH_2CHO$, and the product obtained by reduction of the distillate would be a mixture of homologues of zingerone as shown in the following scheme:

$C_6H_3(OH)(OCH_3)\,CH_2CH_2CO\,CH_2CH(OH)\,C_nH_{2n+1} \xrightarrow{-H_2O} C_6H_3(OH)(OCH_3)\,CH_2CH_2\,CO\,CH:CH\,C_nH_{2n+1} \xrightarrow{H_2} C_6H_3(OH)(OCH_3)\,CH_2CH_2CO\,CH_2\,CH_2\,C_nH_{2n+1}$. As shogaol[2] was obtained by distilling the pungent principles of ginger, the reduction product, dihydroshogaol,[3] may

---

(1) Journ. chem. Soc., **111**, (1917), 789.
(2) Sci. Rep., **7**, (1918), 72.
(3) loc. cit., 77.

also be a homologue of zingerone. It is, therefore, of interest to synthesise the homologues of zingerone and find some readily crystallisable compounds by fully investigating the properties of their derivatives.

The homologues of zingerone were synthesised by condensing vanillin with methyl ketones in the presence of caustic soda and reducing the product suspended in water with sodium amalgam. The condensation of vanillin with methyl ketones was more difficult as the molecular weight of the latter increased. The reduction of the condensation products proceeded in all cases smoothly, and the solubility and pungency of the reduction products were similar to those of zingerone.

As benzoylzingerone and methylzingeroneoxime were readily obtained in the crystalline state, benzoyl derivatives and oximes and semicarbazones of methyl derivatives were first synthesised. A table of the melting points of zingerone, its homologues, and their crystalline derivatives is given below :

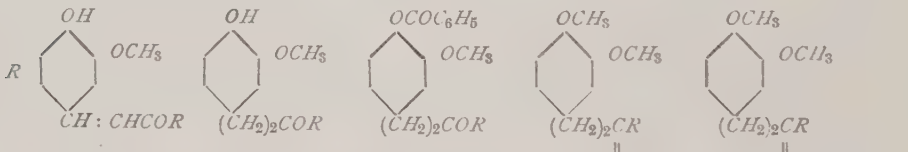

	(I)	(II)	(III)	(IV) *NOH*	(V) *NNHCONH*$_2$
Methyl	128–129°	40–41°	126–127°	93–93.5°	—
Ethyl	91–92°	36–37°	118–119°	120–120.5°	143–144°
n-Propyl	82.5–83.5°	44.5–45°	107.5–108.5°	94.5–95.5°	———
n-Butyl	———	47.5–48°	91–91.5°	111–112°	———
Isobutyl	78–79°	———	81.5–82.5°	114–114.5°	123.5–124.5°
Tertiary Butyl	———	76–80°	57.5–58°	114.5–115.5°	127–128°

As compared with the derivatives with normal chains, the melting points of the condensing products of vanillin and methyl ketones (I) and those of the benzoyl derivatives of their reduction products (III) lower regularly for every increase in number of carbon atoms in the molecule, and the oximes of the methyl derivatives (IV) containing even carbon atoms in *R* have higher melting points than those immediately succeeding them, in which *R* contains an uneven number of carbon atoms.

4-Hydroxy-3-methoxyphenylethyl isobutyl ketone and 4-hydroxy-3-methoxyphenylethyl tertiary butyl ketone are pungent as their isomer, 4-hydroxy-3-methoxyphenylethyl n-butyl ketone. From this, it appears that the pungency of the latter is not greatly influenced by substituting either isobutyl or tertiary butyl for its normal butyl group.

The synthesis of the higher homologues of zingerone is now in progress.

EXPERIMENTAL.

Synthesis of 4-Hydroxy-3-methoxyphenylethyl Ethyl Ketone, $C_6H_3(OH)(OCH_3)CH_2CH_2CO\,C_2H_5$.

This ketone was synthesised by Johei Ichikawa in this laboratory by condensing vanillin with methyl ethyl ketone and reducing the product with hydrogen in the presence of platinum black. He could not continue the investigation before his leaving this laboratory. The authors synthesised the ketone in the following way:

To a mixture of 400 grams of water and 400 grams of a 10 per cent. solution of sodium hydroxide, 60 grams of vanillin and 40 c.c. of methyl ethyl ketone were added, when a yellow solution was obtained, which passed gradually into deep red. After being left for seven days, the product was carefully acidified with concentrated hydrochloric acid, when a brown oil separated. On rubbing with a glass rod, the oil solidified to a dark brown mass which was collected and washed with water. In order to remove the unchanged vanillin, the mass was ground and shaken with a dilute solution of sodium bisulphite for half an hour. The portion insoluble in the sodium bisulphite solution was collected, washed again with water and dried. The yield was 57 grams. The crystals thus obtained were crystallised from dilute alcohol, from which they separated as yellow crystals melting at 91–92°.

Ichikawa gave 91–92[c] as the melting point of 4-hydroxy-3-methoxystyryl ethyl ketone.

Fifteen grams of 4-hydroxy-3-methoxystyryl ethyl ketone were then suspended in 300 c.c. of water and reduced with 130 grams of sodium

amalgam (3 %). After being separated from the mercury, the alkaline solution of the reduction product was carefully acidified with concentrated hydrochloric acid, when an oil separated, which was extracted with ether. The ethereal solution was washed with water, dried over anhydrous sodium sulphate and evaporated. The residual oil was at first purified by distillation under diminished pressure. During the distillation, almost the whole quantity distilled at 201–204° under 28 mm. The yield was 12 grams. The oil was recrystallised from a mixture of ether and petroleum ether, from which it separated in colourless crystals melting at 36–37°:

0.1397 gave 0.3524 CO_2 and 0.0978 H_2O. $C = 68.82$; $H = 7.83$ per cent.

0.1008 gave 0.2544 CO_2 and 0.0706 H_2O. $C = 68.85$; $H = 7.84$ per cent.

$C_{12}H_{16}O_3$ requires $C = 69.23$; $H = 7.75$ per cent.

Ichikawa gave 187–188°/11.5 mm. as its boiling point.

The Benzoyl Derivative, $C_6H_3(OCO\,C_6H_5)(OCH_3)\,CH_2CH_2CO\,C_2H_5$ ——— Two grams of the ketone were shaken with 5 c.c. of benzoyl chloride and 50 c.c. of a 10 per cent. solution of soduim hydroxide for one hour; the precipitate was collected and washed with water. After being dried in the desiccator, the substance was twice recrystallised from absolute alcohol, when it separated in colourless crystals melting at 118–119°. The yield was 2.2 grams after two crystallisations:

0.1080 gave 0.2882 CO_2 and 0.0655 H_2O. $C = 72.80$; $H = 6.79$ per cent.

$C_{19}H_{20}O_4$ requires $C = 73.05$; $H = 6.46$ per cent.

3 : 4-Dimethoxyphenylethyl Ethyl Ketone, $C_6H_3(OCH_3)_2\,CH_2CH_2CO\,C_2H_5$——— 4-Hydroxy-3-methoxyphenylethyl ethyl ketone (10 grams) was shaken with 6 c.c. of methyl sulphate and 30 c.c. of a 10 per cent. solution of sodium hydroxide for two hours. The product was extracted with ether, the ethereal solution washed with water until free from alkali, dried over anhydrous sodium sulphate and evaporated. The residual oil was then distilled under a diminished pressure of 12 mm.,

when 8.4 grams of a colourless oil passed over at 183–184°:

5.167 mg. gave 13.283 mg. CO_2 and 3.861 mg. H_2O. $C = 70.11$; $H = 8.36$ per cent.

$C_{13}H_{18}O_3$ requires $C = 70.24$; $H = 8.16$ per cent.

On cooling with a freezing mixture, the oil solidified and melted at 26.5–27.5°. It was readily crystallisable from a mixture of ether and petroleum ether.

The Oxime, $C_6H_3(OCH_3)_2\,CH_2CH_2\,C(:NOH)\,C_2H_5$——— A mixture of 3 : 4-dimethoxyphenylethyl ethyl ketone (2 grams), hydroxylamine hydrochloride (0.7 gram) and sodium acetate (1.4 grams) was dissolved in dilute alcohol and boiled for two hours under a reflux condenser. In order to isolate the product, the alcohol was removed by gentle evaporation, the oily oxime which solidified on cooling, collected, washed with water and dried. The yield was 2.1 grams. The colourless crystals melted at 120–120.5° after three crystallisations from dilute alcohol:

0.1248 gave 6.48 c.c. N_2 at 20.5° and 751 mm. $N = 5.83$ per cent.

$C_{13}H_{19}O_3N$ requires $N = 5.91$ per cent.

The Semicarbazone, $C_6H_3(OCH_3)_2CH_2CH_2C(:NNH\,CO\,NH_2)\,C_2H_5$ ——— A mixture of 3 : 4-dimethoxyphenylethyl ethyl ketone (1 gram), a solution of semicarbazide hydrochloride (0.5 gram) in water (5 c.c.) and a solution of potassium acetate (0.5 gram) in alcohol (5 c.c.) was allowed to stand overnight. The precipitate thus obtained was collected, washed with water until free from chloride, and dried. The yield was 1.2 grams. It crystallised from dilute alcohol in colourless crystals melting at 143–144°:

0.0473 gave 6.29 c.c. N_2 at 21° and 757 mm. $N = 15.00$ per cent.

$C_{14}H_{21}O_3N_3$ requires $N = 15.05$ per cent.

Synthesis of 4-Hydroxy-3-methoxyphenylethyl n-Propyl Ketone, $C_6H_3(OH)(OCH_3)\,CH_2CH_2CO\,CH_2CH_2CH_3$.

The intermediate product in this synthesis, 4-hydroxy-3-methoxystyryl

n-propyl ketone, $C_6H_3(OH)(OCH_3)CH:CHCOC_3H_7$, was prepared by adding 50 grams of water and 50 grams of a 10 per cent. solution of sodium hydroxide to a mixture of 7.5 grams of vanillin and 5 grams of methyl n-propyl ketone and shaking the whole for fifty hours during ten days. After the removal of the unchanged vanillin in the manner described in the foregoing paragraph, the product was twice recrystallised from dilute alcohol, when it separated in faint yellow crystals melting at 82.5–83.5°. The yield was 4.5 grams after one crystallisation:

0.1149 gave 0.2980 CO_2 and 0.0782 H_2O. $C = 70.76$; $H = 7.62$ per cent.

$C_{13}H_{16}O_3$ requires $C = 70.88$; $H = 7.33$ per cent.

The preparation and purification of 4-hydroxy-3-methoxyphenylethyl n-propyl ketone and its derivatives were carried out in a similar manner to that employed in the case of 4-hydroxy-3-methoxyphenylethyl ethyl ketone and its derivatives.

4-Hydroxy-3-methoxyphenylethyl n-propyl ketone prepared by the reduction of 4-hydroxy-3-methoxystyryl n-propyl ketone with sodium amalgam distilled at 198° under 14 mm. The yield of a colourless oil thus obtained from 6.5 grams of the latter was 4.1 grams. It was further purified by recrystallisation from a mixture of ether and petroleum ether, when colourless crystals melting at 44.5–45° were obtained:

0.1208 gave 0.3126 CO_2 and 0.0879 H_2O. $C = 70.60$; $H = 8.14$ per cent.

$C_{13}H_{18}O_3$ requires $C = 70.24$; $H = 8.16$ per cent.

The Benzoyl Derivative, $C_6H_3(OCO\,C_6H_5)(OCH_3)CH_2CH_2CO\,C_3H_7$. — This compound was obtained in colourless crystals melting at 107.5–108.5° after two crystallisations from absolute alcohol. The benzoyl derivative thus obtained from 2 grams of the ketone amounted to 2.6 grams:

0.1094 gave 0.2944 CO_2 and 0.0683 H_2O. $C = 73.41$; $H = 6.99$ per cent.

$C_{20}H_{22}O_4$ requires $C = 73.59$; $H = 6.80$ per cent.

3 : 4-Dimethoxyphenylethyl n-Propyl Ketone, $C_6H_3(OCH_3)_2CH_2CH_2$

$CO\,C_3H_7$. —— This compound was prepared by shaking 16.5 grams of 4-hydroxy-3-methoxyphenylethyl n-propyl ketone with 10 grams of methyl sulphate and 70 c.c. of a 10 per cent. solution of sodium hydroxide for two hours. After the purification of the crude product, 11.4 grams of a colourless oil boiling at 198–199°/17 mm. were obtained:

0.1267 gave 0.3304 CO_2 and 0.0962 H_2O. $C = 71.14$; $H = 8.50$ per cent.

$C_{14}H_{20}O_3$ requires $C = 71.15$; $H = 8.53$ per cent.

3 : 4-Dimethoxyphenylethyl n-Propyl Ketoxime, $C_6H_3(OCH_3)_2CH_2CH_2C(:NOH)C_3H_7$. —— The crude oxime obtained from 4.4 grams of 3 : 4-dimethoxyphenylethyl n-propyl ketone amounted to 4.5 grams. In order to obtain it in the pure state, it was recrystallised eight times from a mixture of ether and petroleum ether, when it separated in colourless crystals melting at 94.5–95.5°:

11.15 mg. gave 0.570 c.c. N_2 at 17° and 745 mm. $N = 5.97$ per cent.

$C_{14}H_{21}O_3N$ requires $N = 5.58$ per cent.

Synthesis of 4-Hydroxy-3-methoxyphenylethyl n-Butyl Ketone, $C_6H_3(OH)(OCH_3)CH_2CH_2CO\,CH_2CH_2CH_2CH_3$.

In order to obtain the intermediate product in this synthesis, namely, 4-hydroxy-3-methoxystyryl n-butyl ketone, $C_6H_3(OH)(OCH_3)CH:CHCO\,C_4H_9$, a mixture of 7.5 grams of of vanillin and 5.7 grams of methyl n-butyl ketone was shaken with 100 grams of a 5 per cent. solution of sodium hydroxide for seventy three and a half hours during eleven days. After the removal of the unchanged methyl n-butyl ketone by extracting with ether, the aqueous alkaline residue was freed from ether by passing a current of air through it. On acidification with concentrated hydrochloric acid, a brown oil separated, from which the unchanged vanillin was removed by treatment with a dilute solution of sodium bisulphite. The product thus purified was recrystallised three times from dilute alcohol and, finally, from dilute methyl alcohol, when faint yellow crystals melting indefinitely between 66-100° were obtained:

0.1157 gave 0.2822 CO_2 and 0.0824 H_2O. $C = 66.54$; $H = 7.97$ per cent.

$C_{14}H_{18}O_3$ requires $C = 71.76$; $H = 7.75$ per cent.

$C_{14}H_{18}O_3 . H_2O$ requires $C = 66.63$; $H = 7.99$ per cent.

When heated under diminished pressure, it lost 6.94 per cent. in weight, whilst the theoretical loss for 1 H_2O is 7.14.

On reduction with sodium amalgam and subsequent treatment in the manner described in the case of its lower homologues, 4-hydroxy-3-methoxyphenylethyl n-butyl ketone was obtained as a colourless oil boiling at 213–214°/23 mm. The oil obtained from 2 grams of the unsaturated ketone amounted to 1.3 grams. It crystallised from a mixture of ether and petroleum ether in colourless crystals melting at 47.5–48°:

0.1110 gave 0.2876 CO_2 and 0.0847 H_2O. $C = 70.69$; $H = 8.54$ per cent.

$C_{14}H_{20}O_3$ requires $C = 71.15$; $H = 8.53$ per cent.

The benzoyl derivative was colourless and melted at 91–91.5° after twice recrystallising from absolute alcohol:

0.1088 gave 0.2952 CO_2 and 0.0714 H_2O. $C = 74.02$; $H = 7.34$ per cent.

$C_{21}H_{24}O_4$ reqiures $C = 74.09$; H = 7.11 per cent.

3 : 4-Dimethoxyphenylethyl n-Butyl Ketone, $C_6H_3(OCH_3)_2\,CH_2CH_2\,CO\,C_4H_9$.——— This compound was obtained as an oil boiling at 205–206°/20 mm. by shaking 6.6 grams of 4-hydroxy-3-methoxyphenylethyl n-butyl ketone with 4 c.c. of methyl sulphate and 20 c.c. of a 10 per cent. sodium hydroxide solution for two and a half hours and purifying the product as in the case of its lower homologues. The yield was 5.8 grams. The oil was colourless and analysed with the following results:

0.1291 gave 0.3374 CO_2 and 0.1014 H_2O. $C = 71.30$; $H = 8.79$ per cent.

0.1239 gave 0.3238 CO_2 and 0.0952 H_2O. $C = 71.30$; $H = 8.60$ per cent.

The oxime, $C_6H_3(OCH_3)_2CH_2CH_2C(:NOH)C_4H_9$, crystallised from dilute alcohol in colourless crystals and melted at 111–112° after four crystallisations:

9.05 mg. gave 0.429 c.c. N_2 at 15° and 762 mm. $N = 5.63$ per cent.

$C_{15}H_{23}O_3N$ requires $N = 5.28$ per cent.

Synthesis of 4-Hydroxy-3-methoxyphenylethyl Isobutyl Ketone, $C_6H_3(OH)(OCH_3)CH_2CH_2CO\,CH_2CH(CH_3)_2$.

The intermediate product in this synthesis, 4-hydroxy-3-methoxystyryl isobutyl ketone, $C_6H_3(OH)(OCH_3)CH:CH\,CO\,C_4H_9$, was prepared and purified in the following way:

Vanillin (18 grams) and methyl isobutyl ketone (11.3 grams) were added to a mixture of water (132 grams) and a 10 per cent. solution of sodium hydroxide (120 grams). After shaking the whole for 42 hours during nine days, the product was carefully acidified with concentrated hydrochloric acid and extracted with ether. In order to remove the unchanged vanillin, the ethereal solution was shaken with a dilute solution of sodium bisulphite, washed with water, dried and evaporated. On distillation of the residual oil, 10.2 grams of an oil boiling at 233-234.5°/20 mm. were obtained. The oil was three times recrystallised from dilute alcohol, when it separated in faint yellow crystals melting at 78–79°:

0.1224 gave 0.3214 CO_2 and 0.0861 H_2O. $C = 71.61$; $H = 7.87$ per cent.

$C_{14}H_{18}O_3$ requires $C = 71.76$; $H = 7.75$ per cent.

The preparation and purification of the reduction product, 4-hydroxy-3-methoxyphenylethyl isobutyl ketone, $C_6H_3(OH)(OCH_3)CH_2CH_2CO\,C_4H_9$, were carried out in an exactly similar manner to its isomer. During the first distillation, an almost colourless oil passed over at 204.5–206°/16 mm. The oil obtained from 31.5 grams of the unsaturated ketone amounted to 22.5 grams. On repeating the distillation, this oil boiled constantly at 210°/19 mm.:

0.1445 gave 0.3764 CO_2 and 0.1098 H_2O. $C = 71.06$; $H = 8.50$ per cent.

$C_{14}H_{20}O_3$ requires $C = 71.15$; $H = 8.53$ per cent.

Its taste is pungent as its isomer, 4-hydroxy-3-methoxyphenylethyl n-butyl ketone.

The benzoyl derivative, $C_6H_3(O\,CO\,C_6H_5)(OCH_3)\,CH_2CH_2CO\,C_4H_7$, was colourless and melted at 81.5–82.5°:

0.1150 gave 0.3116 CO_2 and 0.0742 H_2O. $C = 73.90$; $H = 7.22$ per cent.

$C_{21}H_{24}O_4$ requires $C = 74.09$; $H = 7.11$ per cent.

3 : 4-Dimethoxyphenylethyl Isobutyl Ketone, $C_6H_3(OCH_3)_2CH_2CH_2\,CO\,C_4H_9$. ——— After three hours' shaking 16.6 grams of 4-hydroxy-3-methoxyphenylethyl isobutyl ketone with 10 c.c. of methyl sulphate and 50 c.c. of a 10 per cent. solution of sodium hydroxide, the product was worked up as its isomer, when an almost colourless oil (14.8 grams) boiling at 204°/19 mm. passed over. On repeating the distillation, the oil distilled at 202°/17 mm.:

0.0978 gave 0.2572 CO_2 and 0.0779 H_2O. $C = 71.74$; $H = 8.92$ per cent.

$C_{15}H_{22}O_3$ requires $C = 71.96$; $H = 8.86$ per cent.

The Oxime, $C_6H_3(OCH_3)_2CH_2CH_2C(:NOH)\,C_4H_9$. ——— The crude oxime was recrystallised from dilute alcohol, from which it separated in colourless crystals melting at 114–114.5°:

0.1090 gave 5.60 c.c. N_2 at 25° and 758 mm. $N = 5.69$ per cent.

$C_{15}H_{23}O_3N$ requires $N = 5.28$ per cent.

The Semicarbazone, $C_6H_3(OCH_3)_2CH_2CH_2C(:NNH\,CO\,NH_2)\,C_4H_9$. ——— 3 : 4-Dimethoxyphenylethyl isobutyl ketone (6 grams), potassium acetate (2.4 grams), and semicarbazide hydrochloride (2.7 grams) were dissolved in a mixture of 30 c.c. of alcohol and 30 c.c. of water, and allowed to stand for two days. As no crystalline precipitate was deposited, the alcohol was evaporated in a vacuum desiccatar. The

residual sirup was extracted with ether, and the ethereal solution washed well with water and dried. After distilling off the ether, the residue was recrystallised several times from dilute alcohol and, once, from a mixture of ether and petroleum ether. The crystals thus purified were colourless and melted at 123.5–124.5°:

0.1040 gave 12.8 c.c. N_2 at 18° and 759 mm. $N = 14.13$ per cent.

$C_{16}H_{25}O_3N_3$ requires $N = 13.68$ per cent.

Synthesis of 4-Hydroxy-3-methoxyphenylethyl Tertiary Butyl Ketone, $C_6H_3(OH)(OCH_3)\,CH_2CH_2CO\,C(CH_3)_3$.

After shaking 46 grams of vanillin and 30 grams of pinacoline with a mixture of 360 grams of water and 300 grams of a 10 per cent. solution of sodium hydroxide for 116 hours during 19 days, the unchanged pinacoline was removed by extracting with ether. The quantity of recovered pinacoline was 12.5 grams. The deep red alkaline residue was carefully acidified with concentrated hydrochloric acid, when a reddish brown oil separated, which was extracted with ether. The ethereal extract was freed from vanillin by shaking with a dilute solution of sodium bisulphite, washed well with water, dried and evaporated. On distillation of the residual oil, a somewhat reddish yellow viscous oil (8.5 grams) passed over at 220–221°/19 mm. The oil thus purified was suspended in water and reduced with sodium amalgam. On isolating and purifying the reduction product as in the case of its isomer, a faint yellow oil boiling at 196.5–198°/16 mm. (6 grams) was obtained, which, after recrystallisation from absolute ether, separated in colourless crystals melting at 76–80°:

0.1010 gave 0.2644 CO_2 and 0.0785 H_2O. $C = 71.40$; $H = 8.70$ per cent.

$C_{14}H_{20}O_3$ requires $C = 71.14$; $H = 8.54$ per cent.

It has a pungent taste similar to its isomer.

The benzoyl derivative, $C_6H_3(OCO\,C_6H_5)(OCH_3)\,CH_2CH_2CO\,C(CH_3)_3$, was obtained as colourless crystals melting at 57.5–58° after recrystallising from absolute alcohol:

0.1130 gave 0.3060 CO_2 and 0.0714 H_2O. $C = 73.88$; $H = 7.07$ per cent.

$C_{21}H_{34}O_4$ requires $C = 74.09$; $H = 7.11$ per cent.

3 : 4-Dimethoxyphenylethyl Tertiary Butyl Ketone, $C_6H_3(OCH_3)_2 CH_2CH_2 CO C(CH_3)_3$.——— This compound was obtained as yellow crystals by shaking 34 grams of 4-hydroxy-3-methoxyphenylethyl tertiary butyl ketone with 2.5 c.c. of methyl sulphate and 20 c.c. of a 10 per cent. solution of sodium hydroxide for one hour, and, after standing overnight, they were collected, washed with water and recrystallised three times from dilute alcohol. The crystals thus purified were colourless and melted at 46.5–47.5°:

0.1353 gave 0.3556 CO_2 and 0.1048 H_2O. $C = 71.70$; $H = 8.67$ per cent.

$C_{15}H_{24}O_3$ requires $C = 71.90$; $H = 8.86$ per cent.

The Oxime, $C_6H_3(OCH_3)_2 CH_2CH_2 C(:NOH) C(CH_3)_3$.——— This oxime was obtained, after recrystallising from dilute alcohol, as colourless crystals melting at 114.5–115.5°, half a degree higher than the melting point of its isomer, 3 : 4-dimethoxyphenylethyl isobutyl ketoxime:

0.1750 gave 8.40 c.c. N_2 at 17° and 757 mm. $N = 5.52$ per cent.

$C_{15}H_{23}O_3N$ requires $N = 5.28$ per cent.

The Semicarbazone, $C_6H_3(OCH_3)_2CH_2CH_2C(:NNH CO NH_2) C(CH_3)_3$. ——— The solution of 3 : 4-dimethoxyphenylethyl tertiary butyl ketone (2.5 grams), semicarbazide hydrochloride (1.1 grams) and potassium acetate (1 gram) in dilute alcohol (25 c.c.) was allowed to stand for seven days. After evaporating the alcohol in a vacuum desiccator, the residue was collected, washed with water, dried and recrystallised once from ether and, three times, from dilute alcohol. The colourless crystals thus obtained melted indefinitely between 108 and 126°, and, after being dried at 100° under reduced pressure, at 127–128°:

0.0672 gave 8.15 c.c. N_2 at 19° and 759 mm. $N = 13.86$ per cent.

$C_{16}H_{25}O_3N_3$ requires $N = 13.68$ per cent.

[June 16th, 1924.]

Preparation of Zingerone, 4-Hydroxy-3-methoxyphenyl-ethyl Methyl Ketone.

By

Hiroshi Nomura.

Lapworth and his collaborator[1] have stated that the synthesis of zingerone, $C_6H_3(OH)(OCH_3)CH_2CH_2CO\,CH_3$, by reduction of 4-hydroxy-3-methoxystyryl methyl ketone, $C_6H_3(OH)(OCH_3)CH:CH\,CO\,CH_3$, with sodium amalgam gave a poor yield. As, in the case of the synthesis of its homologues, the reduction of the condensation products of vanillin with methyl ketones by sodium amalgam and water was effected with satisfactory results, an attempt was made to reduce 4-hydroxy-3-methoxy-styryl methyl ketone by the same method. The yield was about 76 per cent. of the theoretical. The reduction was carried out in the following way.

Vanillalacetone (50 grams) suspended in 1 litre of water was introduced into a bottle, and 420 grams of sodium amalgam (3 %) added in small portions with frequent shaking. When the whole of the amalgam was added and bubbles of gas ceased to be given off, the solution was separated from the mercury. On acidifying the solution with 50 c.c. of concentrated hydrochloric acid, zingerone separated as an oil, which was extracted with ether. A small quantity of substance insoluble in the ether which separated in this operation was filtered off and the ethereal extract (A) and the aqueous solution (B) were treated as follows:

(1) Journ. Chem Soc., **111**, (1917), 790.

(A) The ethereal solution was washed several times with a saturated solution of sodium chloride, dried over anhydrous sodium sulphate and evaporated. The residual oil, on distillation, gave 34 grams of a colourless oil boiling at 190.5–191.5°/15.5 mm., which, after crystallisation from a mixture of ether and petroleum ether, melted at 40–41° and produced no lowering of the melting point by mixing with natural zingerone.

(B) After saturation with sodium chloride, the aqueous residue was extracted with ether, and the ethereal solution washed well with a saturated solution of sodium chloride, dried and evaporated. On distillation of the residual oil under reduced pressure, 4.2 grams of a colourless oil boiling at 185.5°/13 mm. were obtained, which melted at 40–41° after recrystallising from a mixture of ether and petroleum ether and produced no depression of the melting point by admixture with the crystals obtained in the above method (A).

[June 16th, 1924.]

Synthesis of a Homologue of Zingerone, 4-Hydroxy-3-methoxyphenylethyl n-Pentyl Ketone.

By

Junkichi Murai.

In the synthesis of some homologues of zingerone, Nomura and Hotta[1] stated that the lower homologues of 4-hydroxy-3-methoxyphenylethyl n-pentyl ketone have a pungent taste similar to that of zingerone, and that the melting points of their benzoyl derivatives and the intermediate products in their synthesis, 4-hydroxy-3-methoxystyryl n-alkyl ketones, lower with the incease of their molecular weight and the melting points of the oximes of methyl derivatives, $C_6H_3(OCH_3)_2CH_2CH_2C(:NOH)R$, in which R contains even carbon atoms, is higher than those immediately succeeding them, with an odd number of carbon atoms in R.

The author synthesised 4-hydroxy-3-methoxyphenylethyl n-pentyl ketone by the same method as its lower homologue, namely, by condensing vanillin with methyl n-pentyl ketone in the presence of an alkali and reducing the product with sodium amalgam and water, and the properties mentioned in the latter, its lower homologue, were also observed in the case of 4-hydroxy-3-methoxystyryl n-pentyl ketone and the corresponding derivatives of its reduction product.

EXPERIMENTAL.

4-Hydroxy-3-methoxystyryl n-Pentyl Ketone, $C_6H_3(OH)(OCH_3)CH:CH\,CO\,C_5H_{11}$.

(1) Preceding paper.

To a mixture of 125 c.c. of a 10 per cent. solution of sodium hydroxide and 125 c.c. of water, 19 grams of vanillin and 15 grams of methyl n-pentyl ketone were added. After shaking seventy hours during eight days, the product was freed from the unchanged methyl n-pentyl ketone by extraction with ether and acidified with hydrochloric acid, when a dark brown oil separated, which was extracted with ether. In order to remove the vanillin, the ethereal solution was shaken with a dilute solution of sodium bisulphite and washed well with water. The dried ethereal solution was evaporated and the residual oil, on rubbing with a glass rod, solidified to a brown mass. The yield was 12.5 grams. It crystallised from a mixture of ether and petroleum ether in faint yellow crystals melting at 50–50 5°:

0.1143 gave 0.3023 CO_2 and 0.0828 H_2O. $C = 72.15$; $H = 8.11$ per cent.

$C_{15}H_{20}O_3$ requires $C = 72.53$; $H = 8.12$ per cent.

4-Hydroxy-3-methoxyphenylethyl n-Pentyl Ketone, $C_6H_3(OH)(OCH_3)CH_2CH_2CO\,C_5H_{11}$.

Seven grams of 4-hydroxy-3-methoxystyryl n-pentyl ketone suspended in 150 c.c. of water were reduced with sodium amalgam (2.5 %) with occasional shaking. The faintly yellow alkaline solution thus obtained was acidified with hydrochloric acid, when an oily product separated, which was extracted with ether. The ethereal extract was several times washed with water, dried and separated. On distillation of the residual oil under 5.5 m.m., 5.5 grams of a colourless oil boiling at 196–197° passed over. When purified by recrystallisation from a mixture of ether and petroleum ether, it separated in colourless crystals melting at 37.5–38°:

0.1097 gave 0.2897 CO_2 and 0.0910 H_2O. $C = 72.05$; $H = 9.28$ per cent.

$C_{15}H_{22}O_3$ requires $C = 71.96$; $H = 8.86$ per cent.

The compound has a pungent taste similar to that of zingerone.

The Benzoyl Derivative, $C_6H_3(OCO\,C_6H_5)(OCH_3)CH_2CH_2CO\,C_5H_{11}$ ——— When 1 gram of 4-hydroxy-3-methoxyphenylethyl n-pentyl ketone was shaken with 25 c.c. of a 10 per cent. caustic soda solution and

2.5 c.c. of benzoyl chloride for one hour, a colourless precipitate separated, which was collected, washed with water and dried. The precipitate, on recrystallisation from absolute alcohol, separated in colourless crystals and melted at 79.5–80°:

0.1138 gave 0.3095 CO_2 and 0.0754 H_2O. $C = 74.16$; H = 7.41 per cent.

$C_{22}H_{26}O_4$ requires $C = 74.54$; $H = 7.40$ per cent.

3 : 4 Dimethoxyphenylethyl n-Pentyl Ketone, $C_6H_3(OCH_3)_2CH_2\,CH_2\,CO\,C_5H_{11}$.

4-Hydroxy-3-methoxyphenylethyl n-penthyl ketone (7 grams) was dissolved in 65 c.c. of a 10 per cent. solution of sodium hydroxide and shaken with 5 c.c. of methyl sulphate for one hour. The product was extracted with ether and the ethereal solution washed with water until free from alkali, dried and evaporated. The residual oil was subjected to fractional distillation under 7 m.m., when an oil (4.9 grams) boiling at 196–199° was collected. On redistilling this fraction, the oil boiled constantly at 192° under 5 m.m.:

0.1114 gave 0.2953 CO_2 and 0.0898 H_2O. $C = 72.29$; $H = 9.02$ per cent.

$C_{16}H_{24}O_3$ requires $C = 72.68$; $H = 9.17$ per cent.

The Oxime, $C_6H_3(OCH_3)_2CH_2CH_2C(:NOH)\,C_5H_{11}$——— A mixture of this ketone (1 gram), hydroxylamine hydrochloride (0.3 gram) and sodium acetate (0.6 gram) was dissolved in dilute alcohol and boiled for two hours. After the removal of the alcohol, the crude oxime was collected and washed well with water. After recrystallising several times from dilute methyl alcohol, it separated in colourless crystals and melted at 97.5–98°:

7.82 mg. gave 0.343 c.c. N_2 at 9° and 760 m.m. $N = 5.25$ per cent.

$C_{16}H_{25}O_3N$ requires $N = 5.02$ per cent.

The author desires to express his thanks to Dr. Hiroshi Nomura, in whose laboratory this investigation was carried out.

[June 19th, 1924].

Synthesis of m-Hydroxyphenylethyl Methyl Ketone and 3-Hydroxy-4-methoxyphenylethyl Ketone (Isozingerone).

By

Junkichi Murai.

Nomura and Nozawa[1] attempted to synthesise m-hydroxyphenylethyl methyl ketone (I) by condensing m-hydroxybenzaldehyde with acetone in the presence of an alkali, and reducing the product catalytically, with the object of examining whether a phenolic ketone, $C_6H_4(OH)CH_2CH_2CO\,CH_3$, having free hydroxyl group in the meta-position of the side chain, $CH_2CH_2CO\,CH_3$, has a pungent taste, but they could not prepare it in sufficient quantity for analysis, because of the poor yield of the condensation product. Of the isomers of zingerone, 3-hydroxy-4-methoxyphenylethyl methyl ketone (II) has not yet been synthesised.

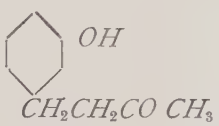

(I)

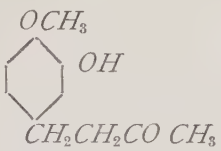

(II)

It would, therefore, be interesting to know whether m-hydroxyphenylethyl methyl ketone and isozingerone are pungent or not.

For the synthesis of the former, m-hydroxystyryl methyl ketone was

(1) Nomura and Nozawa: Sci., Rep., **7**, (1918), 86.

first prepared by the condensation of m-nitrobenzaldehyde with acetone, reduction of the condensation product to the corresponding aminostyryl methyl ketone, and subsequent substitution of the hydroxyl group for its amino group. The intermediate product, 3-hydroxy-4-methoxystyryl methyl ketone, in the latter synthesis, was prepared by condensing isovanillin with acetone in the presence of concentrated hydrochloric acid, since the condensation was difficult as in the case of m-hydroxybenzaldehyde, when sodium hydroxide was used as the condensing agent. The above mentioned two intermediate compounds, m-hydroxystyryl methyl ketone and 3-hydroxy-4-methoxystyryl methyl ketone were readily reduced by water and sodium amalgam to m-hydroxyphenylethyl methyl ketone and 3-hydroxy-4-methoxyphenylethyl methyl ketone (isozingerone) respectively.

As compared the taste of m-hydroxyphenylethyl methyl ketone and isozingerone with that of zingerone, isozingerone was extremely pungent like zingerone, while m-hydroxyphenylethyl methyl ketone was less pungent than isozingerone. It follows, therefore, that the pungency of m-hydroxyphenylethyl methyl ketone is increased by the existence of the methoxy group in the para-position to the side chain, $CH_2CH_2CO\,CH_3$.

EXPERIMENTAL.

Synthesis of m-Hydroxyphenylethyl Methyl Ketone, $C_6H_4(OH)\,CH_2\,CH_2\,CO\,CH_3$.

The starting substance in this synthesis, m-nitrostyryl methyl ketone, was prepared by Vorländer[1] in a similar manner to that employed by Baeyer and his collaborators[2] in the case of its isomers, o-and p-nitrostyryl methyl ketones, namely, by condensing nitrobenzaldehyde with acetone in the presence of an alkali, and then treating the resulting hydroxy-compound, $C_6H_4(NO_2)\,CH(OH)\,CH_2CO\,CH_3$, with acetic anhydride. After examining the condensation under various conditions, the

(1) Vorländer: Ann., **294**, 293.

(2) Baeyer and Becker: Ber, **15**, 2858; Baeyer and Drewsen: Ber., **16**, 1968.

author ultimately synthesised m-nitrostyryl methyl ketone without isolating the intermediate ketol in the following way.

To a solution of m-nitrobenzaldehyde (20 grams) in acetone (200 grams), a mixture of a 10 per cent. solution of sodium hydroxide (20 grams) and water (800 grams) was added in small quantities with frequent shaking. After remaining overnight, two solid substances, which differed in specific gravity from each other, were deposited. The lighter one was first separated by stirring them with the mother liquor, rapidly decanting and pouring off with the liquor, and, then, collected, washed with water, and dried. On recrystallisation from dilute methyl alcohol with the addition of animal charcoal, it separated in faint yellow crystals melting at 94–95° (yield 21 grams).

Vorländer gave 94–95° as its melting point.

In order to prepare m-hydroxystyryl methyl ketone, m-nitrostyryl methyl ketone was first converted into m-aminostyryl methyl ketone by Miller and Rhode's method.[1]

Ten grams of m-nitrostyryl methyl ketone and a solution of ferrous sulphate (90 grams) in water (300 c.c.) were warmed on a water-bath and 50 c.c. of concentrated ammonia slowly run in. The warming was continued for one hour. As the reaction product was weakly acidic, it was made alkaline with a solution of sodium hydroxide and extracted several times with ether. For the purpose of isolation of the basic substance, the ethereal solution was extracted with dilute hydrochloric acid. The acidic solution was well cooled and treated with a solution of sodium nitrite (3 grams) in water (20 c.c.), and, after heating for an hour, and while still hot, a resinous precipitate was filtered off. The cold filtrate was extracted with ether, the ethereal solution washed with water, dried and evaporated. The residue was once crystallised from benzene, when it separated in faint yellow crystals melting at 95–97° (yield 2.8 grams).

Nomura and Nozawa gave 97–98° as its melting point.

---

(1) Miller and Rohde: Ber., **23**, 1885.

Reduction of m-Hydroxystyryl Methyl Ketone.——— m-Hydroxystyryl methyl ketone (6 grams) was suspended in 100 c.c. of water and, to this, 80 grams of sodium amalgam (2.5 %) were added in small quantities and occasionally shaken. After separating the mercury and acidifying carefully with concentrated hydrochloric acid, the precipitate was collected, washed with water, and dried. It crystallised from a mixture of ether and petroleum ether in colourless crystals melting at 85.5–86° and having a slightly pungent taste :

0.1170 gave 0.3133 CO_2 and 0.0784 H_2O $C = 73.05$; $H = 7.50$ per cent.

$C_{10}H_{12}O_2$ requires $C = 73.13$; $H = 7.37$ per cent.

The Benzoyl Derivative, $C_6H_4(OCOC_6H_5)\,CH_2CO_2CO\,CH_3$,——— m-Hydroxyphenylethyl methyl kotone (5.5 grams) dissolved in 45 c.c. of a 10 per cent. solution of caustic soda was shaken with 4.5 c.c. of benzoyl chloride for two hours. The oily product thus separated was extracted with ether, the ethereal extract was washed with water, dried and evaporated. The residual oil was subjected to fractional distillation under diminished pressure, when an oil (6.3 grams) passed over at 220–223°/4.5 m.m.. On repeating the distillation, a colourless oil boiled constantly at 222–223° under the same pressure :

0.1162 gave 0.3243 CO_2 and 0.0635 H_2O $C = 76.12$; $H = 6.12$ per cent.

$C_{17}H_{16}O_3$ requires $C = 76.08$; $H = 6.02$ per cent.

For the preparation of the semicarbazone, $C_6H_4(OCOC_6H_5)\,CH_2\,CH_2C(:N\,NH\,CO\,NH_2)\,CH_3$, the benzoyl derivative (1 gram), sodium acetate (0.6 gram) and semicarbazide hydrochloride (0.4 gram) were dissolved in dilute alcohol and allowed to remain overnight, when a colourless precipitate separated. The precipitate was collected, washed with water and dried. The yield was 1.3 grams. After recrystallising from benzene, it separated in colourless crystals melting at 162–162.5° :

4.90 mg. gave 0.562 c.c. N_2 at 18° and 747 m.m. $N = 12.99$ per cent.

$C_{18}H_{19}O_3N_3$ requires $N = 12.92$ per cent.

Synthesis of Isozingerone, $C_6H_3(OH)(OCH_3)\,CH_2CH_2CO\,CH_3$.

For this synthesis, isovanillin was first synthesised by conversion of piperonal into protocatechuic aldehyde by a slight modification of the process given by Wegscheider[1] and subsequent methylation with methyl iodide.

Fifty six grams of piperonal were heated with 240 grams of phosphorus pentachloride on a salt-bath for three hours and, after standing overnight, 1500 c.c. of water was added and the mixture was boiled for one and a half hours. After cooling, the product was extracted with ether. The ethereal solution was washed with water until free from acid, dried, and evaporated. The residue was recrystallised from xylene, when it separated in grey crystals melting at 152–153° (yield 45.2 grms).

Wegscheider gave 153–154° as its melting point.

In order to prepare isovanillin, the protocatechuic aldehyde thus purified was methylated by Bertram's method.[2]

The condensation of isovanillin with acetone and the subsequent reduction were then carried out in the following way:

Fifteen c.c. of concentrated hydrochloric acid (D. 1.18) were added to a mixture of isovanilin (15 grams) and acetone (80 grams) and left for a week. The product was diluted with water, extracted with ether and the ethereal extract washed with water, dried and evaporated. As the residue (10.1 grams) was difficult to purify, it was suspended in 200 c.c. of water, and reduced with 120 grams of sodium amalgam (2.5 %). After separating the mercury, the alkaline solution was acidified, and extracted with ether. The ethereal solution was washed thoroughly with water dried, and evaporated. The residual oil, on distillation, gave 3.4 grams of an oil boiling at 165–169°/5.5 m.m.. On repeating the distillation, it boiled constantly at 159–160°/4 m.m.. The oil thus purified was almost colourless and analysed with the following results:

0.1126 gave 0.2801 CO_2 and 0.0765 H_2O $C = 67.91$; $H = 7.61$ per cent.

(1) Wegscheider: Monat., **14**, 382.

(2) Bertram: D.R.P., 63007.

$C_{11}H_{14}O_3$ requires $C = 68.00$; $H = 7.27$ per cent.

It has a pungent taste like zingerone.

Benzoylisozingerone, $C_6H_3(OCOC_6H_5)(OCH_3)\,CH_2CH_2CO\,CH_3$——— The above ketone (4 grams) was shaken with 3 c.c. of benzoyl chloride and 30 c.c. of a 10 per cent. solution of caustic soda for two hours. The product was extracted with ether, the ethereal solution washed with water and dried. After evaporating the ether, the residual oil was purified by distillation under diminished pressur, when an oil boiling at 235–237°/4 m.m. (3.2 grams) was obtained. On repeating the operation, an almost colourless oil passed over at 235–236°/4 m.m. :

0.1226 gave 0.3245 CO_2 and 0.0691 H_2O $C = 72.24$; $H = 6.31$ per cent.

$C_{18}H_{18}O_4$ requires $C = 72.45$; $H = 6.09$ per cent.

The Semicarbazone, $C_6H_3(OCO_6H_5)(OCH_3)\,CH_2CH_2C(:N\,NH\,CO\,NH_2)\,CH_3$——— A mixture of the benzoyl derivative (2 grams), sodium acetate (1 gram) and semicarbazide hydrochloride (0.8 gram) was dissolved in dilute alcohol, and allowed to stand overnight. On diluting the product with water, colourless crystals separated, these were collected, washed with water, dried and recrystallised four times from benzene. After being dried at 100° until constant under a diminished pressure of 20 m.m., the substance melted at 140–140.5° and analysed with the following results :

5.00 mg. gave 0.525 N_2 at 20° and 752 m.m. $N = 11.82$ per cent.

$C_{19}H_{21}O_4N_3$ requires $N = 11.83$ per cent.

The author desires to express his thanks to Dr. Hiroshi Nomura, in whose laboratory this investigation was carried out.

[June 30th, 1924.]

Über die (2, 2) deutigen quadratischen Verwandtschaften V.

Von

Tadahiko Kubota.

1. Zerlegung der (2, 2) deutigen quadratischen Punktverwandtschaften.

In den vorigen Mitteiluugen habe ich den folgenden Satz bekommen:

Bezeichnet man die homogenen Punktkoordinaten der einen Ebene mit x_1, x_2, x_3 *und die der anderen Ebene mit* x_1', x_2', x_3', *so kann jede* (2, 2) *deutige quadratische Punktverwandtschaft durch folgendes Gleichungssystem dargestellt werden*:

$$\rho x_1' = L + p\sqrt{S(x_1, x_2, x_3)},\ \rho x_2' = M + q\sqrt{S(x_1,x_2,x_3)}$$
$$\rho x_3' = N + r\sqrt{S(x_1,x_2,x_3)},$$

wobei
$$S = a_1 x_1^2 + a_2 x_2^2 + a_3 x_3^2,$$
$$L = l_1 x_1 + l_2 x_2 + l_3 x_3,$$
$$M = m_1 x_1 + m_2 x_2 + m_3 x_3,$$
$$N = n_1 x_1 + n_2 x_2 + n_3 x_3$$

und p, q, r *Konstanten bedeuten. Sie ist entweder*

$$\rho x_1' = x_1 + p\sqrt{S(x_1,x_2,x_3)},\quad \rho x_2' = x_2 + q\sqrt{S(x_1,x_2,x_3)}$$
$$\rho x_3' = x_3 + r\sqrt{S(x_1,x_2,x_3)}$$

oder
$$\rho x_1' = x_1 + p\sqrt{S(x_1,x_2,x_3)},\quad \rho x_2' = x_2 + q\sqrt{S(x_1,x_2,x_3)},$$
$$\rho x_3' = r\sqrt{S(x_1,x_2,x_3)},$$

wobei
$$S \equiv a_1 x_1^2 + a_2 x_2^2 + a_3 x_3^2 + 2a_{23} x_2 x_3 + 2a_{31} x_3 x_1$$
$$+ 2a_{12} x_1 x_2 = S(x_1,x_2,x_3).$$

Aus diesem Satze herleite ich hier den folgenden Satz:

Jede (2, 2) deutige quadratische Punktverwandtschaft kann als eine zusammengesetzte Verwandtschaft von einer (1, 2) deutigen quadratischen Punktverwandtschaft mit einer (2, 1) deutigen quadratischen Punktverwandtschaft betrachtet werden.

Zuerst diskutieren wir die Verwandtschaft (1). Damit die Umkehrung eindeutig ist, muss eine gewisse Bedingung erfüllt werden. Der Geraden

$$\xi_1 x_1' + \xi_2 x_2' + \xi_3 x_3' = 0$$

entspricht nun

$$(\xi_1 x_1 + \xi_2 x_2 + \xi_3 x_3)^2 - (\xi_1 p + \xi_2 q + \xi_3 r)^2 S = 0.$$

Setzt man

$$x_1 = x_1' + pt, \qquad x_2 = x_2' + qt, \qquad x_3 = x_3' + rt,$$

so erhält man

$$[\xi_1 x_1' + \xi_2 x_2' + \xi_3 x_3' + (\xi_1 p + \xi_2 q + \xi_3 r)t]^2$$
$$-(\xi_1 p + \xi_2 q + \xi_3 r)^2 S(x_1' + pt,\ x_2' + qt,\ x_3' + rt) = 0,$$

d. h.

$$S(x_1', x_2', x_3') + 2S(x_1', x_2', x_3';\ p, q, r)t$$
$$+[S(p, q, r) - 1]t^2 = 0,$$

wobei $S(x_1', x_2', x_3';\ p, q, r)$ die Polarform von S bedeutet.

Damit t eindeutig bestimmbar ist, muss die Bedingung

$$S(p, q, r) - 1 = 0$$

gelten.

Es entsteht nun die Frage, ob die Umkehrung der Verwandtschaft (2) eindeutig sein kann.

Aus den Definitionsgleichungen erhält man

$$\frac{1}{x_1}[rx_1' - px_3'] = \frac{1}{x_2}[rx_2' - qx_3'] = \frac{1}{t}.$$

Nun nehme man die Gerade

$$\xi_1 x_1' + \xi_2 x_2' + \xi_3 x_3' = 0,$$

welche dem Kegelschnitte

$$(\xi_1 x_1 + \xi_2 x_2)^2 - (\xi_1 p + \xi_2 q + \xi_3 r)^2 S = 0$$

entspricht.

Setzt man in die letzte Gieichung

$$x_1 = (rx_1' - px_3')t, \qquad x_2 = (rx_2' - qx_3')t$$

ein, so erhält man

$$\begin{aligned}&[r(\xi_1 x_1' + \xi_2 x_2')t - (\xi_1 p + \xi_2 q)x_3' t]^2\\&-(\xi_1 p + \xi_2 q + \xi_3 r)^2 S(rx_1' - px_3',\ rx_2' - qx_3',\ x_3) = 0,\end{aligned}$$

d. h.

$$\begin{aligned}&[a_{11}(rx_1' - px_3')^2 + 2a_{12}(rx_1' - px_3')(rx_2' - qx_3')\\&+ a_{22}(rx_2' - qx_3')^2 - x_3'^2]t^2\\&+ 2[a_{13}(rx_1' - px_3') + a_{23}(rx_2' - qx_3')]tx_3\\&+ a_{33}x_3^2 = 0,\end{aligned}$$

woraus sich ergibt, dass $a_{33} = 0$ sein muss, damit die Umkehrung eindeutig ist.

Nun nehme man die (2, 1) deutige quadratische Punktverwandtschaft

$$\xi_1 = x_1 + p\sqrt{S(x_1, x_2, x_3)},\ \xi_2 = x_2 + q\sqrt{S(x_1, x_2, x_3)},$$
$$\xi_3 = x_3 + r\sqrt{S(x_1, x_2, x_3)},$$

wobei

$$\begin{aligned}S \equiv\ & a_{11}x_1^2 + a_{22}x_2^2 + a_{33}x_3^2 + 2a_{23}x_2x_3 + 2a_{31}x_3x_1\\&+ 2a_{12}x_1x_2 = S(x_1, x_2, x_3)\end{aligned}$$

und

$$S(p, q, r) = 1$$

Anderseits betrachte man (1, 2) deutige quadratische Verwandtschaft

$$\begin{aligned}x_1' &= \xi_1 S(\xi_1, \xi_2, \xi_3;\ p, q, r),\\x_2' &= \xi_2 S(\xi_1, \xi_2, \xi_3;\ p, q, r),\\x_3' &= S(\xi_1, \xi_2, \xi_3) - k\ S(\xi_1, \xi_2, \xi_3;\ p, q, r)^2.\end{aligned}$$

Setzt man diese Punktverwandtschaft mit der vorigen zusammen, so erhält man

$$\begin{aligned}x_1' &= (x_1 + p\sqrt{S(x_1, x_2, x_3)})(S(x_1, x_2, x_3;\ p, q, r) + S(p, q, r)\sqrt{S(x_1, x_2, x_3)}),\\x_2' &= (x_2 + q\sqrt{S(x_1, x_2, x_3)})(S(x_1, x_2, x_3;\ p, q, r) + S(p, q, r)\sqrt{S(x_1, x_2, x_3)}),\\x_3' &= S(x_1, x_2, x_3) + 2S(x_1, x_2, x_3;\ p, q, r)\sqrt{S(x_1, x_2, x_3)}\\&+ S(p, q, r)S(x_1, x_2, x_3) - k[S(x_1, x_2, x_3;\ p, q, r) + S(p, q, r)\sqrt{S(x_1, x_2, x_3)}]^2,\end{aligned}$$

Da aber $S(p, q, r) = 1$ ist, so erhält man durch Weglassen des gemeinssamen Faktors das folgende Gleichungssystem

$$x_1' = x_1 + p\sqrt{S(x_1, x_2, x_3)}$$
$$x_2' = x_2 + q\sqrt{S(x_1, x_2, x_3)}$$
$$x_3' = (2-k)\sqrt{S(x_1, x_2, x_3)} - k\ S(x_1, x_2, x_3;\ p, q, r).$$

Dies ist die allgemeine (22) deutige quadratische Punktverwandtschaft. Somit ist die Behauptung bewiesen.

Bei der Verwandtschaft

$$x_1' = x_1 + p\sqrt{S(x_1, x_2, x_3)}, \quad x_2' = x_2 + q\sqrt{S(x_1, x_2, x_3)},$$
$$x_3' = x_3 + r\sqrt{S(x_1, x_2, x_3)},$$

entsprechen zwei Punkte $x_1\, x_2\, x_3$ ein und demselben Punkte $x_1'\, x_2'\, x_3'$. Der geometrische Ort der koinzidierenden Punkte $x_1\, x_2\, x_3$, welche einem Punkte $x_1'\, x_2'\, x_3'$ entsprechen, ist

$$S(x_1, x_2, x_3) - S(x_1\, x_2\, x_3;\ p, q, r)^2 = 0 \qquad (3)$$

Wir betrachten nun den Fall, wo der Kegelschnitt

$$S(x_1, x_2, x_3) = 0$$

nicht in zwei Geraden zerfällt. Dann kann man durch geeignete Wahl von Koordinatensystem

$$S \equiv x_1^2 + x_2^2 + x_3^2$$

setzen wenn man in gewissen Fällen imaginäre Transformation ausführt. (3) nimmt in diesem Fall die folgende Form an:

$$(x_1^2 + x_2^2 + x_3^2) - (px_1 + qx_2 + rx_3)^2 = 0 \qquad (4)$$

Deutet man nun x_1, x_2, x_3 als rechtwinklige Koordinaten im Raume an, so wird die Ebene

$$lx_1' + mx_2' + nx_3' = 0$$

dem Kreiskegel

$$(lx_1 + mx_2 + nx_3)^2 - (lp + mq + nr)^2(x_1^2 + x_2^2 + x_3^2) = 0 \qquad (5)$$

entsprechen.

Man kann leicht durch Berechnung beweisen, dass die beiden Kreiskegel (4) und (5) miteinander orthogonal schneiden.

Wenn man die Liebmannsche (1, 2) deutige quadratische Punktverwandtschaft auf die Kugel mit dem Mittelpunkt (0, 0, 0) überträgt und aus dem Mittelpunkt projiziert, so erhält man die obige Verwandtschaft. Dies ist eine andere geometrische Deutung der obigen Verwandtschaft, wenn $S(x_1, x_2, x_3) = 0$ einen nicht-zerfallenden Kegelschnitt bedeutet.

2. Bestimmung aller (2, 2) deutigen involutorischen quadratischen Punktverwandtschaften.

Wenn man zwei Punktfelder auf derselben Ebene betrachtet und auf dasselbe Koordinatensystem bezieht, so entsteht eine Frage, wann unsere (2, 2) deutige quadratische Punktverwandtschaft involutorisch wird.

Durch unsere involutorische Verwandtschaft

$$\rho x_1' = L + p\sqrt{S(x_1, x_2, x_3)}, \quad \rho x_2' = M + q\sqrt{S(x_1, x_2, x_3)},$$
$$\rho x_3' = N + r\sqrt{S(x_1, x_2, x_3)},$$

wobei $S(x_1, x_2, x_3) = 0$ einen nicht-zerfallenden Kegelschnitt bedeutet und zwar

$$S(x_1, x_2, x_3) \equiv x_1^2 + x_2^2 + x_3^2$$

ist, werden alle Geraden in die den Kegelschnitt

$$S(x_1, x_2, x_3) = 0$$

doppelt berührenden Kegelschnitte transformiert und ein den Kegelschnitt

$$S(x_1, x_2, x_3) = 0$$

doppelt berührender Kegelschnitt wird durch unsere Verwandtschaft in zwei Kegelschnitte transformiert, welche den Kegelschnitt

$$S(x_1, x_2, x_3) = 0$$

doppelt berühren.

Deutet man nun $x_1\, x_2\, x_3$ als rechtwinklige Koordinaten im Raume an, so kann man unsere Verwandtschaft beim involutorischen Fall als solche betrachten, bei welcher alle Kreiskegel mit dem Mittelpunkt (0,0,0) in die Kreiskegel mit demselben Mittelpunkt transformiert werden.

Schneidet man dieses Bündel durch die Einheitskugel mit dem Mittelpunkt (0, 0, 0), so erhält man eine Kreisverwandtschaft auf der Kugel. Bekanntlich ist die involutorische Kreisverwandtschaft auf der Ebene entweder eine Inversion oder eine Möbiussche Involution. Gleiches gilt für die involutorische Kreisverwandtschaft auf der Kugel. Dies kann man in folgender Weise beweisen: die Kreisverwandtschaft auf der Kugel mit Erhaltung des Winkelsinnes ist durch

$$z' = \frac{az+b}{cz+d}, \quad ad-bc \neq 0,$$

darstellbar, wobei a, b, c, d komplexe Zahlen bedeuten. Wenn sie involutorisch ist, ist sie durch

$$z' = \frac{az+b}{cz-a} \qquad a^2+bc \neq 0$$

darstellbar. Durch diese Verwandtschaft bleiben die beiden Punkte

$$cz^2-2az-b = 0 \qquad a^2+bc \neq 0$$

ungeändert, welche wir mit P, Q bezeichnen. Die beiden entsprechenden Punkte A, A' und die beiden Punkte P, Q miteinander harmonisch teilen. Daraus kann man leicht zeigen, dass unsere Verwandtschaft aus einer Inversion in Bezug auf einen Kreis, mit dem Durchmesser PQ und aus der Spiegelung in Bezug auf einen Hauptkreis PQ besteht, w. z. b. w.

Auch kann man leicht zeigen, dass die involutorischen Kreisverwandtschaften auf der Kugel mit Umkehrung des Winkelsinnes notwendig eine Inversion ist. Zur Inversion auf der Einheitskugel entspricht auf der projektiven Ebene die involutorische (2, 2) deutige quadratische Punktverwandtschaft

$$\rho x_1' = x_1+p\lambda, \quad \rho x_2' = x_2+q\lambda, \quad \rho x_3' = x_3+r\lambda,$$

wobei $$\lambda = \frac{2}{1-p^2-q^2-r^2}[x_1p+x_2q+x_3r+\sqrt{x_1^2+x_2^2+x_3^2}],$$

d. h.

$$\rho x_1' = x_1+p\lambda, \quad \rho x_2' = x_2+q\lambda, \quad \rho x_3' = x_3+r\lambda,$$

wobei

$$\lambda = \frac{2}{1-a_1p^2-a_2q^2-a_3r^2}[a_1x_1p+a_2x_2q+a_3x_3r+\sqrt{a_1x_1^2+a_2x_2^2+a_3x_3^2}]. \quad (6)$$

Dies ist mit der Verwandtschaft äquivalent, die ich in der ersten Mitteilung S.366 behandelt habe.

Zur Möbiusschen Involution entspricht

$$\rho x_1' = x_1+\frac{2p}{1-p^2-q^2}[x_1p+x_2q+\sqrt{x_1^2+x_2^2+x_3^2}],$$

$$\rho x_2' = x_2 + \frac{2q}{1-p^2-q^2}[x_1 p + x_2 q + \sqrt{x_1^2+x_2^2+x_3^2}],$$

$$\rho x_3' = -x_3,$$

oder $$\rho x_1' = x_1 + \frac{2p}{1-a_1p^2-a_2q^2}[a_1 x_1 p + a_2 x_2 q + \sqrt{a_1 x_1^2 + a_2 x_2^2 + a_3 x_3^2}],$$

$$\rho x_2' = x_2 + \frac{2q}{1-a_1p^2-a_2q^2}[a_1 x_1 p + a_2 x_2 q + \sqrt{a_1 x_1^2 + a_2 x_2^2 + a_3 x_3^2}],$$

$$\rho x_3' = -x_3. \qquad (7)$$

Nun wollen wir den Fall diskutieren, wobei $S(x_1\, x_2\, x_3) = 0$ zwei Geraden darstellt. Man setze

$$S(x_1\, x_2\, x_3) \equiv x_1^2 + x_2^2.$$

Es empfiehlt sich die duale Verwandtschaft zu betrachten.

Bei unserer ursprünglichen Verwandtschaft werden alle die beiden festen Geraden berührenden Kegelschnitte in zwei Kegelschnitte transformiert, welche diese beiden Geraden wieder berühren. Nimmt man bei der dualen Verwandtschaft zwei feste Punkte als Kreispunkte an, so werden alle Kreise in die Kreise transformiert und alle Geraden wieder in die Geraden.

Solcher Transfermation kann man bekanntlich eine Punkttransformation zuordnen lassen, wenn man die Liesche Methode der isotropen Projektion benutzt. Da die obige Verwandtschaft involutorisch und eine Geradentransformation ist, muss die entsprechende Raumtransformation eine Kongruenztransformation sein. Eine involutorische Kollineation, welche den Kugelkreis ungeändert bleiben lässt, muss eine Involution auf dem Kugelkreis definieren. Es gibt also zwei Punkte auf dem Kugelkreis, welche durch unsere Kollineation ungeändert bleiben. Daraus folgert man, dass es mindestens einen Punkt ausserhalb des Kugelkreises auf der unendlich fernen Ebene gibt welcher durch unsere Transformation ungeändert bleibt. Daraus kann man folgern, dass es mindestens eine invariante Gerade gibt, welche keine Minimalgerade ist. Folglich ist unsere Transformation eine Drehung um diese Gerade oder eine Spiegelung in Bezug auf eine Ebene.

Wenn die Kongruenztransformation eine Spiegelung in Bezug auf eine nicht-minimale Ebene ist, so muss die entsprechende Verwandtschaft eine Laguerresche Inversion sein.[1] Die Achse der Laguerreschen Inversion ist die Schnittlinie der Grundebene mit der Spiegelebene. Dies kann man wie folgt ersehen: Die Kreise, welche diese Schnittlinie unter einem gewissen festen Winkel schneiden, bleiben durch unsere Verwandtschaft ungeändert. Alle Punkte dieser Schnittlinie bleiben auch ungeändert. Daraus kann man leicht nachweisen, dass unsere Verwandtschaft notwendig eine Laguerresche Inversion ist.

Wenn die Kongruenztrantformation eine Drehung um eine feste Gerade ist, so muss es in der Ebene zwei feste orentierte Geraden geben, welche durch unsere involutorische Transformationen ungeändert bleiben. Alle orientierten Kreise, welche diese beiden Geraden berühren, bleiben ungeändert. Man betrachte einen Kreis welcher die beiden orientierten Geraden berührt. P, Q seien die beiden Berührungspunkte. Eine Gerade p, welche diesen Kreis berührt, muss durch unsere Verwandtschaft in eine Gerade welche durch den Schnittpunkt von der Geraden PQ und der Geraden p geht und diesen Kreis berührt, transformiert werden. Der Winkelhalbierende des Aussenwinkels der beiden orientierten Geraden sei die Gerade x und der Winkelhalbierende sei y. Dann ist unsere Verwandtschaft eine Laguerresche Inversion, mit der Achse y und mit dem Fundamentalkreise als einem der Kreisen, zusammengesetzt mit der Spiegelung in Bezug auf x.

Nun betrachte man eine duale Verwandtschaft der Laguerreschen Inversion.

Man nehme zwei feste Punkte I und A und einen festen Kegelschnitt. P sei der gegebene Punkt. Nun ziehe man die Gerade PI

(1) Es ist schon von Bateman bemerkt worden, dass die Laguerresche Inversion zur Lorentzschen Transformation in der Relativitätstheorie entspricht Aber es scheint mir nicht stichhaltig zu sein. Denn die Lorentzsche Transformation keine involutorische Verwandtschaft während die Laguerre Inversion eine involutorische Verwandtschaft ist. Um die beiden Verwandtschaften äquivalent zu machen muss man zur Laguerreschen Inversion die Richtungsumkehrung der gerichteten Kreise kombimert werden, Vgl. H. Bateman, American Tourn. of Math. 34, 1912.

welche den gegebenen Punkt P mit dem festen Punkt I verbindet und schneide den Kegelschnitt dadurch in den Punkten M, N. Dann verbinde man AM, AN sodass sie den Kegelschnitt wieder in den Punkten M' N' schneiden. Dann verbinde man IM' IN' und schneide dadurch die Gerade PA in den Punkten Q_1, Q_2. Lässt man sich die Punkte Q_1 Q_2 zum Punkte P beziehen, so erhält man unsere Verwandtschaft.

Die Gleichung des Kegelschnitts sei

$$r^2(a_1 x_1^2 + a_2 x_2^2) + x_3^2 = 0.$$

Die Koordinaten des Punktes I und des Punktes A seien bezw. (001) und $(p\ q\ r)$. Bezeichnet man die Koordinaten des Punktes mit $x_1\ x_2\ x_3$, dann sind die Koordinaten der Punkte M, N

$$x_1 \qquad x_2 \qquad \pm r\sqrt{a_1 x_1^2 + a_2 x^2}.$$

Nun verbinde man die Geraden AM, AN, dann sind die Koordinaten dieser beiden Schnittpunkte M' N'

$$kp + x_1, \qquad kq + x_2 \qquad kr \pm r\sqrt{a_1 x_1^2 + a_2 x_2^2},$$

wobei k die folgende Relation erfüllt;

$$k^2[r^2(a_1 p^2 + a_2 q^2) - r^2]$$
$$+ 2k[r^2(a_1 p x_1 + a_2 q x_2) \pm r^2\sqrt{a_1 x_1^2 + a_2 x_2^2}] = 0,$$

d. h.
$$k = \frac{2}{1 - a_1 p^2 - a_2 q^2}[a_1 p x_1 + a_2 q x_2 + \sqrt{a_1 x_1^2 + a_2 x_2^2}].$$

Folglich erhält man als unsere Verwandtschaft

$$x_1' = x_1 + \frac{2p}{1 - a_1 p^2 - a_2 q^2}[a_1 p x_1 + a_2 q x_2 + \sqrt{a_1 x_1^2 + a_2 x_2^2}],$$

$$x_2' = x_2 + \frac{2q}{1 - a_1 p^2 - a_2 q^2}[a_1 p x_1 + a_2 q x_2 + \sqrt{a_1 x_1^2 + a_2 x_2^2}],$$

$$x_3' = x_3 + \frac{2r}{1 - a_1 p^2 - a_2 q^2}[a_1 p x_1 + a_2 q x_2 + \sqrt{a_1 x_1^2 + a_2 x_2^2}]. \quad (8)$$

Nun wollen wir die involutorische Verwandtschaft bestimmen, welche der zusammengesetzten Verwandtschaft von der Laguerreschen Inversion mit einer gewissen Spiegelung entspricht.

Die Polargerade des Punktes I(100) in Bezug auf diesen Kegelschnitt ist $x_3 = 0$ und die Polargerade des Punktes $(p,\ q,\ r)$ ist

$$r^2(a_1 p x_1 + a_2 q x_2) - r x_3 = 0.$$

Der Schnittpunkt der beiden Geraden ist der Pol H der Geraden AI mit den Koordinaten

$$-a_2 q, \quad a_1 p, \quad 0.$$

Die Verbindungsgerade AI ist

$$q x_1 - p x_2 = 0.$$

Nun verbinde man O mit H und schneide die Gerade AI im Punkte K und bestimme auf dieser Geraden den Punkt Q' derart dass Q, Q' die Punkte H, K harmonisch teilen.

Die Verwandtschaft welche den Punkt P sich dem Punkte Q beziehen lässt, ist durch

$$\begin{aligned} \rho x_1' &= (a_1 p^2 - a_2 q^2) x_1 + 2 a_2 p q x_2, \\ \rho x_2' &= 2 a_1 p q x_1 - (a_1 p^2 - a_2 q^2) x_2, \\ \rho x_3' &= (a_1 p^2 + a_2 q^2) x_3, \end{aligned} \tag{9}$$

darstellbar.

Durch Zusammensetzung der Verwandtschaften (8) und (9) erhält man

$$\begin{aligned} \rho x_1' &= (a_1 p^2 - a_2 q^2) x_1 + 2 a_2 p q x_2 \\ &\quad + \frac{2p(a_1 p^2 + a_2 q^2)}{1 - a_1 p^2 - a_2 q^2} [a_1 p x_1 + a_2 q x_2 + \sqrt{a_1 x_1^2 + a_2 x_2^2}], \\ \rho x_2' &= 2 a_1 p q x_1 - (a_1 p^2 - a_2 q^2) x_2 \\ &\quad + \frac{2q(a_1 p^2 + a_2 q^2)}{1 - a_1 p^2 - a_2 q^2} [a_1 p x_1 + a_2 q x_2 + \sqrt{a_1 x_1^2 + a_2 x_2^2}], \\ \rho x_3' &= (a_1 p^2 + a_2 q^2) x_3 \\ &\quad + \frac{2r(a_1 p^2 + a_2 q^2)}{1 - a_1 p^2 - a_2 q^2} [a_1 p x_1 + a_2 q x_2 + \sqrt{a_1 x_1^2 + a_2 x_2^2}]. \end{aligned} \tag{10}$$

Folglich erhält man den Satz:

Es gibt vier Typen (6) (7) (8) (10) der involutorischen quadratischen (2, 2) deutigen Punktverwandtschaften, deren geometrische Erzeugung ich in diesem Kapitel ausführlich diskutiert habe.

Korrektur zur ersten Mitteilung, These Reports Vol. 6 S.360; man streiche vom siebten Zeile bis zu den neuten Zeile "Alle..... werden" aus. Alle audere Teile bleiben ungeändert,

On the Formation of Martensite in Carbon Steels.[1]

By

Kôtarô Honda.

§ 1. NATURE OF THE A_1 TRANSFORMATION.

Five years ago, the present writer[2] first advanced the theory that the A_1 transformation in carbon steels consists of double or stepped changes, that is,

austenite → martensite → pearlite ;

he has also remarked on several occasions[3] that a large number of observed facts are explained quite satisfactorily by the above theory. Moreover the recent progress in X-ray analysis has established conclusively the correctness of the theory. The present paper deals with the A_1 transformation as viewed in the light of the X-ray analysis and aims at explaining the formation of martensite by quenching.

The Ar_1 transformation is a change from austenite to pearlite, that is, from a solid solution of carbon in iron to a mixture of iron and cementite. By means of the X-ray analysis, it is confirmed that, as

---

(1) The one hundred and third report of the Research Institute of Iron, Steel and Other Metals.

(2) Sci. Rep., **8**, (1919), 181.

(3) Honda and Idei, Sci. Rep., **9**, (1920), 491 ; Honda, Matsushita and Idei, Journ. Iron and Steel Inst., No. 1, (1921); N. Yamada, Sci. Rep., **10**, (1921), 453; Honda, Sci. Rep, **11**, (1922), 19; Trans. of A. S. S. T., Oct. (1923), 450.

(4) Westgren, Journ. Iron and Steel Inst., No. 1, (1921); No. 1 (1922); E. Bain, Chem. & Metallur. Eng., **25**, (1921), 663.

regards iron atoms, the austenite has a face-centred cubic lattice and the martensite a body-centred one as in the case of ferrite, carbon being present in the interspace of these lattices. This is a confirmation of the well-established view that austenite is a solid solution of carbon in γ-iron and martensite one of carbon in α-iron. Then the A_1 transformation consists of two changes :—

(1) The change of the atomic configuration of iron from the face-centred to the body-centred ;

(2) The separation of carbon atoms from the interspace of the lattice as cementite.

These two different processes take place very probably in succession, but not simultaneously ; because in a natural phenomenon it is very difficult to consider two different processes as taking place exactly at the same instant. Admitting that these two processes (1) and (2) take place in succession, the next question is which of the changes (1)→(2) or (2)→(1) is more probable ? The answer is obviously the change (1)→(2). For, if the change in the atomic configuration of the iron from the face-centred to the body-centred lattice is completed, the product is the α-iron dissolving carbon, but α-iron being unable to dissolve so much carbon, most of the carbon is precipitated as cementite. Hence if the first change takes place first, the second one must follow as a necessary consequence ; that is, the order of the changes (1)→(2) is very probable. On the other hand, the second change (2) cannot occur at the first step ; because as the γ-iron has the property of dissolving so much carbon in it, it is very unreasonable to assume the sudden separation of the carbon to occur first without any change of the atomic configuration.

If the above view regarding the order of the succesive changes is assumed to be correct, the process of the A_1 transformation, that is,

austenite → pearlite

consists in :—

γ-iron dissolving carbon → α-iron dissolving carbon → ferrite + Fe_3C,

or

austenite → martensite → pearlite.

That is, the A_1 transformation in process consists of double or stepped changes, as we have already remarked. Thus the correctness of the stepped change is proved.

From the above consideration, the first change of the A_1 transformation is in reality the A_3 transformation, and hence the heat of this transformation, austenite → martensite, must be equal to that of the A_3 transformation in pure iron, a small allowance being made for the presence of the dissolved carbon atoms. Meuthen[1] found by a careful experiment the heat of A_3 transformation in pure iron to be 5.6 calories; while Mr. N. Yamada measured directly the heat of the transformation, austenite → martensite, for a eutectoid steel and found it to be 5.7 calories per gram of iron. The agreement between these two is thus very satisfactory.

§ 2. FORMATION OF MARTENSITE.

As we have shown, the A_1 transformation consists of the changes

austenite → martensite → pearlite.

This way of considering the A_1 transformation does not in the least interfere with the principle of the phase rule; because in the case of equilibrium, for which this rule is only applicable, the martensite is passed over and does not appear at all.

During a slow cooling, at the A_1 point, austenite first changes into martensite, and the latter changes immediately into pearlite, the result being the same as

austenite → pearlite.

During a very rapid cooling, such as quenching in water, the change from austenite to martensite is so far retarded that it begins to take place at a temperature below 300°C, and when this change is completed, the specimen which is subjected to this treatment is nearly at room temperature, and hence the second change from martensite to pearlite

(1) Ferrum, Jahrg. **11**, (1913), 1.

cannot take place, owing to the great viscosity of the specimen at room temperature. Thus martensite can be obtained by quenching the steel in water.

Since during cooling, the change from austenite to pearlite always occurs through an intermediate step—martensite—, it is naturally assumed that during heating, the A_1 transformation, that is, the change from pearlite to austenite takes place through martensite, unless some contradictory facts are found.

According to the above view of quenching, the perfect hardening is obtained, when the first change in the stepped transformation, austenite → martensite, is completed and the second change, martensite → pearlite, is completely suppressed. In the case of a less rapid cooling, the first change occurs at temperature a little higher than in the above case, and therefore the second change partly takes place resulting in a martensitic structure mixed with troostite. Professor C. Benedicks' view that troostite is a dispersed system in which cementite is suspended in iron as very fine colloidal particles, is now generally accepted, and hence troostite is a mechanical mixture of cementite and iron, and does not differ in its nature from pearlite. Hence forward for brevity we shall call the troostite (and sorbite) by the name pearlite. Since the hardness H of austenite, martensite and pearlite satisfy the following relation

$$H_{aust.} < H_{mart.} > H_{pearl.},$$

the hardness of martensite mixed with troostite or pearlite is less than that of pure martensite. This is a case of imperfect hardening.

In the case of an extremely rapid cooling, not only is the second change completely suppressed, but the first change is also partially arrested. We then obtain a martensitic structure mixed with austenite, the hardness of which is also less than that of pure martensite. This is a case of a too severe quenching. In such a case, however, a little tempering at a temperature below 100° C, which accelerates the change of the remaining austenite into martensite, increases its hardness by a

small amount. That in a severely quenched steel, the austenite is present mixed with martensite, is actually confirmed by the X-ray analysis.

It is a well-known fact that in plain carbon steels, martensite can easily be obtained by quenching, but it is very difficult to obtain pure austenite by this means. This is easily understood from the fact that the first change, austenite → martensite consists in the change of atomic configuration, while the second change, martensite → pearlite, is connected with the diffusion of carbon atoms through iron, so that the former change can take place even at low temperatures, but the latter cannot occur at room temperature. We thus see the reason why the pure austenitic structure is very difficult to arrest, while martensite can easily be obtained.

In a previous paper,[1] Dr. T. Matsushita has shown that in carbon steels, there are two kinds of martensites α and β, the α-form being more easily etched than the β form. During a slow heating of a quenched steel, α and β martensites are tempered at about 180° and 330° respectively. Since these martensites have both a body-centred cubic lattice as regards the iron atoms, the difference between them consists very probably in the mode of distribution of the carbon atoms within the space-lattice of the iron atoms. Professor Hanemann in Berlin attributes the difference to that of the concentration of carbon in martensite. In ordinary steels, the concentration of carbon atoms is 1 in 50–150 atoms of iron; since in austenite, these carbon atoms are uniformly distributed throughout the lattice of the iron atoms, it is very difficult to conceive in what way the martensites which have only two different concentrations of carbon, are produced during the rapid cooling, and therefore the present writer does not agree with the view of Professor Hanemann.

In the case of special steels, the velocity of the A_1 transformation becomes very small as compared with that in ordinary steels by virtue of the presence of other elements; hence even at the ordinary rate

(1) Sci. Rep., **7**, (1918), 43.

of cooling, the change, martensite → pearlite, may be arrested, so that we obtain the martensitic structure at room temperature. This is a case of a self-hardening steel.

§ 3. ORIGIN OF THE GREAT HARDNESS OF MARTENSITE.

Since the configuration of the iron atoms in martensite is the same as that in α-iron, the question naturally arises why the carbon atoms in the interspace of the iron lattice give rise to such a great hardness as compared with that of α-iron. The following explanation is probably not far from the actual mechanism of the hardening.

The distribution of the carbon atoms in the martensite has not yet been confirmed by X-ray analysis, but theoretically considered, these atoms cannot approach too near to iron atoms in virtue of the repulsive force coming into play between the two kinds of atoms when they approach very near together; also they must take a symmetrical position in relation to the iron atoms. Hence in order to satisfy these two conditions, the carbon atoms in martensite may take positions in the centre of the face of an elementary cube, distributed here and there according to the law of probability. A local distortion of the lattice may of course result. These carbon atoms will send their lines of force toward six neighbouring atoms and themselves behave like diagonal supporters in a square frame-work, thus giving to the lattice-building a great strength as a whole.

Fig. 1.

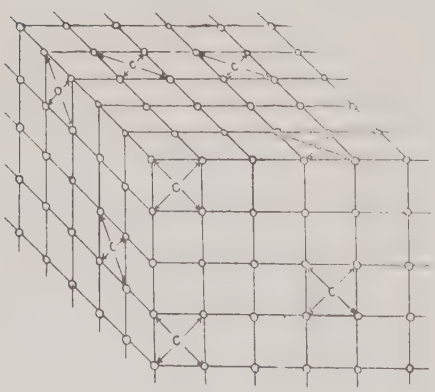

From the above consideration the strength of martensite must increase with the concentration of carbon. This fact is confirmed by experiments as far as a medium carbon steel is concerned. In higher carbon concentra-

tions, the presence of austenite intermingled with martensite causes a decrease of hardnuss. Again, in a complete quenching, the size of the martensite crystals increases with carbon content and consequently causes a decrease of hardness in high carbon steels. These two factors will very probably explain the apparent deviation in high carbon steels from the above theoretical deduction.

If the above view with respect to the positions of the carbon atoms be correct, carbon atoms in the interspace of the lattice cannot produce any interference lines in the X-ray spectrum, for they are distributed quite arbitrarily in space. This conclusion is also actually confirmed by experiments; hence we cannot hope to find the position of the carbon atoms in the iron-lattice by means of the X-ray analysis, however much technics may be improved.

It may be remarked that by quenching iron-nickel alloys containing about 15 to 30 percent of nickel from the austenitic region into water or liquid air, a martensitic structure is obtained, and the hardness greatly increases, though no appreciable content of carbon is present. This is also explained in the same way as in the case of carbon steels. Above the A_3 line, iron atoms assume the distribution of a face-centred cube, some of them being replaced by nickel atoms according to the concentration, but below this line, they take that of a body-centred cube; the sides of the unit cubes in these two cases have a ratio of about 1.3. By quenching the alloys from the austenitic region into water or liquid air, the lattice changes, as a whole, from the face-centred cube to the body-centred, but owing to the very rapid cooling, some of the nickel atoms may not have a sufficient time to assume their proper position and may remain in the centre of the face of the body-centred cube and play the part of carbon atoms in the martensite of carbon steels, thus giving to the alloys a great strength or great hardness.

The great hardness observable in martensitic nickel steels containing carbon requires no farther explanation.

One important point to be noticed is the diffusion of the X-ray spectrum lines of martensite. This is usually explained by assuming that

each individual needle-shaped crystal consists of a very large number of minute crystals orientated at random, their linear dimensions containing only several hundreds of atoms. That explanation does not, however, agree well with the result of microscopic observation, but the following new explanation would very probably express the actual fact.

Owing to a very rapid cooling, the martensite structure is undergoing a great internal stress; a number of martensitic crystals are in a state of tension and numbers of others in a state of compression (not only hydrostatic tension or compression, but also simple tension or compression), their intensities varying from crystals to crystals. Shear being considered as made up of tension and compression, does not require a special consideration. Hence in certain groups of crystals the lattice distance increases in one direction and decreases in the perpendicular direction, and in other groups it is uniformly increased or decreased; the amount of these changes depends on the intensity of stress, being of the order of $\frac{1}{1000}$ of the lattice distance. There are also many groups of crystals whose lattice constant remains unchanged. These micro-strains are probably distributed uniformly throughout the mass of the quenched steel. When such an aggregate of microcrystals is examined by the X-ray, it is to be expected that the spectral lines will be of a diffused nature. Thus the diffusion of the spectral lines is satisfactorily explained by the deformation of the space-lattice by stress, there being no need of assuning a very finely dispersed structure in the martensite crystals.

On the Equilibrium Diagram of the Iron-Carbon-Nickel System.[1]

By

Tsutom Kase.

With 12 Plates.

CONTENTS.

§ 1. Introduction.

§ 2. Binary System of Iron-Nickel.

(1) Thermal analysis.
(2) Polymorphic change in solid state.
(3) Hardness and micro-structures.
(4) Diagram of iron-nickel system.
(5) A_3 points of iron-nickel alloys.

§ 3. Binary System of Nickel-Carbon.

(1) Thermal analysis.
(2) Nickel carbide.

§ 4. Ternary System of Iron-Carbon-Nickel.

(1) Thermal analysis.
(2) Combined or dissolved carbon in iron-carbon-nickel alloys.
(3) Effect of nickel on the A_0 transformation.
(4) Effect of nickel on the A_1 transformation.
(5) Effect of nickel on the A_2 transformation.
(6) Merging of A_1 and A_3 points in iron-carbon-nickel alloys.
(7) Structural diagram of iron-carbon-nickel alloys.
(8) Equilibrium diagram of iron-carbon-nickel system.
(9) Microscopic investigation.

Summary.

(1) The one hundred and fourth report from the Research Institute for Iron, Steel and Other Metals.

§ 1. INTRODUCTION.

Owing to the industrial importance, many papers have been published regarding the nickel steels; but there is as yet no systematic study on the ternary alloys of iron-carbon-nickel system. The present investigation was undertaken to get the equilibrium diagram of the ternary system by means of thermal and magnetic analyses, as well as microscopic and dilatometric methods and to shed further light on the ternary system.

§ 2. BINARY SYSTEM OF IRON-NICKEL.

The binary system, iron-nickel, has been investigated by many authors; among them R. Ruer and E. Schütz,[1] D. Hanson and H. Hanson[2] are specially to be mentioned. While the present paper was being prepared, works on similar subjects by S. Iguchi,[3] D. Hanson and J. Freeman[4] were pulished. At the beginning of the investigation of the ternary system, iron-carbon-nickel, the present writer studied the binary alloys of the iron-nickel system. The iron used in the present investigation was a comparatively pure wrought iron, "Hōchōtetsu." The nickel used to alloy with the iron was a commercial shot nickel. The results of the analysis are given in the following table:—

Material	C (%)	Si (%)	Mn (%)	P (%)	S (%)	Fe (%)
Hōchōtetsu	0.054	0.188	0.015	0.065	0.008	
Shot nickel	0.043	—	0.179	—	—	0.153

(1) Metallurgie, **7**, (1910), 415.
(2) Journ. Iron and Steel Inst., No. II, (1920), 39.
(3) Suiyōkaishi (A Japanese Journal of Metallurgy), **4**, (1922), 1.
(4) Journ. Iron and steel Inst., No. I, (1923), 301.

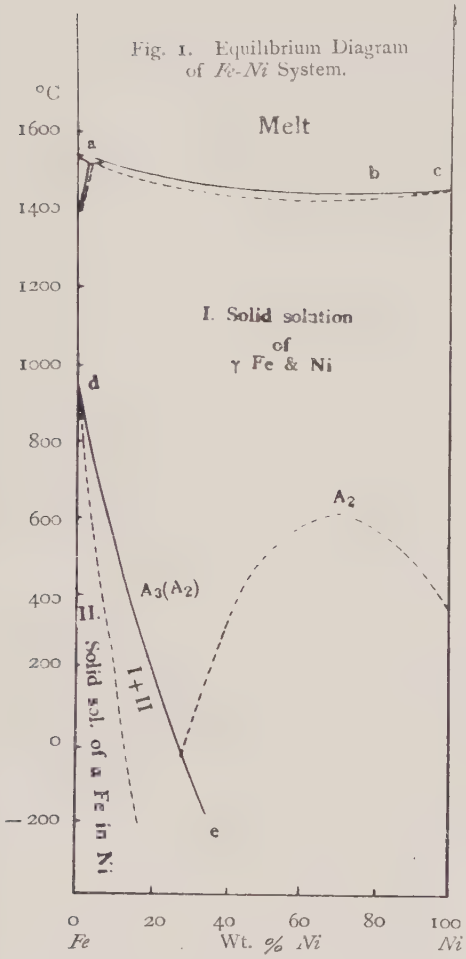

Fig. 1. Equilibrium Diagram of *Fe-Ni* System.

(1) Thermal Analysis.

The metals taken in each experiment were 25 grs. A small kryptol furnace used by the present writer was constructed with two white fire bricks with a hole bored in the centre, filled with a quantity of kryptol, and a porcelain melting tube was set vertically in it. The temperature reading during cooling was taken in every 5 seconds with Le Chatelier's thermo-element with a millivoltmeter. The thermo-element was calibrated with the melting point of tin (231.°9), antimony (630.°6), copper (1083.°0), and nickel (1448°). The melting point of nickel was taken as 1448° C by an extrapolation referred to in the report of the Bureau of Standards of America.

The results of the exepriments are tabulated in Table I; some of the cooling curves are given in Fig. 20, Pl. I, and the equilibrium diagram of iron-nickel system in Fig. 1 (curve a b c.).[1]

(1) The vicinity of the iron side was not thoroughly studied by the present writer, and is referred to the results of D. Hanson and J. Freeman. loc. cit.

TABLE I.

Alloys.	Wt. % of Nickel		Temperature of Arrests (°C)			Remarks
	Cal.	Anal.	First arrest		Second arrest	
			Beginning	Ending		supercooling (°C)
No. 1	0	—	1522		1400	10
2	4	3.72	1516			6
3	6	5.98	1514			8
4	8	7.96	1504	1492		5
5	10	10.90	1493	1480		8
6	20	19.10	1468	1455		13
7	30	29.13	1460	1433		4
8	40	39.23	1448	1436		2
9	50	49.68	1441	1432		14
10	60	60.24	1437	1430		28
11	70	69.36	1434	1431		5
12	80	79.17	1438	1425		18
13	90	90.11	1447	1437		28
14		99.63	1448			7

The liquidus curve *abc* has no discontinuity, but a minimum at 1434° C and about 70 % of nickel. As remarked by Ruer and Shütz, in alloys containing more than 10 % of nickel no break is observable except those due to solidification as shown in Fig. 20, Pl. I. The solidus was determined from the intersection of two tangents drawn on both sides of the change point.

(2) Polymorphic Change in Solid Phase.

In the solid phase, the iron-nickel alloys show polymorphic change. This change was determined by magnetic analysis as well as by differential thermal analysis; the former method was used for all alloys in this system, and the latter for those containing less than 22 percent of nickel. The specimens used for the magnetic analysis were 7 cm. long and 5 mm. thick, as usually employed in our laboratory. The results of the magnetic analysis are shown in Table II, and some of the curves in Fig. 21, Pl. II. In Table II, Ac_2 and Ar_2 show the ending and beginning points of the ferro-magnetic property of the alloys on heating and cooling respectively.

TABLE II.

Alloys	Wt. % of *Ni*		Ac_2 (°C)	Ar_2 (°C)
	Cal.	Anal.		
No. 1	0	—	795	778
2	2	2.41	785	760
3	4	3.89	780	695
4	6	6.35	770	625
5	8	8.04	750	550
6	10	9.93	738	480
7	15	15.21	680	290
8	20	20.20	650	220
9	25	26.36	585	80
10	30	30.25	115(450)*	105(105)*
11	40	39.81	375	350
12	50	49.95	525	490
13	60	58.95	615	570
14	70	69.16	625	600
15	80	78.29	595	550
16	90	88.75	490	475
17		99.62	370	335

(* Quenched in liquid air.)

According to the recent investigation of iron-nickel alloys by X-ray analysis,[1] those containing less than 20 % of nickel have a body centred cubic lattice, and those containing 20 to 30 per cent of nickel consist of two kinds of cubic lattices, body-centred and face-centred, while those containing more than 30 % of nickel have all a face centred cubic lattice alone. In an incomplete equilibrium condition, iron-nickel alloys will contain heterogeneous portions consiting of different concentrations. Thus the magnetic intensity of the chill cast specimen is somewhat

(1) Phys. Rev., **21**, (1923), 402.

less than that of the same specimen annealed, as shown in Fig. 21 curve (2), a and b, Pl. II. This is attributed to the presence of a small quantity of γ solid solution in the former. As the temperature is raised, it changes into α solid solution increasing the magnetic intensity. In annealed specimens, however, this change is not observable in low nickel alloys, containing 4 to 10 per cent of nickel (Fig. 21 (2)–(5), Pl. II); but it is observable as before in high nickel alloys. As the nickel content increases, the Ar_3 (Ar_2) point is gradually lowered and the velocity of the transformation decreases; hence it contains some quantity of the γ solid solution even by a normal cooling. As shown in Fig. 21, (6)–(7), Pl. II, alloys containing 15 to 20 per cent of nickel show the heating curves of the same type as those of the chill cast specimens. As the nickel content further increases, the above phenomenon is invisible, owing to the lowering of the A_3 transformation below the room temperature.

The differential thermal analysis was carried out in the usual way. The heating and cooling curves are given in Fig. 22, (a)–(b), Pl. III, and the transformation points are given in Table III. The Ac_2 and Ar_2 points were taken at the ending or beginning of the heat effect, and Ac_3 and Ar_3 the beginning points of the transformations, as specified with arrows in Fig. 22, (a) (1) and (b) (1), Pl. III.

TABLE III.

Alloys	Wt. % of Nickel		Ac_2 (°C)	Ar_2 (°C)	Ac_3 (°C)	Ar_3 (°C)
	Cal.	Anal.				
No. 1	0	—	800	775	910	890
2	1	—	790	770	870	840
3	2	1.97	790	745	860	790
4	4	3.84	785	700	810	730
5	6	6.11	735	645	760	670
6	8	8.40	730	570	740	610
7	10				710	520
8	15	15.93			650	325
9	20	21.37			620	200
10	27				—	—

The results above mentioned for Ar_3 points are plotted in curve de, Fig. 1. The alloys containing nickel less than 34 per cent are called irreversible alloys. These alloys show a considerable temperature hysteresis during heating and cooling. The cause of this fact has been already explained by Prof. K. Honda and Mr. H. Takagi.[1]

(3) Hardness and Microstructures.

The specimens used for thermal analysis were grinded and polished on two opposite lateral sides and examined microscopically; their hardness was also measured with Shore's scleroscope. The results are shown in Table IV and Fig. 2, (a), (b).

TABLE IV.

Alloys	Wt. % of Nickel		Microstructures	Hardness No.
	Cal.	Anal.		
No. 1	0	—	F *	14
2	2	—	F	14
3	4	3.72	F	17
4	6	5.98	F	18
5	8	7.96	M	19
6	10	10.90	M	20
7	12	12.45	M	34
8	15	15.21	M	36
9	20	19.10	A—M	40
10	25		A—M	30
11	30	29.13	A—M	19
12	40	39.23	A	15
13	50	49.68	A	12
14	60	60.24	A	12
15	70	69.36	A	12
16	80	79.17	A	11
17	90	90.11	A	10
18		99.62	A	9

(* F=Ferrite, M—T=Martensite-Troostite, M=Martensite, A—M=Austenite-Martensite, A=Austenite.)

(1) Sci. Rep. **6**, (1918), 324.

From the figure, we see that the maximum hardness lies between 15 to 20 per cent of nickel. The structure of these alloys having an abnormally high hardness is martensitic. Thus the cause of the high hardness is evident, and there is no necessity to assume any compound between iron and nickel, as proposed by some of the previous investigators. It is here to be noticed that in the case of iron-nickel alloys containing no carbon, the martensitic structure is obtained. D. Hanson and his co-workers proposed a diagram showing the plessite as a eutectoid consisting of camacite and taenite. On this point, some discussion will be given below.

Fig. 2. (a) Hardness of *Fe-Ni* Alloys.
(b) Concentration-structure Diagram of the same Alloys.
(Normally coold from the melt.)

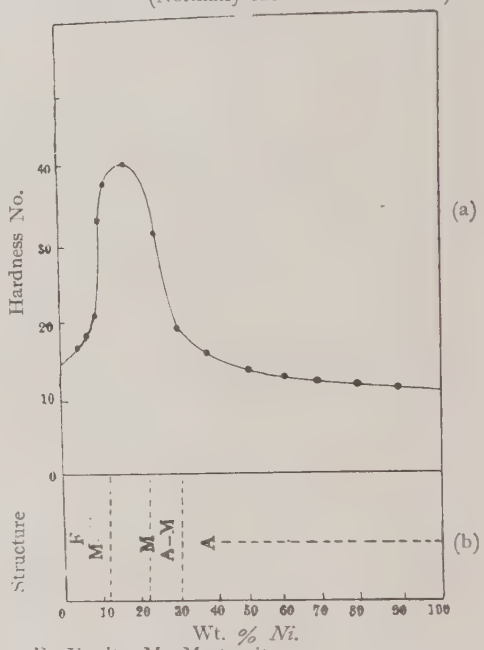

F=Ferrite, M=Martensite,
A–M=Austenite-Martensite,
A=Austenite.

(4) Diagrams of Iron-Nickel System.

Two types of equilibrium diagrams of the iron-nickel system are known. One of these is the eutectoid type,[1] and the other the continuous solid solution type. In support of the first type of diagram, Benedicks pointed out that in the iron-nickel alloy containing 11.70 % of nickel and showing the Widmannstätten structure of a single grain, no granulation occurs at 350° C, but it does decidedly at 490° C.

D. Hanson and H. Hanson[2] also tried to confirm the above view.

(1) Osmond and Cartaud:—Revue de Métallurgie, 1. (1904), 69.
(2) Journ. Iron and Steel Inst., No. II, (1920), 39.

By means of thermal analysis and electric resistance method, no indication of the eutectoid point was observable during a very slow cooling. They also examined the microstructures of the alloys quenched in the course of heating and cooling, and found that in these alloys containing less than 8 per cent of nickel, there is a confined domain giving the mixtures of martensite and ferrite. Further, in the alloys containing 9–30 % of nickel they obtained duplex structures by a prolonged annealing and quenching from about 340° C, and concluded that this fact is a confirmation of the diagram of the eutectoid type as shown in Fig. 3. In this diagram, however, the A_2 curve lying between 30 to 100 percent of nickel does not show any change of phase, like the A_2 point in iron, and hence it should not be included in the equilibrium diagram giving the change of phases; only the lowering of the A_3 point is properly to be taken into consideration.

Fig. 3. *Fe-Ni* Diagram.
(D. Hanson & H. Hanson.)

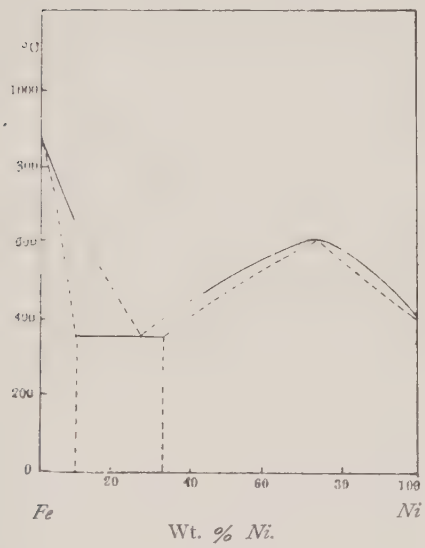

The present writer also investigated the equilibrium diagram of the same system. The stability of the Widmannstätten structure[1] or martensitic structure is available for determination of the said domains on the iron-nickel diagram. Hence, alloys containing 0, 2, 4, 6. 8, 10, 12, 15, 20, 25, 30, 40,.....% of nickel were prepared by chill casting and annealed in vacuum at certain temperatures, quenched in water or cooled in the furnace, and then their microstructures were examined. The results are shown in Table V.

(1) The Widmannstätten structure is considered as that consisting of the regular octahedral cleavages, and is not generally homogeneous; but the martensitic structure is a homogeneous α solid solution. In some cases, these two structures are not easily distinguishable and hence the words "Widmannstätten or martensite is sometimes used.

TABLE V.

Experiments	Wt. % of *Ni*	Annealing temperature (°C)	Annealing time (hours)	Mode of cooling and micro-structure
				Quenched in water.
No. 1	0–30	600	100	No distinct change.
				Quenched in water.
2	<8	890	36	—
	8–25	„	„	Wid. str.
	$\geqq 30$	„	„	Homogeneous austenite.
3				Quenched in water.
	0–25	1000	30	Distinct Wid. str.
	$\geqq 30$	1050	20	Homogeneous austenite.
4				Cooled in the furnace in 3 hours.
	$\leqq 10$	1100	100	Homogeneous α solid solution (ferrite).
	12	„	„	Wid. str., partially decomposed.
	12–25	„	„	Wid. str.
	25	„	„	Wid. str., clearly.
	$\geqq 30$	„	„	Homogeneous austenite.

Thus by long annealing at high temperature (above Ac_3) the grain growth of the alloys takes place, resulting in the characteristic structures by quenching (see Photogr. 4, 5.). In high nickel alloys, we can see the similar structure at the room temperature, by the furnace cooling (see Photogr. 7); while in low nickel alloys, it is hardly visible by the same treatment. This is attributed to the fact that with an increasing content of nickel, the transformation point (Ar_3) lowers very rapidly.

According to the view of the present writer, the so called duplex structure as shown in Photogr. 6 is a partially transformed product of the γ-solid solution of iron-nickel by annealing a quenched austenitic

alloys at a high temperature below Ac_3 point, and hence the conclusion of Hansons is not reasonable.

Next, an experiment was carried out to find the domain of the characteristic structures in the alloys. The specimens were heated to certain temperatures (first annealing tempetature in Table VI), kept there for the required time and slowly cooled to lower temperatures (second annealing tempetatures, in Table VI), again annealed there, and then quenched in water. The results are shown in Table VI and Fig. 4.

TABLE VI.

Experiments	Wt. % of *Ni*	First Annealing		Second Annealing		Structures after quenched in water.
		Temp. (C°)	Time (hours)	Temp. (°C)	Time (hours)	
No. 1	0	1050	15	930	22	Ferrite only.
	2–25	,,	,,	,,	,,	Wid. str.
	≧30	,,	,,	,,	,,	Homogeneous austenite.
2	≦2	1000	21	800	22	Ferrite.
	8–25	,,	,,	,,	,,	Wid. str.
	≧30	,,	,,	,,	,,	Homogeneous aust.
3	≦4	1100	22	670	20	Ferrite.
	8–25	,,	,,	,,	,,	Wid. str.
	≧30	,,	,,	,,	,,	Homogeneous aust.
4	0–4	1000	36	530	85	Ferrite.
	6–10	,,	,,	,,	,,	Ferrite+Wid. str.
	12–25	,,	,,	,,	,,	Wid. str.
	≧30	,,	,,	,,	,,	Homogeneous aust.
5	0–8	1070	16	420	53	Ferrite.
	10–15	,,	,,	,,	,,	Ferrite+Wid. str.
	15–25	,,	,,	,,	,,	Wid. str.
	≧30	,,	,,	,,	,,	Homogeneous aust.
6	≦4	1070	20	240	84	Ferrite.
	12–15	,,	,,	,,	,,	Intermediate str.
	20–25	,,	,,	,,	,,	Wid. str.
	≧30	,,	,,	,,	,,	Homogeneous aust.

Some of the iron-nickel alloys, cooled from the melt, annealed, and slowly cooled in the furnace, were quenched from room temperature in liquid air. The alloys containing nickel less than 25 % gave no

Fig. 4. Relation of Quenching Temperature and Stuructures.

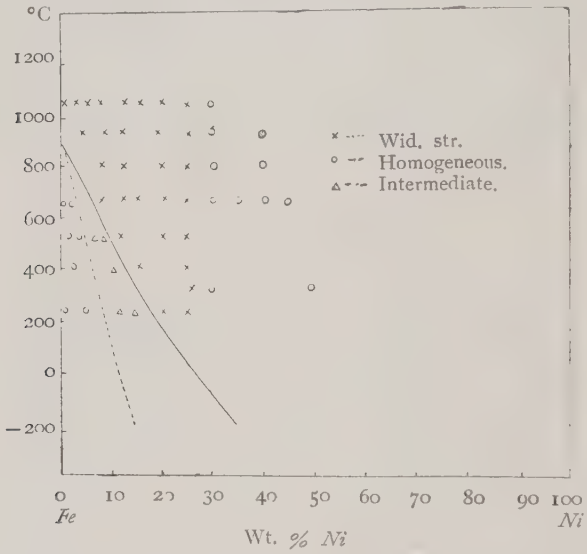

marked change in structures and in scleroscope hardness. But alloys containing nickel more than 25 % changed their structure from austenitic to martensitic, becoming very hard. The results are shown in Table VII and Fig. 5.

TABLE VII.

Wt. % of *Ni*	Structures		Scleroscope Hardness	
	Annealed	Quenched in liquid air	Annealed	Quenched in liquid air.
0	Ferrite	Not changed	16.3	16.5
10.90	Martensitic	Martensitic	23.0	23.5
15.20	,,	,,	27·7	30.7
19.10	,,	,,	35.2	36.5
25.22	,,	,,	28.2	36.4
26.90	Austenitic	,,	25.1	34.2
30.00	,,	,,	12.8	32.5
32.90	,,	,,	13.1	32.2
34.85	,,	Not clear	13.2	13.3
37.10	,,	Not changed	13.2	13.3
39.25	,,	,,	14.7	14.7
50.02	,,	,,	12.1	12.1
60.34	,,	,,	12.2	12.3
69.36	,,	,,	12.1	12.1

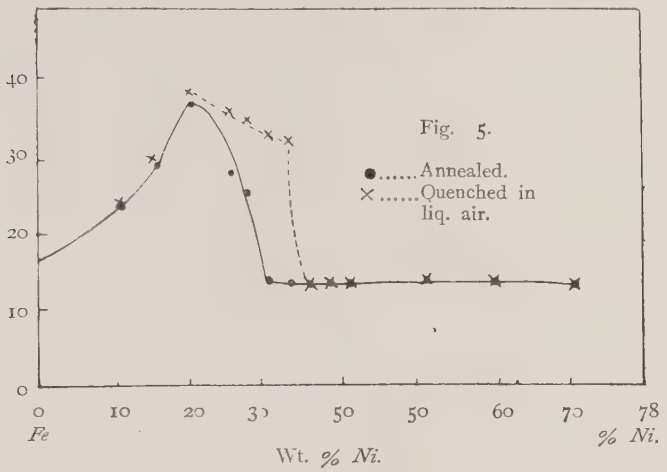

Fig. 5.

The Ar_3 point thus determined microscopically coincides approximately with those obtained by magnetic and thermal analyses. The lowering of the Ar_3 point continues to increase with the content of nickel, until the transformation point reaches below −190° C at 35 % of nickel. The martensitic or Widmannstätten structures are generally observable in quenched alloys, and these alloys undergo increase of magnetization by tempering above 350° C.

(5) A_3 Points of Iron-Nickel Alloys.

In order to find the Ar_3 point lying below the room temperature in some iron-nickel alloys, a dilatometric method was used. The dilatometer used in our laboratory was somewhat modified. A rough sketch is shown in Fig. 6.

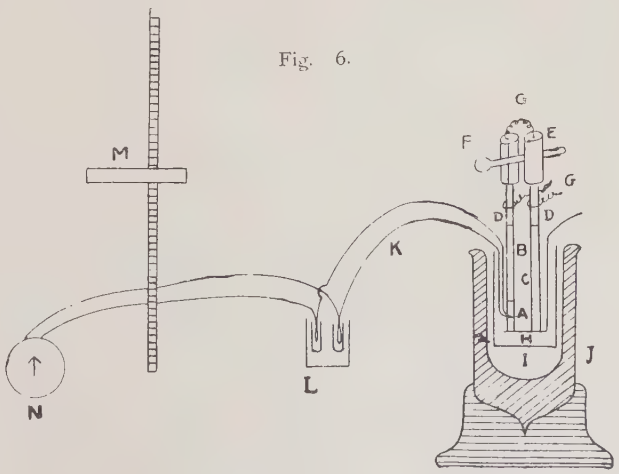

Fig. 6.

In this figure, A is the specimen; B and C, silica tubes; D, iron rod; E, iron cylinders; F, mirror; G, spring to press two short vertical cylinders together; H, brass plate to sustain the specimen A and silica tube C vertically; I, copper cylinder; J, Dewar's vessel; K, copper-constantan junction; L, cold junctions cooled in ice; M, scale and telescope; N, galvanometer.

The specimens used were each 5 mm. thickand 7.5 cm. long. For the measurement of temperature, one junction of a copper-constantan element was placed in contact with the middle part of the specimen. The specimen and the silica tube placed in parallel position were lightly surrounded with cotton wool, put in a cylindrical copper vessel, and placed in a Dewar's vessel. Liquid air was then slowly poured into the latter and thus the specimen was cooled indirectly. If there is a difference in expansion between the specimen and the silica tube, the horizontal axis carrying a small mirror is rotated, the amount of which was read by means of a scale and a telescope placed in front of the mirror. When the temperature of the specimen fell to about −120° C, the further decrease of temperature is difficult, so the liquid air was poured over the cotton; and the specimen was cooled to about −190° C. Afterwards the liquid air in the Dewar's vessel was poured out and the expansion during heating was observed. The heating of specimens above the room temperature was carried out in an electric resistance furnace. The results are shown in Table VIII and Fig. 23, Pl. IV.

TABLE VIII.

Alloys	Wt. % of *Ni*		$Ac_{3,2}$ (°C)	$Ar_{3,2}$ (°C)	Ac_2 (°C)	Ar_2 (°C)
	Cal.	Anal.				
No. 1	28	27.80	470	−20	50	40
2	30	29.71	440	−50	110	100
3	33	33.40	370	−130	170	155
4	35	35.50	—	—	250	240
5	37	36.90	—	—	290	280
6	40	40.01	—	—	360	340
7	100	99.63	—	—	360	345

Some of the specimens were further examined magnetically. The curves are shown in Fig. 24, Pl. V. Comparing the result with that of the dilatometric method, we see that, on heating, the lower transformation in the magnetic curves of quenched alloys containing about 28–33 % of nickel is due to the A_2 transformation of the phase consisting of the face-centred lattice and the higher one the $A_{3,2}$ transformation of the phase consisting of the body-centred lattice; on cooling, this relation is reversed.

From the results so far obtained, we may, regarding the equilibrium diagram of iron-nickel system, conclude as follows:—In the solid phase of this system, the change of the A_3 point only is to be considered, the A_2 point being not a change of phase, and hence the curves showing the magnetic change in alloys containing about 30 to 100 % *Ni* in Fig. 3 should not be drawn in the equilibrium diagram. The A_3 point falls steadily with the increasing content of nickel down to −190° C at 35 % of nickel. In a solid solution, the transformation takes place in a temperature interval, and so is the case for the A_3 change. Hence, the equilibrium diagram of iron-nickel system in the solid phase becomes very simple, as shown in Fig. 1.

§ 3. BINARY SYSTEM OF NICKEL-CARBON.

(1) Thermal Analysis.

This system has been investigated by K. Friedrich and A. Leroux.[1] The nickel used by them was a commercial sample containing about 0.2–0.6 % of iron and about 0.5 % of carbon as impurities. The nickel used in the present investigation was the same as that in the foregoing experiments. A required quantity of nickel was melted in a porcelain melting tube, saturated with graphite, and then cooled in the furnace. This product was used as a mother alloy. For each experiment, 25 grs. of the material were taken. The determination of the solidifying temperature was made for different alloys containing various amounts of carbon up to 2.22 per cent.

(1) Metallurgie, **7**, (1910), 10.

The cooling curves were taken from a temperature 50°–100° above the solidifying points, and the temperatures read at an interval of 5 seconds. The cooling rate of the alloys near the freezing point was about 1° per second. The supercooling at the freezing point was observable in a few samples containing no carbon and in low carbon alloys, the amount being about 30°–130° C. Some of the low nickel alloys were prevented from supercooling by stirring the melt with a silica tube or by inoculation with nickel powder. The alloys were cooled from the melt in the ordinary atmosphere without any protecting oxidation, and after being cooled they were analysed for the contents of carbon. The results are shown in Table IX.

TABLE IX.

Alloys	Wt. % of *Ni.* (°C)	Solidifying temp. (°C)	Eutectic temp. (°C)	Time of arrest (seconds)	Remarks
No. 1	0.05	1448	—		Supercooling 42 (°C)
2	0.10	1440	—		132
3	0.26	1434	—		
4	0.35	1430	—		
5	0.45	1427	—		3
6	0.56	1410	1305	3	
7	0.58	1409	1298	7	2
8	0.82	1318	1310	15	
9	1.07	1363	1313	40	
10	1.10	1315	1315	42	
11	1.24	1381	1314	60	
12	1.30	1349	1313	61	
13	1.83	1330	1317	75	
14	2.22		1318	120	

The above results are graphically shown in Fig. 7. The melting point of nickel is gradually lowered by the addition of carbon. When the content of carbon increases beyond 0.55 per cent, another arrest point is observed in each cooling curve, the time of arrest increasing with the carbon content up to 2.22 per cent. This is attributed to the formation of an eutectic consisting of nickel and nickel-carbide (or carbon), its concentration being 2.22 % of carbon.

Fig. 7. Equilibrium Diagram of *Ni C* System.

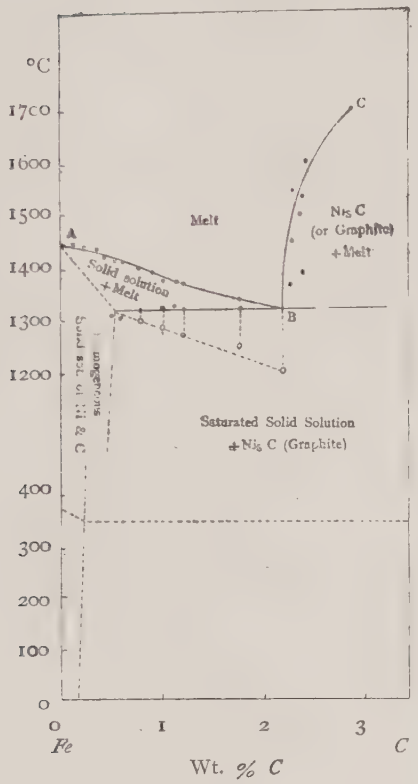

Fig. 8. Temperature-Concentration Diagram of *Ni C* System. O. Ruff and W. Martin.

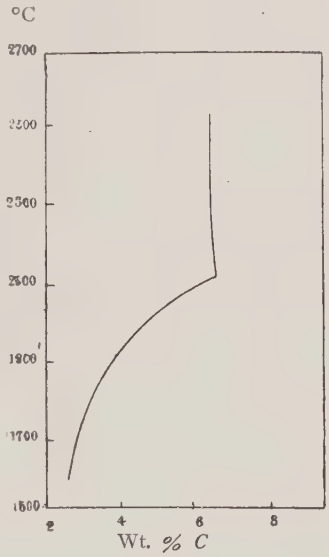

The cooling curves below the eutectic point show no transformation point down to room temperature. It is noticeable that carbon is rather effective for depressing the melting point of nickel, that is, one per cent of carbon lowers the melting point of nickel by about 100° C.

Now examining the specimens microscopically, the result agrees completely with the diagram above given. Nickel dissolves carbon less than 0.55 per cent, giving a homogeneous structure of solid solution (see Photogr. 10). Above this concentration, the eutectic appears, the amount increasing up to 2.22 % of carbon (see Photogr. 11). Alloys containing 0.55 to 2.22 per cent of carbon consist of the solid solution of primary crystals and the eutectic. The eutectic temperature is 1318° C.

(2) Nickel Carbide.

As regards the solubility of carbon in molten nickel, we have a few reports, namely, those of W. Hempel,[1] L, Pebal,[2] Moissan,[3] Jungk,[4] and Gard.[5]

O. Ruff and W. Martin[6] determined the concentration-temperature curve for nickel-carbon alloys from 1550° C to 2500° C. Their method was as follows:— 15 grs. of nickel were melted and covered with graphite in a graphite crucible; the temperature of the furnace was raised to 1500° C, and kept constant for 10 minutes; then it was raised to a required temperature, kept there for 10 minutes more, and quenched in ice water. By analysing the total carbon in the alloys, they obtained a curve as shown in Fig. 8, in which we see a break at 6.42 per cent of carbon and 2100° C. This point corresponds to the composition of trinickel carbide Ni_3C, which is analogous to the iron-carbide Fe_3C. By microscopic examination, they also observed the existence of a brown constituent in the eutectic, which is considered to be the carbide. Thus according to their opinion, nickel carbide exists between 1500° and 2500° C, though it is very easily decomposable.

O. Ruff and E. Gersten[7] also studied the heat of formation of Mn_3C, Fe_3C, and Ni_3C, and obtained the following results:—

Substances	Mn_3C	Fe_3C	Ni_3C
Heat of formation	$+12.9\pm2.14$	-15.3 ± 2	ca. -394 ± 10 Calories

Thus Mn_3C gives the greatest heat of formation, being an exothermic compound, and is the most stable of these carbides. Fe_3C is an end-

(1) Zeit. angew. Chem. **17**, (1904), 300.
(2) Ann. **233**, (1886), 160
(3) Compt. Rend.
(4) Dingler, **222**, 94.
(5) Am. Journ. Sc., (3), **14**, 274.
(6) Metallurgie, **9**, (1912), 143.
(7) Ber. **46**, (1813), 400.

othermic compound, and rather unstable. Ni_3C is a strong endothermic compound, and therefore very unstable. In fact Mn_3C and Fe_3C are obtained by ordinary rate of cooling, but Ni_3C only by a very severe quenching from the melt.

E. Briner and R. Senglet[1] also investigated the carbide of nickel. According to them, a constituent, which is considered to be Ni_3C, is stable above 1600° C and below 900° C, but it is very unstable in the vicinity of 1600° C. The same investigators also treated two grams of a nickel-carbon alloy with hydrochloric acid, and passed the gasses produced through liquid air. But they could detect neither liquid nor gaseous hydro-carbon, as in cases of ordinary carbides. At any rate the existence of Ni_3C is not very certain.

Fig. 9.

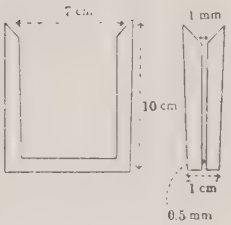

The present writer also made the same investigation. The molten nickel saturated with carbon at a high temperature for 10 minutes was poured into a flat copper mould as shown in Fig. 9. The temperature below 1550° C was measured with a Pt-Pt. Rh thermo-element and above it with an optical pyrometer. The total carbon in the quenched alloys were afterwards analysed. The results are shown in Table X and in Fig. 7, curve BC.

TABLE X.

Alloys	Quenching Temperature (°C)	Total Carbon (%)
No. 1	1366	2.240
2	1383	2.406
3	1444	2.324
4	1500	2.372
5	1529	2.377
6	1537	2.283
7	1600	2.439
8	1700	2.897

(1) Jour. chim. phys., **13**., (1915), 351.

The microscopic examination of these specimens did not, however, show any indication of the formation of carbide (see Photogr. 12). These alloys were also pulverised and put in a silica tube, and examined magnetically to see whether they had a new transformation point; but the result was negative. At any rate, in the equilibrium diagram of the nickel-carbon system, the curve BC represents the solubility of carbon or the carbide in the melt.

After O. Ruff and Wunsch,[1] carbon does not seem to diffuse into nickel or nickel steel at a temperature up to about 100° C below the eutectic point. But by a chemical analysis, which will be referred to afterwards, the present writer found that nickel dissolves about 0.25 per cent of carbon at room temperature. Hence it can be assumed that the solubility curve of carbon in solid nickel is somewhat bent as shown in Fig. 7.

The magnetic analysis of nickel-carbon alloys was also made. Pure nickel loses its magnetic property at 370° C on heating, and restores it at 340° C on cooling, as shown in curve (12), Fig. 21, Pl. II. If nickel dissolves carbon, the transformation point should be lowered and the intensity of magnetization decreases. Curve (1), Fig. 25, Pl. V, shows the curve of magnetic change of a nickel-carbon alloy, containing 0.91 % of total carbon and 0.83 % of dissolved carbon, and chill cast from 1500° C into the iron mould heated to about 300° C. The specimen shows a less intensity of magnetization and lower transformation point than those in pure nickel. Curve (2), Fig. 25, Pl. V, shows heating and cooling curves of an alloy containing more dissolved carbon (1.38 %) than in the former case. From the curve, we see that the dissolved carbon does not separate, by heating to 425° C. Curve (3), Fig. 25, Pl. V, shows the curves of a specimen containing 0.80 % of total carbon and 0.50 % of dissolved carbon. The transformation point in the cooling curve is higher than the heating curve, showing that the dissolved carbon is set free from the solid solution during heating to 650° C. By reheating

(1) Zeit. anorg. Chem. **85**, (1914), 292.

and cooling of the same specimen, the curve does not change (curve 4); A_2 point gradually rises, but is lower than that in pure nickel, showing the presence of a still remaining dissolved carbon. Curves (5), (6), (7) and (8) show the effect of repeated heating and cooling between various temperatures for a specimen containing 1.5 % of total carbon and 1.2 % of dissolved carbon. The same remarks given in the above case are also applicable to this one.

Hence, it is to be concluded that in a quenched specimen, the nickel carbide, if present, is in a dissolved state and hence cannot be detected microscopically.

§ 4. TERNARY SYSTEM OF IRON-CARBON-NICKEL.

(1) Thermal Analysis.

The thermal analysis was first made. The materials used for making alloys were commercial globular nickel, "Hōchōtetsu," and white pig iron. The result of the chemical analyses of the two former has already been cited; that of the white pig iron is given below:—

C	*Si*	*Mn*	*P*	*S*
3.0 %	0.09 %	0.23 %	0.02 %	0.01 %

Temperature readings during cooling from the melt were taken at intervals of 5 seconds with 25 grs. of a mixture of the metals in a porcelain tube, heated in a kryptol furnace. The alloys thus obtained were afterwards analysed with respect to carbon and nickel. The results are shown in Table XI.[1]

---

(1) The binary system of iron-carbon has been investigated by many metallurgists. As to the equilibrium diagram, we have two divergent opinions. The one is the single diagram theory considering the cementite separating as the primary crystal from the melt or austenite, and the double diagram theory, which insists that the graphite or cementite separates primarily according to the circumstance. The former theory was adopted by the present writer in accordance with the views of Professors K. Honda and T. Murakami (Sci. Rep. 10, (1921), 273) as shown in Fig. 10, and some of the trial experiments were carried out as mentioned in places of the present paper.

TABLE XI.

Alloys	Wt. % of *C*	Wt. % of *Ni*		First arrest (°C)	Second arrest		Third arrest (°C)
		Cal.	Anal.		Temp. (°C)	Duration (seconds)	
No. 1	0.05	0		1522	1400		
2	0.10	,,		1510	1411		
3	0.31	,,		1500	1433		
4	0.42	,,		1501	1462		677
5	0.65	,,		1468	—		
6	0.74	,,		1453	—		
7	0.81	,,		1446	—		693
8	1.05	,,		1425	—		707
9	1.70	,,		1410	—		708
10	2.00	,,		1373	1049	4	
11	2.10	,,		1351	1051	5	712
12	2.20	,,		1350	1053	7	707
13	2.21	,,		1347			
14	2.41	,,		1292	1116	20	
15	2.42	,,		1319	1126	20	
16	2.46	,,		1301	1098	25	
17	2.80	,,		1295	1123	35	
18	3.50	,,		1200	1138	70	735
19	4.31	,,		—	1130	100	728
20	0.10	10.00	10.44	1484			
21	0.20	,,		1473			
22	0.25	,,	9.11	1456			
23	0.71	,,		1445			
24	0.80	,,	10.00	1449			
25	0.81	,,	10.91	1448			
26	0.90	,,		1423			
27	1.04	,,	10.36	1399	?		

TABLE XI. *Continued.*

Alloys	Wt. % of *C*	Wt. % of *Ni*		First arrest (°C)	Second arrest		Third arrest (°C)
		Cal.	Anal.		Temp. (°C)	Duration (seconds)	
No. 28	1.58	10.00	10.00	1361	1042	5	
29	1.80	„		1336	1047	8	
30	1.91	„		1335	1071	12	
31	1.93	„	10.94	1340	1054	17	
32	2.00	„	10.76	1336	1037	15	
33	3.24	„	9.68	1182	1164	100	
34	3.82	„			1172	105	
35	0.18	20.08		1462			
36	0.55	„	20.45	1450			
37	0.64	„		1443			
38	0.84	„	20.62	1415			
39	0.92	„	19.23	1406			
40	1.04	„	20.85	1395			
41	1.31	„	21.23	1372			
42	1.40	„	20.10	1372	1183	2	
43	2.70	„	19.75	1237	1191	85	
44	3.50	„	21.46		1200	110	
45	0.12	30.00	30.36	1446			
46	0.19	„	30.82	1443			
47	0.24	„	30.47	1431			
48	0.28	„	30.22	1428			
49	0.40	„	31.31	1420			
50	0.44	„	30.16	1411			
51	0.92	„		1394			
52	1.05	„	31.61	1371			
53	1.45	„	30.05	1314	1193		
54	1.60	„	30.52	1314	1200	50	

TABLE XI. *Continued.*

Alloys	Wt. % of *C*	Wt. % of *Ni*		First arrest (°C)	Second arrest		Third arrest (°C)
		Cal.	Anal.		Temp. (°C)	Duration (seconds)	
No. 55	1.91	30.00	29.54	1294	1171	45	
56	2.15	„		1264	1215	80	
57	2.90	„	29.65		1211	100	
58	0.09	40.00	39.32	1429	1429		
59	0.14	„	40.15	1426			
60	0.33	„	40.90	1435			
61	0.79	„	40.64	1391			
62	0.79	„	40.12	1381			
63	0.98	„	40.70	1407			
64	1.04	„	40.48	1393	1233	10	
65	1.16	„	39.53	1375	1215	20	
66	1.52	„	40.11	1324	1204	30	
67	1.80	„	40.18	1300	1230	55	
68	2.50	„	40.95	1248	1244	110	
69	2.76	„	40.06		1241	120	
70	0.10	50.00	50.60	1421			
71	0.13	„	50.15	1424			
72	0.29	„	50.98	1415			
73	0.53	50.00	50.22	1393			
74	0.57	„	50.12	1392	1071		
75	0.78	„	50.84	1368	1232	5	
76	0.89	„	51.52	1346	1241	10	
77	1.36	„	49.42	1327	1257	45	
78	1.79	„	50.63	1305	1273	80	
79	1.80	„	50.56	1290	1262	70	
80	2.56	„	50.50		1272	115	
81	0.18	60.00	59.26	1426			

TABLE XI. *Continued.*

Alloys	Wt. % of *C*	Wt. % of *Ni*		First arrest (°C)	Second arrest		Third arrest (°C)
		Cal.	Anal.		Temp. (°C)	Duration (seconds)	
No. 82	0.20	60.00	61.11	1414			
83	0.33	„	60.65	1414			
84	0.39	„		1392			
85	0.51	„	60.29	1408			
86	0.59	„	59.15	1379	1253	2	
87	0.62	„	61.28	1401	?		
88	0.96	„	60.75	1344	1283	35	
89	1.19	„	61.01	1328	1290		
90	1.24	„	60.98	1268	?		
91	1.42	„	60.08	1310	1261	75	
92	1.72	„	60.67	1284	1252		
93	2.48	„	60.64		1280	125	
94	0.17	70.00	70.70	1425			
95	0.22	„	70.95	1421			
96	0.25	„	69.65	1417			
97	0.32	„		1401			
98	0.54	„	69.79	1408			
99	0.56	„		1381			
100	0.60	„	70.10	1374			
101	0.85	„	70.51	1378	1302	30	
102	1.16	„	69.60	1370	1310		
103	1.59	„	69.90	1340	1310	75	
104	1.70	„		1325	1305	80	
105	2.35	„	70.23		1310	130	
106	0.03	80.00		1428			
107	0.06	„	80.91	1430			
108	0.13	„	80.60	1426			

TABLE XI. *Continued.*

Alloys	Wt. % of *C*	Wt. % of *Ni*		First arrest (°C)	Second arrest		Third arrest (°C)
		Cal.	Anal.		Temp. (°C)	Duration (seconds)	
No. 109	0.23	80.00		1419			
110	0.30	„	79.90	1417			
111	0.31	„		1417			
112	0.45	„	79.85	1391			
113	0.48	„	80.20	1400			
114	1.01	„	80.50	1387	1308	40	
115	1.76	„	80.45	1324	1315	70	
116	2.26	„	80.73		1315	120	
117	0.17	90.00		1436			
118	0.23	„	89.40	1427			
119	0.27	„	90.36	1435			
120	0.34	„	89.96	1430			
121	0.42	„	89.60	1419			
122	0.66	„	89.70	1398	1311	25	
123	0.95	„	90.00	1382	1315	30	
124	1.13	„	90.56	1358	1315	55	
125	1.14	„	89.56	1374	1308	30(?)	
126	2.25	„	90.36		1312	120	

From the above results, the sections parallel to the iron-carbon side in the space diagam of the ternary system may easily be obtained. Approximate isothermal lines on the liquidus surface are shown in Fig. 11. The curve AB shows the projection of the eutectic curve and DE the solubility of carbon at the eutectic temperature. The isothermal in the field of hyper-eutectic alloys will be shown as dotted lines above AB, though it is not actually determined.

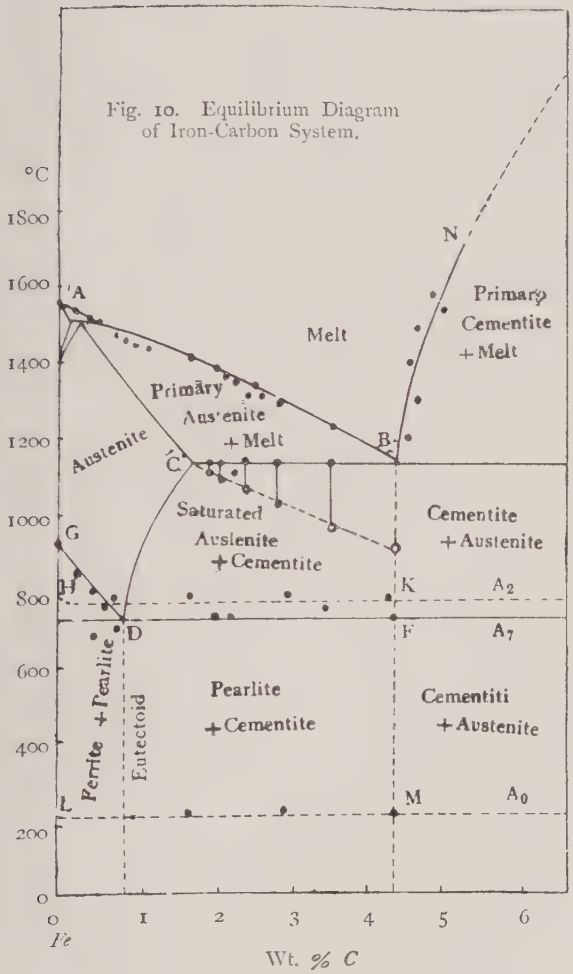

Fig. 10. Equilibrium Diagram of Iron-Carbon System.

(2) Combined or Dissolved Carbon in Iron-Carbon-Nickel Alloys.

The ternary alloys saturated with carbon were cooled from the melt to room temperature in the furnace in 3 hours and analysed for the combined or dissolved carbon. The results are shown in Table XII and graphically in Fig. 12 (a.)

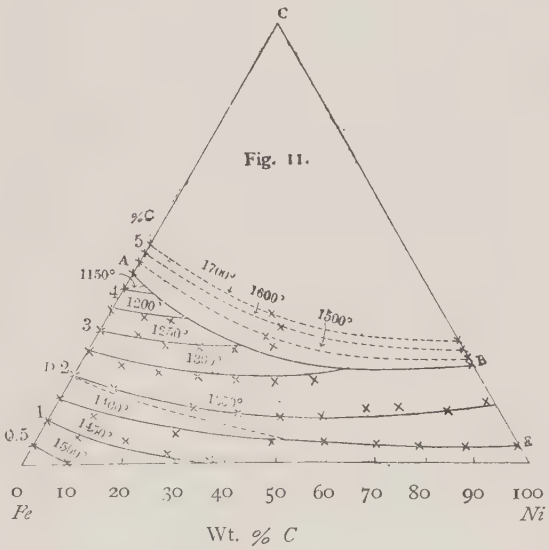

Fig. 11.

TABLE XII.

Alloys	Wt. % of Nickel		Wt. % of Carbon		
	Cal.	Anal.	Total *C*	Graphite	Combined or dissolved *C*
No. 1	0		4.31	—	4.31
2	2.00	1.80	4.10	1.55	2.55
3	6.00	5.88	4.20	1.96	2·24
4	10.00	10.05	3.82	2.82	1.46
5	15.00	15.18	3.63	2.81	0.82
6	20.00	21.46	3.50	2.91	0.59
7	30.00	29.65	2.90	2.62	0.28
8	40.00	40.06	2.76	2.44	0.32
9	50.00	50.50	2.56	2.33	0.23
10	60.00	60.64	2.48	2.16	0.33
11	70.00	70.23	2.35	2.06	0.29
12	80.00	80.73	2.26	1.99	0.27
13	90.00	90.36	2.25	1.98	0.27
14	97.78		2.22	2.02	0.20

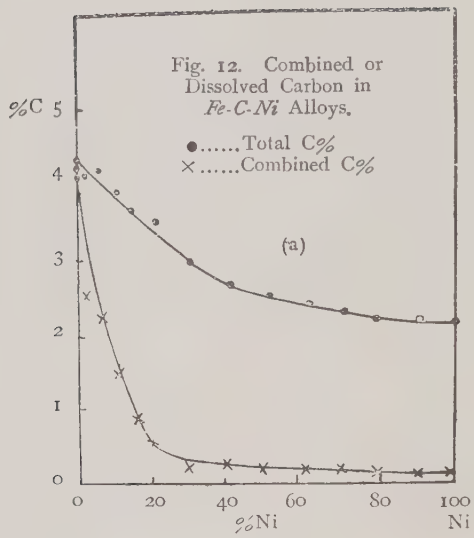

Fig. 12. Combined or Dissolved Carbon in *Fe-C-Ni* Alloys.

The combined or dissolved carbon in the eutectic alloy of iron and carbon is about 4.30 %, provided the rate of cooling is normal; as the nickel content increases, it rapidly diminishes at first and then gradually, and at 30 % of nickel, it contains only 0.25–0.30 % of dissolved carbon, afterwards the amount remaining almost constant. These remarks apply also to hypo-eutectic alloys, as shown in Table XIII and Fig. 12 (b).

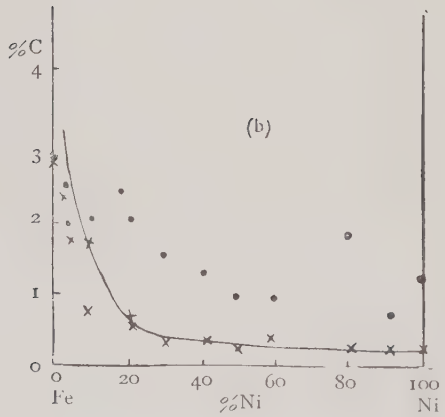

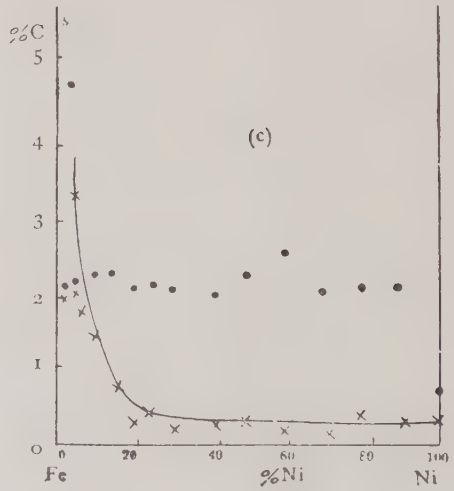

TABLE XIII.

Alloys	Wt. % of Nickel		Wt. % of Carbon		
	Cal.	Anal.	Total *C*	Graphite	Combined or dissolved *C*
No. 1	0		2.790	0.003	2.787
2	2.00		2.338	0.030	2.308
3	4.00		1.861	0.304	1.557
4	8.00	7.96	1.800	1.098	0.702
5	10.00		1.910	0.285	1.625
6	20.00	19.75	2.330	1.693	0.637
7	20.00		0.500	0.018	0.482
8	30.00	30.05	1.450	1.188	0.262
9	40.00	39.53	1.155	0.873	0.282
10	50.00	51.52	0.890	0.749	0.141
11	60.00	60.75	0.955	0.558	0.397
12	70.00		0.316	—	0.316
13	80.00	80.45	1.751	1.496	0.255
14	90.00	89.70	0.660	0.445	0.215
15	98.93		1.070	0.840	0.230
16	99.74		0.260	0.013	0.247

The above results also agree with those of the alloys quenched from the melt into an iron-mould, and annealed at about 1000° C, as shown in Table XIV and Fig. 12 (c).

TABLE XIV.

Alloys	Wt. % of Nickel		Wt. % of Carbon		
	Cal.	Anal.	Total *C*	Graphite	Combined or dissolved *C*
No. 1	2.00	1.78	2.024	2.024	2.000
2	4.00	3.89	2.118	0.088	2.030
3	4.00	3.94	4.735	1.455	3.280
4	6.00	6.12	1.838	0.024	1.814
5	8.00	7.45	2.272	0.446	1.826
6	10.00	10.30	2.174	0.836	1.338
7	15.00	15.47	2.216	1.478	0.738
8	20.00	20.04	2.039	1.790	0.249
9	25.90	25.63	2.092	1.705	0.387
10	30.00	30.47	2.004	1.844	0.160
11	40.00	39.97	2.244	1.965	0.279
12	50.00	52.40	2.226	2.009	0.217
13	60.00	59.52	2.510	2.373	0.137
14	70.00	69.60	2.003	1.802	0.201
15	80.00	80.04	2.126	1.762	0.364
16	90.00	88.67	2.010	1.761	0.249
17	99.27		0.732	0.497	0.235

(3) Effect of Nickel on the A_0 Transformation of Cementite.

The A_0 point (215° C on cooling) is not affected by the content of nickel; but its existence is usually limited to alloys containing a certain amount of the metal. For, the effect of nickel on the iron-carbon alloys is remarkable in its tendency to cause the graphitization of cementite. According to the present investigation, the domain of the existence of cementite, as determined magnetically, is shown in Fig. 13. The A_0 point can be detected in steels containing more than 0.1 per cent of carbon. The quantity of the combined carbon in the steel diminishes as the nickel content increases, and the amount of cementite gradually decreases up to about 25 % of nickel, at which about 0.6 % of carbon dissolves in solid phase. In steels containing more than 10 % of nickel, the lowered and stepped A_1 transformation makes the A_0 transformation of cementite indistinct; but its presence is easily confirmed microscopically.

Fig. 13. The Domain of Existence of Cementite in *Fe-C-Ni* Alloys.

×.....Alloys showing Ar_0 change.
●.....The same change deduced microscopically

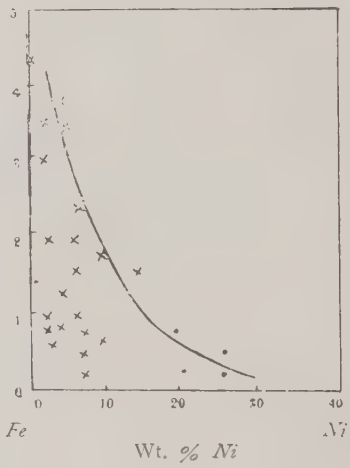

Fig. 14. Effect of Nickel and Carbon on the Position of the Critical Point Ar_1 and Corrésponding Types of Structure. (Sauveur's Book p. 338.)

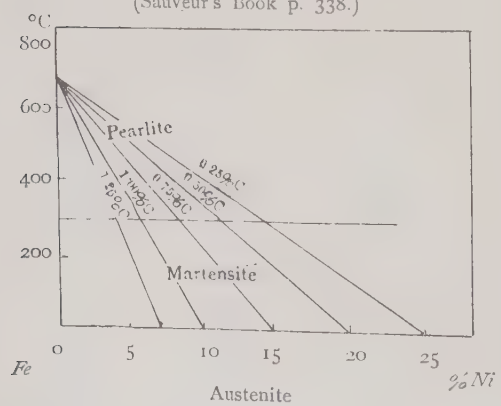

(4) Effect of Nickel on the A_1 Transformation.

The diagram showing the relation of carbon and nickel on the position of the Ar_1 point and corresponding types

of structures has already been constructed by Sauveur as shown in Fig. 14.[1]

The results of the present investingation by means of thermal analysis are given in Table XV and graphically in Fig. 15.

TABLE XV.

Alloys	Wt. % of Nickel		Wt. % of Carbon		Ar_1 (°C)
	Cal.	Anal.	Total *C*	Combined or dissolved *C*	
No. 1	0		4.310	4.300	728
2	2.00	1.80	4.096	2.300	665
3	„		1.205	1.030	672
4	„		0.653	0.601	657
5	6.00	5.88	4.204	1.300	560
6	„		1.290	1.160	552
7	„		0.600		588
8	10.00		3.810	1.512	476
9	„		0.253		476
10	15.00		0.983		332(?)
11	20.00	21.46	3.500	0.601	205(?)
12	25.00		0.611		46(?)
13	28.00	28.76	0.303		—

The diagram shows that the Ar_1 point falls at first rapidly and then gradually, as the nickel content increases, but almost independent of the content of carbon, as it ought to be. As shown in Fig. 14, Sauveur considers the A_1 transformation point to be lowered by the increasing quantity of carbon; but this is only apparent, as in high nickel steels, this transformation is complicated by the stepped transformation, causing apparently much lower transformation; but in equilibrium condition, the A_1 transformation is almost independent of the carbon, as shown in Fig. 15.

(1) The Metallography and Heat-treatment of Iron and Steel, (1920), 338.

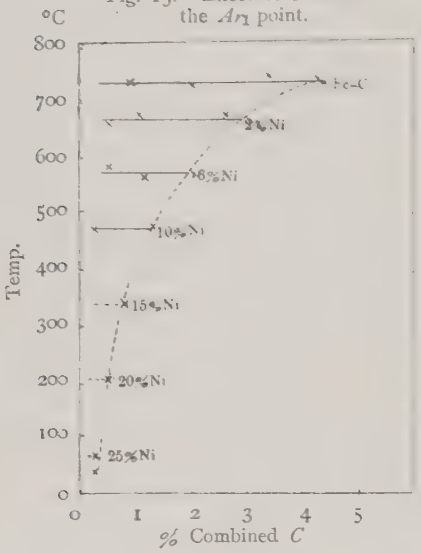

Fig. 15. Effect of Nickel on the Ar_1 point.

(5) Effect of Nickel on the A_2 Transformation.

It is a well known fact that the A_2 point of iron-carbon alloys is nearly constant irrespective of the carbon content. If, however, nickel is added to iron, the A_2 (A_1, A_3) point of the alloys is rapidly lowered with increasing content of nickel. The results of the magnetic investigation made by the present writer are shown in Table XVI.

TABLE XVI.

Alloys	Wt. % of Nickel		Wt. % of Carbon		Ac_2 (Ac_1, Ac_3) (°C)	Ar_2 (Ar_1, Ar_3), (°C)	Remarks
	Cal.	Anal.	Total C	Combined or dissolved C			
No. 1	0		0.05		800	770	
2	,,		0.60		795	700	
3	,,		0.80		788	695	
4	,,		1.69		785	690	
5	,,		3.00		795	680	
6	,,		4.30		785	710	
7	2.00	2.42	0.508		770	685	
8	,,		0.903	0.897	771	620	
9	,,	2.43	0.926	0.450	770	632	
10	,,		1.301	1.021	775	625	
11	,,		2.024	2.000	772	630	
12	,,		4.260		765	635	
13	4.00	4.17	0.288		750	610	
14	,,		0.903	0.897	740	570	
15	,,	4.26	1.521	1.156	740	575	
16	,,	4.25	1.635	1.321	740	500	
17	,,	3.89	2.118	2.030	740	550	
18	,,	3.94	4.357	3.280(?)	740	565, 165	Stepped

TABLE XVI. *Continued.*

Alloys	Wt. % of Nickel		Wt. % of Carbon		Ac_2 (Ac_1, Ac_3) (°C)	Ar_2 (Ar_1, Ar_3) (°C)	Remarks
	Cal.	Anal.	Total *C*	Combined or dissolved *C*			
No. 19	6.00	6.26	0.611	0.490	710	520	
20	„		0.729	0.669	710	525	
21	„	5.30	1.290	0.966	700	500	
22	„		1.553	1.425	710	485, 100	Stepped
23	„	5.42	4.655	3.673	700	500, 100	„
24	8.00	8.67	0.288		710	470, —	
25	„	7.32	0.438		712	485, —	
26	„	7.62	0.870	0.859	705	—, 100	
27	„		1.012		725	485, 100	„
28	„	7.64	1.335		700	—, 90	*
29	„	7.65	2.272	1.826	702	—, 90	
30	„		4.712	2.236	700	492, 115	Stepped
31	10.00	11.30	0.307		710	425, 115	„
32	„	9.91	0.921	0.890	680	—, 68	
33	„		0.790	0.610	680	—, 285	*
34	„	10.43	1.771	1.666	670	—, 60	*
35	„		3.581		675	418, 150	Stepped
36	15.00		0.409	0.391	650	—, 190	
37	„		0.342	0.328	651	—, 95	*
38	„	15.13	0.983	0.410	650	—, —?	*
39	„	15.47	2.216	0.738	655	—, 78	
40	„		3.980	1.616	640	—, 90	
41	„	17.66	0.945	0.918	610	—, 50	*
42	20.00	22.00	0.330	0.310	605	—, 90	*
43	„		0.670	0.520	598	—, —	*
44	„		0.810	0.268	590	—, —	*
45	„	20.04	2.039	0.249	610	—, —	*
46	„		3.685	0.800	600	—, —	*
47	25.00	25.00	0.403	0.312	540	—	*
48	„	25.00	0.910		552	—	*
49	„	25.63	2.092	0.387	560	—	*

Some typical curves are shown in Fig. 26, Pl. VI. The specimens having the transformation points below the room temperature, were immersed in liquid air, and the Ac_2 (Ac_1, Ac_3) points were determined;

these points are marked with asterisks in the above table. Thus the Ac_2 (Ac_1, Ac_3) point is gradually lowered by increasing nickel, carbon being kept constant, and the Ac_2 point curve for alloys containing a constant amount of nickel, first falls and then remains constant as the carbon increases, their forms being all similar to each other, as shown in Fig. 16 (a).

Fig. 16, (a). Effect of Nickel on the Ac_2 (Ac_1 Ac_3) Point.

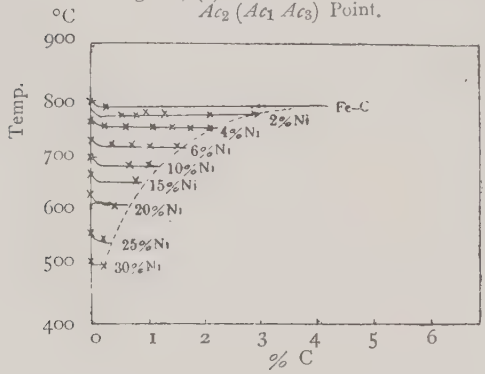

Fig. 16, (b). Effect of Nickel on the Ar_1, (Ar_2, Ar_3) Point.

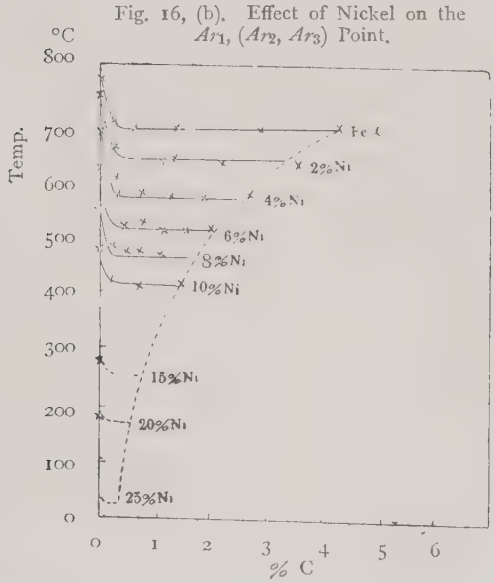

The Ar_2 (Ar_1, Ar_3) point is also affected by nickel in a similar way, but in a more marked degree. When the Ar_1 (A_2, Ar_3) point is lowered between 500° and 150° C, the transformation occurs in two steps, usually denoted by Ar_1' and Ar_2'' points. This stepped transformation has been explained by Professor K. Honda and Mr. T. Kikuta.[1] According to the results of the present writer, Fig. 16 (b) shows the effect of nickel on the Ar_2 (Ar_1, Ar_3) points.

Mr. S. Iguchi[2] investigated the transformations in irreversible nickel steels, and concluded that the Ac_1 point depends on the content of nickel, but not on the carbon, and that Ar_1 and Ar_3 points gradually decrease as the carbon content increases. As mentioned above, the

(1) Sci. Rep. **11**, (1922), 1.
(2) Suiyōkaishi, **4**, (1922), 1.

present investigation also shows that $Ar_{1,3}$ point gradually falls as the nickel content increases, but it is almost independent of carbon. This latter point does not agree with Mr. Iguchi's view. In some high nickel steels, the transformation point is complicated by the stepped changes. In this case, the present writer took always the beginning of the first change. It is, however, to be regretted that Mr. Iguchi has not analysed both for the dissolved and total carbon.

The influence of nickel in high nickel alloys is rather simple, as the solubility of carbon is almost constant, i.e., 0.30–0.25 per cent as stated above. In this case, the A_2 point is lowered by 15°–20° owing to the dissolved carbon, provided the nickel content is constant. This is seen from Table XVII.

TABLE XVII.

Alloys	Wt. % of Nickel		Wt. % of Carbon		Ac_2 (°C)	Ar_2 (°C)
	Cal.	Anal.	Total *C*	Dissolved *C*		
No. 1	30.00	30.68	0.296	0.272	115	100
,,					460 (Ac_3)	105*
2	,,	30.69	2.004	0.260	160	120
,,					150, 460 (Ac_3)	110*
3	,,	31.43	0.473	0.253	170	140
,,					155, 470 (Ac_3)	140*
4	40.00	40.01	0.280	0.250	370	365
5	,,		0.520	0.251	386	346
6	,,		3.858	0.252	390	360
7	50.00	51.23	0.620	0.260	520	495
8	,,		1.320	0.255	540	515
9	,,		1.513	0.253	525	500
10	60.00	60.92	0.270	0.251	605	575
11	,,		0.863	0.258	605	570

TABLE XVII. *Continued.*

Alloys	Wt. % of Nickel		Wt. % of Carobn		Ac_2 (°C)	Ar_2 (°C)
	Cal.	Anal.	Total *C*	Dissolved *C*		
12	60.00		0.925	0.250	610	575
13	70.00	70.33	0.240	0.240	615	590
14	„		0.457	0.258	620	590
15	„		2.117	0.352	625	596
16	80.00	78.45	0.291	0.250	575	560
17	„		0.652	0.303	582	565
18	„	89.16	2.641	0.282	585	550
19	90.00		1.661	0.347	462	440
20	„	86.68	2.636	0.190	488	466
21	99.74		0.260	0.240	355	320
22	97.68		2.320	0.210	365 (?)	320

(* Quenched in liquid air.)

It is here to be noticed that the iron-carbon-nickel alloys containing about 30 % of nickel, when once cooled in liquid air, show the stepped transformations on heating and cooling. They are Ac_2, $Ac_{3,2}$, and Ar_2 and $Ar_{3,2}$ points for the constituents of the alloys having the face-centred and body-centred lattices respectively, as remarked in the former chapter (§ II, 5). It is not considered to be a transformation of a carbide.

(6) Merging of Ar_1 and Ar_3 Points in Iron-Carbon-Nickel Alloys.

As is well known, both Ar_1 and Ar_2 transformations of iron-carbon alloys take place at constant temperatures, irrespective of the carbon content. The Ar_3 point of pure iron falls rapidly with the carbon and reaches a constant temperature above 0.85 % of carbon.

As referred to in § 2 (2), as the nickel increases, both A_3 and A_2 points in iron-nickel alloys fall and coincide at 5 % on cooling, and 10 % on heating. If carbon is present, A_1 point is similarly affected by nickel. By the differential thermal analysis the change of transformation points is observed; the result is shown in Table XVIII, and Fig. 17 (a)-(d).

TABLE XVIII.

Alloys	Wt. % of Nickel		Wt. % of Carbon	Transformation Point (°C)			
	Cal.	Anal.		Ar_1	Ar_2	Ar_3	$Ar_{3,2}$
No. 1	0		0.03		720	890	
2	,,		0.34		715	820	
3	,,		0.50		715	770	
4	,,		0.57		720	745	
5	,,		0.82		730	715	
6	2.00	1.98	0.24	680	720	768	—
7	,,	2.02	0.43	670	700	740	—
8	,,	1.95	0.57	668	720	695	—
9	,,	2.00	0.81	—	740	—	670
10	4.00	3.90	0.28	635	670	695	—
11	,,	4.01	0.41	640	665	680	—
12	,,	3.97	0.78	—	650	—	640
13	,,	3.85	0.95	—	670	—	640
14	6.00	5.86	0.22	575	600(?)	630	—

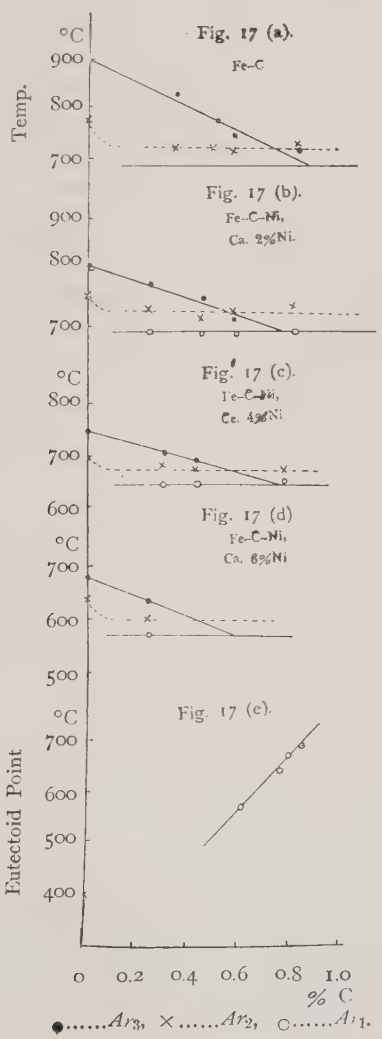

From Fig. 17 (a)-(d), we see that Ar_3 and Ar_1 points coincide at a concentration of about 2 % *Ni* and 0.80 % C, (at 670° C); or about 4 % *Ni* and 0.76 % C, (at 640° C); or 6 % *Ni* and 0.6 % C, (at 570° C); that is, the concentration of carbon at which the eutectoid transformation takes place, gradually diminishes with an increasing content of nickel, as approximately shown in Fig. 17 (e).

(7) Structural Diagram of Iron-Carbon-Nickel Alloys.

The structural diagram of nickel steel after Guillet is given in Fig. 18. By the present writer it was also investigated by means of microscopic observation and scleroscope hardness with the alloys cooled in the furnace. The results are shown in Table XIX and Fig. 19.

TABLE XIX.

Alloys	Wt. % of Nickel		Wt. % of Carbon		Micro-structures	Sclerocope Hardness
	Cal.	Anal.	Total *C*	Combined or dissolved *C*		
No. 1	0		0.30		P, F	23
2	,,		0.60		P, F	—
3	,,		0.81		P, F	25
4	,,		1.05		P, Ce	29
5	,,		1.70		P, Ce	33
6	,,		2.20		P, Ce	36
7	,,		4.31		P, Ce	19
8	2.00		0.24		P, F	—
9	,,		0.81		P	—
10	,,		2.34	2.31	M, Ce	35
11	,,		4.10	2.55	M, Ce	26
12	4.00	3.47	0.78		P	—
13	,,		1.86	1.56	M, Ce	41
14	5.00		1.57		M, Ce	46
15	6.00		2.28		M, Ce	34
16	,,		4.20	2.24	M, G	24
17	8.00		0.31		M, M-T, F	—
18	,,		1.80	0.70	M, Ce, G	29
19	10.00	10.44	0.10		M	26
20	,,		0.25		M	47
21	,,	10.91	0.81		M, A-M	43
22	,,		0.90		A-M	32
23	,,	10.36	1.04		M, A	29
24	,,		1.58		M, G	28
25	20.00		0.18		A-M, A	24
26	,,	10.00	0.64		M, A	29
27	,,	20.45	0.55		M, A	—

TABLE XIX. *Continued*

Alloys	Wt. % of Nickel		Wt. % of Carbon		Micro-structures	Scleroscope Hardness
	Cal.	Anal.	Total *C*	Combined or dissolved *C*		
No. 28	20.00	20.62	0.84		M, A	18
29	„	21.46	3.50		A, G	17
30	30.00	30.36	0.12		A	14
31	„	30.22	0.28		A	14
32	„	31.31	0.40		A	12
33	„		0.92		A, G	17
34	„	29.65	2.90	0.28	A, G	15
35	40.00	39.32	0.09		A	17
36	„	40.90	0.33		A	18
37	„	40.70	0.98		A, G	15
38	„	40.06	2.76	0.32	A, G	12
39	50.00	50.98	0.29		A	
40	„	50.84	0.78		A, G	15
41	„	50.50	2.56	0.23	A, G	12
42	60.00	60.65	0.33		A	13
43	„	61.28	0.62		A, G	18
44	70.00	69.65	0.25		A	13
45	„		2.50		A, G	12
46	80.00		0.31		A	12
47	„		0.23		A	13
48	90.00	90.36	0.27		A	11
49	„		0.33		A	13
50	97.75	99.63	2.25		A, G	11
51			0.05		A	10

(* P=Pearlite, F=Ferrite, Ce=Cementite, M=Martensite, M-T=Martensite-Troostite, A=Austenite, A-M=Austenite-Martensite, G=Graphite.)

The above results roughly agree with those of Guillet, except the terminal region of iron-carbon side.

Fig. 18. Structural Diagram of Nickel Steel.
(Guillet)

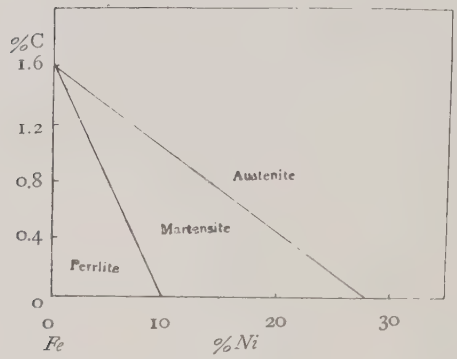

The structural diagram obtained by the present investigation is shown in Fig. 19, in which eight regions consist of the following structural constituents respectively.

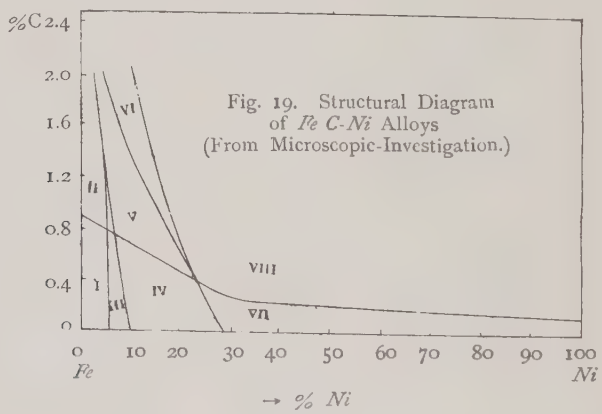

Fig. 19. Structural Diagram
of *Fe C-Ni* Alloys
(From Microscopic-Investigation.)

I. P+F. II. P+Ce.
III. F+M+T. IV. M+A.
V. M+A+Ce. VI. M+A+G.
VII. A. VIII. A+G.

(8) Equilibrium Diagram of Iron-Carbon-Nickel System.

From the foregoing results the equilibrium diagram of the ternary system is constructed as shown in Figs. 27 and 28, Pl. VII, the

former representing a space model and the latter its projection on the basal plane.

In Fig. 27, Pl. VII, ABB'A', AA'D'D and BB'C'C represent the temperature-concentration planes for *Fe-Ni*, *Fe-C* and *Ni-C* respectively. ABFE is the liquidus surface along which the ternary austenite having its composition on the solidus ABGH separates out and CDEF the primary surface of the solid solution of cementite and nickel-carbide.

Curve EF, starting at the eutectic point F of the system *Ni-C*, at 1318° C, and ending at the eutectic point *E* of the system *Fe-C*, at 1130° C, represents the eutectic line of the ternary system, along which the solid solution GH and carbide crystallize simultaneously.

GFKLEH is the eutectic surface showing the beginning of the eutectic crystallization. The surface representing the ending of the same crystallization is obtainable by generating a horizontal line between GH and KL, but for simplicity it is not shown in the diagram.

In the space ABGHEF, there exists the primary austenite and the melt; and in the space CDEFKL, primary carbide and the melt.

Surface GHQPR shows the solubility of the carbide or carbon in the austenite. MQPN is the primary surface of the α solid solution; and so, the intersection QP of these two surfaces is the eutectoid or A_1 line of the system. Hence, above these surfaces, we have a homogeneous solid solution or austenite, but below them, a heterogeneous mixture consisting of the two or three of α solid solution, austenite and the carbide. However, the presence of nickel in the ternary alloys makes easier the decomposition of the carbides. Hence as the content of nickel increases, free cementite gradually decreases, and the alloys containing more than 30 % of nickel actually consist of a mixture of the solid solution iron-nickel and graphite, provided the cooling rate is normal.

The space MSVA' shows a homogeneous α solution consisting of iron, carbon, and nickel, MV is the solubility curve of carbon in iron, and MS that of nickel in iron.

In the iron-carbon system, the A_4 transformation point (ca. 1400° C) is raised as the quantity of carbon increases, and at 1487° C a peritectic

reaction takes place; line *gfe* shows this change. In the iron-nickel system, a similar reaction also occurs at 1500° C; the change is shown by the line *bcd*. Now in the ternary system of *Fe-C-Ni*, the corresponding change will take place along the curve *cf*, the reaction being a monovariant change in the ternary system, though the similar change is nonvariant in the binary system. Hence in the ternary system, no remarkable change in the shape of diagram is observable except an increase of one freedom. Also, it may be reasonably considered that the peritectic temperature gradually lowers from *c* to *f*. The surface *Ade* is the liquidus and *Abg* the solidus for the δ solid solution. Along curve *cf* the melt *de* reacts with the δ solid solution *bg* forming γ solid solution *cf*. The δ solid solution on surface *abg* is in an equilibrium state with the γ solid solution on surface *acf*. That is in, space *Adegb*, the melt and δ solid solution coexist; space *Abga* consisting of δ solid solution, and space *acfgb* of δ and γ solid solutions. In space *BcfEFGH*, melt and γ solid solution coexist.

Some of the sections parallel to the *Fe-Ni* side are shown in Fig. 29 (a)-(d), Pl. VIII.

(9) Microscopic Investigation.

As the etching reagent for nickel steels, several acids have been recommended by previous investigators. Alloys containing less than 15 % of nickel are readily etched with 5 % picric acid in alcohol, those containing 15 to 25 % of nickel by 4 % nitric acid in alcohol, while for those containing more than 25 % of nickel, more concentrated nitric acid is required. In the case of nickel rich alloys, hot hydrochloric acid is generally recommendable as has been remarked by Rawdon and Lorentz,[1] since many pits easily appear in the etching. Some typical structures are shown in Photogr. 1–16, Pl. IX.–X.

Photogr. 1. A microstructure of an iron-nickel alloy containing 10.90 % of nickel and cooled from the melt in the furnace. The whole

(1) Chem. Met. Eng. **25**, (1921), 955.

surface is not simply plain martensitic.

Photogr. 2. That of iron-nickel alloy containing ca. 12 % of nickel and cooled from the melt in furnace. A fine martensitic structure is to be seen.

Photogr. 3. That of iron-nickel alloy containing 19.10 % of nickel and cooled from the melt in the furnace. Austenite-Martensite, that is, martensite developing in the domain of austenite is observable. The grains stand in relief.

Photogr. 4. Hōchōtetsu, annealed at 1050° C for 30 hours, and quenched in water. The structure shows a characteristic Widmannstätten structure.

Photogr. 5. The structure of iron-nickel alloy containing 14.90 % of nickel, after the same treatment as above. The Widmannstätten structure is clearly observable.

Photogr. 6. An iron-nickel alloy containing 14.90 % of nickel, annealed at 1050° C for 30 hours, quenched in water, and then reheated to 500°C for 24 hours. It shows the duplex structure.

Photogr. 7. An iron-nickel alloy containing 25 % of nickel, cooled from the melt in the furnace, annealed at 1000° C for about 24 hours, and cooled in the furnace. The Widmannstätten structure is very clearly developed.

Photogr. 8. The structure of the iron-nickel alloy containing 33.4 % of nickel, immersed in liquid air. The development of the Widmannstätten or martensitic structure by immersion in liquid air shows that the Ar_3 transformation takes place at a low temperature, below the room temperature.

Photogr. 9. The structure of an iron-nickel alloy containing 35.5 % of nickel, similarly treated as above. No Widmannstätten or martensitic structure is observable. But we see some twinned crystals in grains, showing a sign of austenite.

Photogr. 10. A nickel-carbon alloy containing 0.45 % of carbon, cooled from the melt in the furnace. No free carbon or carbide is observable.

Photogr. 11. A nickel-carbon alloy containing 2.22 % of carbon,

cooled from the melt in the furnace. Eutectic mixture of nickel (+dissolved carbon) and graphite is observable.

Photogr. 12. A nickel-carbon alloy, containing 2.44 % of carbon, chill cast into a flat copper mould from 1600° C. Graphite granules and eutectic are seen, but the existence of nickel carbide Ni_3C is not certain.

Photogr. 13. An iron-carbon-nickel alloy containing ca. 2 % of nickel, 2.34 % of total carbon, and 2.31 % of dissolved or combined carbon. The white crystal is eutectic cementite somewhat changed during cooling, the ground mass being troostitic to sorbitic. The Widmanstätten structure due to the acicular cementite separated from the solid solution is observable.

Photogr. 14. An alloy containing 7.96 % of nickel, 1.86 % of total carbon and 0.70 % of dissolved or combined carbon. In the grain boundaries, eutectic graphite formed by the decomposition of cementite is well developed. A small quantity of cementite is also observable in the boundaries. The matrix is martensitic.

Photogr. 15. The martensitic structure of an alloy containing 9.11 % of nickel and 0.25 % of carbon, cooled from the melt in the furnace. Comparing this figure with Photogr. 2, we know that the similar effect of nickel and carbon to form the martensitic structure in nickel steel is noticeable.

Photogr. 16. The structure of an alloy containing ca. 90 % of nickel and 2.5 % of total carbon, cooled from the melt in the furnace. Primary and eutectic graphite are observable.

SUMMARY.

The results of the present investigation may be summarized as follows:—

(1) The equilibrium diagram of the iron-nickel system was newly studied with the result that iron and nickel form a continuous series of solid solution with a break. The A_3 transformation of iron is continuously lowered by the addition of nickel, showing temperature-lags

on heating and cooling, in the case of irreversible nickel steels. A_3 and A_2 points coincide at about 5 % *Ni* on cooling, and at about 10 % *Ni* on heating. The A_3 change has a transformation interval similar as the liquidus and solidus in the case of solidification. At room temperature, the heterogeneous range extends from ca. 15 to 30 % of nickel.

(2) The equilibrium diagram of the nickel-carbon system is determined. Carbon and nickel dissolving carbon form an eutectic; its concentration of carbon is 2.22 % and its temperature 1318° C. The solubility of carbon in nickel is about 0.55 % at the eutectic temperature, and about 0.25 % at room temperature. Below the eutectic point the alloys undergo no change of structure.

(3) Nickel carbide is a dubious compound. The magnetic intensity of the solid solution consisting of nickel and carbon as well as its critical point decrease as the carbon increases.

(4) The equilibrium diagram of iron-carbon-nickel system is constructed. There exists no ternary eutectic, but a binary eutectic of a solid solution consisting of iron-nickel and carbon; its carbon content decreases with increasing nickel.

(5) The sum of the combined and dissolved carbons in the ternary alloys at room temperature rapidly decreases up to ca. 0.30 % in 30 % of nickel steel, and aterwards remains almost constant.

(6) The field representing the existence of cementite in the ternary alloys has been determined. It almost coincides with the range in which combined or dissolved carbon exists, that is, from 0 to about 30% of nickel.

(7) With the addition of nickel, the A_1 transformation of iron-carbon alloys is lowered and tends to be invisible at about 10 % of nickel.

(8) As the nickel content increases, the carbon content in the eutectoid point decreases down to 0.30 % at about 35 % of nickel.

In conclusion, the present writer wishes to express his cordial thanks to Professor K. Honda, under whose kind guidance the present investigation has been carried out, and also to Professor T. Murakami for his valuable advice during the course of the present work, and to Professor T. Ishiwara for his careful corrections throughout this paper.

Plate I.

Fig. 20. Cooling Curves of Thermal Analysis. (Fe-Ni Alloys)

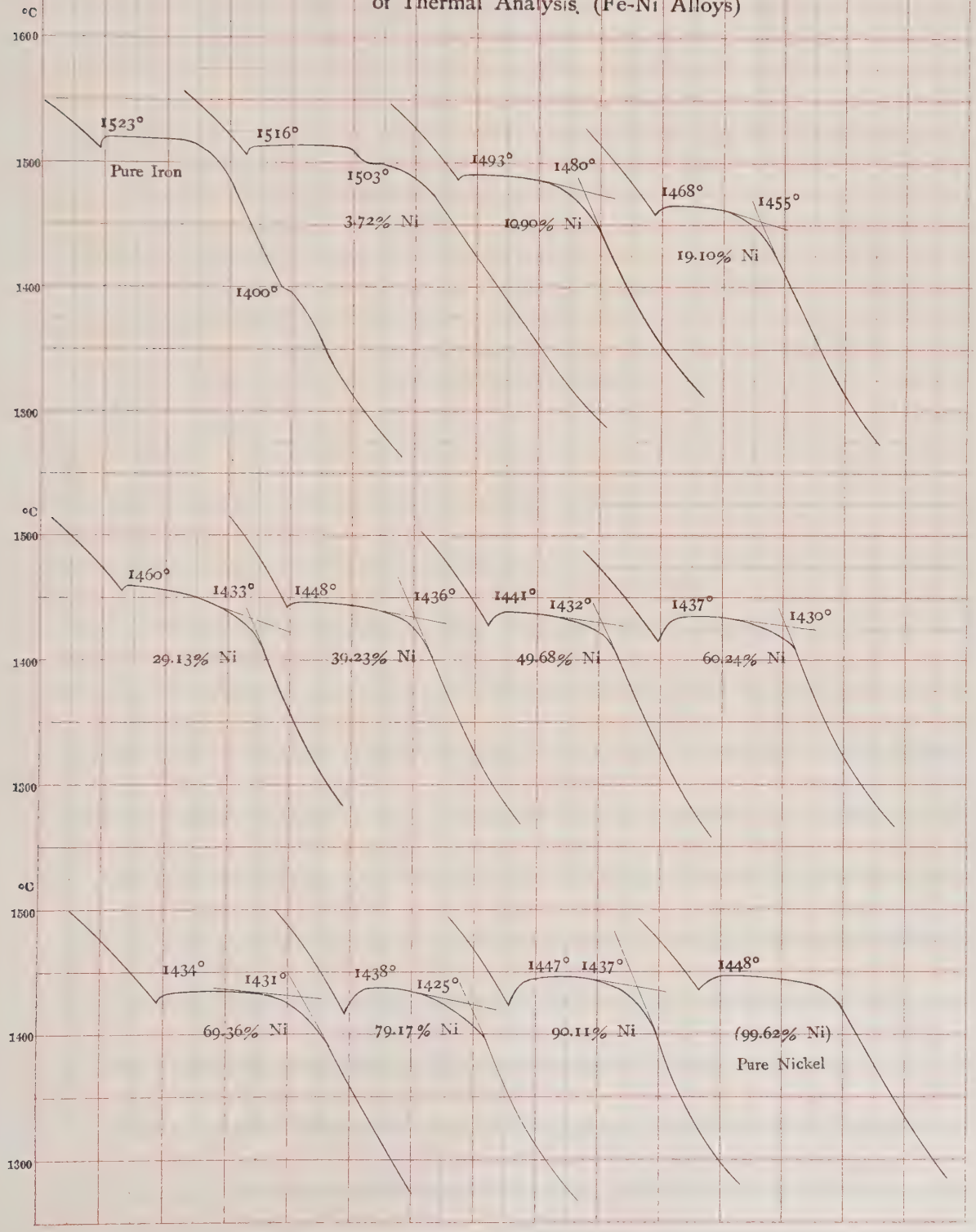

Plate II.

Fig. 21. Curves of Magnetic Analysis.

(Fe-Ni Alloys)

$I = 1.49 \times \delta$ gausses.

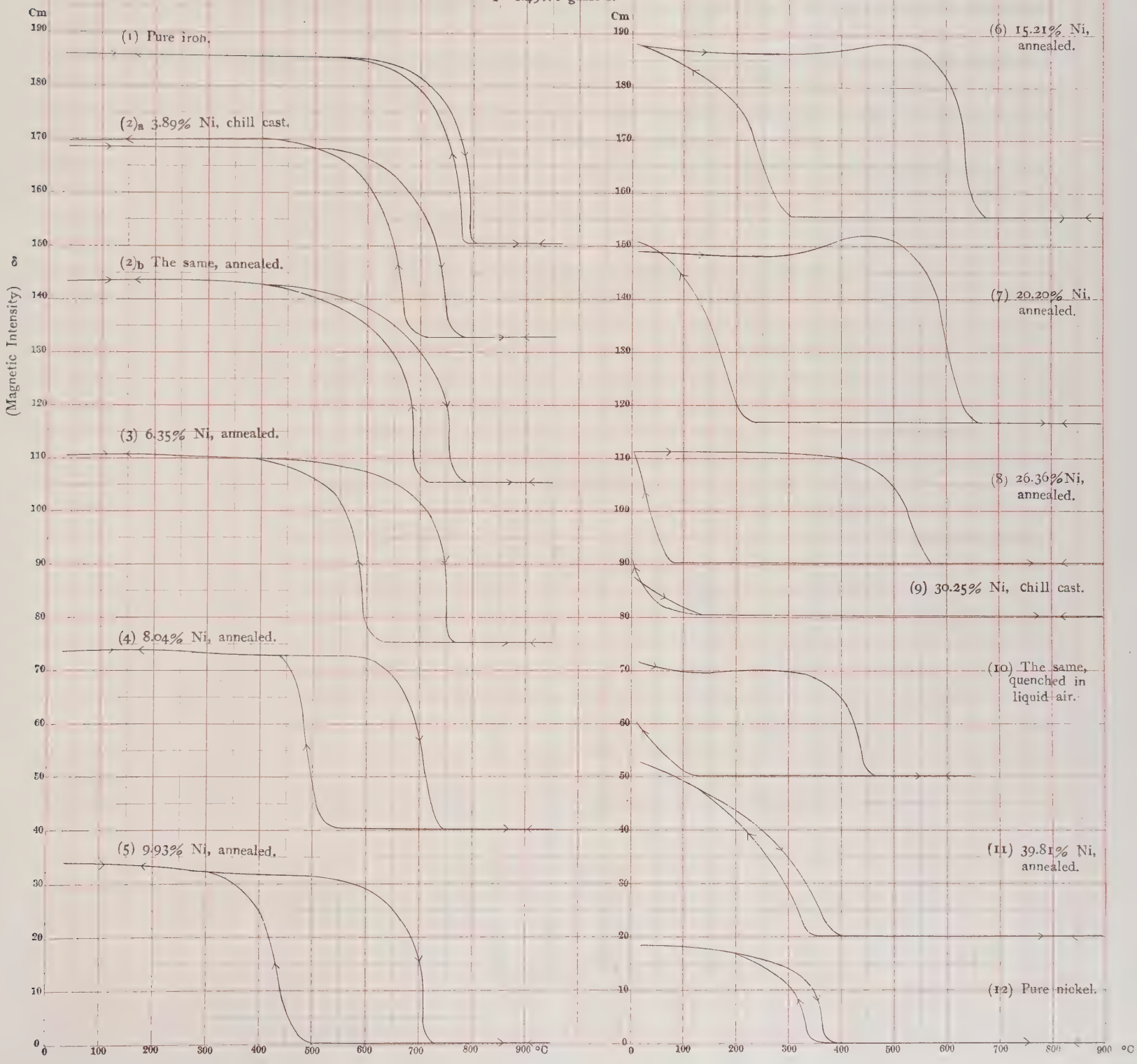
Cm
(Magnetic Intensity) δ
(1) Pure iron.
(2)a 3.89% Ni, chill cast.
(2)b The same, annealed.
(3) 6.35% Ni, annealed.
(4) 8.04% Ni, annealed.
(5) 9.93% Ni, annealed.
(6) 15.21% Ni, annealed.
(7) 20.20% Ni, annealed.
(8) 26.36% Ni, annealed.
(9) 30.25% Ni, chill cast.
(10) The same, quenched in liquid air.
(11) 39.81% Ni, annealed.
(12) Pure nickel.
0 100 200 300 400 500 600 700 800 900 °C

Fig. 22. (a) Heating Curves of Differential Thermal Analysis. (Fe-Ni Alloys)

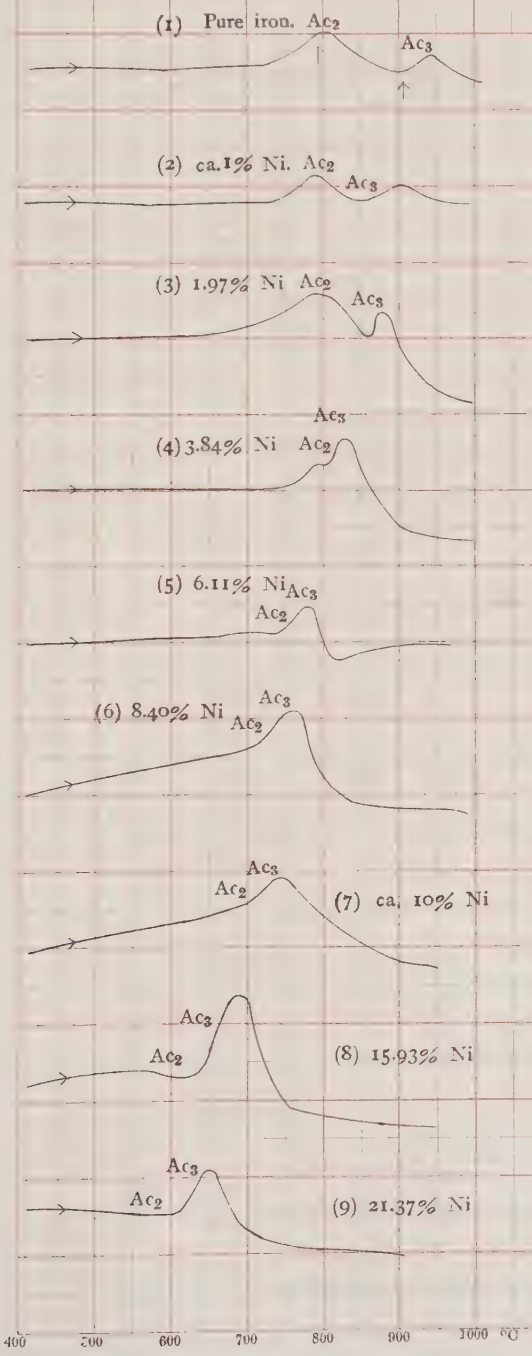

Fig. 22. (b) Cooling Curves of Differential Thermal Analysis. (Fi-Ni Alloys)

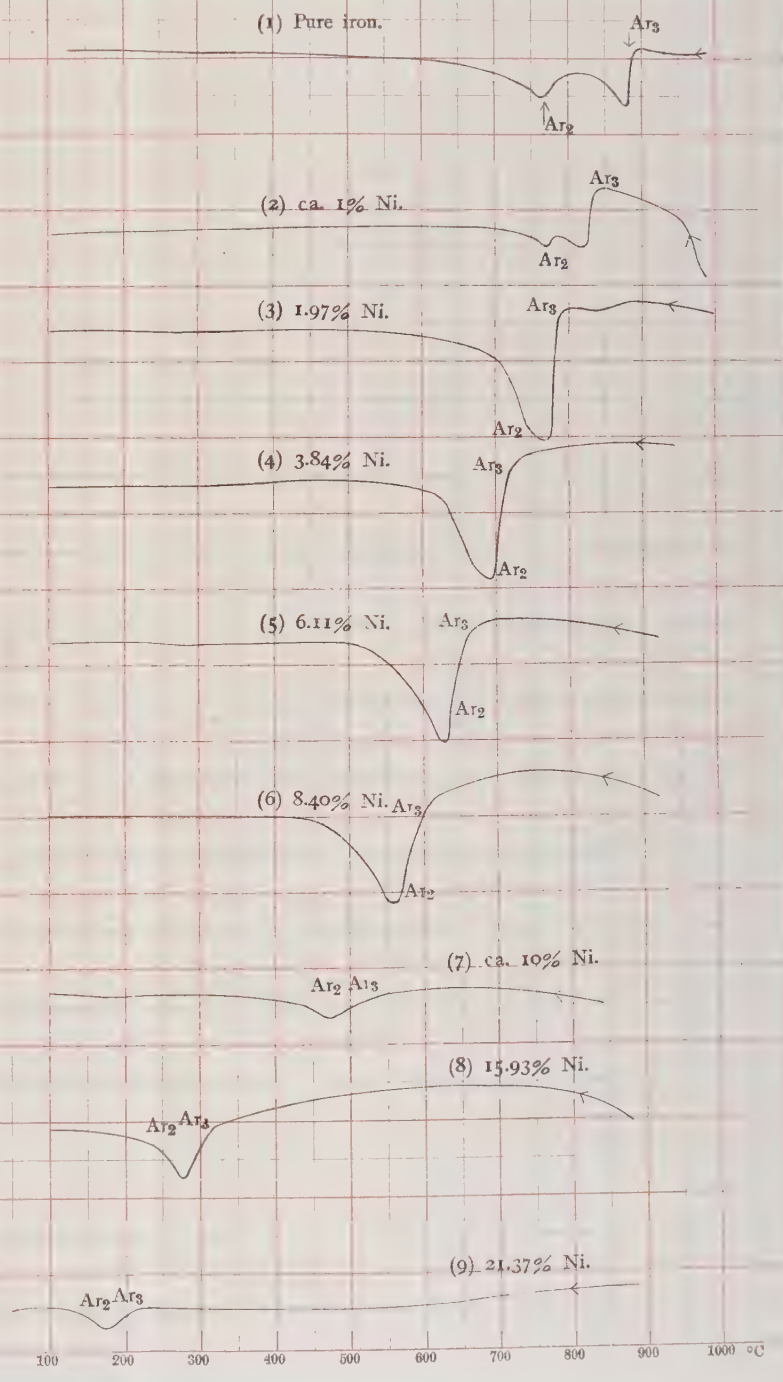

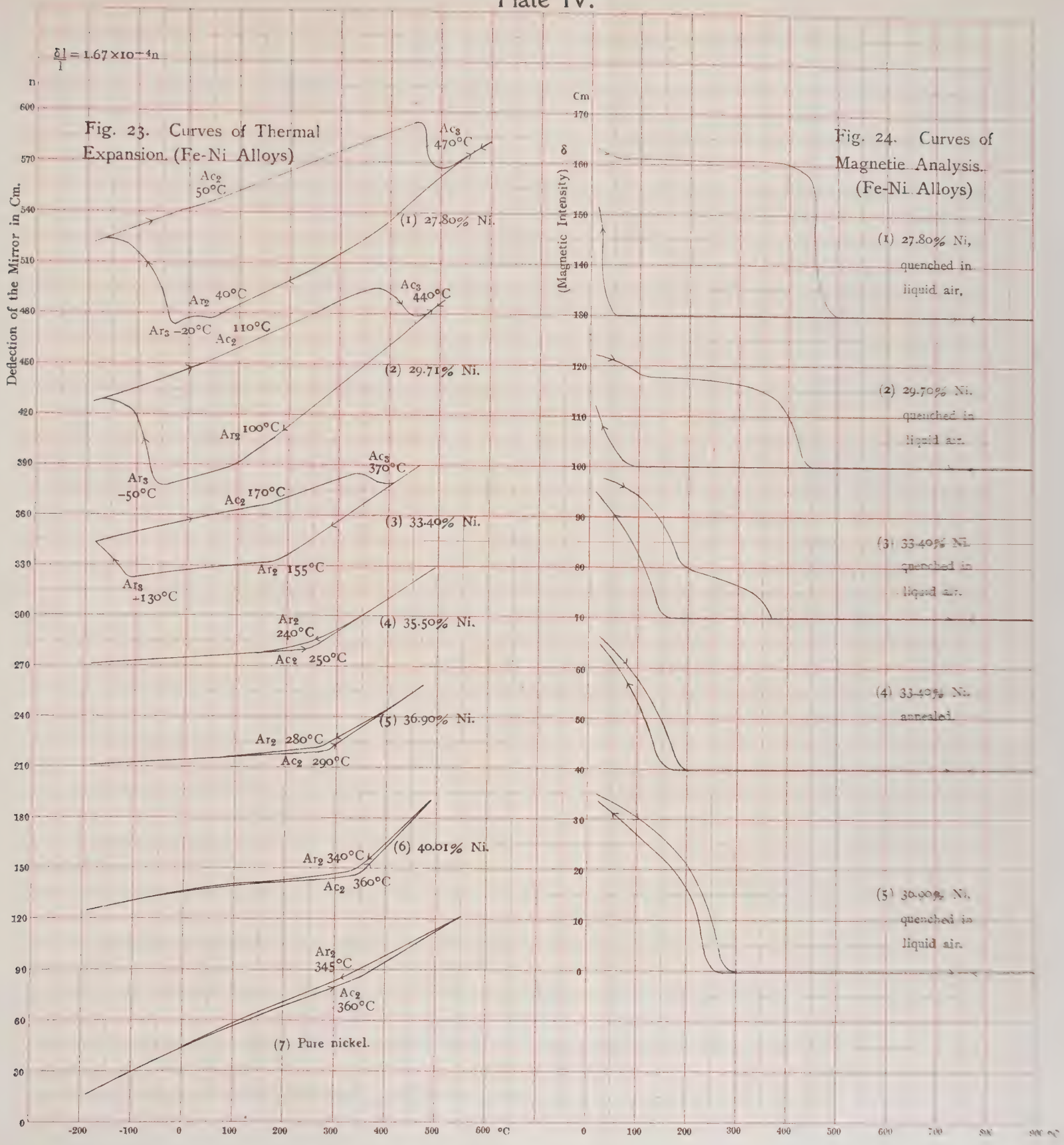

Fig. 23. Curves of Thermal Expansion. (Fe-Ni Alloys)

Fig. 24. Curves of Magnetic Analysis. (Fe-Ni Alloys)

Fig. 25. Curves of Magnetic Analysis. (Ni-C Alloys)

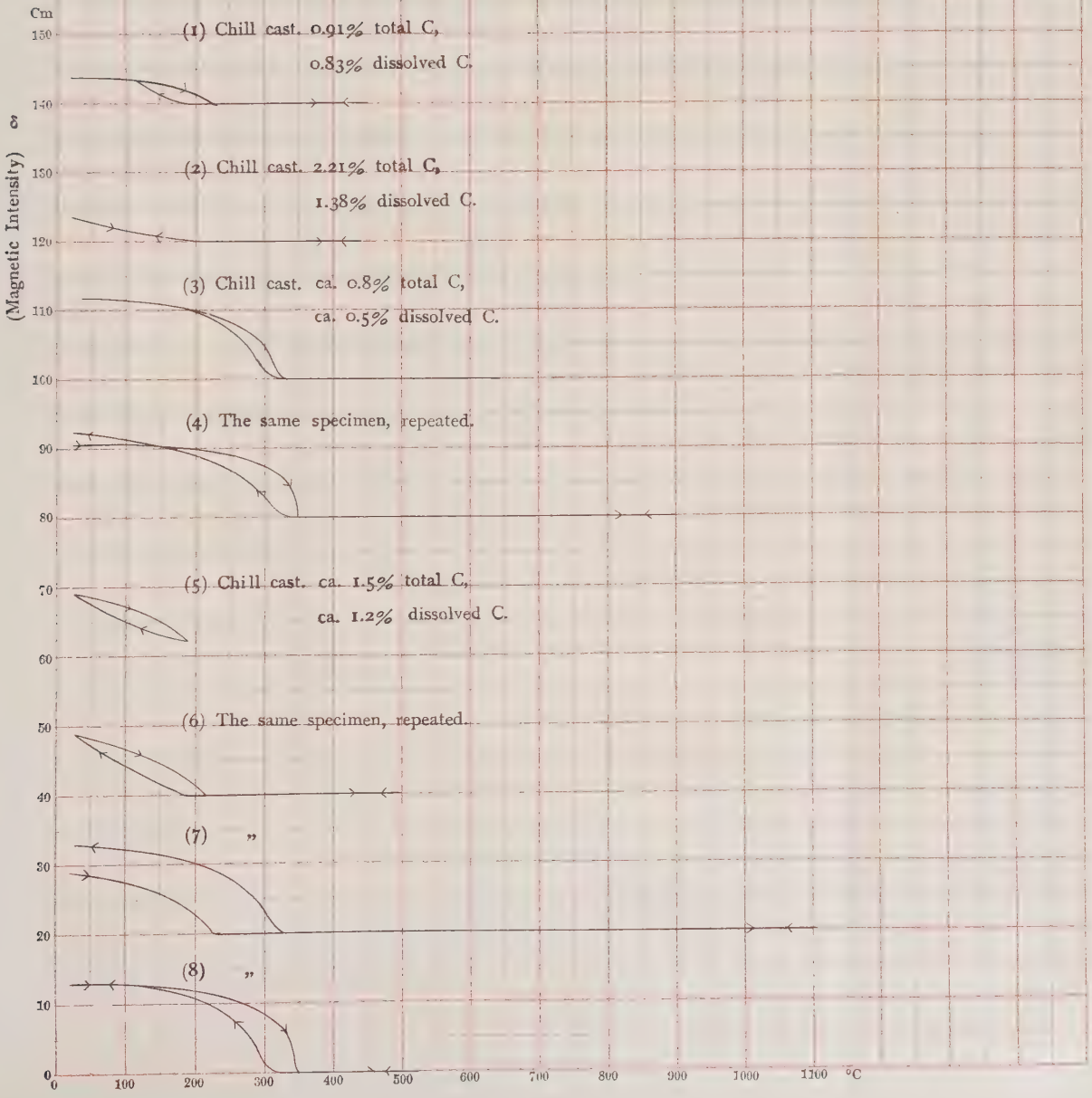

Plate VI.

Fig. 26. Curves of Magnetic Analysis.
(Fe-C-Ni Alloys)

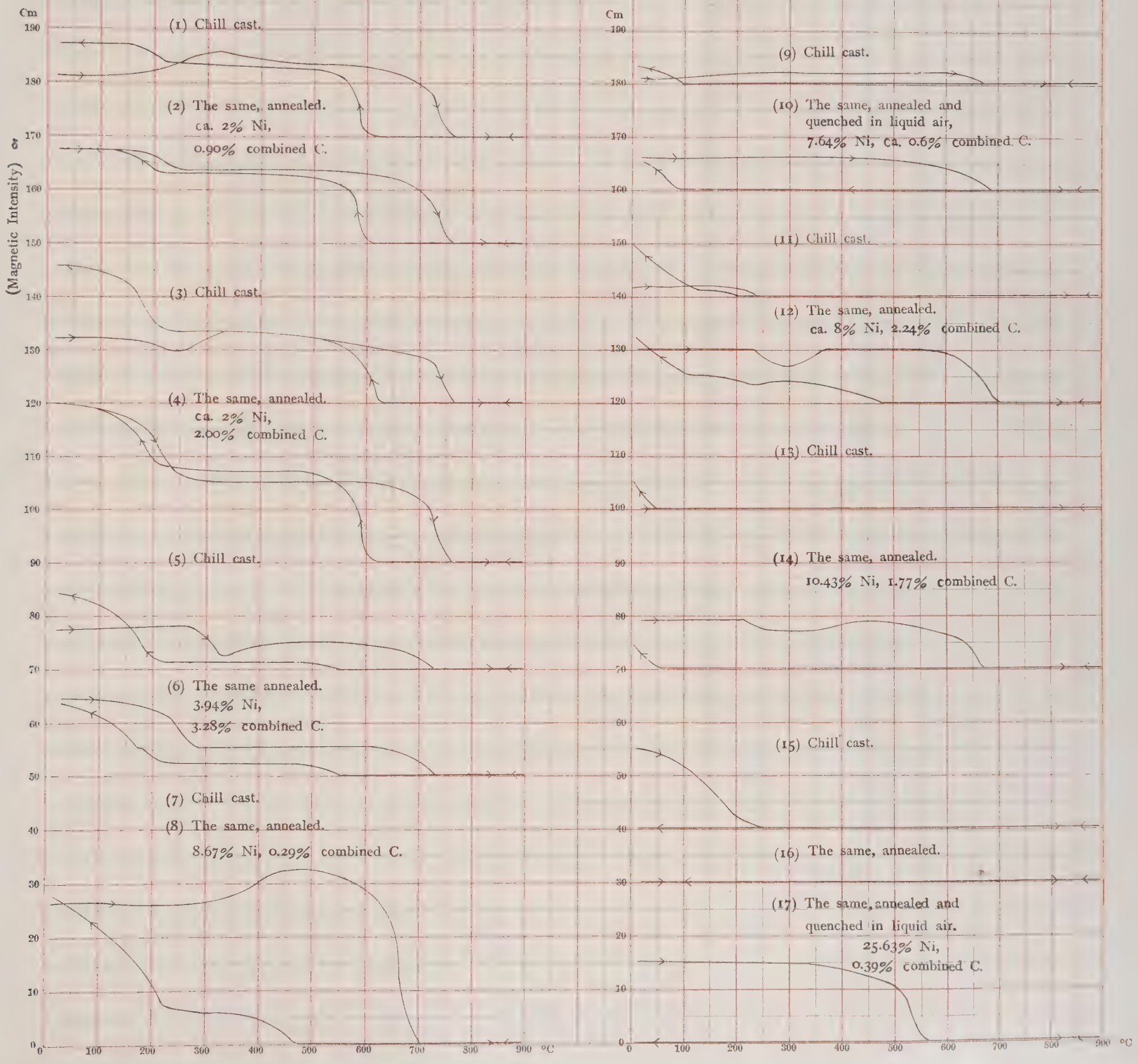

Fig. 27. Equilibrium Diagram of Fe-C-Ni System. (Space model.)

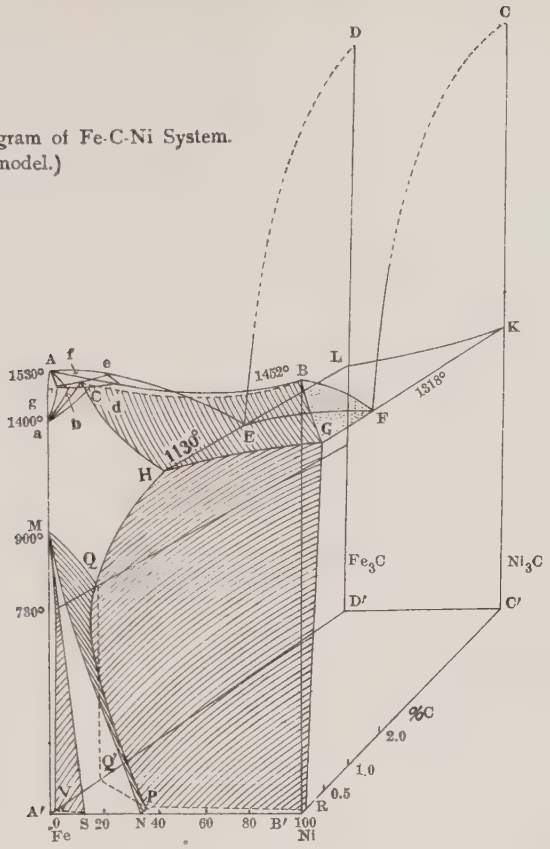

Fig. 28. Equilibrium Diagram of Fe-C-Ni System. (Projection on the basal plane.)

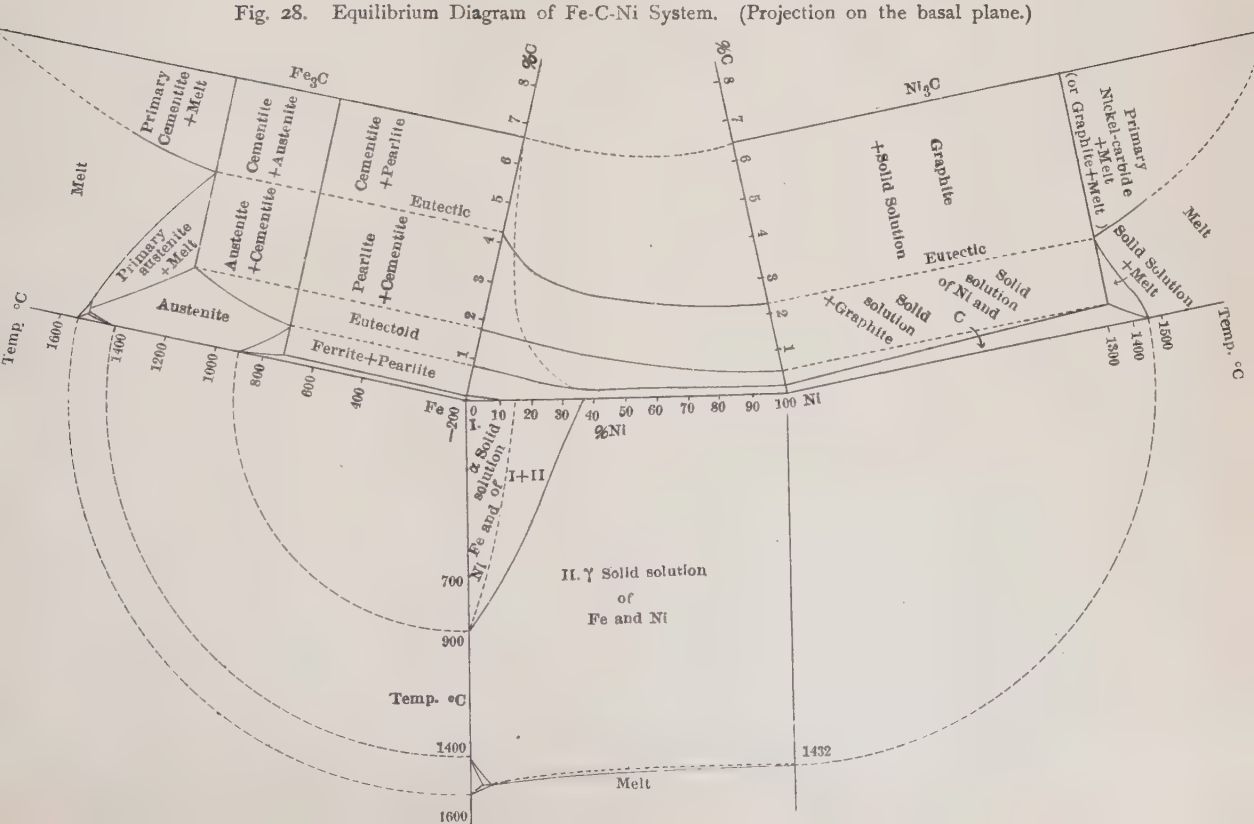

Plate VIII.

Fig. 29.

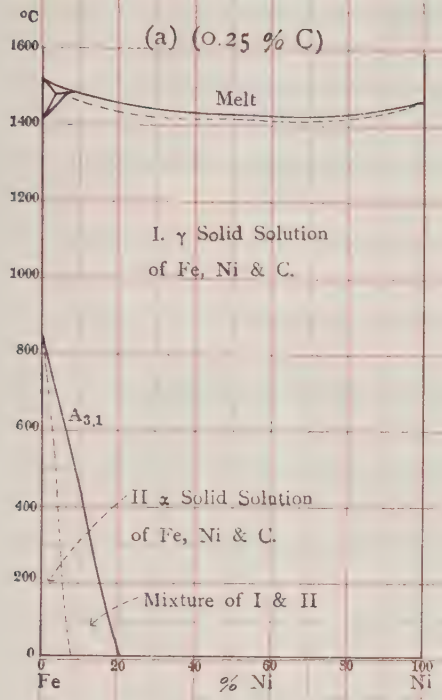

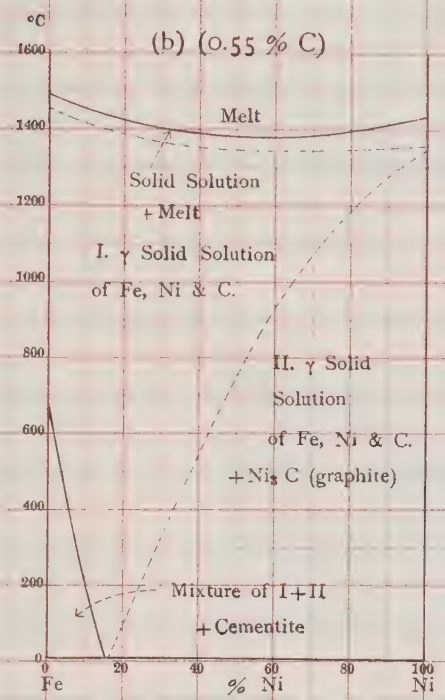

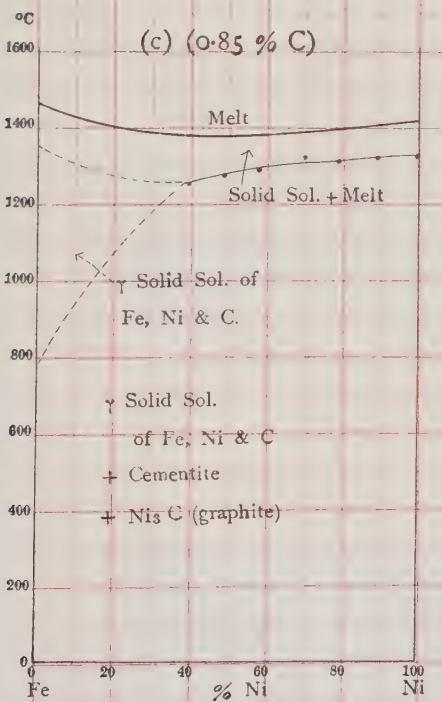

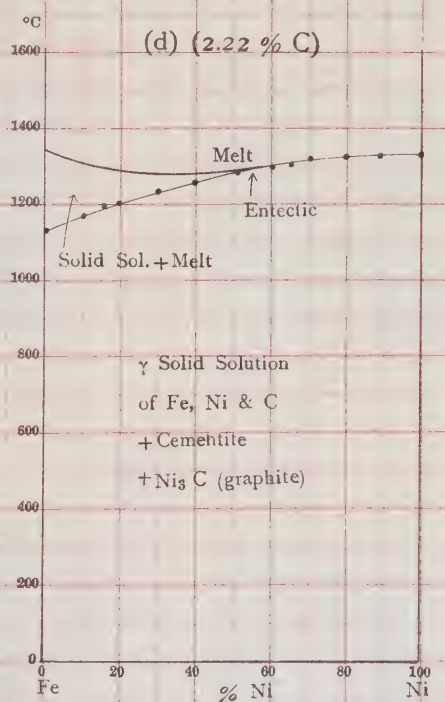

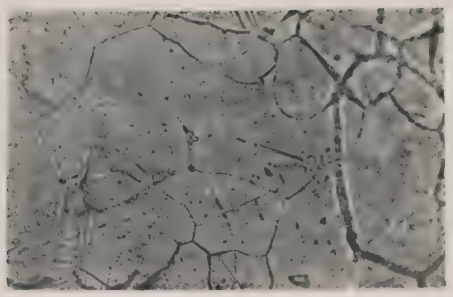

Photogr. 9. Fe-Ni, 35.5% Ni.
Cooled to -190 C. ×100.

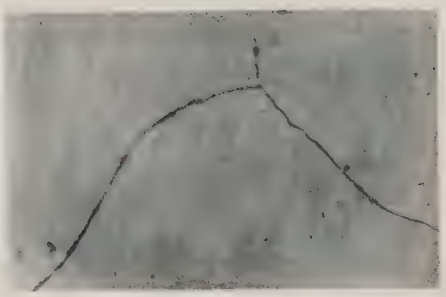

Photogr. 10. Ni-C, 0.45% C.
Normally cooled from melt. ×100.

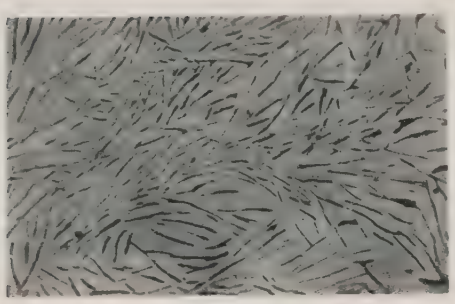

Photogr. 11. Ni-C, 2.22% C.
Normally cooled from melt. ×100.

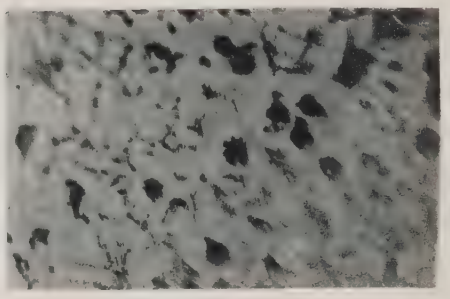

Photogr. 12. Ni-C, 2.44% C.
Chill cast into copper mould. ×500.

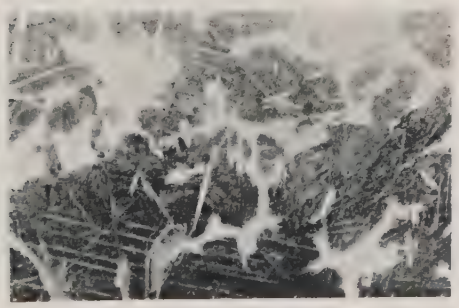

Photogr. 13. Fe-C-Ni, ca. 2% Ni, 2.34% C.
Normally cooled from melt. ×100.

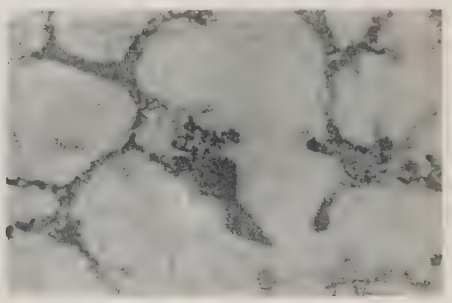

Photogr. 14. Fe-C-Ni, 7.96% Ni, 1.86% C.
Normally cooled from melt. ×100.

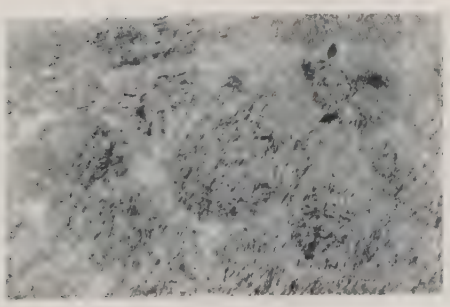

Photogr. 15. Fe-C-Ni, 9.11% Ni, 0.25% C.

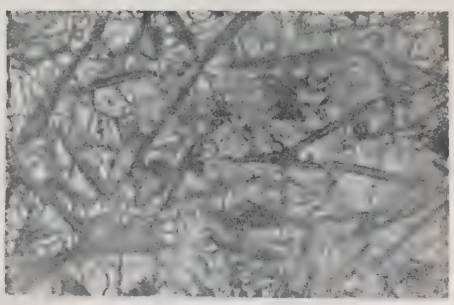

Photogr. 16. Fe-C-Ni, ca. 90%Ni, 2.5% C.

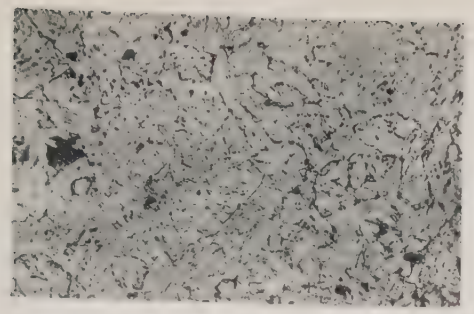

Photogr. 1. Fe-Ni, 10.90% Ni.
Normally cooled from melt. ×100.

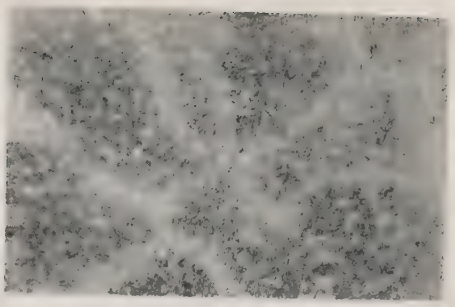

Photogr. 2. Fe-Ni, ca. 12% Ni.
Normally cooled from melt. ×100.

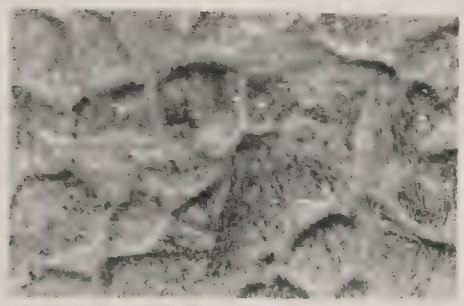

Photogr. 3. Fe-Ni, 19. 10% Ni.
Normally cooled from melt. ×100.

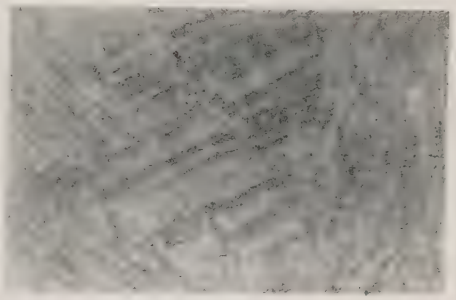

Photogr. 4. Hōchōtetsu. Cast and annealed at 1050°C for 30 fours; quenched in water.
×100.

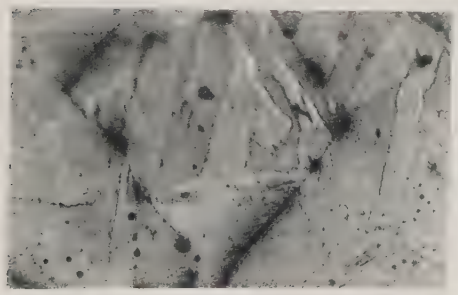

Photogr. 5. Fe-Ni, 14.9% Ni.
Same treatment as Photogr. 4. ×100.

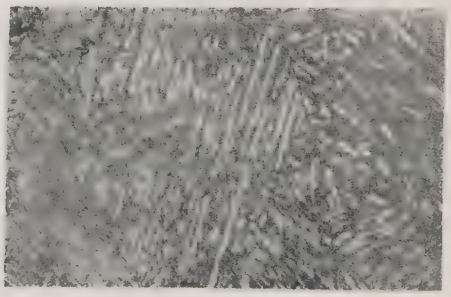

Photogr. 6. Fe-Ni, 14.9% Ni.
After the same treatment as Photogr. 4, annealed at 500°C, for 24 hours. ×100.

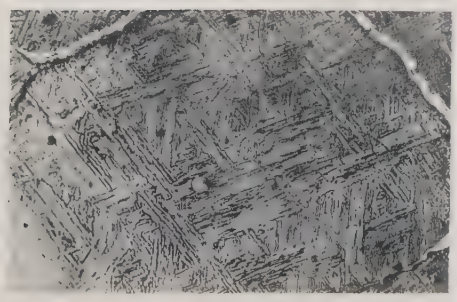

Photogr. 7. Fe-Ni, 25.6% Ni.

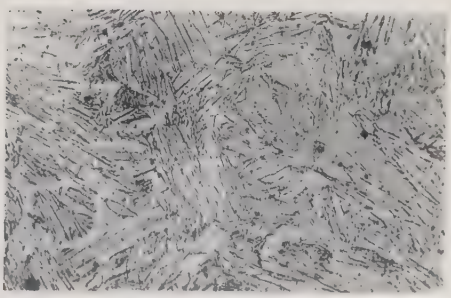

Photogr. 8. Fe-Ni, 33.4% Ni.

On the Law of Depression of Freezing Points in Metallic Alloys.

By

Kôtarô Honda and Toyozô Ishigaki.

§ 1. INTRODUCTION.

It is a well known fact that in solution, the law of depression of the freezing point holds good exactly and is usually employed for the determination of the molecular weight of a solute. In the case of alloys, it is generally believed that the above law does not exactly hold good, though Heycock and Neville[1] have already shown that in the case of binary alloys which form a simple eutectic with each other, this law is fairly well satisfied. In the case of binary alloys forming a solid solution, and also in that of an allotropic change in the solid phase, there is, so far as we are aware, no paper dealing with the confirmation of the law of depression or the elevation of the freezing point or the transformation point.

The theoritical deduction of the law of the depression of the freezing point was first made by Van't Hoff[2] and afterwards extended by M. Planck[3].

In a dilute solution, the change of the freezing point or the trans-

(1) Journ. Chem. Soc. **61**, (1892), 904.
„ „ „ **57**, (1890), 376.
„ „ „ **71**, (1897), 383.
Phil. Trans. (A) **189**, (1897), 25.
(2) Zeitschr. phys. Chem. **1**, (1887), 488.
(3) Thermodynamik, VII Auflage, (1922), 262.

formation point of a solvent due to a solute is given by

$$\delta T = -\frac{RT^2(C_l - C_s)}{m\lambda}$$

where R is the gas-constant, T the melting point or the transformation point of the solvent, C_l and C_s the concentrations of the liquidus and solidus phases coexisting at a given temperature respectively, m the molecular weight of the solute and λ the latent heat of fusion or transformation of the solvent. In the case of binary alloys forming a simple eutectic, C_s is zero and hence

$$\delta T = -\frac{RT^2C}{m\lambda}$$

which is Van't Hoff's law. In the alloys forming a solid solution, C_l may be greater or less than C_s. In the first case, the freezing point is lowered, but in the second case, it is raised. The depression or elevation of the freezing point or of the transformation point for a great number of binary alloys has been already observed mostly in Tammann's Institute in Göttingen, Germany, and is published in "Zeitschrift für anorg. Chemie" and also given Landolt-Börnstein's table. From these data we have selected a number of alloys, whose change of freezing point seems to satisfy the above law. The depression or elevation of the freezing point was estimated from the case of the dilute solution.

Now, since in most cases, the latent heat of fusion of solvent metals is not exactly known, it is more convenient to calculate this from the observed depression of the freezing point, and compare the value so obtained with those previously determined.

Thus for alloys forming a simple eutectic, we use

$$\lambda = -\frac{RT^2C}{m\delta T} = -\frac{RT^2C'}{m_0\Delta T}$$

and for alloys forming solid solutions,

$$\lambda = -\frac{RT^2(C_l - C_s)}{m\,\delta T} = -\frac{RT^2(C'_l - C'_s)}{m_o\,\Delta T}.$$

where C', C'_l and C'_s are all the atomic percentage of the solute, and m_o the atomic weight of the solvent.

TABLE I. Alloys forming simple eutectic.

Alloys		ΔT due to 1 atom. % solute	Atomic weight of solvent	λ in calories (calculated)	λ in calories (observed)
Solv.	Solu.				
Al	Ca	8.14	27.200	78.3	80.0—94.0
Al	Ni	7.65	„	83.5	„
Al	Sn	7.87	„	81.2	„
Ag	Ca	11.50	107.880	24.5	21.1—24.7
Bi	Ag	2.08	208.00	13.5	10.2—12.6
Bi	Au	2.39	„	11.9	„
Bi	Cd	2.37	„	12.0	„
Bi	Sn	2.40	„	11.9	„
Cd	Bi	5.21	112.40	12.2	10.8—13.7
Cd	Sb	5.13	„	12.3	„
Cu	Ca	13.92	63.57	41.8	41.0—43.0
Cu	Cu_2O	12.92	„	44.3	„
Pb	Au	6.10	207.20	5.7	5.3— 6.5
Pb	Sb	5.90	„	5.9	„
Pt	Pb	15.68	195.20	26.5	23.7—27.2
Pt	Sn	15.30	„	26.9	„
Sb	Ag	3.59	120.20	38.0	39.0—40.5
Sb	Ni	3.44	„	39.5	„
Ni	Bi	20.06	58.68	50.7	51.5—56.0
Ni	P	20.01	„	50.8	„
Sn	Ag	2.90	119.00	14.8	13.3—14.6
Sn	Au	3.04	„	14.1	„
Sn	Hg	3.04	„	14.1	„
Zn	Mg	5.98	65.37	24.5	23.1—28.1
Zn	Sb	5.83	„	25.1	„
Zn	Sn	6.05	„	24.2	„

TABLE 2. Alloys forming solid solution.

Alloys		Depr. of Freez. pt. due to 1 atom. % of solu.		$C_l - C_s$	$\frac{\Delta T}{C_l - C_s}$	At. Wt. of solv.	λ (calcul)	λ (observ.)
Solv.	Solu.	Liquidus	Solidus					
Ag	Al	6.35	13.21	0.88	12.20	107.88	23.1	21.1–26.0
Ag	Tl	10.23	73.00	0.86	11.90	„	23.7	„
Ag	Sb	8.84	32.80	0.73	12.10	„	23.3	„
Al	Si	6.24	29.71	0.80	7.90	27.20	80.7	80.0–94.0
Al	Zn	4.06	8.37	0.51	7.63	„	82.5	..
Au	Cu	5.60	10.10	0.45	12.44	197.20	15.3	14.7–15.9
Cu	Au	5.60	9.50	0.41	13.70	63.57	42.3	41.0–43.0
Cu	Pt	15.05	7.22	1.08	13.90	„	41.5	„
Cu	Mn	7.44	16.47	0.55	13.53	„	42.8	„
Ni	Mn	7.97	13.29	0.40	19.91	58.68	51.0	51.5–56.0
Sn	Cu	2.52	18.78	0.87	2.95	119.00	14.8	13.3–14.6
Sn	Zn	1.77	4.03	0.56	3.10	„	13.1	„

The above tables show that the latent heat of fusion calculated in the above manner fall nearly within the range of the observed values, and that for the same solvent, the atomic depression or $\Delta T/(C_l - C_s)$ is nearly independent of the nature of the solute. Thus we see that the law of depression holds good in the cases of these alloys.

We shall add the results of calculation for iron alloyed with carbon. The solidus and the liquidus in the iron-carbon system have been already measured by Rudolf Ruer and Robert Klesper[1] with considerable accuracy. The lowering of the A_3 point has also been repeatedly measured by previous investigators.

According to Ruer and Klesper, the melting point of pure iron is 1528°C, but judging from the depression curve of the iron-carbon system, this seems to be a little too high, at least in connection with the iron-carbon alloys; hence 1523° is here adopted for 1528° (Fig. 1).

(1) Ferrum, 11 Jahrg., Heft 9, 1913/14.

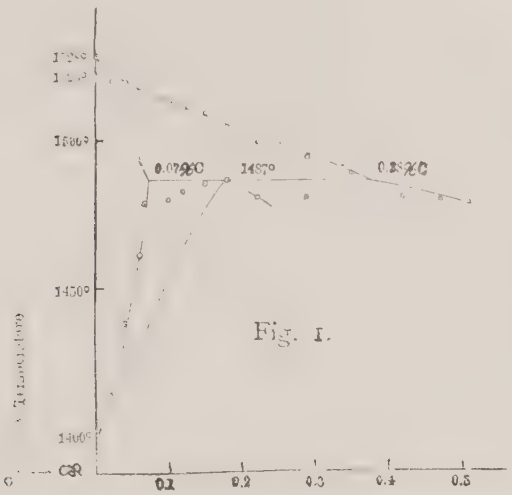

Fig. 1.

Now at 1487°, the concentrations of carbon at the liquidus and solidus points are respectively 0.38 and 0.07 percent; and the depression of the freezing point due to a 0.38 percent concentration of carbon is 36°. Taking the latent heat of pure iron to be 49 calories[1], we get from the formula (1)

$$\delta T = -\frac{RT^2(C_l - C_s)}{m\lambda} = -33.8°$$

which is near the observed value of depression, 36°.

Next, in the same diagram, the A_4 point of pure iron is 1401°C and the rising of the point by the addition of 0.02 percent of carbon is 13° in the upper part of the transformation. Judging from the interval between the upper and lower lines of transition, the concentration $(C_l - C_s)$ becomes nearly equal to 0.005 percent. Taking the heat of transformation to be 1.93 calories,[2] we get

$$\delta T = -\frac{RT^2(C_l - C_s)}{m\lambda} = +13.8°$$

which is also very near the observed value of depression, 13°.

Lastly the A_3 point is also depressed by the addition of carbon; ac-

(1) Landolt-Bernstein Table, II (1923), 1467.
(2) Landolt-Bernstein Table, II (1923), 1486.

cording to the result of an accurate measurement by Assistant Professor S. Konno[1], the A_3 point is 918°C, and δT is 15° by the addition of 0.035 percent of carbon. Taking the heat of transformation to be 5.6 calories, we get

$$\delta T = -\frac{RT^2C}{m\lambda} = -14.7°$$

which is also very near the observed value of depression, 15°.

From the above, we conclude that in the case of these alloys the law of depression is confirmed within experimental error and that at least in the alloys which do not form any intermetallic compound, the solute metals dissolve in the liquid solvents as a monatomic element.

In the other cases, the calculation of the latent heat does not give any reasonable values. This failure is probably due to the following cases :—

1. Impurities contained in metals,
2. Change of freezing point is not determined with a sufficiently dilute solution,
3. The inaccurate determination of the liquidus and solidus.

Hence for a number of cases of previous failure, we have newly determined the change of the freezing point with necessary precautions; the results of our experiment were always found to confirm the said law.

§ 2. METHOD OF EXPERIMENT.

The usual method of thermal analysis is used. The alloy to be tested was melted in an alundum tube placed in a vertical furnace, whose distribution of temperature was uniform over 5 cm. The hot junction of a copper constantan thermo-couple protected by a thin porcelain tube was vertically dipped in the tube. To protect the melt from oxidation, it was covered with a thick layer of asbestos wool, over which fluid paraffin or vaseline was poured, except in the case of zinc and copper, which was melted under a cover of fine graphite powder and in an atmosphere of hydrogen gas.

(1) Sci. Rep. **12**, (1923), 131.

The cold junction of the thermo-couple was invariably placed in a Dewar ice box. The thermoelectromotive force was measured by means of a potentiometer with a drum slide wire, made by the Leeds & Northrup Co. of Philadelphia, and connected with a mirror galvanometer as shown in Fig. 2.

Fig. 2.

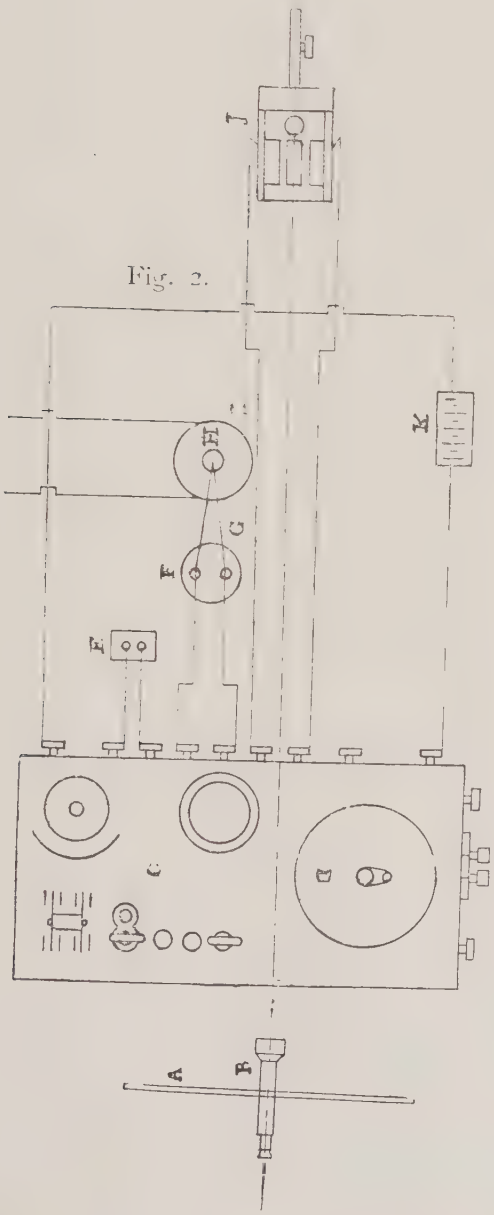

A : Reading scale
B : Telescope
C : Potentiometer
D : Drum slide wire
E : Standard cell
F : Dewar box
G : Thermo-couple
H : Alundum tube
I : Resistance furnace
J : Mirror galvanometer.
K : Battery

By this means we were able to measure a difference of potential up to one thousandth of a millivolt. The calibration of the copper-constantan thermo-couple was made by the melting points of chemically pure metals, such as Sn, Bi, Cd, Pb and Zn, and for Pt-Pt,Rh thermo-couple Cu and Ag prepared by E Merk, Germany, marked "extra pure". Here a great precaution was taken against the contamination of the couple and the metal. If there was

a doubt as to the proper depth of immersion of the hot junction of the thermo-element, several measurements were made at different depths, till a position was found, at which its slight variation did not affect the temperature measurement.

(1) Pure metals.

A favorable rate of cooling for the determination of freezing point was 1.5° per minute and the cooling was started from about 10° above the melting point. The freezing and melting points thus obtained did not differ more than 0.1° from each other.

In our experiment, the undercooling seldom exceeds 0.1° or 0.2°, but this was corrected by means of the heating curve, for which the superheating is negligibly small.

The electromotive forces corresponding to the freezing points of pure metals are given below,

Freezing point of Zn is	419.4°,	21.807	in millivolts.
„ „ Pb is	327.4°,	16.397	„
„ „ Cd is	320.9°,	16.023	„
„ „ Bi is	271.0°,	13.152	„
„ „ Sn is	231.8°,	10.087	„
Boiling point of aniline	182.5°,	8.259	„

For Pt-Pt,Rh thermo-couple, the freezing point of Cu is 1083°, 11.595 in millivolts and that of Ag is 960.5°, 9.785 in millivolts. If we plot the electromotive force against the melting point using the above data, the temperature depression caused by the solute can be found from the corresponding change of electromotive force. Thus, for copper constantan thermoelement, at the melting point of Zn, Pb, Cd, Bi and Sn, 1°C corresponds to 0.0588, 0.0575, 0.0574, 0.0552 and 0.0533 millivolts, and for the Pt-Pt,Rh thermo-element, at the melting point of copper, 1°C to 0.0148 millivolts, respectively. Since we can estimate in the potentiometer up to 0.002 millivolts, about one twenty-fifth of a degree in the copper-constantan thermo-element and one seventh of that in Pt-Pt,Rh thermo-element can be measured.

A certain quantity of the solute metal corresponding to 0.5, 1.0, 1.5, or 2.0 atomic weight was taken in each case and alloyed with the solvent. The method of determination of the freezing points of alloys, whose components did not form any solid solution with each other, was exactly the same as that of pure metals; but for alloys forming solid solutions, to prevent the supercooling of the solidus points, we had to take the heating curves after annealing for 3–17 hours at a temperature a little below its solidus point.

For some alloys, the specimens were analysed after the observation was completed; but we always found, that the quantity of the solute metal does not change within the accuracy required for our investigation. Hence in the tables below, the quantity of the solute taken for alloying is given.

§ 3. RESULTS OF EXPERIMENTS.

I. *Alloys forming a simple eutectic.*

As an example of the present method of measurement, the case of Zn-Cd system is given below:—

TABLE III.

At. % Cd. (Reduced)	Freez. Pt. in M. V.	Freez. Pt. in °C	Depr. in M. V.	Depr. in °C
0	21.807	419.40	—	—
1.0	21.494	414.02	0.313	5.35
2.0	21.186	408.71	0.621	10.69

Thus, at least up to 2 atomic percent of cadmium, the depression of the freezing point is proportional to the concentration of the solute. Here we again calculated the latent heat of fusion of zinc using the above data by means of Van't Hoff's relation and compare the value thus obtained with those previously determined. Thus, we get

$$\lambda = -\frac{RT^2C}{m_0\Delta T} = 27.1 \text{ calories.}$$

Here $T = 419.4 + 273.0 = 692.4°$,

C' = atomic percent $= \frac{1}{100}$, $\Delta T = 5.38°$,

m_0 = molecular weight of the solvent $= 65.37$.

The latent heat of fusion of zinc previously determined varies from 23.1 to 28.1 calories, the greatest value of which nearly coincides with the above calculation. Hence we may conclude that cadmium dissolves in zinc as a monatomic element.

The atomic depression of the freezing point of zinc by an addition of cadmium was found by Heycock and Neville to be 4.6°, which is however too small. The value 5.38° which has been found in the present experiment nearly coincides with the value 5.00° obtained by Lorenz and Plumbridge[1].

The results of observation for six alloys are given in the following table; and the cooling curves from which our results have been obtained, are shown in Pl. I:—

TABLE IV.

Alloys		Mt. Pt. of Solv.	At. % of Solute	Depr. of Freez. Pt. °C	Atomic depression	λ Calc.	λ Observ.
Solv.	Solu.						
Cd	Cu	320.9	0.5 1.5	2.39 7.30	4.84	17.3	10.8—13.7
Cu	Cd	1083.0	1.0 2.0	14.25 29.10	14.45	40.8	41.0—43.0
Cu	Pb	„	1.0 2.0	14.60 29.05	14.55	39.6	„
Pb	Ag	327.4	1.0 2.0	5.88 11.70	5.86	6.0	5.3—6.4
Zn	Cd	419.4	1.0 2.0	5.38 10.09	5.36	27.1	23.1—28.1
Zn	Tl	„	0.25 0.50	1.30 2.70	5.40	27.0	„

Thus, the atomic depression of cadmium by an addition of copper as found by Heycock and Neville was 3.6°; this depression is too small.

(1) Zeitschr. anorg. Chem. **83**, (1913), 233.

the value 4.84° which has been found in the present experiment, approaches considerably to the theoretical value. In the case of thallium dissolved in zinc, the atomic depression of zince as found by Heycock and Neville, that is, 4.95°, is too small. The atomic deperssion of lead by an addition of silver as found by the present experiment nearly coincides with the value 6° which was obtained by Heycock and Neville[1]. According to Friedrich[2] and Sahmen[3], the atomic lowerings of copper by the addition of lead and cadmium are 12.2° and 13.0° respectively, the values of which are a little smaller than ours. From the above table, we see that for the same solvent, the atomic depression is almost independent of the nature of the solute, and that the calculated values of λ, except that from Cd-Cu, approach the mean of the observed values, and that they are probably very close to the true values.

We may therefore conclude, that these solute metals must be present in the solvent as a monatomic element.

II. *Alloys forming a solid solution.*

Let us consider at first the case of Pb-Sn system. As to whether the Pb-Sn system has a solid solubility or not, the investigations by Rudberg[4], Mazzoto, Spring[5], Wiesengrund[6], Kapp[7], Stoffel[8] and Kurnakow[9], are to be mentioned. They found a saturated concentration of each component with the other by means of the eutectic horizontal, the results of which are given in the table below :—

TABLE V.

Name	Sn % in Pb	Pb % in Sn
Rudberg	20	1.0
Mazzoto	6	0.5
Spring	13	10.0
Wiesengrund	4.5—10	13
Kapp	11	1.0
Stoffel	10	?
Kurnakow & Zemczuzuy	8.3	?

(1) Phil. Trans. (A), **189**, (1897), 37.
(2) Metall. **4**, (1907), 300.
(3) Zeitschr. anorg. Ghem. **49**, (1906), 305.
(4) Pogg. Ann. **18**, (1830), 240.
(5) Bull. Sov. Chim. (2), **46**, (1886), 255.
(6) Wied. Ann. **52**, (1894), 777.
(7) Drudes. Ann. **6**, (1901), 754.
(8) Zeitschr. anorg. Chem. **53**, (1909), 139.
(9) Zeitschr. anorg. Chem. **60**, (1908), 1.

From this we see that all these observations agree in the point that the solid solubility of tin in lead is about 10 percent and that of lead in tin is very small. The irregularity of these results may be attributed to the difference in the rates of cooling and to the impurities present. Heycock and Neville measured the atomic depression of lead and tin, and compared them with the theoretical values. Thus:—

Solute	Sn	Pb
Calculated atomic depression	6.5	3.0
Observed atomic depression	1.7	2.8

The above shows that the observed atomic depression of the melting point of lead by the addition of tin is too small as compared with that of the calculated value. In his investigation Stoffel pointed out that this discrepancy is due to the solid solubility of lead for tin. In fact, the depression 1.7° caused by the addition of 1 atomic percent of tin, as found by Heycock and Neville, is the depression of the liquidus point, the value of which nearly coincides with ours, 1.79°. Hence in order to calculate the theoretical depression we must take into consideration the melting interval of the alloy. The following table contains one of our results of observation:—

TABLE VI.

At. % Sn	Freez. pt. in M.V.		Freez. pt. in °C		Its depr. in M.V.		Its dper. in °C	
0	16.397		327.40		—		—	
	Liqui.	Soli.	Liqui.	Soli.	Liqui.	Soli.	Liqui.	Soli.
1.0	16.293	16.246	325.61	324.79	0.104	0.151	1.79	2.61
2.0	16.188	16.086	323.80	322.05	0.209	0.311	3.60	3.35

From the observed value of atomic depression, the latent heat of fusion of lead was calculated from the formula as follows:—

$$\lambda = -\frac{RT^2(C_l' - C_s')}{m_0 \Delta T} \cdot = 5.7 \text{ calories.}$$

Here $T = 327.4° + 273 = 600.4°$,

$C'_l - C'_s = 0.31/100$,

$\delta T = -1.79°$, $m_o = 207.2$.

The previous determinations of the latent heat of fusion of lead vary from 5.3 to 6.4 calories; the above value is nearly their mean. Thus we see that tin dissolves in lead as a monatomic element. The following table contains the results of similar observations for 16 binary alloys, for which the depressions in the liquidus points have been already measured by Heycock and Neville.

TABLE VII.

Alloys		Mt. pt. of solv.	At. % of solu.	Change of freez. pt.		$C'_l - C'_s$	$\frac{\Delta T}{C'_l - C'_s}$	λ Calc.	λ Observ.
Solv.	Solu.			Liqui.	Soli.				
Bi	Pb	271.00	1.0	−1.49	−5.19	0.67	2.24	12.7	10.2–12.6
			2.5	−3.78	−12.58				
Pi	Zn	,,	1.0	−1.46	−4.40	0.66	2.24	12.6	,,
			2.0	−2.98	−8.98				
Cd	Ag	320.90	1.5	+14.20	+5.20	1.73	5.52	11.4	10.8–13.7
			2.0	+19.29	+6.99				
Cd	Hg	,,	0.5	−1.29	−2.47	0.47	5.36	11.7	,,
			1.5	−3.75	−6.98				
Pb	Bi	327.40	0.5	−1.49	−3.09	0.51	5.80	6.0	5.3–6.4
			2.0	−5.90	−12.57				
Pb	Cd	,,	0.5	−2.00	−5.83	0.66	6.04	5.8	,,
			1.0	−3.99	−11.72				
Pb	Hg	,,	1.0	−3.38	−6.50	0.57	6.00	5.9	,,
			2.0	−6.88	−13.17				
Pb	Sn	,,	1.0	−1.79	−2.61	0.31	5.74	5.7	,,
			2.0	−3.60	−5.35				
Cu	Ni	1083.00	1.0	+6.05	+4.23	0.44	13.77	41.7	41.0–43.0
			2.0	+12.15	+8.50				
Cu	Sn	,,	0.5	−5.55	−27.81	0.80	13.92	41.5	,,
			1.0	−11.16	−55.74				
Cu	Sb	,,	0.5	−5.77	−34.80	0.85	13.60	42.6	,,
			1.0	−11.57	−77.00				
Cu	Zn	,,	1.0	−7.30	−14.85	0.51	14.31	40.4	,,
			2.0	−14.58	−29.85				
Sn	Bi	231.80	0.5	−1.19	−6.52	0.81	2.94	14.6	13.3–14.6
			1.0	−2.43	−13.27				
Sn	Cd	,,	1.0	−2.24	−9.21	0.76	2.93	14.5	,,
			2.0	−4.47	−18.88				
Zn	Ag	419.40	0.5	+2.35	+1.27	0.85	5.54	25.7	23.1–28.1
			1.0	+4.72	+2.60				
Zn	Al	,,	0.5	−2.07	−8.36	0.75	5.53	26.5	,,
			1.5	−6.23	−25.14				

The heating curves from which our results have been determined, are shown in Pl. II-IV.

The above table shows that for the same solvents, $\Delta T/(C_i - C_s)$ is almost independent of the nature of the solute, and that the calculated values of λ fall nearly within the range of the observed values.

It is also interesting to compare the atomic depressions of liquidus points (solidus according to them) obtained by Heycock and Neville with ours, as shown below:—

TABLE VIII

Alloys		The depr. of present exper. (Liqui. °C)	The depr. found by Heycock & Neville
Solv.	Solu.		
Bi	Pb	−1.51	−2.1
Bi	Zn	−1.48	−1.5
Cd	Ag	+9.57	+10.3
Cd	Hg	−2.52	−2.7
Pb	Bi	−2.95	−3.0
Pb	Cd	−3.99	−4.1
Pb	Hg	−3.42	−3.4
Pb	Sn	−1.79	−1.7
Sn	Bi	−2.41	−2.4
Sn	Cd	−2.23	−2.4
Zn	Ag	+4.71	+4.4
Zn	Al	−4.15	−4.1
Cu	Ni	−6.06	−6.1
Cu	Sn	−11.14	—
Cu	Sb	−11.56	—
Cu	Zn	−7.29	—

From the above table it is evident that the depressions or elevations as found by Heycock and Neville are all liquidus points, these values almost coinciding with ours. From the results of the present experiment,

we notice that the above values of depression or elevation agree satisfactorily with the theoretical values by taking the solidus points of these alloys into consideration. It is however to be remarked that in the case of an alloy forming a solid solution, the accuracy in measuring the difference $C_l' - C_s'$ is not so large as in the case of an alloy of a eutectic mixture. We can also conclude that even in the case of binary alloys forming a solid solution with each other, the law of the depression of freezing point is valid, and that the solute metals are present in the solvent as the monatomic element.

SUMMARY.

The results of the present experiment may be summarized as follows :—

1. The lowering of the freezing point of pure metals is proportional to the concentration of the other element, which is dissolved in the former, provided the solution is dilute.

2. If the gram molecular weight of a solute is dissolved in a given solvent, then the depression of the freezing point (termed the atomic depression) is constant independent of the nature of the solute, whether it forms a solid solution with the solvent or not.

3. The lowering of the freezing point obeys the law of depression as given by Van't Hoff or Planck, that is,

$$\delta T = -\frac{RT^2 C}{m\lambda}$$

or

$$= -\frac{RT^2(C_l - C_s)}{m\lambda}$$

4. As in the case of usual solution, the law can be used for the determination of the molecular state of the solute present in the solvent.

5. The same law is also applicable to the case of the transformations taking place in the solid phase.

Pl. I.

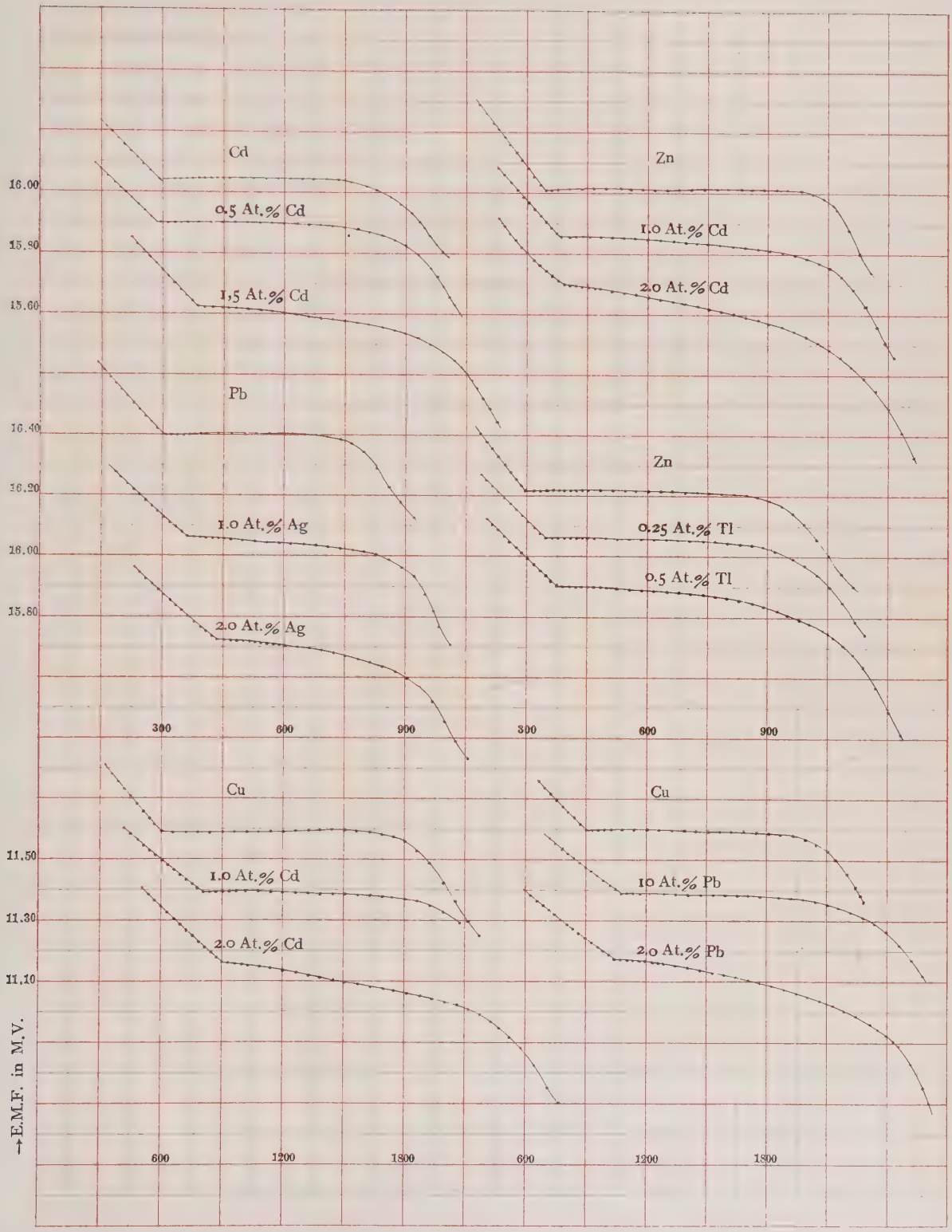
Cd
0.5 At.% Cd
1,5 At.% Cd
Zn
1.0 At.% Cd
2.0 At.% Cd
Pb
1.0 At.% Ag
2.0 At.% Ag
Zn
0.25 At.% Tl
0.5 At.% Tl
Cu
1.0 At.% Cd
2.0 At.% Cd
Cu
1.0 At.% Pb
2.0 At.% Pb
16.00
15.80
15.60
16.40
16.20
16.00
15.80
11.50
11.30
11.10
300
600
900
600
1200
1800
→E.M.F. in M.V.
→Time in Sec.

Pl. II.

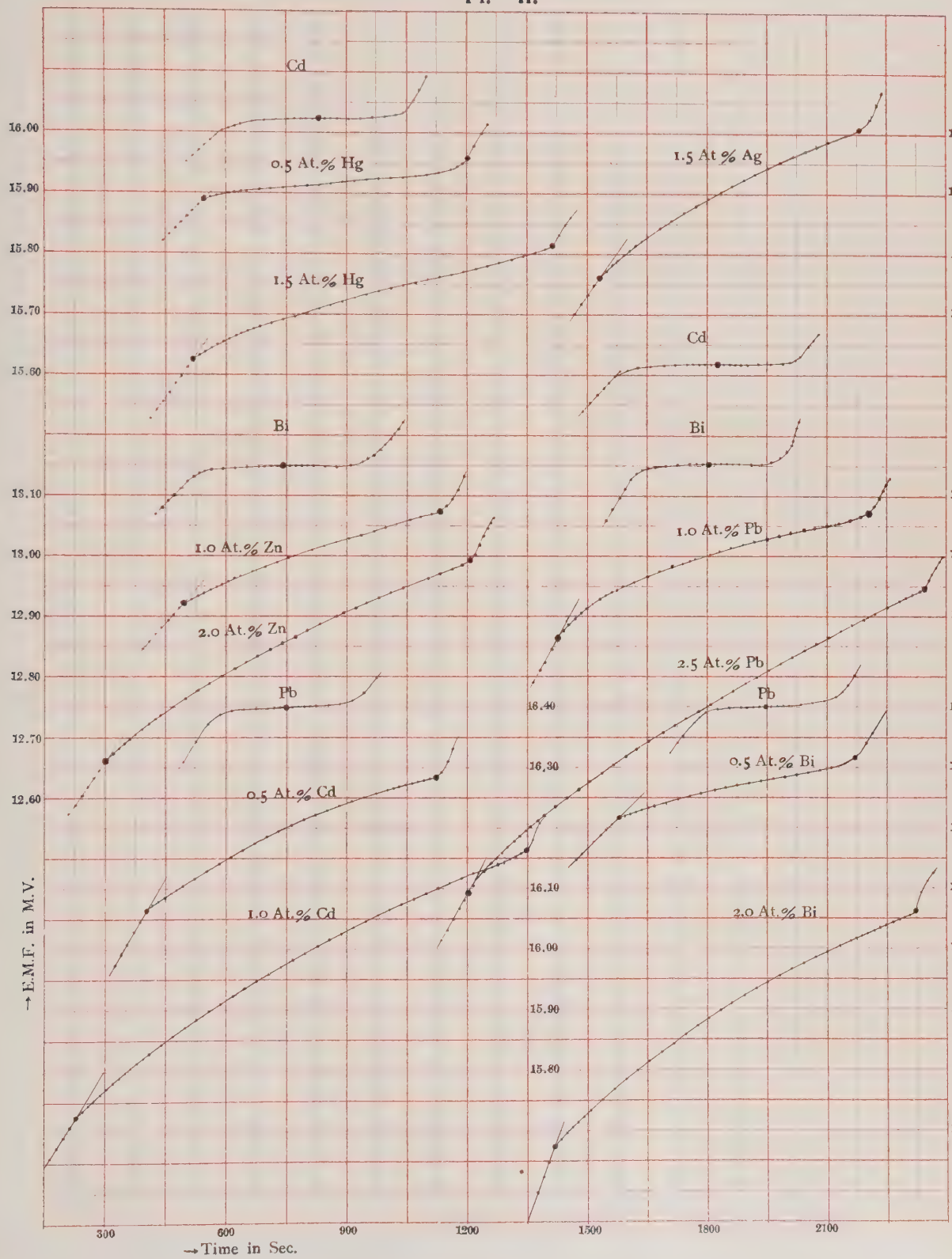
Cd
0.5 At.% Hg
1.5 At.% Hg
Bi
1.0 At.% Zn
2.0 At.% Zn
Pb
0.5 At.% Cd
1.0 At.% Cd
1.5 At % Ag
Cd
Bi
1.0 At.% Pb
2.5 At.% Pb
Pb
0.5 At.% Bi
2.0 At.% Bi
16.00
15.90
15.80
15.70
15.60
13.10
13.00
12.90
12.80
12.70
12.60
16.80
16.60
16.40
16.20
16.00
16.40
16.30
16.20
16.10
16.00
15.90
15.80
15.70
300
600
900
1200
1500
1800
2100
→ E.M.F. in M.V.
→ Time in Sec.

Pl. III.

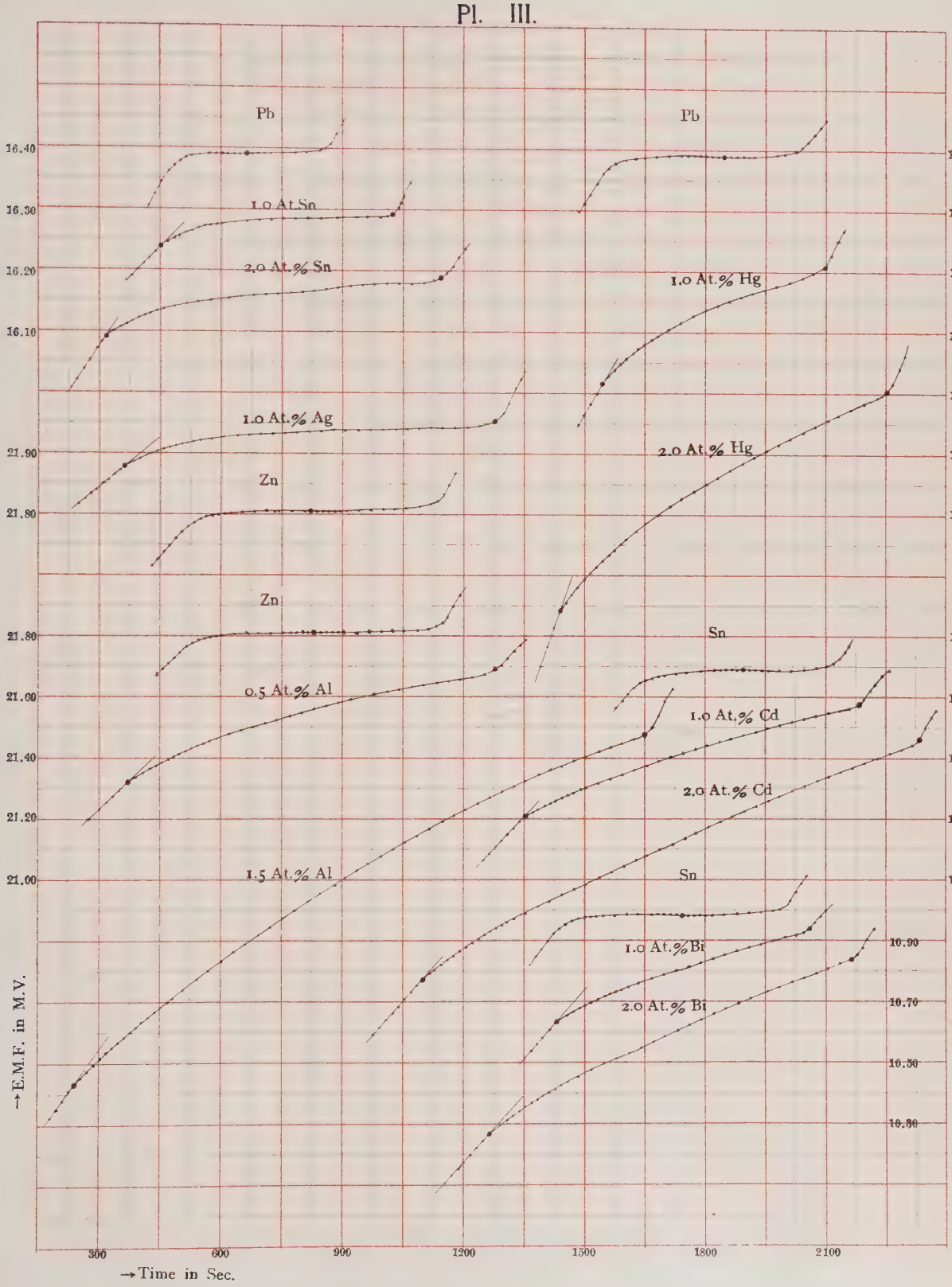
Pb
Pb
1.0 At.Sn
2.0 At.% Sn
1.0 At.% Hg
2.0 At.% Hg
1.0 At.% Ag
Zn
Zn
Sn
0.5 At.% Al
1.0 At.% Cd
2.0 At.% Cd
1.5 At.% Al
Sn
1.0 At.% Bi
2.0 At.% Bi
16.40
16.30
16.20
16.10
21.90
21.80
21.80
21.60
21.40
21.20
21.00
10.90
10.70
10.50
300
600
900
1200
1500
1800
2100
→E.M.F. in M.V.
→Time in Sec.

Pl. IV.

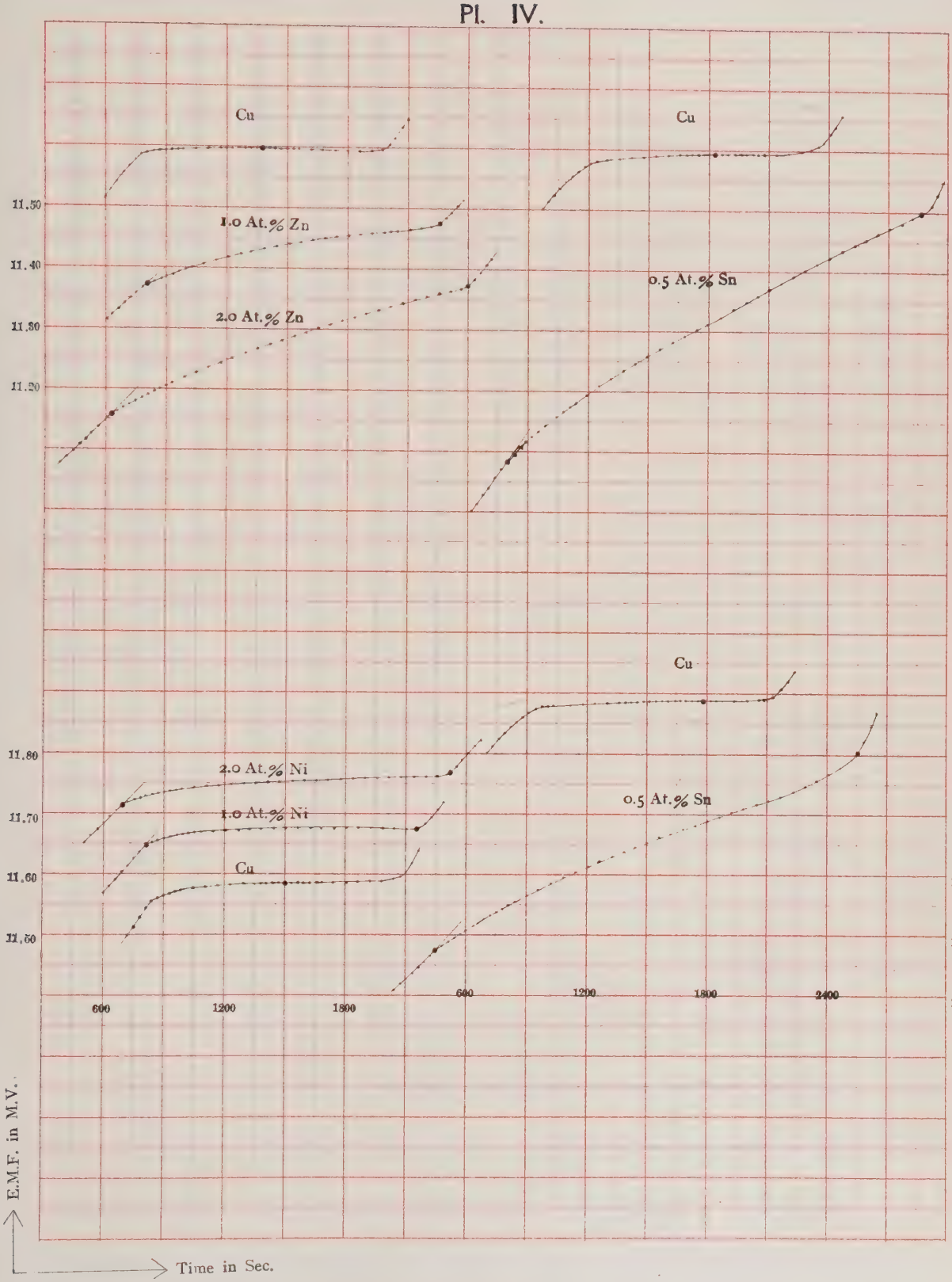
Cu
1.0 At.% Zn
2.0 At.% Zn
Cu
0.5 At.% Sn
Cu
2.0 At.% Ni
1.0 At.% Ni
Cu
0.5 At.% Sn
11.50
11.40
11.30
11.20
11.80
11.70
11.60
11.50
600
1200
1800
600
1200
1800
2400
E.M.F. in M.V.
Time in Sec.

The Use of Liquid Amalgams in Volumetric Analysis, Part II. Oxidimetric Estimation of Tungsten, etc. by Using Lead and Bismuth Amalgams.[1]

By

Kinichi Someya.

I. INTRODUCTION.

In his first communication[2] the writer has described the principles and the methods in the use of liquid amalgams in volumetric analysis, together with some applications of zinc and bismuth amalgams. The present paper deals with some of his further observations on the reducing action of lead and bismuth amalgams, which furnished him a basis for some new methods of oxidimetric determination of iron, titanium, uranium, molybdenum and tungsten.

II. EXPERIMENTAL PART.

Apparatus and methods: Essentially the same as were described in the first communication. Some slight modifications were made according as the circumstances demanded. The symbols A, B, C, etc. refer to the figure of the amalgam reductor described in the first communication.

(a) Preparation of lead amalgam. Pure lead sticks (Kahlbaum made) were washed with a little concentrated hydrochloric acid to remove the surface layer of oxides and were introduced into mercury in a cas-

(1) The one hundred and sixth report of the Research Institute for Iron, Steel and Other Metals.

(2) Zeitschr. f. anorg. Chem., **138**, (1924), 291; Sc. Rep., **1**, (1925), 47.

serole, heated over a wire gauze until the sticks were all dissolved to form a homogeneous liquid. It was cooled, washed with distilled water, and separated from the solid matter by the use of a separating funnel. The solid matter still remaining caused no trouble, since it could easily be separated by putting the amalgam in (A) with the cock (a) under it closed, and opening it and then closing it when nearly all the solid matter remained in (A) while the liquid portion went into (B).

Considering from the investigations of Puschin,[1] Fay and North,[2] and Jänecke,[3] the "liquid" lead amalgam obtained in this way consisted of the solution of lead in mercury and the solid solution of mercury and lead, the percentage of lead in the latter being fairly large and consequently the total percentage of lead in the amalgam also becoming fairly large. The lead in solution and that in solid solution (which latter was, as could be inferred from the appearance of the amalgam, no doubt in very fine suspension) proved to be a very efficient reducing agent. The amalgam could be used a surprizing number of times without impairing its reducing power at all, and the reduction went very smoothly in every applicable case. The writer is convinced that the "liquid" lead amalgam, in cases where it can be applied, is a far superior reducing agent to the amalgamated zinc used in the Jones reductor or to some other things used for like purposes.[4] The same remark applies to the liquid zinc and cadmium amalgams, and, with some reserve, to the bismuth amalgam. The lead amalgam acts very slightly with dilute hydrochloric or sulphuric acid, and can be kept with these acids an indefinite length of time without any appreciable decrease in its reducing power.

(b) In general the reduction of the solution was made in a strongly hydrochloric acid solution, where the reduction went on very rapidly and moreover where the separation of the lead chloride precipitate could

(1) Zeitschr. f. anorg. Chem., **36**, (1903), 213.

(2) Amer. Chem. Journ., **25**, (1901), 230.

(3) Zeitschr. f. anorg. Chem., **60**, (1907), 399.

(4) W. D. Treadwell, M. Lüthy & A. R. Rheiner, Helvelica Chim. Acta., **4**, (1921), 551; W. D. Treadwell, ditto, **5**, (1922), 806.

be entirely prevented. In the case where dilute hydrochloric acid or sulphuric acid was used, this could not be done, but this reduction also went very smoothly though not as rapidly as in the former case. The precipitate, being heavy, easy to settle, and indifferent to the standard solution, was in no way detrimental to the carrying out of the titration.

I. REDUCTION OF IRON WITH LEAD AMALGAM.

The ferric alum solution here used was made and standardized in the same manner as has been described in the previous cowmunication.[1] Suitable quantities were taken and shaken in the amalgam reductor with the lead amalgam and 5–10 cc. of hydrochloric acid (1 : 1) until the solution became perfectly colourless and the lead chloride ceased precipitating. When strong hydrochloric acid was added in large quantity to prevent the formation of the precipitate, the reduction went smoothly but the end of the permanganate titration of the reduced solution could not be so easily discerned owing to the pronounced yellow colour due to ferric iron, and the large quantity of hydrochloric acid present. The addition of phosophoric acid did not reduce the yellow colour appreciably. With the above-mentioned quantity of hydrochloric or sulphuric acid, the reduction also went smoothly and the presence of lead chloride or sulphate did not interfere with the removal of amalgam from the reduction flask (B). The mixture of lead chloride or sulphate and the resulting ferrous solution was titrated in the presence of 5 cc. of concentrated manganous sulphate and 5 cc. of concentrated phosphoric acid (1.7). The results show that the reduction is complete and that the method can be used for the estimation of iron, though it has no great advantage over the zinc, cadmium or bismuth amalgam method.

(1) l. c.

TABLE I. Reduction of Iron with Lead Amalgam.

Exp. No.	Fe_2O_3 taken, g.	$KMnO_4$ req. cc. (Zn-Amalg.)	$KMnO_4$ req. cc. (Pb-Amalg.)	Fe_2O_3 found, g.	Fe_2O_3 error, g.
1.	0.1598	19.94	19.95	0.1599	0.0001
2.	0.1598	19.94	19.96	0.1600	0.0002
3.	0.1598	19.94	19.97	0.1601	0.0003
4.	0.1598	19.94	19.94	0.1598	0.0000
5.	0.0799	9.97	9.95	0.0798	0.0001
6.	0.0799	9.97	9.97	0.0799	0.0000
7.	0.0799	9.97	9.96	0.0798	0.0001

Standard solution, 0.1004 n $KMnO_4$.

II. REDUCTION OF TITANIC SULPHATE WITH LEAD AMALGAM.

The titanic sulphate solution here used was made by fusing pure titanic sulphate (Merck, c. p.) with potassium bisulphate and dissolving the melt in 10 % sulphuric acid. It was standardized by reducing with zinc amalgam and then titrating with potassium permanganate according to the method of Nakazono.[1] For every 10 to 20 cc. of the solution to be reduced 30 cc. of concentrated hydrochloric acid was used. The solution was shaken in the atmosphere of carbon dioxide with the lead amalgam in the cold. The reduction went very quickly and without the separation of any precipitate of lead chloride. The titration was made in the presence of 5 cc. of concentrated manganous sulphate with potassium permanganate taking the perfect colourlessness as its end point or with ferric alum solution until the first excess drop tinged the solution yellow. The latter was standardized by reducing with zinc amalgam and titrating with standard potassium permanganate.[2] The experimental results are very satisfactory, attesting to the usefulness of the lead amalgam. (Tables II and III).

(1) Journ. Jap. Chem. Soc., **42**, (1921), 526; Chem. Abstr., **16**, (1922), 1543.
(2) Nakazono, l. c.

TABLE II. Reduction of Titanic Sulphate with Lead Amalgam, I.

Exp. No.	TiO_2 taken, g.	$KMnO_4$ req. cc. (Zn-Amalg.)	$KMnO_4$ req. cc. (Pb-Amalg.)	TiO_2 found, g.	TiO_2 error, g.
1.	0.1319	16.40	16.38	0.1317	0.0002
2.	0.1319	16.40	16.40	0.1319	0.0000
3.	0.1319	16.40	16.39	0.1318	0.0001
4.	0.0659	8.20	8.18	0.0658	0.0001
5.	0.0659	8.20	8.17	0.0657	0.0002
6.	0.0659	8.20	8.20	0.0659	0.0000

Standard solution, 0.1004 n $KMnO_4$.

TABLE III. Reduction of Titanic Sulphte with Lead Amalgam, II.

Exp. No.	TiO_2 taken, g.	Fe-Alum req. cc. (Zn-Amalg.)	Fe-Alum req. cc. (Pb-Amalg.)	TiO_2 found, g.	TiO_2 error, g.
1.	0.1020	12.64	12.65	0.1020	0.0000
2.	0.1020	12.64	12.63	0.1019	0.0001
3.	0.1020	12.64	12.62	0.1018	0.0002
4.	0.1020	12.64	12.59	0.1015	0.0005
5.	0.1020	12.64	12.64	0.1020	0.0000
6.	0.1020	12.64	12.65	0.1020	0.0000
7.	0.0510	6.32	6.30	0.0508	0.0002
8.	0.0510	6.32	6.33	0.0511	0.0001

Standard solution, 0.10069 n $Fe_2(SO_4)_3.(NH_4)_2SO_4$.

III. REDUCTION OF URANIUM WITH LEAD AMALGAM.

The uranium solution here used was made by dissolving ca. 25 g. of Merck's c. p. uranyl nitrate in water, adding sulphuric acid and evaporating to dryness to convert it into the sulphate. The residue was dissolved in water and diluted to 1 litre. The standardization was made

according to the method of Nakazono[1] by reducing with zinc amalgam in presence of air and then titrating with a decinormal potassium permanganate to the characteristic tint. In the lead smalgam reduction, ca. 20–30 cc. of concentrated hydrochloric acid for 20–30 cc. of the solution was used to prevent the separation of lead chloride. The solution was shaken in the atmosphere of carbon dioxide. The reduction to the uranous condition was found to go very quickly, and even when the solution was heated during the reduction, it went no further. The lead chloride separated during the titration caused no trouble. The table shows that under the adove condition, the reduction to the uranous condition is quantitative. The method is quite satisfactory and possesses all the advantages of the liquid amalgam method in general.

Table IV. Reduction of Uranium with Lead Amalgam.

Exp. No.	UO_2 taken, g.	$KMnO_4$ req. cc. (Zn-Amalg.)	$KMnO_4$ req. cc. (Pb-Amalg.)	UO_2 found, g.	UO_2 error, g.
1.	0.2596	19.23	19.23	0.2596	0.0000
2.	0.2596	19.23	19.22	0.2594	0.0002
3.	0.2596	19.23	19.27	0.2601	0.0005
4.	0.2596	19.23	19.24	0.2597	0.0001
5.	0.2719	20.14	20.12	0.2716	0.0003
6.	0.2719	20.14	20.15	0.2720	0.0001
7.	0.2719	20.14	20.10	0.2713	0.0006
8.	0.1359	10.07	10.07	0.1359	0.0000
9.	0.1359	10.07	10.08	0.1361	0.0002
10.	0.1359	10.07	10.09	0.1362	0.0003
11.	0.1359	10.07	19.05	0.1357	0.0002

Standard solution, 0.0998 n $KMnO_4$.

IV. REDUCTION OF MOLYBDENUM WITH LEAD AMALGAM.

The reduction of molybdic acid by means of zinc or cadmium amalgam carries as far as to the tervalent condition according to the inves-

(1) Journ. Jap. Chem. Soc., **42**, (1921), 751.

tigation of Nakazono[1] and Kano.[2] From the results obtained by such previous workers as Treadwell,[3] who used deposited lead for the molybdic acid reduction, it seemed very probable that lead amalgam also would reduce molybdic acid to the same stage of oxidation under suitable conditions. The molybdic acid solution, prepared as has been described in the first communication was here used again. When concentrated hydrochloric acid solution was used in the reduction, the colour of the solution reduced by lead amalgam was a beautiful reddish brown, while in dilute hydrochloric acid, it was dark green. When made in concentrated hydrochloric acid, the reduction was very quickly completed, while in dilute hydrochloric acid (5 cc. of concentrated hydrochloric acid for ca. 30 cc. of the solution) it was naturally more slow, and the solution had to be warmed and shaken for about 10 minutes. In both cases the titration was made in the presence of concentrated manganous sulphate. The results are perfectly satisfactory.

TABLE V. Reduction of Molybdenum with Lead Amalgam.

Exp. No.	MoO_3 taken, g.	$KMnO_4$ req. cc. (Zn-Amalg.)	$KMnO_4$ req. cc. (Pb-Amalg.)	MoO_3 found, g.	MoO_3 error, g.
1.	0.2193	45.45	45.43	0.2192	0.0001
2.	0.2193	45.45	45.40	0.2190	0.0003
3.	0.2193	45.45	45.44	0.2192	0.0001
4.	0.2193	45.45	45.45	0.2193	0.0000
5.	0.2193	45.45	45.45	0.2193	0.0000
6.	0.1097	22.73	22.71	0.1096	0.0001
7.	0.1097	22.73	22.72	0.1096	0.0001
8.	0.1097	22.73	22.73	0.1097	0.0000
9.	0.1097	22.73	22.72	0.1096	0.0001
10.	0.1097	22.73	22.73	0.1097	0.0000

Standard solution, 0.1005 n $KMnO_4$.

(1) Journ. Jap. Chem. Soc., **42**, (1921) 526; Chem. Abstr., **16**, (1922), 1543.
(2) Journ. Jap. Chem. Soc., **43**, (1922), 173; Chem. Abstr., **16**, (1922), 2818.
(3) Helvetica Chim. Acta, **5**, (1922) 806.

V. REDUCTION OF TUNGSTEN WITH VARIOUS AMALGAMS.

The oxidimetric methods for the estimation of tungsten which appeared in the past literatures are very few and here we are beset with no little difficulty on several points. Otto von der Pfordten[1] proposes the reduction of WO_3 to WO_2 by means of zinc and hydrochloric acid, subsequently titrating back with potassium permanganate. He finds that the reduction does not take place as readily as in the case of molybdenum and admits that it has the drawback in that only a small quantity of the sample can be taken and the percentage error becomes correspondingly large. Herting[2] also finds this method unsatisfactory. Knecht and Hibbert[3] proposes essentially the same method of reduction but titration by means of ferric alum, so as to make the method more convenient in the case of the analysis of steel, by making the separation of iron and tungsten unnecessasy. The difficulty of these methods is obvicus when it is remembered that it is very hard to bring tungstic acid into solution unless we have recourse to some special methods, and even if we succeed in doing so, the rapid action between the strong hydrochloric acid used and the zinc soon lowers the acidity of the solution, which in turn causes the precipitation of tungstic acid, which remains unreduced. E. Kuklin[4] gives directions for determining tungsten in steel, making use of the same principle as von der Pfordten, but dissolving the metal in equal parts of sulphuric acid (1.84) and phosphoric acid (1.7) and determining the tungsten by the difference between the reduction value of Fe+W and that of Fe alone, as determined by the Reinhardt method. He publishes no results obtained in this way. The writer first tried the zinc amalgam reduction of the solution of phosphate complex of tungstic acid, but found that the titration values were very

(1) Ber Dtsch. Chem, Ges., **16**, 508; Liebigs Ann., **282**, 138; Zeitschr. f. anal. Chem., **24**, (1885), 93.

(2) Zeitschr. f. angew. Chem., (1901), 165.

(3) New Reduction Methods in Volumetric Analysis, (1910), 100; Proc. Chem. Soc., **25**, 227.

(4) Stahl u. Eisen, **24**, (1904), 27.

irregular and that no definite results could be obtained. He also warmed the same phosphotungstate complex solution and reduced with cadmium amalgam with the modified amalgam apparatus of Kikuchi,[1] but found that only an apprpximate reduction to the quadrivalent stage occurred within a very small range of acidity and the time of shaking, and when these conditions for reduction were not rigidly controlled, insufficient or execessive reduction always took place and stopped the work without our being able to arrive at any good method for the actual analysis.

It is well known that a soluble tungstate forms a hydrated oxide when dilute acid is added to it, and, apart from converting it into a phosphate or organic acid complex, a great difficulty in the course of the volumetric analysis is encountered first in the preparation of the solution. Recently O. Collenberg and J. Backer[2] published a work in which they reported that they succeeded in preparing a comparatively concentrated hydrochloric acid solution of tungstic acid and in the electrolytic reduction to the pentavalent and the trivalent conditions using different electrodes and suitably regulating the strength of the current. Their sucess in making a hydrochloric acid solution consisted in adding potassium carbonate to the solution, which made tungsten dissolve very easily. The carbonic acid liberated on adding the tungsten solution to the hot hydrochloric acid served probably, according to them, to form very fine particles of tungstic acid which could easily be attacked by hydrochloric acid before they transformed themselves into an insoluble modification. Stimulated by their remarkable success it occurred to the writer to try whether other than electrolytic methods might not be available to bring about the reduction of the tungsten solution prepared in the same way. As it was evident that zinc or any such more electropositive metal would present a difficulty by acting too rapidly with the concentrated acid present, he chose some more electronegative, probably less powerful reducing agent, and moreover in the form of its liquid amalgam, which it has been shown in many other cases to be moderately

(1) Journ. Jap. Chem. Soc., **43**, (1922), 173; Chem. Abstr., **16**, (1922), 1716.
(2) Zeitschr. f. Elektrochem., **30**, (1924), 230.

active and convenient to handle. It was found that liquid bismuth amalgam reduces tungstic acid quantitatively to the pentavalent condition in the strong hydrochlaric acid solution, while lead amalgam also reduces it quantitatively to the trivalent condition.

The tungsten solution here used was prepared by dissolving 1/10 mole of Kahlbaum's purest sodium tungstate crystals in 1 litre of water. It was standardized by taking 20 cc. of the solution and precipitating it with mercurous nitrate and igniting it to the oxide according to the method of Berzelius.[1]

In the preparation of the hydrochloric acid solution to be reduced a slight modification of the Collenberg's procedure was made. The sodium tungstate solution (10 or 20 cc.) was evaporated to a small volume in a conical beaker over wire gauze and then a large volume (about 50 cc.) of hot concentrated hydrochloric acid (1.19) was added *all at once* and the contents shaken and rotated. By proceeding in this way it was very easy to make the tungsten solution of such a small content as is shown in Tables VI, VII, VIII. The contents of the beaker were washed into the amalgam reductor with the same concentrated hydrochloric acid (1.19). If potassium carbonate was added to the sodium tungstate solution before adding hydrochloric acid, the sodium and potassium chlorides formed thereby hindered the smooth reduction of the solution, the amalgam being covered with a dirty black scum which was partly suspended in the solution and made it more or less dark. In the case of the lead amalgam reduetion this phenomenon occurred only to a small extent. But on the whole it was found quite unneecessary to use potassium carhonate.

(a) Reduction of Tungstic Acid with Bismuth Amalgam.

Since in the following experiments the strong hydrochloric acid solution prepared as described above was heated in the amalgam reductor, it was found sometimes very difficult to avoid the loss of a small

(1) Jahresber., **21**, II, 143.

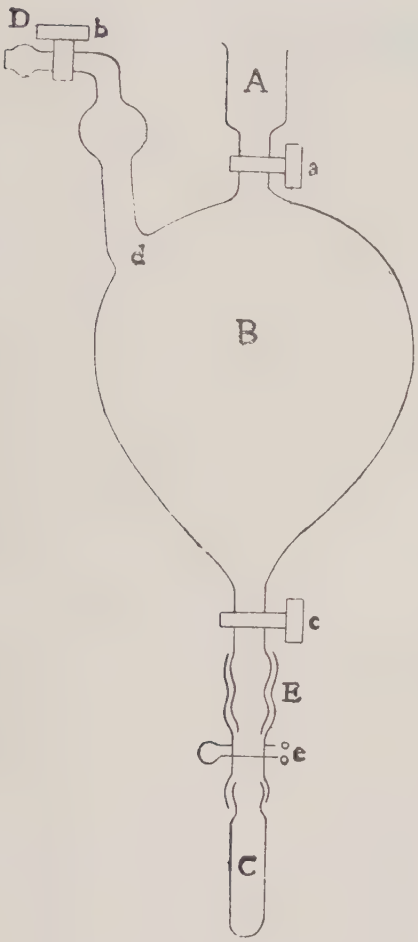

fraction of it which escaped through the stop-cock (b). The slight modification of the appraratus as shown in the annexed figure was found to be sufficient in every case to overcome this difficulty. This appratas was used throughout in the following experiments.

The lower bottle (C) was filled with freshly boiled concentrated hydrochloric acid and the contents were shaken in the atmosphere of carbon dioxide with bismuth amalgam until they became a beautiful blue and the intensity of the colour increased no more, heating the side of the reductor (B) at the same time. The titration was made in the presence of 5 cc. of concentrated manganous sulphate taking the perfect colourlessness as its end point. When too much solution was taken and the acidity was made too low by the permanganate added, hydrolysis occurred making the end point a little obscure. To prevent the formation of the oxide precipitate it was necessary to use so much concentrated hydrochloric acid as will not give rise to the hydrolysis. The results are shown in the following table. It shows that bismuch amalgam reduces tungsten chloride quantitatively to the pentavalent stage and that the results are entirely satisfactory.

TABLE VI. Reduction of Tungstic Acid with Bismuth Amalgam.

Exp. No.	WO_3 taken, g.	$KMnO_4$ req. cc.	WO_3 found, g.	WO_3 error, g.
1.	0.2320	9.90	0.2315	0.0005
2.	0.2320	9.92	0.2320	0.0000
3.	0.2320	9.92	0.2320	0.0000
4.	0.2320	9.93	0.2322	0.0002
5.	0.4640	19.85	0.4642	0.0002
6.	0.4640	19.86	0.4644	0.0004
7.	0.4640	19.84	0.4640	0.0000
8.	0.4640	19.83	0.4638	0.0002

Standard solution, 0.1008 n $KMnO_4$.

(b) Reduction of Tungstic Acid by Means of Lead Amalgam.

Following exactly the same procedure, lead amalgam was used in place of bismuth amalgam. On shaking at 50°, the solution turned first blue, suddenly crimson red and then orange yellow through thick reddish brown, and the reduction was completed in a few minutes. On titration by means of potassium permanganate in the presence of 5 cc. of concentrated manganous sulphate, it was found that the permanganate titer was exactly 3 times as that in the case of the bismuth amalgam reduction, proving that the lead amalgam is capable of reducing tungsten cnloride quantitatively to the trivalent stage under the present condition. The solution was shaken in the atmosphere of carbon dioxide, for in the air, the reduction was a little unsatisfactory (Table VII). The reduced solution was very unstable, but identical titer was obtained as was obtained *in* the amalgam reductor when the titration was rapidly carried out immediately after the solution was brought of the apparatus. The stability increases considerably when the tetravalent stage is passed.

TABLE VII. Reduction of Tungsten with Lead Amalgam.

Exp. No.	WO_3 taken, g.	$KMnO_4$ req. cc. (Pb-Amalg.)	$KMnO_4$ req. cc. (Bi-Amalg.)	WO_3 found, g. (Pb-Amalg.)	WO_3 error, g.	Atmosphere.
1.	0.2320	29.85	9.95	0.2320	0.0000	CO_2
2.	0.2320	29.87	9.95	0.2322	0.0002	CO_2
3.	0.2320	29.88	9.95	0.2322	0.0002	CO_2
4.	0.2320	29.85	9.95	0.2320	0.0000	CO_2
5.	0.2320	29.86	9.95	0.2321	0.0001	CO_2
6.	0.2320	29.85	9.95	0.2320	0.0000	CO_2
7.	0.2320	29.86	9.95	0.2321	0.0001	CO_2
8.	0.2320	29.86	9.95	0.2321	0.0001	CO_2
9.	0.2320	29.20	9.95	0.2269	0.0051	air
10.	0.2320	29.60	9.95	0.2300	0.0020	air
11.	0.2320	29.10	9.95	0.2262	0.0058	air

Standard solution, 0.1005 n $KMnO_4$.

(c) Reduction of Tungsten with Cadmium and Zinc Amalgam.

In the above the lead amalgam was replaced with cadmium amalgam for trial. It acted vigorously with the concentrated hydrochloric acid and the mixture was very inconvenient to handle. This difficulty was nearly overcome by introducing the cadmium amalgam in small portions into the reduction flask (B) each time waiting until the violent action had ceased and occasionally letting out the accumulated hydrogen gas by partly opening the cock (a). The titer, on the whole, making due allowances for the small fraction of the solution which unavoidaly escaped when opening the cock (a), shows itself to be identical with that in the case of the lead amalgam reduction, proving that the cadmium amalgam also reduces tungsten chloride quantitatively to the trivalent condition.

TABLE VIII. Reduction of Tungsten Chloride with Cadmium Amalgam.

Exp. No.	WO_3 taken, g.	$KMnO_4$ req. cc. (Cd-Amalg.)	$KMnO_4$ req. cc. (Bi-Amalg.)	WO_3 found, g.	WO_3 error, g.
1.	0.2320	29.80 a	9.95	0.2316	0.0004
2.	0.2320	29.80 a	9.95	0.2316	0.0004
3.	0.2320	29.84	9.95	0.2319	0.0001
4.	0.2320	29.85	9.95	0.2320	0.0000

a. In all these cases some part of the solution escaped.

Standard solution, 0.1005 n $KMnO_4$.

When zinc amalgam was used, the reaction of the hydrochloric acid with it was even more violent and the consequent loss of some small fraction of the solution could not be avoided in numerous experiments except in one case only. Making allowances for the lost solution, the writer believes that it is quite safe to conclude from the experimental data (Table IX) that the zinc amalgam also reduces tungsten chloride quantitatively to the trivalent condition.

TABLE IX. Reduction of Tungsten Chloride with Zinc Amalgam.

Exp. No.	WO_3 taken, g.	$KMnO_4$ req. cc. (Zn-Amalg.)	$KMnO_4$ req. cc. (Bi-malg.)	WO_3 found, g.	WO_3 error, g.
1.	0.2320	29.37	9.95	0.2283	0.0037
2.	0.2320	29.50	9.95	0.2293	0.0027
3.	0.2320	29.40	9.95	0.2285	0.0035
4.	0.2320	29.85	9.95	0.2320	0.0000

Standard solution, 0.1005 n $KMnO_4$.

From the foregoing experiments it is seen that lead, cadmium and zinc amalgams reduce the hydrochloric acid solution of tungstic acid to the trivalent stage, while bismuth amalgam reduces it to the pentavalent one. For practical application the lead and bismuth amalgams are by far the most convenient and preferable. The results also show that the

method is far more accurate and satisfactory than any one of the above-mentioned oxidimetric volumetric methods heretofore in use. The quantity of tungsten taken can be made fairly large provided the acid concentration is kept large. The reduction is very smooth and always carries to the definite stage of oxidation.

III. SUMMARY.

1. Liquid lead amalgam reduces ferric and uranyl salts to ferrous and uranous ones, and molybdic, titanic and tungstic acids respectively to their tervalent condition, and by utilizing these properties methods for tneir oxidimetric determinations were worked out.

2. Liquid bismuth amalgam reduces tungstic acid quantitatively to the pentavalent condition, which fact can also be utilized in the estimation of tungsten.

3. Cadmium and zinc amalgams also reduce tungstic acid quantitatively to the tervalent condition.

In conclusion the writer wishes to express his heartfelt thanks to Prof. Honda who gave constant interest and encouragement to his work, to Prof. Kobayashi for his useful suggestions and also to Mr. Kato for his enthusiastic help during the course of his work.

Feb. 1925.

The Vapor Pressures of Hydrogen Chloride on aqueous Solutions. Part I.[1]

By

Shinroku Mitsukuri,
Tatsuo Rokkaku and Takeo Watase.

The vapor pressures of hydrogen chloride on aqueous solutions were determined by Dolezalek,[2] R. Gahl[3] and S. J. Bates and H. D. Kirschmann.[4] Their determinations were all limited to concentrated aqueous solutions, say above two normals, and did not include dilute ones. Moreover, their values differed so much one from the other that we can not even estimate the values for dilute solutions by their extrapolations. Several years ago, one of the present authors began making experiments for the determination of vapor pressure of hydrogen chloride on dilute aqueous solutions at the suggestion of Prof. K. Ikeda at the Chemical Laboratory of Tokyo Imperial University, but he had to stop them for certain reasons before he got any definite results. Last year he, with his co-workers, carried them out again in this laboratory and got some results which are to be given in this report.

The vapor pressure of the solute in the solution is usually determined by passing through the solution a known quantity of indifferent gas which, having been saturated by the vapor of the solution, is conducted to the absorber in which the vapor of the solute is absorbed, the absorbing agent then being analysed.

(1) The same results will be published in Japanese in Journ. Chem. Soc. Japan.
(2) Zeit. Physik. Chem., **26**, (1898), 321.
(3) ibid., **33**, (1900), 978.
(4) Journ. Am. Chem. Soc., **41**. (1919), 1991.

But this method is limited by analytical difficulties so that we can not employ it for the determination of very small vapor pressure as in the case of dilute hydrochloric acid at ordinary temperature. Gahl (loc. cit.) used distilled water as the absorbing agent, and determined the concentrations of hydrogen chloride in it by the change of electrolytic conduction before and after the absorption, and calculated the partial pressures of the hydrogen chloride in the saturators. He, however, could not extend his determination to the dilution under two normals.

The present authors used the following method: the air, which is saturated with the vapor of the hydrochloric acid in the saturators, is conducted to the condenser at zero degree centigrade, and the vapor is condensed in it. The condensed liquid is collected in the conductivity cell attached at the end of the condenser. The air, with the water vapor prcssure of 0° C., is freed to the open air. The concentration of the condensed solutions are determined from its electrolytic conduction, and thence the vapor pressure of hydrogen chloride in the vapor phase is calculated. In this method, as the total volume of the air passed through the saturators does not affect the final results, and as the concentration of the solutions of whose electrolytic conductions have to be measured is larger than that of Gahl, the experimental errors are much less than those of the latter, and, therefore, especially suitable for the case of dilute hydrochloric acids.

The apparatus used is sketched diagramatically in fig. 1, which is

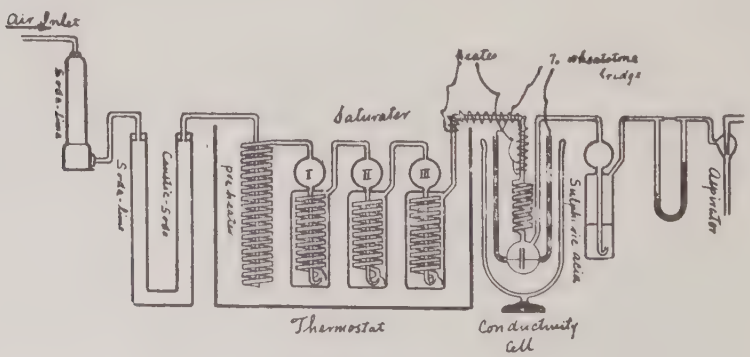

Fig. 1.

self-explanatory. The air, which is freed from carbon dioxide by soda-lime and caustic soda, passing through a glass spiral in the thermostat, takes the temperature of the thermostat and then goes into the saturators. There are three of them in series, their types are quite the same as those used by Gahl. After two months continuous employment of them, we analysed their contents, and found that the concentration of the solution in the first saturator was changed considerably, that in the second slightly, and that in the third not at all. We, therefore, concluded that the air was saturated perfectly in the second saturator. The air thus saturated goes into the hard glass condenser, which is placed in ice-water mixtures and there the vapor condensed. The condensed liquid is collected in the conductivity cell attached at the end of the condenser. The air then is freed to the open air being accompanied only by the water vapor corresponding to the vapor pressure of 0° C. To prevent condensation in the guiding tube between the last saturator and the condenser, this part is wound with resistance wire, and, with a small electric current through it, it was kept at a temperature a few degree above that of the thermostat. A washing bottle which is inserted between the conductivity cell and the aspirator, whose function is to circulate the air current, is to prevent the water vapor coming backwards from the aspirator to the cell.

The conductivity cell is spherical in shape with a volume of about I c. c., and the platinum electrodes are sealed from its sides oppositely, the distance between them being about I mm. All the cells used in our experiments have the cell constants of about 0. 02 in the usual units.

All the parts of the apparatus are connected directly with each other by fusing glass, except the conductivity cell which is connected with ground joints, because it is to be taken off from time to time, and because it is made of hard glass.

The velocity of the air which passes through the apparatus is about a half litre per hour, and it takes about 16–18 hours to get enough of the condensed liquid to measure the conductivity in the cell. The thermostat is regulated to an one twentieth degree during this whole time.

As the cell is imbedded in ice-water mixture in the Dewar vessel, we can not see how far the liquid is collected in it. We, therefore, determine the conductivity from time to time, and, when it reaches the constant value, we take it as the required conductivity.

After the conductivity cell was washed in the usual way, it was connected with the apparatus and the air was passed through continuously for a week. The solution collected in the cell was taken out occasionally so that it was washed thoroughly with the solution whose conductivity was to be measured. Even after these tedious washings the value of the conductivity was still diminishing until finally it reached the constant value after several determinations, which we took as the required one.

The conductivity was measured in the ordinary way with Siemens resistance box, Leeds and Northrup Co.'s slide wire and Noguchi's transformer as the sound origin.

The results thus obtained are given in the following table. (Table I.)

TABLE I.

Conc. HCl.	Sp. Cond.
0.517	3.64×10^{-6}
0.929	4.52×10^{-6}
1.453	6.53×10^{-6}

The figures in the first column in the above table indicate the concentrations of the hydrochloric acids in the saturators expressed in normality, those in the second, specific conductivities of the solutions in the cell. The hydrochloric acid used in the saturators was thrice distilled, was diluted with distilled water and its concentration was determined by the standard alkaline solution.

The calculation of the vapor pressure from the above results is collected in Table 2.

TABLE 2.

Conc. HCl.	Sp. Cond. (0°. C.)	Sp. Cond. (25°. C.)	Conc.	Mol. Fr.	Pres.	Part. P.	Log.
0.517	3.64×10^{-6}	7.79×10^{-6}	1.73×10^{-5}	3.14×10^{-7}	23.5	5.94×10^{-6}	−5.228
0.929	4.52×10^{-6}	9.30×10^{-6}	2.18×10^{-5}	3.96×10^{-7}	23.2	7.37×10^{-6}	−5.130
1.533	6.53×10^{-6}	14.0×10^{-6}	3.30×10^{-5}	5.99×10^{-7}	22.8	10.91×10^{-6}	−4.960

The first and the second column in the table are the same as those in the Table I. The third column is the specific conductivities at 25°. C., which were obtained by multipling 2.14 to the values in the second. As the temperature coefficient of the specific conductivity of very dilute hydrochloric acids such as those used in these experiments is not found in the literature, we measured the specific conductivity of several solutions at 25°.C. directly after the measurements of them at 0°.C., taking the cell out from the ice and putting it into the thermostat. The factor 2.14 does indeed vary with the concentration, but the range of concentration is small enough for the present work to assume it as the constant. In the fourth column are the concentrations in molality whose conductivities are indicated in the third. These values are obtained from the extrapolation of values detetmined by H. C. Parker.[5] In the fifth are the molar fraction corresponding to the molalities in the fourth. In the sixth are the total pressures of the hydrochloric acids of the concentration in the first. These values were obtained from the values of the partial pressures of water on the hydrochlorie acid[6] neglecting the partial pressure of hydrogen chloride, because they were very small. In the seventh are the partial pressures of hydrogen chloride, which were obtained by multipling the molar frations in the fifth by the difference between the total pressure in the sixth and the water vapor pressure at 0°.C , that is 4.6 mm. In the eighth column are the common logarithms

(5) Journ. Am. Chem. Soc., **45**, (1923), 2017.
(6) G. A. Linhart : ibid., **39**, (1917), 2601.

of the values in the seventh. The unit of pressure in the table is the height of the mercury column in mm.

As we have already stated, since there is no experimental values which can be compared with those of ours, we calculated the vapor pressures from the values of the concentrated hydrochloric acids determined by Bates and Kirschmann (loc. cit.) and the activity coefficients of hydrochloric acids determined by Linhart (loc. cit.) from the E. M. F. of the cell, H_2 | HCl | AgCl | Ag. The calculating results are given in table 3.

TABLE 3.

Conc.	γ	$k\gamma$	k	$k\gamma$ (calc.)	Part. press.	Log.
0.1	0.814	—	—	0.0149	2.22×10^{-6}	−5.654
0.5	0.762	—	—	0.0139	4.84×10^{-5}	−4.315
1.0	0.823	—	—	0.01505	2.26×10^{-4}	−3.646
2.0	1.032	—	—	0.0189	1.45×10^{-3}	−2.839
3.0	1.35	—	—	0.0247	5.51×10^{-3}	−2.259
4.0	1.84	0.0337	0.0183	—	—	—
5.0	2.51	0.0460	0.0183	—	—	—
6.0	3.40	0.0624	0.0183	—	—	—
7.0	4.66	0.0843	0.0181		—	—
8.0	6.30	0.15	0.0183	—	—	—

In the first column in the above table the concentrations of hydrochloric acids in molality are indicated, in the second the activity coefficients from Linhart's measurements (loc. cit.), in the third the values $k\gamma$ from the vapor pressure data of Bates and Kirschmann (loc. cit.), in the fourth the values of k obtained from the values in the second and the third, in the fifth the values of $k\gamma$ obtained by multipling 0.0183 into the activity coefficients in the second, assuming that the value of k is constant in the dilute solutions, in the sixth the partial pressures calculated from the values in the fifth, and in the seventh the common logarithms of the values in the sixth.

The comparison of the values of the seventh column in table 3. with those of the eighth column in table 2. is made in table 4, in which concentrations are all recalculated to molality.

TABLE 4.

Conc. (m.)	Part. Press. (obs.)	Part. Press. (calc.)
0.1	—	2.22×10^{-6}
0.5	—	4.84×10^{-5}
0.519	5.94×10^{-6}	—
0.946	7.37×10^{-6}	—
1.0	—	2.26×10^{-4}
1.495	1.091×10^{-5}	—
2.0	—	1.45×10^{-3}
3.0	—	5.51×10^{-3}

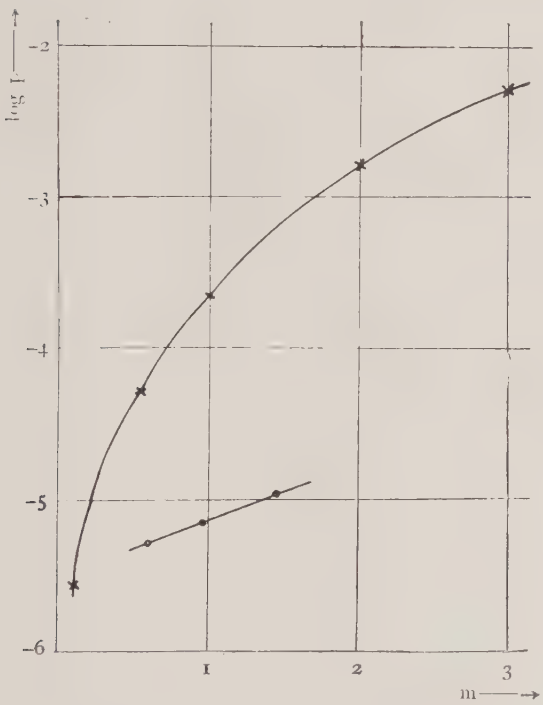

Fig. 2.

The table shows that the observed values are much smaller than those calculated. (see also Fig. 2.) Which are the true values for the partial pressures of hydrogen chloride is a question which can be determined only by further experiments.

After we had reported these results at the annual meeting of the Chemical Society of Japan at Kyoto in April 1924, we found the paper of J. S. Dunn and E. K. Rideal[7] relating to the same subject. Their values are even larger than those

(7) Journ. Chem. Soc., **125**, (1924), 676.

calculated in the above. But their method is so defective that we can not rely upon those values at all. One of the present authors tried the same mothod several years ago, and found that, in that method, there took place a violent surface distillation, and the values thus obtained were far from the true ones.

We were afraid that the same effect might result to some extent in the experiment of Bates and Kirschmann, (loc. cit.) because their saturators were of the kind in which the air was always saturated with the vapor at the surface of the solution. The vapor pressure values in table 3. which were calculated from their data might accordingly be too high.

We express our hearty thanks to Prof. K. Ikeda, by whose suggestion we began this work.

A part of the expense of this experiment was contributed from the Saito Hôon Kai as research fund granted to one of the authors (S. Mitsukuri).

(The Laboratory of Theoretical Chemistry. October, 30, 1924.)

Bemerkungen zu den geodätischen Linien auf Böschungsflächen.

Von

Tsurusaburo Takasu.

In der dritten Auflage von Salkowski-Schell: Allgemeine Theorie der Kurven doppelter Krümmung (1914) ist geodätischen Linien auf Böschungsflächen (d. h. die Evoluten der Schraubenlinie = Aoustsche Cycliden) studiert. In dieser Abhandlung möchte ich einige weitere Eigenschaften hinzufügen.

Satz 1.° Die natürliche Gleichung der geodätischen Linien (E-Kurve nach Salkowski-Schell) ist folgendermassen darstellbar:

$$\cos\rho + \cot\alpha.\,\theta + C = 0,$$

worin C eine Konstante, $\cot\alpha$ = konst. und $\cot\rho$ die beiden winkligen Krümmungen[1] bez. von der Böschungsflächen-gratlinie und den E-Kurven und θ der Windungswinkel der E-Kurve sind.

Beweis I. Salkowski und Schell haben sie folgendermassen gegeben:

$$ds\sqrt{\left(1+\frac{r^2}{\rho^2}\right)^3} = -rd\frac{r}{\rho}\tan\alpha.^{(2)}$$

Num sind

$$-\frac{r}{\rho}\;//\;\cot\rho, \qquad r=\frac{ds}{d\theta}.$$

Also folgt

$$\tan\alpha.\ \sin\rho.\,d\rho = d\theta,$$

d. h.

$$\cos\rho+\cot\alpha.\,\theta+C=0.$$

(1) **Angular curvature** in meiner Terminologie. S. Takasu, Differential Geomerty of Curves in Plane-space, I. These Reports, vol. XI (1922), S. 379.

(2) L. c. S. 134.

Beweis II. Ich habe bewiesen, dass[1]

$$-\sin\rho\frac{d\rho}{d\theta}=\tan\rho_i,$$

woraus folgt unsre Behauptung unmittelbar, da $\rho_i=\frac{\pi}{2}-\alpha$ ist.

Satz 2.° Die Gratlinie (G) der abwickelbaren Fläche, die durch die Achsenebene der winkligen Krümmung[2] der E-Kurve beschrieben wird, ist eine Schraubenlinie.[3]

Beweis I. Ich habe bewiesen, dass[4] die notwendige und hinreichende Bedingung dafür, dass die Gratlinie der abwickelbaren Fläche, die durch die Achsenehene der winkligen Krümmung irgend einer Raumkurve eine Schraubenlinie sei, besteht darin, dass $\cos\rho$ eine lineare Funktion von θ ist. Dies ist jetzt und nur jetzt der Fall, woraus folgt unsre Behauptung unmittelbar.

Beweis II. Ich habe bewiesen, dass[5] die Schmiegungsebene der Evolute parallel zur Achsenebene der winkligen Krümmung der Evolute ist. Nun ist die E-Kurve eine Evolute einer Schraubenlinie. Also ist G parallel zur genannten Schraubenlinie. Nun ist eine parallele Kurve zu einer Schraubenlinie wieder eine Schraubenlinie, woraus folgt unsre Behauptung.

Beweis III. Ich habe bewiesen, dass[6]

$$\tan\alpha=\tan\rho',$$

worin $\cot\rho'$ die winklige Krümmung von G ist, woraus folgt unmittelbar unsre Behauptung.

Satz 3.° Die Gratlinie ber Böschungsfläche und G besitzen dieselbe winklige Krümmung,

Satz 4.° Die rektifizierende Gratlinie der E-Kurve ist auch eine Schraubenlinie, deren winklige Krümmung $\cot\bar{\rho}$ gleich

(1) Takasu, l. c., Part II, vol. XII (1923), S. 79.
(2) **Axtal plane of angular curvature** in meiner Terminologie. Takasu, I, l. c.
(3) Also ist dies die charakteristische Eigenschaft von der E-Kurve.
(4) Takasu, II, l. c. S. 109.
(5) Ebenda, S. 77.
(6) Ebenda, S. 99.

$$\tan \alpha = \tan \rho'$$

ist.

Dies folgt unmittelbar aus

$$\tan \alpha = \tan \rho' = \cot \bar{\rho}.^{(1)}$$

Satz 5.° Die Polarkurve der Gratschraubenlinie der Böschungsfläche (d. h. die rektifizierende Gratlinie von der E-Kurve) und G sind Schraubenlinien derart, dass die erste die Umkehrung $\tan \rho'$ der winkligen Krümmung von der zweiten als ihre winklige Krümmung besitzt.

Beweis. In der Tat ist die winklige Krümmung der genannten Polarkurve gleich

$$\tan \alpha = \tan \rho'.$$

Satz 6.°(2) Die Polarkurve einer E-Kurve ist wieder eine E-Kurve.

Analytischer Beweis. Beziehen ρ_1, θ_1, σ_1 etc. sich auf die genannte Polarkurve, so sind

$$\sin \rho = \cos \rho_1, \qquad d\rho = -d\rho_1.$$

Nun ist

$$\tan \alpha \sin \rho \, d\rho = d\theta.$$

Daraus folgt:

$$\tan \alpha \cos \rho_1 \, d\rho_1 = -d\theta = d\sigma_1,$$

wo σ_1 den Kontingenzwinkel darstellt. Also

$$\tan \alpha \, d \sin \rho_1 = -\frac{d\sigma_1}{d\theta_1} d\theta_1 = -\cot \rho_1 \, d\theta_1,$$

$$\frac{1}{2} \tan \alpha \, (1-\sin^2 \rho_1)^{-\frac{1}{2}} \, d \, (1-\sin^2 \rho_1) = d\theta_1,$$

d. h. $$\tan \alpha \, (1-\sin^2 \rho_1)^{\frac{1}{2}} = \theta_1 + C',$$

d. h. $$\tan \alpha \cos \rho_1 = \theta_1 + C',$$

woraus folgt unsre Behauptung.

Satz 7.° $$\rho = \theta_i + c,$$

worin das Symbol i die sich auf die Gratlinie der Böschungsfläche

(1) Ebenda, S. 99.

(2) Salkowski-Schell, l. c. S. 134.

beziehenden Grössen zeigt und c eine Konstante derart ist, das $\theta_i + c$ der Winkel zwischen den entsprechenden Schmiegungsebenen der beiden Kurven ist.(1)

Satz. 8.° $R_i = \text{con}\,\rho\,(s+k)$,

worin k eine Konstante derart, dass $s+k$ der Abstand zwischen den entsprechenden Kurvenpunkten ist, und R_i^{-1} die erste Krümmung der Gratlinie der Böschungsfläche bedeutet.(2)

8atz 9.° $$T_i = \tau_i^{-1} = -\frac{s+k}{\frac{d}{d\theta} log \sec \rho}$$

$$= \frac{R^2 + T^2}{R\left(T\frac{dR}{ds} - R\frac{dT}{ds}\right)},$$(3)

wo τ_i^{-1} die duale Torsion bedeutet.

Satz 10.° $$T = \tau^{-1} = \frac{\tan\alpha}{\cos(\theta_i+c)}\left\{\frac{dR_i}{d\theta_i}\,\text{cosec}\,(\theta_i+c) - R_i \sec(\theta_i+c)\right\}$$

$$= \frac{\tan\alpha}{\cos(\theta_i+c)\,\tau_i}\left\{\frac{d\tau_i}{d\theta_i}\,\frac{\tan\alpha}{\tau_i}\,\text{cosec}\,(\theta_i+c) + \tan\alpha \sec(\theta_i+c)\right\}$$(4)

Satz 11.° $$R = -\frac{\tan\alpha \sin(\theta_i+c)}{\cos^2(\theta_i+c)}\left\{\text{cosec}\,(\theta_i+c)\,\frac{dR_i}{d\theta_i} - \sec(\theta_i+c)\,R_i\right\}$$

$$= -\frac{\tan^2\alpha \sin(\theta_i+c)}{\tau_i^2 \cos^2(\theta_i+c)}\left\{\text{cosec}\,(\theta_i+c)\,\frac{d\tau_i}{d\theta_i} + \sec(\theta_i+c)\right\}.$$(5)

Satz 12.° Die in der natürlichen Gleichung der E-Kurve auftretende Konstante C ist durch die folgenden Beziehungen verbunden:

$$\cos\rho = -\cot\alpha.\,\theta + C = \cos(\theta_i+c) = R_i/(s+k).$$

N. B. Wir könnten einige noch weitere Eigenschaften als die der Evolute einer Kurve hinzufügen.

---

(1) (2) (3) (4) (5) Takasu, II, l. c., S. 76 etc.

On the Relation between the Intrinsic Equations of Analytic Functions under Linear Transformations and Curves under Inversions &c.

By

Tsurusaburo Takasu.

Prof. Wilczinski has studied some differential properties of functions of a complex variable, which are invariant under linear transformations[1] introducing the concepts of *intrinsic equations of analytic functions of a complex variable under linear transformations*. In one of my foregoing papers[2], I have discussed the intrinsic equations of non-Euclidean minimal curves as well as of plane curves under inversions, which are both abstractly identical with those of curves on the Absolute quadric. In this paper, after giving another method of forming the intrinsic equations of such curves, it will be shown that there is a close relation between the theory of Wilczinski and my own, each affording another method of the other.

§ 1. INTRINSIC EQUATIONS OF CURVES ON THE ABSOLUTE QUADRIC.

1. If $(xx) = 0$ be the equation to the Absolute, we may put

$$(1) \qquad x_1 \equiv \sigma(1-st), \quad x_2 \equiv \sigma i(1+st), \quad x_3 \equiv -\sigma(s+t),$$

$$x_4 \equiv \sigma i(s-t).$$

(1) Liouville's Journal de Mathématiques pures et appliquées, 9. Série, 1 (1922), 2 (1923).

(2) Takasu, Natural Equations of Curves under Circular Point-transformation Groups and their Duals. (Under press). For its abstract see Japanese Journal of Mathematics, vol. 1 (1924), etc.

Then s and t are the projective parameters of the two systems of generating lines, and the motions are composed of the transformations of the types

$$(2)\qquad \begin{cases} \bar{s} = \dfrac{\alpha s+\beta}{\gamma s+\delta}, & \alpha\delta-\beta\gamma\neq 0, \\ \bar{t} = \dfrac{at+b}{ct+d}, & ad-bc\neq 0, \end{cases}$$

and the symmetry transformations are given by

$$(3)\qquad \begin{cases} \bar{t} = \dfrac{\alpha' s+\beta'}{\gamma' s+\delta'}, & \alpha'\delta'-\beta'\gamma'\neq 0, \\ \bar{s} = \dfrac{a' t+b'}{c' t+d'}, & a'd'-b'c'\neq 0. \end{cases}$$

Let us now normalize x in such a way that

$$(4)\qquad (x'x')_p = 1$$

by an adequate choice of σ and p.

From the Cayley's identity[3]

$$(5)\qquad \{t, s\} \equiv \left(\frac{dp}{ds}\right)^2 [\{t, p\}-\{s, p\}],$$

where $\{t, s\} \equiv \dfrac{t'''}{t'} - \dfrac{3}{2}\left(\dfrac{t''}{t'}\right)^2$ is the so-called Schwarzian derivative, by taking $p = t$, we obtain the identity

$$(6)\qquad \{s, t\} \equiv -\frac{\{t, s\}}{\left(\dfrac{dt}{ds}\right)^2},$$

When s undergoes a linear transformation, we have

$$(7)\qquad \{\bar{s}, t\} = \{s, t\},$$

so that

$$(8)\qquad \frac{\{t, s\}}{\left(\dfrac{dt}{ds}\right)^2} = \frac{\{t, \bar{s}\}}{\left(\dfrac{dt}{d\bar{s}}\right)^2},$$

or

(3) Cayley, Collected Mathematical Papers, vol. XI, p. 152.

$$\sqrt{\{t, s\}}\, ds = \sqrt{\{t, \bar{s}\}}\, d\bar{s}. \tag{9}$$

Let us put

$$dp = \frac{1}{2}\sqrt{\{t, s\}}\, ds = \frac{i}{2}\sqrt{\{s, t\}}\, dt. \tag{10}$$

Then p *is an integral invariant under motions and* dp^2 *changes its sign by a symmetry transformation.* Let us call p the *length* of the curve $x = x(p)$ on the Absolute.

When p is so determined, from (5), we have

$$\{t, p\} - \{s, p\} \equiv 4. \tag{11}$$

For the purpose of normalization of x in such a way that (4) holds, we are lead to take

$$\sigma = \frac{1}{2\sqrt{s't'}}, \tag{12}$$

so that

$$\left\{\begin{array}{ll} x_1 = \dfrac{1-st}{2\sqrt{s't'}}, & x_2 = \dfrac{i(1+st)}{2\sqrt{s't'}}, \\ x_3 = -\dfrac{s+t}{2\sqrt{s't'}}, & x_4 = \dfrac{i(s-t)}{2\sqrt{s't'}}. \end{array}\right. \tag{13}$$

Here we see that all $x's$ receive the factor i *when* x *have undergone a symmetry transformation.*

Then we have

$$|x\ x'\ x''\ x'''|_p \equiv -1, \tag{14}$$

which is seen to be equivalent to (10) or (11).

Hence we have

$$dp = (dxdx)^{\frac{1}{2}} = i\,|x\ dx\ d^2x\ d^3x|^{\frac{1}{6}} \tag{15}$$

which again shows that dp receives the factor i, when x have undergone a symmetry transformation.

If we interpret the semi-invariant

$$|x\ dx\ d^2x\ d^3x|$$

as the *sine-amplitude of four-consecutive points of the curve,* dp *may be*

interpreted as i-times the six-th root of the sine-amplitude of four consecutive points of the curve.

The quantity

$$\{t, p\}+\{s, p\} \tag{16}$$

is an absolute invariant under motions and changes its sign by a symmetry transformation and is seen to be equal to $(x''x'')_p$.

When a twice continuously differentiable function $\phi(p)$ *is given, the curve on the Absolute having*

$$\{t, p\}+\{s, p\} \equiv (x''x'')_p = \phi(p)^{(4)}, \tag{17}$$

is uniquely determined. For, from (11) and (17), we have

$$\begin{cases} \{t, p\} = \frac{1}{2}\phi(p)+2. \\ \{s, p\} = \frac{1}{2}\phi(p)-2, \end{cases} \tag{18}$$

which are equivalent to

$$\begin{cases} \frac{dX}{dp} = -1-\frac{1}{4}\phi(p)+X^2, \qquad X \equiv \frac{t''}{2t'i}, \\ \frac{dY}{dp} = \quad 1-\frac{1}{4}\phi(p)+Y^2, \qquad Y \equiv \frac{s''}{2s'i}. \end{cases} \tag{19}$$

When (18) are solved

$$t = t(p), \qquad s = s(p)^{(5)}, \tag{20}$$

substituting in (13), we obtain

$$x = x(p).$$

Therefore we may consider (17) as *an intrinsic equation of the curve* $x = x(p)$ *on the Absolute under motions.*

It changes its sign by a symmetry transformation.

Eliminating p between (20), we have

---

(4) This is equivalent to $x^{IV}+\phi x''+\frac{3}{2}\phi' x'+\left(\frac{1}{2}\phi''+1\right) = 0$.

(5) p and so $\phi(p)$ are each an automorphic function of t as well as of s.

$$s = s(t), \tag{21}$$

which we may consider as an equation of the curve

$$x = x(p).$$

2. *Second Method.* First let us introduce *an integral invariant.* The determinant

$$|\, x \;\; dx \;\; d^2x \;\; d^3x \,|$$

is an absolute invariant under motions and changes its sign by a symmetry transformation. The expression $(dxdx)$ is an absolute invariant under any congruent transformation, motion or symmetry transformation. Under the transformation

$$\xi = h\bar{\xi}, \tag{22}$$

we have

$$|\,(h\bar{x}) \;\; d(h\bar{x}) \;\; d^2(h\bar{x}) \;\; d^3(h\bar{x})\,| = h^4\,|\,\bar{x} \;\; d\bar{x} \;\; d^2\bar{x} \;\; d^3\bar{x}\,|\,,$$

$$(d(h\bar{x})d(h\bar{x})) = h^2(d\bar{x}d\bar{x}).$$

Therefore *the expression*

$$-dp^2 = \frac{|\, x \;\; dx \;\; d^2x \;\; d^3x \,|}{(dxdx)^2} = \frac{|\,\bar{x} \;\; d\bar{x} \;\; d^2\bar{x} \;\; d^3\bar{x}\,|}{(d\bar{x}d\bar{x})^2} \tag{23}$$

is an absolute invariant under motions and changes its sign by a symmetry transformation and is an absolute invariant under the transformations (22).

If we consider x as having been so normalized, that

$$dp^2 = (dxdx), \tag{24}$$

since

$$-dp^2 = \frac{|\, x \;\; dx \;\; d^2x \;\; d^3x \,|}{(dxdx)^2} = \left| x \;\; \frac{dx}{dp} \;\; \frac{d^2x}{dp^2} \;\; \frac{d^3x}{dp^3} \right| dp^2, \tag{25}$$

we have

$$|\, x \;\; x' \;\; x'' \;\; x''' \,|_p \equiv -1. \tag{26}$$

If we put

$$i^n x = \frac{\varepsilon\,|\,\bar{x} \;\; d\bar{x} \;\; d^2\bar{x} \;\; d^3\bar{x}\,|^{\frac{1}{2}}}{i(d\bar{x}d\bar{x})^{3/2}}\bar{x} = \frac{\varepsilon\,|\, x \;\; dx \;\; d^2x \;\; d^3x\,|^{\frac{1}{2}}}{i(dxdx)^{3/2}}, \quad \varepsilon = \pm 1,$$

where $n = 1$ or 0 according as x has or has not undergone a symmetry transformation, we succeed in assuring (24). In the following, we will drop the factor i^n, but *it should always be understood.*

The coordinates

$$x = x(p)$$

should satisfy the following differential equation

$$\left|x^{IV}\ x'''_1\ x''_2\ x'_3\ x_4\right| \cdot \begin{vmatrix} 1 & 0 & 0 & 0 & 0 \\ 0 & x'''_1 & x''_1 & x'_1 & x_1 \\ 0 & x'''_2 & x''_2 & x'_2 & x_2 \\ 0 & x'''_3 & x''_3 & x'_3 & x_3 \\ 0 & x'''_4 & x''_4 & x'_4 & x_4 \end{vmatrix}$$

$$\equiv \begin{vmatrix} x^{IV} & x''' & x'' & x' & x \\ (43) & (33) & (23) & (13) & (03) \\ (42) & (32) & (22) & (12) & (02) \\ (41) & (31) & (21) & (11) & (01) \\ (40) & (30) & (20) & (10) & (00) \end{vmatrix} = 0,$$

where

$$(i\ j) \equiv (x^{(i)}x^{(j)}),$$

$$x^{IV} + \phi x'' + \frac{3}{2}\phi' x' + \left(\frac{1}{2}\phi'' + 1\right)x = 0 \tag{27}$$

by virtue of the identity:

$$\left|x'''\ x''\ x'\ x\right|^2 \equiv \phi^2 - (33) \equiv 1, \tag{28}$$

where

$$\phi \equiv (22).$$

When twice continuously differentiable function $\phi(p)$ is given the equations of the curves for which

$$(22) = \phi(p) \tag{29}$$

are determined uniquely from (27) and the accompanying condition

$$(xx) \equiv 0, \tag{30}$$

except under motions. Therefore *we may consider* (29) *as an intrinsic equation of the curve* $x = x(p)$ *on the Absolute* (30) *under motions. It changes its sign by a symmetry transformation.*

It will readily be seen that *the last two theories are equivalent.*

3. *The treatment of the same problem in terms of the planecoordinates is equivalent to that in Art.* 4.

§ 2. INTRINSIC EQUATIONS OF NON-EUCLIDEAN MINIMAL CURVES.

4. If $X_i = X_i(p)$, $i = 1, 2, 3, 4$ such that

$$(XX) \equiv k^2 \tag{31}$$

be the Weierstrassian coordinates of a point of a non-Eucliclean minimal curve, then

$$(X'X')_p \equiv 0, \tag{32}$$

so that we may put

$$\begin{cases} X_1' \equiv \sigma(1-st), & X_2' \equiv \sigma i(1+st), \\ X_3' \equiv -\sigma(s+t), & X_4' \equiv \sigma i(s-t). \end{cases} \tag{33}$$

If we take

$$\sigma = \frac{1}{2}(s't')^{-\frac{1}{2}}, \tag{34}$$

we have

$$(X''X'')_p \equiv 1, \tag{35}$$

$$|X\ X'\ X''\ X'''|_p \equiv -k, \tag{36}$$

$$|X'\ X''\ X'''\ X^{IV}|_p \equiv -k^{-1}, \tag{37}$$

so that

$$dp = ik^{-\frac{1}{6}}\,|X\ dX\ d^2X\ d^3X|^{\frac{1}{6}} = (d^2X\ d^2X)^{\frac{1}{4}}. \tag{38}$$

The condition (31) or (36) becomes

$$\{t, p\} - \{s, p\} = 4k^{-1}, \tag{39}$$

while we have

$$\{t, p\}+\{s, p\}\equiv(X'''X''')_p^{(6)}. \tag{40}$$

From (5), we have

$$\{t, s\}=\left(\frac{dp}{ds}\right)^2 4k^{-1}, \tag{41}$$

so that (38) may be replaced by

$$dp=\frac{1}{2}\sqrt{k\{t, s\}}\,ds=\frac{i}{2}\sqrt{k\{s, t\}}\,dt \tag{42}$$

as in (10).

I have called p the *natural parameter* and

$$(X'''X''')_p=\phi(p) \tag{43}$$

the *intrinsic* (*natural*) *equation of the minimal curve under the motion-group, dp^2 and $(X'''X''')$ change their signs by a symmetry transformation.*

When (43) is given, by (39) and (40), we have to solve the differential equations

$$\begin{cases} \{t, p\}=\dfrac{1}{2}\phi(p)+\dfrac{2}{k}, \\ \{s, p\}=\dfrac{1}{2}\phi(p)-\dfrac{2}{k}. \end{cases} \tag{44}$$

When these equations are solved, we have equations of the forms

$$s=s(p), \qquad t=t(p), \tag{45}$$

which are equivalent to an equation of the form

$$s=s(t) \quad \text{or} \quad t=t(s). \tag{46}$$

Hence *we may take an equation of the form* (46) *for an equation of the minimal curve.*

5. Hitherto we have referred to a curve $X=X(p)$ such that $(X'X')\equiv 0$ as a *minimal curve* (*of the first kind*). Now I will refer to a curve whose osculating planes are minimal as a *minimal curve of the second kind. For a three-dimensional space-curves, it is a necessary*

(6) Takasu, Natural Equations etc., l. c.

consequence of belonging to the first kind, that they belong to the second kind. For,

$$\Sigma \left| X\ X'\ X'' \right|^2 \equiv \begin{vmatrix} (XX) & 0 & -(X'X') \\ 0 & (X'X') & 0 \\ -(X'X') & 0 & (X''X'') \end{vmatrix}$$

$$\equiv (XX)(X'X')(X''X'') - (X'X')^3.$$

Therefore *the treatment of the same problem in terms of the plane-coordinates*

$$u = |\ X\ X'\ X''\ |, \quad (uu) \equiv 0,$$

is equivalent to that in Art. 1 *or in Art.* 2.

§ 3. INTRINSIC EQUATIONS OF PLANE CURVES UNDER CIRCULAR POINT-TRANSFORMATION GROUPS.

6. If we interpret x in § 1 as the tetracyclic point-coordinates of a point on a plane curve

$$x = x(p), \tag{47}$$

the theories given there afford *us its intrinsic equation under the circular point-transformation group.*[7]

7. If we interpret X in § 2 as the tetracyclic (doubly oriented) circle-coordinates of the osculatlng circle of a plane curve, *the theories given there afford us its intrinsic equation under the circular point transformation group.*[8]

8. If x and X have the meanings stated in the last two articles and p the corresponding common natural parameter, *it will readily be seen that*

$$x = \frac{dX}{dp}, \tag{48}$$

which makes clear the relation between the two theories of § 1 *and* § 2.

(7) Cfr. Takasu, Fundamentalsäze der Kurventheorie in den Euklidischen tetrazyklischen, pentasphärischen und Laguerreschen Räumen. (Under press).

(8) Takasu, Natural Equations etc., l. c.

§ 4. INTRINSIC EQUATIONS OF ANALYTIC FUNCTIONS OF A COMPLEX VARIABLE UNDER LINEAR TRANSFORMATIONS.

9. Wilczinski[9] has shown that

$$\varphi = \int \sqrt{\{w, z\}}\, dz \tag{49}$$

and

$$\theta = \frac{\sqrt{\{w, z\}}}{\frac{dw}{dz}} \tag{50}$$

are *integral* and *differential invariants* of the analytic function

$$w = f(z) \tag{51}$$

of a complex variable z under the parameter group of the linear transformations

$$\bar{z} = \frac{\alpha z + \beta}{\gamma z + \delta}, \qquad \alpha\delta - \beta\gamma \neq 0 \tag{52}$$

respectively and called

$$\theta = F(\varphi) \tag{53}$$

an *intrinsic equation of the analytic function*

$$w = f(z)$$

under the said 3-parameter group.

10. Hes has also shown that

$$\varphi = \int \sqrt{\{w, z\}}\, dz \tag{54}$$

and

$$\begin{aligned} I = \{w, \varphi\} &= \{z, \varphi\} + 1 \\ &= -\frac{1}{\theta^2}\left[\frac{d^2 \log \theta}{dw^2} - \frac{1}{2}\left(\frac{d \log \theta}{dw}\right)^2\right] \\ &= -\left[\frac{d^2 \log \theta}{d\varphi^2} + \frac{1}{2}\left(\frac{d \log \theta}{d\varphi}\right)^2\right] \\ &= -\frac{1}{(w')^2\theta^2}\left[\frac{d^2 \log \theta}{dz_2} - \frac{1}{2}\left(\frac{d \log \theta}{dz}\right)^2 - \frac{w''\theta'}{w'\theta}\right] \end{aligned} \tag{55}$$

(9) Loc. cit.

are the *integral* and the *differential invariants* of the analytic fuuction

$$w = f(z)$$

of a complex variable z under the six-parameter group of the linear transformations:

$$(56) \qquad \bar{z} = \frac{\alpha z + \beta}{\gamma z + \delta}, \qquad \bar{w} = \frac{\alpha w + b}{c w + d},$$

$$\alpha\delta - \beta\gamma \neq 0, \qquad ad - bc \neq 0$$

respectively and called

$$(57) \qquad I = G(p)$$

an *intrinsic equation of the analytic function*

$$w = f(z)$$

under the said 6-parameter group.

§ 5. COMPARISON OF THE FOUR FOREGOING THEORIES.

11. *The theories in* § 1, § 2 *and* § 3 *are all abstractly identical, so that any proposition obtained in one of the four theories can always be transferred into any other giving rise to a new proposition.*

The theory of § 1 affords us a *geometrical interpretation of that of Wilczinski.* Thus if we interpret w and z as the projective parameters of the two systems of generating lines of the Absolute, the function

$$w = f(z)$$

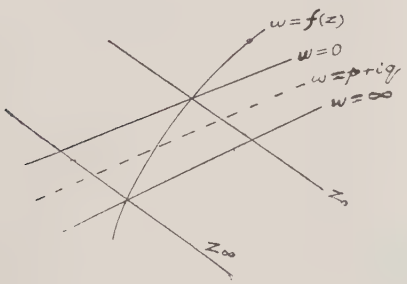

expresses a curve on the Absolute. The zeros z_0 and poles z e. g. of the function w are the parameters of the z-system of the generating lines, which meet the generating lines $w = 0$ and $w = \infty$ at the points on the curve

$w = f(z)$ respectively, &c.

Let us stay upon § 1 only for a while. If we take

$$w = t, \quad z = s, \quad k = 4,$$

we see that we may take

$$\varphi = 2p, \tag{57}$$

$$I = \{w, \varphi\} = \frac{1}{4}\{t, p\} = \frac{1}{8}\phi(p) + \frac{1}{2}. \tag{58}$$

Thus it seems to me to be *a little more natural* to take

$$J = \frac{1}{4}\{t, p\} + \frac{1}{4}\{s, p\} = \frac{1}{4}\phi(p) \tag{59}$$
$$\equiv \{w, \varphi\} + \{z, \varphi\} = H(\varphi)$$

for the canonical form of the intrinsic equation of the analytic function under the six parameter group (55) instead of taking $I = G(\varphi)$.

Then in order to find $w = f(z)$ whose intrinsic equatton is $J = H(\varphi)$, we are lead to integrate the two Schwarzian differential equations

$$\begin{cases} \{w, \varphi\} = \frac{1}{2}H(\varphi) + \frac{1}{2}, \\ \{z, \varphi\} = \frac{1}{2}H(\varphi) - \frac{1}{2}, \end{cases} \tag{60}$$

and then to eliminate φ.

Let U_1 and U_2 be two linearly independent solutions of the linear differential equation

$$\frac{d^2U}{d\varphi^2} + \frac{1}{4}\{H(\varphi) + 1\}U = 0. \tag{61}$$

Then $\frac{U_2}{U_1}$ will be a solution of the first equation of (60) and any solution of the latter equation will be a linear fractional equation of $\frac{U_2}{U_1}$. Similarly, any linear function $\frac{V_2}{V_1}$, where V_1 and V_2 are linearly independent solutions of

$$\frac{d^2V}{d\varphi_2} + \frac{1}{4}\{H(\varphi) - 1\}V = 0, \tag{62}$$

will be a solution of the second equation of (60).

From (61), we have

$$U_1\frac{dU_2}{d\varphi}-U_2\frac{dU_1}{d\varphi}=\text{const.}=c,\ \text{say.}$$

Let $\varphi=\varphi_0$ be a value of φ for which $H(\varphi)$ is analytic and let

$$(63)\qquad \begin{cases} U_1=1, & \dfrac{dU_1}{d\varphi}=0 \quad \text{for} \quad \varphi=\varphi_0, \\ U_2=0, & \dfrac{dU_2}{d\varphi}=1 \quad \text{for} \quad \varphi=\varphi_0, \end{cases}$$

so that

$$w=\frac{U_2}{U_1}=0 \qquad \text{for } \varphi=\varphi_0,$$

and

$$\frac{dw}{d\varphi}=\frac{d}{d\varphi}\left(\frac{U_2}{U_1}\right)=\frac{1}{U_1^2}=1 \quad \text{for } \varphi=\varphi_0.$$

Then

$$(64)\qquad U_1\frac{dU_2}{d\varphi}-U_2\frac{dU_1}{d\varphi}=c=1.$$

It may be verified that any solution of (62) satisfies the equation

$$V=c_1U_1(\varphi)+c_2U_2(\varphi)+\frac{1}{2}\int_{\varphi_0}^{\varphi}[U_1(\psi)U_2(\varphi)-U_1(\varphi)U_2(\psi)]V(\psi)d\psi.$$

If V_1 and V_2 denote the solution of (62), which are defined by the same initial conditions (63) which determine U_1 and U_2, V_1 and V_2 will satisfy the two integral equations

$$(65)\qquad V_k(\varphi)=U_k(\varphi)+\frac{1}{2}\int_{\varphi_0}^{\varphi}[U_1(\psi)U_2(\varphi)-U_1(\varphi)U_2(\psi)]V_k(\psi)d\psi,$$

$$(k=1,\ 2)$$

and we shall have

$$(66)\qquad z=\frac{\alpha V_1+\beta V_2}{\gamma V_1+\delta V_2}, \qquad \alpha\delta-\beta\gamma\neq 0,$$

as the most general expression for the independent variable z which

corresponds to the given intrinsic equation. The common kernel of the two integral equatiohs (65) is *skew symmetric*

$$K(\varphi, \psi) = -K(\psi, \varphi).$$

Thus *the general problem of finding the functions which correspond to a given intrinsic equation has been reduced to a problem in linear integral equations of the Volterra type with a skew symmetric kernel.*

12. Wilczinski[1] has given the following theorem. The fundamental invariants of two inverse functions have unity for their sum. Now it should be restated as follows: *The sum of the "fundamental invariants" of two mutually inverse functions is equal to zero.*

For,

$$J = \{w, \varphi\} + \{z, \varphi\},$$

$$\bar{J} = \{z, i\varphi\} + \{w, i\varphi\}$$

$$= -\{z, \varphi\} - \{w, \varphi\} = -J.$$

$$J + \bar{J} = 0. \tag{67}$$

The consideration of the inverse function $\bar{w} = f^{-1}(\bar{z})$ of $w = f(z)$ is now equivalent to a transformation

$$\bar{w} = z, \qquad \bar{z} = w. \tag{68}$$

But this transformation is a special case of (3). Therefore we may state: *The sums of the fundamental invariants*

$$J + \bar{J} \qquad \text{and} \qquad d\varphi^2 + d\bar{\varphi}^2$$

of two functions w and $\bar{w}$ such that

$$w = f(z),$$

$$\frac{a\bar{w} + b}{c\bar{w} + d} = f^{-1}\left(\frac{a\bar{z} + \beta}{\gamma\bar{z} + \delta}\right)$$

are both equal to zero.

13. By Art. 6, we conclude that the equation

(1) Wilczinski, l. c. Part II (1923), p. 42,

$$\frac{dp}{dt} = F(p)$$

serves as an intrinsic equation of a curve on the Absolute under the transformation subgroup

$$\bar{s} = \frac{\alpha s + \beta}{\gamma s + \delta}, \qquad \alpha\delta - \beta\gamma \neq 0,$$

where

$$p = \frac{1}{2}\int \sqrt{\{t, s\}}\, ds,$$

$$s = \frac{-x_3 - ix_4}{x_1 - ix_2} = \frac{x_1 + ix_2}{x_3 - ix_4},$$

$$t = \frac{-x_3 + ix_4}{x_1 - ix_2} = \frac{x_1 + ix_2}{x_3 + ix_4},$$

and

$$F(p) = \textit{an analytic function of } p.$$

This theorem may be transferred into two other theories.

14. The Wilczinski's essay, l. c., consists chiefly of the theory, of *osculating functions*, which transferred into the theories § 1 and § 3, *gives rise to the theory of osculating curves leading to interesting theorems.* But the detail will be left to the readers.

N. B. when a group of linear transformation on z is operated upon a function $w = f(z)$, we obtain a *class of functions* including w. The study of the common properties of such functions is a generalization of that of the automorphic functions and must lead to a vast field, Wilczinski's results being only a part of it. Especially the theory must be interesting, when the group is *discrete* or *finite*. The intrinsic equations of such functions *under discrete* or *finite groups* are much desirable.

Geometry of Doubly Oriented Spheres in Non-Euclidean Space.

By

Tsurusaburo Takasu.

In two of my foregoing papers[1], I have stated that the true theory of doubly oriented circles and spheres, which obey the law of Lie's higher sphere geometry, would be developed later in a separate paper. It is the purpose of this paper to fulfil this promise and make an introduction to the said theory.

1. Assume that the following theories have appropriately been founded up:

1°. Projective geometry, oriented points and planes as elements.[2]

2°. Non-Euclidean geometry, doubly oriented points, lines and planes as elements[3].

3°. Pentaspherical geometries in Non-Euclidean space.[4]

2. If (y) be the special correlatively oriented circle coordinates such that

$$y_m = a_m,\ m = 1,\ 2,\ 3,$$

If (z) be the special directly oriented circle coordinates such that

$$z_m = a_m,\ m = 1,\ 2,\ 3,$$

(1) T. Ota (my former family name), Pentaspherical Geometries in Non-Euclidean Space, I. The Tôhoku Mathematicel Journal, vol. 19, (1921), pp. 249–250. T. Takasu, the same topic, Part II. The same journal, vol. 21 (1922), p. 68, foot-note. Part III, vol. 21 (1922). Part IV, vol. 24 (1924). Cfr. the Euclidean case.

(2) (3) Takasu, Natural Non-Euclidean Geometry, Doubly Oriented Points Lines and Planes as Elements. (Under press.) Artt. 1–2. For its abstract see the Japanese Journal of Math., vol. 1 (1924).

(4) See (1).

$$y_4 = \varepsilon i \cos\frac{r}{k}\bar{\varepsilon}\sqrt{(aa)_3}$$

of the correlatively oriented circle

$$(ax)_3 + \left(\varepsilon i \cos\frac{r}{k}\bar{\varepsilon}\sqrt{(aa)_3}\right) \times (\varepsilon_0 i\sqrt{(xx)_3}) = 0,$$

$$\varepsilon,\ \bar{\varepsilon},\ \varepsilon_0 = \pm 1,$$

we have

$$\frac{(yy)_4}{(yy)_3} = 1 - \cos^2\frac{r}{k} = \sin^2\frac{r}{k},$$

$$\frac{\varepsilon\sqrt{(yy)_4}}{\sqrt{(yy)_3}} = \epsilon \sin\frac{r}{k} = \epsilon\cos\psi.$$

Let us take

$$y_5 = \epsilon i\sqrt{(yy)_4} = \epsilon i \sin\frac{r}{k}\sqrt{(yy)_3},$$

$$= \epsilon i \cos\psi\sqrt{(yy)_3},$$

and call the ratios $(y)_5$ the *special doubly oriented circle coordinates of the first kind.*

$$z_4 = \epsilon i \cos\psi\,\bar{\epsilon}\sqrt{(aa)_3}$$

of the directly oriented circle

$$(au)_3 + (\epsilon i \cos\psi\,\bar{\epsilon}\sqrt{(aa)_3}) \times (\epsilon_0 i\sqrt{(uu)_3}) = 0,$$

$$\epsilon,\ \bar{\epsilon},\ \epsilon_0 = \pm 1,$$

we have

$$\frac{(zz)_4}{(zz)_3} = 1 - \cos^2\psi = \sin^2\psi,$$

$$\frac{\varepsilon\sqrt{(zz)_4}}{\sqrt{(zz)_3}} = \varepsilon\sin\psi = \varepsilon\cos\frac{r}{k}.$$

Let us take

$$z_5 = \varepsilon i\sqrt{(zz)_4} = \varepsilon i \sin\psi\sqrt{(zz)_3},$$

$$= \varepsilon i \cos\frac{r}{k}\sqrt{(zz)_3},$$

and call the ratios $(z)_5$ the *special doubly oriented circle coordinates of the second kind.*

Thus the doubly oriented circle is given by the equations:

$$(y\ \boldsymbol{x})_4 = 0,$$

$$y_5 = \epsilon i\sqrt{(yy)_4}.$$

Its radius is given by

$$\frac{y_5}{i\sqrt{(yy)_3}} = \frac{\epsilon\sqrt{(yy)_4}}{\sqrt{(yy)_3}} = \epsilon\sin\frac{r}{k}.$$

$$(z\ \boldsymbol{y})_4 = 0,$$

$$z_5 = \varepsilon i\sqrt{(zz)_4}.$$

Its radial angle is given by

$$\frac{z_5}{i\sqrt{(zz)_3}} = \frac{\varepsilon\sqrt{(zz)_4}}{\sqrt{(zz)_3}} = \varepsilon\sin\psi.$$

3. If we take $y_m = z_m$ $(m = 1, 2, 3)$, we have

$$(yy)_3 + y_5^2 + z_5^2 = 0,$$

$$(zz)_3 + y_5^2 + z_5^2 = 0,$$

$$y_4^2 + (zz)_4 = 0,$$

$$z_4^2 + (yy)_4 = 0,$$

$$z_5 = y_4, \qquad y_5 = z_4.$$

Thus the two kinds spoken of in the last article are not distinct from each other. Hereafter let us call the ratios $(y)_5$ such that

$$y_m = a_m (m = 1, 2, 3)$$

$$y_4 = \varepsilon i \cos\frac{r}{k}, \quad y_5 \equiv z_4 \equiv \epsilon i \cos\psi$$

the special doubly oriented circle coordinates.

4. If (η) be the general correlatively oriented circle coordinates of the correlatively oriented circle (y), we have

$$(\eta\eta)_4 = K(yy)_4 \qquad (1),$$

If (ζ) be the general directly oriented circle coordinates of the directly oriented circle (z), we have

$$(\zeta\zeta)_4 = K(zz)_4 \qquad (1),$$

where $K \neq 0$ is a function of the transformation only. Without loss of generality, we my assume $K = 1$.

5. Let us put

$$\eta_5 \equiv \epsilon i \sqrt{(\eta\eta)_4} \qquad \zeta_5 \equiv \varepsilon i \sqrt{(\zeta\zeta)_4}$$

and call the ratios

$(\eta)_5$ the *general doubly oriented circle coordinates of the first kind.*

$(\zeta)_5$ the *general doubly oriented circle coordinates of the second kind.*

6. If we adopt the convention in Art. 3, we have

$$\eta_m (m = 1, 2, 3), \qquad \eta_5 = y_5 = z_4,$$

$$\zeta_m (m = 1, 2, 3), \qquad \zeta_5 = z_5 = y_4.$$

7. The angle of intersection θ_{yx} $(\theta_{\eta\xi})$ of two doubly oriented circles (y) $((\eta))$ and (x) $((\xi))$ will be given by

$$\cos\theta_{yx} = \frac{(yx)_4}{(iy_5)(ix_5)},$$

$$\cos\theta_{\eta\xi} = \frac{(\eta\xi)_4}{(i\eta_5)(i\xi_5)}.$$

$$\sin^2\frac{\theta_{yx}}{2} = \frac{(yx)_5}{2y_5x_5}, \text{ etc.}$$

The common tangential segments S_{zx} $(S_{\zeta\xi})$ of two doubly oriented circles (z) $((\zeta))$ and (x) $((\xi))$ will be given by

$$\cos\frac{S_{zx}}{k} = \frac{(zx)_4}{(iz_5)(ix_5)},$$

$$\cos\frac{S_{\zeta\xi}}{k} = \frac{(\zeta\xi)_4}{(i\zeta_5)(i\xi_5)},$$

$$\sin^2\frac{S_{zx}}{2k} = \frac{(zx)_5}{2z_5x_5}, \text{ etc.}$$

(1) TAKASU, I, l. c. p. 264.

8. The doubly oriented circles whose coordinates (y) satisfy a linear equation

$$(ay)_5 = 0$$

is called a *linear congruence of doubly oriented circles.* They have the followlng interpretations:

$(aa)_4 \neq 0, \quad \epsilon = \pm 1.$

$$\sin^2\frac{\theta_{ay}}{2} = \frac{(ay)_4 + \epsilon i\sqrt{(aa)_4}\,y_5}{2\epsilon i\sqrt{(aa)_4}\,y_5},$$

$$= \frac{-a_5 + \epsilon\sqrt{(aa)_4}\,i}{2\epsilon\sqrt{(aa)_4}\,i}.$$

$(aa)_3 + a_5^2 \neq 0, \quad \varepsilon = \pm 1.$

$$\sin^2\frac{S_{ay}}{2k}$$

$$= \frac{(ay)_3 + a_5 y_5 + \varepsilon i\sqrt{(aa)_3 + a_5^2}\,y_4}{2\varepsilon i\sqrt{(aa)_3 + a_5^2}\,y_4},$$

$$= \frac{-a_4 + \varepsilon i\sqrt{(aa)_3 + a_5^2}}{2\varepsilon\sqrt{(aa)_3 + a_5^2}\,i}.$$

The doubly oriented circles of the linear congruence

meet a doubly oriented circle at a fixed angle, which will be null, if

$$(aa)_4 = 0.$$

lie to a doubly oriented circle at a fixed tangential distance, which will be line, if

$$(aa)_3 + a_5^2 = 0.$$

When $(aa)_5 = 0$ holds, the congruence is said to be *special*, even when

$$(aa)_4 = 0$$

or when

$$(aa)_3 + a_5^2 = 0.$$

It consists in the doubly oriented circles properly tangent to one doubly oriented circle.

9. The expression

$$I = \frac{(ab)_5}{\sqrt{(aa)_5}\,\sqrt{(bb)_5}}$$

is an absolute invariant of the two linear congruences of doubly oriented circles

$$(ay)_5 = 0 \qquad \text{and} \qquad (by)_5 = 0$$

under the pentacyclic group spoken of in Art. 24.

10.

$$I = \frac{\cos\phi - \cos\phi_1 \cos\phi_2}{\sin\phi_1 \sin\phi_2},$$

where ϕ_1 and ϕ_2 are the angles associated with the definition of the congruences, and ϕ the angle of their (first) fundamental doubly oriented circles.

$$I = \frac{\cos\frac{S}{k} - \cos\frac{S_1}{k}\cos\frac{S_2}{k}}{\sin\frac{S_1}{k}\sin\frac{S_2}{k}},$$

where S_1 and S_2 are the common tangential segments associated with the definition of the congruences, and S the common tangential segment of their (second) fundamental doubly oriented circles.

Proof.

$$\cos\phi_1 = \frac{(a\,y)_4}{\epsilon\sqrt{(aa)_4(-iy_5)}} = \frac{a_5}{\epsilon i\sqrt{(aa)_4}}, \text{ etc.}$$

$$\sin\phi_1 = \frac{\sqrt{(aa)_5}}{\epsilon\sqrt{(aa)_4}}, \text{ etc.}$$

$$\cos\phi = \frac{(ab)_4}{\epsilon\sqrt{(aa)_4}\,\bar{\epsilon}\sqrt{(bb)_4}}.$$

$$\frac{\cos\phi_1\cos\phi_2 - \cos\phi}{\sin\phi_1\sin\phi_2} = \left(\frac{a_5}{\epsilon i\sqrt{(aa)_4}}\cdot\frac{b_5}{\bar{\epsilon} i\sqrt{(bb)_4}} - \frac{(ab)_4}{\epsilon\sqrt{(aa)_4}\,\bar{\epsilon}\sqrt{(bb)_4}}\right) \Big/ \left(\frac{\sqrt{(aa)_5}}{\epsilon\sqrt{(aa)_4}}\cdot\frac{\sqrt{(bb)_5}}{\bar{\epsilon}\sqrt{(bb)_4}}\right),$$

$$= \frac{-(ab)_5}{\sqrt{(aa)_5}\sqrt{(bb)_5}} = -I.$$

Cor. $$\frac{\cos\phi_1\cos\phi_2 - \cos\phi}{\sin\phi_1\sin\phi_2} = \frac{\cos\frac{S_1}{k}\cos\frac{S_2}{k} - \cos\frac{S}{k}}{\sin\frac{S_1}{k}\sin\frac{S_2}{k}}.$$

11. The two linear congruences

$$(ay)_5 = 0 \qquad \text{and} \qquad (by)_5 = 0$$

are said to be *in involution*, when

$$I = 0$$

i. e. when

$$(ab)_5 = 0$$

12. If one of two linear congruences in involution be special, its (first) fundamental doubly oriented circle is a member of the other congruence ;

If one of two linear congruences in involution be special, its (second) fundamental doubly oriented circle is a member of the other congruence ;

if both be special, their fundamental doubly oriented circles are tangent.

Proof. $(ab)_5 = 0.$

If $(aa)_5 = 0$, the coordinates of the first fundamental doubly oriented circle

$$\frac{a_1}{\epsilon\sqrt{(aa)_4}}, \ldots\ldots\ldots\ldots, \frac{a_4}{\epsilon\sqrt{(aa)_4}}, \; i$$

satisfy the equation of the other congruence

$$(by)_5 = 0.$$

If both be special, so that

$$(aa)_5 = 0, \qquad (bb)_5 = 0,$$

their fundamental circles

$$\frac{a_1}{\epsilon\sqrt{(aa)_4}}, \ldots\ldots\ldots\ldots, \frac{a_4}{\epsilon\sqrt{(aa)_4}}, \; i$$

and

$$\frac{b_1}{\epsilon\sqrt{(bb)_4}}, \ldots\ldots\ldots\ldots, \frac{b_4}{\epsilon\sqrt{(bb)_4}}, \; i$$

are tangent, since

$$(ab)_5 = 0.$$

13. We obtain the following correspondences :

Plane π.	*Space* Σ_3.	*Space* Σ'_3.
Linear congruence	Dir. or. sphere	Cor. or. sphere
Invariant I	Cos. of angle of 2 dir. or. spheres	Cos. of common tangential segment by k of 2 cor. or. spheres.
Congruences in invol.	Orthogonal dir. or. spheres.	Tangentially orthogonal cor. or. spheres.

14. These analogies lead us to consider the doubly oriented circle transformation, which corresponds to an inversion in Σ_3 and a dual inversion in Σ'_3 each as a special case.

We start with a nonspecial linear congruence $(a)_5$ and define as

an *inversion* | a *dual inversion*

therein the following transformation:

$$\rho y'_i = (a_5^2 - a_5^2) y_i + 2(ay)_5 a_i, \qquad \rho y'_i = (a_4^2 - a_4^2) y_i + 2(ay)_5 a_i,$$

$$i = 1, 2, 3, 4, 5, \qquad i = 1, 2, 3, 4, 5,$$

where

$$a_5^2 - a_5^2 \equiv -(aa)_5, \qquad a_4^2 - a_4^2 \equiv -(aa)_5,$$

which is seen at once to correspond to

inversion in space[1]. | dual inversion in space[1].

We have the following relative invariants:

$$(y'y')_5 = \rho^{-2}(a_5^2 - a_5^2)(yy)_5, \qquad (y'y')_5 = \rho^{-2}(a_4^2 - a_4^2)(yy)_5,$$

$$(ay')_5 = -\rho^{-2}(a_5^2 - a_5^2)(ay)_5. \qquad (ay')_5 = -\rho^{-2}(a_4^2 - a_4^2)(ay)_5.$$

When $a_5 = 0$, | When $a_4 = 0$,

we fall back to the ordinary

inversion: | dual inversion:

$$\frac{y_i'}{-iy_5'} = \frac{y_i}{iy_5} - 2\frac{(ay)_4}{iy_5'(aa)_4}a_i, \qquad \frac{y_i'}{-iy_4'} = \frac{y_i}{iy_4} - 2\frac{(ay)_3 + a_5 y_5}{iy_4\{(aa)_3 + a_5^2\}}a_i,$$

$$i = 1, 2, 3, 4. \qquad i = 1, 2, 3, 5.$$

The doubly oriented circles (y) and (y') are coaxal with the doubly oriented circle $(a)_5$. | The doubly oriented circles (y) and (y') are homocentric with the doubly oriented circle $(a)_5$.

The product of the tangents of the halves of their

angles therewith is | tangential distances by k therefrom is

$$\tan\frac{(ay)}{2}\tan\frac{(ay')}{2} = \tan^2\frac{\phi}{2}, \qquad \tan\frac{S_{ay}}{2k}\tan\frac{S_{ay}'}{2k} = \tan^2\frac{S}{2k},$$

(1) TAKASU, III, l. c., Art. 262.

where ϕ is the fundamental angle associated with the linear congruence.

where S is the fundamental segment associated with the linear congruence.

For,

$$\sin^2\frac{(ay)}{2} = \frac{a_5y_5+(ay)_4}{2a_5y_5},$$

$$\cos^2\frac{(ay)}{2} = \frac{a_5y_5-(ay)_4}{2a_5y_5}.$$

$$\tan^2\frac{(ay)}{2} = \frac{a_5y_5+(ay)_4}{a_5y_5-(ay)_4} = \frac{(a_5-a_5)y_5+(ay)_5}{(a_5+a_5)y_5-(ay)_5}.$$

$$\tan^2\frac{(ay')}{2} = \frac{a_5y'_5+(ay')_4}{a_5y'_5-(ay')_4} = \frac{(a_5-a_5)y'_5+(ay')_5}{(a_5+a_5)y'_5-(ay')_5},$$

$$= \frac{(a_5-a_5)[(a_5^2-a_5^2)y_5+2(ay)_5a_5]-(a_5^2-a_5^2)(ay)_5}{(a_5+a_5)[(a_5^2-a_5^2)y_5+2(ay)_5a_5]+(a_5^2-a_5^2)(ay)_5},$$

$$= \left(\frac{a_5-a_5}{a_5+a_5}\right)^2\frac{(a_5+a_5)y_5-(ay)_5}{(a_5-a_5)y_5+(ay)_5}.$$

$$\therefore\quad \tan\frac{(ay)}{2}\tan\frac{(ay')}{2} = \frac{a_5-a_5}{a_5+a_5} = \frac{\epsilon i\sqrt{(aa)_4}-a_5}{\epsilon i\sqrt{(aa)_4}+a_5} = \tan^2\frac{\phi}{2}.$$

Hence, if a general linear congrunce consist in doubly oriented circles

meeting a fixed doubly oriented circle at a fixed angle not zero, then two doubly oriented circles are mutually inverse in the congruence, when and only when they are coaxal with the fixed doubly oriented circle, and the product of the tangents of half their angles therewith is equal to the square of the tangent of half the angle associated with the congruence.

lying at a fixed tangential distance not zero to a fixed doubly oriented circle, then two doubly oriented circles are mutually dual inverse in the congruence, when and only when they are homocentric with the fixed doubly oriented circle, and the product of the tangents of half their tangential distances thereto by k is equal to the square of the tangent of half the tangential segment associated with the congruence by k.

15. When the angle associated with a linear congruence of doubly oriented circles is $\frac{\pi}{2}$, the inversion in the congruence is a doubly oriented circle inversion.

For, then and only tnen $a_5 = 0$.

When the tangential segment associated with a linear congruence of doubly oriented circles is $\frac{\pi}{2}k$, the dual inversion in the congruence is a doubly oriented circle dual inversion.

For, then and only then $a_4 = 0$

16. Inversion in the linear congruence of all null doubly oriented circles is the reversal of the sign either of the radius or the radial angle of each doubly oriented circle (i. e. the reversal of the direct or the correlative orientation).

Dual inversion in the linear congruence of all line doubly oriented circles is the reversal of the sign either of the radial angle or the radius of each doubly oriented circle (i. e. the reversal of the correlative or the direct orientation).

For, $a_1 = a_2 = a_3 = a_4 = 0$. $\therefore \quad a_5 = 0$.

$$\rho y_i' = (a_5^2 - a_5^2) y_i + 2(ay)_5 a_i.$$

$$i = 5 : \rho y_5' = -a_5^2 y_5 + 2(a_5 y_5) a_5 = a_5^2 y_5.$$

$$i = 4 : \rho y_4' = -a_5^2 y_4.$$

$$\therefore \quad y_5' : y_4' = -y_5 : y_4.$$

$$\therefore \quad \varepsilon'\epsilon' \tan \frac{r'}{k} = -\varepsilon\epsilon \tan \frac{r}{k}.$$

Hence the result.

17. Inversion in the linear congruence of all doubly oriented circles of given radius (i. e. of given radial angle) will change each doubly oriented circle into a concentric one, whose radius (with sense) differs from the negative of that of the given doubly oriented circle by a constant.

Dual inversion in the linear congruence of all doubly oriented circles of given radial angle (i. e. of given radius) will change each doubly oriented circle into a coaxial one, whose radial angle (with sense) differs from the negative of that of the given doubly oriented circle by a constant.

Proof. $a_1 = a_2 = a_3 = 0. \qquad \therefore \quad a_4^2 = -a_4^2.$

$$\rho y'_i = -(a_4^2 + a_5^2)y_i + 2(ay)_5 a_i.$$

$$i = 1: \quad \rho y_1' = -(a_4^2 + a_5^2)y_1,$$

$$i = 2: \quad \rho y_2' = -(a_4^2 + a_5^2)y_2,$$

$$i = 3: \quad \rho y_3' = -(a_4^2 + a_5^2)y_3.$$

$$y_1' : y_2' : y_3' = y_1 : y_2 : y_3$$

Hence the concentricity takes place.

$$i = 4: \quad \rho y_4' = -(a_4^2 + a_5^2)y_4 + 2(a_1 y_1 + a_5 y_5)a_4 = (a_4^2 - a_5^2)y_4 + 2a_4 a_5 y_5.$$

$$i = 5: \quad \rho y_5' = -(a_4^2 + a_5^2)y_5 + 2(a_4 y_4 + a_5 y_5)a_5 = (a_5^2 - a_4^2)y_5 + 2a_4 a_5 y_4.$$

$$\frac{y_4'}{y_5'} = \frac{(a_4^2 - a_5^2)y_4 + 2a_4 a_5 y_5}{-(a_4^2 - a_5^2)y_5 + 2a_4 a_5 y_4} = \left(-\frac{y_4}{y_5} + \frac{2a_4 a_5}{a_5^2 - a_4^2}\right) \Big/ \left(1 + \frac{2y_4 a_4 a_5}{y_5(a_5^2 - a_4^2)}\right),$$

$$\tan\frac{\varepsilon' \epsilon' \gamma'}{k} = \tan\left(\alpha - \frac{\varepsilon \epsilon \gamma}{k}\right),$$

where

$$\tan\alpha \equiv \frac{2a_4 a_5}{a_5^2 - a_4^2}.$$

18. A necessary and sufficient condition that the product of the inversions (dual inversions) in two linear congruences should be commutative is that the congruences should be in involution.

Proof. $\rho \equiv a_5^2 - a_5^2.$

$$\rho y'_i = (a_5^2 - a_5^2)y_i + 2(ay)_5 a_i, \qquad i = 1, 2, 3, 4, 5.$$

$$\rho y''_i = (\beta_5^2 - b_5^2)y'_i + 2(by')_5 b_i, \qquad i = 1, 2, 3, 4, 5.$$

$$\rho^2 y''_i = (\beta_5^2 - b_5^2)[(a_5^2 - a_5^2)y_i + 2(ay)_5 a_i] + 2b_i[(a_5^2 - a_5^2)(by)_5 + 2(ay)_5(ab)_5],$$

$$\rho y''_i = (a_5^2 - a_5^2)y'_i + 2(ay')_5 a_i,$$

$$\rho y'_i = (\beta_5^2 - b_5^2)y_i + 2(by)_5 b_i,$$

$$\rho^2 y''_i = (a_5^2 - a_5^2)[(\beta_5^2 - b_5^2)y_i + 2(by)_5 b_i] + 2a_i[(\beta_5^2 - b_5^2)(ay)_5 + 2(by)_5(ab)_5].$$

In order that the two results may be the same, it is necessary and sufficient that

$$b_i(ay)_5(ab)_5 = a_i(by)_5(ab)_5$$

for all (y), for which it is again necessary and sufficient that

$$b_i(ab)_5 - a_i(ab)_5 = 0, \qquad i = 1, 2, 3, 4, 5,$$

for which it is once more necessary and sufficient that

$$(ab)_5 = 0.$$

19. Every pentacyclic group of daubly oriented circles can be factored into the product of five or less inversions (dual inversions) in linear congruences.

20. If $(A^{(i)})$, $i = 1, 2, 3, 4, 5$, be five linear congruences mutually in involution and (a) and (a') any two others, then

$$I_{aa'} = \sum_{n=1}^{n=5} I_{aA^{(n)}}\ I_{a'A^{(n)}},$$

where

$$I_{aa'} \equiv \frac{\cos\theta - \cos\phi\cos\phi'}{\sin\phi\sin\phi'} \equiv \frac{\cos\dfrac{T}{k} - \cos\dfrac{S}{k}\cos\dfrac{S'}{k}}{\sin\dfrac{S}{k}\sin\dfrac{S'}{k}},$$

where θ is the angle between the first fundamental doubly oriented circles of (a) and (a'), and ϕ, ϕ' the angles associated to (a) and (a') respectively; T the tangential distance between the second fundamental doubly oriented circles of (a) and (a'), and S, S' the tangential distances associated to (a) and (a') respectively.

Proof. Multiplying

$$\begin{vmatrix} A_1^{(1)} & A_2^{(1)} & A_3^{(1)} & A_4^{(1)} & A_5^{(1)} & 0 \\ A_1^{(2)} & A_2^{(2)} & A_3^{(2)} & A_4^{(2)} & A_5^{(2)} & 0 \\ A_1^{(3)} & A_2^{(3)} & A_3^{(3)} & A_4^{(3)} & A_5^{(3)} & 0 \\ A_1^{(4)} & A_2^{(4)} & A_3^{(4)} & A_4^{(4)} & A_5^{(4)} & 0 \\ A_1^{(5)} & A_2^{(5)} & A_3^{(5)} & A_4^{(5)} & A_5^{(5)} & 0 \\ a_1 & a_2 & a_3 & a_4 & a_5 & 0 \end{vmatrix} \text{ and } \begin{vmatrix} A_1^{(1)} & A_2^{(1)} & A_3^{(1)} & A_4^{(1)} & A_5^{(1)} & 0 \\ A_1^{(2)} & A_2^{(2)} & A_3^{(2)} & A_4^{(2)} & A_5^{(2)} & 0 \\ A_1^{(3)} & A_2^{(3)} & A_3^{(3)} & A_4^{(3)} & A_5^{(3)} & 0 \\ A_1^{(4)} & A_2^{(4)} & A_3^{(4)} & A_4^{(4)} & A_5^{(4)} & 0 \\ A_1^{(5)} & A_2^{(5)} & A_3^{(5)} & A_4^{(5)} & A_5^{(5)} & 0 \\ a'_1 & a'_2 & a'_3 & a'_4 & a'_5 & 0 \end{vmatrix}$$

together, we get

$$\begin{vmatrix} (A^{(1)}A^{(1)}) & 0 & 0 & 0 & 0 & (A^{(1)}a) \\ 0 & (A^{(2)}A^{(2)}) & 0 & 0 & 0 & (A^{(2)}a) \\ 0 & 0 & (A^{(3)}A^{(3)}) & 0 & 0 & (A^{(3)}a) \\ 0 & 0 & 0 & (A^{(4)}A^{(4)}) & 0 & (A^{(4)}a) \\ 0 & 0 & 0 & 0 & (A^{(5)}A^{(5)}) & (A^{(5)}a) \\ (A^{(1)}a') & (A^{(2)}a') & (A^{(3)}a') & (A^{(4)}a') & (A^{(5)}a') & (aa') \end{vmatrix} = 0,$$

i. e.

$$\sum_{n=1}^{n=5} \frac{(aA^{(n)})}{\sqrt{(A^{(n)}A^{(n)})}\sqrt{(aa)}} \cdot \frac{(a'A^{(n)})}{\sqrt{(A^{(n)}A^{(n)})}\sqrt{(a'a')}} = \frac{(aa')}{\sqrt{(aa)}\sqrt{(a'a')}}.$$

Hence the result.

21. When $(A^{(n)})$, $n = 1, 2, 3, 4, 5$, are five linear congruences mutually in involution, and (a) any other, then

$$\sum_{n=1}^{n=5} I^2_{aA^{(n)}} = 1.$$

22. When $(A^{(n)})$, $n = 1, 2, 3, 4, 5$, are five linear congruences mutually in involution, and (a) any other, then we interpret the ratios

$$(a) = (I_a A^{(n)})$$

as the *coordinates of the linear congruence* referred to $(A^{(n)})$, $n = 1, 2, 3, 4, 5$.

When

$$a_n = I_a A^{(n)},$$

we call (a) the *normal form* of (a).

23. Let five linear congruences in involution be $(A^{(i)})$, $i = 1, 2, 3, 4, 5$; the angle associated with the congruence $(A^{(j)})$ be ϕ_j, the angle at which an arbitrary doubly oriented circle cuts the fundamental doubly oriented circle of $(A^{(j)})$ shall be θ_j. Let us then write

the common tangential segment associated with the congruence $(A^{(j)})$ shall be S_j the tangential distance at which an arbitrary doubly oriented circle lies to the fundamental doubly oriented circle of $(A^{(j)})$ shall be T_j.

Let us then write

$$X_j' \equiv \frac{\cos\theta_j - \cos\phi_j}{\sin\phi_j}, \qquad X_j' \equiv \frac{\cos\frac{T_j}{k} - \cos\frac{S_j}{k}}{\sin\frac{S_j}{k}},$$

$$= \frac{i(A^{(j)}y)_5}{y_5\sqrt{(A^{(j)}A^{(j)})_5}}. \qquad = \frac{i(A^{(j)}y)_4}{y_4\sqrt{(A^{(j)}A^{(j)})_5}}.$$

Then $$(X'X')_5 = 0.$$

For, $$\cos\phi_j = \frac{A_5^{(j)}}{\epsilon_j i\sqrt{(A^{(j)}A^{(j)})_4}}, \quad \sin\phi_j = \frac{\sqrt{(A^{(j)}A^{(j)})_5}}{\epsilon_j\sqrt{(A^{(j)}A^{(j)})_4}},$$

$$\sin\theta_j = \frac{(A^{(j)}y)_4}{\epsilon_j\sqrt{(A^{(j)}A^{(j)})_4}\,\epsilon_y\sqrt{(yy)_4}}.$$

$$\begin{vmatrix} A_1^{(1)} & A_2^{(1)} & A_3^{(1)} & A_4^{(1)} & A_5^{(1)} & 0 \\ A_1^{(2)} & A_2^{(2)} & A_3^{(2)} & A_4^{(2)} & A_5^{(2)} & 0 \\ A_1^{(3)} & A_2^{(3)} & A_3^{(3)} & A_4^{(3)} & A_5^{(3)} & 0 \\ A_1^{(4)} & A_2^{(4)} & A_3^{(4)} & A_4^{(4)} & A_5^{(5)} & 0 \\ A_1^{(5)} & A_2^{(5)} & A_3^{(5)} & A_4^{(5)} & A_5^{(5)} & 0 \\ y_1 & y_2 & y_3 & y_4 & y_5 & 0 \end{vmatrix}^2 \equiv 0,$$

$$\begin{vmatrix} (A^{(1)}A^{(1)}) & 0 & 0 & 0 & 0 & (A^{(1)}y) \\ 0 & (A^{(2)}A^{(2)}) & 0 & 0 & 0 & (A^{(2)}y) \\ 0 & 0 & (A^{(3)}A^{(3)}) & 0 & 0 & (A^{(3)}y) \\ 0 & 0 & 0 & (A^{(4)}A^{(4)}) & 0 & (A^{(4)}y) \\ 0 & 0 & 0 & 0 & (A^{(5)}A^{(5)}) & (A^{(5)}y) \\ (A^{(1)}y) & (A^{(2)}y) & (A^{(3)}y) & (A^{(4)}y) & (A^{(5)}y) & 0 \end{vmatrix} \equiv 0,$$

$$\begin{vmatrix} 1 & 0 & 0 & 0 & 0 & X_1' \\ 0 & 1 & 0 & 0 & 0 & X_2' \\ 0 & 0 & 1 & 0 & 0 & X_3' \\ 0 & 0 & 0 & 1 & 0 & X_4' \\ 0 & 0 & 0 & 0 & 1 & X_5' \\ X_1' & X_2' & X_3' & X_4' & X_5' & 0 \end{vmatrix} \equiv 0,$$

$$(X'X')_5 \equiv 0.$$

Thus if five linear congruences in involution of doubly oriented circles consist in the doubly oriented circles

meeting five fundamental doubly oriented circles at five fundamental angles,

lying to five fundamental doubly oriented circles at five fundamental tangential distances,

then we may take for the coordinates of every proper doubly oriented circle five quantities each proportional to the quotient of the difference of the cosine of a fundamental

angle and the cosine of the angle made with the corresponding fundamental doubly oriented circle divided by the sine of that fundamental angle. The sum of the squares of these coordinates will in every case be zero.

tangential distance and the cosine of the tangential distance by k to the corresponding fundamental doubly oriented circle divided by the sine of that fundamental tangential distance by k. The sum of the squares of these coordinates will in every case be zero.

24. The most general analytic transformation that carries a doubly oriented circle into a doubly oriented circle and the doubly oriented circles of a linear congruece into doubly oriented circles of a linear congruence is given by a quinary orthogonal transformation. Let us refer to it as a *pentacyclic group.*

25. The quinary orthogonal transformation just spoken of may be interpreted as follows:

$$a_m' = I_{\alpha\,(m)} = \sum_{n=1}^{n=5} I_{\alpha A(n)}\, I_{\beta\,m) A(n)}, \quad m = 1, 2, 3, 4, 5.$$

$$\sum_{n=1}^{n=5} I_{\beta^2(m) A(n)} = 1,$$

$$\sum_{n=1}^{n=5} I_{\beta(m) A(n)}\, I_{\beta(m') A(n)} = 0, \quad m \neq m', \quad m,\ m' = 1, 2, 3, 4, 5,$$

since $(\beta^{(m)})$, $m = 1, 2, 3, 4, 5$ are mutually in involution.

26. If (x), (y), (z), (t) be four doubly oriented circles, then

If (x), (y), (z), (t) be any four doubly oriented circles, then

$$\frac{(xy)(zt)}{(xt)(zy)} = \frac{\sin^2\frac{(xy)}{2}\sin^2\frac{(zt)}{2}}{\sin^2\frac{(xt)}{2}\sin^2\frac{(zy)}{2}}$$

is an absolute invariant for the pentacyclic group.

$$\frac{(xy)(zt)}{(xt)(zy)} = \frac{\sin^2\frac{S_{xy}}{2k}\sin^2\frac{S_{zt}}{2k}}{\sin^2\frac{S_{xt}}{2k}\sin^2\frac{S_{zy}}{2k}}$$

is an absolute invariant for the pentacyclic group.

27. The analogies to Art. 2—Art. 7 are to be stated here for *doubly oriented spheres.*

28. The doubly oriented spheres, whose coordinates $(y)_6$ satisfy a linear equation

$$(ay)_6 = 0.$$

is called a *linear complex of doubly orinted spheres.* They have the interpretations analogous to Art. 8.

29. The most general analytic transformation, which carries a doubly oriented sphere into a doubly oriented sphere and doubly oriented spheres of a linear complex into doubly oriented spheres of a linear complex is a 6-ary orthogonal transformation; they form a group, which we will call the *hexaspherical group.* It consists of a *subgroup of direct transformations,* whose determinants are positive and a *subset of indirect transformations,* whose determinants are negative.

30. The anlogies to Art. 9—Art. 25 are to be stated here.

31. Putting

$$p_{12} \equiv y_1 + iy_4, \qquad p_{34} \equiv y_1 - iy_4,$$
$$p_{13} \equiv y_2 + iy_5, \qquad p_{42} \equiv y_2 - iy_5,$$
$$p_{14} \equiv y_3 + iy_6, \qquad p_{23} \equiv y_3 - iy_6,$$

so that

$$\Sigma p_{12}p_{34} \equiv (yy)_6 \equiv 0,$$
$$\Sigma p_{12}p'_{34} \equiv (yy')_6 \equiv 0,$$

we obtain an analogy to LIE's line-sphere transformation[1].

August 1923.

---

(1) Prof. BECK has cited my discovery of the analogy of LIE's higher sphere geometry in his paper: Zur LIE-schen Kugelgeometrie im Nicht-Euclidischen Raum. Jahresbericht der DEUTSCHEN Mathdmatiker-Vereinigung, 32. Bd. (1923). For the date of mine, see the introductry note.

N. B. Just as the non-Euclidean geometry was capable of being finished in *two* ways, the tetracyclic (pentaspherical) geometry may be treated in *two* different ways, one of which is to insert it in the pentacyclic (hexaspherical) geometry. For the detail, see the last § of the paper cited in the foot-note (2) of Art. 1.

The Influence of Metallic Elements on the Corrosion of Iron and Steel.[1]

By

Yuhatirô Utida and Makoto Saitô.

With Nine Plates.

§ 1. INTRODUCTION.

From the technical point of view, it is very important to obtain a ferrous metal or alloy, which has a high resistivity against corroding action of various media. Concerning this problem, numerous investigations have already been made and various non-corroding alloys, such as high nickel steel, stainless steel etc., discovered. A systematic study on the corrosion of iron and steel alloyed with various special elements were made by Messrs. Newton Friend,[2] Leslie Aitchison,[3] Robert Hadfield[4] and W. H. Hatfield[5] and many other investigators.

The present work was commenced to study systematically the influence of various metallic elements on the corrosion of iron and steel

(1) The one hundred and fifth report of the Research Institute of Iron, Steel and Other Metals.

(2) Jour. of Iron and Steel Inst., No. 1, (1912).
Iron and Steel Inst., Carnegie Scholarship Memoirs, 11, (1922).

(3) A paper read before the Faraday Soc., May and Dec., 1915.
Iron and Coal Trade Rev., Nov. 1921.

(4) Jour. of Iron and Steel Inst., No. II, (1892).
Opening address at a general discussion on "Corrosion of Metals," held before the Faraday Soc., Dec., 1915. A paper published in 1922.

(5) The Engineer, Dec. 1922.

in acids, as well as, the oxidation in atmospheric oxygen at 1100° C. It is here to be noted that in all cases, special elements were added in the range of concentration forming a solid solution with the mother alloys.

The specimens used in the present investigation may be classified into two series :—

(I). Iron containing a small amount of carbon and varying proportion of one special element ;

(II). Iron containing a constant percentage of carbon and varying two other elements.

§ 2. METHOD OF EXPERIMENTS.

The test samples were prepared by casting an alloy of Hôchôtetsu (nearly pure iron) with various metallic elements in a metallic mould having a bore, 5 mm diameter and 20 cm length.

From these rods, samples of 4 to 5 cm long were taken ; thier surfaces were first ground, and then polished with emery papers. They were then washed in water, benzene and alcohol, and finally dried in desiccator : After that, they were weighed and immersed in the beakers containing corrosion medium, such as nitric, hydrochloric or sulphuric acid, and left for twenty-four hours at room temperature. They were then taken out from the liquid, cleaned with a brush, washed in distilled water and alcohol, dried in desiccator and weighed again. In every case, the weight of the specimens was from 5 to 7 grams and the area exposed to the action of solution from 6 to 8 sq. cm. The corrosion degree is given as the loss of weight per sq. cm. of the surface area of the specimen.

In measuring oxidation degree at high temperatures, the cleaned and dried specimen was put in a porcelain boat and weighed. The boat containing the specimen was placed in a platinum electric furnace heated to 1100° C, and remained there for one hour. The boat was then taken out from the furnace, cooled in a dry desiccator to room temperature and

weighed. The oxidation degree is given as the increase of the weight of the specimen per sq. cm. of its surface.

§ 3. RESULTS OF EXPERIMENTS.

EXPERIMENT I.

Iron containing a small amount of carbon and varying proportion of one special elements, such as nickel, chromium, silicon, copper, manganese or tungsten.

The analysis of materials, from which the test specimens were prepared, is given below :—

Materials.	C (%)	Si (%)	Mn (%)	S (%)	P (%)	Al (%)	Other element. (%)
Hôchôtetsu. . . .	0.05	0.047	0.15	0.010	0.040	—	—
Nickel.	0.18	0.15	0.20	0.025	—	—	Ni=98,98
Chromium. . . .	0.12	90.78	tr.	(Fe=2.80)	—	0.98	Cr=95,12
Silicon.	0.39	6.38	90.33	—	—	—	—
Copper.	—	—	—	—	—	—	Cu=99,9
Manganese. . . .	0.02	0.07	6.10	—	—	—	
Ferro-tungsten. . .	0.21	0.12	0.08	—	0.05	—	W=81,46
Ferro-chrominm . .	3.20	4 71	0.34	—	—	—	Fe=30,02 Cr=61,83

The results of observation are graphically given in Tables 1–6 and Figs. 1–4, Pl. I, II.

TABLE I. Influence of Nickel.

Composition.		Loss of weight per sq. cm.			Weight of oxygen combined per sq. cm. at 1100° C.
C (%)	Ni (%)	HNO_3	HCl	H_2SO_4	
0.05	0	0.9380 gr.	0.0712 gr.	0.0990 gr.	0.0212 gr.
0.08	8.21	0.5090	0.0602	0.0112	0.0369
0.08	15.59	0.4183	0.0371	0.0091	0.0318
0.06	23.57	0.4087	0.0342	0.0037	0.0227
0.08	33.92	0.3360	0.0040	0.0011	0.0170
0.07	42.99	0.3125	0.0028	0.0003	0.0160
0.06	54.50	0.2552	0.0016	0.0005	0.0133
0.07	60.09	0.1050	0.0012	0.0006	0.0077
0.09	75.81	0.0560	0.0008	0.0005	0.0055
0.12	81.06	0.0275	0.0009	0.0005	0.0046
0.14	86.56	0.0254	0.0014	0.0006	0.0040
0.18	98.98	0.0221	0.0015	0.0006	0.0030

TABLE II. Influence of Chromium.

Composition.		Loss of weight per sq. cm.			Weight of oxygen combined per sq. cm. at 1100° C.
C (%)	Cr (%)	HNO_3	HCl	H_2SO_4	
0.06	0.97	0.6240 gr.	0.2465 gr.	0.1002 gr.	0.0455 gr.
0.10	4.86	0.5400	—	0.1110	0.0510
0.12	8.33	0.0181	0.2801	0.2166	0.0498
0.10	13.55	0.0002	0.3055	0.1248	0.0407
0.10	18.71	0.0001	0.4847	0.1252	0.0056
0.11	27.85	0.0000	0.6158	0.0710	0.0017
0.11	35.88	0.0000	0.7160	0.0132	0.0004

TABLE III. Influence of Silicon.

Composition.		Loss of weight per sq. cm.			Weight of oxygen combined per sq. cm. at 1100° C.
C (%)	Si (%)	HNO_3	HCl	H_2SO_4	
0.04	1.33	0.6830 gr.	0.1115 gr.	0.1762 gr.	0.0405 gr.
0.05	4.16	0.4775	0.1038	0.1256	0.0025
0.06	7.00	0.4485	0.0648	0.1041	0.0019
0.06	9.88	0.2818	0.0397	0.0513	0.0012
0.07	13.02	0.1897	0.0274	0.0167	0.0009

TABLE IV. Influence of Tungsten.

Composition.		Loss of weight per sq. cm.			Weight of oxygen combined per sq. cm. at 1100° C.
C (%)	W (%)	HNO_3	HCl	H_2SO_4	
0.07	0.40	0.5890 gr.	0.1427 gr.	0.9796 gr.	0.0397 gr.
0.08	0.73	—	0.1222	0.0638	0.0344
0.07	2.85	0.5642	0.0576	0.0476	0.0291
0.08	4.63	0.5207	0.0335	0.0328	0.0221
0.07	6.63	0.4545	0.0183	0.0278	0.0227
0.07	8.24	0.3175	0.0117	0.0172	0.0306

TABLE V. Influence of Manganese.

Composition.		Loss of weight per sq. cm.		
C (%)	Mn (%)	HNO_3	HCl	H_2SO_4
0.04	0.95	0.5090 gr.	0.2191 gr.	0.1854 gr.
0.06	4.36	0.6464	0.5015	0.3055
0.08	8.41	0.7720	0.5520	0.5999
0.08	13.75	0.8263	0.8930	2.5850×
0.08	16.55	0.7570	0.8570	3.0120×

Table VI. Influence of Copper.

Composition.		Loss of weight per sq. cm.		
C (%)	Cu (%)	HNO_3	HCl	H_3SO_3
0.05	0.55	0.2410 gr.	0.0025 gr.	0.0220 gr.
0.05	1.06	0.3820	0.0027	0.0162
0.06	1.60	0.4355	0.0037	0.0117
0.07	2.10	0.4875	0.0031	0.0098
0.06	2.88	0.5875	0.0026	0.0107

In the Table V, the numbers marked by × are the reduced value after four hours' immersion in the acid.

In Figs. 1–4, the ordinate is the loss of weight in grams per sq. cm, and the abscissa the percentage of an alloyed element, except Fig. 4 in which the ordinate is the weight of oxygen combined in grams per sq. cm.

It is remarked that the scale of the ordinate of the portions of the curves shown by chain lines is one-tenth of that shown by full lines.

From these figures, the following conclusions may be drawn:—

(i) Nitric acid, 10 per cent solution, Pl. I, Fig. 1.

With an increasing amount of an alloyed element, the resistivity against the corrosion in the acids increases; but for copper and manga-

nese, their amount should not exceed one per cent. Especially, the effect of chromium is very large; for example, iron containing about 14 per cent of this element is scarcely corroded and retains almost its original metallic luster, after twenty-four hours' immersion in the acid. The effect of nickel is not so large as that of chromium. Though the resistivity of iron against the nitric acid somewhat increases by the addition of a small amount of copper or manganese, it decreases with an increasing amount of the element. The resistivity of iron containing manganese against acids is least.

(ii) Hydrochloric acid, 10 per cent solution, Pl. I, Fig. 2.

The corrosion diminishes by alloying the elements mentioned above with iron, except manganese and chromium, which cause an increase of corrosion. The effect of copper and tungsten is most prominent. The iron containing a large proportion of nickel resists the corrosion very strongly.

The results of experiment made by Henry S. Rawdon and Alexander I. Krynitsky[1] show that "addition of chromium to iron and steel increases the rate of attack by hydrochloric acid and that of nickel is much effective in diminishing the attack by the same acid."

(iii) Sulphuric acid, 10 per cent solution, Pl. II, Fig. 3.

Nickel, tungsten and copper increase greatly the resistivity of iron against the corrosion in this acid.

Lislie Aitchison[2] shows that tungsten steel containing 0.7 per cent carbon increases its resistivity against the corrosion by 10 per cent sulphuric acid, till the content of tungsten reaches 15 per cent. In the case of copper, the solubility[3] of iron in dilute sulphuric acid (1 : 3) decreases at first and reaches a minimum and then increases with increasing content of this element.

A small quantity of silicon and chromium diminishes the resistivity, but their high content considerably increases it.

(1) Chem. and Met. Eng. July 26, 1922.

(2) A paper read before the Faraday Soc., May 11, 1915.

(3) G. Howell Clevenger and Bhlupendranath Ray, St. u Eisen, 1, (1914).

Sir R. Hadfield[1] obtained the results on the corrosion of metallic chromium containing 99.35 per cent chromium in the three acids that this metal is readily soluble in dilute and strong hydrochloric acid, insoluble in dilute and strong nitric acid, and soluble or slightly soluble in dilute and strong sulphuric acid. In agreement with expectation from his results, the present experiment also shows that in the 10 per cent acid, chromium promotes the solubility of iron in hydrochloric acid and gives a strong resistivity against nitric acid, but in the case of sulphuric acid, the tendency is somewhat different. Namely, though the corrosion of iron in this acid increases by the addition of a small amount of chromium, it decreases when a certain limit of the concentration is reached. The results obtained by J. Newton Friend[2] show also this increase of solubility in 0.5 per cent sulphuric acid. In his experiment, nickel considerably decreases the corrosion of iron in the same acid as in the present one.

The effect of manganese is always to increase the corrosion.

(iv) Oxidation of the specimens in the atmosphere at 1100° C, Fig. 4, Pl. II.

For the addition of a small quantity of silicon, chromium, and tungsten, the oxidation degree of iron is increased, but when their amount exceeds a certain limit, it diminishes very rapidly. With regard to the resistivity against oxidation, silicon is the most effective amoung the four elements above mentioned, next chromium and nickel follow in their effect.

EXPERIMENT II.

Iron containing a constant percentage of carbon and varying amount of two other elements.

In the present case, the authors investigated the resistivity of iron containing constant percentages of carbon and nickel and varying proportion of chromium against the acids and the oxidation degree at 1100° C.

The results of experiments are given in Tables VIII to XI and Figs. 5 to 7, Pl. III.

---

(1) Iron Age, Jan. 20, 1916.

(2) J. Own, Iron and Steel Inst., No. 1, (1921).

TABLE VIII.

Composition.			Loss of weight per sq. cm.			Wt. of oxygen per sq. cm. at 1100° C.
C (%)	Ni (%)	Cr (%)	HNO_3	HCl	H_2SO_4	
0.10	4.00	8.89	0.0045 gr.	0.0412 gr.	0.0470 gr.	0.0460
0.13	4.05	11.20	0.0007	0.0460	0.0569	0.0451
0.12	3.80	13.66	0.0000	0.0570	0.0440	0.0377
0.13	3.88	15.36	0.0000	0.0682	0.0372	0.0118
0.14	3.81	18.12	0.0000	0.0870	0.0368	0.0014
0.15	3.38	22.80	0.0000	0.0430	0.0323	0.0007
0.16	3.38	28.36	0.0000	0.0455	0.0054	0.0005

TABLE IX.

Composition.			Loss of weight per sq. cm.			Wt. of oxygen per sq. cm. at 1100° C.
C (%)	Ni (%)	Cr (%)	HNO_3	HCl	H_2SO_4	
0.10	6.21	9.58	0.0055 gr.	0.0366 gr.	0.0435 gr.	0.0476
0.12	5.66	11.68	0.0006	0.0233	0.0296	0.0407
0.12	5.94	13.83	0.0000	0.0229	0.0206	0.0294
0.12	6.68	17.78	0.0000	0.0258	0.0105	—
0.14	5.82	20.55	0.0000	0.0342	0.0050	0.0010
0.14	5.86	26.01	0.0000	0.0378	0.0042	0.0007
0.15	6.42	32.04	0.0000	0.0648	0.0038	0.0009

TABLE X.

Composition.			Loss of weight per sq. cm.			Wt. of oxygen per sq. cm. at 1100° C.
C (%)	Ni (%)	Cr (%)	HNO_3	HCl	H_2SO_4	
0.06	10.21	10.18	0.0087 gr.	0.0182 gr.	0.0047 gr.	0.0275
0.09	10.55	12.60	0.0004	0.0092	0.0034	0.0220
0.09	10.66	15.83	0.0000	0.0060	0.0031	0.0098
0.10	10.50	18.67	0.0000	0.0053	0.0031	0.0012
0.13	9.66	21.95	0.0000	0.0058	0.0037	0.0010
0.10	10.33	25.32	0.0000	0.0066	0.0048	0.0010
0.10	10.32	27.98	0.0000	0.0076	0.0039	0.0008

TABLE XI.

Composition.			Loss of weight per sq. cm.			Wt. of oxygen per sq. cm. at 1100° C.
C (%)	Cr (%)	Ni (%)	HNO_3	HCl	H_2SO_4	
0.08	13.71	9.04	0.0046 gr.	0.0035 gr.	0.0017 gr.	0.0334 gr.
0.08	13.51	12.51	0.0002	0.0033	0.0019	0.0190
0.09	13.98	14.95	0.0000	0.0037	0.0022	0.0026
0.10	13.36	18.72	0.0000	0.0042	0.0023	0.0011
0.11	13.20	21.80	0.0000	0.0048	0.0024	0.0006
0.12	13.61	25.59	0.0000	0.0086	0.0023	0.0006
0.09	13.61	28.10	0.0000	0.0094	0.0032	0.0006

The following tables which are derived from the above ones, show the influence of chromium or nickel, when the contents of carbon and nickel, or those of carbon and chromium, are kept constant.

TABLE XII.

Composition.			Loss of weight per sq. cm.			Wt. of oxygen per sq. cm. at 1100° C.
C (%)	Cr (%)	Ni (%)	HNO_3	HCl	H_2SO_4	
0.12	8.33	0	0.0181 gr.	0.2801 gr.	0.2166 gr.	0.0498 gr.
0.10	8.89	4.00	0.0045	0.0412	0.0472	0.0460
0.10	9.58	6.21	0.0055	0.0366	0.0435	0.0476
0.06	10.18	10.21	0.0087	0.0182	0.0047	0.0275
0.08	9.04	13.71	0.0046	0.0035	0.0017	0.0334

TABLE XIII.

Composition.			Loss of weight per sq. cm.			Wt. of oxygen per sq. cm. at 1100° C.
C (%)	Cr (%)	Ni (%)	HNO_3	HCl	H_2SO_4	
0.10	13.55	0	0.0002 gr.	0.3055 gr.	0.1248 gr.	0.0407 gr.
0.12	13.66	3.80	0.0000	0.0570	0.0440	0.0377
0.12	13.83	5.94	0.0000	0.0229	0.0206	0.0294
0.09	12.60	10.55	0.0004	0.0092	0.0034	0.0220
0.08	12.51	13.51	0.0002	0.0033	0.0019	0.0190

TABLE XIV.

Composition.			Loss of weight per sq. cm.			Wt. of oxygen per sq. cm. at 1100° C.
C (%)	Cr (%)	Ni (%)	HNO_3	HCl	H_2SO_4	
0.10	15.13	0	0.0001 gr.	0.2370 gr.	0.2400 gr.	0.0274 gr.
0.13	15.36	3.88	0.0000	0.0682	0.0372	0.0118
0.12	15.44	6.22	0.0000	0.0276	0.0155	0.0118
0.09	15.83	10.66	0.0000	0.0060	0.0031	0.0098
0.09	14.95	13.98	0.0000	0.0037	0.0022	0.0026

TABLE XV.

Composition.			Loss of weight per sq. cm.			Wt. of oxygen per sq. cm. at 1100° C.
C (%)	Cr (%)	Ni (%)	HNO_3	HCl	H_2SO_4	
0.10	18.71	0	0.0001 gr.	0.4847 gr.	0.1252 gr.	0.0056 gr.
0.14	18.12	3.81	0.0000	0.0870	0.0368	0.0014
0.12	17.78	6.68	0.0000	0.0250	0.0105	—
0.10	18.67	10.50	0.0000	0.0053	0.0031	0.0012
0.10	18.72	13.36	0.0000	0.0042	0.0023	0.0011

TABLE XVI.

Composition.			Loss of weight per sq. cm.			Wt. of oxygen per sq. cm. at 1100° C.
C (%)	Cr (%)	Ni (%)	HNO_3	HCl	H_2SO_4	
0.13	21.81	0	0.0000 gr.	0.3954 gr.	0.0631 gr.	0.0021 gr.
0.15	22.80	3.38	0.0000	0.0430	0.0323	0.0007
0.14	20.55	5.82	0.0000	0.0342	0.0050	0.0010
0.13	21.95	9.66	0.0000	0.0058	0.0037	0.0010
0.11	21.80	13.20	0.0000	0.0048	0.0024	0.0006

In Figs. 5 to 7, the mark number in each curve corresponds to the table number. From the tables and figures, the following conclusions may be drown :—

(i) Nitric acid, 10 per cent solution.

As it is clear from the tables, the nitric acid corrosion of the specimens in this series is almost negligible except those in which chromium content is under 12 per cent and it is too simple to be shown in curves.

From the tables in Series II, it is seen that when chromium content exceeds 12 per cent, the resistibity to the corrosion by 10 per cent nitric acid is already so high that the improving effect of nickel does not almost appear. The luster of the specimens after examination is the same as that before.

(ii). Hydrochloric acid, 10 per cent solution, Fig, 5, Pl. III.

As stated before, chromium increases the corrosion of iron in this acid as shown in the curve in Fig, 2, Pl. I; but the addition of nickel to the chromium steels causes a large influence on the corrosion by the hydrochloric acid of 10 per cent solution. With increasing nickel content, the corrosion diminishes very rapidly as shown in the figures and each set of the specimens containing this element shows a minimum point of corrosion, except the specimens containing the smallest amount of nickel (Table VIII), which show a maximum point at 18 per cent chromium.

(iii) Sulphuric acid, 10 per cent solution, Fig. 6, Pl. III.

The general tendency of the corrosion of the specimen in this acid is almost similar till 6 per cent nickel. The curve X (10 per cent nickel) has a minimum point, and the curve XI (13 per cent nickel) shows that the amout of chromium between 9 and 28 per cent does not almost affect the degree of corrosion.

(iv) Oxidation of the specimens in the atmosphere at 1100° C for one hour, Fig. 7, Pl. III.

The general tendency of the oxidation of each set of the specimens in the atmosphere at 1100° C is almost similar irrespective of nickel content from zero to 13 per cent, that is, when the amount of chromium in the specimens, reaches about 12 per cent, their resistance against the oxidation increases very rapidly and becomes almost constant above 20 per cent, even if the nickel contents are varied. In this experiment, specimens belonging to Table XI shows the greatest resistivity against the oxidation.

EXPERIMENT III.

According to the above investigations, the alloys containing nickel, a small amount of carbon and 15 per cent chromium show a maximum resistivity against the corrosion of 10 per cent hydrochloric acid.

In the following experiments, the corrosion degrees of the alloys in the acids are measured when they contain 0.1 to 0.7 per cent carbon, 0 to 12 per cent nickel and 15 per cent chromium.

Carbon in the specimens was added by ferro-chrome. As the certain amounts of chromium and carbon were lost during melting, several specimens were made in order to obtain the required chemical compositions.

The results of the experiments are shown in Tables XVII to XX and Figs. 8 and 9, Pl. IV.

TABLE XVII.

Composition.			Loss of weight per sq. cm.		
C (%)	Cr (%)	Ni (%)	HNO_3	HCl	H_2SO_4
0.09	14.55	0	0.0002 gr.	0.3060 gr.	0.1651 gr.
0.10	15.11	2.11	0.0001	0.1090	0.1830
0.11	14.56	4.56	0.0000	0.0720	0.0823
0.08	14.61	6.35	0.0000	0.0509	0.0608
0.09	15.08	8.21	0.0000	0.0355	0.0177
0.12	14.16	10.66	0.0000	0.0155	0.0049
0.11	14.28	12.50	0.0000	0.0035	0.0034

TABLE XVIII.

Composition.			Loss of weight per sq. cm.		
C (%)	Cr (%)	Ni (%)	HNO_3	HCl	H_2SO_4
0.30	14.92	0	0.0000 gr.	0.0402 gr.	0.1492 gr.
0.28	14.55	2.31	0.0000	0.0321	0.1541
0.32	15.02	4.25	0.0000	0.0214	0.0340
0.30	15.11	6.60	0.0001	0.0136	0.0110
0.28	14.74	8.69	0.0001	0.0040	0.0088
0.32	14.62	10.69	0.0001	0.0026	0.0044
0.33	15.12	12.20	0.0001	0.0036	0.0035

TABLE XIX.

Composition.			Loss of weight per sq. cm.		
C (%)	Cr (%)	Ni (%)	HNO_3	HCl	H_2SO_4
0.51	14.32	0	0.0000 gr.	0.0202 gr.	0.1258 gr.
0.52	15.11	2.16	0.0001	0.0250	0.1305
0.47	14.56	4.32	0.0015	0.0207	0.1138
0.50	14.61	6.48	0.0026	0.0105	0.0700
0.49	14.95	8.50	0.0002	0.0051	0.0363
0.52	15.16	10.31	0.0001	0.0020	0.0158
0.51	14.28	12.48	0.0001	0.0020	0.0066

TABLE XX.

Composition.			Loss of weight per sq. cm.		
C (%)	Cr (%)	Ni (%)	HNO_3	HCl	H_2SO_4
0.70	15.18	0	0.0000 gr.	0.0150 gr.	0.1470 gr.
0.72	14.82	2.20	0.0000	0.0216	0.2001
0.74	15.20	4.20	0.0000	0.0209	0.1580
0.71	14.93	6.32	0.0056	0.0058	0.1117
0.69	14.87	8.14	0.0001	0.0043	0.0518
0.69	15.66	10.08	0.0001	0.0014	0.0271
0.72	15.53	12.31	0.0001	0.0011	0.0131

In the above tables, carbon and chromium contents in the specimens are kept constant and the amount of nickel is varied.

In order to see the influence of carbon on the corrosion of the specimen in the acids, the curves derived from the above ones are given in Fig. 10 to 11, Pl. IV.

From the above results, the following conclusions may be drawn:

(i) Nitric acid, 10 per cent solution.

As the corrosion of the specimen in this acid is very slight, the figures are not given, but it is to be noted that the corrosion of the alloys containing 0.5 to 0.7 per cent carbon, 4 to 6 per cent nickel and 15 per cent chromium is relatively considerable, as shown in Tables XIX and XX. The reason of the considerable corrosion of the specimens in the above ranges is unknown.

In short, except this range, nickel and carbon exerts only a least influence on the corrosion of the iron-chromium alloys in the 10 per cent nitric acid, when the amount of chromium is above 13 per cent, as shown in the last experiment and Table II.

(ii) Hydrochloric acid, 10 per cent solution.

In Table XVIII and Fig. 8, Pl. IV, it is found that the resistance against the corrosion by this acid greatly increases by adding nickel to the specimen, when this contains 10 per cent chromium and 0.1 per cent carbon. The effect of nickel gradually decreases by increasing carbon content, but it is to be noted that the resistance rather decreases, when nickel and carbon content are 2 to 4 and 0.3 to 0.5 per cent respectively. Fig. 10, Pl. IV, shows that carbon in each series of the specimens containing constant chromium and nickel increases almost uniformly their resistance against the acid and its degree becomes smaller as nickel increases. When the nickel content is 12 per cent, the corrosion in each series is nearly the same notwithstanding the content of carbon.

(iii) Sulphuric acid, 10 per cent solution.

The resistance of the specimen against this acid slightly decreases at first and after reaching a minimum, rapidly increases, with the increasing content of nickel, as shown in Fig. 9, Pl. IV. It is to be remarked that the decrease of resistance up to 2 per cent of nickel is promoted by increasing carbon. Specimens No. XIX and XX also show the same effect in the 10 per cent hydrochloric acid. The influence of carbon on the sulphuric acid corrosion of the sample containing constant percentage of nickel and chromium is shown in Fig. 11, Pl. IV. When nickel content is large or small, a minimum corrosibility occurs respectively at 0.3 and 0.5 per cent of carbon. This effect of carbon becomes less and less as the content of nickel increases.

EXPERIMENT IV.

Finally the corrosion of the alloys in the mixed acids was investigated. Eight specimens belonging to the class of alloys which greatly resisted

to the corrosion of single acids, were choosen; their chemical compositions were as follows:—

Specimens.	Alloyed compositions.			
	C.	Si.	Cr.	Ni.
A	0.3	—	15.0	10.0
B	0.1	—	20.0	10.0
C	0.3	—	15.0	—
D	0.3	2.0	16.0	12.0
E	0.1	3.0	20.0	6.0
F	0.1	3.0	20.0	10.0
G	0.4	—	20.0	8.0
H	0.7	—	13.0	10.0

At first the corrosions in nitric acid (sp. gr. = 1.057), hydrochloric acid (sp. gr. = 1.05) and sulphuric acid (sp. gr. = 1.07) were tested. Then two acids mixed in various proportions were used for the test of corrosion. The results are given in the following table XXI to XXV and in Fig. 12.

TABLE XXI.

Specimens.	24 hours' corrosion. Loss of weight per sq. cm.		
	HCl (Sp. gr. = 1.05)	HNO_3 (Sp. gr. = 1.057)	H_2SO_4 (Sp. gr. = 1.07)
A	0.00204	0.000075	0.00249
B	0.0218	0.0001475	0.00587
C	0.0286	0.0001415	0.1995
D	0.00227	0.00754	0.00172
E	0.028	0.0000	0.0109
F	0.0349	0.0000	0.00376
G	0.00102	0.0000241	0.00145
H	0.000624	0.00207	0.00318

TABLE XXII.

Spicimens.	24 hours' corrosion. Loss of weight per sq. cm.		
	sp. gr. = 1.05 HCl 7 : sp. gr. = 1.057 HNO_3 1	HCl 3 : HNO_3 1	HCl 1 : HNO_3 1
A	0.00834	0.0037	0.0357
B	0.0671	0.0416	0.200
C	0.0149	0.0864	0.2140
D	0.00462	0.0259	0.0398
E	0.0199	0.0192	0.047
F	0.0413	0.0362	0.1086
G	0.00868	0.00468	0.01484
H	0.00422	0.0168	0.0173

TABLE XXIII.

Specimens.	24 hours' corrosion. Loss of weight per sq. cm.		
	HCl 1 : HNO_3 3	HCl 1 : HNO_3 7	sq. gr. = 1.057 HNO_3 7 : sq. gr. = 1.07 H_2SO_4 1
A	0.0964	0.2050	0.0000878
B	0.1075	0.0383	0.0000
C	0.3050	0.1485	0.00012
D	0.091	0.1575	0.083
E	0.0298	0.0229	0.0000
F	0.0411	0.00856	0.0000656
G	0.0124	0.024	0.000172
H	0.01745	0.0267	0.0706

TABLE XXIV.

Specimens.	24 hours' corrosion. Loss of weight per sq. cm.		
	HNO_3 3 : H_2SO_4 1	HNO_3 1 : H_2SO_4 1	HNO_3 1 : H_2SO_4 1
A	0.001955	0.00736	0.0190
B	0.0000	0.00288	0.00369
C	0.00135	0.0172	0.0363
D	0.0626	0.0887	0.196
E	0.00072	0.00196	0.044
F	0.0000	0.0227	0.0014
G	0.000172	0.000052	0.000795
H	0.0941	0.1335	0.12

TABLE XXV.

Specimens.	24 hours' corrosion. Loss of weight per sq. cm.		
	HNO_3 1 : H_2SO_4 7	sp. gr. = 1.07 H_2SO_4 7 : sq. gr. = 1.05 HCl 1	H_2SO_4 3 : HCl 1
A	0.0452	0.00346	0.00105
B	0.00996	0.00806	0.01165
C	0.1315	0.1620	0.1410
D	0.1605	0.000854	0.000516
E	0.01325	0.0249	0.0383
F	0.0029	0.02	0.0193
G	0.00164	0.00302	0.00386
H	0.0674	0.000706	0.000841

TABLE XXVI.

Specimens.	24 hours' corrosion. Loss of weight per sq. cm.		
	H_2SO_4 1 : HCl 1	H_2SO_4 1 : HCl 3	H_2SO_4 1 : HCl 3
A	0.000833	0.00104	0.00562
B	0.0377	0.026	0.0161
C	0.1475	0.0750	0.0406
D	0.000574	0.000734	0.001155
E	0.0234	0.0300	0.0414
F	0.0246	0.0265	0.0264
G	0.001165	0.00101	0.00121
H	0.00064	0.000638	0.000732

From Pl. V, Fig. 12, we see clearly that for all alloys, the corrosion in mixed acids is considerably greater than that in pure acids, except alloy C. The specimens D, G, H are all very strong against the corrosion of pure acids, but not so good in the mixed acids. Silicon has a tendency to increase the resistivity of an alloy against three acids, but its content must not be greater than three percent; otherwise it imparts a bad effect on its mechanical properties. Of eight specimens tested, the specimen G has the highest resistivity against both pure and mixed acids. This alloy has nearly the same composition as Krupp's rustless steel V_2 A.

5. SUMMARY.

The general summary of the results of our experiments is as follows:—

(1) The resistivity of cast specimens of iron or steel containing special elements against the acids was studied. The corrosibility is not the same for three acids tested. For example, specimen containing chromium has a least corrosibility in 10 per cent nitric acid, but it is easily corroded by hydrochloric acid of the same concentration. Nickel and silicon give a high resistivity to the corrosion of iron against the acids.

(2) It is very interesting to see the combined effect of nickel and chromium contained in iron with a small amount of carbon on the corrosion of these acids. Iron containing chromium is easily corroded by the hydrochloric acid and that containing nickel resists very strongly against the same acid; but the combined effect of the two elements on the corrosion give a better result than that obtained by the specimen containing one of these elements. In the case of the sulphuric acid, the same results are also obtained. The combined effect of nickel, chromium and carbon shows that in hydrochloric acid, the better results are given by increasing carbon when it is contained in the range of 0.1 to 0.7 per cent and in the sulphuric acid, 0.3 per cent carbon give the best results.

(3) The corrosibility in mixed acids is considerably greater than that in pure acids. Generally speaking, alloys containing high chromium and nickel and a low corbon have a high resistibity against pure and mixed acids.

In conclusion, the present writers express their cordial thanks to Professer K. Honda, under whose direction the present work was carried out.

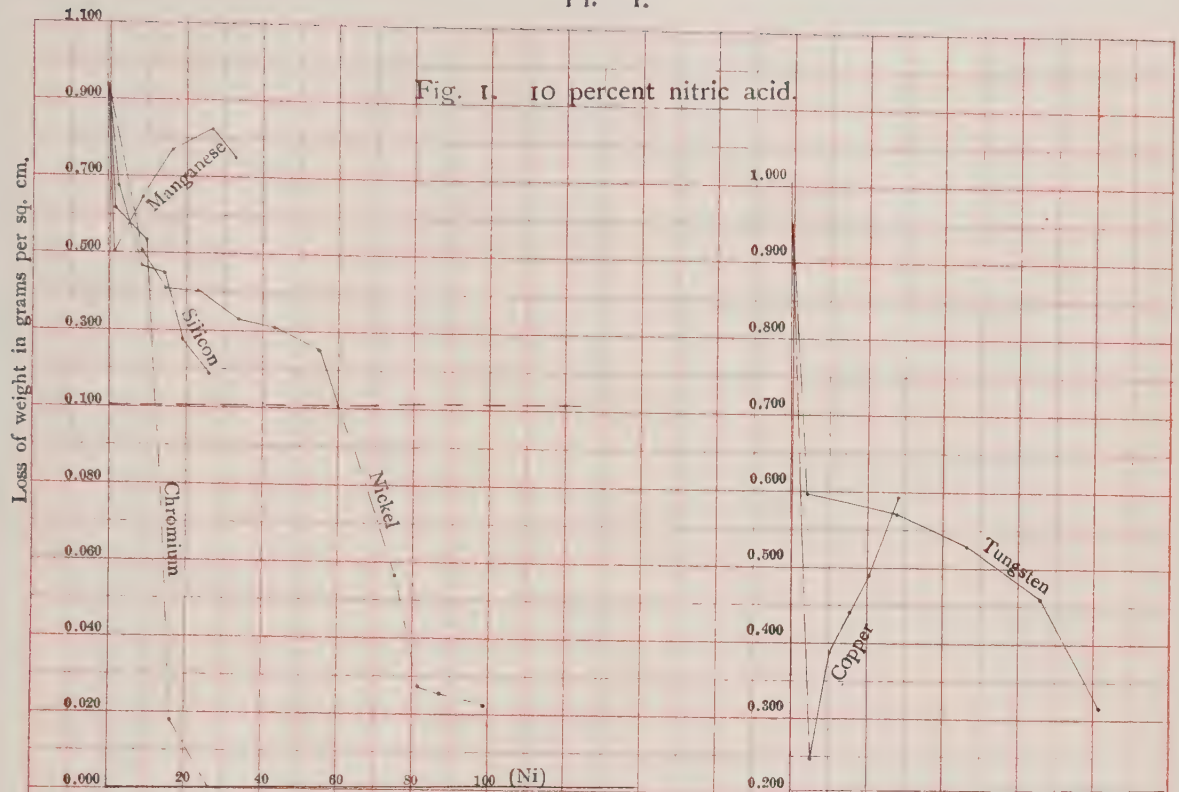

Fig. 1. 10 percent nitric acid.

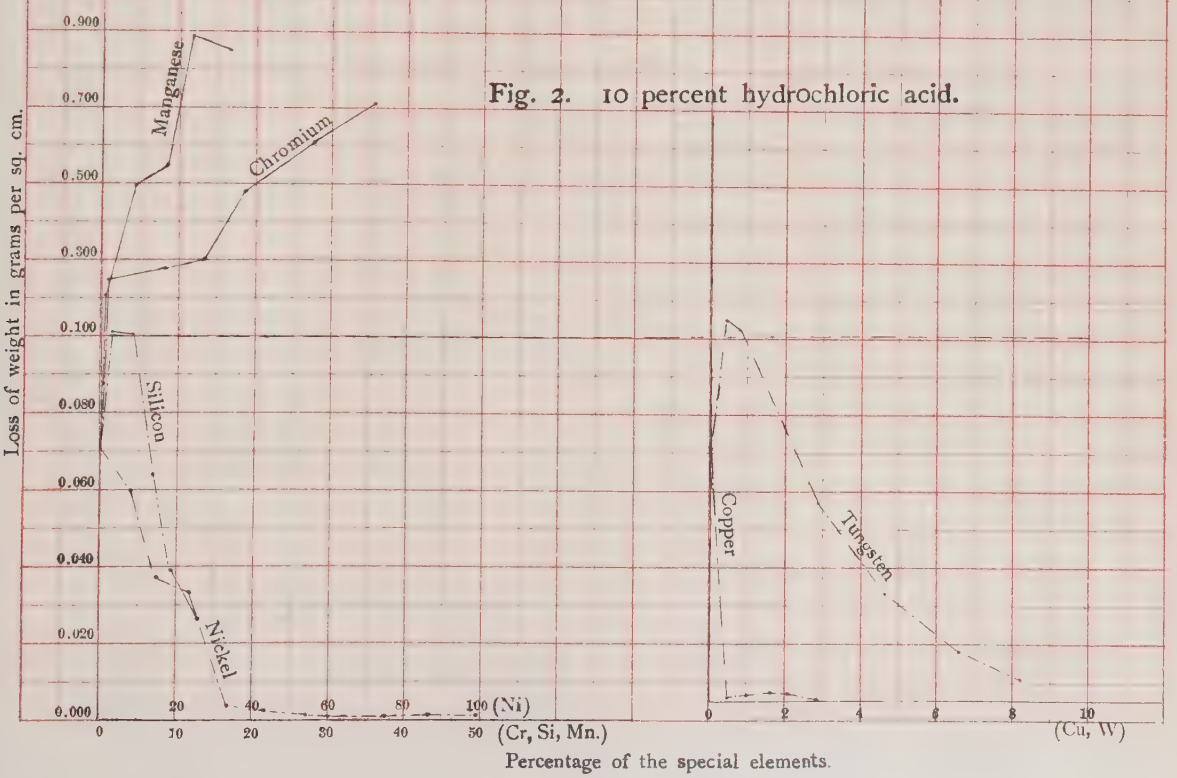

Fig. 2. 10 percent hydrochloric acid.

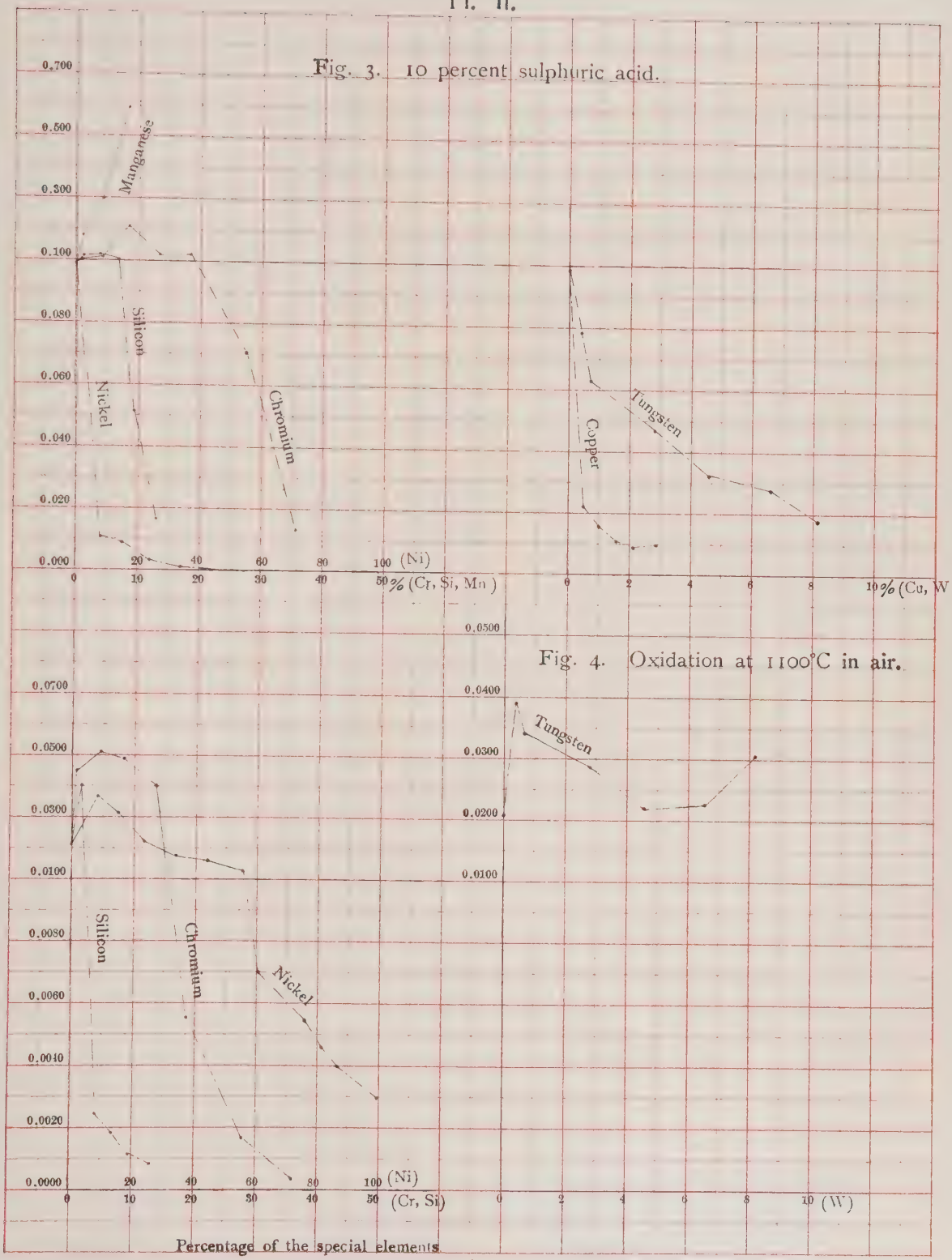
Fig. 3. 10 percent sulphuric acid.
Loss of weight in grams per sq. cm.
0.700
0.500
0.300
0.100
0.080
0.060
0.040
0.020
0.000
Manganese
Silicon
Nickel
Chromium
Copper
Tungsten
0 20 40 60 80 100 (Ni)
0 10 20 30 40 50 % (Cr, Si, Mn)
0 2 4 6 8 10 % (Cu, W)
Fig. 4. Oxidation at 1100°C in air.
Increase of weight in grams per sq. cm.
0.0700
0.0500
0.0300
0.0100
0.0080
0.0060
0.0040
0.0020
0.0000
0.0500
0.0400
0.0300
0.0200
0.0100
Tungsten
Silicon
Chromium
Nickel
0 20 40 60 80 100 (Ni)
0 10 20 30 40 50 (Cr, Si)
0 2 4 6 8 10 (W)
Percentage of the special elements

Fig. 5. Corrosion in 10 percent hydrochloric acid.

Fig. 6. 10 percent sulphuric acid.

Fig.

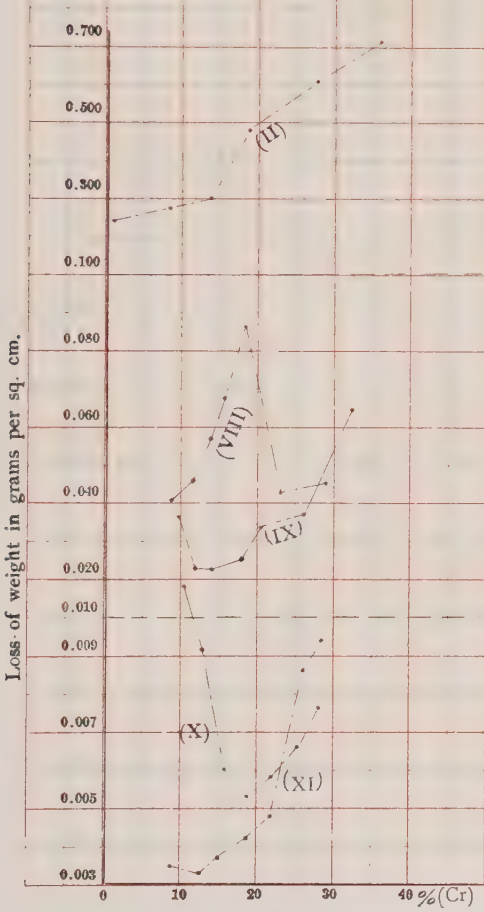

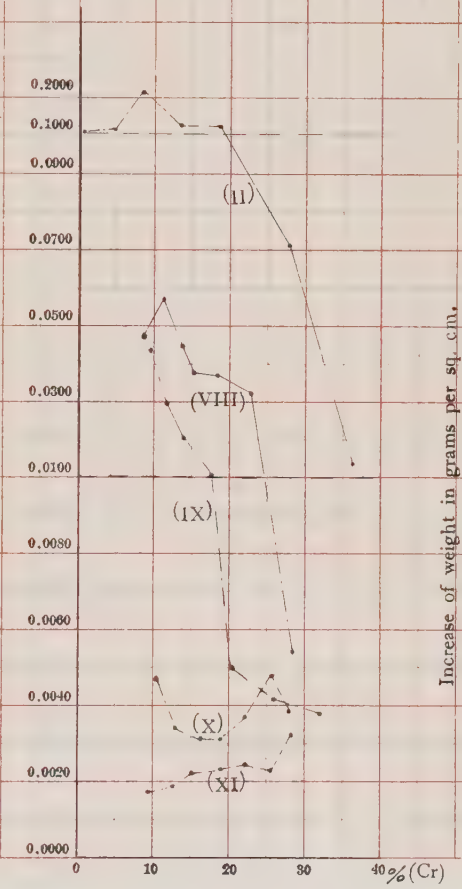

E F

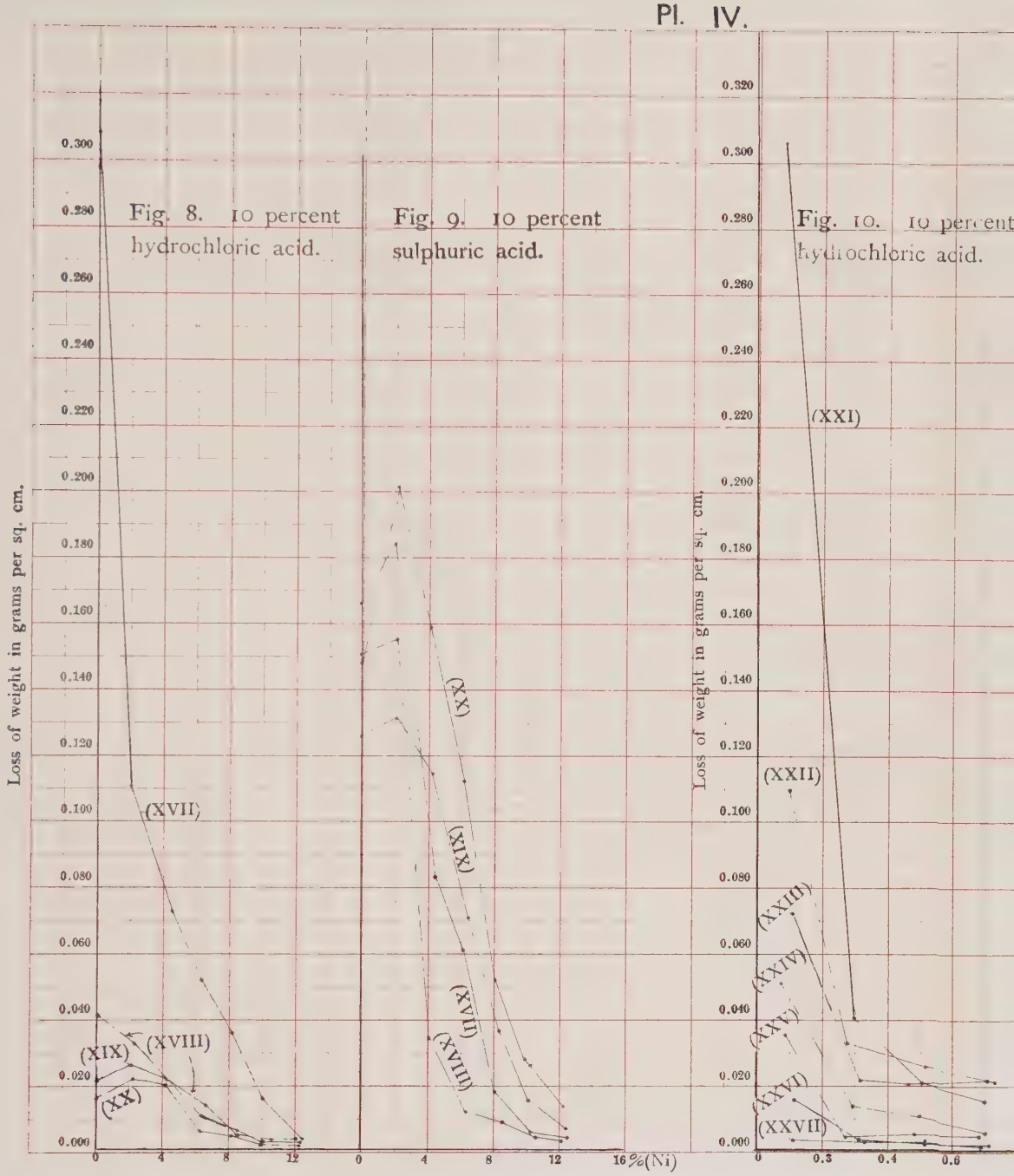

Fig. 8. 10 percent hydrochloric acid.

Fig. 9. 10 percent sulphuric acid.

Fig. 10. 10 percent hydrochloric acid.

E F

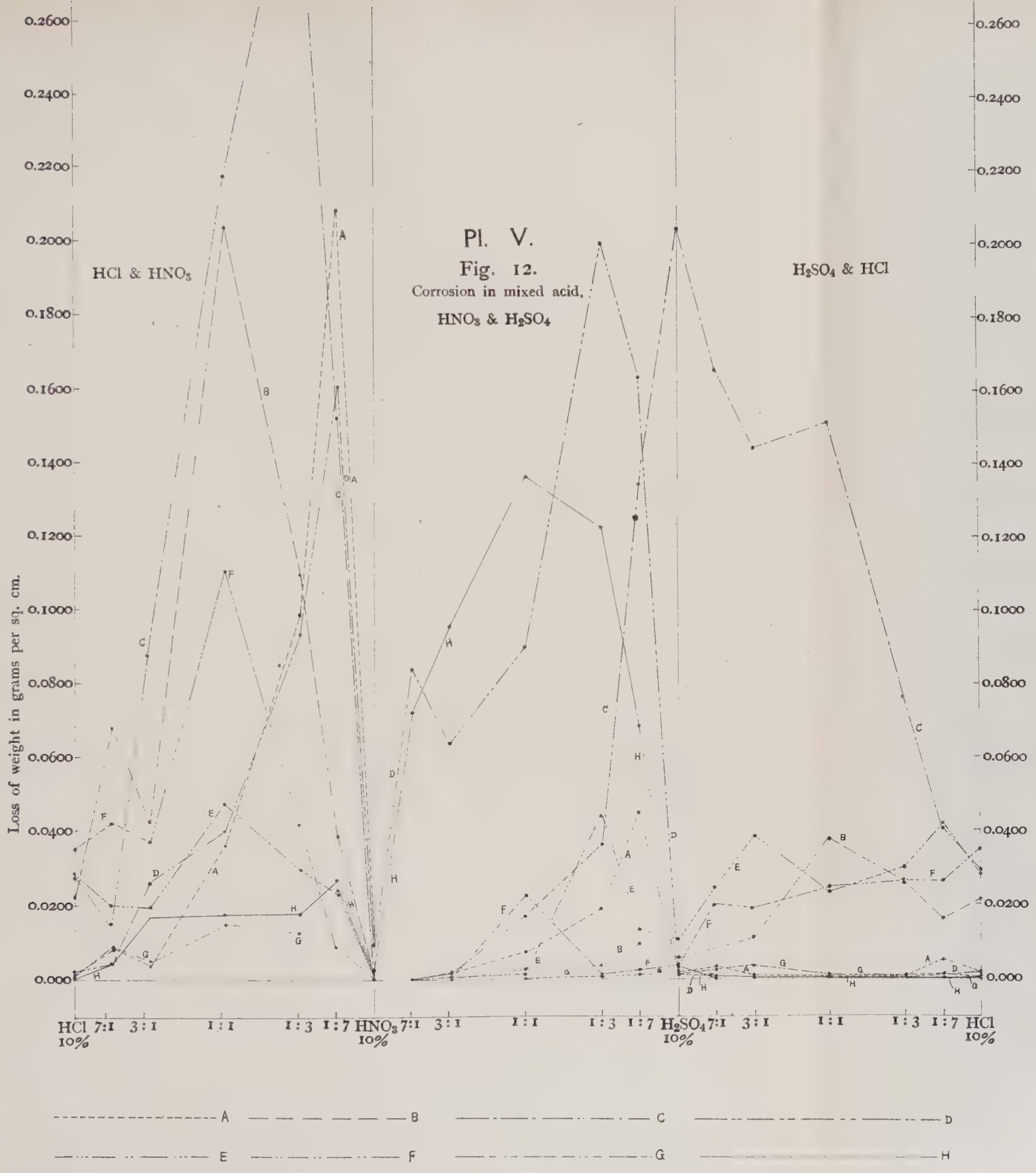
Pl. V.
Fig. 12.
Corrosion in mixed acid.
HNO3 & H2SO4
HCl & HNO3
H2SO4 & HCl
Loss of weight in grams per sq. cm.
0.2600
0.2400
0.2200
0.2000
0.1800
0.1600
0.1400
0.1200
0.1000
0.0800
0.0600
0.0400
0.0200
0.000
HCl 10%
7:1
3:1
1:1
1:3
1:7
HNO3 10%
H2SO4 10%
HCl 10%
A
B
C
D
E
F
G
H

Some Experiments on the Contact Electric Layers.

By

Mitsuru Satô.

In his previous paper,[1] the writer has reported that when certain melted dielectrics, such as wax or resin, are solidified on a metallic plate, and then separated from it, some surface charge appears on the contact surface of the dielectrics. This seems to be a sort of contact electric effect. The present experiment has been undertaken to make the nature of this charge clearer. Since this charge, also its quantity, is greatly affected by the state of the contact surface of the metal, the metallic surface was always carefully polished with sand paper, before the dielectrics were brought into contact with it.

First, the signs and the relative values of the surface densities of the charge when resin or wax is brought into contact with several metals were determined. In the case of resin, since it adhered firmly to the glass surface as it solidified, the following method was devised for separating it from the metals. As depicted in Fig. 1, a thin metallic plate M was pressed tightly between the two ends of the glass tubes A and B. Melted resin was poured into A to the depth of about 1 cm. When the resin solidified at a moderate rate, A was

Fig. 1.

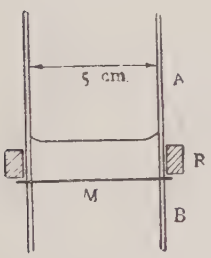

(1) Sci. Rep. **11**, (1922), 161.

detached from B, the plate M still adheredes to A, and holding A on a metallic plate, M was pushed by an insulated rod and allowed to fall on another metallic plate.

The plate was connected electrically with a Wilson's tilted electroscope, so that the charge given by M to the plate might be measured by Townsend's induction method.[1] To make sure that M might be uniformly detached, a metallic ring R was placed on it. Again in the case of Carnaüba-wax, since it contracted considerably as it solidified and separated by itself easily from the glass surface, the following method was adopted for measuring the charge. A glass tube D, 1 cm. long and 3 cms. in diameter, was placed in A on the middle part of M as depicted in Fig. 2. Melted Carnaüba-wax was poured into A, as far as the upper end of the glass tube D. Before the wax began to solidify, two ends of a string s were dipped into D. When solidification was complete, the wax block D was taken out of A by means of the string s. To avoid the effect of the charge on the curved surface of D, it was covered with tin foil. The total charge in D was measured by dropping it into a metallic can. The can was placed on an insulated stand, and was connected electrically as before with a Wilson's tilted electroscope so that the charge in D might be measured by the induction method.

Fig. 2.

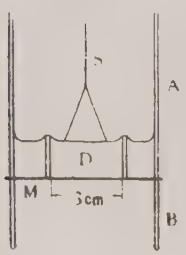

In spite of such precautions as have just been mentioned, the quantity of the charge in each experiment did not come out quite constant. This is perhaps due to the fact that the state of contact between the insulators and the metals was not the same in each experiment at the time when the separation took place. The numerical values in Table I represent the relative values of the surface electricity on the contact surface of metals, based on the assumption that they are equal and opposite to those of the insulators.

(1) Sci. Rep. **11**, (1922), 161.

TABLE I.

Metal	Al	Zn	Fe	Sn	Cu
Resin	4.9	4.1	−0.2	−2.6	−3.6
Carnaüba wax . . .	*6.6	9.6	−0.96	−7.5	−10.45

Henning[1] has made an accurate measurement of the contact electric potential. In his experiment the metals to be tested were placed in a high vacuum during the whole process. He shaved off the metallic surface and then the metal was borught into contact with another metal, the potential difference being measured at the same time. The rusults of his experiments are shown in the following table.

TABLE II.
(In contact with Brass.)

Metal	Al	Zn	*Sn	Fe	Cu
Contact P. D's Before Scraping	0.293	0.193	0.216	0.053	−0.106
Contact P. D's After Scraping	1.04	0.64	0.32	0 24	0 1

Comparing tables I and II, the order of the series of metals shows approximate coincidence except those marked with a star. Hence it is very probable that we are dealing with a contact electric effect.

Next, to test whether the surface charge just mentioned was distributed only over the surface of the dielectrics or penetrated them to some extent, the following experiments were made. The substance used was a mixture of equal parts of resin and Carnaüba-wax. To obtain specimens as uniform as possible the following method was devised. To the end of a glass cylinder of 12.8 cms. in diameter and 1 cm. in length a thin metallic plate *M* was clamped with three screws, so that the whole formed a cylindrical vessel with *M* as its bottom as shown in Fig. 3.

(1) Phys. Rev. **2**, No. 3, (1914), 228.

Fig. 3.

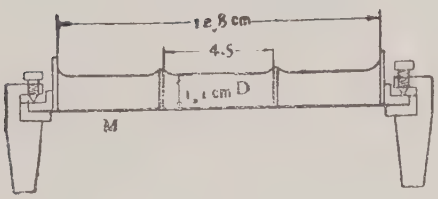

The metallic plate *M* was held horizontally, and on the middle part of it another glass cylinder 4.5 cms. in diameter and 1.1 cms. long was placed. The melted mixture was poured into the vessel as far as the upper end of the inner glass cylinder. After the mixture had solidified the block *D* was taken out of the vessel. The distribution of the charge was tested in the following way: In the first place the total charge in *D* was measured by means of the method mentioned above. Then a very thin layer of the contact surface was shaved off with a sharp knife. The total charge of what was left of the specimen was measured. In the second place another very thin layer was shaved off and then the total residual charge was measured. The process was repeated to the depth at which no variation of the total residual charge was to be recognized. Then the same method was applied to the upper surface of *D*, i. e. the surface which had been freely in contact with air during solidification.

The thickness of the layer shaved off every time was calculated from the weight of the powder, the density of the specimen and the

Fig. 4.

Resin-wax (Solidified on a Cu-plate).

diameter of the block *D*. The relation between the charge in the remaining part at each step and the depth from the surface which was originally in contact with the metal or air is shown in Figs. 4 and 5.

Fig. 5.

Resin-wax (Solidified on a Zn-plate).

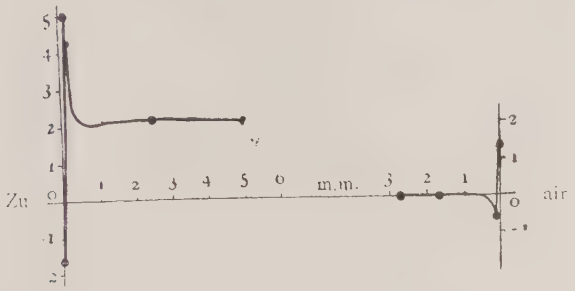

From these results it may be inferred that the apparent surface charge consists of double electric layers; one nearer to the contact surface is more intense and its thickness is very small; the other, further from the contact surface, is opposite in sign to that of the former and is weaker and the thickness is very large. The phenomenon occurs not only in the contact surface between the insulator and the metal, but also in that of the dielectrics and air, i. e. in both the contact surfaces of two different dielectrics.

The above mentioned experiments, however, are not sufficient to decide whether the electric layers are caused by bringing the solid dielectrics and metals into contact. The following experiment was undertaken to clarify this point. The plane surfaces of the specimen made by the method shown in Fig. 3 were carefully polished with sand paper and then silvered. The resulting silver surface was then coppered electrolytically. It was washed in running water for about 20 minutes and was kept in a desiccator for about 7 days. Then the metallic film which formed was removed from the specimen and its charge was measured as mentioned above. The results are shown in Fig. 6.

Fig. 6.

Total residual charge.
Resin-wax (silvered.)

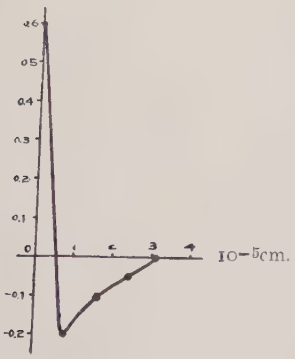

The charge contained in a layer at a certain depth of the specimen may be calculated from

Fig. 7.

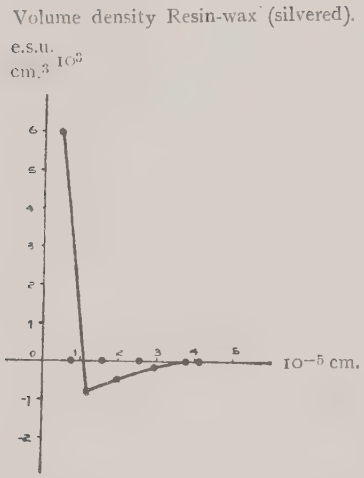

the gradient of the curve shown in the figure. The volume of the layer may be calculated from the mass of the powder of the dielectric and its density: Consequently the volume density of the charge in the layer may be determined. The results of the calculation are shown in Fig. 7.

From these results it may be concluded that the contact electric phenomenon in question occurs as the result of bringing into contact solid dielectrics and metals.

In order to see further if there be some difference in the two cases, i. e. solidification on a metallic plate and silvering on solid dielectrics, the following experiment was made.

Melted resin was solidified on a piece of silvered copper foil. On the other hand, a solid resin was silvered and then coppered electrolytically. The distribution of the charge in the two cases was compared. The results are shown in Figs. 8, 9, 10 and 11. The difference in the

Fig. 8.

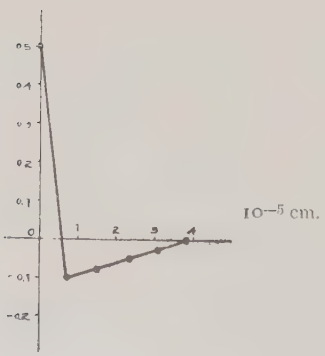

Fig. 9.

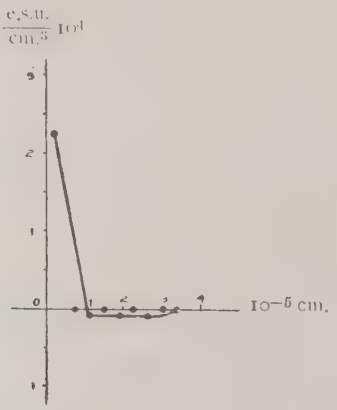

Fig. 10.

Total residual charge.
Resin (solidified on a silvered cu-plate).

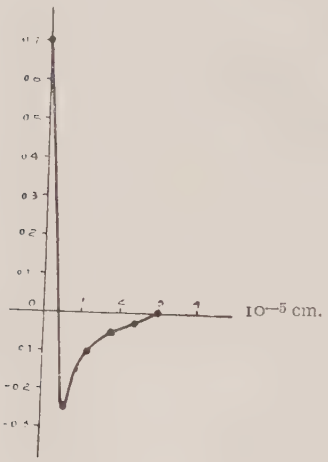

Fig. 11.

Volume density.
Resin (solidified on a silvered cu-plate).

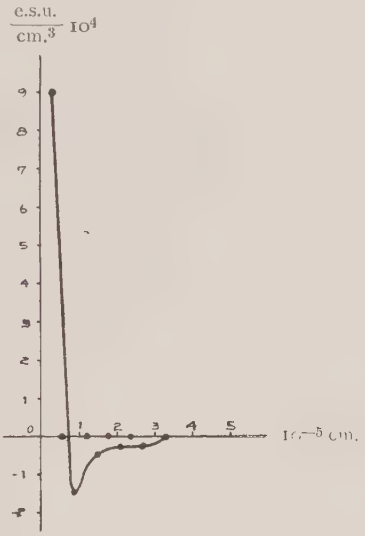

two cases is only quantitative. Hence it may be concluded that the electric layers are caused only by the contact of dielectrics with metals or other dielectrics.

In the case of this contact electricity, the distribution of electricity in the metal cannot be determined by the method mentioned above. But it is most probable that a similar distribution of electricity occures in the metallic side. Hence the electric layers, when produced by the contact of two different substances, consists of quadruple layers as shown diagramatically in Fig. 12, where the y-axis shows a section of the contact surface of two different substances *A* and *B* and is also used at the same time to represent the volume density of the charge, and the abscissa represents the depth from the contact surface.

Fig. 12.

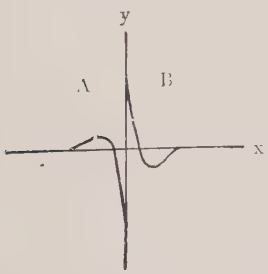

The phenomenon of contact electric layers has been studied by a number of physicists and chemists. But most of the experimental methods employed are very

indirect and the nature of the layers is still entirely hidden in obscurity. The results here obtained, though very rough, will be some contribution to a knowledge of contact electric layers in as much as the method of experiment is very direct.

In conclusion the writer wishes to express his hearty thanks to Prof. K. Honda for his kind advice in the course of the present investigation. He is also indebted to Messrs. S. Komubo and Y. Hara for their zealous collaboration during the experiment.

On the Variation of Residual Charge and the Ratio of Electrical Conductivity to Capacity due to Temperature.[1]

By

Hikoo Saegusa.

With 8 Plates.

CONTENTS.

§ 1. Introduction.
§ 2. Apparatus and Method of Experiment.
§ 3. Variation of Residual Charge due to Temperature.
(1) Effect of Temperature on Accumulation of Residual Charge.
(2) Relation between the Saturated Value of Residual Charge and Temperature.
§ 4. Variation of the Ratio of Conductivity to Capacity due to Temperature.
§ 5. Concluding Remarks.

§ 1. INTRODUCTION.

The temperature effect on the residual charge and the electrical conductivity of solid dielectrics has been studied by some physicists, but their results are not conclusive. A. Zeleny[2] studied with mica, paraffin-paper and ozokonite-paper within a range of temperatures from $-70°$ to 30°C. He found that the liberated charge increases with the temperature, but the rate of the increase appears to follow no general law. The

(1) The eighth report from the investigation staff for dielectrics was conducted by the late Prof. K. Aichi; read before the Annual Meeting of Math. Phys. Soc. Japan, April, 2, 1923; April 3, 1924.

(2) A. Zeleny, Phys. Rev. **6**, (1915), 478.

author[1] also studied with some crystalline dielectrics such as calcite, quartz, and mica, in a narrow range of 6°-25°C, and found that the residual charge increases with the temperature and the time required to accumulate a stationary value of the residual charge is shortened with a rise of temperature. H.L. Curtis[2] studied with a mica condenser within a narrow range of 15°-30°C, and found that the absorbed charge increases with the temperature, and that the insulation resistance decreases as the temperature rises. M. Pirani and W.v. Siemens[3] studied the conductivity of insulators such as porcelain, quartz and marquadmass at a high temperature up to 1600°C, and deduced the empirical formula, viz. $\log w = a + b/T$; where w is the resistance, T the absolute temperature and a, b the constants.

From the above results, we can conclude that the temperature affects the residual charge and the electrical conductivity of a solid dielectric in the same way. It is thus worth while to study more exactly the temperature-effect on these two quantities for a much wider range of temperatures.

For this purpose, the present experiment, was undertaken with crystalline dielectrics belonging to different crystallographic systems.

§ 2. APPARATUS AND METHOD OF EXPERIMENT.

(1) Apparatus.

The skeleton view of the apparatus used in the present experiment is shown in the annexed figure. The symbols in the figure are as follows:—

(1) H. Saegusa, Sci. Rep. **10**, (1921). 101.
(2) H.L. Curtis, Bull. Bureau, Stand. **6**, (1910), 431.
(3) M.v. Pirani & W.v. Siemens, Zeitschr. Elektrochem. **15**, (1909), 969.

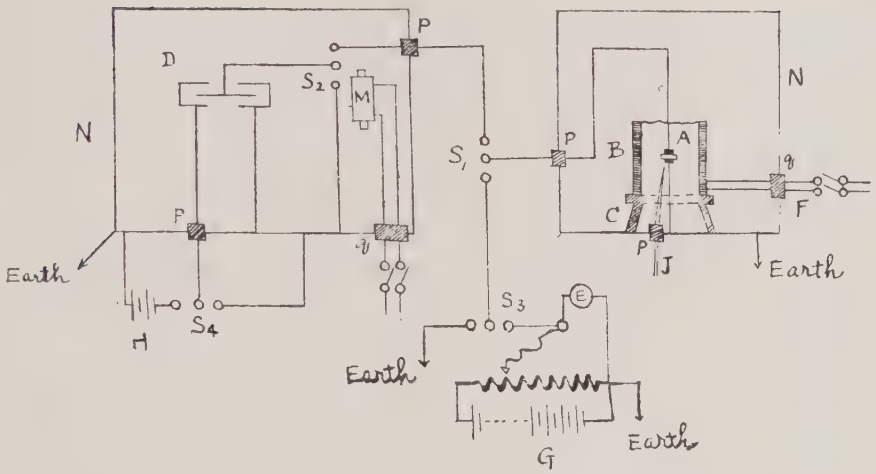

A :—Condenser made of test-specimens (one side earthed).
B :—Heating furnace.
C :—Porcelain stand.
D :—Dolezalek quadrant electrometer.
E :—Siemen's precision voltmeter.
F :—Heating lead wires.
G :—Batteries for charging the test-condenser A.
H :—Batteries for charging one pair of quadrants.
J :—Copper constantan thermo-junction for measuring the temperature.
M :—Electromagnet for operating the locker.
s_1 s_2 s_3 s_4 :—Lockers.
p :—Ambroid serving for the insulation of the leading wires.
q :—Ebonite.
N :—Metallic boxes enclosing the apparatus.

We maintained the interior of these metallic boxes in a nearly perfectly dry state by constantly circulating dry air through them, the air being previously dried by passing it through several bottles containing pure $H_2 SO_4$ and U tubes filled with $P_2 O_5$; moreover, dehydrating agents $P_2 O_5$ and $H_2 SO_4$ were placed in the interior of the boxes.

As test-specimens, thin plates of crystalline dielectrics, silvered on both sides, or inserted tightly between two sheets of very thin aluminium foil, were used. The dimensions of the plates were as follows:—

TABLE I.

Dielectrics[1]	Thickness	C/C′	Remarks
Quartz II ($10\bar{1}0$)	0.48cmm	0.615 (13°C)	Hexagonal, transparent, parallel to optical axis.
Quartz ⊥ (0001)	0.243mm	1.282 (19°C)	Hexagonal, transparent, perpendicular to optical axis.
Mica	0.012mm	60.7 (23°C)	Monoclinic, transparent, parallel to cleavage plane.
Rock salt (100)	0.86mm	0.77 (28°C)	Isometric, transparent, parallel to cleavage plane.
Selenite (010)	0.15mm	0.636 (23°.5C)	Monoclinic, (transparent gypsum) parallel to cleavage plane.
Microcline (001)	0.41mm	0.95 (19°C)	Triclinic, (Amazon stone) parallel to cleavage plane.
Scheelite (101)	0.67mm	0.95 (17°C)	Tetragonal, yellowish containing few cracks.
Barite (001)	0.69mm	1.11 (14°.5C)	Orthorhombic, transparent, perpendicular to principal axis, containing few cracks.

In the table, C is the electrical capacity of the test-specimen, and C′ that of the apparatus excluding the test specimen, which has a value of 39.3 cm. in electrostatic unit at 18°C, and the figures in the bracket in the third column show the temperatures in degrees Centigrade at which the capacity ratio was measured.

(2) Method of Experiment.

Before the commencement of the observation of residual charge, the capacity ratio, C/C′ was measured at the ordinary temperature with the results shown in the above table. The sum of the capacities C and C' when multiplied by the residual charge measured in volts, gives approximately the magnitudes of residual charge at various temperatures and for different dielectrics.

The residual charge was observed in the following order:—

At first, the specimen A was heated two or three hours at a con-

(1) The crystals are the same materials as those used in our former investigation. Sci. Rep. **10**; (1921), 101, 437; **11** (1922), 463.

stant temperature. Next, operating the locker S_1, S_3, A was charged at a suitable voltage during a certain time (A was always earthed except when the observation was being taken). It was then connected to the earth during a given time by operating the locker S_3, and then disconnected from the earth by the locker S_1, and simultaneously connected to the quadrant electrometer by the locker S_2 which is operated by the electromagnet M. From this instant the potential rise in the test-condenser due to residual charge was observed with respect to time.

The potential of the condenser A rises gradually from zero, and then tends to a saturation value. After about 20 or 30 minutes, the potential of the condenser A decreases gradually, and at last the rate of decrease becomes nearly proportional to the potential of the test-condenser; this last rate of potential decrease was taken as the measure of the leakage at the temperature at which the observation of the residual charge was taken.

Dividing the above time rate of potential decrease by the potential at which it was taken, the ratio of conductivity to capacity at various temperatures was deduced, assuming that the decrease of potential in the specimen was caused by the conduction of electricity through the dielectric and the apparatus, following Ohm's law.

Thus, we have

$$i = \left(\frac{\sigma}{d} + \sigma'\right) e,$$

$$i = (C + C') \frac{de}{dt},$$

were i is the conduction current, σ the conductivity and d the thickness of dielectric, σ' the conductivity of the apparatus divided by its conducting path, C, C' the capacities of the test condenser, and the apparatus including the electrometer, respectively, e the potential difference of the condenser. From the above relation, we have

$$\frac{\sigma + \sigma' d}{C + C'} = \frac{1}{e} \frac{de}{dt} d.$$

In the above calculation, we neglected the surface leakage, since its

path was much longer than that of the thickness, and moreover the specimen had been perfectly dried.

In the experiment, the charging time was always 4 minutes, and the discharging time 10 seconds.

§ 3. VARIATION OF RESIDUAL CHARGE DUE TO TEMPERATURE.

(1) Effect of Temperature on the Accumulation of Residual Charge.

The experimental results of the accumulation of residual charge (corrected for leakage) are graphically given for quartz || in Figs. 1-6, Pl. I. for quartz ⊥ in Figs. 9-14, Pl. II, for mica in Figs 17-19, Pl. III, for rock salt in Figs. 22-25, Pl. IV, for selenite in Figs. 28-32, Pl. V, for microcline in Figs. 35-38, Pl. VI, for scheelite in Figs. 41-44, Pl, VII, for barite in Figs. 47-52, Pl. VIII. From the above figures, we see that the accumulation time i.e., the time required for the saturated value of residual charge, decreases as the temperature rises; and with a further rise of temperature, the potential of the specimen due to residual charge reaches a maximum with respect to time; afterwards it decreases and tends to a certain stationary value; and the accumulation time up to the maximum point and the maximum value of residual charge also decreases as the temperature rises. The effect of temperature on the accumulation of residual charge is entirely equivalent to that of a good conducting dielectric, such as tourmaline for the ordinary temperature, used in our former investigation[1].

(2) Relation between the Saturated Value of Residual Charge and Temperature.

The relations between the saturated value of residual charge and the temperature, are graphically given for quartz || in Fig. 7, Pl. I, for quartz ⊥ in Fig. 15, Pl. II, for mica in Fig. 20, Pl. III, for rock salt in Fig. 26, Pl. IV, for selenite in Fig. 33, Pl. V, for microcline in Fig. 39, Pl. VI, for scheelite in Fig. 45, Pl. VII, for barite in Fig. 53, Pl. VIII.

(1) H. Saegusa, l.c.

From these figures, we see that the saturated value of residual charge at first gradually increases with temperature up to a certain point, then rapidly and reaches a maximum at a certain temperature, after which it decreases considerably, tending grandually to an asymptotic value. All these curves were plotted by the saturated value of residual charge and temperature taken from the accumulation curves of residual charge, reducing the charging potential into the whole number and assuming as the residual charge to be proportional to the charging potential, other conditions being the same. For the high temperature above the maximum, the stationary value of residual charge was taken against the temperature, and figures in the curves show the reduced charging potentials in volts.

In a given material, the saturated value of residual charge becomes maximum nearly at the same temperature for various values of applied potentials below and above the limit potential[1]. The limit potential for quartz || lies between 200 volts and 350 volts, for quartz perpendicular, between 50 volts and 150 volts, for mica, selenite, microcline, above the highest charging potential; and for rock salt, scheelite, barite, their limit potential is between the two charging potentials in their curve. Hence, we may say that the residual charge will be maximum at the same temperature for various thickness of the same material under a constant charging potential. This temperature is characteristic for different materials and also for different direction of crystals.

Table II contains the maximum temperatures and the maximum residual charge in cm. for 100 volts charging, deduced from the curves above referred to :—

TABLE II.

Dielectrics	Max. Temperature	Max. Residual charge in cm for 100 volts charging	Dielectrics	Max. Temperature	Max. Residual charge in cm for 100 volts charging
Quartz ||	165°C	1.35 cm	Selenite	285°C	0.80 cm
Quartz ⊥	55°C	1.84 cm	Microcline	62°C	1.60 cm
Mica	320°C	0.85 cm	Scheelite	198°C	0.55 cm
Rock salt	176°C	0.37 cm	Barite	192°C	2.55 cm

(1) H. Saegusa, l.c.

From table II, we see that generally speaking the lower the maximum temperature the greater the magnitude of the maximum residual charge, except in the case of selenite and barite.

Fig. 33. Pl. V, the variation of selenite is somewhat different. For the fresh specimen, (A curves) the saturated value of residual charge gradually increases up to about 130°C, then it remains nearly constant up to about 230°C, after which it increases rapidly and reaches a maximum; afterwards it follows a similar variation as in the cases of other materials. After this experiment, we found that selenite had entirely lost its water of crystallization and had become anhydrite.[1]

With this anhydrite specimen (B curve), we observed that the saturated value of the residual charge increases gradually with the temperature and reaches a maximum at the same temperature as in the case of the fresh specimen, after which the variation is similar to that of the latter; and shows no constant part as in the case of the fresh specimen.

Thus, we conclude that selenite begins to lose its water of crystallization at about 130°C and entirely loses it at about 230°C under a heating rate of the present experiment.

It is also of a very different nature in the case of barite, as shown in Fig. 53, Pl. VIII. For the fresh specimen (A curves), the saturated value of the residual charge decreases from about 20°C as the temperature rises, and then tends to an asymptotic value; but for an old specimen which has been previously heated in the first series of experiments, the variation of the residual charge with the temperature is exactly the same as in the cases of other materials. Thus, it seems to be that in the case of fresh heating, some absorbed gas was driven off and this modified temporarily the surface of the barite and caused the electrical conductivity of the latter to increase.

It is a noticeable fact that for two plates of quartz, one parallel to

(1) The chemical composition of selenite being $Ca\,SO_4 + 2\,H_2O$, it is a pure hydrous calcium sulphate. When it is heated to a temperature below 130°C, until one molecule of the water of crystallization is driven off, it forms a cement known as "plaster of Paris"; and when all the water of crystalization is driven off, it at last forms anhydrite, $Ca\,SO_4$.

the optical axis and the other perpendicular to it, we observe a marked difference in the variation of the saturated value of the residual charge due to temperature. It is a general rule that at the lower temperature the residual charge becomes maximum the lower the temperature at which the maximum point of accumulation of the residual charge occurs. The maximum temperature i.e. the temperature at which the saturated value of the residual charge becomes maximum, is almost independent of the charging potential below and above the limit potential.

It is also a noteworthy fact that the residual charge remains constant till the whole water of crystallization is driven off.

From the above results, we may conclude that the crystals of the monoclinic system such as mica, and selenite generally have a higher maximum temperature, than the crystal of other systems, and the crystals of the hexagonal and the isometric systems, such as quartz, and rock salt, generally have a lower maximum temperature than the crystals of the other systems. These facts quite coincide with the variety of the limit potential.(1)

§ 4. VARIATION OF THE RATIO OF CONDUCTIVITY TO CAPACITY DUE TO TEMPERATURE.

The relations between the ratio of conductivity to capacity and temperature are graphically shown in Fig. 8, Pl. I for quartz parallel, in Fig. 16 Pl. II. for quartz perpendicular, in Fig. 21 Pl. III for mica, in Fig. 27, Pl. IV for rock salt, in Fig. 34, Pl. V for selenite, in Fig. 40, Pl. VI for microcline, in Fig. 46, Pl. VII for scheelite, in Fig. 54, Pl. VIII for barite.

In these curves, $\frac{1}{e}\frac{de}{dt}60 = \frac{\sigma+\sigma' d}{C+C'}\frac{60}{d}$ is plotted against the

(1) The crystals of the monochinic system generally have a larger limit potential and a smaller residual charge, than the crystals of the other systems, and the crystals of the hexagonal and isometric system generally have a smaller limit potential and a larger residual charge than the crystals of the other systems.

(See, H. Saegusa, Sci. Rep. 10 (1921), 101, 439; 11 (1922) 463.)

temperature. As seen from these figures the ratio of conductivity to capacity increases slowly with the temperature up to a certain point and then it increases rapidly within a certain range of temperauture, afterwards it gradually tends to a saturation value.

The maximum rate of the increase occurs at about the maximum temperature, i.e. the temperature at which the saturated value of the residual charge becomes maximum.

In the expression

$$\frac{\sigma+\sigma' d}{C+C'},$$

C', σ' are independent of temperature, and the variation of C (capacity of the specimen) with temperature is very small, for example as shown in Fig. 27 for rock salt, although the variation of $\frac{\sigma+\sigma' d}{C+C'}\frac{60}{d} = \frac{1}{e}\frac{de}{dt}60$ is very great. Hence the variation of the above expression with temperature might be attributed mainly to that of conductivity σ of the specimen.

As shown in the above figures, the variation of the conductivity is far greater than that of the residual charge. This seems to be quite reasonable, since the maximum accumulated value of the residual charge decreases as the conductivity increases, or as the temperature rises. Thus, we may conclude that the variation of the residual charge due to temperature may be attributed to the increase of the temperature coefficient of conductivity.

The inflexion point of the variation of the ratio of conductivity to capacity due to temperature, nearly coincides with the maximum temperature of the residual charge. Thus we may conclude that the variation of residual charge due to temperature can generally be expressed as a function of the temperature coefficient of the variation of the ratio of conductivity to capacity.

It is a noticeable fact that the conductivity of quarts $\perp$ is greater than that of quartz $\parallel$ at the ordinary temperature, but the increase with temperature is much greater for quartz $\parallel$ than for quartz $\perp$, and at a

high temperature, about 300°C, the conductivity of quartz || is several times greater than that of quartz ⊥.

For selenite, as in the case of the residual charge, the variation of conductivity is somewhat different. The conductivity is nearly constant up to about 240°C, then it rapidly increases and gradually tends to a saturation value. Thus, it shows that until the crystallization water is entirely driven off, the conductivity does not increase. For the anhydrite selenite, as shown in Fig. 34, B, curve, the increase of conductivity follows that of ordinary materials.

For barite, as shown in Fig. 54, Pl. VIII, the variation of cunductivity of the fresh specimen shows a complex nature, but for that previously heated, the variation is similar to that of other materials.

The above results show that the conductivity of dielectrics generally increases with temperature, and tends to a certain saturation value. Thus, we may say that the increase of conductivity of dielectrics due to temperature has a certain limit according to the difference of materials and the direction of the crystals.

From the above results, we may conclude that the rapidly increasing temperature of the conductivity of the crystals belonging to the hexagonal and isometric systems, such as quartz and rock salt, is much lower than that of the crystals belonging to the monoclinic system such as mica, and selenite.

§ 5. CONCLUDING REMARKS.

The increase of the residual charge mainly depends on the increase of conductivity of the material i.e. increase of the temperature coefficient of the latter; the residual charge increases with the conductivity and reaches a maximum, after which, with greatly increasing conductivity, the bodily conduction through dielectric takes place manifestly, and the residual charge decreases rapidly, and tends to a certain stationary value as the conductivity tends to a saturation value.

Thus the variation of the residual charge closely coincides with the variation of the temperature coefficient of conductivity.

The increase of conductivity and the residual charge of dielectrics due to temperature may be explained as follows. Some free electrons[1] contained in dielectrics become kinetic owing to the external thermal agitation; hence the conductivity increases as the temperature rises. As the free electrons become energetic beyond a certain limit, the collisions between some of the free electrons and atoms take place. And some parts of the energy of the free electron will be given to the atoms, hence the rate of increase of conductivity becomes small as the number of collisions increases. Thus the conductivity gradually tends to a saturation value as the rate of increase of kinetic energy due to the thermal agitation cancels the rate of increase of dissipation of energy due to collision.

When the conductivity of dielectrics increases with temperature, a charged energy of the condenser made of the dielectrics increases owing to an easy displacement of the free electrons, and also the discharged energy of the condenser must increase. Hence the residual energy of the condeneser will also be increased. Thus the residual charge increases with the temperature. With further rise of temperature, while the rate of increase of conductivity due to temperature reaches a maximum, the residual charge also reaches a maximum with respect to temperature, after which the residual charge decreases owing to the conduction of electricity through dielectrics as much as the conductivity increases further. And when the conductivity tends to a saturated value, the residual charge also tends to a stationary constant value.

Thus, the variation of the residual charge may be explained by the variation of the temperature coefficient of conductivity as a thermal motion of free electrons and their collisions with atoms.

In the case of selenite, the fact that the residual charge and the conductivity remain constant, till the whole of the water of crystallization is driven off, may also be explained as follows. When the water of crystallization has begun to be driven off, a disturbance takes place in

(1) Generally speaking, some doublets with a constant electrical moment must be taken into account in addition to free electrons.

the atomic arrangement, and the disturbed atoms will bind the free electrons more rigidly than when there was no disturbance. This binding force increases as the disturbance becomes greater by virtue of a further rise of temperature, while the free electrons also become energetic. Thus the facts above mentioned may probably be the result of cancelling of the effect of the increase of the binding force of disturbed atoms and the increase of kinetic energy of the free electrons.

Hence, when the whole of the water of crystallization is driven off, the disturbed atoms are set in an amorphous state; and their binding force also sets in nearly a constant value, therefore the residual charge and the conductivity increase rapidly owing to the increase of the kinetic energy of the free electrons as the temperature rises.

The fact that crystals belonging to the monoclinic system have a small rate of increase of the residual charge and conductivity may probably be attributed to the stability of their atomic arrangement, i.e. the greatness of the binding force of the atoms on the free electrons.

SUMMARY.

The present investigation may be summarized as follows:—

1. The accumulation of the residual charge is greatly affected by temperature, i.e. the accumulation time at which the residual charge is saturated, is shortened as the temperature increases.; with a further rise of temperature, the residual charge reaches a maximum with respect to the accumulation time, and then decreases and tends to a stationary value. The maximum magnitude and its accumulation time decrease as the temperature rises.

2. The saturation value or the stational value of the residual charge increases with the temperature and reaches a maximum; then it decreases and tends to a stationary value.

The maximum temperature is characteristic for materials and for the orientation of crystals. As shown in the case of selenite, the accumulated residual charge remains a constant value, though the temperauture rises, till the whole water of crystallization is driven off. As shown in

the case of barite, some freshly heated crystals, show a somewhat different feature of variation of the residual charge, but in reheated crystals the variation becomes similar to that of ordinary materials.

3. The ratio of conductivity to capacity increases gradually with the temperature, and then rapidly increases from the maximum temperature of the residual charge, and then it gradually tends to a saturation value. The rate of increase of the ratio of conductivity to capacity is generally far greater than that of the saturation value of the residual charge. As shown in the case of selenite, the ratio of conductivity to capacity remains constant, till the water of crystallization is wholly driven off, and afterwards it rapidly increases with the temperature. As shown in the case of barite, for freshly heated specimen, the variation is quite different from that of other crystals, but for reheated, it is quite similar to that of other crystals.

The variation of conductivity of dielectrics due to temperature is quite opposite to that of conductors. Dielectrics generally become greatly conductive with a rise of temperature.

4. For the crystals of the monoclinic system, such as mica and selenite, the residual charge becomes maximum at a higher temperature than for those of the crystals belonging to the hexagonal and isometric systems, such as quartz and rock salt, and the rapidly increasing temperature of conductivity for the former crystals is much higher than for those of the latter. The crystals belonging to the other systems are intermediate for these effects.

5. The variation of the residual charge with temperature, seems to be due mainly to the variation of conductivity, since the variation of capacity due to temperature is very small as compared with that of conductivity. Thus we conclude that the mechanisms of the residual charge and of its variation due to temperature, may be satisfactorily explained by the conductivity and the variation of its temperature coefficient.

March, 1924.

EXPLANATION OF FIGURES.

Figs. 1–6, Pl. I. Accumulation of residual charge by various charging potentials and under various temperatures for quartz ||. The figures to the curves show the temperature and the charging potentials in volts. (charging time 4 min., discharging time 10 sec.)

Fig. 7. Relation between the saturated value of the residual charge (stationary value from the maximum of residual charge) and the temperature for quartz ||. Reduced charging potentials are 100, 200 and 350 volts.

Fig. 8. Relation between the ratio of conductivity to capacity (divided by the thickness of the specimen and multiplied by 60) and temperature for quartz ||. Ordinate represents $\frac{1}{c}\frac{dc}{dt}60$ and abscissa the temperature.

Figs. 9–14, Pl. II. Accumulation of residual charge by various charging potentials and under various temperatures for quartz ⊥.

Fig. 15. Relation between the saturated value of residual charge and the temperature for quartz ⊥. Reduced charging potentials are 50, 150 and 250 volts.

Fig. 16. Relation between the ratio of conductivity to capacity and the temperature for quartz ⊥.

Figs. 17–19, Pl. III. Accumulation of residual charge by various charging potentials and under various temperatures for mica.

Fig. 20. Relation between the saturated value of residual charge and temperature for mica. Reduced charging potentials are 100 and 300 volts.

Fig. 21. Relation between the ratio of conductivity to capacity and temperature for mica.

Figs. 22–25, Pl. IV. Accumulation of residual charge by various charging potentials and under various temperatures for rock salt.

Fig. 26. Relation between the saturated value of residual charge and temperature for rock salt. Reduced charging potentials are 100 and 250 volts.

Fig. 27. Relation between temperature and respectively the ratio of conductivity to capacity, the ratio of capacity to that of the electrometer, and its inverse, for rock salt.

Figs. 28–31, Pl. V. Accumulation of residual charge by various charging potentials and under various temperatures for selenite.

Fig. 32. Accumulation of residual charge under various temperatures for anhydrite selenite.

Fig. 33. Relation between the saturated value of residual charge and temperature for selenite. Reduced charging potentials are 100 and 250 volts. (A) is the relation for fresh selenite and (B) for anhydrite selenite.

Fig. 34. Relation between the ratio of conductivity to capacity and temperature for selenite. (A) is the relation for fresh selenite and (B) for anhydrite selenite.

Figs. 35–38, Pl. VI. Accumulation of residual charge by various charging potentials and under various temperatures for microcline.

Fig. 39. Relation between the saturated value of residual charge and the temperature for microcline. Reduced charging potentials are 100 and 250 volts.

Fig. 40. Relation between the ratio of conductivity to capacity and the temperature for microcline.

Figs. 41-44, Pl. VII. Accumulation of residual charge by various charging potentials and under various temperatures for scheelite.

Fig. 45. Relation between the saturated value of residual charge and the temperature for scheelite. Reduced charging potentials are 100 and 300 volts.

Fig. 46. Relation between the ratio of conductivity to capacity and the temperature for scheelite.

Figs. 47-52, Pl. VIII. Accumulation of residual charge by various charging potentials and under various temperatures for barite.

Fig. 47–48, are the relations for the first heating experiment and figs. 49-52 the second heating.

Fig. 53. Relation between the saturated value of residual charge and the temperature for barite. Reduced charging potentials are 100 and 250 volts. A curves are the relations for fresh barite and B curves for second heatings.

Fig. 54. Relation between the ratio of conductivity to capacity and the temperature. A is the relation for the fresh barite and B the second heating.

Pl. I.

Quartz II (10$\bar{1}$0) Thickness: 0.480 mm.
Sensibility: 1 cm = 11.32 volts

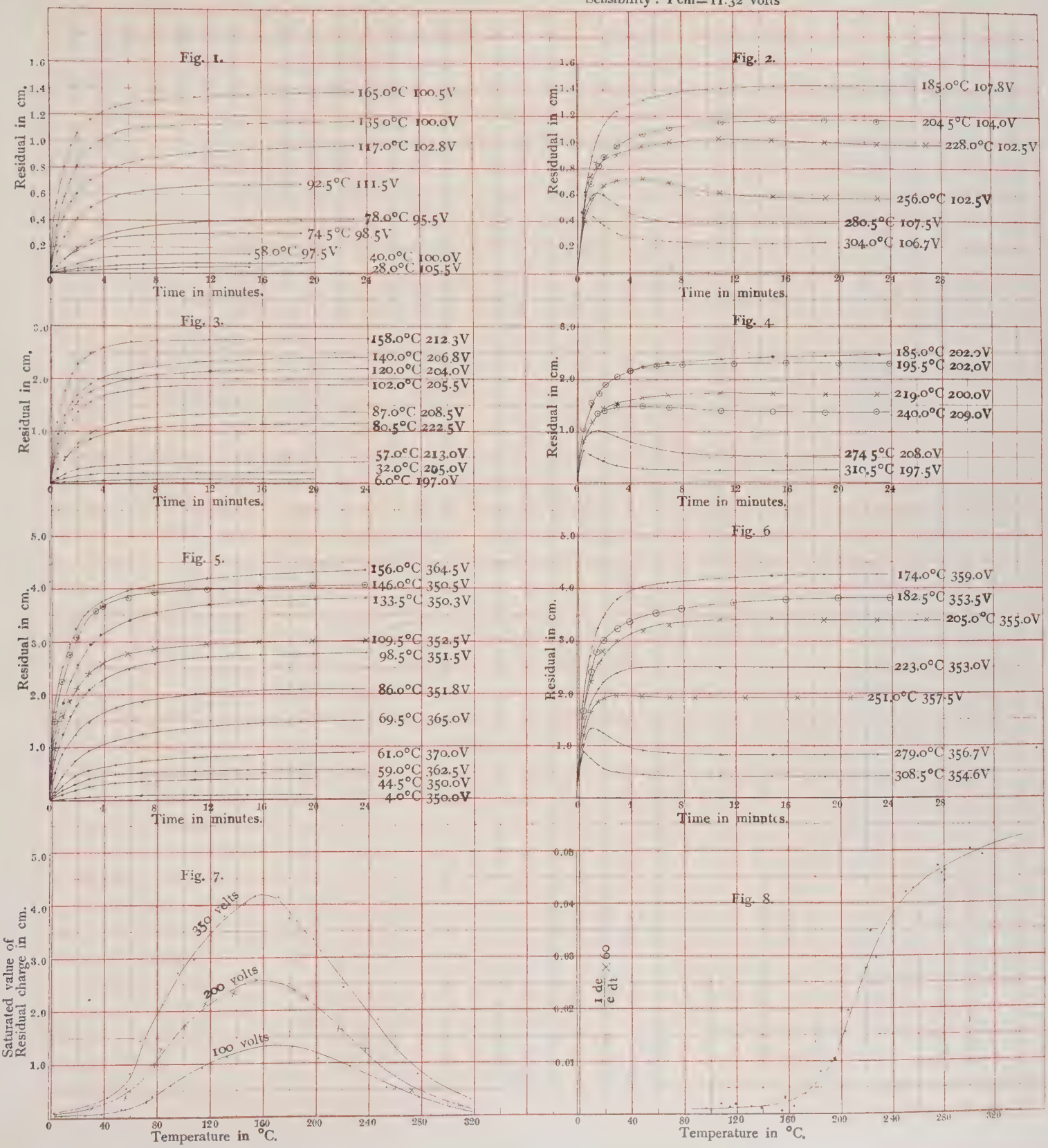

Pl. II.

Quartz 1. (0001) Thickness: 0.243 mm.
Sensibility: 1 cm = 11.32 volts

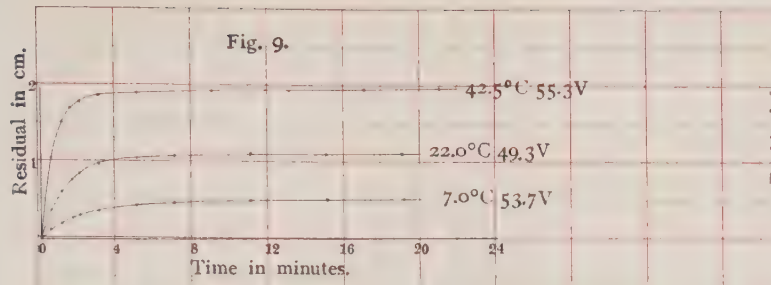

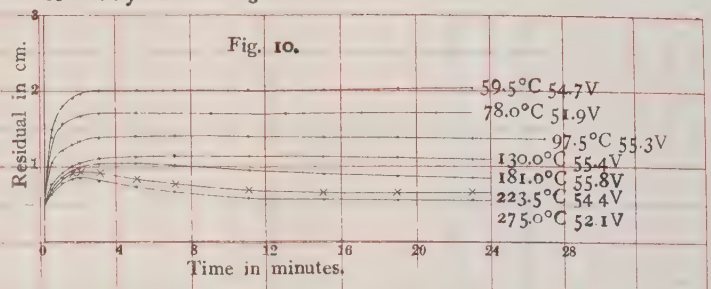

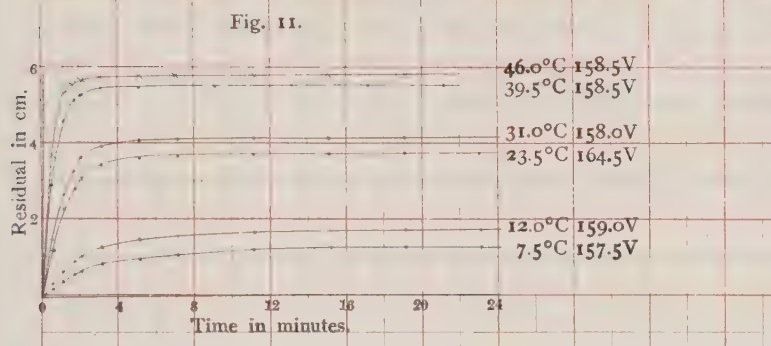

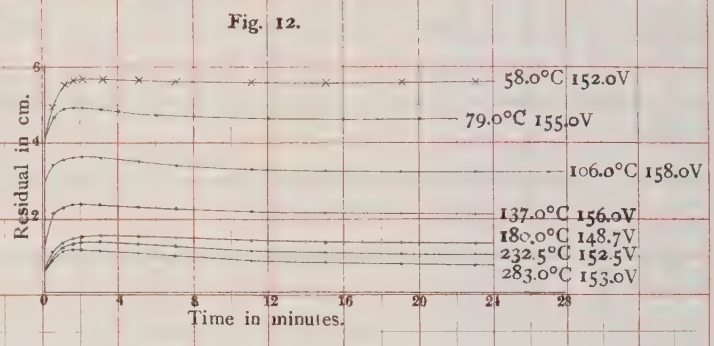

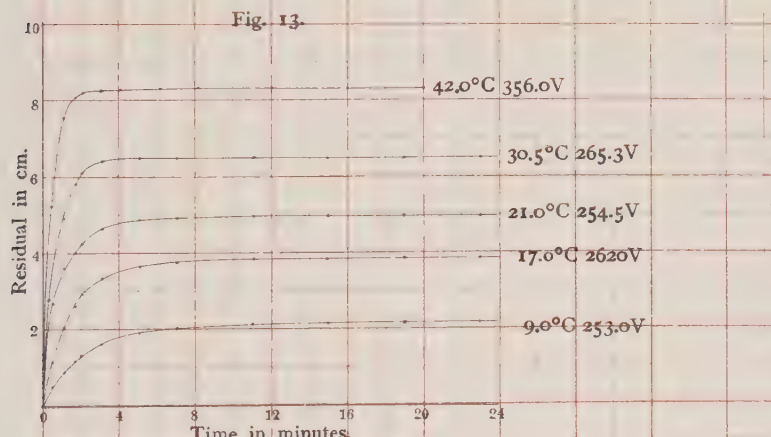

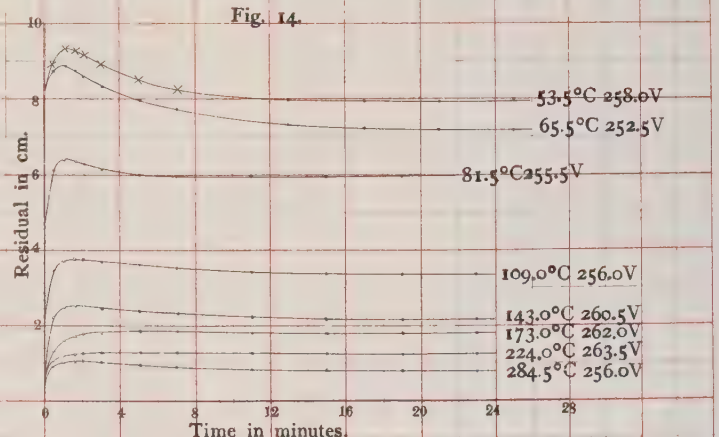

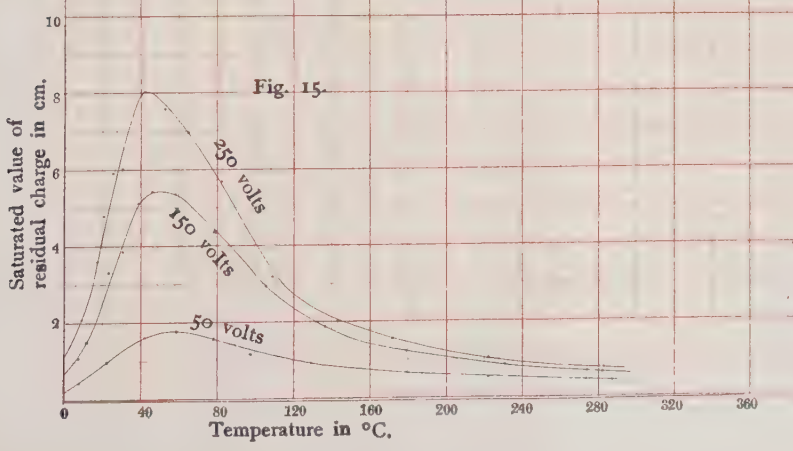

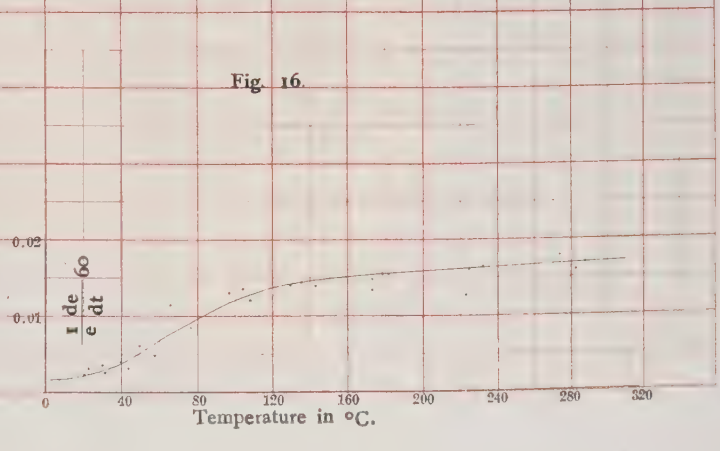

Pl. III.

Mica. Thickness: 0.012 mm.
Sensibility: 1 cm = 11.20 volts

Fig. 17.

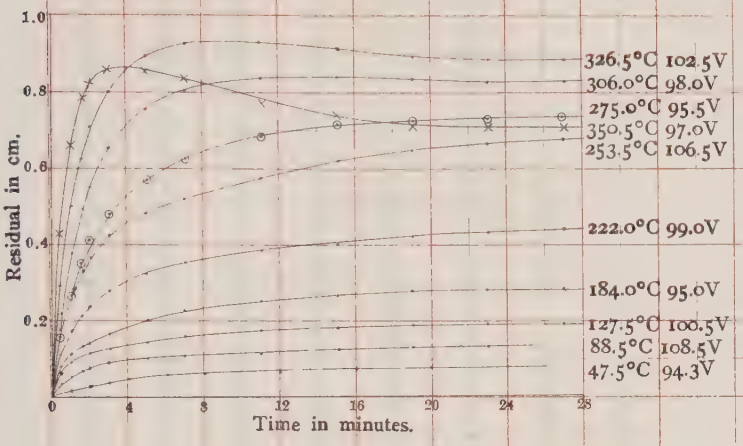

Fig. 18.

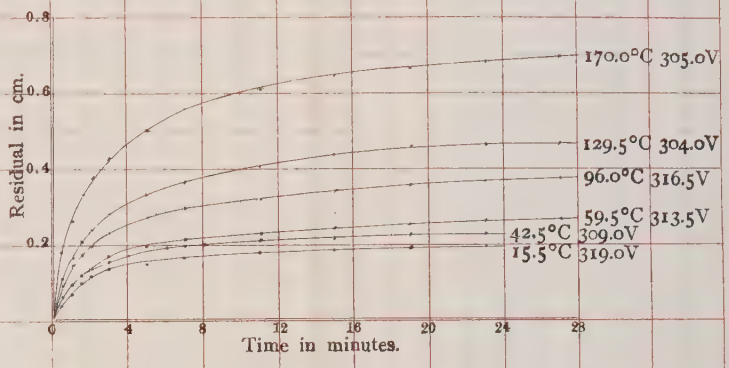

Fig. 19.

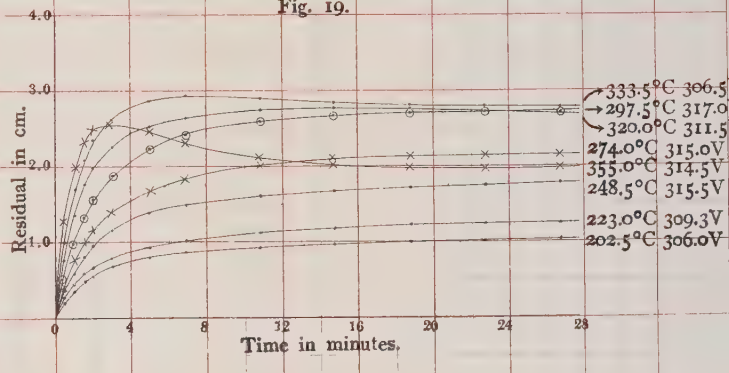

Fig. 20.

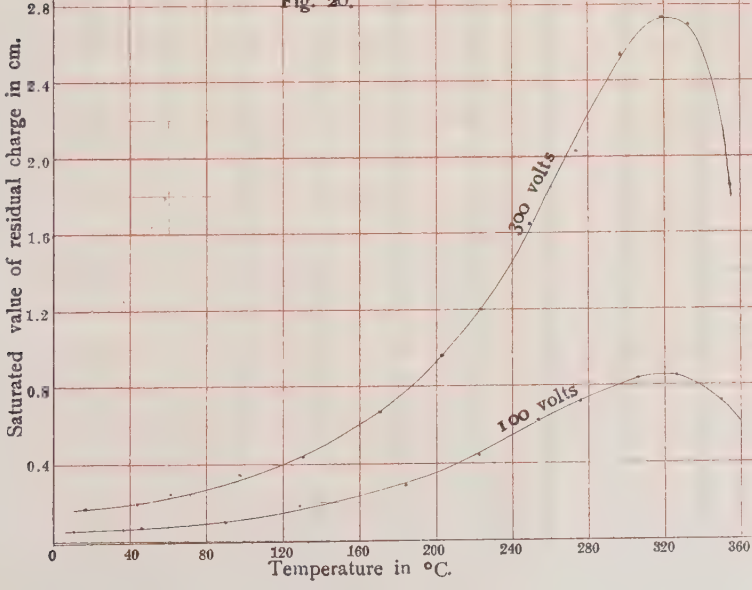

Fig. 21.

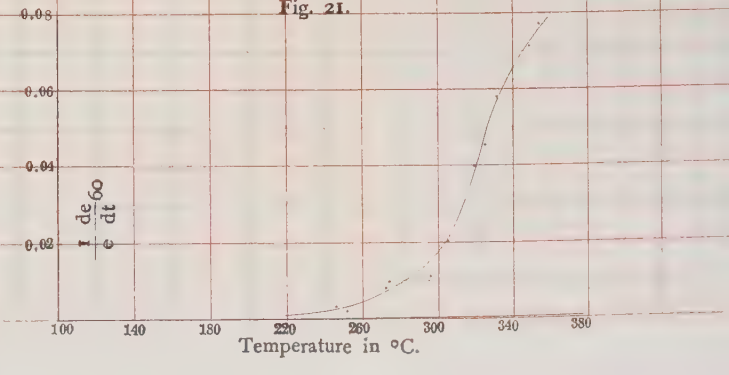

Pl. IV.

Rock Salt (100)., Thickness: 0.86 mm.
Sensibility: 1 cm = 11.24 volts.

Fig. 22.

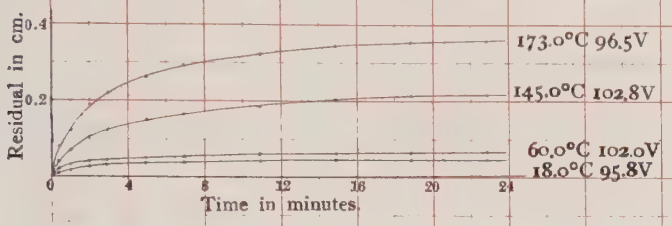

Fig. 23.

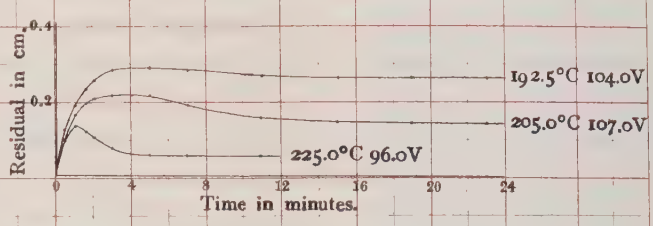

Fig. 24.

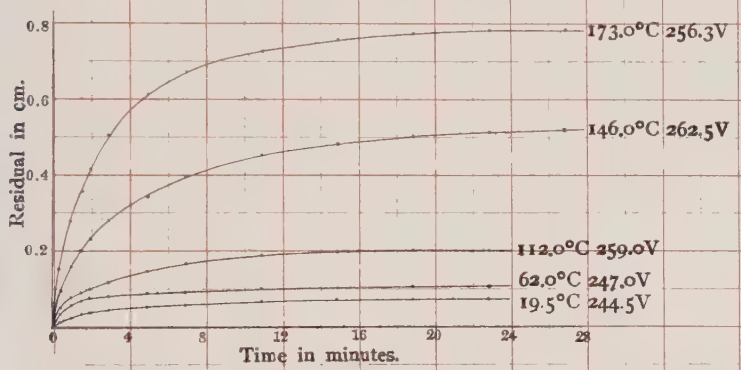

Fig. 25.

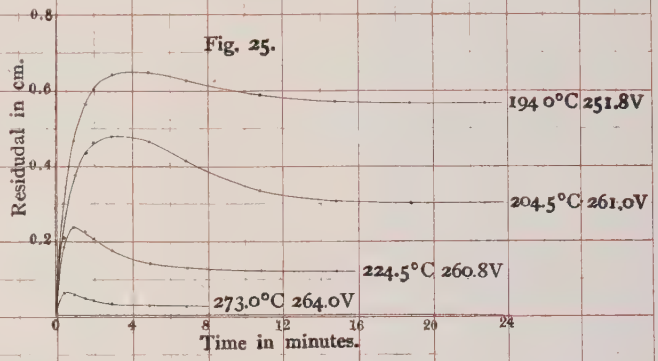

Fig. 26.

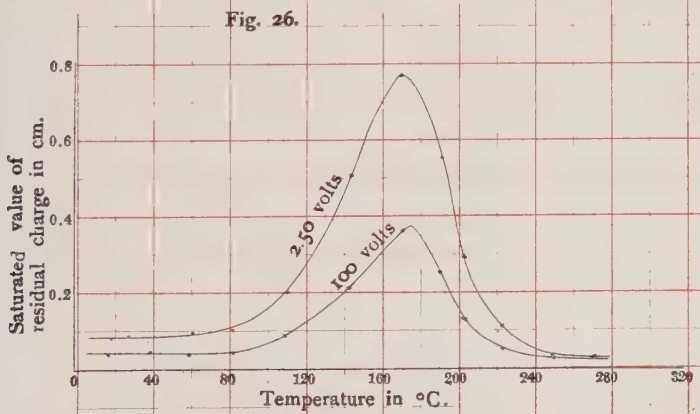

Fig. 27.

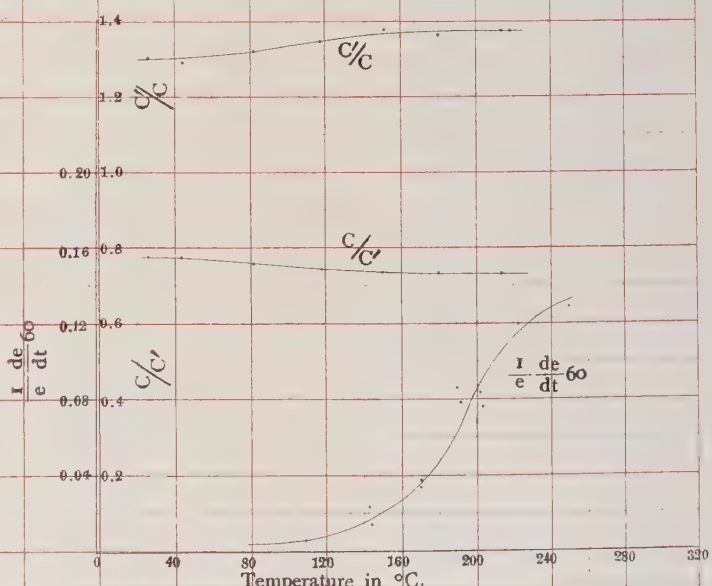

Pl. V.

Selenite (010) Thickness: 0.15 mm.
Sensibility: 1 cm = 11.20 volts

Fig. 28.

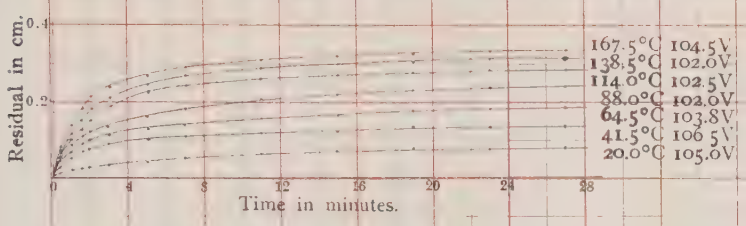

Fig. 29.

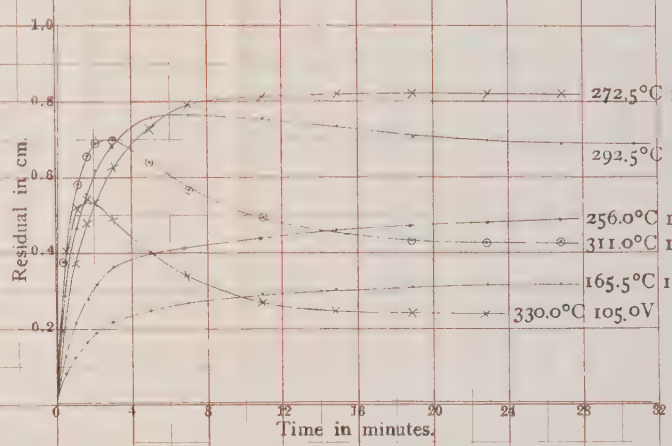

Fig. 30.

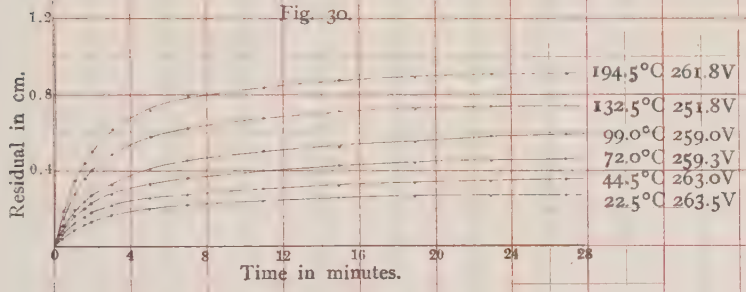

Fig. 31.

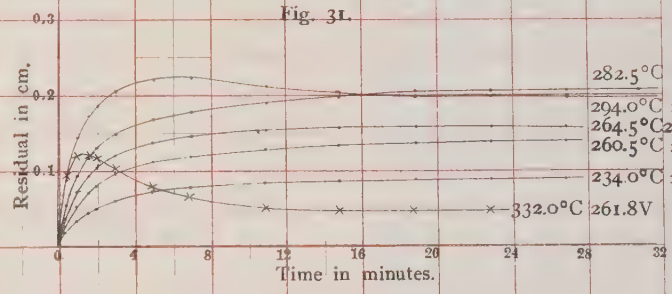

Fig. 33.

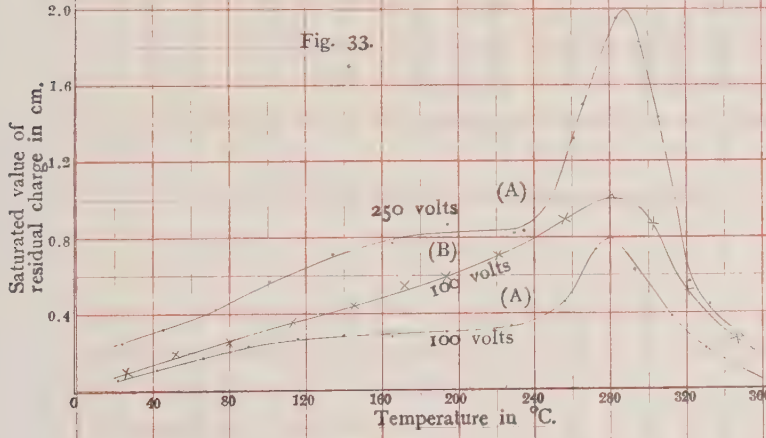

Fig. 32.

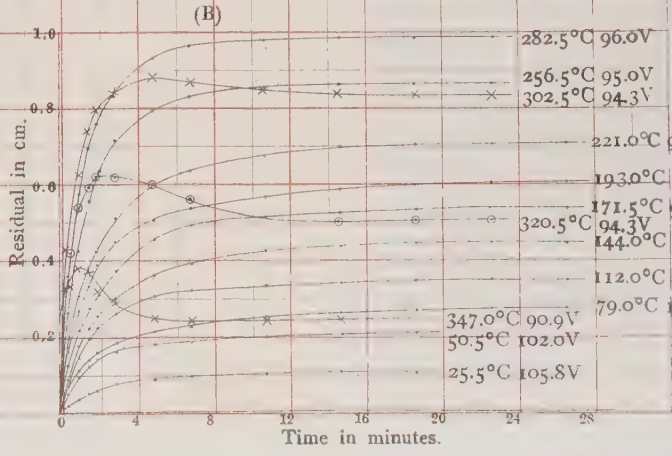

Fig. 34.

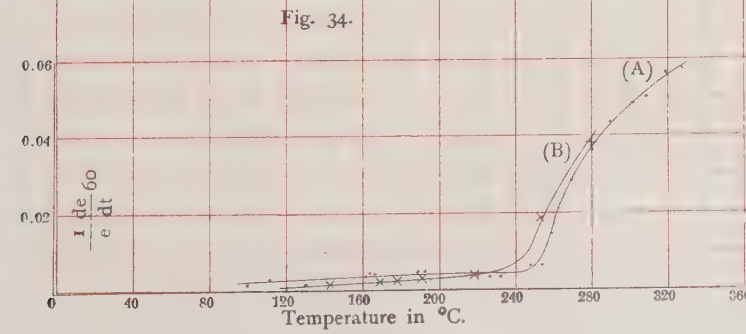

Pl. VI.

Microcline (001) Thickness: 0.41 mm
Sensibility: 1 cm = 11.20 volts

Fig. 35.

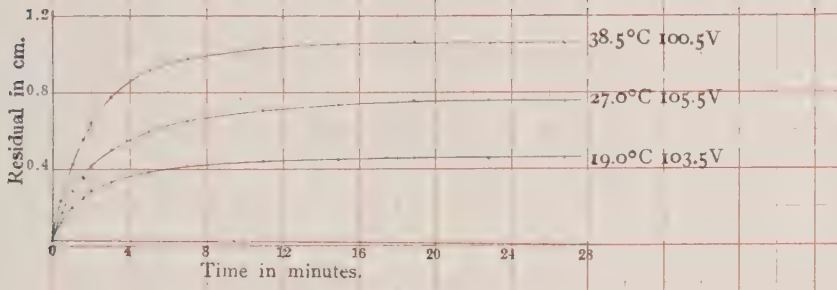

Fig. 36.

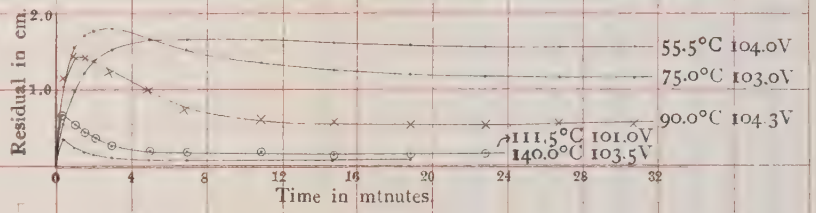

Fig. 37.

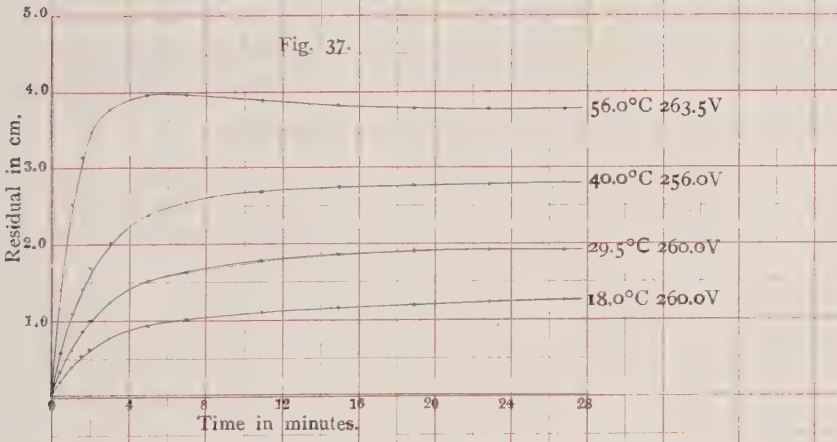

Fig. 38.

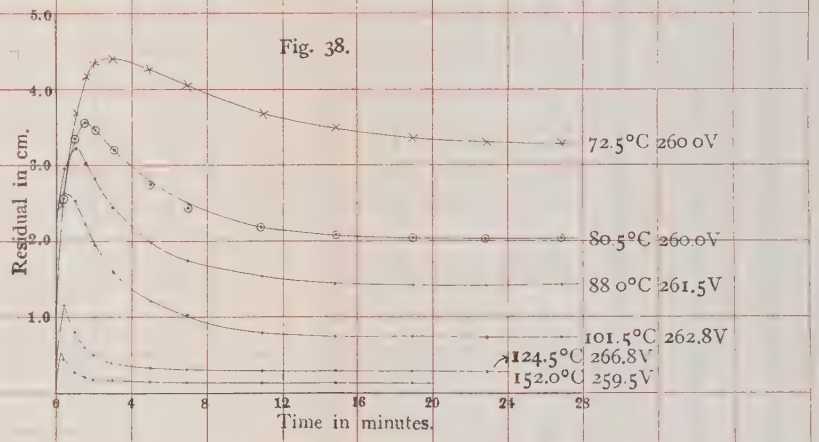

Fig. 39.

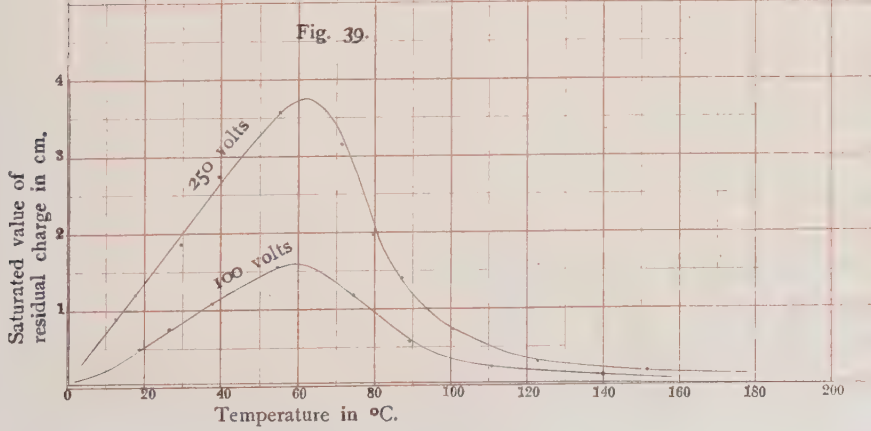

Fig. 40.

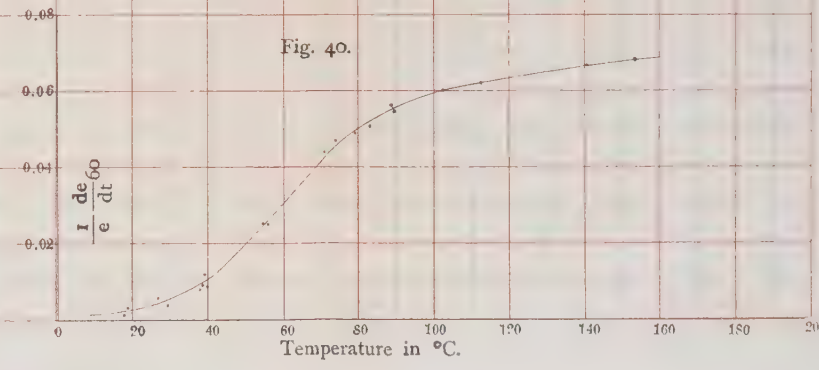

Pl. VII.

Scheelite (101)., Thickness: 0.67 mm
Sensibility: 1 cm = 11.0 volts

Fig. 41.

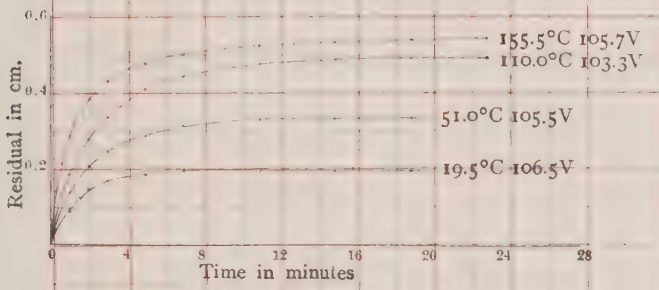

Fig. 42.

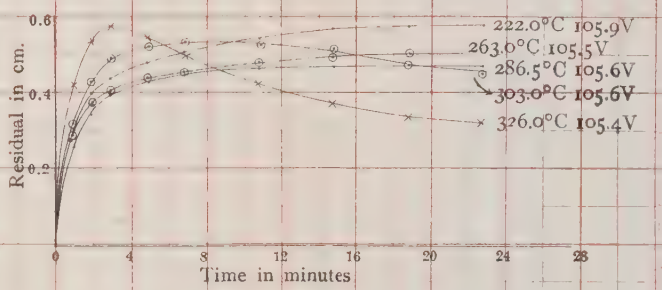

Fig. 43.

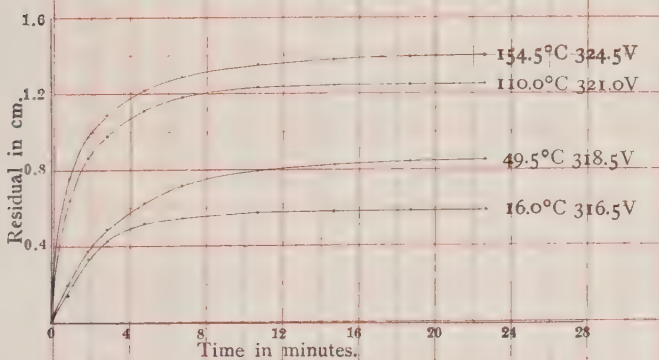

Fig. 44.

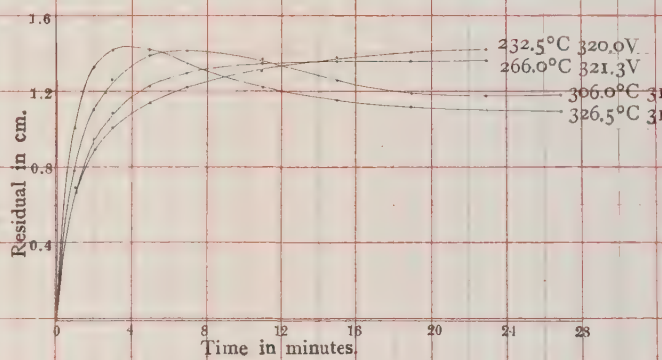

Fig. 45.

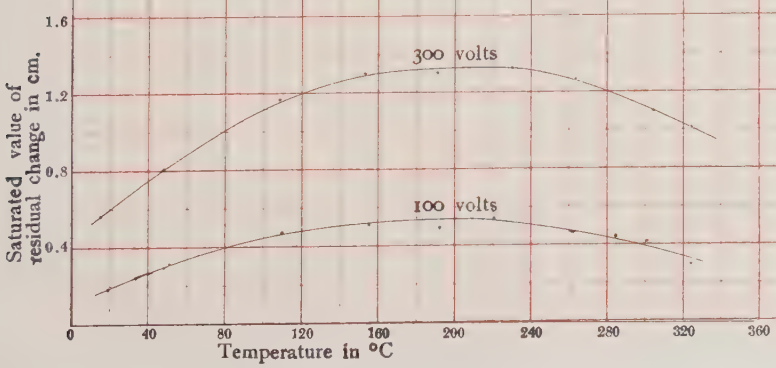

Fig. 46.

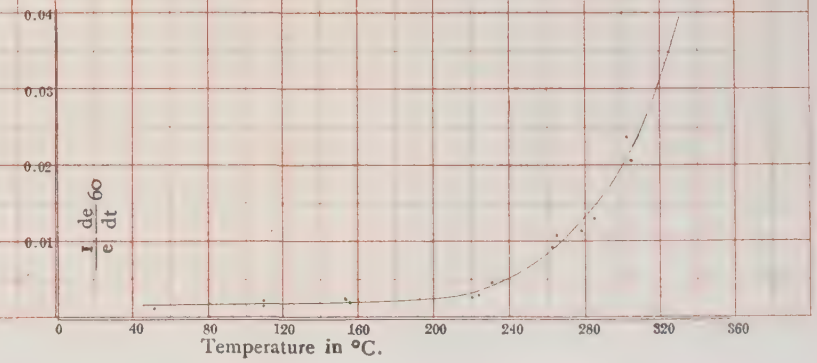

Pl. VIII.

Barite (001) Thickness : 0.69 mm.
Sensibility : 1 cm = 111 volts

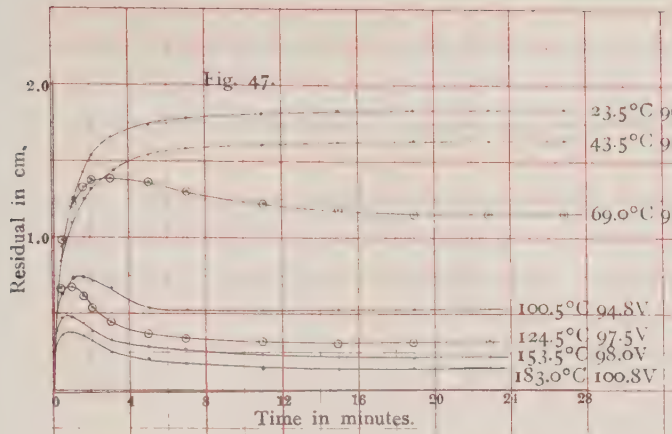

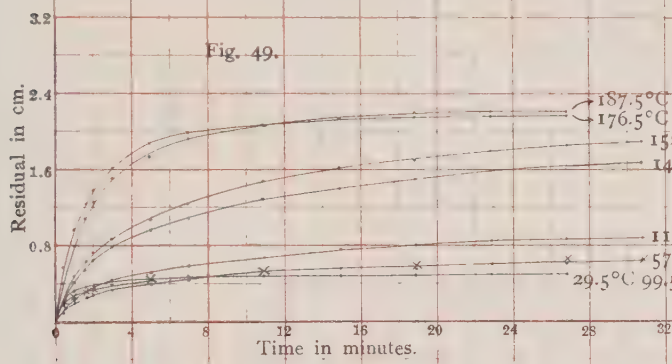

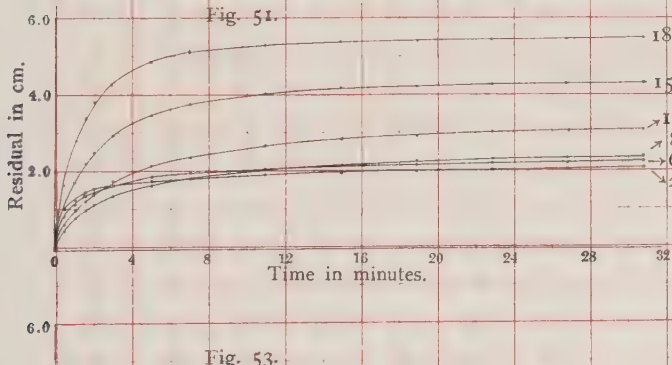

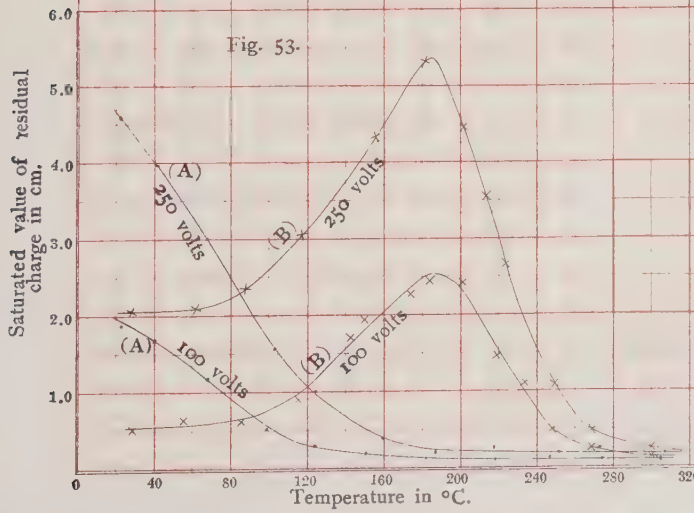

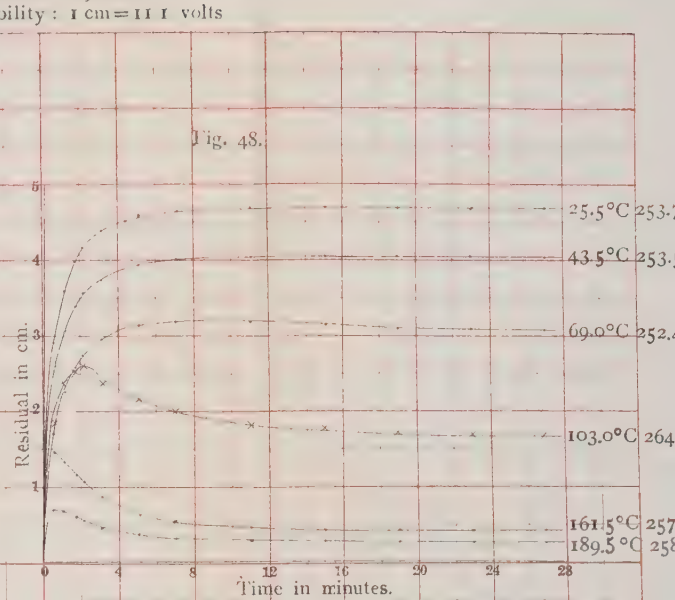

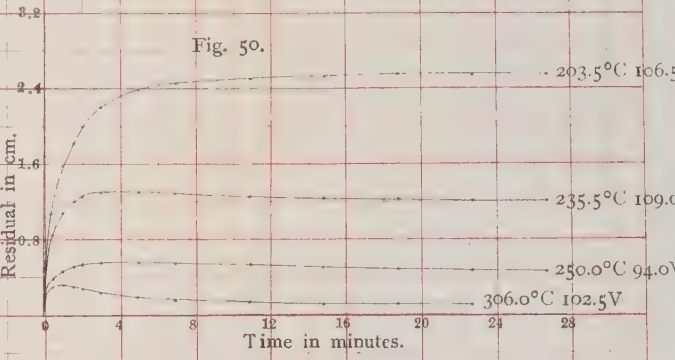

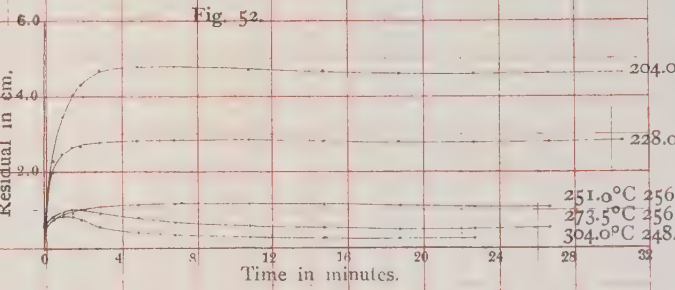

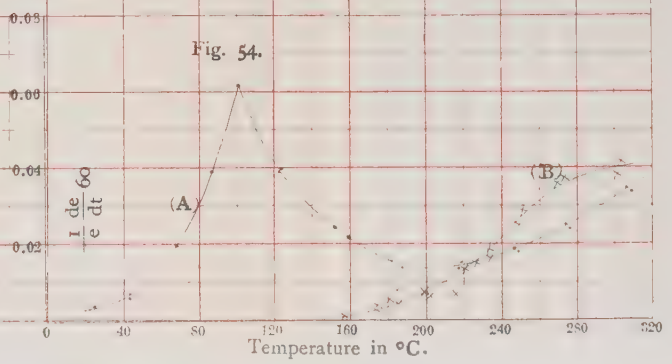

Further Studies on the Variation of Residual Charge and the Ratio of Electrical Conductivity to Capacity due to Temperature.[1]

By

Hikoo Saegusa.

With 5 Plates.

CONTENTS.

§ 1. Introduction.

§ 2. Variation of Residual Charge due to Temperature.

(1) Effect of Temperature on the Accumulation of Residual Charge.

(2) Relation between the Saturated Value of Residual Charge and Temperature.

§ 3. Variation of the Ratio of Conductivity to Capacity due to Temperature.

Summary

§ 1. INTRODUCTION.

It is worth while to study the above mentioned problem with the object of ascertaining, first whether there is any difference in the variation of the residual charge and the ratio of electrical conductivity to capacity due to temperature, between the crystalline[2] and amorphous dielectrics and secondly the relation between the insulating power and the above mentioned phenomena for amorphous materials.

(1) The ninth report from the investigation staff for dielectrics was conducted by the late professor K. Aichi; read before the annual meeting of Math. Phys. Soc. Japan, April 3, 1924.

(2) H. Saegusa, Sci. Rep. **14**, (1925), 319.

For this purpose, we investigated the following materials by the same method and apparatus, as those used in our former investigations.[1] The materials in the form of plates had the following dimensions :—

Dielectrics	Thickness	C/C′	Remarks
Ambroid	0.19 mm	0.59 (22.5°C)	Yellowish brown colour, made in Germany
Paper	0.17 mm	0.23 (19.0°C)	Ashless filter paper (in a perfectly dried state)
Paraffin	0.28 mm	0.31 (19°C)	Semi-transparent plate, Filtered several times
Ebonite	0.29 mm	0.54 (18°C)	Black colour, made in Japan
Glass	0.29 mm	1.34 (16°C)	Deck glass

In the above table, C is the electrical capacity of the test-specimens, C′ that of the apparatus excluding the test-specimen and equal to 39.3 cm. in electro-static unit at 18°c and the figures in brackets in the third column show the temperature at which the capacity was measured.

§ 2. VARIATION OF RESIDUAL CHARGE DUE TO TEMPERATURE.

1. Effect of Temperature on Accumulation of Residual Charge.

The experimental results of the accumulation of residual charge (corrected for leakage) are graphically given for ambroid in Figs, 1–4, Pl. I, for paper in Figs. 7–10, Pl. II, for paraffin in Figs. 13–15, Pl. III, for ebonite in Figs. 18–21, Pl. IV, for glass in Figs. 24–27, Pl. V. As seen from the above figures, the accumulation time up to the saturated value of residual charge decreases as the temperature rises, and the saturated value increases with the temperature. At a further rise of temperature, the residual charge reaches a maximum, and afterwards it decreases gradually and tends to a certain constant value. The

(1) H. Saegusa. loc. cit.

accumulation time up to the maximum point and the magnitude of the residual charge at the maximum point decrease as the temperature rises.

The accumulation of the residual charge of the amorphous dielectrics is quite similar to that of isolated crystals in our former investigation.

The figures in the curves show the temperature and the charging potentials in volts.

2. Relation between the Saturated Value of Residual Charge and the Temperature.

The relations between the saturated value of the residual charge and the temperature are graphically given for ambroid in Fig. 5, Pl. I. for paper in Fig. 11, Pl. II, for paraffin in Fig. 16, Pl. III, for ebonite in Fig. 22, Pl. IV, for glass in Fig. 28, Pl. V. As shown in the above figures, the saturated value of the residual charge gradually increases with the temperature, then it rapidly increases and reaches a maximum, after which it decreases rapidly to a certain temperature, and then gradually tends to an asymptotic value.

In the case of amorphous substances, the residual charge does not become maximum at the same temperature for charging potentials lying above and below the limit potential, for the same material, as in the case of crystals. The maximum temperature for the residual charge is characteristic for different materials. The figures in the curves show the reduced charging potentials in volts, and the limit potential for materials used in the present experiments lies between the potentials given in the curves.

The following table contains the maximum temperatures and the maximum residual charge in cm. for 100 volts charging as deduced from the curves above referred to :—

Dielectrics	Max. temperature for 100 volts charging	Max. Residual charge for 100 volts charging
Ambroid	333°C	1.75 cm
Paper	100°C	0 52 cm
Paraffin	59°C	1.30 cm
Ebonite	120°C	1.85 cm
Glass	20°C	1.50 cm

As shown in the above table, good insulating materials such as ambroid and paper have generally a higher maximum temperature and a comparatively small value of maximum residual charge; but this does not hold so rigorously as in the case of isolated crystals.

It was observed that at the highest temperature heated, materials, suffered a change, i. e. ambroid became black coloured at about 320°C, paper brown coloured at about 190°C, paraffin was melted at about 85°C, ebonite began to melt at about 250°C.

It is a noticeable fact that the variation of the residual charge for ambroid is quite similar to that for mica.

§ 3. VARIATION OF THE RATIO OF CONDUCTIVITY TO CAPACITY DUE TO TEMPERATURE.

The relation between the ratio of conductivity to capacity and the temperature is graphically shown in Fig. 6, Pl, I for ambroid, in Fig. 12, Pl. II for paper, in Fig. 17, Pl. III for paraffin, in Fig. 23, Pl. IV for ebonite, in Fig. 29, Pl. V for glass. They are $\frac{\sigma+\sigma' d}{C+C'}\frac{60}{d}$ or $\frac{1}{e}\frac{de}{dt}$ 60—temperature curves, where σ is the conductivety of the test-specimen, σ' the equivalent conductivity of the apparatus, C the capacity of the test-condenser, C' that of the apparatus, which is nearly equal to the capacity of the electrometer, d the thickness of the specimen, e the potential difference at the test-condenser and $\frac{de}{dt}$ the time rate of the potential decrease of the test-condenser.

As seen from these figures, the ratio of conductivity to capacity increases at first slowly with the temperature, then rapidly, and the curve has an inflexion point at about the maximum temperature and then it gradually tends to a saturation value. The maximum rate of variation occurs at about the maximum temperature.

In the expression

$$\frac{\sigma+\sigma' d}{C+C'},$$

C' σ' are independent of temperature and the variation of capacity of the test-condenser C is generally very small. Thus the variation of the above expression with the temperature might be attributed mainly to that of conductivity σ of the test-specimen. Hence the variation of the residual charge due to temperature might be attributed to the variation of the temperature coefficient of conductivity.

For glass, the variation of conductivity due to temperature is somewhat different, as shown in Fig. 29, Pl. V, i.e. the ratio of conductivity to capacity increases with the temperature and reaches a maximum at about 50°C, and then decreases to about 80°C, afterwards it remains nearly constant up to about 220°C. The first variation up to about 80°C is probably due to the effect of water vapour on the surface of the test-specimen.

It is a noticeable fact that the variation for ambroid is similar to that for mica as in the case of residual charge.

The variation of the residual charge with temperature mainly depends on the variation of the electrical conductivity and coincides with that of the temperature coefficient of the conductivity as in the case of isolated crystals. Hence the variation of the residual charge with temperature can be represented by a certain function of the temperature coefficient of the electrical conductivity. Both variations may be caused by the increase of thermal energy of free electrons and the collision with atoms as we have explained in our former paper.

SUMMARY.

The present investigation may be summarized as follows:—

1. The accumulation of the residual charge for amorphous materials is greatly affected by temperature as in the case of crystals, and the features of the accumulation are similar to those in the latter.

2. The residual charge increases with the temperature and reaches a maximum, and then decreases, tending to an asymptotic value.

The maximum temperature, i.e. the temperature at which the saturated value of the residual charge becomes maximum, is characteristic to

materials, and it is different for charging potentials; and the maximum temperature is comparatively higher for good insulating materials than poor insulators.

3. The ratio of conductivity to capacity increases with the temperature and from about the maximum temperature, it gradually tends to a saturated value as in the case of crystals. The maximum rate of increase of the conductivity occurs at a higher temperature in good insulating materials than for poor insulators.

4. The electrical conductivity of the amorphous dielectrics greatly increases at the temperature in the neighbourhood of the point at which the dielectrics suffer a change. Thus, a good insulator at the ordinary temperature becomes poor as the temperature increases.

5. The variation of the residual charge and the conductivity due to temperature for ambroid are similar to those for mica.

April, 1924.

Explanation of Figures.

Fig. 1–4, Pl. I. Accumulation of residual charge by various charging potentials and under various temperatures for ambroid. The figures to the curves show the temperature and the charging potentials in volts. (charging time 4 min., discharging time 10 sec.).

Fig. 5. Relation between the saturated value of residual charge (stationary value from the maximum of residual charge) and the temperature for ambroid. Reduced charging potentials are 100 and 300 volts.

Fig. 6. Relation between the ratio of conductivity to capacity (divided by the thickness of the specimen and multiplied by 60) and the temperature for ambroid. Ordinate represents $\frac{1}{e}\frac{de}{dt}$ 60 and abscissa the temperature.

Fig. 7–10, Pl. II. Accumulation of residual charge by various charging potentials and under various temperatures for paper.

Fig. 11. Relation between the saturated value of residual charge and the temperature for paper. Reduced charging potentials are 100 and 300 volts.

Fig. 12. Relation between the ratio of conductivity to capacity and the temperature for paper.

Fig. 13–15, Pl. III. Accumulation of residual charge by various charging potentials and under various temperatures for paraffin.

Fig. 16. Relation between the saturated value of residual charge and the temperature for paraffin. Reduced charging potentials are 100 and 300 volts.

Fig. 17. Relation between the ratio of conductivity to capacity and the temperature for paraffin.

Figs. 18–21, Pl. IV. Accumulation of residual charge by various charging potentials and under various temperatures for ebonite.

Fig. 22. Relation between the saturated value of residual charge and the temperature for ebonite. Reduced charging potentials are 100 and 300 volts.

Fig. 23. Relation between the ratio of conductivity to capacity and the temperature for ebonite.

Figs. 24–27, Pl. V. Accumulation of residual charge by various charging potentials and under various temperatures for glass.

Fig. 28. Relation between the stational value of residual charge and the temperature for glass. Reduced charging potentials are 100 and 300 volts.

Fig. 29. Relation between the ratio of conductivity to capacity and the temperature for glass.

Pl. I.

Ambroid. Thickness: 0.19 mm Sensibility: 1 cm = 11.1 volts

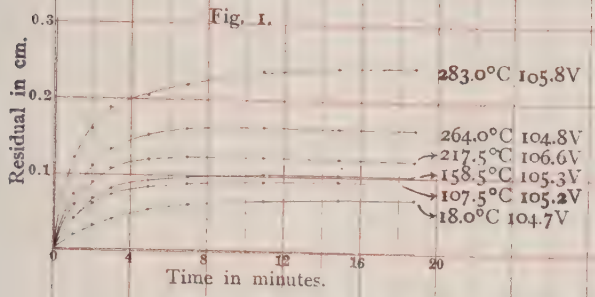

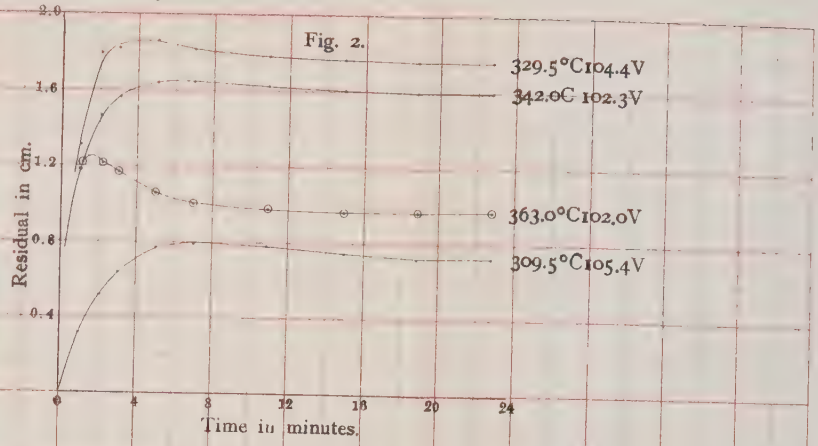

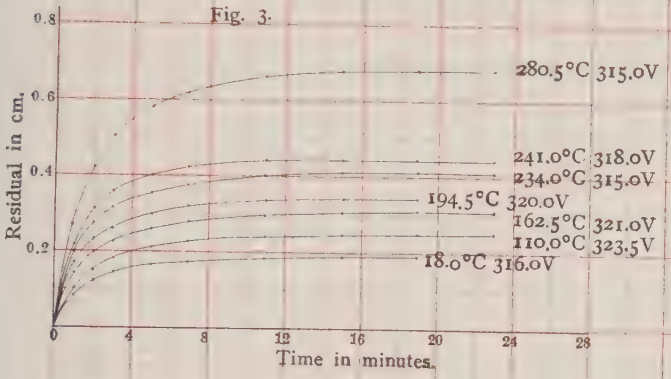

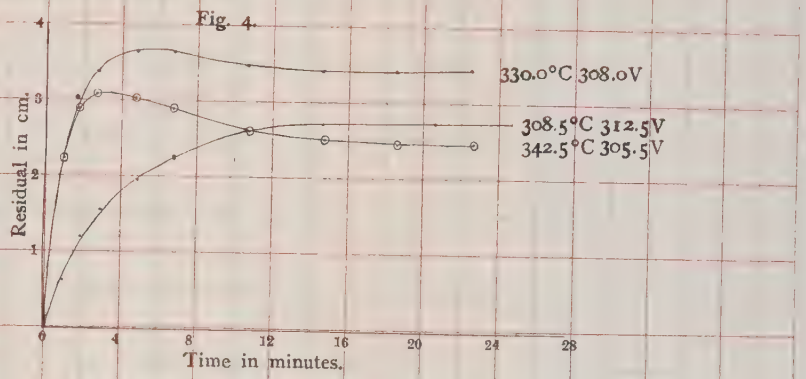

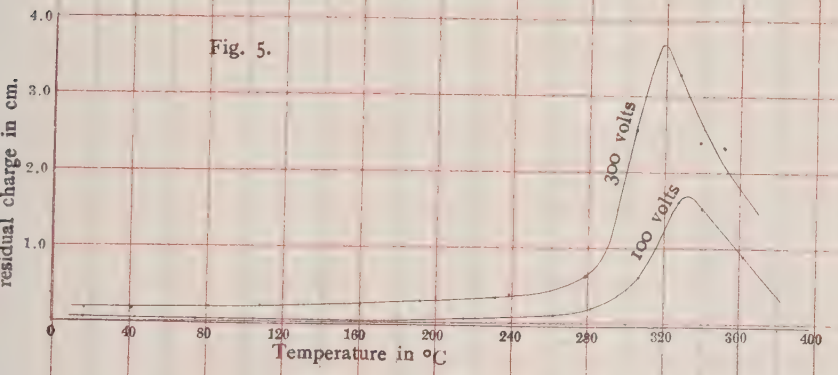

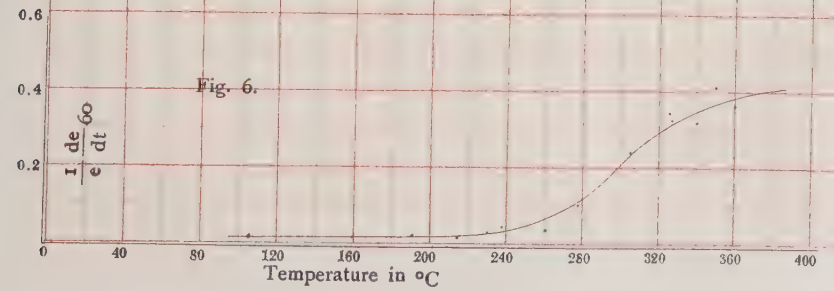

Pl. II.

Paper. Thickness: 0.17 mm. Sensibility: 1 cm = 11.0 volts

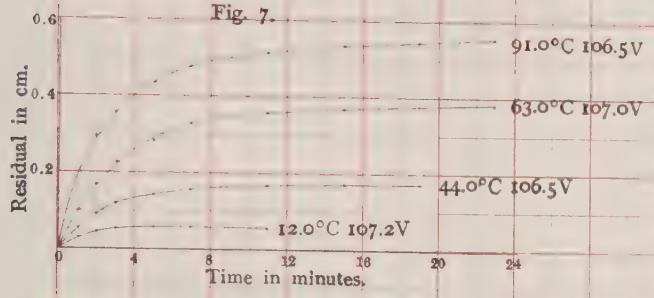

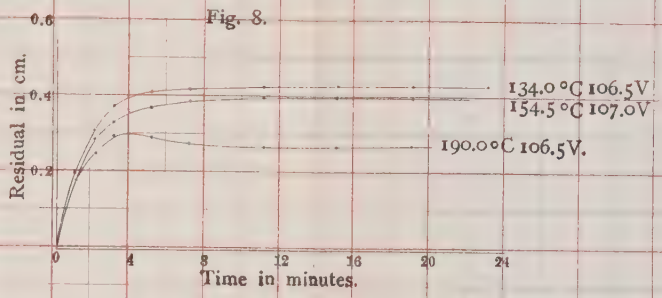

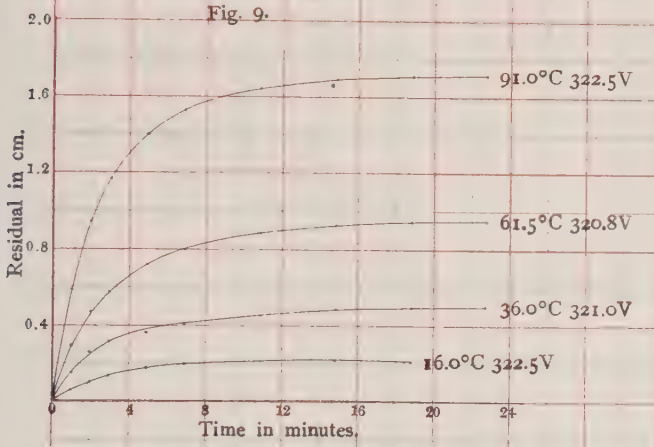

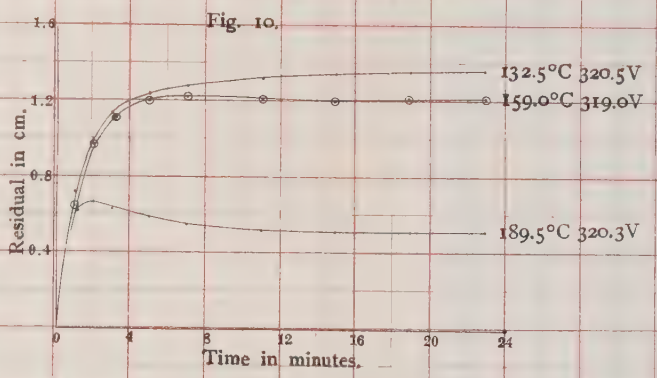

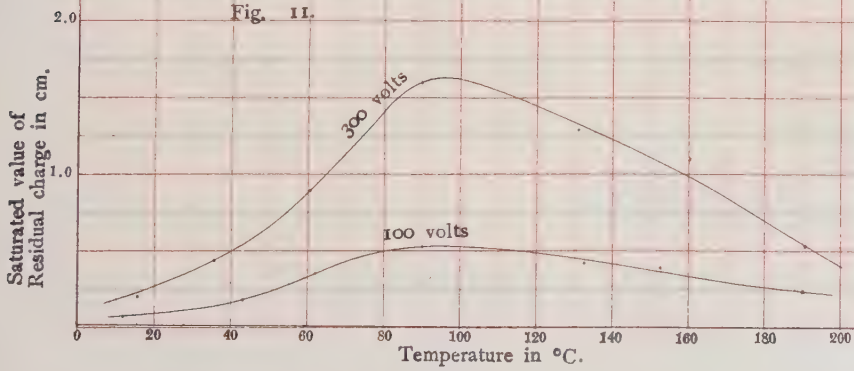

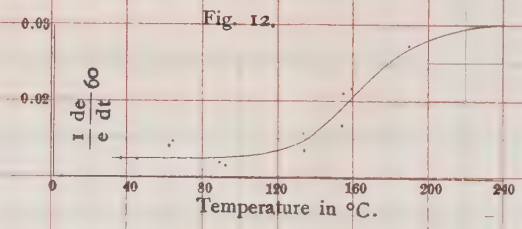

Pl. III.

Paraffin, Thickness: 0.28 mm. Sensibility: 1 cm = 11.1 volts

Fig. 13.

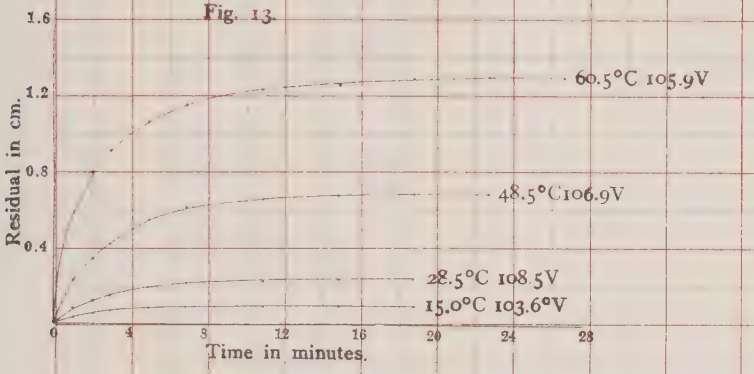

Fig. 14.

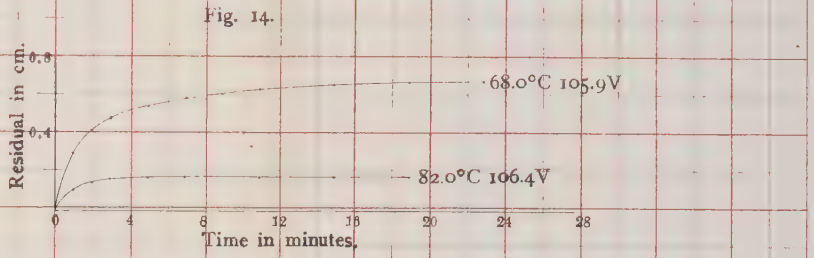

Fig. 15.

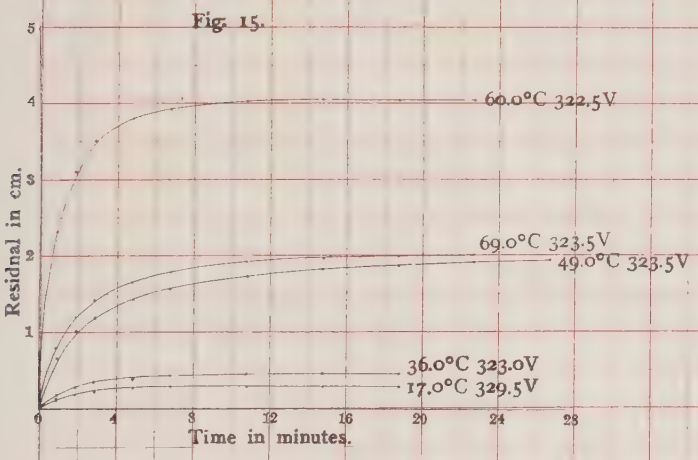

Fig. 17.

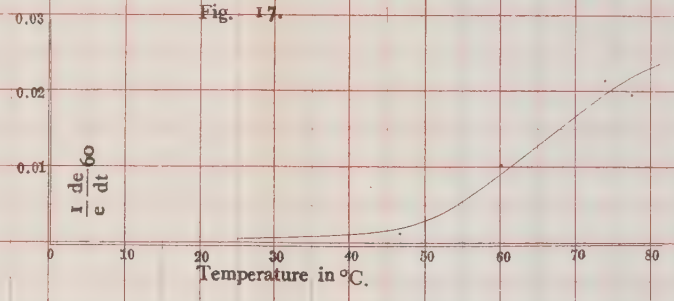

Fig. 16.

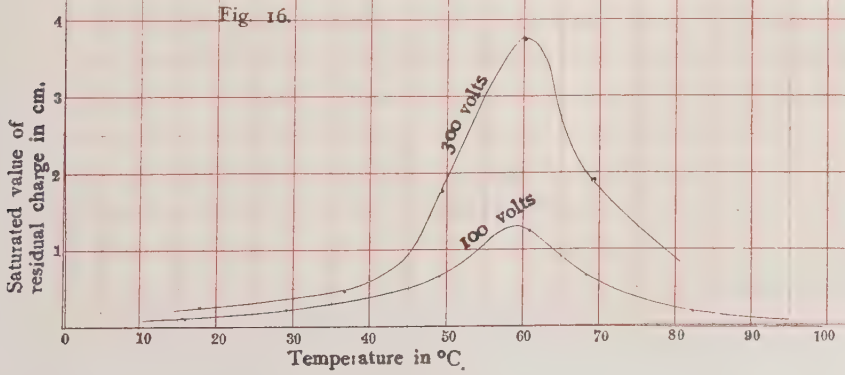

Pl.IV.

Ebonite, Thickness: 0.29 mm Sensibility: 1 cm = 10.8 volts

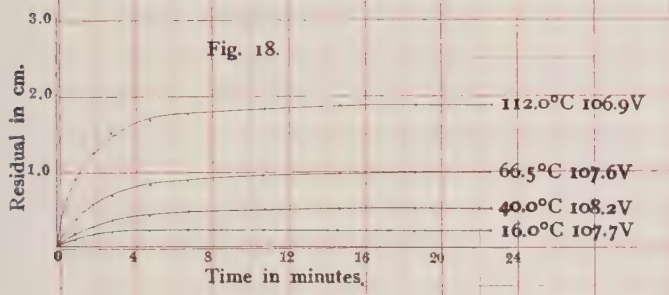

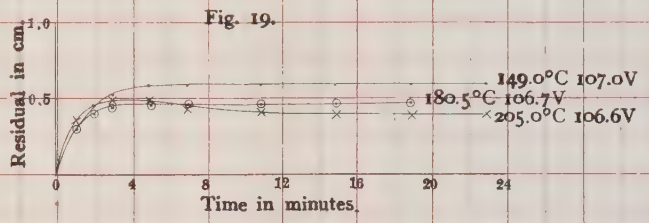

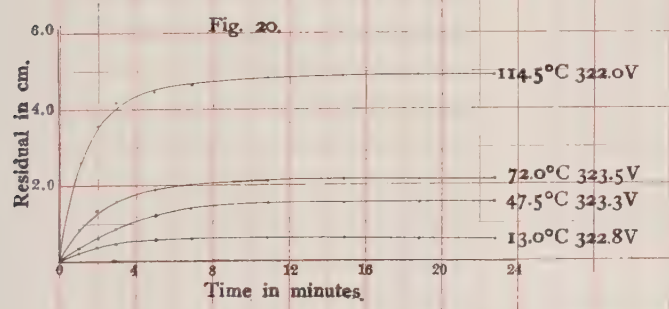

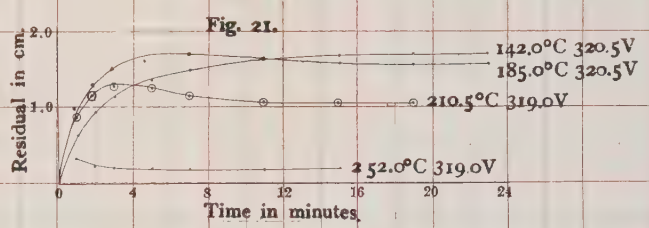

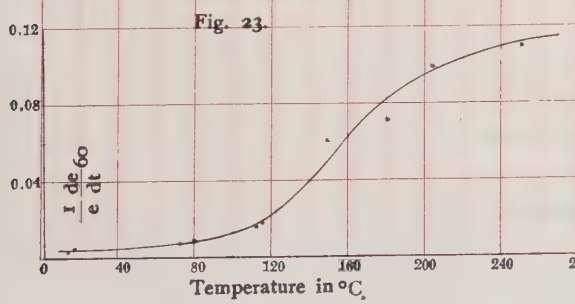

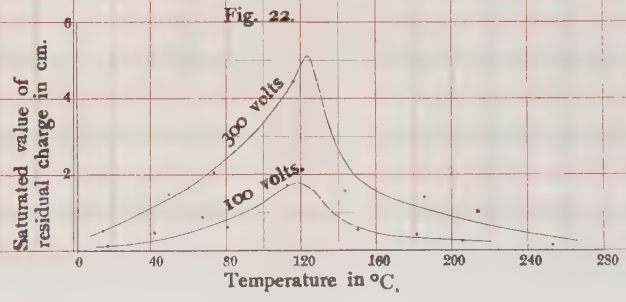

Pl. V.

Glass, Thickness: 0.29 mm. Sensibility: 1 cm = 111 volts

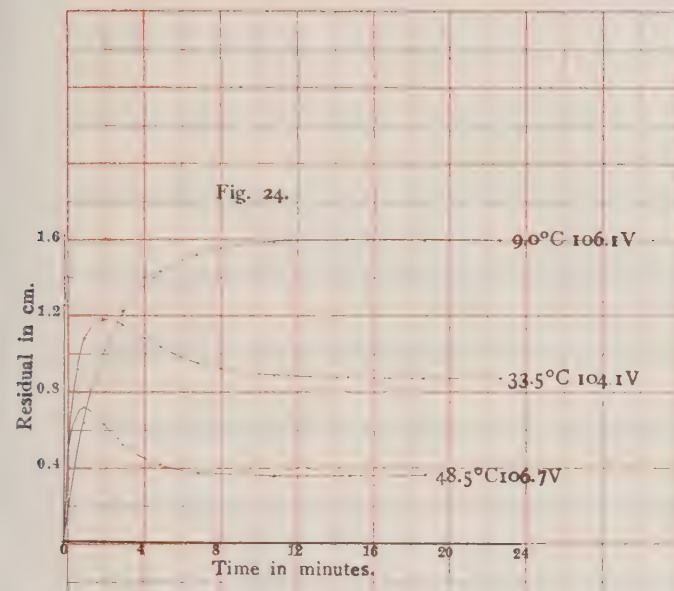

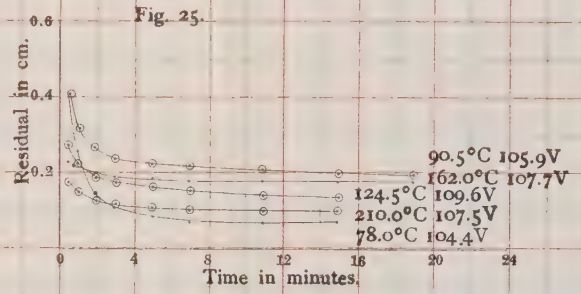

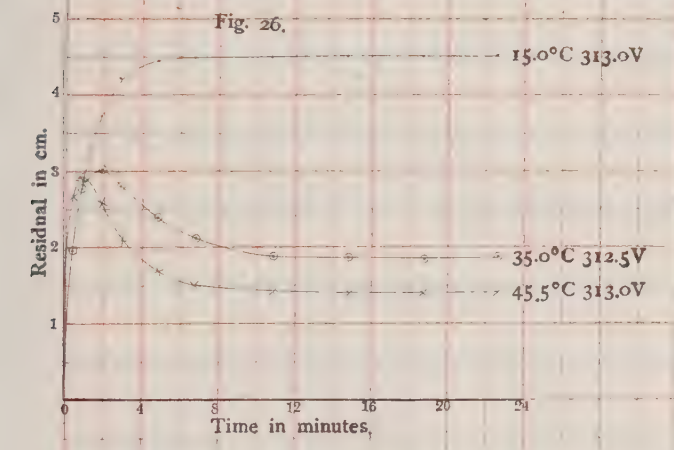

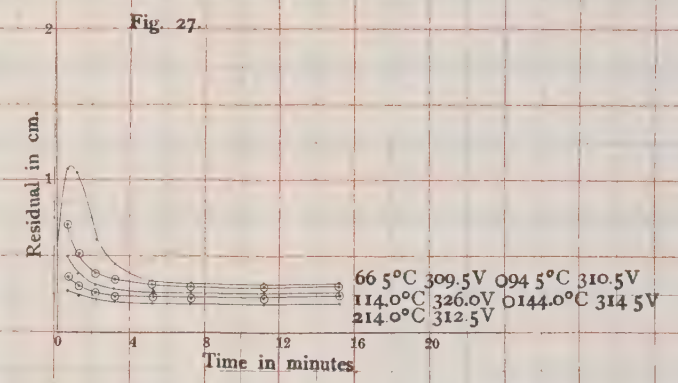

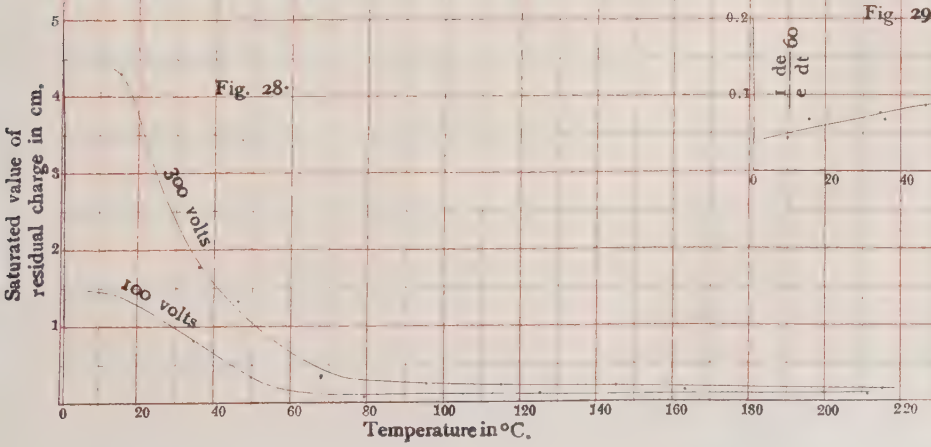

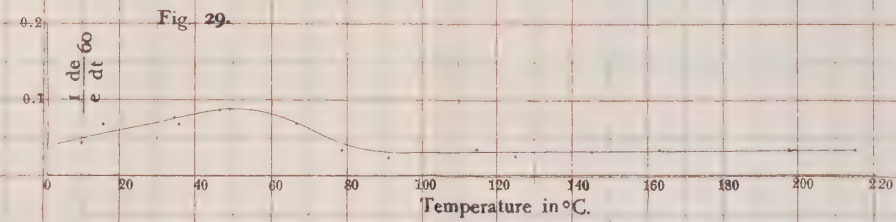

The Effect of Cold-Working and Annealing on some Physical Properties of Copper, Aluminium and their Alloys.

By

Tsutomu Matsuda.

CONTENTS.

Introduction.

Part I. Effect of Cold-Working on Mechanical Properties and Electric Resistance

I. Effect of Cold-rolling.
II. Effect of Cold-drawing.
III. Effect of Cold-twisting.

Part II. Effect of Annealing on the Electric Resistance and Mechanical Properties of Cold-worked Metals.

I. Variation of the Electric Resistance during Heating of Cold-rolled Plates.
II. Effect of Annealing on the Electric Resistance and Mechanical Properties of Cold-rolled Plates.
III. Variation of the Electric Resistance during Heating of Cold-drawn Rods.
IV. Effect of Annealing on the Electric Resistance and Mechanical Properties of Cold-drawn Rods.
V. Discussion of Results.

Part III. Effect of Heating on the Length of Cold-worked Metals.

I. Introduction.
II. Results of Experiments.
(1) Cold-rolled Plates.
(2) Cold-drawn Rods.
III. Discussion of Results.

Summary.

INTRODUCTION.

The effect of cold-working on the mechanical properties of metals and alloys has been examined by many workers Among recent

investigations in this line, those of Alkins,[1] Johnson,[2] Ellis,[3] and Koeber and Wieland[4] may be mentioned. The first and the second investigators examined the effect of drawing and rolling on some mechanical and physical properties of copper, and the third and the fourth investigators the effect of rolling on brass. The physical properties, such as electric resistance and density, are also affected by cold-working, though in lesser extent as compared with mechanical properties. As a classical research in this direction that of Kahlbaum and Sturm[5] is to be noted. Further data may be found in papers recently published by Alkins, Johnson, and Guillet and Ballay.[6]

The present research has been undertaken to examine the effect of cold-working and of subsequent low-temperature annealing on some physical and mechanical properties of copper, aluminium and their commercial alloys to supply further data in this line.

PART I. EFFECT OF COLD-WORKING ON MECHANICAL PROPERTIES AND ELECTRIC RESISTANCE.

As the method of cold-working, rolling, drawing and twisting were used. The materials subjected to rolling were copper, brasses (Cu = 71, 60 and 54 %), aluminium-bronze (Al = 7 %), phosphor-bronzes (Sn = 3 and 9 %), manganese-copper (Mn = 3.6 %), aluminium and duralumin, and those subjected to drawing were copper, brasses (Cu = 70 and 60 %), phosphor-bronze (Sn = 3 %) and duralumin, while thirteen kinds of brass wires containing 5 to 46 percent of zinc were subjected to twisting. These alloys had the composition as given in Tables I and II, and consisted of single solid solution α, with the exception of 60 : 40 brass, β-brass (Cu = 54 %) and duralumin.

(1) J. Inst. Met. (1918), No. 2, 33; (1920), No. 1, 381.
(2) *ibid.* (1919), No. 1, 335; (1920), No. 1, 443; (1921), No. 2, 173.
(3) Met. Ind. **15**, (1919), 495.
(4) Mit. K. W. Inst. Eisenf., III, 1, (1921), 57.
(5) Z. anorg. Chem. **46**, (1905), 215.
(6) A full bibliography will be given in later sections.

I. Effect of Cold-Rolling.

By rolling a large ingot, four kinds of plates having the thickness varying from 10 to 20 mm were prepared. They were well annealed and then cold-rolled down to 8 mm without intermediate annealing. The initial and final thickness of these plates and the reduction in thickness are given in the following table:

Mark.	Initial thickness in mm (d_0).	Final thickness in mm (d).	Reduction in thickness in percent $\left(\frac{d_0-d}{d_0} \times 100\right)$.
1	10	8	20.0
2	13	8	38.4
3	16	8	50.0
4	20	8	60.0

From the plates thus obtained, test-specimens having proper dimensions were taken and subjected to tests. The tensile strength, elongation and electric resistance were determined on two groups of test-specimens each taken parallel or right angles to the direction of rolling. In the following pages, the former group is called "longitudinal" or L-specimen and the latter "transversal" or T-specimen. Thus by "4 L-specimen" we mean the specimen taken parallel to the direction of rolling from the plate, which received 60 percent reduction.

(1) *Mechanical properties.* The tensile strength, elongation and hardness were determined in the cold-rolled or annealed state, and the results obtained are given in Table I. Specimens for the tensile test had the sectional area of about 40 sq. mm and the elongation was measured on 50 mm. The impression for Brinell hardness test was made on the surface of plate by using a 10 mm ball under the load of 500 kg, with the exception of aluminium for which the load was 300 kg. From these results it was confirmed that as the degree of cold-deformation proceeds the tensile strength of either L- or T-specimens increases regularly while the elongation decreases, and that the L-specimen has lower strength but higher elongation than the T-specimen. If the specimens are

annealed at 350° (for aluminium and duralumin), 450° (for copper and 60 : 40 brass), 500° (for other alloys) or at higher temperatures for 30 minutes, the difference between the mechanical properties of L- and T-specimens, and also that of plates subjected to varying degrees of deformation almost completely vanish as shown in the table, although some differences are still notice able in the elongation of aluminium-bronze and duralumin.

(2) *Electric Resistance.* Before discussing the results obtained by the present writer, the researches hitherto published will be briefly referred to. Kahlbaum and Sturm[1] and Credner[2] examined the effect of cold-drawing on the electric resistance of various metals, while Addicks,[2] Gewecke,[2] Alkins[3] and others made similar tests on copper. Recently an extensive research was made by Guillet and Ballay.[4] All these researches show that the resistivity of metals and alloys increases by cold-drawing, and that the amount of increase is widely different in different metals and alloys. Generally speaking, however, the effect on pure metals is smaller as compared with that on alloys ; in the former the increase seldom amounts to 4 percent, while in the latter it sometimes exceeds 10 percent.

The results obtained by the present writer will be next considered. Square rods, 8 mm in width and 20 cm in length, were taken parallel and right angles to the direction of rolling, and their resistance was determined. The difference between the specific resistance of L- and T-specimens, which received varying degree of deformation, falls within experimental error after proper annealing. The annealing was made at 350° to 500° or at higher temperatures for 30 minutes as already remarked in the previous section. The mean value of the specific resistances is given in Table I. The resistance of cold-rolled L- and T-specimens was next determined, and the percentage difference between this and that of

(1) *loc. cit.*
(2) Tammann, Lehrbuch der Metallographie, (1923), 147–9.
(3) J. Inst. Met. (1924), No. 1, 157.
(4) Rev. Mét. **20**, (1923), 398. A further test on aluminium has been published by Guillet, (Rev. Mét. **21**, (1924), 12).

annealed ones was calculated by the following formula,

percentage difference in specific resistance

$$= \frac{\sigma_r - \sigma_a}{\sigma_a} \times 100,$$

where σ_r = specific resistance of cold-rolled specimen,

σ_a = ,, ,, ,, annealed specimen.

The values thus obtained are given in Table I and also graphically in Fig. 1, where the ordinate represents the percentage difference in specific resistance, and the abscissa the reduction of thickness in percent. From these results it may be concluded that by cold-rolling the electric resistanee of metals increases, and that the increase is marked in aluminium-bronze, duralumin, 70 : 30 brass and phosphor-bronze (Sn = 3 %), and also that no systematic difference can be found in the specific resistance of L- and T-specimens.

As already remarked, the increase of specific resistance due to cold-working has been well established, but its cause has not yet been made fully clear. Tammann[1] considers that the electric resistance of a metal is a vectorial property, and varies with the orientation of the metallic crystallites. He further considers that, by cold-drawing and rolling, the metallic crystallites assume a definite orientation, which bears a certain relation to the direction of working, and therefore the electric resistance of a cold-worked metal along a certain direction, e. g., along the axis of cold-drawn wire, is higher than that of annealed one, in which the orientation of crystallites is quite irregular. As predicted by Tammann, the regurality in the orientation of crystallites in cold-rolled or drawn metals has been conclusively confirmed by recent investigations.[2] More-

(1) *loc. cit.* 145–54.

(2) Polanyi; (Zs. Phys. **17**, (1923), 42), summarises as follows: By drawing metals having face-centred cubic lattice, [111] and less frequently [100] become parallel to the direction of drawing, while by rolling [112] and [100] become parallel to the direction of rolling and (101) and (100) to the surface of plate. Details and further researches may be found in papers published by Ettisch, Polanyi and Weissenberg, Zs. Phys. **7**, (1921), 181; Zs. phy. Chem. **99**, (1921), 332; Mark, Polanyi and Schmid, Zs. phys. **12**, (1922), 58; Burger, Phys. Zs. **23**, (1922), 24; Koerber, Mit. K. W. Inst. Eisenforschung, III, 2, (1922); Ono, Mem. Coll. Eng. Kyushu Imp. Univ. (1922); Mark and Weissenberg, Zs. Phys. **14**, (1923), 328; **16**, (1923), 314; Uspenski and Konojewski, *ibid*, **16**, (1923), 215; Mark and Polanyi, *ibid*, **18**, (1923), 75; Wever, St. Eis. **44**, (1924), 51; Zs. Phys. **28**, (1924), 69.

over the electric resistance should be a vectorial property as considered by Tammann, but in metals and alloys having cubic space lattice, such as tested in the present research,[1] the difference in the electric resistance along various crystallographic axes of a metallic crystallite may not be so large as to account for the large increase due to cold-working. Quite recently Grueneisen and Goens[2] have shown that at 0° the electric resistance measured along a direction parallel to the hexagonal axis of single crystals of zinc and cadmium exceeds only 8 and 19 percent that measured perpendicular to it. This affords a further support to the above view, as in metals and alloys having the lattice form of high degree of symmetry such as cubic, the difference in specific resistance along various crystallographic axes is considered to be very small. Moreover the present research shows that no systematic difference exists between the electric resistances of L- and T-specimens. If the view of Tammann be correct, there must exist some systematic differences.

From the above considerations it may be concluded that the regularity in the orientation of crystallites in cold-worked metals does not contribute to the increase of electric resistance to any appreciable degree.[3] As shown later, the results of test on the effect of cold-twisting on the electric resistance afford a further support to the writer's above view.

---

(1) Copper and aluminium have the lattice form of face-centred cubic type, and all the alloys tested in the present research, with the exception of β-brass, have also similar form as already confirmed by Andrews (Phys. Rev. **18,** (1921), 251), Bain (Chem. Met. Eng. **28,** (1923), 21), Owen and Preston (Proc. Phy. Soc. London, **36**. (1923), 14, 49) and Jette, Phragmén and Westgren (J. Inst. Met. (1924), No. 1, 193).

(2) Phys. Zs. **24,** (1923), 506; Zs. Phys. **26,** (1924), 260.

(3) After the present paper had been prepared, the writer noticed that a similar view has also been expressed by Geiss and Liempt (Zs. anorg Chem. **133,** (1924), 107).

TABLE I. Plate.

(a) Copper (Cu = 99.78 %).

Mark.	Tensile strength in kg. per sq. mm.		Elongation percent on 50 mm.		Brinell hardness.	Percentage diff. in spec. resist.		
	L	T	L	T		L	T	mean
1	30.8	31.9	12	8	84	1.3	1.3	1.3
2	36.2	37.0	7	6	96	2.1	1.6	1.9
3	35.9	39.0	7	5	103	1.4	1.9	1.7
4	37.7	39.7	6	5	107	2.1	2.1	2.1
annealed at 450°	24.7	24.9	44	44	46	spec. resist. = 1.95(1)		

(b) 70 : 30 brass (Cu = 71.20, Pb = 0.02, Fe = 0.02 %).

1	...	...	...	...	...	...	...	...
2	59.5	63.1	12	10	160	6.7	6.8	6.8
3	64.1	67.6	11	9	162	9.4	8.8	9.1
4	68.3	71.3	10	8	167	10.0	9.6	9.8
annealed at 500°	36.9	36.4	48	49	78	spec. resist. = 6.15		
„ 600°	34.5	34.5	55	55	59	„ „ = 6.17		

(c) 60 : 40 brass (Cu = 60.26, Pb = 0.03, Fe = 0.02 %).

1	49.7	49.3	21	21	132	1.7	1.9	1.8
2	57.9	58.3	12	11	146	2.7	3.1	2.9
3	62.5	65.2	10	9	164	4.9	5.2	5.1
4	65.3	68.9	8	8	175	7.2	7.3	7.3
annealed at 450°	42.6	42.2	45	46	73	spec. resist. = 6.22		
„ 600°	37.6	37.0	46	46	61	„ „ = 6.32		

(d) Beta-brass (Cu = 54.49 %).

1	...	...	...	...	...	...	...	...
2	59.4	64.8	8	9	169	1.4	1.4	1.4
3	61.9	66.0	7	7	170	1.9	1.9	1.9
4	64.3	67.0	7	6	170	2.0	2.6	2.3
annealed at 500°	51.1	52.4	33	32	90	spec. resist. = 4.95		
„ 600°	50.9	50.8	31	33	91	„ „ = 4.94		

(1) Spec. resist. was measured at 20–23° and expressed in microohms.

TABLE I. (*Continued*).

(e) Aluminium-bronze (Cu = 92.99, Al = 7.03 %).

Mark.	Tensile strength in kg. per sq. mm.		Elongation percent on 50 mm.		Brinell hardness.	Percentage diff. in spec. resist.		
	L	T	L	T		L	T	mean
1	...	...	...	...	...	...	...	...
2	...	...	...	...	...	...	...	...
3	74.0	74.4	10	9	183	12.1	12.0	12.1
4	79.6	80.2	9	4	205	13.8	13.6	13.7
annealed at 500°	50.5	50.6	46	40	111	spec. resist. = 11.17		
„ 600°	46.0	45.7	57	51	75	„ „ = 11.30		

(f) Phosphor-bronze (Cu = 96.27, Sn = 3.35, P = 0.13 %).

1	53.7	53.9	11	9	141	3.2	3.5	3.4
2	55.6	57.4	10	7	151	10.0	9.1	9.6
3	63.0	67.6	9	7	164	9.0	8.3	8.7
4	63.7	71.1	9	7	169	8.8	9.1	9.0
annealed at 500°	45.3	45.0	27	26	118	spec. resist. = 7.18		
„ 600°	39.4	39.2	39	38	76	„ „ = 7.55		

(g) Phosphor-bronze (Cu = 90.45, Sn = 9.23, P = 0.04 %).

1	58.1	58.6	26	15	157	1.8	1.9	1.9
2	67.7	70.4	14	7	180	4.4	4.6	4.5
3	79.4	81.3	8	3	204	3.2	3.6	3.4
4	84.6	88.6	7	3	209	4.8	3.9	4.4
annealed at 500°	47.5	46.1	55	50	108	spec. resist. = 14.47		
„ 600°	45.5	43.7	60	60	81	„ „ = 14.67		

(h) Manganese-copper (Cu = 95.69, Mn = 3.60 %).

1	...	...	...	...	...	...	...	...
2	44.8	45.2	11	8	131	1.1	1.1	1.1
3	45.4	46.2	10	8	135	0.9	0.9	0.9
4	46.4	...	10	...	144	1.1	1.1	1.1
annealed at 500°	34.6	34.7	39	38	73	spec. resist. = 15.13		
„ 600°	34.5	33.8	40	40	63	„ „ = 15.12		

TABLE I. (*Continued*).

(i) Aluminium (Fe = 0.52, Si = 0.56, Cu = 0.26 %).

Mark.	Tensile strength in kg. per sq. mm.		Elongation percent on 50 mm.		Brinell hardness.	Percentage diff. in spec. resist.		
	L	T	L	T		L	T	mean
1	14.0	14.8	14	10	38	4.9	5.5	5.2
2	15.1	15.6	10	9	42	5.5	5.8	5.7
3	16.9	17.0	8	10	45	6.1	5.5	5.8
4	17.4	18.3	8	8	49	6.1	6.6	6.4
annealed at 350°	12.1	12.1	26	24	25	spec. resist. = 3.11		

(j) Duralumin (Cu=4.02, Mn=0.84, Fe=0.65, Si=0.60, Mg=0.46%).

1	36.8	33.8	5	5	99	7.0	8.1	7.6
2	38.5	38.3	4	3	104	9.9	10.9	10.4
3	38.9	39.3	4	3	109	10.7	12.3	11.5
4	40.1	38.6	3	2	106	11.4	13.0	12.2
annealed at 350°	28.3	28.7	8	5	60	spec. resist. = 3.99		

II. Effect of Cold-Drawing.

By drawing a large ingot, three kinds of rods having the diameters varying from about 8 to 11 mm in. were prepared. They were well annealed and then cold-drawn down to 6.35 mm without further annealing. The details are given in the following table :—

Mark	Initial diameter in mm (d_0).	Final diameter in mm (d).	Reduction in sectional area in percent $\left(\frac{d_0^2-d^2}{d_0^2}\times 100\right)$.
1	7.94	6.35	36.0
2	9.53	6.35	55.6
3	11.12	6.35	67.3

Specimens were taken from these rods and their tensile properties, hardness and electric resistance were determined. The sectional area of the tensile test-piece was about 25 sq. mm and the hardness was measured on the transversal section. The results obtained are given in Table II, and also graphically in Fig. 1.

TABLE II. Rod.

(a) Copper (Cu = 99.83 %).

Mark.	Tensile strength in kg per sq. mm.	Elongation percent on 50 mm.	Brinell hardness	Percentage diff. in spec. resist.
1	40.0	9	...	1.7
2	45.0	7	...	2.3
3	49.1	6	...	2.5
annealed at 450°	25.8	43	...	spec. resist. = 1.80

(b) 70 : 30 brass (Cu = 69.59, Pb = 0.03, Fe = 0.02 %).

1	59.5	10	142	6.8
2	73.4	7	185	12.0
3	81.5	6	194	13.2
annealed at 500°	40.2	47	...	spec. resist. = 6.33
„ 600°	37.3	53	44	„ „ = 6.34

(c) 60 : 40 brass (Cu = 60.42, Pb = 0.03, Fe = 0.03 %).

1	68.5	12	166	2.9
2	76.2	8	175	6.8
3	88.2	6	187	8.3
annealed at 450°	45.2	35	...	spec. resist. = 6.69
„ 650°	43.2	41	70	„ „ = 6.66

(d) Phosphor-bronze (Cu = 96.23, Sn = 3.40, P = 0.13 %).

1	55.6	9	141	3.0
2	64.2	7	164	4.1
3	72.1	6	170	2.5
annealed at 500°	39.5	42	...	spec. resist. = 7.79
„ 600°	37.6	43	55	„ „ = 7.90

(e) Duralumin (Cu = 3.96, Mn = 0.52, Fe = 0.54, Si = 0.61, Mg = 0.50 %).

1	34.5	6	85	4.6
2	37.3	5	98	5.9
3	39.5	5	103	8.0
annealed at 350°	25.1	17	54	spec. resist. = 3.63

III. Effect of Cold-Twisting.

Brass wires, which were 3.3 mm thick and contained 5 to 46 percent of zinc, were prepared by cold-drawing. Test-specimens taken from these wires were then subjected to the test after the following treatments :—

(1) Annealed at 600° for 30 minutes and then cooled slowly in the furnace ;

(2) After annealing, twisted 10 turns on 20 cm ;

(3) After twisting, once more annealed at 600° and slowly cooled ;

(4) Specimens subjected to the treatment (1) were twisted 20 turns on 20 cm ;

(5) After twisting, once more annealed at 600° and slowly cooled.

The results obtained are shown in Table III and also graphically in Fig. 2. As the twisting could not follow too far without causing breaking down of the specimens, especially of those rich in zinc, the increase in tensile strength and electric resistance was not so large as in the case of rolling and drawing. Yet regular rise in strength and resistance and the almost complete recovery of the original value by annealing are well established from these results.

Tammann[1] considers that the increase of electric resistance due to bending or twisting may be ascribed to the formation of fine cracks by these treatments, and therefore the original low value can not be restored by annealing. Thus according to his view the increase due to these treatments is essentially different from that due to rolling and drawing. The writer's results however show that his view is not probable at least within the degree of cold-twisting so far tested.

As shown above, tensile strength and electric resistance increase with the degree of cold-deformation, whether the deformation is produced by rolling, drawing or twisting. As shown in Fig. 3, a simple relation holds between the tensile strength and the increase of electric resistance

(1) *loc. cit.* 151–2.

of the metals. This shows that the methods of deformation and consequently the orientation of metallic crystallites have little effect on the increase of the electric resistance.

From the results so far obtained, the present writer considers that the increase of electric resistance by cold-working can not be ascribed neither to the "Umorientierung" of metallic crystallites, nor to the formation of minute cracks, as considered by Tamman, but may be due to the straining of space lattices caused thereby. These points will be more fully discussed in a later section.

TABLE III, 1.

Effect of Cold-Twisting and Annealing on the Tensile Strength of Brass Wires.

Alloy.	Tensile strength in kg. per sq. mm.					
	Cu (%)	(1) Annealed.	(2) Twisted 10 turns.	(3) Annealed.	(4) Twisted 20 turns.	(5) Annealed.
No. 1	99.97	26.4	31.1	25.6	33.2	.....
2	95.15	27.6	31.7	27.0	36.3	.....
3	89.46	29.6	33.8	28.8	40.9	29.1
4	84.73	31.9	37.2	30.5	43.9	31.7
5	79.66	34.7	40.5	33.5	47.4	34.0
6	74.85	37.3	42.7	37.2	48.5	36.7
7	67.70	35.6	41.7	34.9	48.8	35.7
8	65.50	35.0	41.1	35.0	47.9	34.8
9	63.76	35.1	40.8	34.7	46.3	35.2
10	61.53	40.8	48.0	38.5	55.2	41.4
11	59.32	43.5	53.0	43.4	57.1	43.5
12	57.48	48.2	54.0	47.3	.....	.....
13	55.72	51.6	54.3	.....	.....	.....
14	53.93	48.6	55.5	.....	.....	.....

Table III, 2.

Effect to Cold-Twisting and Annealing on the Specific Resistance of Brass Wires.

Alloy.	(1) Spec. resist. at 30° in microohms.	Increase of spec. resist. in percent.			
		(2) Twisted 10 turns.	(3) Annealed.	(4) Twisted 20 turns.	(5) Annealed.
No. 1	1.79	1.3	0.0	2.2	...
2	3.13	1.4	0.0	2.4	0.5
3	4.20	1.6	0.1	2.5	0.6
4	4.87	1.8	0.0	3.2	0.5
5	5.52	1.9	0.3	3.6	0.2
6	5.98	1.8	0.4	5.1	0.3
7	6.48	1.4	0.3	3.6	0.8
8	6.60	1.9	0.4	3.8	1.0
9	6.69	1.6	0.3	3.5	0.7
10	6.48	1.7	−0.3	4.3	0.8
11	6.06	2.3	0.2	4.4	...
12	5.66	2.3	0.4	...	...
13	5.20	2.9	−0.2	...	...
14	4.91	3.0	0.3	...	...

PART II. EFFECT OF ANNEALING ON THE ELECTRIC RESISTANCE AND MECHANICAL PROPERTIES OF COLD-WORKED METALS.

As remarked in the preceding sections, the electric resistance of cold-worked metals may be reduced to its normal value if they are annealed at proper temperatures. Systematic researches in this line have hitherto been almost entirely confined in copper,[1] with the exception of

(1) Gewecke (Martens-Heyn, Materialienkunde, II A, 305–6); Credner (Tammann, Lehrbuch d. Metallog. (1923), 149); Bardwell (Bureau of Standards, Copper, 52).

those of Lea, Collins and Reeve[1] and Guillet and Ballay,[2] who have studied the effect of annealing on the resistance of brass. Guillet and Ballay have also studied the variation of electric resistance of cold-drawn brasses (Cu = 68 and 60 %) and nickel-copper (Ni = 40 %) during heating. The present writer considers that the test in this line has practical importance for metals to be used as electrical conductors or resistance wires, and further supplies some valuable informations as regards the internal changes to be produced in metals by working and annealing. The present research has been undertaken to make these points clear by the following tests :—

(1) Variation in electric resistance during heating of cold-worked metals was measured;

(2) After annealing at various temperatures for short period the electric resistance was determined;

(3) The specimens used for the preceding test were subjected to tensile test;

(4) After annealing at various temperatures Brinell hardness and microstructure were examined.

Results of tests such as (3) and (4) have been frequently published by many investigators, but the change at lower temperature range has not been made so fully clear as that at higher temperature range.

I. Variation of the Electric Resistance during Heating of Cold-Rolled Plates.

Test-pieces, 8 mm wide and 20 cm long, were taken from cold-rolled plates parallel and right angles to the direction of rolling and the variation of the resistance during heating was determined. The procedure of the test was as follows: The specimen was introduced into a horizontal tube furnace, and constant current was passed the specimen through copper leads attached to its both ends. Two thin soft copper

(1) J. Inst. Met. (1923), No. 1, 223.
(2) *loc. cit.*

wires served as potential leads, the one pair of their ends being fastened to two points 15 cm apart on the specimen, while the other pair to a Leeds and Northrup's potentiometer. The potential difference was first determined at ordinary temperatures and then heating current was put on the furnace and the potentials were determined at various temperatures during heating. The rate of heating was about 3° per minute. The specimens subjected to this test were cold-rolled 4 L-, 4 T-, 3 L-, 2 L- and annealed 1 L-specimens, and some results obtained are graphically shown in Fig. 4, where the ordinate represents the specific resistance and the abscissa the temperature. As the results of tests, the following points were noticed:—

1. In the case of 70 : 30 and 60 : 40 brasses, aluminium-bronze, bronzes (Sn = 3 and 9 %) and duralumin, abnormal changes beginning to take place at the following temperatures were noticed:—

Alloys.		Beginning temperature of abnormal change.			
		2 L	3 L	4 L	4 T
70 : 30 brass	(1)	190°	190°	190°	190°
	(2)	320	315	310	310
60 : 40 brass	(1)	185	180	165	170
	(2)	330	310	305	305
Aluminium-bronze	(1)	...	180	180	180
	(2)	...	345	340	340
Phosphor-bronze (Sn=3%)	(1)	205 320	200 310	195 300	200 300
	(2)	?	390	395	390
Phosphor-bronze (Sn=9%)	(1)	205	200	200	200
	(2)	320	320	320	320
Duralumin	(1)	200	200	200	200
	(2)	...	...	...	...

In the above table, (1) refers to the beginning temperature of an abnormal change, which takes place at lower temperature range, while (2) to that at higher temperature range. If such abnormal change does not take place, the resistance-temperature curve should take the

course as shown by the dotted line in the figure. The second change is obviously due to the "recrystallisation" of cold-worked metals; this was confirmed by microscopic and other tests as will be shown later. The first change has never been remarked except by Guillet and Ballay,[1] and the nature of which will be discussed in later sections.

2. The changes in L- and T-specimens are quite similar, as shown in Fig. 4. This was true for all the alloys tested.

3. In the case of copper, β-brass, manganese-copper and aluminium, no abnormal change could be detected by this method. But it could be found in the resistance-annealing temperature curve as will be shown in the next section.

4. The resistance-temperature curves of annealed specimens were quite smooth and no abnormal change could be found.

A further test was made on aluminium-bronze, in which the heating rate was considerably reduced. The result obtained is graphically shown in Fig. 4, from which it may be concluded that a marked decrease in the electric resistance takes place as the result of the abnormal change and that the course of the curve in the temperature range, at which the abnormal change takes place, is somewhat different, the curve being convex against the temperature axis in this case, instead of being concave as in the previous case: This shows that the progress of the abnormal change becomes quite appreciable at lower temperature if sufficient time is allowed for.

II. Effect of Annealing on the Electric Resistance and Mechanical Properties of Cold-Rolled Plates.

Though the method above described is quite simple, it is not suitable to detect small changes such as to be found in copper, aluminium and others, and also to determine the magnitude of the decrease in electric resistance due to the abnormal change. Moreover the temperature from

(1) Rev. Mét. **20,** (1923), 398; they noticed similar changes in 68:32 and 60:40 brasses, but gave no explanation about them.

which the abnormal change begins to take place cannot be accurately determined. The writer therefore examined the electric resistance of 3 L-specimens after annealing at various temperatures for 10 minutes. The specimens were allowed to cool in an open air after annealing. The results obtained are shown in Table IV and Fig. 5.

TABLE IV.

Effect of Annealing on the Specific Resistance and Tensile Properties of Plate.

σ = specific resistance in microohm,
T. S. = tensile strength in kg per sq. mm,
elong = elongation in percent on 50 mm.

Annealing temp.	(a) Copper.			(b) 70 : 30 brass.			(c) 60 : 40 brass.		
	$\sigma_{23°}$	T. S.	elong.	$\sigma_{25°}$	T. S.	elong.	$\sigma_{26°}$	T. S.	elong.
as rolled	1.99	40.0	4	6.87	65.2	8	6.54	64.4	12
60°	1.99	39.9	5	6.86	65.3	8	6.52	64.3	13
100	1.99	38.9	4	6.88	65.0	8	6.52	63.7	14
135	1.99	39.6	5	6.84	64.1	8	6.51	62.7	14
155	1.99	39.5	5	6.76	64.8	8	6.53	61.8	16
180	1.99	39.5	5	6.70	65.8	8	6.38	61.5	15
210	1.99	39.5	5	6.63	68.4	7	6.34	60.6	19
230	1.98	37.6	5.5	6.61	68.1	7.5	6.33	60.7	18
260	1.98	37.0	6	6.58	66.9	8	6.32	60.0	19
285	1.97	38.0	5	6.54	64.0	8	6.32	59.0	20
305	1.97	37.8	6	6.53	62.2	8	6.32	58.2	20
335	1.96	30.4	16	6.36	48.0	31	6.22	51.6	29
360	1.95	25.9	38	6.26	43.4	40	6.23	47.6	36
385	1.95	25.5	39	6.22	42.9	40	6.22	45.6	37
410	1.65	25.1	38	6.23	41.1	43	6.21	44.8	40
435	...	...	...	...	...	...	...	....	...
460	1.95	25.0	40	6.20	40.1	43	6.23	42.9	44
510	1.96	24.6	40	6.22	39.2	45	6.28	42.1	45
560	1.96	25.1	40	6.21	37.5	49	6.36	41.0	47
615	...	...	...	6.23	36.7	48	6.36	40.6	46
720	1.97	24.9	40	...	...	...	...	...	...

TABLE IV. (*Continued*).

Annealing temp.	(d) β-brass.	(e) Al-bronze.			(f) P-bronze (3 %).			(g) P-bronze (9 %).		
	$\sigma_{26°}$	$\sigma_{25°}$	T. S.	elong.	$\sigma_{25°}$	T. S.	elong.	$\sigma_{21°}$	T. S.	elong.
as rolled	5.05	12.66	75.8	8	7.86	64.9	8.5	15.07	82.2	6
60°	5.04	.....	.....	...	.....	.....	...	15.08	83.3	6
100	5.02	12.68	76.3	7	7.84	65.5	9	15.07	82.5	6
135	5.00	.....	.....	...	.....	.....	...	15.07	82.1	6
155	4.99	12.59	77.2	8	7.77	65.4	8	15.05	82.5	8
180	5.00	12.42	77.2	7	7.69	65.5	9	15.06	81.3	8
210	4.97	12.18	78.6	6	7.66	64.2	11	14.82	78.6	9
230	.....	12.15	79.7	6	7.66	64.2	11	14.78	78.6	9
260	5.00	11.87	79.7	6	7.66	63.7	12	14.70	76.9	10
285	.....	11.86	79.7	5	7.64	62.2	14	14.68	74.6	13
305	4.97	11.90	79.0	6	7.57	62.1	14	14.65	74.9	15
335	4.95	11.74	76.9	6	7.42	62.5	14	14.60	70.9	16
360	4.95	11.58	67.4	13	7.25	62.0	14	14.50	62.9	17
385	.....	11.43	62.7	17	7.20	61.7	15	14.43	54.2	19
410	4.92	11.32	55.4	30	7.04	60.1	15	14.38	48.4	23
435	.....	.....	.....	...	6.99	58.7	16	.....	... ..	...
460	4.90	11.17	52.3	40	7.00	57.0	17	14.47	47.5	34
510	4.94	11.23	51.1	40	7.07	50.3	21	14.50	46.1	39
560	.....	.....	.....	...	7.36	43.7	26	14.57	45.8	42
615	.....	.....	.....	...	7.58	41.1	36	14.63	43.8	44
720	.....	.....	.....	...	.....	.....	...	.....	.....	...

Annealing temp.	(h) Mn-copper.			(i) Duralumin.			Annealing temp.	(j) Aluminium.		
	$\sigma_{22°}$	T. S.	elong.	$\sigma_{25°}$	T. S.	elong.		$\sigma_{24°}$	T. S.	elong.
as rolled	15.27	47.8	8	4.44	40.3	6	as alloed	3.32	18.6	7
60°	.....	.....	...	.....	.....	...	70°	3.32	18.3	6
100	15.25	47.6	8	.....	.....	...	120	3.33	18.2	6
135	.....	.....	...	4.41	40.1	6	170	3.34	17.5	7
155	15.26	48.0	9	4.42	40.9	7	195	3.28	17.1	8
180	15.25	48.2	8	4.41	40.8	7	215	3.22	16.4	9
210	15.26	48.0	8	4.15	37.7	7	240	3.20	15.8	8
230	15.23	45.8	9	4.08	37.2	7.5	265	3.16	14.7	8
260	15.18	45.8	9	3.88	31.1	7	290	3.14	14.9	9
285	15.14	46.2	10	3.87	28.3	8	315	3.12	12.9	14
305	15.13	45.5	11	3.84	29.4	8	340	3.10	12.0	18
335	15.12	45.5	11	3.88	27.0	9	365	3.19	11.9	26
360	15.15	46.0	11	3.89	26.2	10	415	3.21	12.3	25
385	15.13	46.0	11	3.93	26.7	12	465	3.22	12.2	24
410	15.09	44.6	11	4.08	29.3	16				
435	15.09	44.0	13	.....	.....	...				
460	15.08	42.2	16	4.57	35.2	15				
510	15.09	34.6	36	4.67	39.0	14				
560	15.09	33.2	38	.....	.....	...				
615	15.07	33.1	38	.....	.. ...	...				
720	.....	.....	...	.....	.....	...				

These specimens were then subjected to the tension test and the tensile strength and elongation thus obtained are also given in the preceding table and Fig. 5. For the hardness and microspcoic tests, specimens were taken from 4-plates. The results of hardness test are given in Table V and also in Fig. 5.

TABLE V.

Effect of Annealing on the Hardness of Plate.

Annealing temp.	Copper.	70 : 30 brass.	60 : 40 brass.	Al bronze.	P-bronze (3 %)	P-bronze (9 %)	Aluminium.	Duralumin.	Annealing temp.	β-brass.	Mn.-copper.
as rolled	107	167	175	205	169	209	49	100	as rolled	167	146
70°	109	168	177	204	169	212	49	...	70°	167	151
120	108	171	177	206	173	213	49	...	110	166	146
145	110	...	...	...	...	...	...	101	135	150	147
170	110	174	171	209	173	218	48	100	160	137	150
195	109	179	167	210	173	216	47·5	99	180	123	144
215	109	181	161	209	169	216	46	94	210	110	146
240	110	177	159	216	171	218	44	84	240	106	149
265	108	174	158	217	169	208	42	80	265	107	135
290	108	171	157	222	166	204	39	74	290	108	132
315	106	137	139	218	162	199	33	72	320	109	131
340	84	104	105	192	163	190	27	62	340	106	130
365	51	92	87	152	161	125	25	60	370	92	130
390	45	...	85	138	...	119	...	62	395	91	124
415	45	87	82	123	155	117	25	76	425	93	123
465	45	82	74	114	140	109	...	...	445	...	118
515	45	78	73	111	118	108	...	...	470	91	96
600	...	...	...	...	76	...	...	...	520	92	63
									570	91	65
									625	91	64
									730	89	...

From these results the following points were noticed :—

1. In the resistance-annealing temperature curves, we notice the decrease in resistance beginning from the temperatures given below :—

Metals.	Peginning temperature of		$\Delta\sigma_1/(\Delta\sigma_1+\Delta\sigma_2)$
	first decrease	second decrease	
Copper	200°	320°	0.45
70 : 30 brass	160	310	0.51
60 : 40 brass	150	310	0.58
β-brass	110	330	0.46
Aluminium-bronze	160	330	0.54
Phosphor-bronze (Sn = 3 %) . . .	150 300	390	0.75
„ „ (Sn = 9 %) . . .	180	330	0.62
Manganese-copper	230	400	0.67
Aluminium	170	.....	.....
Duralumin	180	.....	.....

If the above temperatures are compared with those given in the preceding section, we find satisfactory agreements in the temperatures from which the second change begins to occur, while the beginning temperatures of the first change were found to be lower than those given before. This may be partly because the annealing time is somewhat longer in this case and partly the beginning of the first change is less marked in the former case, as the first change takes place more gradually as compared with the second.

2. The magnitudes of abnormal changes in electric resistance corresponding to the first and second changes are nearly equal as shown in the preceding table.[1] But in the case of aluminium and duralumin, the second change is so small that its magnitude could not be accurately determined.

3. Corresponding to the first decrease in electric resistance, a gradual rise followed by a fall is found in the tensile strength and

(1) Where $\Delta\sigma_1$ represents the decrease of resistance from the beginning of the first change to that of the second, and $\Delta\sigma_2$ the decrease from the beginning of the second change to the minimum resistance.

hardness of 70 : 30 brass and aluminium-bronze,[1] and a gradual fall in those of other metals and alloys (Fig. 5). A gradual increase in elongation is also noticed in most metals and alloys, with the exception of 70 : 30 brass and aluminium-bronze. Corresponding to the second decrease in resistance, very pronounced decrease in the tensile strength and hardness and marked increase in elongation are found in copper and its alloys.[2] A similar change is also noticed in aluminium and duralumin, though in less marked degree. That the process of annealing occurs in two stages in most metals has already been remarked by Rosenhain.[3] Here it is shown by the writer that corresponding to the change in mechanical properties the electric resistance also changes in two steps.

4. From the examination of the microstructure of annealed specimens it may be concluded that the second change is due to the recrystallisation. But the change in microstructure corresponding to the first change could not be found at all.

5. As already remarked, the increase in hardness and tensile strength by low-temperature annealing is observable in 70 : 30 brass,[4] aluminium-bronze and phosphor-bronze (Sn = 9 %). But the writer's present investigation was not extended so far as to make the nature of this change fully clear.

III. Variation of the Electric Resistance during Heating of Cold-drawn Rods.

The method of test was similar to the case of plates. The results obtained are graphically shown in Fig. 6, which show that abnormal changes begin to take place from the following temperatures :—

---

(1) Similar change may be noticed in the hardness of phosphor-bronze (Sn = 9 %).

(2) With the exception of β-brass, in which the first change is more marked than the second.

(3) "Introduction to the Study of Physical Metallurgy." 266–8.

(4) Slight hardening of 70 : 30 brass by a proper low-temperature annealing has been confirmed and discussed by many workers (Carpenter and Traverner, J. Inst. Met. (1918), No. 1, 117–25, de Forest, Proc. Am. Soc. Test. Mat. 1918, Part 2, 207–8; Howe, *ibid*, 218; Moore and Beckinsale, J. Inst. Met. (1920), No. 1, 225; (1922), No. 1, 149; Upthengrove and Harbert, Trans. A. I. M. M. E. **68**, (1923), 725; Jeffries and Archer, Science of Metals, 189–91).

Alloys.	Beginning temperature of abnormal change.		
	1	2	3
70 : 30 brass . . . . . (1)	190°	185°	185°
(2)	340	315	305
60 : 30 brass . . . . . (1)	190	170	160
(2)	330	325	300
Phosphor-bronze (Sn = 3 %) (1)	195	195	200
(2)	315	315	320
	405	390	395
Duralumin . . . . . (1)	200	200	200
(2)	...	...	...

These temperatures agree well with those obtained in the case of plates, from which it may be concluded that the methods of cold-working have little effect on these temperatures.

IV. Effect of Annealing on the Electric Resistance and Mechanical Properties of Cold drawn Rods.

The method of test was also similar to that used in the case of plates. Some results obtained are given in Table VI and graphically in Fig. 7.

TABLE VI.

Effect of Annealing on the Specific Resistance and Tensile Properties of Rod.

σ = specific resistance in microohm,
T. S. = tensile strength in kg per sq. mm,
elong = elongation in percent on 50 mm.

Annealing temp.	Copper (2).			ann'g temp.	70 : 30 brass (1).		
	$\sigma_{23°}$	T. S.	elong.		$\sigma_{23°}$	T. S.	elong.
as drawn	1.83	41.7	7.5	as drawn	6.75	59.5	10
60°	1.83	40.6	8	70°	6.75	60.5	9
100	1.83	41.5	8	120	6.74	60.8	8
135	1.83	41.5	7	145	6.75	.....	...
155	1.83	41.6	8	170	6.68	60.1	9

TABLE VI. (*Continued*).

Annealing temp.	Copper (2).			Annealing temp.	70 : 30 brass (1).		
	σ_{230}	T. S.	elong.		σ_{230}	T. S.	elong.
180°	1.83	41.2	8	195	6.67	59.8	9
210	1.83	41.5	7.5	215	6.58	.....	...
230	1.83	40.8	7	240	6.60	59.0	9
260	1.83	41.5	8	265	6.57	.....	...
285	1.82	40.4	9.5	290	6.58	57.9	11
305	1.82	37.3	10	315	6.57	57.3	13
335	1.82	37.0	12	340	6.49	56.0	15
360	1.81	25.9	39	365	6.34	43.3	37
385	1.80	25.9	41	390	6.31	.....	...
410	1.80	25.6	42	415	6.30	41.6	47
460	1.80	25.5	41	465	6.31	40.7	51
510	1.80	25.2	40	515	6.29	39.8	50
615	1.80	25.2	42	565	6.31	38.1	50
720	1.82	25.5	42	615	6.31	36.4	54

Annealing temp.	70 : 30 brass (2).			70 : 30 brass (3).			60 : 40 brass (3).		
	σ_{220}	T. S.	elong.	σ_{220}	T. S.	elong.	σ_{220}	T. S.	elong.
as drawn	7.10	73.4	7	7.32	81.5	6	7.36	88.2	6
70°	7.10	72.8	6.5	7.32	82.2	6	7.37	88.5	5
120	7.08	74.3	6.5	7.33	83.6	5.5	7.38	88.0	6
145	.....	.....	...	.....	.....	...	7.32	.....	...
170	7.00	74.3	6 5	7.20	84.8	5.5	7.15	87.7	5
195	6.94	76.8	6	7.15	87.9	5.5	7.14	84.4	6
215	6.87	76.7	6	6.97	88.0	6	7.07	83.7	8.5
240	6.79	75.2	6.5	6.94	86.4	6	7.03	82.0	9
265	6.75	74.3	6	6.91	84.0	6	6.97	.....	...
290	6.73	70.7	7	6.85	75.2	6	6.84	80.4	10
315	6.38	52.9	25	6.38	47.1	32	6.60	63.9	22
340	6.38	44.8	37	6.38	46.0	37	6.57	60.4	27
365	6.38	44.1	41	6.38	44.9	38	6.63	58.9	33
390	.....	.....	...	.....	.....	...	6.65	57.0	34
415	6.36	42.3	42	6.36	44.3	40	6.67	55.3	35
465	6.36	41.2	44	6.36	42.2	43	6.75	53.9	35
515	6.35	40.5	48	6.35	40.2	44	6.82	50.3	35
565	6.34	37.8	51	6.34	38.8	48	6.76	51.0	33
615	6.35	38.3	52	6.35	37.3	52	.....	.....	...

TABLE VI. (*Continued*).

Annealing temp.	P-bronze (1).			P-bronze (2).		P-bronze (3).		Duralumin (2).		
	$\sigma_{30°}$	T. S.	elong.	T. S.	elong.	T. S.	elong.	$\sigma_{22°}$	T. S.	elong.
as drawn	8.15	54.2	9	64.2	7	72.1	6	3.75	37.3	5
70°	8.13	54.3	10	63.9	7	.....	...	3.74	36.9	5
120	8.14	53.5	10	64.9	7	71.9	6	3.74	36.5	6
145	8.14	54.1	10	.....	...	.....	...	.....	.....	...
170	8.14	.....	...	64.9	7	.....	...	3.73	36.6	6
195	8.11	54.2	14	64.2	8	71.6	6	3.67	35.8	8
215	8.05	53.2	14	62.2	10	69.5	6	3.60	32.5	8
240	8.05	.....	...	61.9	10	66.3	9	3.58	30.3	8.5
265	8.05	52.2	17	59.3	12	66.1	10.5	3.54	28.3	8
290	8.05	51.8	18	59.6	13	65.7	13	3.54	28.1	10
315	8.05	51.3	19	58.4	15	63.3	14	3.57	27.1	11.5
340	7.93	49.6	20	57.1	15	62.0	14	3.61	25.7	16
365	7.92	49.6	20	56.8	17	61.6	16	3.68	24.7	17
390	7.93	49.8	20	56.6	17	60.1	15	3.77	28.8	21
415	7.87	49.2	21	55.5	18	54.1	20	3.87	31.9	20
465	7.83	45.0	27	47.3	25	41.8	38			
515	7.80	38.6	40	38.9	41	39.7	43			
565	7.83	36.8	45	38.4	42	39.3	43			
615	7.88	36.7	45	37.8	44	38.0	42			

From these results the following table was obtained:—

Metals.	Beginning temperature of		$\Delta\sigma_1/(\Delta\sigma_1+\Delta\sigma_2)$.
	first decrease	second decrease	
Copper (2)	260°	330°	0.37
70:30 brass (1)	160	330	0.39
„ „ (2)	150	290	0.49
„ „ (3)	140	290	0.48
60:40 brass (3)	150	290	0.48
Phosphor-bronze (1)	200 320	400	0.67
Duralumin (2)	180	—	—

From these results we know that the conclusion arrived at in the case of plates holds fairly well in this case too.

V. Discussion of Results.

The results so far obtained may be summarised as follows:— The electric resistance of cold-worked copper and its alloys decreases in two steps by annealing. The decrease corresponding to the latter step is obviously due to the recrystallisation and the mechanical properties also suffer a considerable change. From a lower temperature range, however, the decrease in the electric resistance beings to occur, the magnitude of which amounting nearly the half of the total decrease. A small and gradual change in mechanical properties corresponding to this decrease is also observable. In aluminium and duralumin similar changes may be noticed. These were established both in the case of plates and rods.

As the results of the present research the following facts are established as regards the change in electric resistance: (1) the electric resistance increases as the result of cold-deformation, whether the deformation is produced by rolling, drawing or twisting; (2) there exists no systematic difference between the electric resistances of cold-rolled plates measured along and perpendicular to the direction of rolling; (3) when metals are annealed, the resistance decreases in two steps.

It has been already remarked by the present writer that the increase of electric resistance may be ascribed to the straining of space lattice caused by cold-deformation. Recently Bridgman,[1] Fukuta[2] and Lees and Calthrop[3] have shown that longitudinal or torsional stress causes to increase the electric resistance of some metal wires, though the stress remains within the elastic limit. If the stress increases still further and metals are plastically deformed, the increase in resistance also becomes considerable. When the external forces are removed, the most part of strain may be released and the resistance also decreases and approaches

(1) Proc. Amer. Acad. **57,** (1922), 41; **59,** (1923), 119.
(2) Sci. Rep. **11,** (1922), 131.
(3) Proc. Phy. Soc. London. **35,** (1923), 225; Engg. **117,** (1924), 288.

to its original value. But some portion of strain and consequently of increased resistance remain as such, as there exists "concealed stress"[1] within metals. Similar phenomena may occur in cold-worked metals. Moreover, in a certain stage of cold-deformation, heterogenous strain[2] may be produced in the space lattice. This contributes to the increase in electric resistance too. When the metals are heated, the strains thus produced begin to decrease from temperatures far below the beginning temperature of the recrystallisation. The first change in electric resistance corresponds to this stage of release in strain. This proceeds at first rapidly and then more slowly with the rise of temperature and the last trace of strain may be completely removed by the recrystallisation; this later stage corresponds to the second change in the electric resistance.

PART III. EFFECT OF ANNEALING ON THE LENTH OF COLD WORKED METALS.

I. Introduction.

The effect of cold-working on the density of metals has been frequently investigated. Kahlbaum and Sturm,[3] Spring,[4] Johnston and Adams[5] determined the densities of various metals before and after cold-deformation, while Heyn and Bauer,[6] Goerens,[7] Landon[8] and O'Neill[9] determined the density of iron or mild steel after drawing, twisting or stretching. On the other hand, Alkins[10] and Johnson[11] have systematically investigated the effect of cold-drawing and rolling on

(1) "Verborgene spannung" (Heyn, Festschrift d. Kaiser Wilhelm Gesellschaft, (1921), 121).

(2) *cf.* Czochralski, Zs. Metallk. **15**, (1923), 128–32.

(3) Zs. anorg. Chem. **46**, (1905), 215.

(4) *cf. ibid.* **76**, (1912), 293–4.

(5) *ibid.* **76**, (1912), 274.

(6) Int. Zs. Metallog. **1**, (1911), 36–42.

(7) Ir. St. Inst. Carnegie Mem. 1913.

(8) J. Ir. St. Iust. (1923), No. 2, 455.

(9) J. Ir. St. Inst. (1924), No. 1, 93.

(10) J. Inst. Met. (1920), No. 1, 403–17.

(11) *ibid*, (1920), No. 1, 473; (1921), No. 2, 175.

the density of copper. The results of these investigations, with the exception of that of Johnson, conclusively show that the density of metals decreases as the result of cold-working. To explain this decrease various theories have been proposed: among them those of Kahlbaum and Sturm,[1] Spring,[2] Heyn and Bauer[3] and of Tammann[4] may be mentioned. Johnson however have clearly shown that rolling produces the increase of density of copper. This can not be explained by the theories above mentioned, according to which the decrease is to be expected in this case too. Moreover, the results of tests of Heyn and Bauer, Goerens, and Lee, Collins and Reeve[5] on the effect of annealing on the density of cold-worked metals show that the effect is already noticeable by annealing at temperatures so low as the recrystallisation can not take place at all. This is also not easy to explain by most theories hitherto advanced, according to which the change in density by annealing, at least most part of it, is to be expected to accompany the recrystallisation. So it seems to the writer that a further test in this line is desirable to understand the nature of the change.

As already well known, the variation in density due to working is very small and seldom exceeds 0.2 percent, so the test may be subjected to unavoidable experimental errors. The writer therefore determined to investigate the change from an another direction which has never been tried. The method was as follows:—Test-specimens which were taken from cold-rolled plates, lengthwise along and perpendicular to the direction of rolling, and also from cold-drawn rods, were introduced into a horizontal tube furnace and the variation of the length of the specimen was determined up to 500.° This method allows to trace the changes during heating in one and the same specimen and is suitable to determine such a minor change as under consideration. But the results so far

(1) *loc. cit.*
(2) *loc. cit.*
(3) *loc. cit.*
(4) Lehrbuch der Metallographie, (1923), 137.
(5) J. Inst. Met. (1923), No. 1, 217.

obtained only give the variation in length in one (for rod) or two (for plate) directions in cold-worked metals, and the cubical expansion or contraction, i. e., the variation of specific volume, can not be determined there-from, as the cold-worked metal may not behave as an isotropic substance as regards the thermal expansion. This is a serious disadvantage of the present method, but the results obtained may throw some light on the discussion of the problem under consideration.

The apparatus used was constructed by the writer with slight modification of a differential dilatometer devised by Dr. Konno.[1] The specimens, about 6 mm thick[2] and 5 cm long, were taken from plates and rods most severely deformed. As the neutral body the annealed metal having the same composition with the specimen under test was used and the rate of heating was about 3° per minute.

II. Results of Experiments.

(i) *Cold-rolled plates.* As already remarked, the effect of cold-working on the density is so small that in some metals and alloys no distinct change could be detected even by the present method. Some typical results are graphically shown in Fig. 8, where the ordinate represents the percentage increase or decrease in length[3] and the abscissa the temperature. As the length of the specimen and of the neutral body were not strictly identical, the elongation-temperature curve sometimes takes upward or downward course as shown in the figure.

---

(1) Sci. Rep. **12**, (1923), 127.

(2) The specimens taken from plates were made to the size by turning 8 mm square rods.

(3) As calculated by the following formula,

$$\text{percentage change in length} = \frac{\delta l - \delta l_0}{l} \times 100 = \frac{nd}{2Dl} \times 100,$$

where δl = length change of specimen,
δl_0 = „ „ „ neutral body,
n = scale reading,
d = diameter of roller carrying mirror = 1.42 mm,
D = scale distance = 180 cm,
l = length of specimen = 5 cm.

From these results we may notice abnormal changes beginning to take place from the temperatures below :—

Alloys.		Beginning temperature of abnormal change.	
		4 L	4 T
70 : 30 brass	(1)	200°	200°
	(2)	310	315
60 : 40 brass	(1)	140	160
	(2)	310	315
Aluminium-bronze	(1)	190	180
	(2)	340	350
Phosphor-bronze (Sn = 3%)	(1)	150	210
	(2)	385	400
Phosphor-bronze (Sn = 9%)	(1)	190	190
	(2)	330	340

These temperatures agree well with those obtained by the similar test in electric resistance, except the first changes in 4 L-specimens of 60 : 40 brass and phosphor-bronze (Sn = 3 %). This discrepancy will be discussed in a later section.

As clearly shown in the figure, very remarkable differences may be noticed between the L- and T-specimens : In the L-specimen abnormal *expansions* are found while in the T-specimen *contractions*,[1] and the magnitude of the second abnormal change is generally smaller in the T-specimens.

The change in length after the recrystallisation is completed is not appreciable with the exception of 60 : 40 brass, in which large expansion is found in either L- or T-specimen. This large expansion is also found in the cold-drawn 60 : 40 brass rod.

(2) *Cold-drawn rods.* A similar test was made on rods and the results obtained are shown in Fig. 9, a. In this case too abnormal changes beginning from the following temperatures may be noticed :—

(1) Price and Davidson (Trans. Amer. Inst. Met. **10**, (1916), 151) have shown that L-specimens taken from cold-rolled brass plates, which contain 64.7 percent of copper and were reduced more than 40 percent in thickness, elongate after annealing at about 300°, while T-specimens contract after similar treatment.

Alloys.	Beginning temperature of abnormal change.
70 : 30 brass	{110° 315
60 : 40 brass	{130 315
Phosphor-bronze (Sn = 3%)	{150 ...

In this case the beginning temperature of the first change is quite low and the second change is scarcely observable in 70 : 30 and 60 : 40 brasses. This point will be discussed in the following section.

To confirm the above results, a further test was made on thin brass wires containing 69.71 and 60.13 percent of copper respectively. They were 3.2 mm thick and reduced 55.6 percent in sectional area by cold-drawing. Specimens having the length of 20 cm were taken from these wires and annealed for 30 minutes at the temperatures given in the table below. The length of the specimen was determined before and after annealing, and the results obtained are shown in Fig. 9, b and the following table :—

Annealing temperature.	Percentage decrease in length.	
	70 : 30 brass.	60 : 40 brass.
120°	0.03	0.05
215	0.05	0.09
265	0.07	0.16
315	0.07	0.15
360	0.06	0.14
410	0.10	0.12
460	0.08	0.05
510	0.09	+ 0.07

These results confirm those already obtained; slight difference between them may be attributed to the difference in the degree of deforma-

tion, the thickness of specimens and particularly to the difference in length of annealing time.

III. Discussion of Results.

The results so far obtained may be summed up as follows:—

The length of cold-worked metals varies in two steps by heating. The beginning temperatures of these changes agree well with those found in the case of electric resistance, except the first change in 4 L-specimens of 60 : 40 brass and phosphor-bronze (Sn = 3%) plates and in cold-drawn rods. The changes found in the T-specimen and the rod are contraction while those in the L-specimen expansion, and the percentage decrease or increase seldom exceeds 0.05 percent in plates while it reaches 0.1 to 0.15 percent in rods.

Since the change in length taking place during heating of cold-rolled plate is quite similar to that in electric resistance as regards the beginning temperature of abnormal change and other aspects, it is natural to consider that the change under consideration is also due to the release of strain, which is produced in space lattice by cold working. But a essential difference in the changes in length and resistance during heating may not be over-looked: While the changes in electric resistance to be found in L- and T-specimens are quite similar to each other, those in length occur in opposite sense.

The change in length observable in rods is quite different from that in plates; the abnormal change begins to occur from much lower temperature and its magnitude is three or four times larger as compared with that in plates. These may be attributed to the differences in the internal mechanism of rolling and drawing, and consequently to the difference in the intensity and mode of distribution of the "internal stress" ("Eigenspannung" as considered by Heyn[1]).

---

(1) Int. Zs. Metallog. **1**, (1911), 16; J. Inst. Met. (1914), No. 2, 3; St. Eis. **37**, (1917), 442, 475, 497.

The difference in the condition of experiments,—i. e., specimens taken from plates were turned from 8 mm square to 6 mm round rod—may also affect to some degree. The lowering of the beginning temperature of the first change may be noticed in 4 L-specimens of 60 : 40 brass and phosphor bronze, in which it was found that "internal stress" exists in some marked degree. Thus the changes taking place in the T-specimens, which is believed to be free from "internal stress," is quite similar to those found in the case of electric resistance with respect to its beginning temperature. The "internal stress" which so much affects the change of length is believed to have little effect on the electric resistance, as there is no systematic difference in resistances of L- and T-specimens.(1)

In summarising, strain produced in space lattice by cold-working contributes to the variation in electric resistance and length. By heating, the release of strain begins to occur from low temperature and terminates as recrystallisation is complete. "Internal stress" also contributes to the change of length in rods and some L-specimens taken from plates. In this case the change is large and begins to take place from much lower temperature.

SUMMARY.

The present research may be summarised as follows :—

1. The effect of cold-working on some physical properties of copper, aluminium and their alloys was studied.

2. By cold-working (rolling, drawing and twisting), the electric resistance of metals becomes larger, but there exists no systematic difference between the resistance of the specimens taken parallel and right angles to the direction of rolling.

---

(1) This was also confirmed by a test on 70 : 30 brass sheet, 0.1 mm thick, in which the abnormal change in electric resistance on heating takes place quite similarly to that in plate and rod, notwithstanding the wide difference existing in the intensities and perhaps in the modes of distribution of internal stress between them.

3. The increase in resistance by twisting disappears by proper annealing.

4. Neither the regularity in the orientation of metallic crystallites nor the formation of minute cracks within metals, as considered by Tammann, should not be the principal cause of the increase of resistance by cold-working. It may be ascribed to the straining in space lattice produced by cold-working.

5. Specimens taken parallel to the direction of rolling have lower strength and higher elongation than those taken right angles to the said direction.

6. By annealing, the electric resistance of cold-worked metals decreases in two steps. The decrease corresponding to the latter step is obviously due to the recrystallisation, and the mechanical properties also suffer a considerable change. From lower temperature range, however, the decrease in the resistance begins to occur, the magnitude of which amounting nearly the half of the total increase. A small and gradual change in mechanical properties corresponding to this decrease is also noticeable.

7. When metals are heated, the strain in space lattice set up by cold-working begin to disappear from temperatures far below the beginning temperature of the recrystallisation. The first step of the decrease in electric resistance corresponds to this stage of release in strain. This proceeds at first rapidly and then more slowly with the rise of temperature, and the last trace of strain may be completely removed by the recrystallisation; this later stage corresponds to the second change in the resistance.

8. The length of cold-rolled or drawn metals also varies in two steps by heating. The change is *expansion* in the specimens taken parallel to the direction of cold-rolling, while *contraction* is found in cold-drawn rods and the specimens taken from plates right angles to the direction of rolling. The general feature of the change is quite similar to that in the electric resistance. But in some specimens taken parallel to the direction of rolling and in cold-drawn rods, in which "internal

stress" exists in some marked degree, the change in the length begins to take place from much lower temperatures.

9. The "internal stress" which so much affects the change of length is believed to have little effect on the electric resistance.

(Research Laboratory, Sumitomo Copper Works, Osaka, Feb. 1925.)

Pl. I.

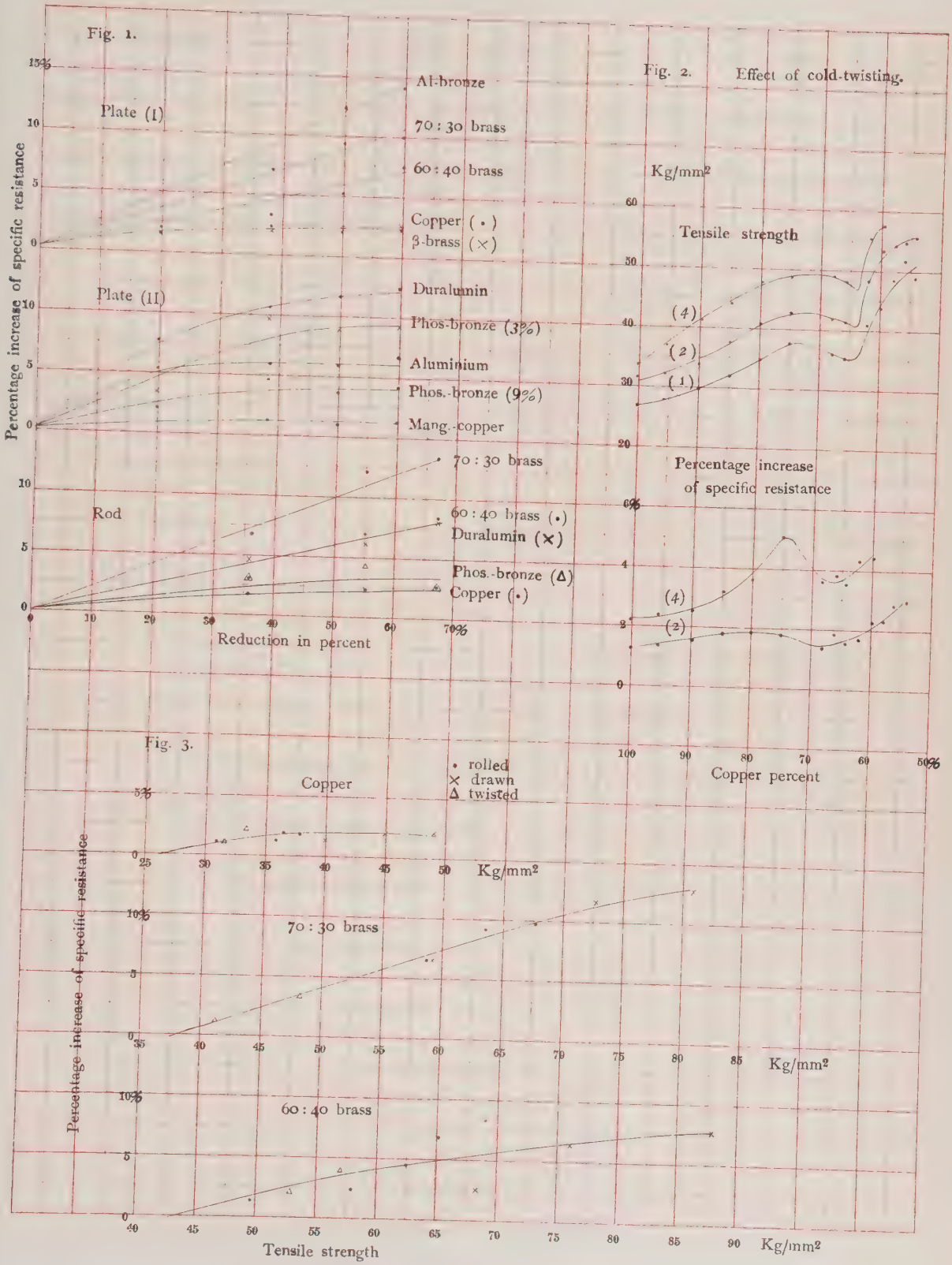
Fig. 1.
Plate (I)
Al-bronze
70 : 30 brass
60 : 40 brass
Copper (•)
β-brass (×)
Plate (II)
Duralumin
Phos-bronze (3%)
Aluminium
Phos.-bronze (9%)
Mang.-copper
Rod
70 : 30 brass
60 : 40 brass (•)
Duralumin (×)
Phos.-bronze (Δ)
Copper (•)
Percentage increase of specific resistance
Reduction in percent
Fig. 2. Effect of cold-twisting.
Kg/mm²
Tensile strength
(4)
(2)
(1)
Percentage increase of specific resistance
(4)
(2)
Copper percent
Fig. 3.
Copper
• rolled
× drawn
Δ twisted
Kg/mm²
70 : 30 brass
60 : 40 brass
Percentage increase of specific resistance
Tensile strength
Kg/mm²

Pl. II.

Fig. 4. Electric resistance-temperature curve.

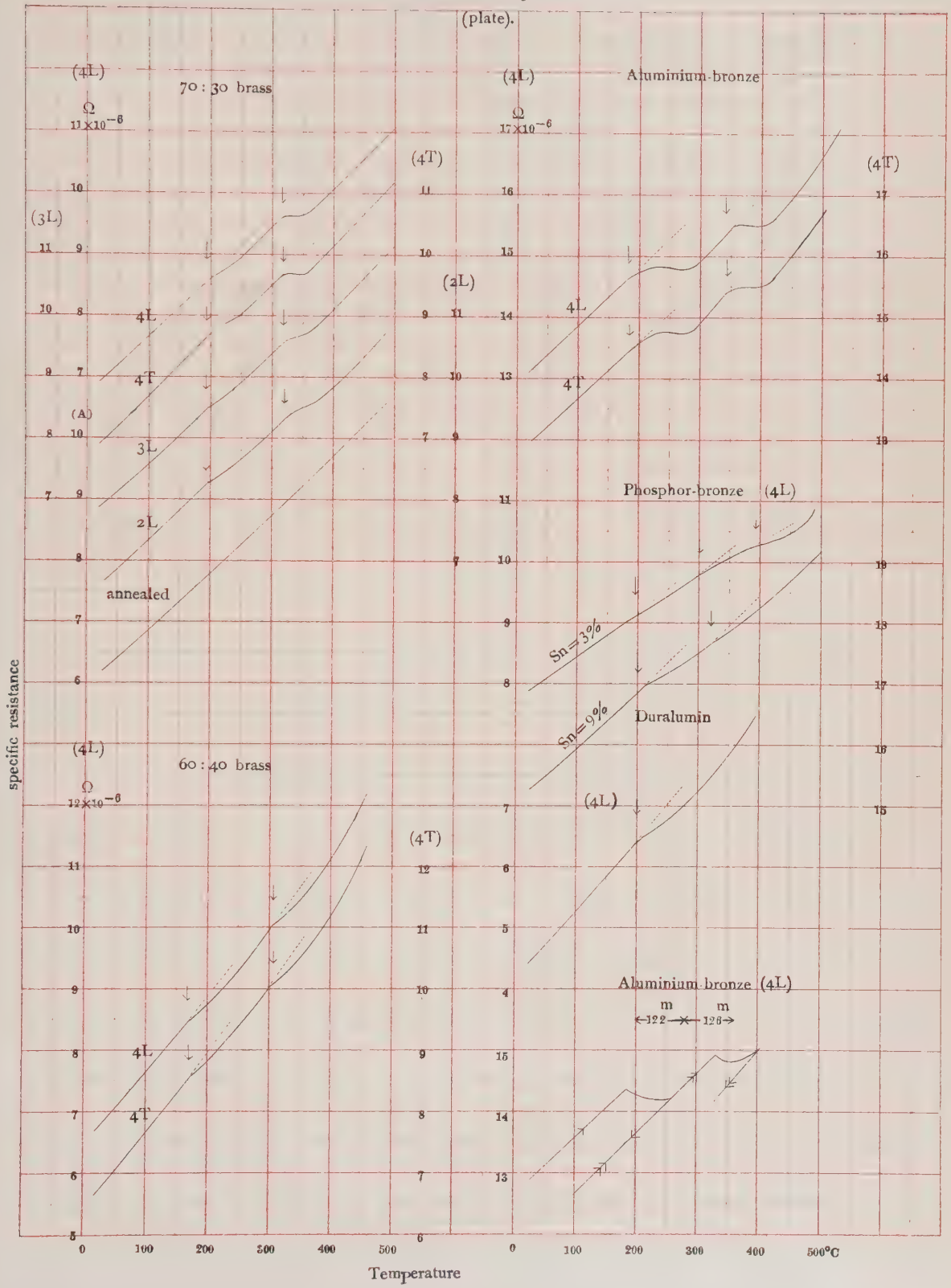

Fig. 5, a. Effect of annealing (plate).

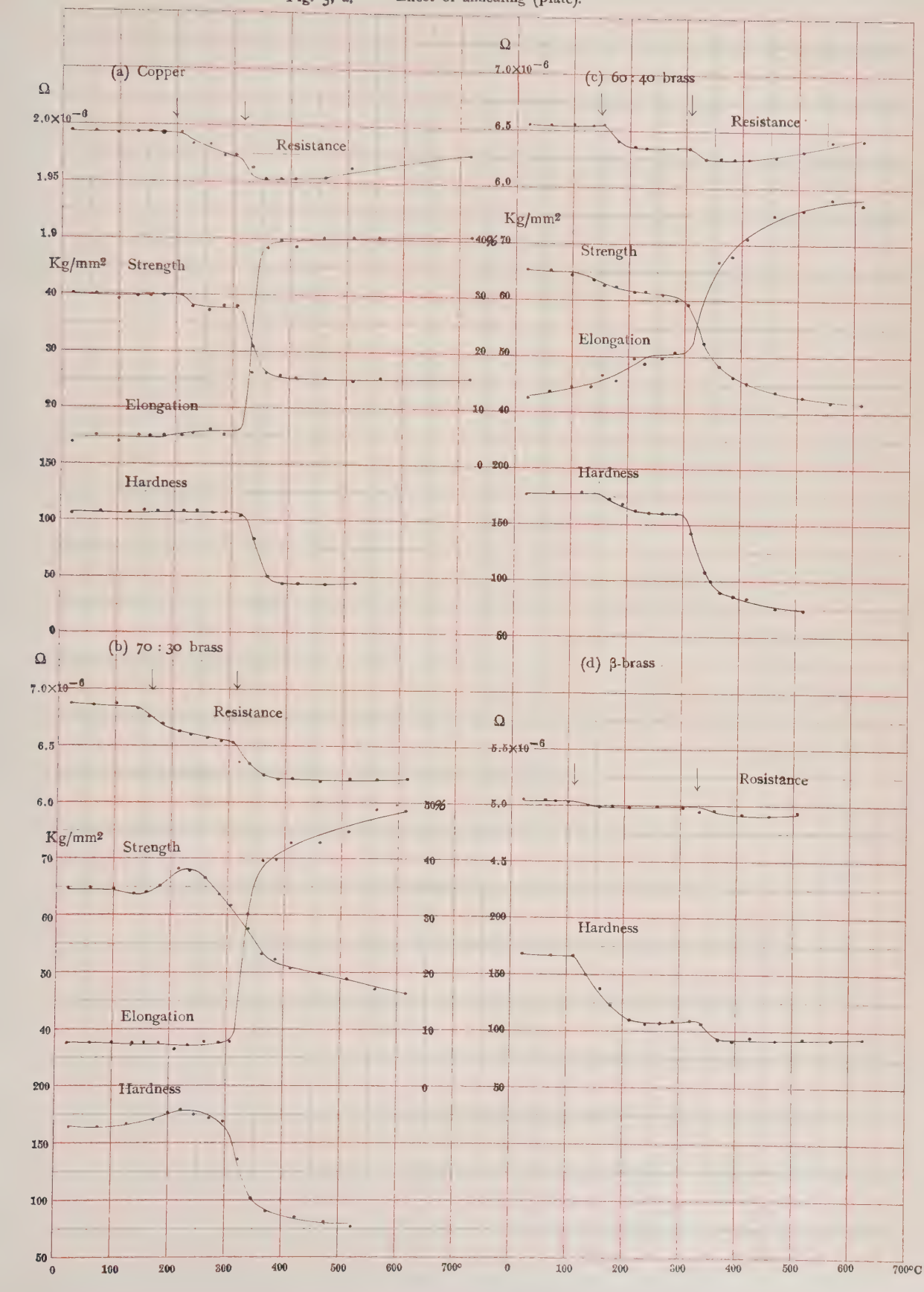

Pl. IV.

Fig. 5, b. Effect of annealing (plate).

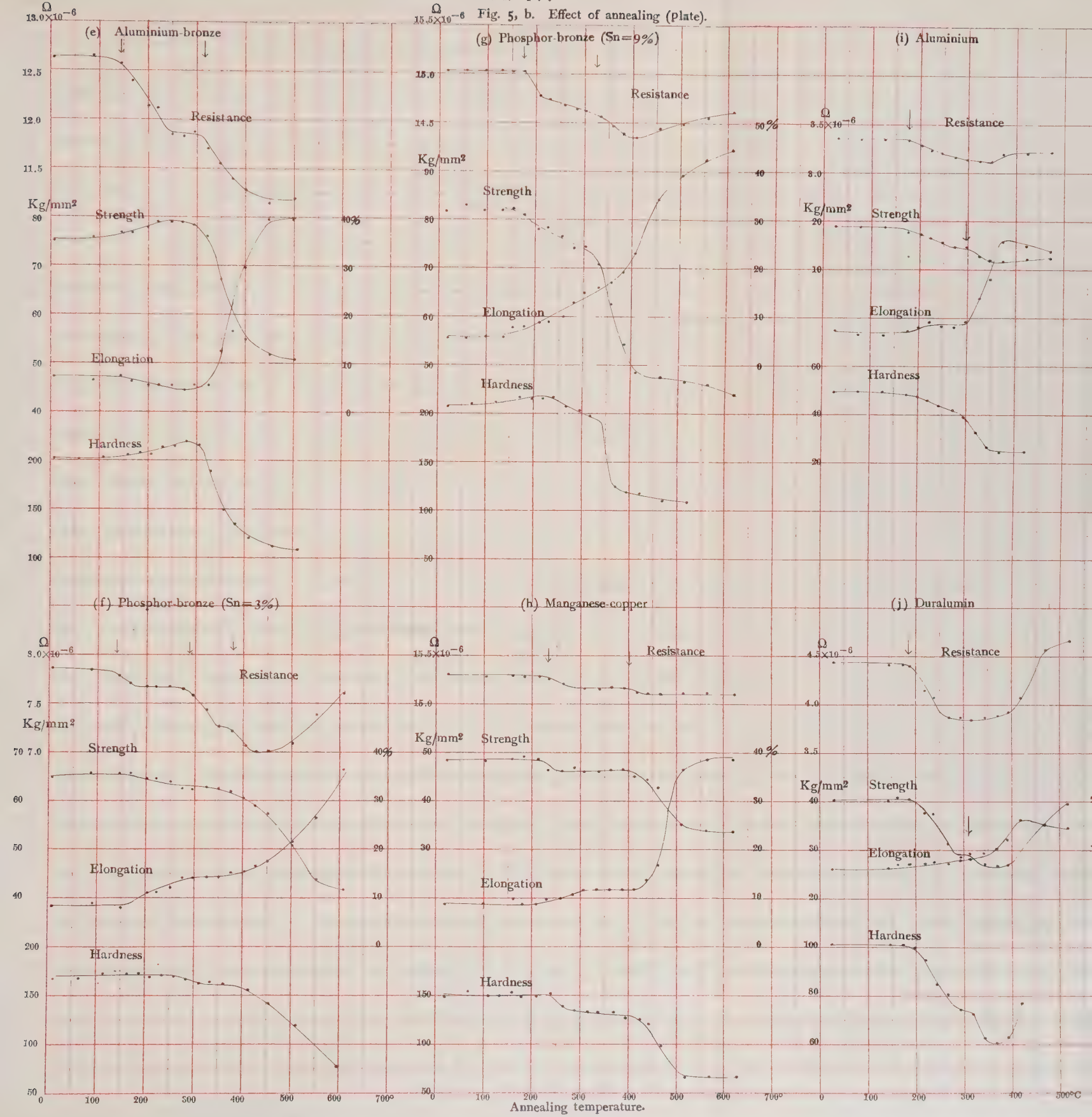

Pl. V.

Fig. 6. Electric resistance-temperature curve (rod).

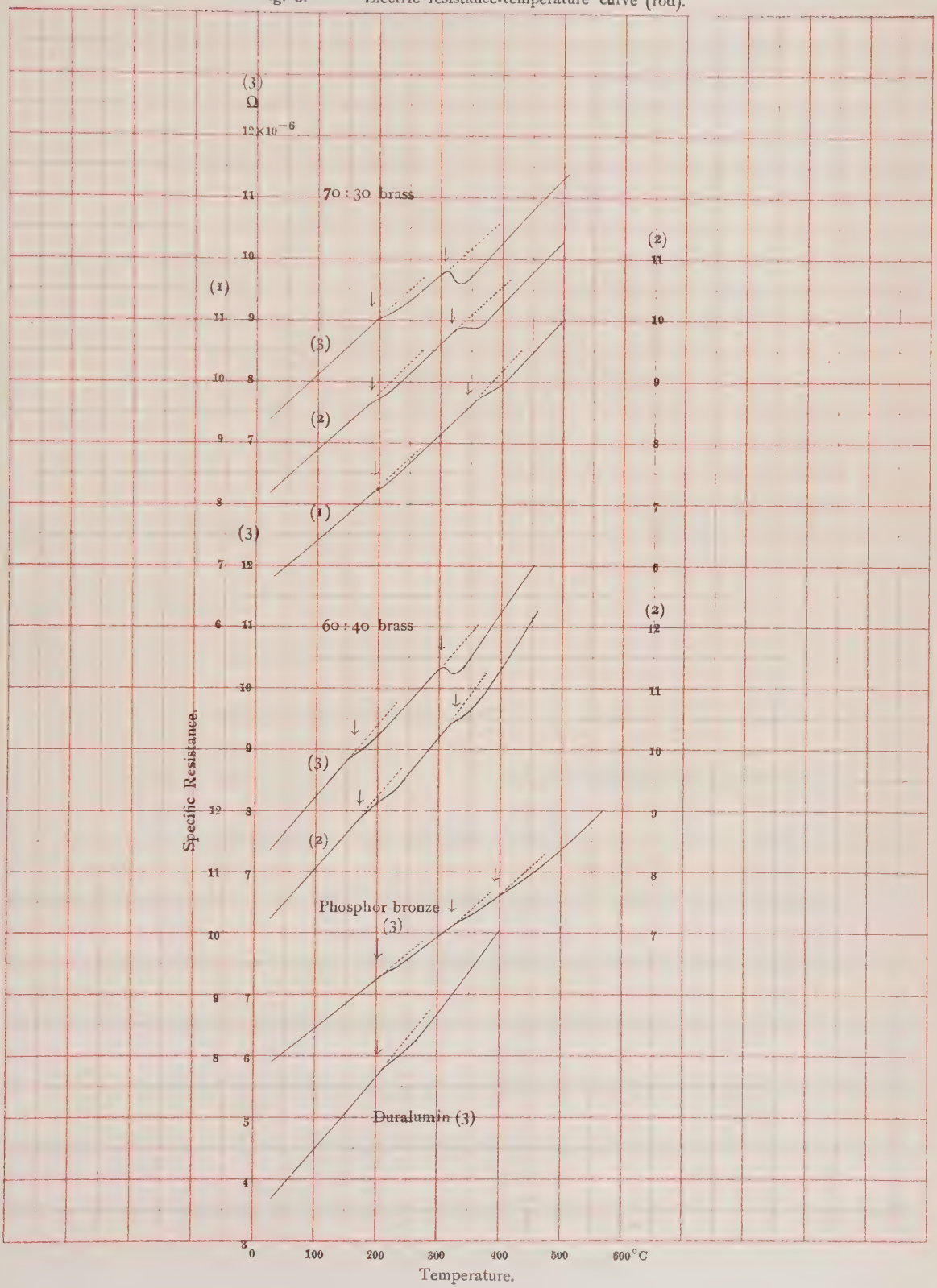

Pl. VI.

Fig. 7. Effect of annealing (rod).

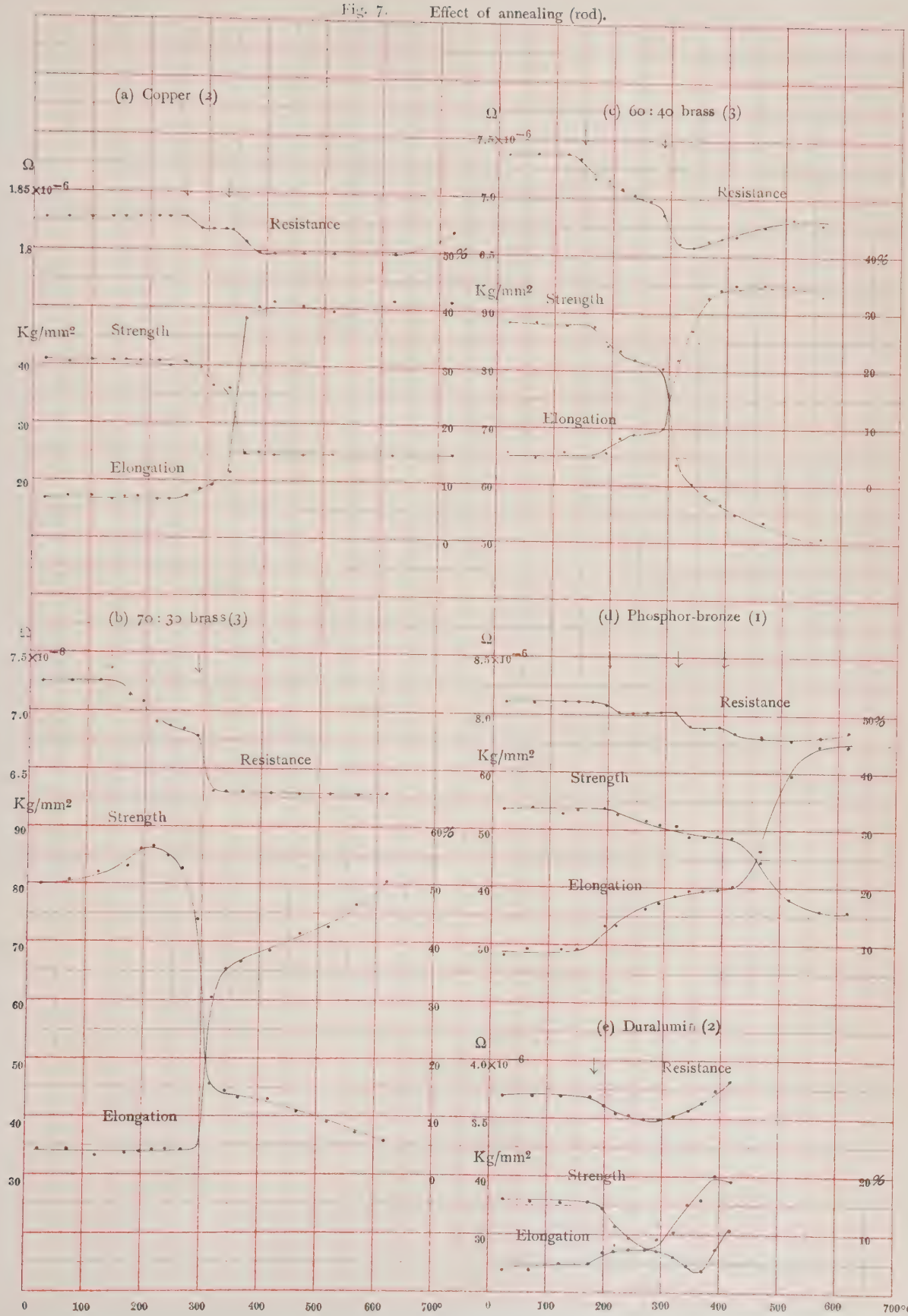

Fig. 8. Differential elongation-temperature curve. (plate).

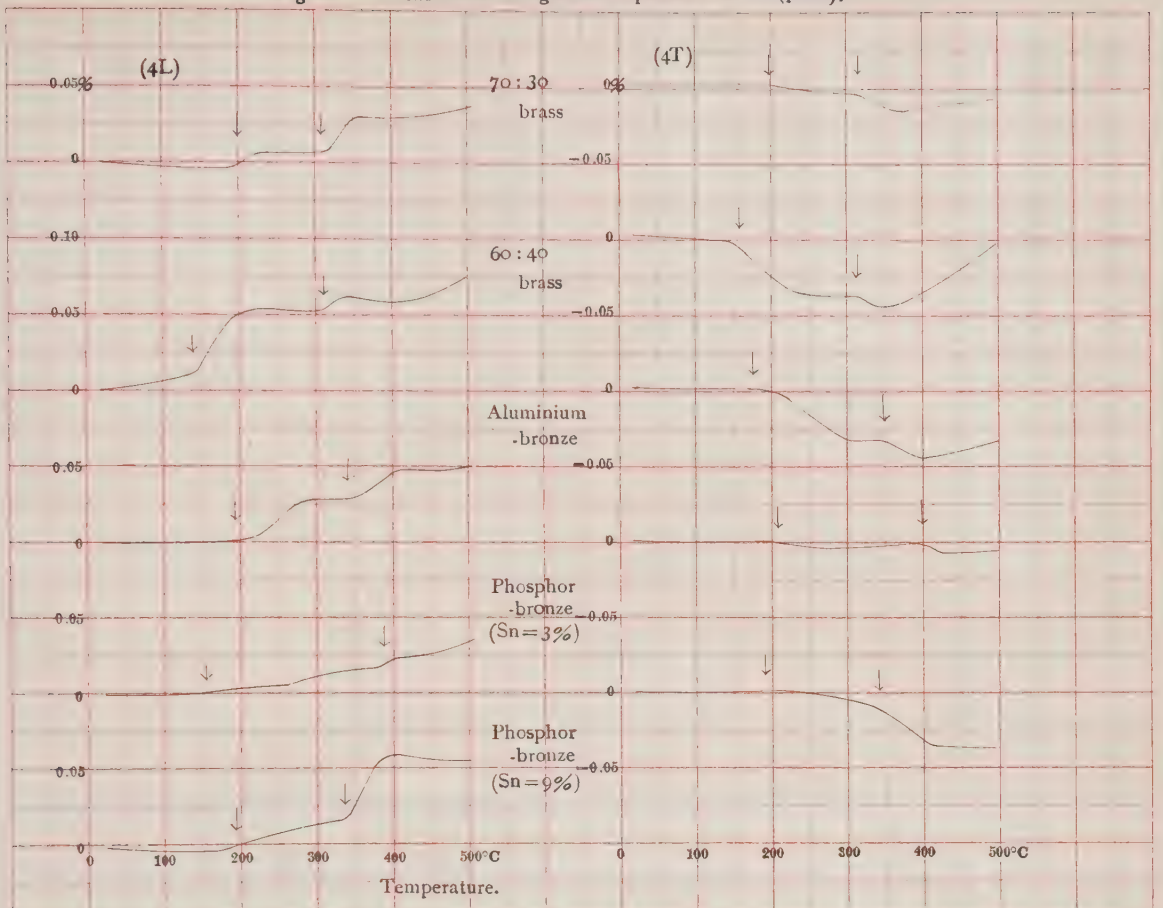

Fig. 9. Rod.

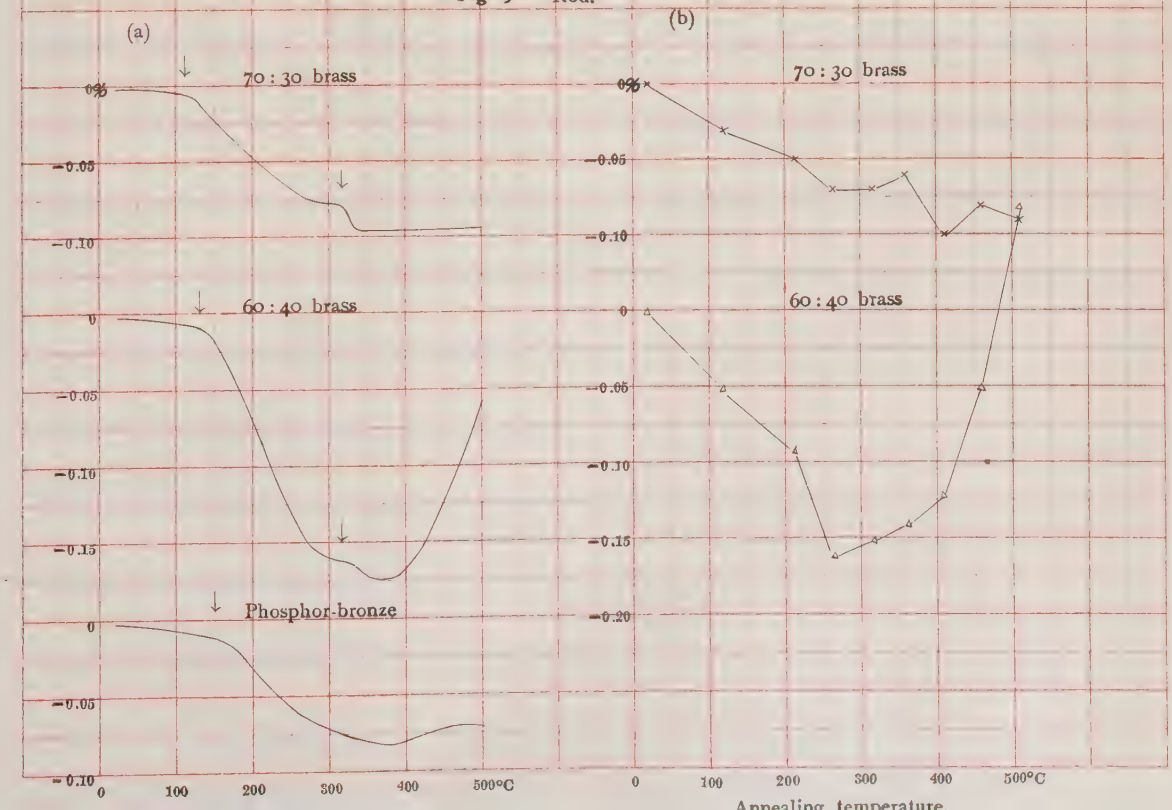

On the Influence of Some Elements on the Spheroidization of Carbides in Steels.[1]

By

Tomimatu Isihara.

§ 1. INTRODUCTION.

Many investigations have already been made on the formation of spheroidized cementite in steels, as this structure being the softest and the most ductile state which the steel can assume at room temperature, is very important from the practical point of view. According to the conclusions of previous investigators such as Osmond,[2] Goerens,[3] Hanemann and Morawe,[4] K. Honda and S. Saito,[5] the spheroidized cementite can be obtained by four different methods :— (1) Reheating of quenched or severely forged steels to a temperature just below the A_1 point ; (2) a very slow cooling through the A_1 range ; (3) repeated heating and cooling through the A_1 range ; (4) a long annealing of lamellar pearlite at a temperature just below the A_1 point. But the results of observation made by Professor K. Honda do not confirm the last mentioned case. According to him, if we heat a lamellar pearlite up to the temperature of Ac_1, the lamellar cementite begins to dissolve into γ–iron ; but since the degree of dissolution cannot be the

(1) The one hundred and eighth report of the Research Institute of Iron, Steel and Other Metals.

(2) Osmond, Rev. de Met., **1**, (1904), 349.

(3) Goerens, Metallkunde, **4**, (1907), 182.

(4) Hanemann-Morawe, Stahl und Eisen, **33**, (1913), 1350.

(5) K. Honda and S. Saito, Sci. Rep , **9**, (1922), 311.

same for different portions of the same lamellar, the latter is divorced into isolated islands as the dissolution goes on. These islands are then rounded into a globular form by the surface tension acting on the bounding surface of the cementite and thus spheroidization takes place. The divorcing of a lamellar into isolated islands by a prolonged heating below the A_1 point by the surface tension alone, as is frequently assumed, seems to be very unlikely to occur in virtue of the great viscosity of the solid cementite.

If the globularized steel is further heated beyond the Ac_1 point, the globules gradually decrease in number, till they dissolve into γ–iron and completely disappear. On the other hand, at the moment of the dissolution of cementite at the A_1 point, its concentration in austenite is not uniform; because the diffusion of carbon in austenite requires some duration of time. Hence, if the steel be cooled from the A_1 point or a little above it, the cementite is first precipitated from the numerous centres of the concentrated portions, the deposits themselves agglomerating by virtue of the surface tension and thus resulting in numerous globules.

In short, the divorcing of lamellar carbide or cementite into small isolated islands is the important factor for the spheroidization by a prolonged heating below the A_1 point. Whether this divorcing is caused by a heat treatment or a mechanical treatment makes no difference as regards spheroidization.

Recently, Whiteley[1] published an interesting paper, in which he examined the effect of the presence of cementite nuclei on the nature of the pearlite formed and on the position of the Ar_1 point, when the steel was slowly cooled down. According to his result, the formation of lamellar pearlite in hypo-eutectoid steel, by a slow cooling, indicates the absence of carbide nuclei, but this conclusion seems to me unsound. As a matter of fact, to get a structure containing lamellar pearlite the rate of cooling must be fairly rapid in the range of the A_1 transformation. If, on the other hand, the rate of cooling be much diminished in the A_1

(1) J. H. Whiteley, Jour. Iron and Steel Inst. (1922), 1, 239.

range, very fine spheroidized cementite will more or less appear during a very slow separation of cementite from the γ–solution. In other words, the presence of a spheroidized cementite indicates a very slow rate of cooling through the A_1 range irrespective of whether the nuclei were present or not. If the nuclei be present, during a very slow cooling through the A_1 range, the spheroidization of cementite takes place easily ; i, e, the formation of spheroidized cementite is accelerated by the presence of cementite nuclei. From the same point of view, an easy formation of spheroidized cementite in both hypo- and hyper-eutectoid steels can be expected ; because α–iron transformed from γ–iron by the A_3 change in hypo-eutectoid steel, and also the cementite separated along the A_{cm} line in hyper-eutectoid steel will act as an exciting cause of the Ar_1 change and consequently the under-cooling does not occur, while the eutectoid steel, not being subject to any such exciting cause, undergoes its lowering and consequently the γ–iron changes into lamellar pearlite in virtue of the rapid reaction. Hence the spheroidization of cementite in a eutectoid steel is not so likely to occur as in the other two cases.

The velocity of the Ac_1 transformation or the dissolution of cementite in iron depends on the size of the cementite or carbide. The finer its size the greater the velocity of dissolution. Hence in a structure containing fine cementites, the interval of temperature above the A_1 point during which spheroidal cementite appears, is comparatively small. This temperature interval depends of course more or less on the duration of heating above the A_1 point, being less as the heating duration increases.

When a steel contains other elements such as, manganese, chromium, copper, &c, the velocity of the A_1 transformation of the steel is diminished, i. e., the dissolution of carbon in γ–iron requires a much longer time than is required in a pure carbon steel, and consequently it is to be expected that the interval of temperature above the A_1 point, in which spheroidal cementite or carbide appears, increases with the amount of elements added.

The present investigation was undertaken to confirm the above conclusion.

§ 2. EXPERIMENTAL METHOD.

As the test specimen, the present writer used cylindrical rods, 6 mm in diameter and 2 cm in length, which were annealed beforehand for two hours at 1100°C and then cooled in the furnace to make the structure lamellar. The specimens were heated at a rate of 2° per minute, kept at the maximum temperature for 20 minutes, and then slowly cooled at the same rate, till the temperature reached 50° below the Ac_1 point.

In the case of the present investigation, it was necessary to know the exact temperatures of the Ac_1 and Ar_1 points of the specimens. This was done by means of magnetic analysis and dilatometric measurements, which have constantly been used in our laboratory. We investigated three kinds of steels containing manganese, chromium, and copper, and compared the effects of these elements in spheroidizing the carbides with the case of plain carbon steels, such as were studied by Prof. K. Honda and Dr. S. Saito.

§ 3. RESULTS OF EXPERIMENTS.

Twenty kinds of manganese steels, chromium steels and copper steels were prepared from Swedish iron and metallic manganese, chromium and copper.

A. Effect of Manganese.

The composition of specimens and the A_1 point found by magnetic analysis are shown in Table I.

TABLE I.

Alloy No.	C (%)	Mn (%)	Ac_1(°C)	Ar_1(°C)	Alloy No.	C (%)	Mn (%)	Ac_1(°C)	Ar_1(°C)
1	0.51	1.02	705	655	11	0.41	3.00	685	625
2	0.68	1.03	705	650	12	0.71	3.04	685	625
3	0.86	1.02	710	650	13	0.89	3.01	685	630
4	1.31	1.09	705	650	14	1.28	3.04	685	630
5	2.0	1.04	700	660	15	2.03	3.03	685	630
6	0.46	1.94	695	640	16	0.45	4.02	675	610
7	0.72	2.02	695	640	17	0.76	4.01	675	610
8	0.90	2.05	695	640	18	0.93	4.12	675	610
9	1.28	2.02	695	640	19	1.29	4.16	675	605
10	2.02	2.05	690	640	20	2.00	4.09	675	600

In these steels, manganese is present as a carbide Mn_3C, which is isomorphous to the cementite, and hence the carbide as seen under a microscope is not a pure cementite, but an isomorphous mixture of Mn_3C and Fe_3C; but for the sake of simplicity we shall call the mixture the cementite. The results of experiments are shown in the following Tables II to V. In the tables, letters G and L represent globular and lamellar respectively.

TABLE II.

Max. temp. (°C)	No. 1	No. 2	No. 3	No. 4	No. 5	Max. temp. (°C)	No. 1	No. 2	No. 3	No. 4	No. 5
670	L	L	L	L	L	730	L+G	L+G	L+G	G	G
680	,,	,,	,,	,,	,,	744	,,	,,	,,	,,	,,
688	,,	,,	,,	,,	,,	754	,,	,,	,,	,,	,,
696	L+G	L+G	L+G	L+G	L+G	773	,,	,,	,,	G+L	,,
704	G+L	G+L	G+L	G+L	G+L	810	L	L	L	L+G	,,
712	,,	,,	,,	,,	,,	875	,,	,,	,,	,,	,,
721	,,	,,	,,	G	G	900	,,	,,	,,	L	L+G

TABLE III.

Max. temp. (°C)	No. 6	No. 7	No. 8	No. 9	No. 10	Max. temp. (°C)	No. 6	No. 7	No. 8	No. 9	No. 10
670	L	L	L	L	L	730	L+G	L+G	G+L	G	G
680	„	„	„	„	„	744	„	„	„	„	„
688	L+G	L+G	L+G	L+G	L+G	754	„	„	L+G	„	„
696	L+G	L+G	L+G	L+G	L+G	773	„	L+G	„	G+L	„
704	G+L	G+L	„	„	„	810	L	L	L	„	„
712	„	„	G+L	„	„	875	„	„	„	„	„
721	„	G	„	G	G	900	„	„	„	L	L+G

TABLE IV.

Max. temp. (°C)	No. 11	No. 12	No. 13	No. 14	No. 15	Max. temp. (°C)	No. 11	No. 12	No. 13	No. 14	No. 15
670	L	L	L	L	L	730	L+G	L+G	G+L	G	G
680	L+G	L+G	L+G	L+G	L+G	744	„	„	„	G+L	„
688	„	„	G+L	„	„	754	L+G	„	„	„	G+L
696	G	G	„	„	„	773	L	„	„	„	„
704	L+G	L+G	„	„	„	810	„	L	„	„	„
712	„	„	„	„	G+L	875	„	„	„	„	„
721	„	„	„	„	„	900	„	„	L	L	L+G

TABLE V.

Max. temp. (°C)	No. 16	No. 17	No. 18	No. 19	No. 20	Max. temp. (°C)	No. 16	No. 17	No. 18	No. 91	No. 20
650	L	L	L	L	L	721	L+G	L+G	G	G	G+L
663	L	„	L+G	L+G	L+G	730	„	„	„	„	„
670	L+G	L+G	„	„	„	744	„	„	„	„	„
680	„	„	„	„	G+L	754	„	„	„	„	„
688	„	„	„	„	„	773	L	L	„	L+G	„
696	„	„	„	„	„	810	„	„	L+G	„	L+G
704	„	„	„	„	„	875	„	„	„	„	„
712	„	„	„	„	„	900	„	„	L	L	„

The temperature interval above the Ac_1 point, in which spheroidized carbides occur, varies slightly with the content of carbon and considerably with that of manganese as seen from Figs. 1 and 2. In these figures, the two lines represent the upper and lower limits of the spheroidizing interval, and the dotted lines the Ac_1 and Ar_1 lines.

If the content of carbon be the same, the spheroidizing interval of temperature increases slightly with the content of manganese. The Ac_1 or Ar_1 point is lowered by 10° by an addition of 1 percent of manganese. On the other hand, if the content of manganese be kept constant, the spheroidizing interval remains constant or increases slightly up to the eutectoid concentration, and then rapidly increases, with the increasing content of carbon. This rapid increase is to be expected from the form of the solubility line of cementite in iron.

In comparing the above result with the case of carbon steel,[1] we find a considerable increase in the spheroidizing range above the Ac_1 point. This result agrees with that of Monypenny.[2] From these results, we conclude that the presence of manganese in steels decreases the velocity of the dissolution of cementite or carbide in iron, and consequently widens the spheroidizing interval; and consequently the spheroidization becomes easier to effect from a practical point of view. Some photographs are given in Pl. IV.

According to the theoretical consideration before referred to, the line of the lower limit of the spheroidizing interval should coincide with the Ac_1 line (dotted line), but actually it lies a little below the Ac_1 line, i. e., from 5° to 10° below the latter line. This discrepancy between the theory and experiments is very probably attributable to the difference between the rate of heating in the determinations of the Ac_1 line and the spheroidizing interval. For, the position of the Ac_1 line depends on the rate of heating, being lower as the rate is smaller. In the magnetic determination of the Ac_1 line, the rate of heating, though

(1) K. Honda and S. Saito, Sci. Rep., **9**, (1920), 311.
(2) Monypenny, Jour. Iron and Steel, Inst. No. 1, (1920), 493.

slow, is not so slow as in the case of the spheroidizing of the cementite, where the temperature of the specimens is kept constant for 20 minutes. In order to confirm this view a few specimens were reexamined at a very slow rate of heating, and it was found that the true Ac_1 point is really lower by 2° to 5° than the lower limit of the spheroidizing interval.

B. Effect of Chromium.

Twenty kinds of specimens were also prepared from Swedish iron and metallic chromium by means of a Tammann furnace. Their compositions and the A_1 points found by magnetic analysis are given in Table VI.

TABLE VI.

Alloy No.	C (%)	Cr (%)	Ac_1(°C)	Ar_1(°C)	Alloy No.	C (%)	Cr (%)	Ac_1(°C)	Ar_1(°C)
1	0.45	0.99	765	715	11	0.40	3.07	775	715
2	0.71	1.25	765	720	12	0.76	3.14	765	710
3	0.93	1.04	765	715	13	0.93	3.02	770	710
4	1.32	0.97	765	715	14	1.29	3.00	765	710
5	2.02	1.02	755	700	15	2.02	3.18	770	705
6	0.50	2.18	767	720	16	0.44	3.96	765	720
7	0.69	1.92	770	725	17	0.76	3.80	770	715
8	0.94	1.95	775	720	18	0.97	3.86	770	710
9	1.33	1.91	765	710	19	1.31	3.77	765	700
10	2.00	2.14	770	700	20	1.85	3.95	765	690

It is a well known fact that chromium slightly raises the Ac_1 point of steel and diminishes the velocity of the dissolution of carbide, the solubility of carbon in iron being decreased. Hence as in the case of manganese steel, the practice of the spheroidizing of carbide will be easy to effect in chromium steel. The result of experiments are shown in Tables VII to X and Figs. 3 and 4.

TABLE VII.

Max. temp. (°C)	No. 1	No. 2	No. 3	No. 4	No. 5	Max. temp. °C)	No. 1	No. 2	No. 3	No. 4	No. 5
953	L	L	L	L	L+G	736	L	L	L	L	L
905	„	„	„	L+G	„	729	L	L	„	„	L
865	„	„	„	L+G	„	721	„	„	„	„	„
810	L+G	G+L	G+L	„	G	712	„	„	„	„	„
800	L+G	G+L	G+L	„	„	704	„	„	„	„	„
791	„	„	„	„	„	696	„	„	„	„	„
782	„	„	„	„	G+L	688	„	„	„	„	„
773	G+L	L+G	„	„	G+L	679	„	„	„	„	„
763	„	„	„	G+L	„	670	„	„	„	„	„
754	„	L	L	G+L	„	660	„	„	„	„	„
743	L	L	L	L	L+G						

TABLE VIII.

Max. temp. (°C)	No. 6	No. 7	No. 8	No. 9	No. 10	Max. temp. (°C)	No. 6	No. 7	No. 8	No. 9	No. 10
953	L	L	L	L+G	L+G	782	L+G	L+G	G	G	G
905	L+G	L+G	L+G	„	„	773	„	L+G	G+L	G+L	L+G
865	„	L+G	G+L	G+L	G	763	„	„	L+G	L+G	„
810	„	„	G	G	„	754	L	L	L	L	„
800	„	„	„	„	„	743	„	„	„	„	„
791	„	„	„	„	„	736	„	„	„	„	„

TABLE IX.

Max. temp. (°C)	No. 11	No. 12	No. 13	No. 14	No. 15	Max. temp. (°C)	No. 11	No. 12	No. 13	No. 14	No. 15
953	L	L	L	L+G	G+L	773	G+L	G+L	L+G	G+L	G+L
905	G+L	G+L	G+L	„	„	763	L+G	„	„	„	„
865	„	G	G	G	G	754	„	L+G	„	L+G	L+G
818	G	„	„	„	„	744	L	L	L	L	„
810	„	„	„	„	„	736	„	„	„	„	L
800	„	„	G+L	G+L	G+L	729	„	„	„	„	„
791	G+L	G+L	„	„	„	721	„	„	„	„	„
782	„	„	„	„	„	712	„	„	„	„	„

TABLE X.

Max. temp. (°C)	No. 16	No. 17	No. 18	No. 19	No. 20	Max. tamp. (°C)	No. 16	No. 17	No. 18	No. 19	No. 20
953	L+G	L+G	L+G	G+L	G+L	782	G+L	G+L	L+G	G+L	G+I
905	L+G	„	„	G	G	773	„	„	„	„	„
865	„	G+L	„	„	„	763	L+G	L+G	„	L+G	„
818	G+L	„	„	„	„	754	L	L	L	L	„
810	„	„	„	G+L	„	744	„	„	„	„	L
800	„	„	„	„	„	736	„	„	„	„	„
791	„	„	„	„	G+L	729	„	„	„	„	„

From these results, we see that the spheroidizing interval of temperature is larger than that of manganese and carbon steels. If the content of carbon be kept constant, the interval rapidly increases with chromium ; and if the content of chromium be kept constant, the interval remains nearly constant up to the eutectoid concentration and then increases rapidly, with increasing carbon.

Microscopically observed, the size of spheroidized carbide is also smaller than in the case of carbon and manganese steels.

Thus the spheroidization of chromium steels begins to take place at the Ac_1 point, an allowance of 20° being made as previously mentioned in the case of manganese steel ; this interval extends to a much wider range of temperature than in the case of manganese steels. The practice of the spheroidization is then much easier to effect in chromium steels than in the case of carbon and manganese steels.

C. Effect of Copper.

Twenty kinds of steels were also made from electrolytic copper and Swedish iron. The composition and the A_1 point found by a dilatometer are given in Table XI.

TABLE XI.

Alloy No.	C (%)	Cu (%)	Ac_1(°C)	Ar_1(°C)	Alloy No.	C (%)	Cu (%)	Ac_1(°C)	Ar_1(°C)
1	0.41	1.01	720	670	11	0.45	2.96	710	670
2	0.70	1.10	730	680	12	0.72	2.95	710	670
3	0.89	1.05	725	675	13	0.91	3.02	710	670
4	1.28	1.00	730	680	14	1.32	2.97	710	680
5	2.02	1.03	730	680	15	2.00	3.01	710	670
6	0.43	2.00	710	670	16	0.41	3.96	720	660
7	0.68	1.98	710	680	17	0.72	3.90	720	685
8	0.88	1.97	710	670	18	0.89	4.10	720	670
9	1.28	2.03	710	670	19	1.29	4.02	715	680
10	1.98	2.01	720	680	20	1.98	3.98	720	670

In these steels carbon is present as plain cementite, and the structure is much more distinct in comparison with those of chromium and manganese steels. The results of observations are given in Tables XII to XV and Figs. 5 to 6.

TABLE XII.

Max. temp. (°C)	No. 1	No. 2	No. 3	No. 4	No. 5	Max. temp. (°C)	No. 1	No. 2	No. 3	No. 4	No. 5
680	L	L	L	L	L	763	G+L	G+L	G	G+L	G+L
689	,,	,,	,,	,,	,,	773	,,	,,	G+L	,,	,,
696	,,	,,	,,	,,	,,	782	,,	,,	,,	,,	,,
704	,,	,,	,,	,,	,,	791	,,	,,	,,	,,	,,
712	L+G	L+G	L+G	,,	L+G	800	,,	,,	,,	,,	,,
721	G+L	G+L	G+L	L+G	G+L	810	L	L	,,	,,	,,
729	,,	,,	,,	G+L	,,	865	,,	,,	L	,,	,,
736	,,	,,	,,	,,	,,	905	,,	,,	,,	L	,,
743	,,	,,	,,	,,	,,	953	,,	,,	,,	,,	,,
754	,,	,,	,,	,,	,,						

TABLE XIII.

Max. temp. (°C)	No. 6	No. 7	No. 8	No. 9	No. 10	Max. temp. (°C)	No. 6	No. 7	No. 8	No. 9	No. 10
680	L	L	L	L	L	763	L+G	G+L	L+G	G	G+L
689	„	„	„	„	„	773	„	„	„	„	„
696	„	„	„	„	„	782	„	„	„	L+G	„
704	L+G	L+G	L+G	L+G	L+G	791	„	„	„	„	„
712	„	G+L	G+L	G+L	G+L	800	„	„	„	„	„
721	„	„	„	„	„	810	L	„	„	„	„
729	G	„	„	„	„	865	„	L	L	„	„
736	G+L	„	„	„	„	905	„	„	„	„	„
743	G	„	„	G	„	953	„	„	„	L	L+G
754	L+G	„	G	„	„						

TABLE XIV.

Max. temp. (°C)	No. 11	No. 12	No. 13	No. 14	No. 15	Max. temp. (°C)	No. 11	No. 12	No. 13	No. 14	No. 15
680	L	L	L	L	L	763	G+L	G+L	G+L	G+L	G+L
689	„	„	„	„	„	773	„	„	G	„	„
696	„	„	„	„	„	782	„	„	G+L	„	„
704	L+G	L+G	L+G	L+G	„	791	„	„	„	„	„
712	G+L	G+L	G+L	G+L	G+L	800	„	„	„	„	„
721	„	„	„	„	„	810	L	L	„	„	„
729	„	„	„	„	„	865	„	„	L	„	„
736	„	„	„	„	„	905	„	„	„	L	„
743	„	„	„	„	„	953	„	„	„	„	L+G
754	„	„	„	„	„						

TABLE XV.

Max. temp. (°C)	No. 16	No. 17	No. 18	No. 19	No. 20	Max. temp. (°C)	No. 16	No. 17	No. 18	No. 19	No. 20
680	L	L	L	L	L	763	G	G+L	G+L	G	G+L
689	„	„	„	„	„	773	G+L	„	„	„	„
696	„	„	„	„	„	782	„	„	„	„	„
704	L+G	L+G	L+G	L+G	L+G	791	„	„	„	„	„
712	G+L	G+L	„	G+L	G+L	800	„	„	„	„	„
721	„	G	G	„	„	810	L	L	„	„	„
729	„	„	„	G	„	865	„	„	L	„	„
736	G	„	G+L	„	„	905	„	„	„	„	„
743	„	„	„	„	„	953	„	„	„	G	L+G
754	„	„	„	„	„						

The spheroidizing interval of temperature is a little larger than that of manganese or carbon steel, but is a little smaller than that of chromium steel. If the content of carbon be the same, this interval remains nearly constant, and if the content of copper be kept constant, the interval also remains nearly constant up to the eutectoid concentration and then increases rapidly, with increasing carbon.

Microscopically observed, the size of spheroidized cementite is larger than that found in manganese and chromium steels.

From the results, we see that the spheroidization of copper steel begins to take place at the Ac_1 point, a small allowance being made, and this interval extends to a wider range of temperature than in the case of manganese steel, but is less than in the case of chromium steel. Thus the spheroidization of copper steel takes place in the same degree as in the case of manganese steel.

Some typical photomicrographs are given in Pl. V by way of examples with brief explanations.

In these photomicrographs, sodium picrate was used as an etching reagent, but in two other cases, alcoholic solution of picric acid was used instead of it.

SUMMARY.

From the results so far described, the following conclusions may be drawn :—

(1) Manganese, chromium, and copper have each a considerable influence on the formation of spheroidal carbides, differing each in its degree.

(2) In manganese steel, the spheroidizing interval of temperature above the Ac_1 point is slightly increased with the content of manganese. In chromium and copper steels, it increases considerably with the content of chrominm and copper.

(3) If the content of these elements in steels be kept constant, the spheroidizing interval remains nearly constant up to the eutectoid concentration and then increases rapidly, with the content of carbon.

In conclusion, the present writer expresses his cordial thanks to Professor K. Honda, under whose kind guidance the present investigation has been carried out, and also to Professor T. Murakami for his useful advices. His thanks are also due to Mr. M. Mikami for his zealous assistance throughout the present investigation.

Pl. I.

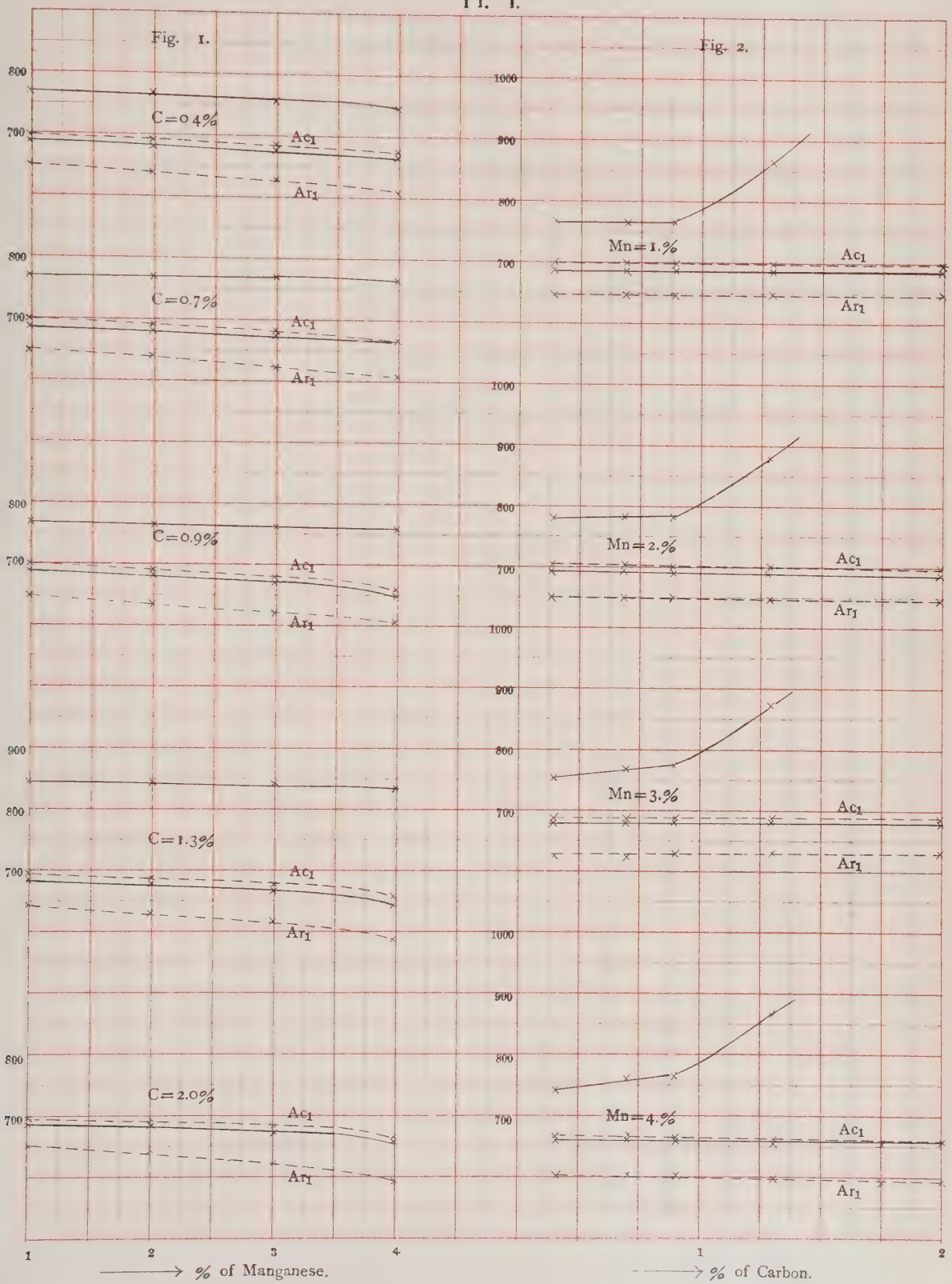
Fig. 1.
C=0.4%
Ac1
Ar1
C=0.7%
Ac1
Ar1
C=0.9%
Ac1
Ar1
C=1.3%
Ac1
Ar1
C=2.0%
Ac1
Ar1
800
700
900
1
2
3
4
→ % of Manganese.
Fig. 2.
Mn=1.%
Mn=2.%
Mn=3.%
Mn=4.%
Ac1
Ar1
1000
900
800
700
1
2
- - → % of Carbon.

Pl. II.

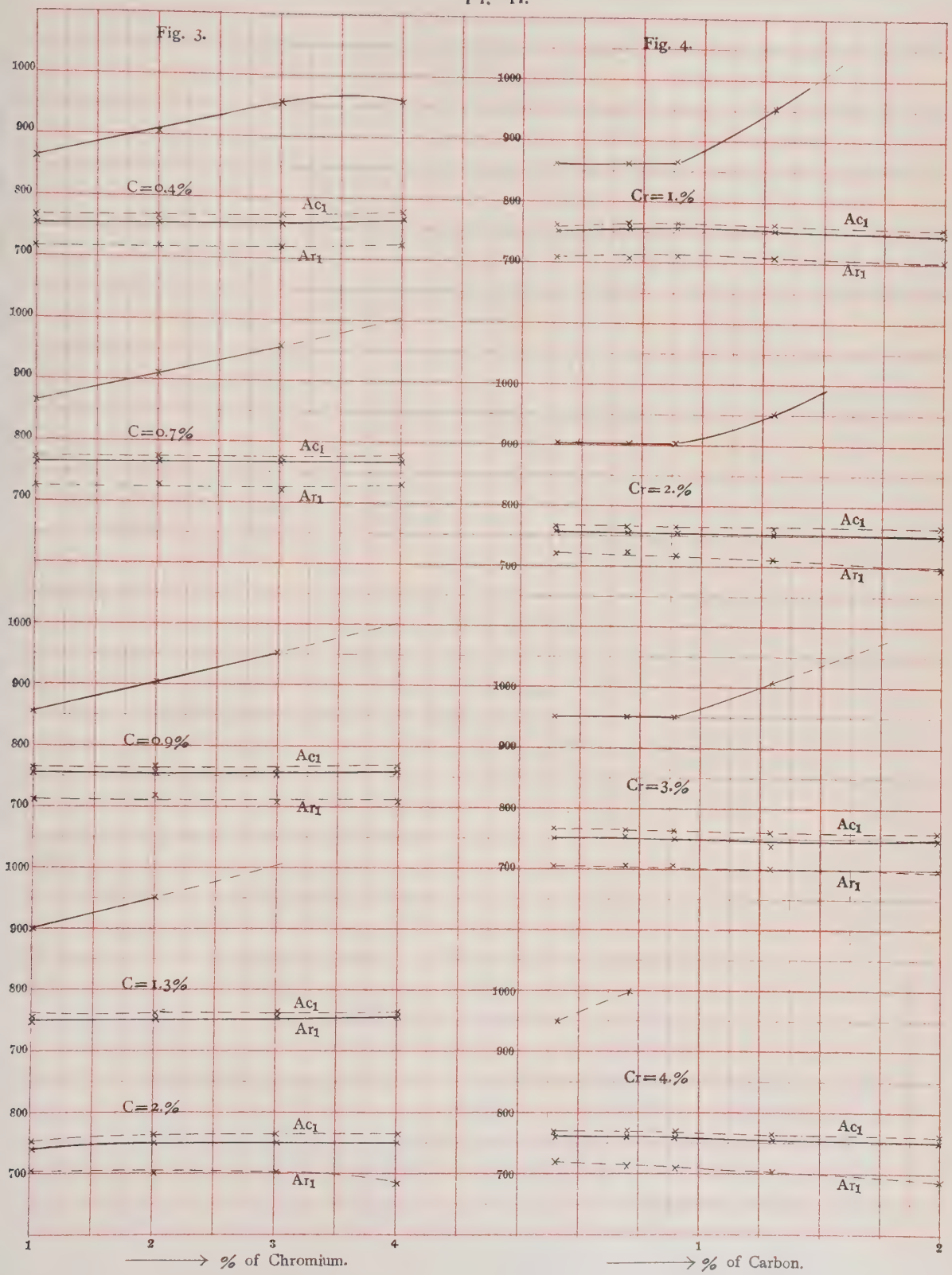
Fig. 3.
C=0.4%
Ac1
Ar1
C=0.7%
Ac1
Ar1
C=0.9%
Ac1
Ar1
C=1.3%
Ac1
Ar1
C=2.%
Ac1
Ar1
1000
900
800
700
1
2
3
4
% of Chromium.
Fig. 4.
Cr=1.%
Ac1
Ar1
Cr=2.%
Ac1
Ar1
Cr=3.%
Ac1
Ar1
Cr=4.%
Ac1
Ar1
1000
900
800
700
1
2
% of Carbon.

Pl. III.

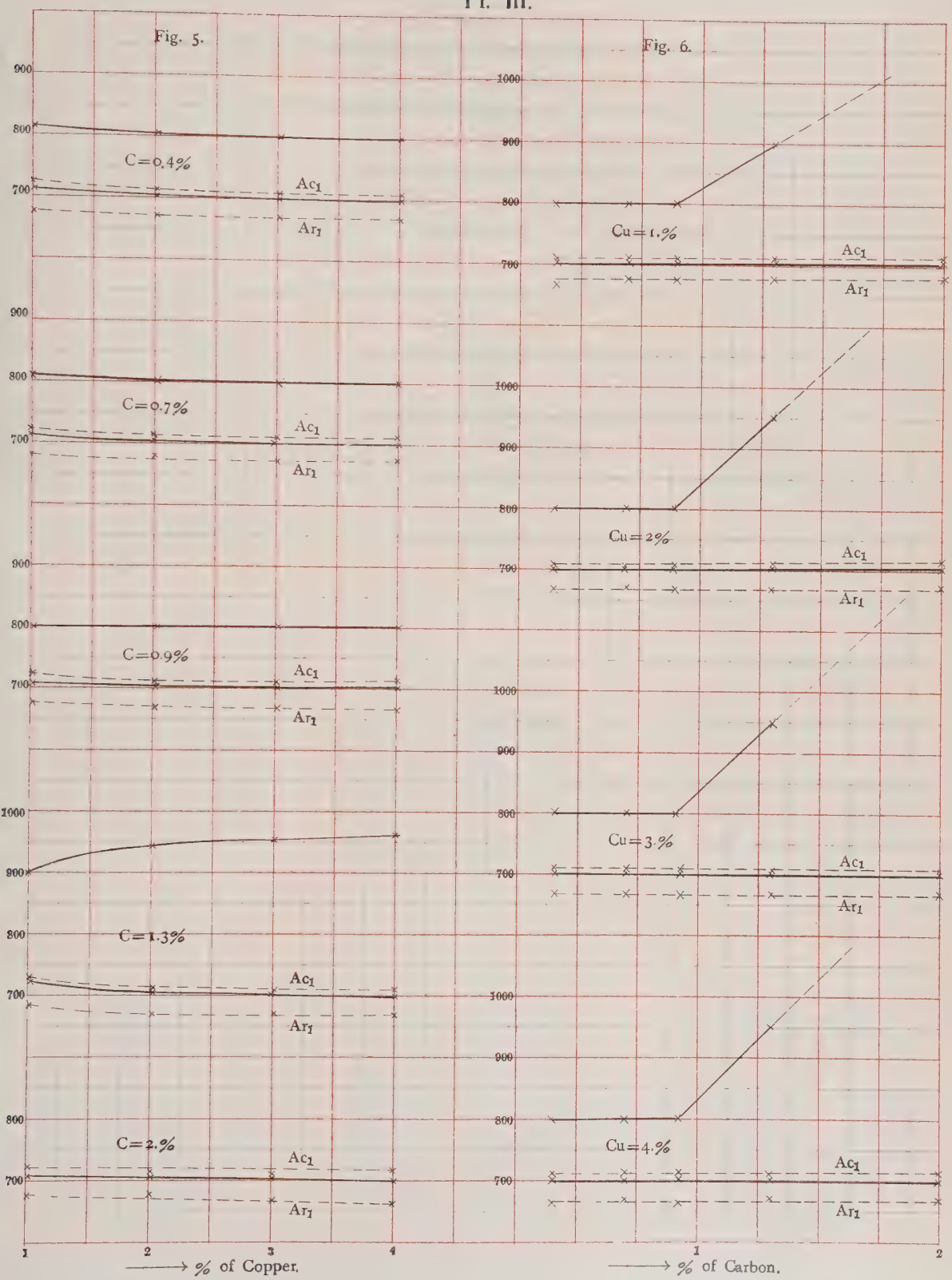
Fig. 5.
C=0.4%
C=0.7%
C=0.9%
C=1.3%
C=2.%
Ac1
Ar1
900
800
700
1000
1
2
3
4
% of Copper.

Fig. 6.
Cu=1.%
Cu=2%
Cu=3.%
Cu=4.%
Ac1
Ar1
1000
900
800
700
1
2
% of Carbon.

Plate IV.

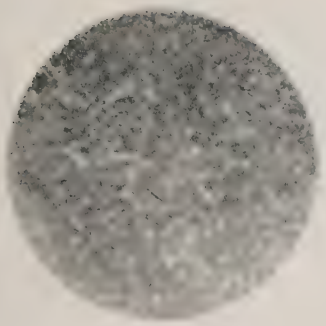

C = 2 %, Mn = 1 %. ×800
Heated to 750°C

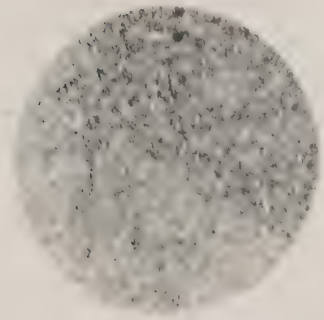

C = 2 %, Mn = 2 %. ×800
Heated to 780°C

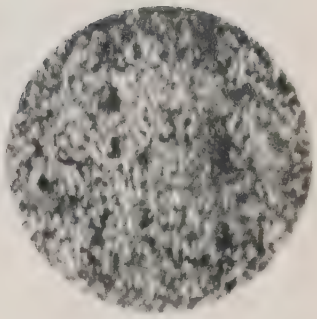

C = 0.9 %, Mn = 3 %. ×800
Heated to 780°C

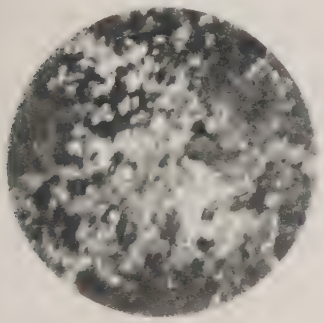

C = 0.7 %, Mn = 2 %. ×800
Heated to 750°C

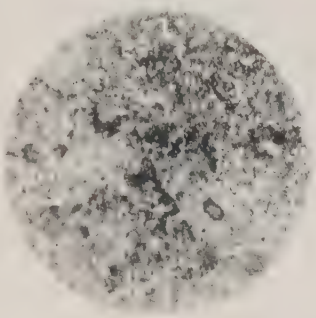

C = 1.3 %, Mn = 3 %. ×800
Heated to 780°C

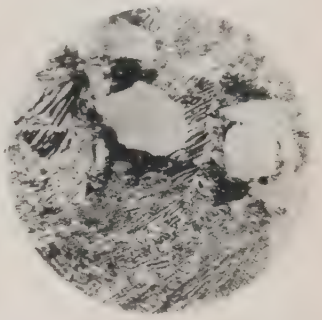

Cr = 1 %, C = 0.7 %. ×750
Heated to 800°C

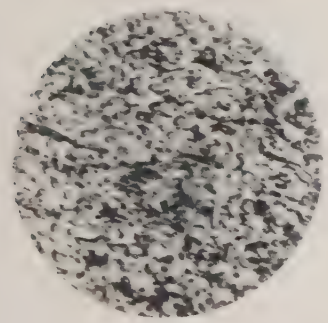

Cr = 1%, C = 2%. ×1200
Heated to 800°C

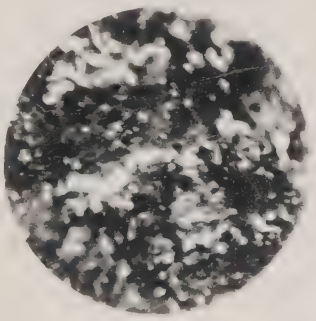

Cr = 2 %, C = 2 %. ×1200
Heated to 810°C

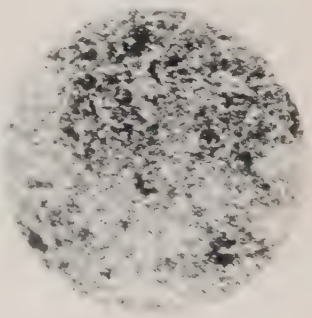

Cr = 3 %, C = 0.9 %. ×1200
Heated to 810°C

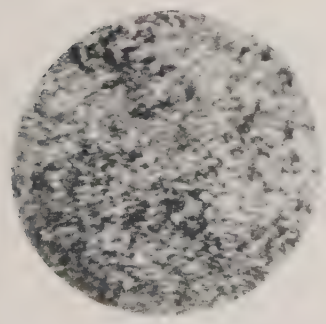

Cr = 3 %, C = 1.3 %. ×1000
Heated to 880°C

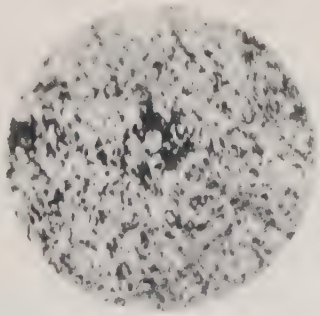

Cr=4%, C=0.7%. ×1000
Heated to 860°C

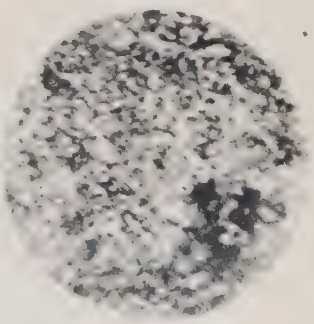

Cr = 4 %, C = 0.9 %. ×1500
Heated to 840°C

Plate V.

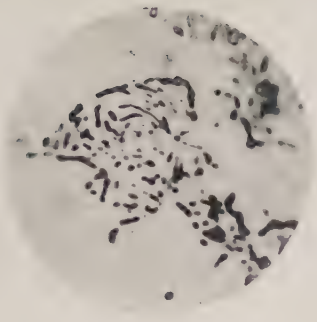

Cu = 1 %, C = 0.4 %. ×750
Heated to 780°C

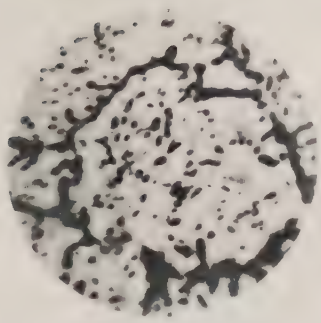

Cu = 1 %, C = 1.3 %. ×780
Heated to 800°C

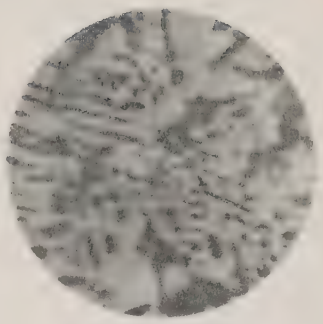

Cu = 1 %, C = 2 %. ×750
Heated to 770°C

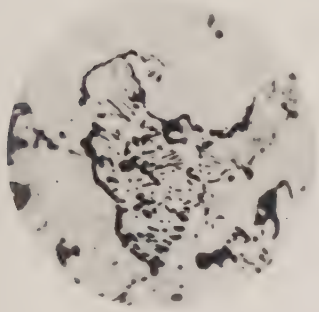

Cu = 2 %, C = 0.4 %. ×750
Heated to 790°C

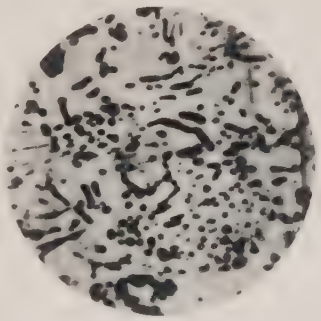

Cu = 2 %, C = 1.3 %. ×750
Heated to 790°C

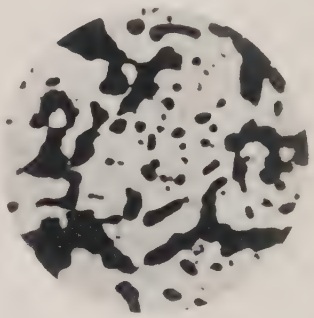

Cu = 2 %, C = 2 %. ×750
Heated to 780°C

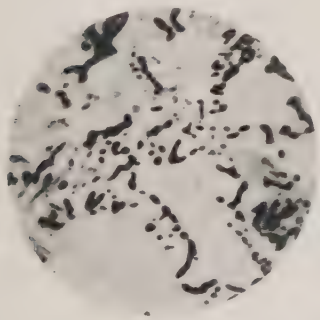

Cu = 3 %, C = 0.7 %. ×750
Heated to 820°C

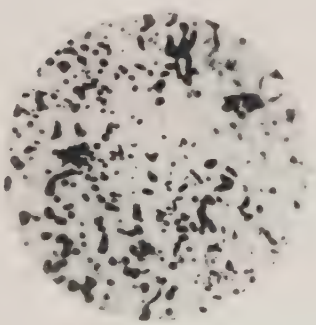

Cu = 3 %, C = 0.9 %. ×750
Heated to 800°C

Cu = 3 %, C = 1.3 %. ×750
Heated to 820°C

Cu = 4 %, C = 0.7 %. ×750
Heated to 790°C

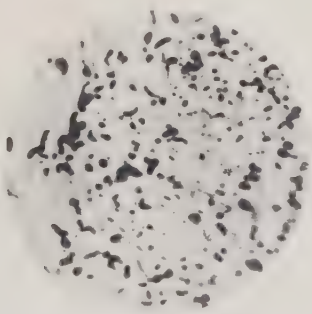

Cu = 4 %, C = 0.9 %. ×750
Heated to 780°C

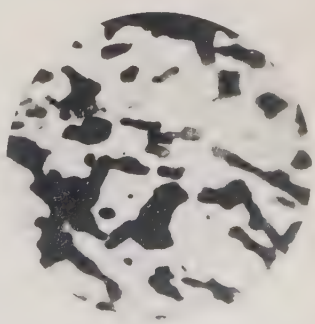

Cu = 4 %, C = 2 %. ×750
Heated to 950°C

Über die Doppelsechs.

Von

Tadahiko Kubota.

Im Folgenden möchte ich den Schläflischen Satz sowie den Grace-Wrenschen Satz über die Doppelsechs durch eine einheitliche Methode beweisen und zwar mit Hilfe der darstellenden Geometrie.

Es ist bei perspektiver Darstellung in der darstellenden Geometrie wohl bekannt, dass eine Gerade g im Raume durch zwei Punkte G_1, G_2 in der Ebene dargestellt werden kann; in diesem Falle wird die Bedingung dafür, dass die beiden durch G_1, G_2 und H_1, H_2 dargestellten Geraden sich schneiden, durch den Parallelismus der Geraden $G_1 H_1$ und $G_2 H_2$ ausgedrückt.

Transformiert man durch die obige Methode den Schläflischen Satz über die Doppelsechs in die Ebenengeometrie so erhält man den Satz:

Nimmt man sechs Punktepaare $A_1 A_2$, $B_1 B_2$, $C_1 C_2$, $D_1 D_2$, $E_1 E_2$ *und* $F_1' F_2'$ *derartig, dass*

$$A_1F_1' // A_2F_2',\ B_1F_1' // B_2F_2',\ C_1F_1' // C_2F_2',\ D_1F_1' // D_2F_2',\ E_1F_1' // E_2F_2'$$

und bestimme man fünf andere Punktepaare

$$A_1' A_2',\quad B_1' B_2',\quad C_1' C_2',\quad D_1' D_2',\quad E_1' E_2'$$

derartig dass

$A_1' B_1 // A_2' B_2$	$A_1' C_1 // A_2' C_2$
$A_1' D_1 // A_2' D_2$	$A_1' E_1 // A_2' E_2$
$B_1' A_1 // B_2' A_2$	$B_1' C_1 // B_2' C_2$
$B_1' D_1 // B_2' D_2$	$B_1' E_1 // B_2' E_2$
$C_1' A_1 // C_2' A_2$	$C_1' B_1 // C_2' B_2$

$C_1' D_1 // C_2' D_2$ $\quad$ $C_1' E_1 // C_2' E_2$

$D_1' A_1 // D_2' A_2$ $\quad$ $D_1' B_1 // D_2' B_2$

$D_1' C_1 // D_2' C_2$ $\quad$ $D_1' E_1 // D_2' E_2$

$E_1' A_1 // E_2' A_2$ $\quad$ $E_1' B_1 // E_2' B_2$

$E_1' C_1 // E_2' C_2$ $\quad$ $E_1' D_1 // E_2' D_2$

sind, dann existiert ein Punktepaar $F_1 F_2$ derartig, dass
$A_1' F_1 // A_2' F_2$, $B_1' F_1 // B_2' F_2$, $C_1' F_1 // C_2' F_2$, $D_1' F_1 // D_2' F_2$, $E_1' F_1 // E_2' F_2$ *sind.*

Wenn man diesen Satz in der ebenen Geometrie beweisen kann, so kann man die Richtigkeit des Schläflischen Satzes über die Doppelsechs behaupten.[1]

Hilfssatz 1. *Man nehme zwei Punktepaare $A_1 A_2$, $B_1 B_2$ auf der Ebene derartig, dass $A_1 B_1$ und $A_2 B_2$ nicht-parallel sind. Nimmt man einen Punkt X_1 in der Ebene beliebig, so kann man zu diesem Punkte X_1 den Punkt X_2 derartig zuordnen lassen, dass*

$$A_1 X_1 // A_2 X_2, \quad B_1 X_1 // B_2 X_2$$

sind. Bewegt sich der Punkt X_1 auf einem durch A_1, B_1 hindurchgehenden Kegelschnitt, so bewegt sich der entsprechende Punkt X_2 auf einem durch A_2, B_2 hindurchgehenden Kegelschnitte, welcher mit dem ursprünglichen ähnlich und und ähnlich gelegen ist. Dies ist eine Art der (1, 1) deutigen quadratischen Punktverwandtschaften.

Hilfssatz 2. *Man nehme drei feste Punktepaare $A_1 A_2$, $B_1 B_2$, $C_1 C_2$ auf der Ebene und lasse sich den Punkt X_1 derartig bewegen, dass die drei zu $A_1 X_1$ $B_1 X_1$ $C_1 X_1$ parallelen Geraden, welche bzw. durch A_2, B_2, C_2 hindurchgehen, sich in demselben Punkte X_2 schneiden. Dann ist der geometrische Ort des Punktes X_1 ein Kegelschnitt, welcher durch $A_1 B_1 C_1$ hindurchgeht. Dieser Kegelschnitt ist mit dem entsprechenden Kegelschnitte, dem geometrischen Orte des Punktes X_2, ähnlich und ähnlich gelegen.*

Aus dem obigen Hilfssatz erhält man den Hilfssatz 3.

---

(1) Diese Methode ist durch Umformung der Bakerschen gebildet, Vgl. Baker Princeples of geometry III.

Wenn nun vier Punktepaare $A_1 A_2$, $B_1 B_2$, $C_1 C_2$, $D_1 D_2$, *gegeben sind, so existieren zwei Punktepaare* X_1, X_2 *derartig, dass*

$$A_1 X_1 // A_2 X_2,\ B_1 X_1 // B_2 X_2,\ C_1 X_1 // C_2 X_2,\ D_1 X_1 // D_2 X_2$$

sind.

Hilfssatz 4. *Wenn das Kegelschnittpaar* $\mathfrak{K}_1 \mathfrak{K}_2$ *und das mit* $\mathfrak{K}_1 \mathfrak{K}_2$ *ähnliche und ähnlich gelegene Kegelschnittpaar* $\mathfrak{L}_1 \mathfrak{L}_2$ *sich in zwei Punktquadrupeln* $P Q R S$ *und* $P' Q' R' S'$ *schneiden, sodass die beiden Verbindungslinien* $P Q$ *und* $P' Q'$ *zueinander parallel sind, so müssen auch die Verbindungslinien* $R S$, $R' S'$ *zueinander parallel sein.*

Schneidet man diese vier Kegelschnitte durch die unendlich ferne Gerade, so erhält man zwei Paare von Schnittpunkten, welche für ähnliche und ähnlich gelegene Kegelschnitte dieselben sind. Diese beiden Paare von Schnittpunkten bestimmen ein und dieselbe Involution. Die Schnittpunkte der Geraden $R S$ bzw. $R' S'$ mit der unendlich fernen Geraden müssen bei dieser Involution der konjugierte Punkt vom Schnittpunkte der Geraden $P Q$ bezw. $P' Q'$ mit der unendlich fernen Geraden sein, und folglich müssen sie ein und derselbe Punkt sein. Damit ist der Hilfssatz bewiesen.

Hilfssatz 5. *Zieht man beim obigen Hilfssatz zwei Paare von parallelen Geraden* $P M$, $P' M'$ *und* $Q N$, $Q' N'$, welche $\mathfrak{K}_1 \mathfrak{K}_2$ *bezw.* $\mathfrak{L}_1 \mathfrak{L}_2$ *in den Punkten* M, M', N, N' *schneiden, und sind die Verbindungslinien* $M N$ *und* $M' N'$ *zueinander parallel, so müssen die Geradenstrecken* $M N$ *und* $M' N'$ *inbezug auf die Geraden* $R S$ *und* $R' S'$ *ähnlich und ähnlich gelegen sein.*

Bezeichnet man nun die Schnittpunkte der Geraden $P M$, $P' M'$ mit den Kegelschmitten $\mathfrak{L}_1 \mathfrak{L}_2$ bzw. mit T, T', dann ist nach dem Hilfssatz 5

$$N T // N' T'.$$

Die Punktepaare $M M'$; $T T'$; $W W'$, wobei $W W'$ die Schnittpunkte der Geraden $P M$, $P' M'$ bzw. mit den Geraden $R S$, $R' S'$ bedeuten, sind die entsprechenden Punkte einer gewissen Projektivität. Bezeichnet man den Schnittpunkt eines Kegelschnitts $\mathfrak{M}$ des Büschels $P Q R S$ mit der Geraden $P M$ durch X und den Schnittpunkt des zu $\mathfrak{M}$ ähnlichen und

ähnlich gelegenen Kegelschnittes $\mathfrak{M}'$ des Büschels $P'\,Q'\,R'\,S'$ durch X', dann wird die obige Projektivität durch Zuordnung der Punkte X, X' entstehen. Da aber bei dieser Projektivität der unendlich ferne Punkt sich selbst entspricht, so muss diese Projektivität eine Ähnlichkeit sein. Bezeichnet man nun die Schnittpunkte der Geraden $M\,N$ und $M'\,N'$ mit der Geraden $R\,S$ bzw. $R'\,S'$ durch U, U', so sind die Dreiecke $M\,W\,U$ und $M'\,W'\,U'$ ähnlich und ähnlich gelegen,

d. h. $$M\,T:\ T\,W = M'\,T' : T'\,W'$$

und $$M\,N:\ N\,U = M'\,N' : N'\,U'.$$

Damit ist der Satz bewiesen.

Nun gehen wir zum Beweis des Hauptsatzes über. Man bestimme das Punktepaar $F_1\,F_2$ derartig, dass

$$A_1'\,F_1 // A_2'\,F_2,\ B_1'\,F_1 // B_2'\,F_2,\ C_1'\,F_1 // C_2'\,F_2,\ D_1'\,F_1 // D_2'\,F_2.$$

Zuerst betrachte man zwei Tripel von Punkten

$$B_1\,C_1\,E_1 \quad \text{und} \quad B_2\,C_2\,E_2$$

und die daraus durch den Hilfssatz 2 bestimmten Kegelschnitte $\mathfrak{H}_1\,\mathfrak{H}_2$ und ferner die beiden Tripel von Punkten

$$B_1'\,C_1'\,D_1' \quad \text{und} \quad B_2'\,C_2'\,D_2'$$

und die daraus durch den Hilfssatz 2 bestimmten Kegelschnitte $\mathfrak{L}_1, \mathfrak{L}_2$. Da aber E_1, E_2 und $D_1'\,D_2'$ die Beziehungen

$$B_1'\,E_1 // B_2'\,E_2 \qquad C_1'\,E_1 // C_2'\,E_2$$
$$D_1'\,E_1 // D_2'\,E_2 \qquad D_1'\,B_1 // D_2'\,B_2$$
$$D_1'\,C_1 // D_2'\,C_2$$

erfüllen, so müssen $E_1\,E_2\ D_1'\,D_2'$ bzw. auf den Kegelschnitten $\mathfrak{L}_1, \mathfrak{L}_2, \mathfrak{H}_1, \mathfrak{H}_2$ liegen. Ferner ist

$$E_1\,D_1' // E_2\,D_2'.$$

Wendet man auf diese Figur den Hilfssatz 5 an, so folgt dass $B_1'\,C_1$ und $B_2'\,C_2$, $B_1\,C_1'$ und $B_2\,C_2'$, $A_1'\,F_1$ und $A_2'\,F_2$, $A_1\,F_1'$ und $A_2\,F_2'$ inbezug auf die Verbindungslinien von zwei anderen Schnittpunkten von $\mathfrak{H}_1\,\mathfrak{H}_2$ und $\mathfrak{L}_1, \mathfrak{L}_2$ ähnlich und ähnlich gelegen sein müssen.

Nun betrachte man in gleicher Weise zwei Paare von Punkttripeln

$$A_1\, C_1\, E_1 \quad \text{und} \quad A_2\, C_2\, E_2$$
$$A_1'\, C_1'\, D_1' \quad \text{und} \quad A_2'\, C_2'\, D_2'$$

und die daraus durch den Hilfssatz 2 bestimmten Kegelschnittpaare $\mathfrak{C}_1, \mathfrak{U}_1$ und $\mathfrak{C}_2\, \mathfrak{U}_2$. Diese beiden Kegelschnittpaare $\mathfrak{C}_1\, \mathfrak{C}_2$ und $\mathfrak{U}_1\, \mathfrak{U}_2$ gehen durch $D_1'\, E_1$ bzw. $D_2'\, E_2$ hindurch. Folglich sind die Streckenpaare $A_1'\, C_1$ und $A_2'\, C_2$, $A_1\, C_1'$ und $A_2\, C_2'$, $B_1'\, F_1$ und $B_2'\, F_2$, $B_1\, F_1'$ und $B_2\, F_2'$ in-bezug auf die Verbindungslinien der anderen Schnittpunkte von $\mathfrak{C}_1\, \mathfrak{C}_2$ und $\mathfrak{U}_1\, \mathfrak{U}_2$ ähnlich und ähnlich gelegen.

Ferner betrachte man zwei Paare von Punkttripeln

$$A_1\, B_1\, E_1 \quad \text{und} \quad A_2\, B_2\, E_2$$
$$A_1'\, B_1'\, D_1' \quad \text{und} \quad A_2'\, B_2'\, D_2'$$

und die daraus durch den Hilfssatz 2 bestimmten Kegelschnittpaare $\mathfrak{W}_1\, \mathfrak{V}_1$, $\mathfrak{W}_2\, \mathfrak{V}_2$.

Diese Kegelschnitte $\mathfrak{W}_1\, \mathfrak{W}_2$ und $\mathfrak{V}_1\, \mathfrak{V}_2$ gehen durch $D_1'\, E_1$ bzw. $D_2'\, E_2$ hindurch.

Folglich sind die Streckenpaare $A_1'\, B_1$ und $A_2'\, B_2$, $A_1\, B_1'$ und $A_2\, B_2'$, $C_1'\, F_1$ und $C_2'\, F_2$, $C_1\, F_1'$ und $C_2\, F_2'$ ähnlich und ähnlich gelegen inbezug auf die Verbindungslinien der anderen Schnittpunkte von $\mathfrak{W}_1\, \mathfrak{W}_2$ und $\mathfrak{V}_1\, \mathfrak{V}_2$.

Also sind die Strecken $B_1'\, C_1$ und $B_2'\, C_2$, $B_1\, C_1'$ und $B_2\, C_2'$, $A_1'\, F_1$ und $A_2'\, F_2$, $A_1\, F_1'$ und $A_2\, F_2'$ inbezug auf zwei parallele Geraden ähnlich und ähnlich gelegen. Auch sind die Strecken $A_1'\, C_1$ und $A_2'\, C_2$, $A_1\, C_1'$ und $A_2\, C_2'$, $B_1'\, F_1$ und $B_2'\, F_2$, $B_1\, F_1'$ und $B_2\, F_2'$, inbezug auf zwei parallele Geraden ähnlich und ähnlich gelegen. Ferner sind die Strecken $A_1'\, B_1$ und $A_2'\, B_2$, $A_1\, B_1'$ und $A_2\, B_2'$ $C_1'\, F_1$ und $C_2'\, F_2$, $C_1\, F_1'$ und $C_2\, F_2'$ ähnlich und ähnlich gelegen inbezug auf zwei parallele Garaden.

Bestimmt man nun aus den Parallelitätsbedingungen

$$A_1'\, F_1 // A_2'\, F_2,\ B_1'\, F_1 // B_2'\, F_2,\ C_1'\, F_1 // C_2'\, F_2,\ E_1'\, F_1 // E_2'\, F_2$$

das Punktepaar $F_1\, F_2$, so müssen diese Punkte $F_1\, F_2$ auch dieselben Bedingungen erfüllen, denn die obigen Bedingungen ändern sich nicht durch Vertauschung von D und E, D' und E'.

Die parallelen Garaden, bezüglich welcher die Strecken $B_1' C_1$ und $B_2' C_2$, $B_1 C_1'$ und $B_2 C_2'$, $A_1 F_1'$ und $A_2 F_2'$ ähnlich und ähnlich gelegen sind, sind eindeutig bestimmbar.

Zu diesem Zwecke bestimme man den Schnittpunkt von $B_1' B_2'$ und $C_1 C_2$ mit L und den Schnittpunkt von $B_1 B_2$ und $C_1' C_2'$ mit M und den Schnittpunkt von $A_1 A_2$ und $F_1' F_2'$ mit N, dann bestimme man auf der Verbindungslinie $L M$ zwei Punkte $P Q$ derartig, dass

$$P L : Q L = B_1' C_1 : B_2' C_2$$
$$P M : Q M = B_1 C_1' : B_2 C_2'.$$

Durch diese beiden Bedingungen sind P und Q eindeutig bestimmbar. Nun bestimme man auf der Verbindungslinie von $M N$ die Punkte $P' Q'$ derartig, dass

$$P' M : Q' M = B_1 C_1' : B_2 C_2',$$
$$P' N : Q' N = A_1 F_1' : A_2 F_2'$$

dann sind $P' Q'$ daraus eindeutig bestimmbar. Verbindet man nun $P P'$ und $Q Q'$, so sind sie einander parallel und die gesuchten Geraden.

In gleicher Weise sind die beiden parallelen Geraden, bezüglich welcher die Strecken $A_1' C_1$ und $A_2' C_2$, $A_1 C_1'$ und $A_2 C_2'$, $B_1 F_1'$ und $B_2 F_2'$ ähnlich und ähnlich gelegen sind, eindeutig bestimmbar, und die beiden parallelen Geraden, bezüglich welcher die Strecken $A_1' B_1$ und $A_2' B_2$, $A_1 B_1'$ und $A_2 B_2'$, $C_1 F_1'$ und $C_2 F_2'$ ähnlich und ähnlich gelegen sind, auch eindeutig bestimmbar.

Nun sind die Strecken $A_1' F_1$ und $A_2' F_2$, $B_1' F_1$ und $B_2' F_2$, $C_1' F_1$ und $C_2' F_2$ bezw. inbezug auf diese drei Paare paralleler Geraden ähnlich und ähnlich gelegen. Durch diese Bedingung ist das Punktepaar $F_1 F_2$ eindeutig bestimmbar. Also müssen die beiden auf zweierlei Weisen bestimmten Punktepaare $F_1 F_2$ vollständig übereinstimmen. Damit ist vorliegender Satz bewiesen.

Über den Grace-Wrenschen Satz habe ich in einer früheren Arbeit den folgenden Satz bewiesen,[1] aus welchem der Wrensche Satz unmittelbar hergeleitet wird.

---

(1) Science Reports Tôhoku Imp. Univ. VI, p. 89.

Wenn die sechs Geraden p, q, a_1, a_2, a_3, a_4 *die Gerade* g *schneiden und man die andere Schnittlinie von* $(p\,q\,a_1\,a_2)$, $(p\,q\,a_1\,a_3)$, $(p\,q\,a_2\,a_3)$, $(p\,q\,a_3\,a_4)$, $(p\,q\,a_2\,a_4)$ *und* $(p\,q\,a_1\,a_4)$ *bezw. mit* β_{34}, β_{24}, β_{14}, β_{12}, β_{13} *und* β_{23} *bezeichnet, dann besitzen die Regelscharen*

$$(\beta_{12}\ \beta_{13}\ \beta_{14})\quad (\beta_{21}\ \beta_{23}\ \beta_{24})\quad (\beta_{31}\ \beta_{32}\ \beta_{34})\quad (\beta_{41}\ \beta_{42}\ \beta_{43})$$

ein und dieselbe Erzeugende.

Diesen Satz werde ich hier durch die Methode der darstellenden Geometrie beweisen.

Es seien zwei Punkte $G_1\,G_2$ und sechs Punktepaare $P\,P'$, $Q\,Q'$, $A_1\,A_1'$, $A_2\,A_2'$, $A_3\,A_3'$ und $A_4\,A_4'$ derartig gegeben, dass

$$\begin{array}{ll} G_1\,P//G_2\,P' & G_1\,Q//G_2\,Q' \\ G_1\,A_1//G_2\,A_1' & G_1\,A_2//G_2\,A_2' \\ G_1\,A_3//G_2\,A_3' & G_1\,A_4//G_2\,A_4' \end{array}$$

sind.

Nun bestimme man aus

$$\begin{array}{ll} P\,Q\ A_1\,A_2, & P'\,Q'\ A_1'\,A_2' \\ P\,Q\ A_1\,A_3, & P'\,Q'\ A_1'\,A_3' \\ P\,Q\ A_2\,A_3, & P'\,Q'\ A_2'\,A_3' \\ P\,Q\ A_3\,A_4, & P'\,Q'\ A_3'\,A_4' \\ P\,Q\ A_2\,A_4, & P'\,Q'\ A_2'\,A_4' \\ P\,Q\ A_1\,A_4, & P'\,Q'\ A_1'\,A_4' \end{array}$$

durch den Hilfssatz 3 sechs neue Punktepaare

$$B_{34}\ B_{34}';\quad B_{24}\ B_{24}';\quad B_{14}\ B_{14}';\quad B_{12}\ B_{12}';\quad B_{13}\ B_{13}'\quad B_{23}\ B_{23}',$$

und diese sind nun die Schnittpunkte zweier Kegelschnitte, welche bzw. durch

$$\begin{array}{ll} P\,Q\,A_1 & P'\,Q'\,A_1' \\ P\,Q\,A_2 & P'\,Q'\,A_2' \\ P\,Q\,A_3 & P'\,Q'\,A_3' \\ P\,Q\,A_4 & P'\,Q'\,A_4' \end{array}$$

bestimmt werden, und durch G_1, G_2 hindurchgehen.

Nun bestimme man nach dem Hilfssatz 2 durch

$$\begin{array}{ll} (B_{12}\ B_{13}\ B_{14}) & (B_{12}'\ B_{13}'\ B_{14}') \\ (B_{21}\ B_{23}\ B_{24}) & (B_{21}'\ B_{23}'\ B_{24}') \\ (B_{31}\ B_{32}\ B_{34}) & (B_{31}'\ B_{32}'\ B_{34}') \\ (B_{41}\ B_{42}\ B_{43}) & (B_{41}'\ B_{42}'\ B_{43}') \end{array}$$

vier Kegelschnittpaare. Diese Kegelschnittpaare gehen durch P, Q bezw. durch P', Q' hindurch.

Daraus kann man folgern, dass diese vier Kegelschnittpaare durch ein und dasselbe Punktepaar hindurchgehen. Dies kann man beweisen, indem man die Punkte P, Q als imaginäre Kreispunkte im Unendlichen annimmt und die ganze Figur inbezug auf G_1 durch Transformation reziproker Radien transformiert und den vorgelegten Satz in den Miquelschen Satz transformiert.

Bezeichnet man nun dieses Schnittpunktepaar durch $X_1\ X_2$, dann gehören $X_1\ X_2$ zu den Reihen von Punkten, denen B_{12}, $B_{13}\ B_{14}$ bezw. B_2', B_{13}' und B_{14}' angehören, d. h. $PX_1 // P'X_2$, $Q\,X_1 // Q'\,X_2$.

Dieses Punktepaar $X_1\ X_2$ bestimmt also eine Gerade, welche gleichzeitig den Regelscharen

$$\begin{array}{lll} \beta_{12} & \beta_{13} & \beta_{14} \\ \beta_{21} & \beta_{23} & \beta_{24} \\ \beta_{31} & \beta_{32} & \beta_{34} \\ \beta_{41} & \beta_{42} & \beta_{43} \end{array}$$

angehört. Damit ist vorliegender Satz bewiesen.

Über die Eibereiche im n-dimensionalen Raume.

Von

Tadahiko Kubota.

In meiner vorigen Arbeit[1] habe ich einige Ungleichheitsbeziehungen über die Eibereiche im n-dimensionalen Raume beim Gebrauch der Hyperkugelfunktionen hergeleitet. Hier möchte ich die Minkowskische Ungleichheit auf den n-dimensionalen Raum übertragen und zwar durch Verallgemeinerung der Methode der Fourier-Reihen von W. Blaschke.[2]

Verallgemeinerung des Minkowskischen Satzes.

Es seien zwei Eibereiche $\mathfrak{K}$, $\mathfrak{K}'$ *im n-dimensionalen Raume vorgelegt und sei der Bereich* $\mathfrak{K}+t\mathfrak{K}'$ *daraus hergeleitet. Wenn die Grösse* V_{n-2} *für diesen Bereich* $\mathfrak{K}+t\mathfrak{K}'$

$$V_{n-2}(\mathfrak{K}+t\mathfrak{K}') = V_{n-2}(\mathfrak{K}) + 2\,V_{n-2}(\mathfrak{K},\mathfrak{K}')\,t + V_{n-2}(\mathfrak{K}')\,t^2,$$

ist, dann gilt die Ungleichheit

$$V_{n-2}(\mathfrak{K}\ \mathfrak{K}')^2 - V_{n-2}(\mathfrak{K})\,V_{n-2}(\mathfrak{K}') \geqq 0,$$

wobei die Gleichheit dann und nur dann gilt, wenn die beiden Eibereiche ähnlich und ähnlich gelegen sind.

Der erste Beweis. Die Stützhyperebenenfunktionen H, H' der beiden Eibereiche $\mathfrak{K}$, $\mathfrak{K}'$ seien in die Reihe der Hyperkugelfunktionen entwickelbar:

$$H \sim X_0 + X_1 + X_2 + \cdots\cdots + X_m + \cdots\cdots,$$
$$H' \sim Y_0 + Y_1 + Y_2 + \cdots\cdots + Y_m + \cdots\cdots,$$

---

(1) Diese Reports, Series I, Vol. XIV, (1925).

(2) Jahresberichte der D. M. V., Bd. 23 (1914).

dann ist die Stützhyperebenenfunktion $H+tH'$ für den Eibereich $\mathfrak{K}+t\mathfrak{K}'$

$$H+tH' \sim \sum_{m=0}^{\infty}(X_m+tY_m).$$

Daraus ergeben sich nach der zitierten Arbeit:

$$V_{n-2}(\mathfrak{K}) = -\frac{1}{2}\sum_{m=0}^{\infty}(m-1)(m+n-1)\iint\cdots\cdots\int X_m^2\,d\omega,$$

$$V_{n-2}(\mathfrak{K}') = -\frac{1}{2}\sum_{m=0}^{\infty}(m-1)(m+n-1)\iint\cdots\cdots\int Y_m^2\,d\omega,$$

$$V_{n-2}(\mathfrak{K}+t\mathfrak{K}') = -\frac{1}{2}\sum_{m=0}^{\infty}(m-1)(m+n-1)\iint\cdots\cdots\int (X_m+tY_m)^2\,d\omega,$$

woraus folgt

$$V_{n-2}(\mathfrak{K},\mathfrak{K}') = -\frac{1}{2}\sum_{m=0}^{\infty}(m-1)(m+n-1)\iint\cdots\cdots\int X_m Y_m\,d\omega.$$

Nun ist

$$Y_0^2\{V_{n-2}(\mathfrak{K},\mathfrak{K}')^2 - V_{n-2}(\mathfrak{K})\,V_{n-2}(\mathfrak{K}')\}$$
$$= V_{n-2}(\mathfrak{K}, Y_0\mathfrak{K}-X_0\mathfrak{K}')^2 - V_{n-2}(Y_0\mathfrak{K}-X_0\mathfrak{K}').\ V_{n-2}(\mathfrak{K}).$$

Anderseits ist

$$V_{n-2}(\mathfrak{K}, Y_0\mathfrak{K}-X_0\mathfrak{K}')$$
$$= -\frac{1}{2}\sum_{m=2}^{\infty}(m-1)(m+n-1)\iint\cdots\cdots\int X_m(Y_0X_m-X_0Y_m)\,d\omega,$$

$$V_{n-2}(Y_0\mathfrak{K}-X_0\mathfrak{K}')$$
$$= -\frac{1}{2}\sum_{m=2}^{\infty}(m-1)(m+n-1)\iint\cdots\cdots\int (Y_0X_m-X_0Y_m)^2\,d\omega.$$

Folglich ist

$$Y_0^2\{V_{n-2}(\mathfrak{K},\mathfrak{K}')^2 - V_{n-2}(\mathfrak{K})\,V_{n-2}(\mathfrak{K}')\}$$
$$= \left\{-\frac{1}{2}(m-1)(m+n-1)\iint\cdots\cdots\int X_m(Y_0X_m-X_0Y_m)\,d\omega\right\}^2$$
$$+ V_{n-2}(\mathfrak{K}) \times -\frac{1}{2}\sum_{m=2}^{\infty}(m-1)(m+n-1)\iint\cdots\cdots\int (Y_0X_m-X_0Y_m)^2\,d\omega \geqq 0,$$

wobei die Gleichheit dann und nur dann gilt wenn

$$\frac{X_0}{X_m} = \frac{Y_0}{Y_m}, \quad m = 2, 3, 4 \ldots\ldots\ldots$$

sind, d. h. wenn die beiden Eibereiche ähnlich und ähnlich gelegen sind.

Damit ist der vorgelegte Satz bewiesen.

Der zweite Beweis. Da im Allgemeinen

$$V_{n-2}(Y_0 \mathfrak{K} - X_0 \mathfrak{K}') < 0$$

ist, so muss

$$V_{n-2}(\mathfrak{K}) + 2\, V_{n-2}(\mathfrak{K}, \mathfrak{K}')\, t + V_{n-2}(\mathfrak{K}')\, t^2$$

zwei reelle Wurzeln besitzen. Somit gilt

$$V_{n-2}(\mathfrak{K}, \mathfrak{K}')^2 > V_{n-2}(\mathfrak{K})\, V_{n-2}(\mathfrak{K}')$$

im Allgemeinen.

$$V_{n-2}(\mathfrak{K}, \mathfrak{K}') = V_{n-2}(\mathfrak{K})\, V_{n-2}(\mathfrak{K}')$$

kann dann und nur dann gelten wenn

$$V_{n-2}(Y_0 \mathfrak{K} - X_0 \mathfrak{K}') = 0$$

d. h. wenn

$$\frac{X_0}{X_m} = \frac{Y_0}{Y_m} \quad m = 2, 3, 4 \ldots\ldots\ldots$$

Damit ist der vorgelegte Satz bewiesen.

Folgerung. Aus dieser Ungleichheit kann man den Brunn-Minkowski-Fujiwaraschen Satz auf den n-dimensionalen Raum übertragen:

$$V_{n-2}\left(\frac{\mathfrak{K}+\mathfrak{K}'}{2}\right) \geqq \left(\frac{\sqrt{V_{n-2}(\mathfrak{K})} + \sqrt{V_{n-2}(\mathfrak{K}')}}{2}\right)^2,$$

wobei die Gleichheit dann und nur dann gilt, wenn die beiden Eibereiche ähnlich und ähnlich gelegen sind.

Der Beweis: Aus dem obigen Satz erhält man

$$V_{n-2}\left(\frac{\mathfrak{K}+\mathfrak{K}'}{2}\right) = \frac{1}{4} V_{n-2}(\mathfrak{K}) + \frac{1}{2} V_{n-2}(\mathfrak{K}, \mathfrak{K}') + \frac{1}{4} V_{n-2}(\mathfrak{K}')$$

$$\geqq \frac{1}{4} V_{n-2}(\mathfrak{K}) + \frac{1}{2}\sqrt{V_{n-2}(\mathfrak{K})\, V_{n-2}(\mathfrak{K}')} + \frac{1}{4} V_{n-2}(\mathfrak{K}')$$

$$= \frac{1}{4}\left\{\sqrt{V_{n-2}(\mathfrak{K})} + \sqrt{V_{n-2}(\mathfrak{K}')}\right\}^2,$$

wobei die Gleichheit dann und nur dann gilt wenn die beiden Eibereiche ähnlich und ähnlich gelegen sind, w. z. b. w.

Endlich möchte ich noch einen Satz hinzufügen.

Wenn die Summe der Hauptkrümmungsradien $R_1 R_2 \ldots\ldots R_{n-1}$ einer konvex-geschlossenen Hyperfläche im n-dimensionalen Raume konstant ist, so ist die Fläche notwendig eine Hyperkugel.

Entwickelt man die Stützhyperebenenfunktion der konvex-geschlossenen Hyperfläche in die Reihe:

$$H \sim X_0 + X_1 + X_2 + \ldots\ldots X_m + \ldots\ldots,$$

so ist

$$R_1 + R_2 + R_3 + \ldots\ldots + R_{n-1} = -\sum_{m=0}^{\infty} (m-1)(m+n-1) X_m.$$

Nach der Voraussetzung ist

$$R_1 + R_2 + \ldots\ldots + R_{n-1} = \text{konst.}$$

Folglich ist

$$X_m = 0, \quad m = 2, 3\ldots\ldots,$$

und

$$H = X_0 + X_1,$$

was eine Hyperkugel bedeutet.

Damit ist der Satz bewiesen.

Sendai, den 1. Juni, 1925.

A Kinetic Theory of the Viscosity of Liquids.

By

Mitsuru Satô.

1. INTRODUCTION.

The kinetic theory of the viscosity of gases was, as is well known, first treated by Maxwell. According to him the viscosity is due to the momentum transfer which is caused by the migration of molecules. Hence the viscosity must increase with the rise of temperature, which conclusion is in good agreement with the facts. This theory has been studied by many physicists since the time of Maxwell and become an effeetive means of calculating the molecular diameter. But regarding the viscosity of liquids the writer is unaware of any thorough and well-framed theory. The remarkable difference in the viscosity of liquids as compared with that of gases consists in the manner of the variation with respect to temperature; i. e., the viscosity decreases greatly with the rise of temperature. When this fact is considered the mechanism which gives rise to viscosity in the case of liquids must be very different from that in the case of gases. There have been attempts to explain this phenomenon by the momentum transfer due to molecular impact[1] or molecular migration[2] in the same manner as in the case of gases but none of them has yet been favoured with success. According to the idea entertained by the writer the more important part of the liquid viscosity

(1) J. D. Van der Waals. Jr. Akad. Amsterdam Proc. **21**, (1919), 743, 1283. G. Jäger, Die Fortschritte der kinetischen Gastheorie, 126.

(2) Kleemann, Kinetic Theory of Gases and Liquids, 113.

has its origin in the mutual action among molecules, i.e. in the molecular force, the effect due to the momentum transfer being very small compared with the above one.

To explain viscosity by this idea, we must assume some law of mutual action between molecules. The simplest law is the one assumed in the gas theory, in which as a first approximation, the molecule is considered to be the centre of attraction. But this assumption fails to explain the liquid viscosity. A second approximation is to consider molecules as dipoles of a constant moment. With this assumption P. Debye treated the dielectric constant of liquids.(1) Also M. Born studied the ionic motion in liquids and the moment of force to which dielectrics are subject by the revolving electric field.(2) Judging from the fact that with many liquids the calculations of P. Debye and M. Born are in good agreement with experiments,(3) this assumption must be regarded as representing well the characteristic properties of the mutual action between molecules. The object of the present paper is to explain viscosity of liquids on the assumptions of Debye and Born.

To treat the molecular impact purely electrically we have to trace to the origin of the repulsive force. But since that force varies inversely as the higher power of the distance between molecules in comparison with the attractive force, it may, as a first approximation be assumed, as is done in the case of the gas theory, that molecules have rigid boundaries. As to the form of the rigid boundary the simplest way is to suppose it to be a simple sphere. But this is a first approximation; actually molecules will not be symmetrical in all directions. One step in advance of this assumption is to suppose something which is long and thin in one direction, and among its possible shapes the one mathematically simplest is a system of two small spheres connected by a thin rigid rod, where, however, the diameters of the spheres are considered to be small in comparison with the length of the rod. This assumption will

(1) P. Debye, Phys. Zs. **13**, (1912), 1.
(2) M. Born Zs. f. Phys. **1**, (1920), 221.
(3) Peter Lertes, Zs. f. Phys. **4**, (1921), 315.

be very different from the actual molecules but it will be sufficient to represent the characteristic property of molecules which are long and thin.

The relation between the geometrical form of molecules and their dipole axes will only be definite when the molecular structure becomes definite. But for simplicity it will here be assumed that the dipole axis and the longitudinal axis of the geometrical form coincide with each other.

The rectangular axes x, y, z which define the position of a molecule in a liquid are taken and the liquid is considered to make a mass motion in the positive direction of x and the velocity to increase in the positive direction of z. (Fig. 1.) Also the velocity gradient is assumed to be constant. Each molecule will make a mass motion and is subject to a thermal agitation as well, so that the actual motion will be very complicated. But when considering the mean effect of the mutual action between molecules, it may be assumed that the centre of each molecule are in a layer of definite thickness which is parallel to the xy plane. Further it is here assumed that the velocity of the mass motion changes discontinuously from one layer to another. Thus if the mean distance of the centres of the adjacent molecules be z_0, the velocity of mass motion changes discontinuously by $z_0 \frac{dv}{dz}$. Where v is the velocity of the mass motion.

Fig. 1.

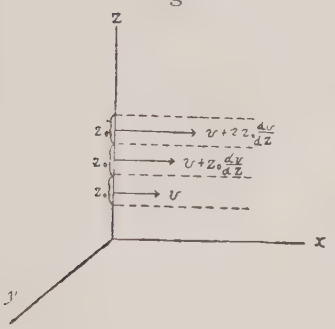

2. THE FIELD OF FORCE DUE TO MOLECULAR IMPACT.

If we now consider a molecule in a certain layer, the momentum which it receives from the surrounding molecules, is not the same for all directions. The momentum in the positive direction of x which it receives from the positive side of z must be greater than that which it receives from the negative side of z. Consequently a couple which tends to bring the long axis of the molecule parallel to the x-axis comes into play. But since this action is due to the molecular impact, it is independent of the sign of the pole.

The force due to impact is equal to the momentum given in unit time and this is determined by the momentum given every time and the number of impacts per unit time ν. The momentum given every time varies with the velocity difference of mass motion of molecules in neighbouring layers or $z_0\frac{dv}{dz}$. Hence if the force of the couple be f, we may put

$$f = \Phi\left(\nu, z_0\frac{dv}{dz}\right).$$

We are unable to determine the functional form of the function Φ, but in extreme cases it is easy to do so. If $\frac{dv}{dz}$ be so large that any molecule comes into collision with different molecules in every collision, the number of collisions is proportional to the product of the density ρ and $z_0\frac{dv}{dz}$, and as the momentum given every time is proportional to $z_0\frac{dv}{dz}$, it may be considered that

$$f = \text{const} \times \rho\left(z_0\frac{dv}{dz}\right)^2.$$

If however $\frac{dv}{dz}$ is so small that any molecule comes into collision with a different molecule after it has collided with the same molecule a very large number of times, the number of giving momentum will be proportional to the number of collisions of the molecule with the surrounding molecules due to thermal agitation. The momentum given every time will be proportional to $z_0\frac{dv}{dz}$. So that

$$f = \text{const. } \nu\, z_0\frac{dv}{dz}.$$

Since hitherto the investegation of the viscosity in liquids has been largely limited to the case where their velocity gradient is very small, the same condition will be assumed below.

To find out what relation exists between the number of collision of molecules ν and the molecular orientation, let the angle which the molecular axis makes with x-axis be θ (Fig. 2), and that the

Fig. 2

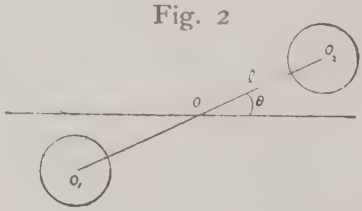

axes which are parallel to x, y, z and have their origin at the centre of one of the spheres of a molecule be ξ, η, ζ respectively. (Fig. 3).

Let the polar angle φ be measured from the axis ζ and the azimuthal angle ψ from the negative direction of ξ, and the radius of the sphre a. Then the elementary area of the spherical surface is expressed by $a^2 \sin\varphi \, d\varphi \, d\psi$. If the number of molecules which impinge upon the unit area in unit time be n, that for the elementary area in unit time is

Fig. 3.

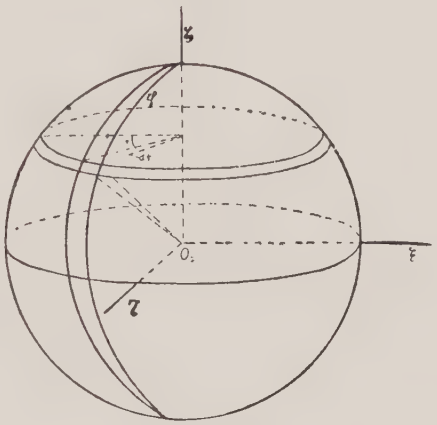

$$n \, a^2 \sin\varphi \, d\varphi \, d\psi.$$

The direction cosines of the surface normal, at a point on the spherical surface are

$$\sin\varphi \cos\psi, \qquad \sin\varphi \sin\psi, \qquad \cos\varphi.$$

If in one impact the momentum given be $mz_0 \dfrac{dv}{dz}$ and the impact be elastic, then its component in the direction of the surface normal is

$$mz_0 \frac{dv}{dz} \sin\varphi \cos\psi,$$

where m is the mass of a molecule.

Hence the x-component of the given momentum is

$$m z_0 \frac{dv}{dz} \sin^2\varphi \cos^2\psi.$$

Accordingly the x-componet of the force due to the velocity gradient of mass motion, and acting on the elementary area, is

$$df = n \, a^2 \, m \, z_0 \frac{dv}{dz} \sin^3\varphi \cos^2\psi \, d\varphi \, d\psi.$$

If we take the elementary area, mentioned above on the negative side of x-aixis on the sphere O_2 in Fig. 2, we may consider an element-

ary area on the sphere O_1 that is symmetrical with the former with respect to O. In the latter case the force df acts in the negative direction of x. Hence if now $OO_1 = OO_2 = l$ the moment of the couple is

$$dc = 2(l\sin\theta + a\cos\varphi)\,df$$

$$= 2\,m\,n\,a^2 z_0 \frac{dv}{dz}(l\sin\theta\sin^3\varphi\cos^2\psi + a\sin^3\varphi\cos\varphi\cos^2\psi)\,d\varphi\,d\psi.$$

Accordingly, the moment of the force acting on the whole surface of the molecule is

$$C = 2\,m\,n\,a^2 z_0 \frac{dv}{dz}\int_{\psi=-\frac{\pi}{2}}^{\frac{\pi}{2}}\int_{\varphi=0}^{\pi}(l\sin\theta\sin^3\varphi\cos^2\psi + a\sin^3\varphi\cos\varphi\cos^2\psi)\,d\varphi\,d\psi$$

$$= \frac{4\pi}{3}a^3 m\,n\,z_0 l\sin\theta\,\frac{dv}{dz}.$$

If the total number of molecules falling on the whole surface of the molecule in unit time be ν, $\nu = 8\pi a^2 n$.

Hence

$$C = \frac{\nu}{6}m z_0 \frac{dv}{dz} l\sin\theta.$$

If we put for simplicity

$$\beta = \frac{\nu}{6}m z_0 \frac{dv}{dz} l \quad \ldots\ldots\ldots\ldots\ldots\ldots\ldots\ldots(1)$$

then

$$C = \beta\sin\theta.$$

When θ becomes small the above argument does not apply. But since the extent to which it does not apply is very small, it will here be assumed that the error introduced by applying the above expression to all possible values of θ is on the whole very small.

If a straight line drawn parallel to the axis of a molecule O_1O_2 through the centre of a unit sphere O and its intersection with the spherical surface be P (Fig. 4), the orientation of the molecule is determined by the position of P on the spherical surface. If now P be on the upper hemisphere initially and θ becomes smaller and smaller and finally zero, by the impacts of molecules in the neighbouring layers and

Fig. 4.

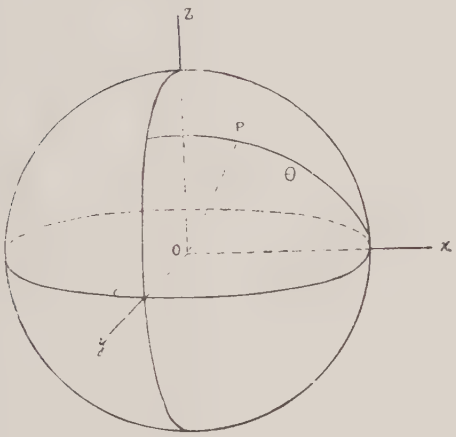

further comes down to the lower hemisphere by virtue of its inertia, then the molecule will be turned again by impacts. Thus the molecule will make continual rotations. But within the limit in which θ is small, the rotating moment C is very small, compared with the disturbing effect due to thermal agitation. So it may be assumed that the number of points coming above the xy-plane and that coming below it, is equal, i.e. macroscopically speaking, we may regard the intersection of the sphere and the xy-plane as the diaphragm line. Thus assumed, the field of the force that turns molecules becomes a conservative one.

In such a field the work necessary for turning the molecule from $\theta = 0$ to θ is

$$u = \beta \int_0^\theta \sin\theta \, d\theta = \beta (1 - \cos\theta).$$

In determining the sense of the molecular axis, if we take the direction from the negative to the positive pole

$$u = \beta (1 \mp \cos\theta),$$

when $\quad 0 \leqq \theta \leqq \pi, \quad -$

and when $\quad \pi \leqq \theta \leqq 2\pi, \quad +.$

3. MEAN POTENTIAL ENERGY BETWEEN TWO MOLECULES AT A GIVEN DISTANCE.

Let the centres of two molecules be O and O′, and their distane r, the dipole intensity of each molecule $\pm e$, the pole distance $2a$, the angles between OO′ and the positive direction of the dipole axis (that is

the direction from $-e$ towards $+e$) λ_1, and λ_2 and ψ_1 and ψ_2 the angles between the xz-plane and the plane defined by each dipole axis and oo′, then the potential energy between the dipoles is

$$u' = -\frac{\mu^2}{2r^3}\left\{-2\cos\lambda_1\cos\lambda_2+\sin\lambda_1\sin\lambda_2\cos(\psi_1-\psi_2)\right\}. \quad \ldots\ldots(2)$$

where μ is the moment of dipole i.e. $\mu = 2ae$.

If we now consider any arbitrary two molecules in the liquid and their central distance be r, and the angles between the positive direction of their axes and the positive direction of the x-axis be θ_1 and θ_2 respectively, the probability of the directions of the axes of the two molecules being within the solid angles $d\omega_1$, and $d\omega_2$ is proportional to

$$e^{-\frac{1}{kT}(u'+u_1+u_2)}d\omega_1\,d\omega_2$$

where k is Boltzmann's constant, T the absolute temperature, u' the mutual potential energy between the two molecules, u_1 and u_2 the potential energy of the two molecules with respect to the field of force due to the impact of the surounding molecule i.e.

$$u_1 = \beta(1\mp\cos\theta_1), \quad u_2 = \beta(1\mp\cos\theta_2),$$

where the double sign must be $-$, when $0 < \theta_1, \theta_2 < \pi$ and $+$ when $\pi < \theta_1,\ \theta_2 < 2\pi$.

Hence the mean potential energy between the two molecules having a certain central distance is

$$\bar{u} = C\int_{(\omega_1)}\int_{(\omega_2)} u' e^{-\frac{1}{kT}(u'+u_1+u_2)}d\omega_1\,d\omega_2, \quad C = \frac{1}{\int_{(\omega_1)}\int_{(\omega_2)} e^{-\frac{1}{kT}(u'+u_1+u_2)}d\omega_1\,d\omega_2},$$

where the integration is to be carried out in all direction, and this may be expressed by notations (ω_1), (ω_2) hereafter. u_1 and u_2 are proportional to $\frac{dv}{dz}$ and as $\frac{dv}{dz}$ is assumed to be very small, we may assume that u_1 and u_2 are also very small and their second and higher powers can be neglected.

Hence

$$\bar{u} = C\int_{(\omega_1)}\int_{(\omega_2)} u' e^{-\frac{u'}{kT}}\left(1-\frac{u_1}{kT}-\frac{u_2}{kT}\right) d\omega_1\, d\omega_2$$

$$= C\left\{\left(1-\frac{2\beta}{kT}\right)\int_{(\omega_1)}\int_{(\omega_2)} u' e^{-\frac{u'}{kT}} d\omega_1\, d\omega_2 + \frac{\beta}{kT}\int_{(\omega_1)}\int_{(\omega_2)} u' e^{-\frac{u'}{kT}} (\pm\cos\theta_1 \pm\cos\theta_2) d\omega_1 d\omega_2.\right.$$

Also

$$\int_{(\omega_1)}\int_{(\omega_2)} e^{-\frac{1}{kT}(u'+u_1+u_2)} d\omega_1\, d\omega_2 = \int_{(\omega_1)}\int_{(\omega_2)} e^{-\frac{u'}{kT}} d\omega_1\, d\omega_2 - \frac{u_1+u_2}{kT}\int_{(\omega_1)}\int_{(\omega_2)} e^{-\frac{u'}{kT}} d\omega_1\, d\omega_2.$$

The second term can be neglected in comparision with the first; consequently

$$\int_{(\omega_1)}\int_{(\omega_2)} e^{-\frac{1}{kT}(u'+u_1+u_2)} d\omega_1\, d\omega_2 = \int_{(\omega_1)}\int_{(\omega_2)} e^{-\frac{u'}{kT}} d\omega_1\, d\omega_2.$$

Therefore

$$\bar{u} = \frac{\left(1-\frac{2\beta}{kT}\right)\int_{(\omega_1)}\int_{(\omega_2)} u' e^{-\frac{u'}{kT}} d\omega_1\, d\omega_2}{\int_{(\omega_1)}\int_{(\omega_2)} e^{-\frac{u'}{kT}} d\omega_1\, d\omega_1} + \frac{\frac{\beta}{kT}\int_{(\omega_1)}\int_{(\omega_2)} u' e^{-\frac{u'}{kT}} (\pm\cos\theta_1 \pm\cos\theta_2) d\omega_1 d\omega}{\int_{(\omega_1)}\int_{(\omega_2)} e^{-\frac{u'}{kT}} d\omega_1\, d\omega_2}$$

$$= A(r) + \frac{D}{B(r)} \quad \ldots\ldots (4)$$

where

$$A(r) = \frac{\left(1-\frac{2\beta}{kT}\right)\int_{(\omega_1)}\int_{(\omega_2)} u' e^{-\frac{u'}{kT}} d\omega_1\, d\omega_2}{\int_{(\omega_1)}\int_{(\omega_2)} e^{-\frac{u'}{kT}} d\omega_1\, d\omega_2} \quad \ldots\ldots (5)$$

$$B(r) = \int_{(\omega_1)}\int_{(\omega_2)} e^{-\frac{u'}{kT}} d\omega_1\, d\omega_2 \quad \ldots\ldots (6)$$

$$D = \frac{\beta}{kT}\int_{(\omega_1)}\int_{(\omega_2)} u' e^{-\frac{u'}{kT}} (\pm\cos\theta_1 \pm \cos\theta_2)\, d\omega_1\, d\omega_2 \ldots\ldots\ldots\ldots (7)$$

A and B depend upon the magnitude of r and not upon its direction, D depends upon both.

Now $u' e^{-\frac{u'}{kT}}$ must be a symmetrical function of a coordinate which determines the orientation of one of molecules and the corresponding one which belongs to the other molecule.

Hence

$$\int_{(\omega_1)}\int_{(\omega_2)} u' e^{-\frac{u'}{kT}} (\pm\cos\theta_1)\, d\omega_1\, d\omega_2 = \int_{(\omega_1)}\int_{(\omega_2)} u' e^{-\frac{u'}{kT}} (\pm\cos\theta_2)\, d\omega_1\, d\omega_2.$$

Accordingly,

$$D = \frac{2\beta}{kT}\int_{(\omega_1)}\int_{(\omega_2)} u' e^{-\frac{u'}{kT}} (\pm\cos\theta_1)\, d\omega_1\, d\omega_2 \ldots\ldots\ldots\ldots\ldots (8)$$

Thus physically speaking, the result is double the calculated value on the assumption that only the molecule (1) is subjected to the force due to the velocity gradient and the molecule (2) is not. Expanding the integrand into a power series,

$$D = 2\beta\int_{(\omega_1)}\int_{(\omega_2)} \left\{\left(\frac{u'}{kT}\right) - \frac{1}{1!}\left(\frac{u'}{kT}\right)^2 + \frac{1}{2!}\left(\frac{u'}{kT}\right)^3 - \ldots\right\} (\pm\cos\theta_1)\, d\omega_1\, d\omega_2$$

$$= D^{(1)} + D^{(2)},$$

where

$$D^{(1)} = 2\beta\int_{(\omega_1)}\int_{(\omega_2)} \left\{\left(\frac{u'}{kT}\right) + \frac{1}{2!}\left(\frac{u'}{kT}\right)^3 + \ldots\ldots\ldots\ldots\right\} (\pm\cos\theta_1)\, d\omega_1\, d\omega_2,$$

$$D^{(2)} = -2\beta\int_{(\omega_1)}\int_{(\omega_2)} \left\{\left(\frac{u'}{kT}\right)^2 + \frac{1}{3!}\left(\frac{u'}{kT}\right)^4 + \ldots\ldots\ldots\ldots\right\} (\pm\cos\theta_2)\, d\omega_1\, d\omega_2.$$

Consider at first $D^{(1)}$. In integrating with respect to ω_1, we consider $d\omega_1'$ which is diametrically opposite to the elementary solid angle

$d\omega_1$. By interchanging $d\omega_1$ with $d\omega_1'$ the one of the factors of the integrand

$$\left(\frac{u'}{kT}\right)+\frac{1}{2!}\left(\frac{u'}{kT}\right)^3+\cdots\cdots\cdots\cdots$$

change its sign, while the other $\pm\cos\theta_1$ does not.

Hence

$$D^{(1)}=0$$

Also in $D^{(2)}$, the signs of the two factors of the integrand as well as their absolute values does not vary by interchanging $d\omega_1$ with $d\omega_1'$. Therefore $D^{(2)}$ is twice the value calculated for the positive direction of z above the xy-plane and we may put this as follows

$$D^{(2)}=-4\beta\int_{(\omega_2)}\int_{(\omega_2)}\left\{\sum_{n=1}^{\infty}\frac{1}{(2n-1)!}\left(\frac{u'}{kT}\right)^{2n}\right\}\cos\theta_1\,d\omega_1\,d\omega_2$$

where the symobol (ω_2) denotes that the integration is taken over the upper hemisphere.

Consequently

$$D=-4\beta\int_{(\omega_2)}\int_{(\omega_2)}\left\{\sum_{n=1}^{\infty}\frac{1}{(2n-1)!}\left(\frac{u'}{kT}\right)^{2n}\right\}\cos\theta_1\,d\omega_1\,d\omega_2.$$

Later we shall consider in the liquid a plane XY perpendicular to z-axis, and calculate the component of the force acting on the molecules which are situated on the negative side of XY-plane from the liquid on the positive side. But $A(r)$ depends only on the magnitude of r and is independent of the direction of it, so that the resultant of the component of the force in the x-direction coming from this term is zero, so that for our purpose there is no need of calculating $A(r)$.

4. EVALUATION OF $B(r)$.

First we will evaluate $B(r)$.

$$B(r)=\int_{(\omega_1)}\int_{(\omega_2)}e^{-\frac{u'}{kT}}\,d\omega_1\,d\omega_2$$

$$=\int_{(\omega_1)}\int_{(\omega_2)}\left\{1-\frac{u'}{kT}+\frac{1}{2!}\left(\frac{u'}{kT}\right)^2-\cdots\cdots\right\}d\omega_1\,d\omega_2.$$

Considering as before $d\omega_1'$ which is diametrically opposite to the elementary solid angle $d\omega_1$, we see that the sign of u' changes, so that the integral of the odd power terms of the integrand vanishes.

Accordingly,

$$B(r) = \int_{(\omega_1)} \int_{(\omega_2)} \left\{ 1 + \frac{1}{2!}\left(\frac{u'}{kT}\right)^2 + \frac{1}{4!}\left(\frac{u'}{kT}\right)^4 + \cdots\cdots \right\} d\omega_1\, d\omega_2.$$

Since

$$d\omega_1 = \sin\lambda_1\, d\lambda_1\, d\psi_1 \text{ and } d\omega_2 = \sin\lambda_2\, d\lambda_2\, d\psi_2,$$

putting the expression (2) into the above integral,

$$B(r) = 16\pi^2 + \frac{\mu^4}{2!\,2^2 k^2 T^2 r^6} \int\int\int\int \Big\{ -2\cos\lambda_1 \cos\lambda_2 + \sin\lambda_1 \sin\lambda_2 \cos(\psi_1 - \psi_2) \Big\}^2 \sin\lambda_1 \sin\lambda_2\, d\lambda_1\, d\lambda_2\, d\psi_1\, d\psi_2 + \cdots\cdots$$

$$= 16\pi^2\left(1 + \frac{\mu^4}{36 k^2 T^2 r^6} + \cdots\cdots\right)$$

$$= 16\pi^2\Big(1 + \triangle(r)\Big). \quad \cdots\cdots\cdots\

So that calculating u' in the mean distance between molecules, the 2nd. and higher terms are small in comparison with the first term and can be neglected.

But it must be considered that the central distance between molecules may possibly become smaller than their mean distances. Therefore the mutual potential energy possessed by a molecule which is very near to another molecule must be regarded to decrease in the ratio $1 : \{1+\triangle(r)\}$ with the ones which are far apart. But considering the density of the distribution of other molecules with respect to a molecule, it increases in the ratio,

$$\frac{\left[\int\int\int\int e^{-\frac{u'}{kT}} \sin\lambda_1 \sin\lambda_2 \, d\lambda_1 \, d\lambda_2 \, d\psi_1 \, d\psi_2\right]_{r=r}}{\left[\int\int\int\int e^{-\frac{u'}{kT}} \sin\lambda_1 \sin\lambda_2 \, d\lambda_1 \, d\lambda_2 \, d\psi_1 \, d\psi_2\right]_{r=\infty}} = 1+\triangle(r)$$

so that if we consider that the position which the centre of a molecule occupies with respect to another molecule is distributed with equal probability within the range in which it is allowed to occupy, there is no objection in considering for $B(r) = 16\pi^2\{1+\triangle(r)\}$,

$$B = 16\pi^2 \quad \ldots\ldots (11)$$

5. EVALUATION OF D.[1]

Put

$$D = \sum_{n=1}^{\infty} D_{2n} \quad \ldots\ldots (12)$$

or

$$D_{2n} = -\frac{4\beta}{(kT)^{2n}(2n-1)!}\int_{\omega_2}\int_{\omega_2} u'^{2n}\cos\theta_1 \, d\omega_1 \, d\omega_2$$

$$= -\frac{4\beta\mu^{4n}}{(kT)^{2n}(2n-1)!\,2^{2n}r^{6n}}\int_{\omega_2}\int_{\omega_2}\Big\{-2\cos\lambda_1\cos\lambda_2$$

$$+\sin\lambda_1\sin\lambda_2\cos(\psi_1-\psi_2)\Big\}^{2n}\cos\theta_1 \, d\omega_1 \, d\omega_2 \quad \ldots\ldots (13)$$

(1) The following calculation is very laborious. It may be much more simplified, by making use of the spherical function. The writer has an intention of working on this line.

Let X, Y and Z be the points of intersections of the straight lines drawn parallel to the axes x, y and z through the centre O of a unit sphere with the spherical surface, and R, P_1, and P_2 the intersections of the lines drawn parallel to the direction of r and the axes of the molecules (1) and (2) respectively. (Fig. 5). Let also the polar angles of R, P_1 and P_2 measured from the positive direction of the x-axis be $\textcircled{H}$, θ_1 and θ_2 respectively, and the azimuthal angle of R measured from the plane OXY be Φ, then we have from the spherical triangle RP_1X

Fig. 5

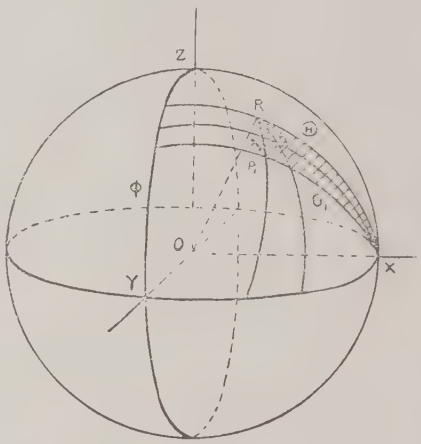

$$\cos\theta_1 = \cos\lambda_1 \cos\textcircled{H} + \sin\lambda_1 \sin\textcircled{H} \cos\psi_1.$$

Consequently

$$D_{2n} = -\frac{4\beta\mu^{4n}}{(kT)^{2n}(2n-1)!\,2^{2n}r^{6n}} \int_{\textcircled{\omega_2}} \int_{\textcircled{\omega_1}} \Big\{ -2\cos\lambda_1 \cos\lambda_2 + \sin\lambda_1 \sin\lambda_2 \cos(\psi_1-\psi_2) \Big\}^{2n} (\cos\lambda_1 \cos\textcircled{H} + \sin\lambda_1 \sin\textcircled{H} \cos\psi_1)\, d\omega_1\, d\omega_2 \quad \ldots\ldots (13)$$

Since

$$d\omega_1 = \sin\lambda_1\, d\lambda_1\, d\psi_1$$

$$d\omega_2 = \sin\lambda_2\, d\lambda_2\, d\psi_2$$

we have

$$D_{2n} = D_{2n}^{(1)} + D_{2n}^{(2)}$$

where

$$D_{2n}^{(1)} = -\frac{4\beta\mu^{4n}}{(kT)^{2n}(2n-1)!\,2^{2n}r^{6n}} \iint_{\textcircled{1}} \iint_{\textcircled{2}} \Big\{ -2\cos\lambda_1 \cos\lambda_2 + \sin\lambda_1 \sin\lambda_2 \cos(\psi_1-\psi_2) \Big\}^{2n} \sin\lambda_1 \sin\lambda_2 \cos\textcircled{H}\, \cos\lambda_1\, d\lambda_1\, d\lambda_2\, d\psi_1\, d\psi_2$$

$$D_{2n}^{(2)} = -\frac{4\beta\,\mu^{4n}}{(kT)^{2n}(2n-1)!\,2^{2n}\,r^{6n}}\iint_{(1)}\iiint_{(2)}\Big\{-2\cos\lambda_1\cos\lambda_2$$

$$+\sin\lambda_1\sin\lambda_2\cos(\psi_1-\psi_2)\Big\}^{2n}\sin^2\lambda_1\sin\lambda_2\sin\textcircled{H}\cos\psi_1\,d\lambda_1\,d\lambda_2\,d\psi_1\,d\psi_2.$$

For convenience we will at first treat $D_{2n}^{(2)}$.

If the angles which the plane of the great circle ZR makes with the plane RX, RP_1 and RP_2 be ψ_0, ψ_1' and ψ_2' respectively, (Fig. 6), then

Fig. 6

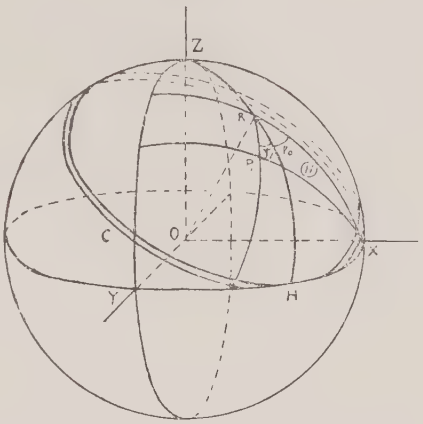

$$\psi_1 = \psi_0 + \psi_1'$$

$$\psi_2 = \psi_0 + \psi_2'$$

$$\psi_1 - \psi_2 = \psi_1 - \psi_2'$$

$$d\psi_1 = d\psi_1 \quad d\psi_2 = d\psi_2'.$$

Therefore

$$D_{2n}^{(2)} = -\frac{4\beta\,\mu^{4n}\sin\textcircled{H}}{(kT)^{2n}(2n-1)!\,2^{2n}\,r^{6n}}\iint_{(1)}\iiint_{(2)}\Big\{-2\cos\lambda_1\cos\lambda_2$$

$$+\sin\lambda_1\sin\lambda_2\cos(\psi_1'-\psi_2')\Big\}^{2n}\sin^2\lambda_1\sin\lambda_2\cos(\psi_0+\psi_1')\,d\lambda_1\,d\lambda_2\,d\psi_1'\,d\psi_2'$$

$$= -\frac{4\beta\,\mu^{4n}\sin\textcircled{H}}{(kT)^{2n}(2n-1)!\,2^{2n}\,r^{6n}}\iint_{(1)}\iiint_{(2)}\Big\{\sum_{p=o}^{2n} A\cos^p\lambda_2\sin^q\lambda_2\cos^q(\psi_1'-\psi_2')\Big\}$$

$$B\sin\lambda_2\cos(\psi_0+\psi_1')\,d\lambda_1\,d\lambda_2\,d\psi_1'\,d\psi_2'$$

where $p+q=2n$ and A and B are independent of λ_2, ψ_1' and ψ_2'. First considering the integral with respect to λ_2, we see that the limits of integration are o and π, and when p is odd, q also becomes odd.

So that $$\int_0^{\pi}\sin^{q+1}\lambda_2\cos^p\lambda_2\,d\lambda_2 = 0.$$

Therefore removing the terms which reduce to zero,

$$D_{2n}^{(2)} = -\frac{4\beta\,\mu^{4n}\sin\textcircled{H}}{(kT)^{2n}(2n-1)!\,2^{2n}\,r^{6n}}\iint_{\textcircled{1}}\iiint_{\textcircled{2}}\left\{\sum_{t=0}^{n} A\cos^{2t}\lambda_2\sin^{2s}\lambda_2\cos^{2s}(\psi_1'-\psi_2')\right\}$$
$$B\sin\lambda_2\cos(\psi_0+\psi_1')\,d\lambda_1\,d\lambda_2\,d\psi_1'\,d\psi_2'$$

where $\qquad 2t+2s=2n.$

Next considering the integral with respect to ψ_1', if λ_1 be made constant the path of the integral becomes an arc C of a small circle which is perpendicular to OR. Hence the limits of integral can be taken $\psi_1^{(0)}$ and $2\pi-\psi_1^{(0)}$ where $\psi_1^{(0)}$ is a function os λ_1. Thus

$$\int_{\psi_1^{(0)}}^{2\pi-\psi_1^{(0)}}\cos^{2s}(\psi_1'-\psi_2')\cos(\psi_0+\psi_1')\,d\psi_1'$$
$$=\int_{\psi_1^{(0)}}^{2\pi-\psi_1^{(0)}}(\cos\psi_1'\cos\psi_2'+\sin\psi_1'\sin\psi_2')^{2s}(\cos\psi_0\cos\psi_1'-\sin\psi_0\sin\psi_1')\,d\psi_1'$$
$$=\int_{\psi_1^{(0)}}^{2\pi-\psi_1^{(0)}}\left\{\sum E\cos^{l}\psi_1'\sin^{m}\psi_1'\right\}(\cos\psi_0\cos\psi_1'-\sin\psi_0\sin\psi_1')\,d\psi_1'$$
$$=\int_{\psi_1^{(0)}}^{2\pi-\psi_1^{(0)}}\sum(F\cos^{l+1}\psi_1'\sin^{m}\psi_1'+G\cos^{l}\psi_1'\sin^{m+1}\psi_1')\,d\psi_1'$$

where $l+m=2s$, and E, F and G are independent of ψ_1'.

Now l and m are both odd or both even. So that one of $l+1$ and m is even and the other is odd. The same remark applies to l and $m+1$. Hence the above integral is zero, i.e.,

$$D_{2n}^{(2)}=0.$$

Accordingly

$$D_{2n}=-\frac{4\beta\,\mu^{4n}\cos\textcircled{H}}{(kT)^{2n}(2n-1)!\,2^{2n}\,r^{6n}}\iint_{\textcircled{1}}\iiint_{\textcircled{2}}\Big\{-2\cos\lambda_1\cos\lambda_2$$
$$+\sin\lambda_1\sin\lambda_2\cos(\psi_1-\psi_2)\Big\}^{2n}\cos\lambda_1\sin\lambda_1\sin\lambda_2\,d\lambda_1\,d\lambda_2\,d\psi_1\,d\psi_2\quad\ldots\ldots\ldots\ldots(14)$$

To evaluate this, first consider the integral with respect to λ_2. Now the odd power terms of $\cos\lambda_2$ in the expansion of $\{\ \}^{2n}$ has the form

$$A \cos^{2p+1}\lambda_2 \sin^{2q+1}\lambda_2,$$

where $$2p+2q+2 = 2n.$$

Hence if we integrate after multiplying with $\sin\lambda_2$,

$$A\int_0^{\pi} \cos^{2p+1}\lambda_2 \sin^{2q+2}\lambda_2 \, d\lambda_2 = 0.$$

Hence in the expansion of $\{\ \}^{2n}$ we have to take only the even power terms of $\cos\lambda_2$. Thus

$$D_{2n} = -\frac{4\beta\mu^{4n}\cos(H)}{(kT)^{2n}(2n-1)!\,2^{2n}r^{6n}} \iint_{(1)} \iiint_{(2)} \Big[\sum_{p=0}^{n} \frac{(2n)!}{(2n-2p)!\,(2p)!} \Big\{2\cos\lambda_1\cos\lambda_2\Big\}^{2n-2p}$$

$$\Big\{\sin\lambda_1\sin\lambda_2\cos(\psi_1-\psi_2)\Big\}^{2p}\Big]\sin\lambda_1\sin\lambda_2\cos\lambda_1\, d\lambda_1\, d\lambda_2\, d\psi_1\, d\psi_2$$

$$= -\frac{2^3 n\mu^{4n}\cos(H)}{(kT)^{2n}r^{6n}} \iint_{(3)} \iiint_{(4)} \Big[\sum_{p=0}^{n} \frac{1}{2^{2p}(2n-2p)!\,(2p)!}$$

$$\cos^{2n-2p+1}\lambda_1 \sin^{2p+1}\lambda_1 \cos^{2n-2p}\lambda_2 \sin^{2p+1}\lambda_2 \cos^{2p}(\psi_1-\psi_2)\, d\lambda_1\, d\lambda_2\, d\psi_1\, d\psi_2. \quad (15)$$

But

$$\int_0^{\pi} \cos^{2n-2p}\lambda_2 \sin^{2p+1}\lambda_2 \, d\lambda_2 = \frac{(2p)(2p-2)(2p-4)\ldots\ldots 4.2}{(2n+1)(2n-1)\ldots\ldots(2n-2p+1)}.\ 2.$$

For simplicity puting

$$(2p)(2p-2)\ldots\ldots 4.2 = E(2p)!$$

$$(2n+1)(2n-1)\ \ldots\ldots 3.1 = O(2n+1)!,$$

we have

$$\int_0^{\pi} \cos^{2n-2p}\lambda_2 \sin^{2p+1}\lambda_2 \, d\lambda_2 = \frac{E(2p)!\,O(2n-2p-1)!}{O(2n+1)!}\ .\ 2 = \frac{2^{p+1}p!\,O(2n-2p-1)!}{O(2n+1)!}.$$

Consequently

$$D_{2n} = -\frac{2^3 n\beta\mu^{4n}\cos(H)}{(kT)^{2n}r^{6n}} \iint_{(1)} \int_{(3)} \sum_{p=0}^{n} \frac{1}{2^{2p}(2n-2p)!\,(2p)!}\cdot$$

$$\frac{2^{p+1}p!\,O(2n-2p-1)!}{O(2n+1)!} \cos^{2n-2p+1}\lambda_1 \sin^{2p+1}\lambda_1 \cos^{2p}(\psi_1-\psi_2)\, d\lambda_1\, d\psi_1\, d\psi_2$$

$$= -\frac{n\beta\mu^{4n}\cos(H)}{2^{n-4}\,O(2n+1)!\,(kT)^{2n}\,r^{6n}}\iint_{(\lambda)}\int_{(\psi)}\sum_{p=0}^{n}\frac{p!}{(n-p)!\,(2p)!}$$

$$\cos^{2n-2p}\lambda_1\sin^{2p+1}\lambda_1\cos\lambda_1\cos^{2p}(\psi_1-\psi_2)\,d\lambda_1\,d\psi_1\,d\psi_2. \quad \ldots\ldots\ldots\ldots\ldots(16)$$

The integration with respect to ψ_2 from 0 to 2π may easily be transformed to that with respect to $\psi=\psi_1-\psi_2$ from 0 to 2π and

$$\int_0^{2\pi}\cos^{2p}\psi\,d\psi=\frac{(2p-1)(2p-3)\ldots\ldots3.1}{(2p)(2p)-2\ldots\ldots\ldots4.2}.\,2\pi=\frac{O(2p-1)!}{2^p\,p!}.\,2\pi.$$

Hence

$$D_{2n}=-\frac{n\beta\mu^{4n}\cos(H)}{2^{n-4}\,O(2n+1)!\,(kT)^{2n}\,r^{6n}}\iint_{(\lambda)}\sum_{p=0}^{n}\frac{p!}{2^{2p}(n-p)!\,(2p)!}\cdot$$

$$\frac{O(2p-1)!}{2^p\,p!}.\;2\pi\cos^{2n-2p}\lambda_1\sin^{2p}\lambda_1\cos\lambda_1\,d\lambda_1\,d\psi_1$$

$$=-\frac{\pi n\beta\mu^{4n}\cos(H)}{2^{n-5}\,O(2n+1)!\,n!\,(kT)^{2n}\,r^{6n}}\iint_{(\lambda)}(1-\frac{3}{4}\sin^2\lambda_1)^n\sin\lambda_1\cos\lambda_1\,d\lambda_1\,d\psi_1. \quad (17)$$

Now if ψ_1 is first kept constant and λ_1 is changed from R to the great circle XY (Fig. 7), and it at XY, $\lambda_1=\lambda_1'$, and moreover we put

$$1-\frac{3}{4}\sin^2\lambda_1=y$$

then

$$dy=-\frac{3}{2}\sin\lambda_1\cos\lambda_1\,d\lambda_1.$$

Hence

$$D_{2n}=\frac{n\pi\beta\mu^{4n}\cos(H)}{3.2^{n-6}\,O(2n+1)!\,n!\,(kT)^{2n}\,r^{6n}}\int_{\psi_1=0}^{2\pi}\int_{y=0}^{1-\frac{3}{4}\sin^2\lambda_1'}y^n dy\,d\psi_1$$

$$=\frac{\pi n\beta\mu^{4n}\cos(H)}{3.2^{n-6}\,O(2n+1)!\,n!\,(kT)^{2n}\,r^{6n}}\int_{\psi_1=0}^{2\pi}\left\{(1-\frac{3}{4}\sin^2\lambda_1')^{n+1}-1\right\}d\psi_1$$

If $\widehat{HK} = l$, $\widehat{RH} = \lambda_0$, from the spherical triangle RKH (Fig. 7)

Fig. 7

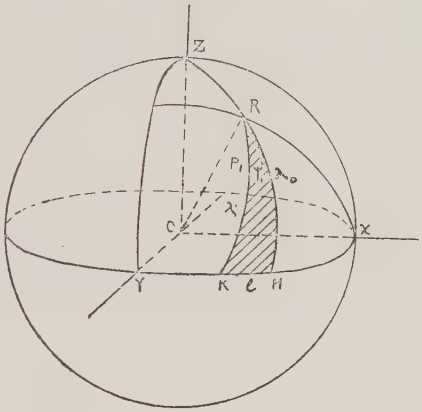

$$\sin \lambda_1' = \frac{\sin l}{\sin \psi_1'},$$

$$\cos\lambda_1' = \cos l \cos \lambda_0.$$

Eliminlating λ_1',

$$\sin^2\psi_1' = \frac{\sin^2 l}{1 - \cos^2 l \cos^2\lambda_0}.$$

Differentiating both sides

$$\sin \psi_1' \cos \psi_1' \, d\psi_1' = \frac{\sin l \cos l \sin^2\lambda_0}{\sin^4\lambda_1'} dl.$$

Also

$$\cos_2\psi_1' = 1 - \frac{\sin^2 l}{\sin^2\lambda_1'} = \frac{\cos^2 l \sin^2\lambda_0}{\sin^2\lambda_1'}.$$

Hence

$$\cos \psi_1' = \frac{\cos l \sin \lambda_0}{\sin\lambda_1'}, \quad \sin \psi_1' \cos \psi_1' = \frac{\sin l \cos l \sin \lambda_0}{\sin^2\lambda_1'}, \quad d\psi_1' = \frac{\sin \lambda_0}{\sin^2\lambda_1'} dl.$$

Since $d\psi_1 = d\psi_1'$, if we put l in place of ψ_1,

$$D_{2n} = \frac{n\pi\beta\mu^{4n}\cos \textcircled{H}}{3.2^{n-6}O(2n+1)!(n+1)!(kT)^{2n}r^{6n}} \int_{l=0}^{2\pi} \left\{ \left(1 - \frac{3}{4}\sin^2\lambda_1'\right)^{n+1} - 1 \right\} \frac{\sin \lambda_0}{\sin^2\lambda_1'} dl$$

$$= - \frac{n\pi\beta\mu^{4n}\cos \textcircled{H}}{3.2^{n-6}O(2n+1)!\,(n+1)!\,(kT)^{2n}r^{6n}4^{n+1}} \int_0^{2\pi} \Big\{ 4^{n+1} - (1 + 3\cos^2\lambda_1')^{n+1} \Big\} \frac{\sin \lambda_0 \, dl}{4 - (1 + 3\cos^2\lambda_0)}$$

$$= - \frac{n\pi\beta\mu^{4n}\cos \textcircled{H}}{2^{n-6}4^{n+1}O(2n+1)!\,(n+1)!\,(kT)^{2n}r^{6}} \int_0^{2\pi} \sum_{i=0}^{n} 4^{n-i}(1 + 3\cos^2\lambda_1')^i \sin \lambda_0 dl. \tag{18}$$

The integrand can be expanded and arranged in the following manner :

$$\sum_{i=0}^{n} 4^{n-i}(1+3\cos^2\lambda_1')^i = 4^n + 4^{n-1}(1+3\cos^2\lambda_1') + 4^{n-2}(1+3\cos^2\lambda_1')^2 + \cdots\cdots$$

$$+ 4^{n-i}(1+3\cos^2\lambda_1')^i + \cdots\cdots + (1+3\cos_2\lambda_1')^n$$

$$= 4^n$$

$$+ 4^{n-1} + 4^{n-1}.3.\cos^2\lambda_1'$$

$$+ 4^{n-2} + 4^{n-2}.2.3\cos^2\lambda_1' + 4^{n-2}.3^2\cos^4\lambda_1'$$

$$+ \cdots\cdots$$

$$+ 4^{n-i} + 4^{n-i}.i.3\cos^2\lambda_1' + 4^{n-i}\frac{i(i-1)}{2!}.3^2\cos^4\lambda_1'$$

$$+ 4^{n-i}\frac{i(i-1)(i-2)}{3!}.3^3\cos^6\lambda_1' + \cdots\cdots$$

$$+ \cdots\cdots$$

$$+ 1 + n.3.\cos^2\lambda_1' + \frac{n(n-1)}{2!}3^2\cos^4\lambda_1' + \frac{n(n-1)(n-2)}{3!}3^3\cos^6\lambda_1' + \cdots\cdots$$

Adding this column by column

$$\sum_{i=0}^{n} 4^{n-i}(1+3\cos^2\lambda_1')^i = S_0 + S_1(3\cos^2\lambda_1') + S_2(3\cos^2\lambda_1')^2 + \cdots\cdots$$

$$+ S^i(3\cos^2\lambda_1')^i + \cdots\cdots + S_n(3\cos^2\lambda_1')^n$$

where

$$S_0 = 4^n + 4^{n-1} + 4^{n-2} + \cdots\cdots + 4^{n-i} + 4^{n-i-1} + \cdots\cdots + 1$$

$$S_1 = 4^{n-1} + 2.4^{n-2} + 3.4^{n-3} + \cdots\cdots + i4^{n-i} + (i+1)4^{n-i-1} + \cdots\cdots + n$$

$$S_2 = 4^{n-2} + 3.4^{n-3} + \frac{4.3}{2!}4^{n-4} + \ldots + \frac{i(i-1)}{2!}4^{n-i} + \frac{(i+1)i}{2!}4^{n-i-1} + \ldots + \frac{n(n-1)}{2!}$$

$$S_i = 4^{n-i} + (i+1)4^{n-i} + \frac{(i+2)(i+1)}{2!}4^{n-i-1} + \cdots\cdots + \frac{n(n-1)\cdots(n-i+1)}{i!}.$$

$$\cdots\cdots$$

$$S_n = 1.$$

Between these S there are the following relations

$$3\,S_1 = S_0 - \frac{(n+1)!}{n!\,1!}$$

$$3\,S_2 = S_1 - \frac{(n+1)!}{(n-1)!\,2!}$$

$$3\,S_3 = S_2 - \frac{(n+1)!}{(n-2)!\,3!}$$

.....

$$3\,S_{i-1} = S_{i-2} - \frac{(n+1)!}{(n-i+2)!\,(i-1)!}$$

$$3\,S_i = S_{i-1} - \frac{(n+1)!}{(n-i+1)!\,i!}$$

.....

Eliminating S_1, S_2, ..., S_{i-1} from them,

$$3^{i+1}S_i = 3\,S_0 + 1 - \left\{1 + \frac{(n+1)!}{(n+1-1)!\,1!}\,3 + \frac{(n+1)!}{(n+1-2)!\,2!}\,3^2 + \cdots\cdots\right.$$

$$\left. \cdots\cdots + \frac{(n+1)!}{(n+1-i)!\,i!}\,3^i\right\}.$$

But what is in the parenthesis is the sum of the first $i+1$ terms in the expansion of $(1+3)^{n+1}$. If this be denoted bo $T_{i+1}(1+3)^{n+1}$

$$3^{i+1}S_i = 3\,S_0 + 1 - T_{i+1}\,(1+3)^{n+1}$$

But

$$S_0 = \frac{4^{n+1}-1}{4-1} = \frac{4^{n+1}-1}{3}.$$

Therefore

$$3^{i+1}\,S_i = 4^{n+1} - T_{i+1}(1+3)^{n+1}$$

The right-hand side is the sum of the last $n-i+1$ terms in the exponsion of $(1+3)^{n+1}$ which results on subtracting the first $i+1$ terms from the $n+2$ terms of the expansion of $(1+3)^{n+1}$ i.e. the sum of the first $n-i+1$ terms in the expansion of $(3+1)^{n+1}$ Thus,

$$S_i = \frac{1}{3^{i+1}} T_{n-i+1}(3+1)^{n+1}$$

Now, since $\cos\lambda_1' = \cos\lambda_0 \cos l$,

$$D_{2n} = -\frac{n\pi\beta\mu^{4n}\cos\textcircled{H}}{2^{n-6}4^{n+1}O(2n+1)!\,(n+1)!\,(kT)^{2n}r^{6n}}\int_0^{2\pi}\sum_{i=0}^{n} S_i\, 3^i \cos^i\lambda_1' \sin\lambda_0\, dl$$

$$= -\frac{n\pi\beta\mu^{4n}\cos\textcircled{H}}{2^{n-6}4^{n+1}O(2n+1)!\,(n+1)!\,(kT)^{2n}r^{6n}}\int_0^{2\pi}\sum_{i=0}^{n} S_i\, 3^i \cos^{2i}\lambda_0 \cos^{2i} l \sin\lambda_0\, dl$$

$$= -\frac{n\pi\beta\mu^{4n}\cos\textcircled{H}}{2^{n-6}4^{n+1}O(2n+1)!\,(n+1)!\,(kT)^{2n}r^{6n}}\left\{\sum_{i=0}^{n} S_i\, 3^i \frac{O(2i-1)!}{E(2i)!}\cdot 2\pi\cos^{2i}\lambda_0\right\}\sin\lambda_0$$

$$= -\frac{n\pi^2\beta\mu^{4n}\cos\textcircled{H}}{2^{n-7}4^{n+1}O(2n+1)!\,(n+1)!\,(kT)^{2n}r^{6n}}\left\{\sum_{i=0}^{n} X_i \cos^{2i}\lambda_0\right\}\sin\lambda_0$$

$$= -\frac{n\pi^2\beta\mu^{4n}\cos\textcircled{H}}{2^{n-7}4^{n+1}O(2n+1)!\,(n+1)!\,(kT)^{2n}r^{6n}}\left\{\sum_{i=0}^{n}(1-\sin^2\lambda_0)^i X_i \sin\lambda_0\right\} \quad \cdots\cdots (19)$$

where

$$X_i = \frac{O(2i-1)!}{E(2i)} S_i\, 3^i$$

$$= \frac{1}{3}\frac{O(2i-1)!}{E(2i)!} T_{n-i+1}(3+1)^{n+1} \quad \cdots\cdots (20)$$

But

$$\sum_{i=0}^{n}(1-\sin^2\lambda_0)^i X_i$$

$$= X_0$$

$$+ X_1(1-\sin^2\lambda_0)$$

$$+ X_2(1-2\sin^2\lambda_0 + \sin^4\lambda_0)$$

$$+ X_3(1-3\sin^2\lambda_0 + 3\sin^4\lambda_0 - \sin^6\lambda_0)$$

$$+ \cdots\cdots$$

$$+X_i\Big(1-i\sin^2\lambda_0+\frac{i(i-1)}{2!}\sin^4\lambda_0+\frac{i(i-1)(i-2)}{3!}\sin^6\lambda_0+\ldots\ldots$$
$$+(-1)^i\sin^{2i}\lambda_0\Big)$$

$$+X_{i+1}\Big(1-(i+1)\sin^2\lambda_0+\frac{(i+1)\,i}{2!}\sin^4\lambda_0-\frac{(i+1)\,i\,(i-1)}{3!}\sin^6\lambda_0+\ldots\ldots$$
$$+(-1)^i(i+1)\sin^{2i}\lambda_0+(-1)^{i+1}\sin^{2i+1}\lambda_0\Big)$$

$$+X_{i+2}\Big(1-(i+2)\sin^2\lambda_0+\frac{(i+2)(i+1)}{2!}\sin^4\lambda_0-\frac{(i+2)(i+1)}{3!}\sin^6\lambda_0+\ldots.$$
$$+(-1)^i\frac{(i+2)(i+1)}{2!}\sin^{2i}\lambda_0+\ldots\ldots\ldots\Big)$$

$$+\ldots\ldots\ldots\ldots\ldots\ldots\ldots\ldots\ldots\ldots\ldots\ldots\ldots\ldots\ldots\ldots\ldots\ldots\ldots\ldots$$

$$+X_n\Big(1-n\sin^2\lambda_0+\frac{n(n-1)}{2!}\sin^4\lambda_0-\frac{n(n-1)(n-2)}{3!}\sin^6\lambda_0+\ldots\ldots$$
$$+(-)^i\frac{n(n-1)\ldots(n-i+1)}{i!}\sin^{2i}\lambda_0+\ldots\ldots\Big)$$

Adding column by column, we have

$$\sum_{i=0}^{n}(1-\sin^2\lambda_0)^i X_i=Y_0^{(n)}-Y_1^{(n)}\sin^2\lambda_0+Y_0^{(n)}\sin^4\lambda_0+\ldots\ldots$$
$$+(-1)^i Y_i^{(n)}\sin^{2i}\lambda_0+\ldots\ldots+(-1)^n\sin^{2n}\lambda_0,$$

where

$$Y_i^{(n)}=X_i+(i+1)X_{i+1}+\frac{(i+2)(i+1)}{2!}X_{i+2}+\ldots+\frac{n(n-1)\ldots(n-i+1)}{i!}X_n.$$

But from the spherical triangle RXH in the Fig. 7, we have

$$\sin\lambda_0=\sin\Phi\sin\textcircled{H}.$$

Hence

$$D_{2n}=-\frac{n\pi^2\beta\mu^{4n}\sin\Phi\sin\textcircled{H}\cos\textcircled{H}}{2^{n-2}4^{n+1}\Gamma(2n+1)!\,(n+1)!\,(kT)^{2n}r^{6n}}\sum_{i=0}^{n}(-1)^i Y_i^{(n)}\sin^{2i}\Phi\sin^{2i}\textcircled{H}$$

$$=-\frac{\pi^2\beta H_n\mu^{4n}}{(kT)^{2n}r^{6n}}\sin\Phi\sin\textcircled{H}\cos\textcircled{H}\sum_{i=0}^{n}(-1)^i Y_i^{(n)}\sin^{2i}\Phi\sin^{2i}\textcircled{H}\ldots(21)$$

where

$$H_n = \frac{n}{2^{n-7}4^{n+1}\,O(2n+1)!\,(n+1)!} \qquad (22)$$

6. NUMERICAL CALCULATION OF H_n AND $Y_i^{(n)}$.

For convenience the formula for calculation H_n and $Y_i^{(n)}$ are enumerated in this section. H_n may be calculated directly from (22), and result is shown in the following table.

TABLE I.

n	1	2	3	4	5	6	7
H_n	0.667	$1.111.10^{-2}$	$7.442.10^{-5}$	$2.756.10^{-7}$	$6.521.10^{-10}$	$1.076.10^{-12}$	$1.307.10^{-15}$

Also $Y_i^{(n)}$ can be calculated by the following method, step by step.

I. $T(3+1)^{n+1}$ is calculated by following formula,

3^{n+1}	$\binom{n+1}{1}3^n$	$\binom{n+1}{2}3^{n-1}$	$\binom{n+1}{i}3^{n-i+1}$	$\binom{n+1}{2}3^2$	$\binom{n+1}{1}3$
	T_1	T_2	T_i	T_{n-2}	T_{n-1}
T_1	T_2	T_3	T_{i+1}	T_{n-1}	T_n

II. X_i is calculated by (20).

III. $Y_i^{(n)}$ is calculated by following formula,

X_0							
X_1	X_1						
X_2	$2X_2$	X_2					
X_3	$3X_3$	$3X_3$	X_3				
⋮	⋮	⋮	⋮	⋮	⋮	⋮	
X_n	nX_n	$\frac{n(n-1)}{2!}X_n$	$\frac{n(n-1)(n-2)}{3!}$ ⋮	⋮	⋮	⋮	1
$Y_0^{(n)}$	$Y_1^{(n)}$	$Y_2^{(n)}$	$Y_3^{(n)}$ ⋮	⋮	⋮	⋮	1

The result is shown in the following table.

TABLE II.

	0	1	2	3	4	5	6	7
$Y^{(1)}$	6.5	1.5						
$Y^{(2)}$	33.4	15.8	3.38					
$Y^{(3)}$	157.6	113.0	49.0	8.44				
$Y^{(4)}$	713.3	689.0	450.0	156.1	22.14			
$Y^{(5)}$	3150.8	3824.7	3351.4	1750.9	498.7	59.8		
$Y^{(6)}$	13689.7	20026.9	22011	15377	6589.5	1584.7	164.4	
$Y^{(7)}$	58593	100120	132638	116486	66825	33813	5027	459

7. COEFFICIENT OF VISCOSITY.

Consider a plane XY in the liquid perpendicular to the z-axis, and a molecule P_1 on one side B and P_2 on the other side A (Fig. 8). The x-component of force acting on P_1 by P_2 is

Fig. 8.

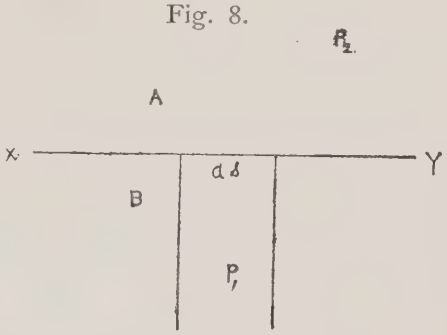

$$f = -\frac{\partial \bar{u}}{\partial x}$$

$$= -\frac{\partial \bar{u}}{\partial r}\cos\textcircled{H} + \frac{1}{r}\frac{\partial \bar{u}}{\partial \textcircled{H}}\sin\textcircled{H}$$

where r denotes $P_1 P_2$. If F' be the x-component of force exerted by all the molecules of the A side on P_1, then

$$F' = -\sum_A \frac{\partial \bar{u}}{\partial r}\cos\textcircled{H} + \sum_A \frac{1}{r}\frac{\partial \bar{u}}{\partial \textcircled{H}}\sin\textcircled{H}.$$

But from (4) we know that $\bar{u}$ consists of $A(r)$ and $\frac{D}{B}$ amongst which $A(r)$ depends upon the distance only and is independent of its

direction. So there is no x-component of force acting on P_1 which comes from this term. Hence for calculating F' we may put $\frac{D}{B}$ instead of $\bar{u}$.

Thus

$$F' = -\sum_A \frac{1}{B}\frac{\partial D}{\partial r}\cos\textcircled{H} + \sum_A \frac{1}{Br}\frac{\partial D}{\partial \textcircled{H}}\sin\textcircled{H} \quad \ldots\ldots\ldots\ldots(23)$$

Next consider a cylinder which stands on XY and whose width is ds, and sum up F' for the molecules within this,

$$F = \frac{1}{B}\sum_B \left\{ -\sum_A \frac{\partial D}{\partial r}\cos\textcircled{H} + \sum_A \frac{\partial D}{r d\textcircled{H}}\sin\textcircled{H} \right\}.$$

If the coefficient of viscosity be η,

$$\eta = \frac{F}{ds\frac{dv}{dz}} = \frac{1}{B\,ds\frac{dv}{dz}}\sum_B \left\{ -\sum_A \frac{\partial D}{\partial r}\cos\textcircled{H} + \sum_A \frac{1}{r}\frac{\partial D}{\partial \textcircled{H}}\sin\textcircled{H} \right\} \ldots.(24)$$

In order to evaluate the right-hand side of this expression we assume that the centre of the molecule P_2 exists with equal probability everywhere throughout the region A. In the case where the distance between the centre P_1 and the XY plane is large, the centre P_2 can occuply all the positions in the region A. But when the centre P_1 is close to the XY plane, the positions which can be occupied by the centre of P_2 can not be all, but some small portion of A must be ex-excluded. If now we adopt the model shown by Fig. 2, the portion which has to be excluded will vary with the orientations of P_1 and P_2, so that the calculation of the mutual action between A and B will be so involved that it may almost be impossible to carry out. Hence we shall here introduce a provisional quantity r_0. r_0 will be such that, when we assume that we replace the real molecules by points having the same mutual action as the real molecules but no dimension, and a sphere is drawn with P_1 as its centre and r_0 as its radius, within which no above-mentioned points exist, but outside of which they are uniformly distributed, the same effect will be produced by the points on P_1 as is actually done by the molecules themselves (Fig. 9). r_0 is, in fact,

Fig. 9.

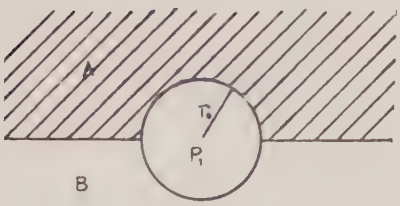

analogous to molecular diameter defined in gas theory, but is, of course, not the same. Hence we will call it equivalent molecular diameter for convenience. When P_1 approaches the plane XY, we draw a sphere of radius r_0 with P_1 as its centre, and this portion is excluded from the region A. Also P_1 is assumed to exist with equal probability everywhere throughout the region B. Take an elementary volume dV in the region A and let N be the number of molecules in unit volume. Then the number of P_2 in dV is $N\,dV$. Hence from (23) the force in the x-direction exerted on P_1 by the molecules in the region A is

$$F' = -\frac{N}{B}\int_A \left(\frac{\partial D}{\partial r}\cos\Theta - \frac{1}{r}\frac{\partial D}{\partial \Theta}\right) dV.$$

But

$$dV = r^2 \sin\Theta\, d\Theta\, d\Phi\, dr.$$

Hence

$$\int \frac{1}{r}\frac{\partial D}{\partial \Theta}\sin\Theta\, dV = \iiint r\sin^2\Theta\,\frac{\partial D}{\partial \Theta}\, d\Theta\, d\Phi\, dr.$$

Fig. 10.

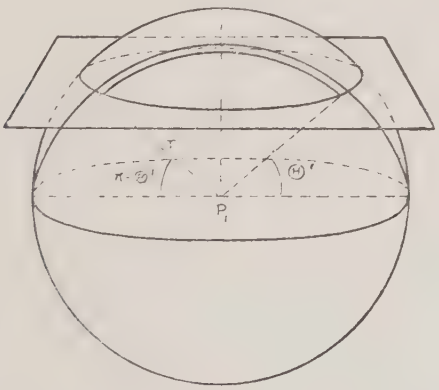

In the right-hand side expression, making r and Φ constant and integrating by parts from Θ' to $\pi-\Theta'$ with respect to Θ, (Fig. 10).

$$\int \frac{1}{r}\frac{\partial D}{r\,\textcircled{H}} \sin \textcircled{H}\, dV = \iint r\, dr\, d\Phi \Big\{ |\sin^2 \textcircled{H} \cdot D|_{\textcircled{D}'}^{\pi-\textcircled{E}'} - 2\int_{\textcircled{D}'}^{\pi-\textcircled{D}'} \sin \textcircled{H} \cos \textcircled{H} \cdot D \cdot d\textcircled{H} \Big\}.$$

$$= -\iiint 2\, r \sin \textcircled{H} \cos \textcircled{H}\, D\, dr\, d\textcircled{H}\, d\Phi$$

$$= -2\int \frac{D}{r} \cos \textcircled{H}\, dV.$$

Consequently

$$F' = -\frac{N}{B}\int \left\{ \frac{\partial D}{\partial r} + \frac{2D}{r} \right\} \cos \textcircled{H}\, dV \qquad \ldots\ldots (25)$$

Putting

$$A_n = -\frac{\pi^2 \beta\, \mu^{4n}}{(kT)^n} H_n \sin \Phi \sin \textcircled{H} \cos \textcircled{H} \sum (-1)^i\, Y_i^{(n)} \Phi \sin^{2i} \textcircled{H} \qquad \ldots\ldots (26)$$

from (21)

$$D_n = \frac{A_n}{r^{6n}} \qquad D = \sum \frac{A_n}{r^{6n}}.$$

Substituting them in (25)

$$F' = -\frac{N}{B}\int \left\{ -\sum \frac{6n\, A_n}{r^{6n+1}} + \sum \frac{2A_n}{r^{6n+1}} \right\} \cos \textcircled{H}\, dV$$

$$= \frac{N}{B}\int \left\{ \sum \frac{(6n-2)\, A_n}{r^{6n+1}} \right\} \cos \textcircled{H}\, dV$$

$$= \frac{N}{B}\iiint \left\{ \sum \frac{(6n-2)\, A_n}{r^{6n-1}} \right\} \sin \textcircled{H} \cos \textcircled{H}\, d\textcircled{H}\, d\Phi\, dr \qquad \ldots\ldots (27)$$

To evaluate this we have to distinguish the case where the distance of P_1 from XY plane, Z is greater than r_0, and that where it is not so.

I. $Z \leqq r_0$.

Fig. 11.

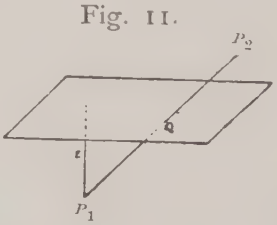

To integrate with respect to r making $\textcircled{H}$ and Φ constant. Let Q be the point where $P_1 P_2$ meets XY plane, and $P_1 Q = r'$, (Fig. 11) then we have to integrate from r' to ∞. Thus

$$F' = \frac{N}{B}\iint \sum \frac{A_n}{r'^{6n-2}} \sin \textcircled{H} \cos \textcircled{H}\, d\textcircled{H}\, d\Phi.$$

But

$$\frac{1}{r'} = \frac{\sin \Theta \sin \Phi}{Z}.$$

Consequently

$$F' = \frac{N}{B}\iint\sum \frac{A_n \sin^{6n-2}\Theta \sin^{6n-2}\Phi}{Z^{6n-2}} \sin \Theta \cos \Theta \, d\Theta \, d\Phi \ldots\ldots(28)$$

Putting

$$A_n = G_n \sin \Phi \sin \Theta \cos \Theta \sum (-1)^i Y_i^{(n)} \sin^{2i}\Phi \sin^{2i}\Theta, \ldots\ldots(29)$$

or

$$G_n = -\frac{\pi^2 \beta \mu^{4n}}{(kT)^{2n}} H_n, \ldots\ldots(30)$$

we have

$$F' = \frac{N}{B}\left\{\sum \frac{G_n}{Z^{6n-2}}\left(\sum (-1)^i Y_i^{(n)} \iint \sin^{6n+2i}\Theta \cos^2\Theta \sin^{6n+2i-1}\Phi \, d\Theta \, d\Phi\right)\right\}.$$

With respect to Θ and Φ we have to integrate from 0 to π each. But

$$\int_0^\pi \sin^{2m}\Theta \cos^2\Theta \, d\Theta = \frac{O(2m-1)!}{E(2m+2)!}\pi, \quad \int_0^\pi \sin^{2m+1}\Phi \, d\Phi = \frac{E(2m)!}{O(2m+1)!}.2. \quad (31)$$

Hence

$$F' = \frac{N}{B}\left\{\sum \frac{G_n}{Z^{6n-2}}\left(\sum (-1)^i Y_i^{(n)} \frac{O(6n-2i-1)!}{E(6n+2i+2)!} \cdot \frac{E(6n+2i-2)!}{O(6n+2i-1)!}\right)\right\}$$

$$= \frac{2\pi N}{B}\left\{\sum \frac{G_n}{Z^{6n-2}}\left(\sum (-1)^i Y_i^{(n)} \frac{1}{(6n+2i+2)(6n+2i)}\right)\right\}. \ldots(32)$$

Putting

$$L_n = \sum (-1)^i \frac{Y_i^{(n)}}{(6n+2i+2)(6n+2i)}, \ldots\ldots(33)$$

we have,

$$F' = \frac{2N\pi}{B}\sum \frac{G_n L_n}{Z^{6n-2}} \ldots\ldots (34)$$

II. $Z < r_0$

Fig. 12.

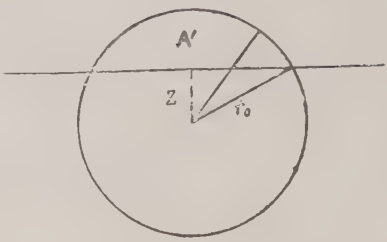

In this case we have to subtract the integration for the region A' which is in the part A when a sphere is drawn with P_1 as centre and r_0 as radius, from the integration for the whole region of A. (Fig. 12). Thus,

$$F'' = F_1'' - F_2'' \quad \cdots\cdots (35)$$

where

$$F_1'' = \frac{N}{B}\iiint_A \left\{\sum \frac{(6n-2)\,A_n}{r^{6n-1}}\right\} \sin \textcircled{H} \cos \textcircled{H}\, d\textcircled{H}\, d\Phi\, dr \quad \cdots\cdots (36)$$

$$F_2'' = \frac{N}{B}\iiint_{A'} \left\{\sum \frac{(6n-2)\,A_n}{r^{6n-1}}\right\} \sin \textcircled{H} \cos \textcircled{H}\, d\textcircled{H}\, d\Phi\, dr \quad \cdots\cdots (37)$$

The integral F_1'' is quite the same as in the case (I). To integrate F_2'' with respect to r we transform the expression by the polar angle θ measured from Z-axis and the azimuthal angle φ measured from XZ-plane. The relation between $\textcircled{H}$, Φ and θ, φ are as follows;

$$\left.\begin{aligned} &\cos \textcircled{H} = \sin\theta \cos\varphi \\ &\sin \textcircled{H} \cos \Phi = \sin\theta \sin\varphi \\ &\sin \textcircled{H} \sin \Phi = \cos\theta. \end{aligned}\right\} \quad \cdots\cdots (38)$$

Since

$$dV = r^2 \sin\theta\, d\theta\, d\varphi\, dr,$$

$$F_2'' = \frac{N}{B}\iiint \left\{\sum \frac{(6n-2)\,G_n}{r^{6n-1}} \left(\sum (-1)^i Y_i^{(n)} \cos^{2i+1}\theta \sin^3\theta \cos^2\varphi\right)\right\} d\theta\, d\varphi\, dr. \quad (39)$$

We have to integrate with respect to φ from 0 to 2π keeping r and θ constant, and since

$$\int_0^{2\pi} \cos^2\varphi\, d\varphi = \pi$$

$$F'' = \frac{N\pi}{B}\iint \sum \frac{(6n-2)\,G_n}{r^{6n-1}} \left(\sum (-1)^i Y_i^{(n)} \cos^{2i+1}\theta \sin^3\theta\right) d\theta\, dr \ldots (40)$$

Next, we have to integrate with respect to θ from 0 to θ' and since

$$\int_0^{\theta'} \cos^{2i+1}\theta \sin^3\theta \, d\theta = \frac{2}{(2i+2)(2i+4)} - \frac{\cos^{2i+2}\theta'}{2i+2} + \frac{\cos^{2i+4}\theta'}{2i+4},$$

$$F_2'' = \frac{N\pi}{B}\int \frac{(6n-2)\,G_n}{r^{6n-1}}\left\{\sum (-1)^i Y_1^{(n)}\left(\frac{2}{(2i+2)(2i+4)} - \frac{\cos^{2i+2}\theta'}{2i+2} + \frac{\cos^{2i+4}\theta'}{2i+4}\right)\right\} dr.$$

But

$$\cos\theta' = \frac{Z}{r}.$$

Hence

$$F_2'' = \frac{N\pi}{B}\int (6n-2)\,G_n\left\{\sum (-1)^i Y_i^{(n)}\left(\frac{2}{(2i+2)(2i+4)\,r^{6n-1}} - \frac{Z^{2i+2}}{(2i+2)\,r^{6n+2i+1}} + \frac{Z^{2i+4}}{(2i+4)\,r^{6n+2i+3}}\right\} dr.$$

With respect to r we have to integrate from Z to r_0. Therefore

$$F_2'' = \frac{N\pi}{B}\sum (6n-2)\,G_n\left\{\sum (-1)^i Y_i^{(n)}\right.$$
$$\left[\frac{2}{(2i+2)(2i+4)(6n-2)}\left(\frac{1}{Z^{6n-2}} - \frac{1}{r_0^{6n-2}}\right)\right.$$
$$- \frac{Z^{2i+2}}{(2i+2)(6n+2i)}\left(\frac{1}{Z^{6n+2i}} - \frac{1}{r_0^{6n+2i}}\right)$$
$$\left.\left. + \frac{Z^{2i+4}}{(2i+4)(6n+2i+2)}\left(\frac{1}{Z^{6n+2i+2}} - \frac{1}{r_0^{6n+2i+2}}\right)\right]\right\}.$$

From (33)

$$F_2'' = \frac{N\pi}{B}\sum G_n\left\{\frac{2L_n}{Z^{6n-2}} - \sum (-1)^i Y_i^{(n)}\left[\frac{2}{(2i+2)(2i+4)}\cdot\frac{1}{r_0^{6n-2}}\right.\right.$$
$$- \frac{(6n-2)}{(2i+2)(6n+2i)}\cdot\frac{Z^{2i+2}}{r_0^{6n+2i}}$$
$$\left.\left. + \frac{(6n-2)}{(2i+4)(6n+2i+2)}\cdot\frac{Z^{2i+4}}{r_0^{6n+2i+2}}\right]\right\} \quad (41)$$

Hence

$$F''=F_1''-F_2''$$

$$=\frac{N\pi}{B}\sum(6n-2)\,G_n\Big\{\sum(-1)^i Y_i^{(n)}\Big(\frac{2}{(2i+2)(2i+4)(6n-2)}\cdot\frac{Z^{2i+2}}{r_0^{6n-2}}$$

$$-\frac{1}{(2i+2)(6n+2i)}\cdot\frac{1}{r_0^{6n+2i}}$$

$$+\frac{1}{(2i+4)(6n+2i+2)}\cdot\frac{Z^{2i+4}}{r_0^{6n+2i+2}}\Big)\Big\}\quad(42)$$

Consider a cylinder standing on XY and whose base is ds. (Fig. 13).

The number of P_1 contained in the elementary volume bounded by the cylindrical surface and two sectional planes whose distances from XY are Z and $Z+dZ$ respectively, is $N\,ds\,dZ$.

Fig. 13.

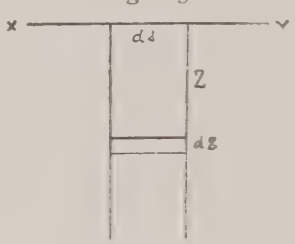

Hence the x-component of the force acting on the molecules in A from the molecules in the cylinder is

$$F=N\,ds\Big[\int_0^{r_0}F''\,dZ+\int_{r_0}^{\infty}F'\,dZ\Big]\quad(43)$$

From (42)

$$\int_0^{r_0}F''\,dZ=\frac{N\pi}{B}\sum(6n-2)\,G_n\sum_i(-1)^i Y_i^{(n)}$$

$$\Big\{\frac{2}{(2i+2)(2i+4)(6n-2)}\cdot\frac{1}{r_0^{6n-2}}\int_0^{r_0}dZ$$

$$-\frac{1}{(6i+2)(6n+2i)}\cdot\frac{1}{r_0^{6n+2i}}\int_0^{r_0}Z^{2i+2}dZ$$

$$+\frac{1}{(2i+4)(6n+2i+2)}\cdot\frac{1}{r_0^{6n+2i+2}}\int_0^{r_0}Z^{2i+4}dZ\Big\}$$

$$=\frac{2N\pi}{B}\sum(6n-2)\,G_n\sum(-1)^i Y_i^{(n)}\frac{36n^2+6n(4i+3)+4i^2+5i+5}{(2i+3)(2i+5)(6n+2i)(6n+2i+2)}.$$

Putting

$$M_n = \sum (-1)^i Y_i^{(n)} \frac{36n^2+6n(4i+3)+4i^2+5i+5}{(2i+3)(2i+5)(6n+2i)(6n+2i+2)},$$

$$\int_0^{r_0} F'' \, dZ = \frac{2N\pi}{B} \sum \frac{M_n G_n}{r_0^{6n-3}} \quad \ldots\ldots (44)$$

Also

$$\int_{r_0}^{\infty} F' \, dZ = \frac{2\pi N}{B} \sum \int_{r_0}^{\infty} \frac{G_n L_n}{Z^{6n-2}} \, dZ = \frac{2\pi N}{B} \sum \frac{G_n L_n}{6n-3} \cdot \frac{1}{r_0^{6n-3}} \quad \ldots\ldots (45)$$

Consequently

$$F = ds \frac{2\pi N^2}{B} \sum \frac{G_n}{r_0^{6n-3}} \left(\frac{L_n}{6n-3} + M_n \right).$$

If we put for simplicity

$$R_n = \frac{L_n}{6n-3} + M_n \quad \ldots\ldots (46)$$

$$F = ds \frac{2\pi N^2}{B} \sum \frac{G_n R_n}{r_0^{6n-3}} \quad \ldots\ldots (47)$$

L_n, $\frac{L_n}{6n-3}$, M_n and R_n are as shown in Table III.

TABLE III.

n	1	2	3	4	5	6	7
L_n	0.1166	0.1400	0.2601	0.5874	1.489	4.206	11.76
$\frac{L_n}{6n-3}$	0.0389	0.01556	0.01735	0.0283	0.0552	0.1274	0.302
M_n	0.4837	2.029	8.50	35.17	144.8	585.7	2345
R_n	0.5226	2.045	8.52	35.20	144.9	585.8	2345

Substituting (1) for β in the expression (30)

$$G_n = -\frac{\pi^2 \mu^{4n}}{(kT)^{6n}} \cdot H_n \cdot \frac{\nu}{6} m Z_0 \frac{dv}{dz} \cdot l$$

Since ν is proportional to the linear velocity of the molecules and the linear velocity is proportional to the square root of the absolute temperature T, we can put

$$\nu = c\sqrt{T}.$$

Hence

$$G_n = -\frac{\pi^2 c l m Z_0}{6} \cdot \frac{dv}{dz} \cdot \sqrt{T}\, \frac{\mu^{4n} H_n}{(kT)^{2n}} \quad \cdots\cdots (49)$$

If m_H be the mass of the hydrogen atom and w and ρ the molecular weight and the density of the liquid respectively,

$$m = m_H w, \qquad Z_0 = \sqrt[3]{\frac{w m_H}{\rho}}.$$

Hence

$$G_n = -\frac{\pi^2 c l}{6} \cdot \frac{(m_H w)^{\frac{4}{3}}}{\rho^{\frac{1}{3}}} \cdot \frac{dv}{dz} \cdot \sqrt{T} \cdot \frac{\mu^{4n} H_n}{(kT)^{2n}} \quad \cdots\cdots (50)$$

Substituting this in (47)

$$F = -ds \frac{dv}{dz} \cdot \frac{2\pi^3 l}{6} \cdot \frac{N^2}{B} \frac{(m_H w)^{\frac{4}{3}}}{\rho^{\frac{1}{3}}} \sqrt{T} \sum \frac{\mu^{4n} H_n R_n}{(kT)^{2n}} \cdot \frac{1}{r_0^{6n-3}}.$$

But

$$N = \frac{\rho}{m} = \frac{\rho}{w m_H}.$$

Also if we put as the value of B, $16\pi^2$ from (11)

$$F = -ds \frac{dv}{dz} \cdot \frac{\pi c l}{48} \cdot \frac{\rho^{\frac{5}{3}}}{(m_H w)^{\frac{2}{3}}} \sqrt{T} \sum \frac{\mu^{4n} H_n R_n}{(kT)^{2n}} \cdot \frac{1}{r_0^{6n-3}}.$$

$$\eta = -\frac{F}{ds \frac{dv}{dz}} = \frac{\pi c l}{48} \cdot \frac{\rho^{\frac{5}{3}}}{(m_H w)^{\frac{2}{3}}} \cdot \sqrt{T} \sum \frac{\mu^{4n} H_n R_n}{(kT)^{2n}} \cdot \frac{1}{r_0^{6n-3}} \quad \cdots (51)$$

Putting

$$P_n = H_n R_n$$

$$\eta = \frac{\pi c l}{48} \cdot \frac{\rho^{\frac{5}{3}}}{(m_H w)^{\frac{2}{3}}} \sqrt{T} \sum \frac{P_n \mu^{4n}}{(kT)^{2n}} \cdot \frac{1}{r_0^{6n-3}} \quad \cdots\cdots (52)$$

The values of P_n are shown in Table IV.

TABLE IV.

n	1	2	3	4	5	6	7
H_n	0.6667	$1.111.10^{-2}$	$7.442.10^{-5}$	$2.756.10^{-7}$	$6.521.10^{-10}$	$1.076.10^{-12}$	$1.307.10^{-14}$
R_n	0.5226	2.045	8.520	35.20	144.9	585.8	2345
P_n	0.3486	$2.272.10^{-12}$	$6.344.10^{-4}$	$1.019.10^{-5}$	$9.442.10^{-8}$	$6.302.10^{-10}$	$1.3035.10^{-11}$

In the expression (52) cl and r_0 are unknown molecular constants. If now at $T = T_0$, $\eta = \eta_0$ $\rho = \rho_0$

$$\frac{\eta}{\eta_0} = \frac{\sqrt{T}\,\rho^{\frac{5}{3}} \sum \frac{P_n\,\mu^{4n}}{(kT)^{2n}} \cdot \frac{1}{r_0^{6n-3}}}{\sqrt{T_0}\,\rho_0^{\frac{5}{3}} \sum \frac{P_n\,\mu^{4n}}{(kT_0)^{2n}} \cdot \frac{1}{r_0^{6n-3}}} = \frac{\rho^{\frac{5}{3}} \sum \frac{P_n\,\mu^{4n}}{T^{2n-\frac{1}{2}}} \cdot \frac{1}{k^{2n} r_0^{6n}}}{\rho_0^{\frac{5}{3}} \sum \frac{P_n\,\mu^{4n}}{T^{2n-\frac{1}{2}}} \cdot \frac{1}{k^{2n} r_0^{6n}}},$$

or

$$\sum \left(\frac{\eta \rho_0^{\frac{5}{3}}}{T_0^{2n-\frac{1}{2}}} - \frac{\eta_0 \rho^{\frac{5}{3}}}{T^{2n-\frac{1}{2}}} \right) P_n\,\mu^{4n} \frac{1}{k^{2n} r_0^{6n}} = 0.$$

Putting

$$\frac{\eta \rho_0^{\frac{5}{3}}}{T_0^{2n-\frac{1}{2}}} - \frac{\eta_0 \rho^{\frac{5}{3}}}{T^{2n-\frac{1}{2}}} = Q_n, \quad \frac{\mu^4}{k^2 r_0^6} = x, \quad \ldots\ldots\ldots\ldots (53)$$

x can be found by solving the equation

$$P_1 Q_1 + P_2 Q_2 x + P_3 Q_3 x^2 + P_4 Q_4 x^3 + \ldots\ldots = 0 \ldots\ldots\ldots (54)$$

and r_0 can be determined by

$$r_0 = \sqrt[6]{\frac{\mu^4}{x k^2}}. \quad \ldots\ldots\ldots\ldots (55)$$

cl can be determined by substituting its value in (51).

8. COMPAPISON WITH EXPERIMENTS.

I. Ethyl Alcohol.

At $T=273$, $\eta_0=0.017716$, $\rho_0=0.8065$ and at $T=343$, $\eta=0.005098$, $\rho=0.7446$.

Calculating Q_n from (53) by making use of these values, we have following table.

TABLE V.

n	1	2	3	4	5	6	7
Q_n	$-0.916.10^{-6}$	$-0.391.10^{-11}$	$0.289.10^{-16}$	$0.860.10^{-21}$	$1.669.10^{-26}$	$2.678.10^{-31}$	$3.952.10^{-36}$

Calculating $P_n Q_n$ from the value of P_n and Q_n in the Table IV and V, we have following Table.

TABLE VI.

n	1	2	3	4	5	6	7
P_nQ_n	$-0.3193.10^{-6}$	$-0.8881.10^{-13}$	$1.833.10^{-20}$	$0.876.10^{-26}$	$15.76.10^{-34}$	$16.87.10^{-41}$	$5.164.10^{-47}$

Hence the equation (54) becomes

$$-0.3193.10^{-6}-0.8881.10^{-13}x+1.833.10^{-20}x^2+0.876.10^{-26}x^3 +15.76.10^{-34}x^4+16.87.10^{-41}x^5+5.164.10^{-47}x^6+\ldots\ldots=0$$

or

$$-0.3193-0.8881.10^{-7}x+1.833.10^{-14}x^2+0.876.10^{-10}x^3 +15.76.10^{-28}x^4+16.87.10^{-35}x^5+5.164\,10^{-41}x^6+\ldots\ldots=0.$$

If we put

$$x\,.\,10^{-6}=X \qquad \text{consequently } r_0=\sqrt[6]{\frac{\mu^4}{Xk^2 10^6}} \quad \ldots\ldots\ldots\ldots\ldots (56)$$

$$-31930-8881X+1833X^2+876X^3+157.6X^4+16.875X^5+5.164X^6+\ldots=0.$$

To make clear the degree of accuracy of solution, first we take 5 first terms of the equation, and next 6 terms, and so on.

$X^4+5.53X^3+11.64X^2-56.4X-202.5=0$ $\qquad X=3.1$

$X^5+9.34X^4+51.94X^3+108.6X^2-526.4X-1894=0$ $\qquad X=3.04$

$X^6+3.26X^5+30.52X^4+169.7X^3+364.7X^2-1721X-6091=0$ $\qquad X=3.00.$

Making use of the last value of X and Debye's value of $\mu(=4.3.10^{-19})$[1]

$$r_0 = \sqrt[6]{\frac{(4.3.10^{-19})^4}{3\times(1.37.10^{-16})^2.10^6}} = 9.202.10^{-9}\text{ cm.}$$

But the molecular diameter in its vapour state is

$$\sigma = 33.10^{-9}\text{ cm.}^{(2)}$$

and is about 3.5 times great as r_0. As has been already remarked, r_0 and σ are analogous, but not quite the same. That they are in the same order of magnitude shows the reliability of our theory.

Now (52) can be writen in the following form

$$\eta = \frac{\pi cl}{48}\,\frac{\rho^{\frac{5}{3}}}{(m_H w)^{\frac{2}{3}}}\,r_0^3\sqrt{T}\sum P_n\left(\frac{X.10^6}{T^2}\right)^n \quad \ldots\ldots\ldots\ldots\ldots\ldots(58)$$

Putting $T = 343$ and substituting the above value into X, using the value in Table IV as the value of P_n.

$$\sum P_n\left(\frac{X10^6}{T^2}\right)^n = 8.889+14.77+10.52+4.309+1.018+0.1733+0.09142$$
$$= 39.77.$$

Putting

$$m_H = 1.66.\ 10^{-24}\,gr., \qquad w = 46, \qquad \eta = 0.005098,$$
$$cl = 4\times 10^5$$

Now l is of the order of 10^{-8} cm, so that c becomes of the order of 10^{12}.

Hence from $\nu = C\sqrt{T}$, ν is of the order of 10^{13}.

The mean velocity of molecule at 0°C in the vapour state is

$$\Omega = 35440\,\frac{cm.}{sec.}^{(3)}$$

---

(1) loc. cit.
(2) Landolt-Börnstein, 141 (1912).
(3) Landolt-Bornstein (1912).

Also the mean free path is, under 1 atmospheric pressure

$$L = 341.10^{-8} \text{ cm.}^{(1)}$$

Hence the number of collision in this state

$$\nu' = \frac{\Omega}{L} = \frac{35440}{341} . 10^8 = 1.025.10^{10}.$$

But the densities of the gas and the liquid at 0°C and under 1 atmosphric pressure is

$$\rho_g = 2.054.10^{-3} \frac{gr.}{cm^3}^{(2)}$$

$$\rho_l = 0.8065 \frac{gr.}{cm^3}.$$

respectively.

Hence if we calculate the number of collislons assuming it to be proportional to the density

$$\nu = \nu' \frac{0.8065}{2.054} . 10^3 = 4.04 \times 10^{12}$$

which is near to the value above obtained. Hence our result is probably a reliable one.

Now if we put numerical values for the factors which is independent of temperature, (58) becomes

$$\eta = 11.313\, \rho^{\frac{5}{3}} \sqrt{T} \left(1.0458 \frac{1}{T^2} + 2.0448.10^5 \frac{1}{T^4} + 1.713.10^{10} \frac{1}{T^6} + 8.256.10^{14} \frac{1}{T^8} + 2.29.10^{19} \frac{1}{T^{10}} + 4.595.10^{23} \frac{1}{T^{12}} + 2.851.10^{28} \frac{1}{T^{14}} + \ldots\ldots \right). \quad (59)$$

If we put $T = 273$, $\rho_0 = 0.8065$ in this expression

$$\eta_{273} = 11.313 \times 0.8065 \times \sqrt{273} \times 10^{-5} \left(1.403 + 3.682 + 4.138 + 2.676 + 0.998 + 0.268 + 0.244 + \ldots\ldots \right).$$

But since the last term in ( ) is 0.2, the final result when the terms

(1), (2). Landolt-Börn stein (1912).

are taken as far as this, can not be free from the error as great as 2%. Calculating the right-hand side of the above expression,

$$\eta_{273} = 0.01751.$$

The result of experiment is 0.01771 and is in error which is as great as the one expected. This is due to the insufficiency of terms. Calculated values of η at every 10 degrees between 273 and 343 from (59) is shown in comparision with experimental data.

TABLE VII.

$t°C$	ρ	η_{cal}	η_{obs} [1]
0	0.8065	0.01751	0.01771
10	0.7979	0.01415	0.01451
20	0.7894	0.01154	0.01194
30	0.7810	0.00968	0.00992
40	0.7722	0.00814	0.00831
50	0.7633	0.00691	0.00701
60	0.7541	0.00591	0.00596
70	0.7446	0.00510	0.00510

II. Methyl Alcohol.

At $T = 273, \eta_0 = 0.008166, \rho_0 = 0.8100$ and at $T = 333, \eta = 0.005098, \rho = 0.7446$.[1] By similar calculations as I, we have

$$X^6 + 3.325X^5 + 32.4X^4 + 203.5X^3 + 554X^2 + 736X + 2725 = 0.$$

Solving this equation

$$X = 1.671$$

By (56), making use of Debye's value of $\mu (= 3.4.10^{-19})$[2] and the above value of X

$$r_0 = 8.675.10^{-9}\ cm.$$

Putting $T = 333$, $w = 32$ in (51) and substituting the above value of X, we have

$$cl' = 7.83.10^5.$$

(1) Landolt-Börnstein, 79 (1912).

(2) loc. cit.

$$\eta = 2.357\,\rho^{\frac{5}{3}}\sqrt{T}\left(5.825\,\frac{1}{T^2}+6.344.10^{5}\,\frac{1}{T^4}+2.960.10^{10}\,\frac{1}{T^6}+7.96.10^{4}\,\frac{1}{T^8}\right.$$
$$\left.+1.230.10^{19}\,\frac{1}{T^{10}}+4.744.10^{27}\,\frac{1}{T^{14}}+\ldots\ldots\right).$$

In the following table are shown the values of η calculated by the above formula to compare with the experimental data.

TABLE VIII.

t°C	ρ	η_{cal}	η_{obs} [2]
0	0.8100	0.008144	0.008166
10	0.8008	0.006958	0.006901
20	0.7915	0.005995	0.005957
30	0.7825	0.005213	0.005204
40	0.7740	0.004574	0.004565
50	0.7650	0.004030	0.004028
60	0.7550	0.003571	0.003571

9. FURTHER EXPERIMENTAL EVIDENCES SUPPORTING THE ABOVE THEORY.

1. Variation of Viscosity of Liquids in an Electric Field.

The molecules of non-conducting liquids placed in a strong electric field are forced to tend, to some extent, to arrange themselves lengthwise along the lines of force. Hence, as a necessary consequence of the above theory, it follows that the viscosity of liquids must vary in an electric field. Some experiments have been carried out by *A.* Sellerio to test this point.[2] He measured the variation of viscosity in an electric field by making use of the method of damped vibration, obtaining the following results.

(1) Landolt-Börnstein 76 (1912)
(2) A. Sellerio, N. Cimento **11**, (1916), 395.

Substance	Increase of viscostty in %	Electric field (volt per cm)
Castor oil	2.4	23000
Carbon disulphide	5.3	12000
Vaseline oil	6.0	16000

These results are clearly in favour of our theory, at least in a qualitative manner.

II. Variation of Dielectric Constant due to the Velocity Gradient in a Flow of Liquid.

According to the above theory, there exists a tendency that the molecules in a flowing of liquids are forced to arrange lengthwise along the direction of the stream when there is a velocity gradient. Hence the dielectric constant of liquids must also vary. Some experimental evidence has already been obtained by Maxwell in support of the above theory.[1] His experiment was made for the purpose of ascertaining the state of strain in a viscous fluid in motion. Into a cylindrical box with a glass bottom is introduced some viscous liquid such as Canada balsam. Within the liquid a solid cylinder was rotated about its vertical axis. Polarized light was passed vertically through the liquid. He observed the phenomenon of a double refraction due to strain occurring in the Canada balsam which had such a fluidity that it very rapidly assumed a level surface after being disturbed. Maxwell's method is not accurate enough to enable us to detect the variation of dielectric constant due to strain in the case of ordinary viscous liquids. But if we were to apply some suitable method for the measurement of the dielectric constant, it is very probable that we could detect the same effect.

10. POSSIBLE FEATURES OF THE STRUCTURE OF STREAM WHICH MAY BE REVEALED BY *X*-RAY EXAMINATION.

As a consequence of the above theory, it must follow that the

(1) Clerk Maxwell, Scientific Papers Vol. II, 379.

molecules of a viscous fluid in flowing must have a somewhat regular arrangement i.e. fibrous structure. Hence we may expect this to have some effect on the *X*-Ray pattern[1].

In conclusion the writer wishes to express his hearty thanks to Professor K. Honda for his continued encouragement throughout the course of this investigation, also, to Proffessor I. Kobayashi for his kind advices with regard to the mathematical treatment.

Sendai, September, 1924.

---

(1) Some of the experiments for the elucidation of the phenomena mentioned in 9,10 are in progress in our laboratory.

Dielectric Constants of Liquids.
Part I.
On the Method of Measuring Dielectric Constants of Liquids.

By

Yoshikatsu Matsuike.

Among many methods of measuring dielectric constants, the so-called "Resonance Method"[1], it is said, gives the most accurate results.

The present author improved several points in this method, and finally got a nearly perfect apparatus for the measurements which are to be given in this paper.

1. PRINCIPLE OF THE METHOD.

When a certain potential difference is applied on the plate circuit and some current on the filament of a triod valve in whose plate circuit certain capacity and impedance have been inserted and in whose grid

---

(1) Scott Taggart; Electrician, 72, (1919), 466.
J. Herweg; Ber. Deut. Physik. Ges., 21, (1919), 572.
G. Falckenberg; Ann. Physik., 61, (1920), 167.
K. Whiddington; Proc. Camb. Phys. Soc. 20, (1921), 445.
L. C. Jackson; Phil. Mag., 255, (1922), 481.
M. Jezewski; Journ. Phpsiq. Rad., 3, (1922), 293.
M. H. Beltz; Phil. Mag., 261, (1922), 479.
K. Theoportschick; Physik. Z., 621, (1922), 344.
W. Kast; Ann. Physik., 73½, (1923), 145.
T. E. P. Wagstoff; Phil. Mag., 282 (1924), 66.
Edwin C. Filts; Phys. Rev., 23, (1924), 345.
Ross Gunn; Phil. Mag., 283, (1924), 224.
C. T. Zahn; Phys Rev., 24, (1924), 400.

circuit certain impedance has been inserted, there an oscillation current is set up. The frequency of that current is given by the formula,

$$n = 1/2\pi\sqrt{LC}$$

where L is the self-inductance, C the capacity and n the frequency.

We can, therefore, by changing the value L or C, obtain current of any frequeney at will.

If two such circuits with high but nearly equal frequencies are coupled, there occur beats corresponding to the difference between them. But when the capacity C is changed by $\triangle C$ in one of the circuits under constant L, n of that circuit will change twice as much as C, that is

$$2\triangle n/n = \triangle C/C$$

and naturally the frequency of the beat changes.

Hence by adjusting the capacity in one of the coupled circuits, it is possible to have a point of resonance between them where the beat dies.

Now when a cell is inserted paralled to the condenser of one of these circuits and its medium changed while other conditions are kept constant, the total capacity of this circuits changes, and its amount can be determined by the displacement of the resonance point or by the change of the number of beats. The dielectric constant of the medium of the cell can be calculated easily from the data of this capacity change.

2. DETAILS OF THE APPARATUS.

The apparatus consists of three parts: (I & I′) a pair of radio frequency circuits, (II), a detector, and (III), an audio frequency circuit, which are coupled one to the other as shown in fig. 1.

Both in I and I′ circuits, the valves are operated with 100-200 volts on the plates, and 0.6-1 0 amperes on the filaments. Their negative poles are earthened. The impedance coils, L_1 and L_1', are wound 400 turns with 3 cm. radii with silk-covered wire of No. 24; L_2 and L_2', 100 turns with 4.5 cm. radii, with silk-covered wire of No. 22; L_3 and L_3', 50

Fig. 1

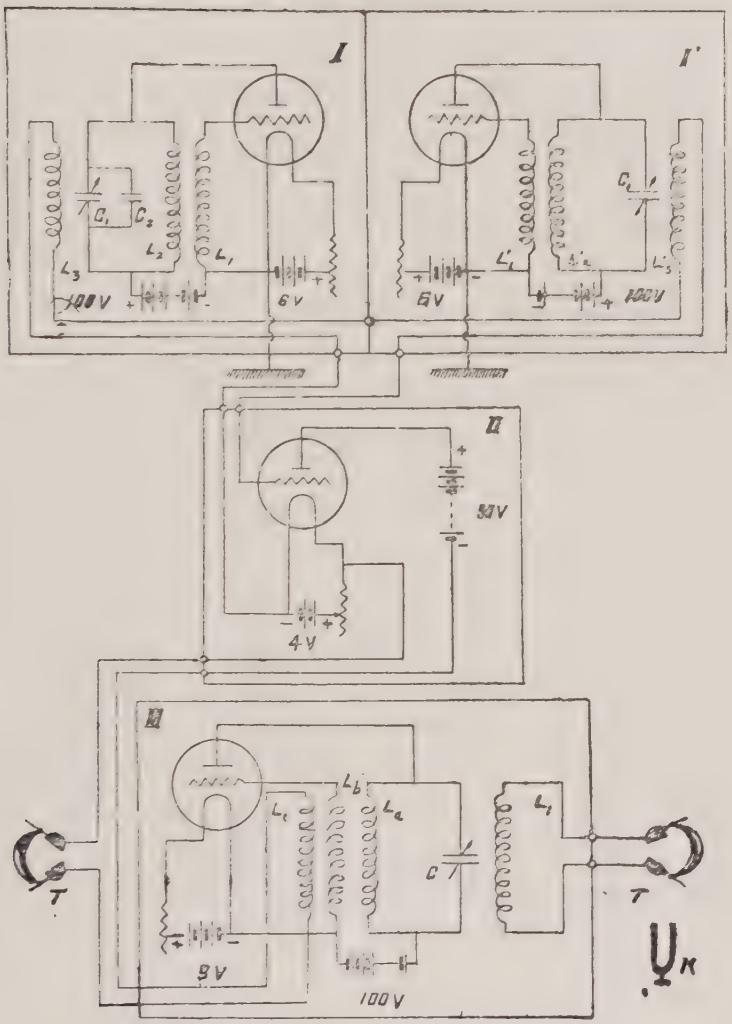

turns with 6 cm. radii, with silkcovered wire of No. 22; and these are loosely coupled one to the other.

C_1' is a variable air condenser of about 0.002 $\mu\mu F.$ of total capacity. C_1 consistes of two condensers. One of them is a step variable condenser, made up of ten small condensers, the capacity of each being about 10^{-5} $\mu\mu F.$; the other is a sliding variable condenser with a piece of glass plate, 5 cm. long, 2 cm. width and 0.5 mm. thick-

ness, which can slide in and out between two parallel brass plates separated by a distance of 1 mm. In the latter condenser even as small a change as 10^{-9} $\mu\mu F.$ can be read by means of the precision screw vernier fitted to the glass plate, and its total change of capacity is nearly 10^{-5} $\mu\mu F.$ C_2 is a cell to be filled with samples: its construction will be described later. With the design above mentioned, it is possible to have a circuit oscillated with a frequency of about a million per second.

The calibration of the condensers is, of course, carefully done.

In the detector (II), the valve is operated with 50 V. on the plate and 0.6 amp. on the filament. This circuit serves to detect and amplify the waves which come from I and I′, and at the same time to change the alternating current to the direct for the sake of getting a clear sound in the telephone receiver.

Fig. 2

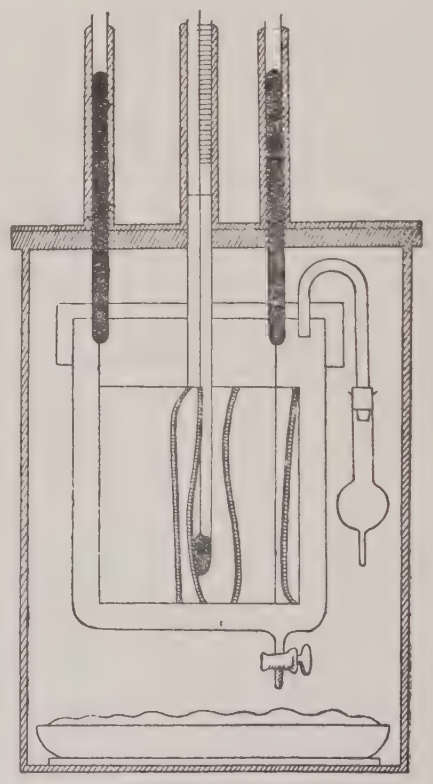

In the low frequency circuit (III), the valve is operated with 100 V. on the plate, and with 0.6 amp. on the filament. The coil is wound 2000 turns with 15 cm. radi us with cotton covered wire of No. 36. Its total self-inductance is 0.21 henry, which is divided into 2 parts, one for the use of L_a and the other for the use of L_b. L_c is also a coil of the same dimension with 500 turns. These are coupled with one another. C is a group of variable condensers with a total capacity of 1 $\mu\mu F.$ By adjusting this capacity, an audible note of the frequency of about 2000 per second can be excited. This note is tuned to a standard tuning

fork from time to time during the experiments, to maintain the frequency constant.

The receiver fitted to the detector has very high impedance, specially designed for the use of wireless.

A cell is shown in Fig. 2. The concentric cylinders of nickel plate are placed vertically in a glass bottle which is to be filled with liquid samples. To maintain its temperature constant, the bottle is placed in a brass bomb together with P_2O_5 or $CaCl_2$ as shown in the figure, to keep the space dry; and then they are put in a thermostat.

In the case of a liquid such as water, whose conductivity is comparatively large, the nickel electrodes are covered with paraffin.

3. PROCEDURE OF THE MEASUREMENT.

The beats produced by the two oscillating circuits I and I' of nearly equal frequencies, say about a million per second, is again coupled with the audible circuits III of a constant frequency of about 2000, and the two points on the variable condensers of the circuit I, where the final beat dies, are determined, while keeping other conditions constant.

The mean position of these two points is taken as the resonance point.

Next, the standard liquid benzene, is put in the cell, and the resonance point is determined in exactly the same way as above stated.

Finally, the sample, of which the dielectric constant is to be measured, is put in to the cell, and again the resonance point is determined.

The dielectric constant of the sample ε is then calculated by the formula,

$$\varepsilon = (\varepsilon_0 - 1)\frac{S-a}{s-a} + 1.$$

where ε_0 is the dielectric constant of the standard liquid, and a, s and S are the reading of the variable condenser at the point of resonance when air, the standard liquid and the sample respectively are put in to the cell.

The following precautions are taken for the experiments to secure good results.

(1) All the apparatus are covered with metallic boxes which are earthened, for the sake of protecting them from external electrical disturbances.

(2) Spaces inside the boxes are kept dry with $CaCl_2$.

(3) All the connecting wires are kept fixed and all the joints are soldered.

(4) As the constancy of the frequency depends much upon the quality of valves, they are carefully selected.

(5) To get the constant frequency current, the oscillations are generated for several hours before the experiment is undertaken.

4. PURIFICATION OF THE SAMPLES.

The starting substances are all obtained as pure chemicals from Kahlbaum in Gemany. They are then treated as follows.

(1) Benzene:—After several recrystalizations, it is dehydrated with with metallic sodium and then is distilled. m.p., 5.4°C: b.p., 80.08°C.

This is adopted as a standard liquid, and its dielectric constant is assumed to be 2.277 at 25°C., according to Turner

(2) Ether:—It is dehydrated with metallic sodium, kept in contact with mercury, and then distilled. b.p., 34.58°.C.

(3) Carbon bisulphide:—It is soaked with CaO_2 to remove all sulphur, distilled, shaken with $KMnO_4$, mercury and mercuric sulphate, and then redistilled. b.p., 46.28°. C.

(4) Chloroform:—It is kept in contact with $CaCl_2$ several days, then distilled. b.p., 61.20°C.

(5) Acetone:—It is crystallized with NaI at $-8.°C$ and then they are decomposed by distillation. b.p., 56.06°.C.

(6) Ethyl-alcohol:—It is dehydrated with $CaCl_2$ and metallic Ca thoroughly, then distilled carefully.

(7) Water:—Ordinary conductivity water.

5. THE RESULTS OF THE EXPERIMENTS.

The measurements are carried on with the above several pure liquids at 25°C., and their results are tabulated in Table. 1.

TABLE 1.

	Ether $(C_2H_5)_2O$	Carbon bisulphide CS_2	Chloroform $CHCl_3$	Acetone $(CH_3)_2CO$	Ethyl alcohol C_2H_5OH	Water H_2O
Reading when air is in the condenser	4.125	11.981	11.784	4.384	4.384	6.41
Reading when standard liquid benzene is in the cond.	5.458	18.219	17.124	5.600	5.600	(C_2H_2OH) 11.66
Reading when liquid sample is in the cond.	7.418	20.202	29.032	23.870	24.926	28.51
Dielectric constant of liquid sample	4.156	2.675	5.135	21.45	22.62	84.08
Notes.	4.227 (Turner)	2.64 (Drude)	5.2 (Turner) 4.93 (Drude)	20.9 (Walden)	26.8 (Turner) 20.8 (Walden) 20.5 (Abeggs)	76 (Cohn) 81 (Turner) 88 (Drude) 87.2 (Jewski)

In this table, ethyl alcohol is used for standardizing the cell, with paraffinized electrodes, which is used for the determination of the dielectric constant of water.

6. SUMMARY.

(1) An apparatus for the measurements of dielectric constants of liquids by means of resonance of two high oscillators is described.

(2) Dielectric constants of several liquids are given with the accuracy of about one-thousandth.

In conclusion, the present author wishes to express his grateful thanks to Assistant-Professor Shinroku Mitsukuri, under whose kind

guidance and encouragement the present work was carried on, and also to Mr. Mishio Ishimoto of the Mitsubishi Ship Building Co. for his valuable advices.

A part of the expense of this experiment was paid by the research fund granted to Prof. S. Mitsukuri from the Department of Education, and also by the research fund granted to the present author from the Kuzuhara Cold Storage Co. at Tokyo.

(The Laboratory of Theoretical Chemistry,
Feb. 20th. 1925)

On the Structural Diagrams of Some Special Steels.[1]

By

Tsutom Kasé.

With 5 Plates

Contents :—

§ 1. Introduction.
§ 2. Nickel Steel.
§ 3. Manganese Steel.
§ 4. Chromium Steel.
§ 5. Microscopic Investigation.
Summary.

§ 1. INTRODUCTION.

The present writer has recently investigated the diagram of the iron-carbon-nickel system.[2] It was found that iron-nickel alloys containing about 30–34 per cent of nickel, when cooled from a very high temperature, have an austenitic structure at room temperature, and on a further cooling down to −190°C, they undergo the A_3 transformation, their structure changing from austenite to martensite, and further that during this transformation these alloys increase in volume and hardness in a marked degree. Hence, if the iron-carbon-nickel alloys be examined by means of a dilatometer and a hardness tester, the structural diagram of the ternary system can be easily studied. The object of the present investigation was to determine by the above methods, the structural diagrams of nickel, manganese, and chromium steels.

(1) The one hundred and eighth report of the Research Institute for Iron, Steel and Other Metals.

(2) Sci. Rep., **14** (1925), 173.

% Ni	% C	Scleroscope Hardness and Microstructure							
		Cooled from melt in the furnace		Immersed in liquid air		Annealed		Immersed in liquid air	
4	0.8	51.0	M	37.9	M	26.2	S	26.4	S
8	„	43.0	M	58.5	M	29.3	M	30.2	M
10	„	26.6	M	58.4	M	47.3	M	60.0	M
12	„	18.3	A	55.1	M	44.7	A	58.2	M
15	„	18.1	A	56.1	M	33.1	A	57.0	M
20	„	17.9	A	55.7	M	31.7	A	58.8	M
25	„	18.6	A	28.7	M	18.0	A	44.8	M
30	„	18.5	A	20.8	A	17.1	A	37.8	M, (G)
32	„	17.4	A	17.8	A	17.4	A	18.1	A
35	„	16.5	A	16.7	A	16.3	A	16.5	A
2	4.1	64.3	P	64.4	P	47.6	P	49.6	P
4	4.0	30.4	S, G	35.8	S, G	18.6	S, G	20.9	S, G
6	4.0	34.7	M, G	43.8	M, G	17.8	S, G	18.1	S, G
8	3.9	36.2	M, G	45.7	M, G	26.0	A, G	30.8	M, G
10	3.8	44.3	M, G	53.7	M, G	37.5	A, G	43.9	M, G
12	3.7	25.4	A, G	45.4	M, G	30.6	A, G	39.0	M, G
15	3.6	17.4	A, G	37.9	M, G	27.6	A, G	39.0	M, G
20	3.5	16.8	A, G	38.2	M, G	16.7	A, G	40.7	M, G
25	3.2	16.0	A, G	29.2	M, G	14.0	A, G	36.3	M, G
30	2.9	14.2	A, G	18.4	M, G	12.8	A, G	24.1	M, G
32	2.9	14.4	A, G	17.7	A, G	13.6	A, G	19.9	A, G
35	2.8	16.5	A, G	16.8	A, G	13.4	A, G	16.1	A, G
40	2.8	15.1	A, G	15.3	A, G	15.0	A, G	15.0	A, G

(* F=Ferrite, P=Pearlite, M=Martensite, A=Austenite, T=Troostite, G=Graphite)

In Table II, the chief structures such as pearlite, martensite, and austenite are given, the details of the other intermediate structures being omitted for simplicity.

From the above table, we see that austenitic and austenite-martensitic structures are transformed into a martensitic state by quenching

the specimen in liquid air. As the alloys of a martensitic structure are much harder than those of an austenitic structure, the composition-hardness curves in Fig. 2, a~c are to be expected. In Fig. 2, the full and dotted lines correspond to the hardness curves of the alloys before and after being immersed in liquid air.

Thus, the annealed iron-nickel alloys containing 20–34 per cent of nickel increase in hardness after being immersed in liquid air. A similar effect, however, is produced in those containing carbon, in cases where the alloys contain 10 per cent or less of nickel. As the cooling rate becomes more rapid the nickel concentration of maximum hardness is lowered. An alloy containing about 30 per cent of nickel and ca. 0.8 per cent of carbon does not increase in hardness, after an immersion in liquid air; further if it has been previously annealed at a high temperature for a long duration of time to cause a slight decrease of its hardness, there is, after an immersion in liquid air, an abnormal increase in hardness, the microstructure being at the same time changed from austenite to martensite. This peculiar phenomenon is explained in the following way:— The alloy cooled somewhat rapidly from the melt contains comparatively much dissolved carbon, and hence its transformation point is lowered below −190°C, but after a prolonged annealing graphite separates as a decomposition product of cementite; consequently the transformation point is raised, and the alloy, when immersed in liquid air, changes from austenite to martensite.

Further the eutectic alloy containing 2 % of nickel has an abnormally high degree of hardness as compared with the alloys containing higher content of nickel. This is attributed to the fact that the cementite contained in the latter alloys is decomposed.

(*b*) *Magnetic and Dilatometric Analyses.*

The magnetic analysis of the iron-nickel and iron-carbon-nickel system has been already made by the present writer in his investigation of the equilibrium diagram of iron-carbon-nickel alloys. Although all

% Ni	% C	Scleroscope Hardness and Microstructure							
		Cooled from melt in the furnace		Immersed in liquid air		Annealed		Immersed in liquid air	
4	0.8	51.0	M	37.9	M	26.2	S	26.4	S
8	„	43.0	M	58.5	M	29.3	M	30.2	M
10	„	26.6	M	58.4	M	47.3	M	60.0	M
12	„	18.3	A	55.1	M	44.7	A	58.2	M
15	„	18.1	A	56.1	M	33.1	A	57.0	M
20	„	17.9	A	55.7	M	31.7	A	58.8	M
25	„	18.6	A	28.7	M	18.0	A	44.8	M
30	„	18.5	A	20.8	A	17.1	A	37.8	M, (G)
32	„	17.4	A	17.8	A	17.4	A	18.1	A
35	„	16.5	A	16.7	A	16.3	A	16.5	A
2	4.1	64.3	P	64.4	P	47.6	P	49.6	P
4	4.0	30.4	S, G	35.8	S, G	18.6	S, G	20.9	S, G
6	4.0	34.7	M, G	43.8	M, G	17.8	S, G	18.1	S, G
8	3.9	36.2	M, G	45.7	M, G	26.0	A, G	30.8	M, G
10	3.8	44.3	M, G	53.7	M, G	37.5	A, G	43.9	M, G
12	3.7	25.4	A, G	45.4	M, G	30.6	A, G	39.0	M, G
15	3.6	17.4	A, G	37.9	M, G	27.6	A, G	39.0	M, G
20	3.5	16.8	A, G	38.2	M, G	16.7	A, G	40.7	M, G
25	3.2	16.0	A, G	29.2	M, G	14.0	A, G	36.3	M, G
30	2.9	14.2	A, G	18.4	M, G	12.8	A, G	24.1	M, G
32	2.9	14.4	A, G	17.7	A, G	13.6	A, G	19.9	A, G
35	2.8	16.5	A, G	16.8	A, G	13.4	A, G	16.1	A, G
40	2.8	15.1	A, G	15.3	A, G	15.0	A, G	15.0	A, G

(* F=Ferrite, P=Pearlite, M=Martensite, A=Austenite, T=Troostite, G=Graphite)

In Table II, the chief structures such as pearlite, martensite, and austenite are given, the details of the other intermediate structures being omitted for simplicity.

From the above table, we see that austenitic and austenite-martensitic structures are transformed into a martensitic state by quenching

the specimen in liquid air. As the alloys of a martensitic structure are much harder than those of an austenitic structure, the composition-hardness curves in Fig. 2, a~c are to be expected. In Fig. 2, the full and dotted lines correspond to the hardness curves of the alloys before and after being immersed in liquid air.

Thus, the annealed iron-nickel alloys containing 20–34 per cent of nickel increase in hardness after being immersed in liquid air. A similar effect, however, is produced in those containing carbon, in cases where the alloys contain 10 per cent or less of nickel. As the cooling rate becomes more rapid the nickel concentration of maximum hardness is lowered. An alloy containing about 30 per cent of nickel and ca. 0.8 per cent of carbon does not increase in hardness, after an immersion in liquid air; further if it has been previously annealed at a high temperature for a long duration of time to cause a slight decrease of its hardness, there is, after an immersion in liquid air, an abnormal increase in hardness, the microstructure being at the same time changed from austenite to martensite. This peculiar phenomenon is explained in the following way:— The alloy cooled somewhat rapidly from the melt contains comparatively much dissolved carbon, and hence its transformation point is lowered below −190°C, but after a prolonged annealing graphite separates as a decomposition product of cementite; consequently the transformation point is raised, and the alloy, when immersed in liquid air, changes from austenite to martensite.

Further the eutectic alloy containing 2 % of nickel has an abnormally high degree of hardness as compared with the alloys containing higher content of nickel. This is attributed to the fact that the cementite contained in the latter alloys is decomposed.

(*b*) *Magnetic and Dilatometric Analyses.*

The magnetic analysis of the iron-nickel and iron-carbon-nickel system has been already made by the present writer in his investigation of the equilibrium diagram of iron-carbon-nickel alloys. Although all

Fig. 2.

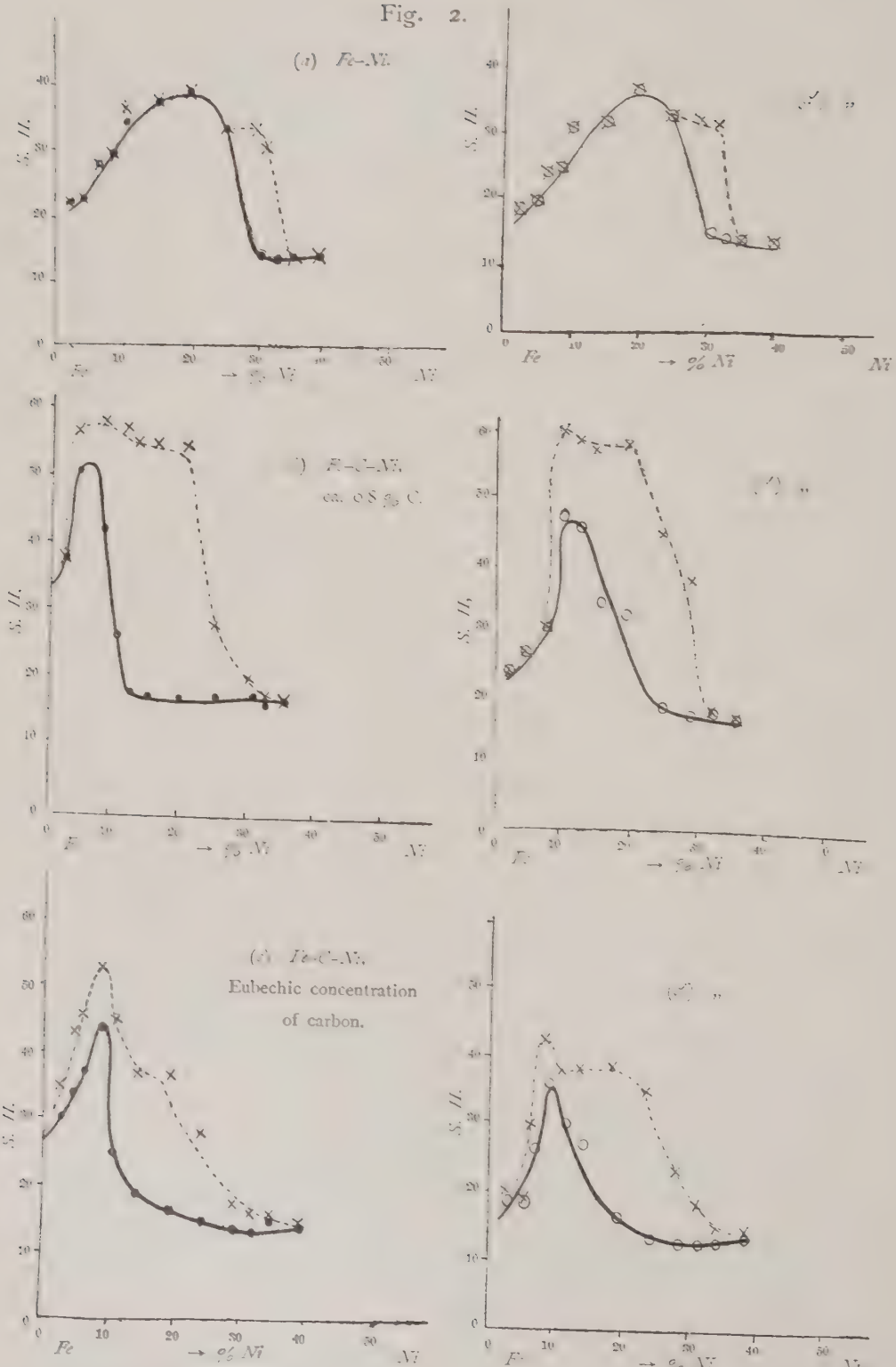

S.H.=Scleroscope Hardness.

● Cooled from the melt in the furna-

iron-nickel alloys which contain no carbon are ferro-magnetic at room temperature, the Ar_3 point of these alloys falls rapidly with an increasing content of nickel; in the case of a 26 % Ni alloy, it falls below room temperature, and in that of a 35 % Ni alloy, below −190° C. The fact that alloys containing more than 26 per cent of nickel are strongly magnetic above the A_3 point, is attributed to the face-centred distribution of the nickel atoms, some of which are replaced by iron atoms. The magnetic intensity curve of iron-nickel alloys (length =7 cm., diameter =5 mm., H =221 Gausses) is given for reference, in Fig. 3.

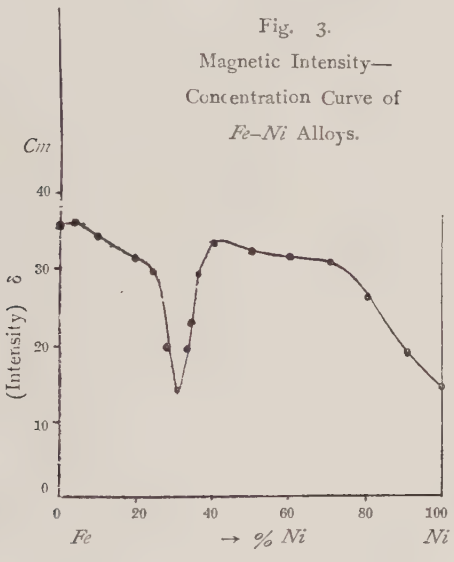

Fig. 3.
Magnetic Intensity—
Concentration Curve of
Fe–Ni Alloys.

In the case of iron-carbon-nickel alloys, however, as the alloy contains 8 % Ni, (4 % Ni, in high carbon nickel steel), the transformation appears often as a stepped change in the normal cooling; this phenomenon continuing as long as the alloy contains nickel up to about 10 per cent. In a 15 % Ni alloy (10 % Ni in high carbon nickel steel) the upper transformation does not generally appear, but only the lower transformation giving rise to the martensitic structure. Higher nickel alloys, containing about 20–27 % Ni, have an austenitic structure and are paramagnetic; but they become ferro-magnetic after being immersed in liquid air.

The transformations below room temperature in iron-carbon-nickel alloys were examined by means of a dilatometer. About sixty specimens were examined by this method and the results are shown in Table III, some of the curves being given in Figs. 1, (1)~(9), Pl. I. Also, the curves of magnetic analysis for the same alloys as those in Fig. 1 (immersed in liquid air) are shown in Figs. 2, (1)~(7).

TABLE III.

% Ni		% C		A3,2 (°C) (Beginning)	$\frac{\delta v}{v}$ (%) at 15° C
Cal.	Anal.	Cal.	Anal.		
2~20		Trace		—	—
25	25.50	,,		90, (A'_3−16)	(0.57)
26	26.42	,,		75, (A'_3−22)	0.45
27	26.91	,,		45 (A'_3−27)	0.67
28	27.80	,,		−22	1.33
29		,,		−25	2.55
30	29.71	,,		−50	3.59
31	31.92	,,		−72	2.26
33	33.40	,,		−130	1.18
35~100		,,		—	0
2~6		0.3		—	0
8	8.01	,,	0.37	−5	0.16
10		,,		−26	0.56
15	14.09	,,		−10	0.33
20		,,		7	4.04
25		,,			4.88
27		,,		−25	4.21
30	30.25	,,	0.40	−85	2.38
2~4		0.8		—	0
8		,,		−8	0.62
10	11.70	,,		−15	1.75
15	15.30			0	3.55
20		,,		6	6.11
25		,,		−25	4.56
30	29.70	,,	0.84	−90	2.34
2~6		1.80		—	0
8	8.27	,,	1.62	−20	0.24
10		,,	1.86	−10	1.28

% Ni		% C		A_3 (Beginning)	$\frac{\delta v}{v}$ (%) at 15° C
Cal.	Anal.	Cal.	Anal.		
15		1.80	1.57	−5	1.96
20		„	1.79	0	2.22
25	25.08	„	1.44	−25	3.50
30	29.72	„	1.67	−70	1.78
2~6		(Saturated)		—	0
8	7.82	„	3.99	−9	0.36
10	9.82	„	4.25	−20	0.65
15		„	4.62	−5	1.49
20		„	3.16	+5	2.38
25		„	3.56	+20	3.99
30		„	3.70	−90	2.91

Between room temperature and −190°C, an austenitic structure generally undergoes an abnormal irreversible expansion in changing to a martensitic structure. $\frac{\delta v}{v}$ in the above table represents this irreversible change of volume at room temperature, which is caused by immersing the alloys in liquid air; the values are calculated from the dilatometric data.

From the magnetic and dilatometric observations, we have constructed a structural diagram of nickel steel as shown in Fig. 4. In Fig. 4, region P comprises those alloys which undergo a complete Ar_1 and no abnormal expansion during cooling to −190°C; region M, a stepped or incomplete Ar_1, and a weak or strong abnormal expansion at low temperature; region Aq is non-magnetic when annealed at 1000° C, but magnetic after being immersed in liquid air, and undergoes a strong expansion at a low temperature; region A is magnetic, but with no abnormal expansion at a low temperature.

Of the iron-carbon-nickel alloys, those containing a small amount of carbon and nickel (less than about 4 % Ni) have normal Ar_1 transforma-

tions, those containing an intermediate amount of carbon and nickel, stepped Ar_1 transformations, and those containing a large amount of carbon and nickel no transformation point i. e., they are paramagnetic at room temperature. The domain in which the iron-carbon-nickel alloys have stepped transformations is the martensitic region (M) as shown in Fig. 4. The lower transformation can take place at the upper transformation point, if the alloys are exposed to the temperature of the latter during a suitably long interval of time (see also Fig. 2, (2), Plate I). In this case, the weak abnormal expansion vanishes as shown in Fig, 1, (2), Plate I. This result agrees with the view of Professor K. Honda and Mr. T. Kikuta.[1] If the stepped transformation exists the weak abnormal expansion is observable on cooling the alloys down to −190°C (see Figs. 1, (3), (4) and Figs. 2, (2), (3), Plate I). A small abnormal expansion shows a slight development of martensitic structure, a large abnormal expansion a strong development of the same structure, and no abnormal expansion no change of structure. Though in the alloys which undergo no abnormal expansion twinned crystals are sometimes formed, the latter have no effect on the hardness.

The maximum hardness in the annealed alloys containing a constant content of carbon is found in alloys containing from 10 % to 20 % Ni according to the content of carbon ; after being immersed in liquid air, the alloys containing 6 to 10 per cent of nickel (about 25 % Ni, for the low carbon nickel steel) undergo a small abnormal change of expansion and hardness, their structure changing from martensitic or austenite-martensitic to fine martensitic ; those containing 10 to 30 per cent of nickel (and also containing carbon) show a large change of expansion and hardness, and the structure changes from austenite-martensite or austenite to martensite or austenite-martensite.

Thus, the structural diagram of the annealed and slowly cooled nickel steels, as shown in Fig. 4, should be correct. From Fig. 4, we can easily deduce the percentage structural composition of nickel steel as shown in Fig. 5.

(1) Sci. Rep. **II** (1922), 1.

Fig. 4. Structural Diagram of Nickel Steel.

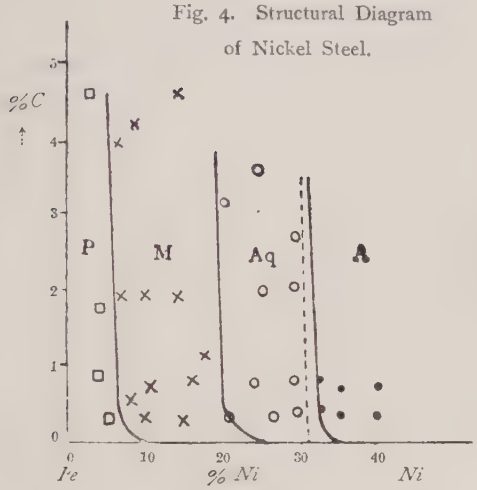

Fig. 5. Percentage Structural Composition of Nickel Steel.

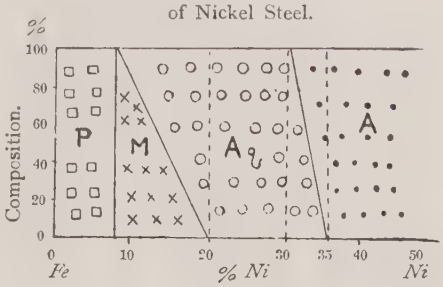

§ 3. MANGANESE STEEL.

According to Guillet, the structural diagram of manganese steel is as shown in Fig. 6. The present writer tried to examine the structural diagram of this alloy by means of the scleroscope hardness, microstructure, magnetic analysis, and dilatometric method as in the case of nickel steels.

Fig. 6. Structural Diagram of Manganese Steel. (Guillet.)

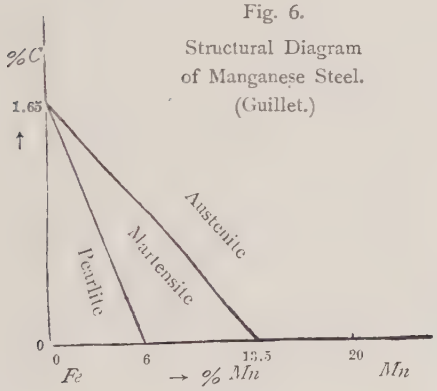

(*a*) *Hardness and Structure.*

The results of observation are shown in Table IV and, graphically, in Figs. 7, a~c.

TABLE IV.

% Mn	% C	Scleroscope Hardness and Microstructure							
		Cooled from melt in the furnace		Immersed in liquid air		Annealed		Immersed in liquid air	
2	Trace	16.5	F	16.7	F	12.5	F	12.6	F
4	„	22.8	F	23.5	F	22.7	F	23 0	F
6	„	42.0	M	42.6	M	32.5	M	32.8	M

% Mn	% C	Scleroscope Hardness and Microstructure							
		Cooled from melt in the furnace		Immersed in liquid air		Annealed		Immersed in liquid air	
8	Trace	42.2	M	42.1	M	33.3	M	33.5	M
10	„	43.1	M	42.9	M	34.5	M	34.4	M
12	„	36.9	M	36.2	M	26.2	M	26.2	M
15	„	34.1	M	34.0	M	27.5	A	27.3	A
20	„	20.8	A	20.9	A	20.4	A	20.4	A
30	„	16.7	A	17.0	A	15.3	A	15.8	A
40	„	13.8	A	13.9	A	12.4	A	12.5	A
50	„	13.8	A	13.8	A	12.1	A	12.1	A
60	„	13.6	A	13.6	A	13.5	A	13.5	A
1	0.8	33.6	T	36.7	T	30.6	T, S	33.0	T, S
2	,	57.2	M	66.1	M	32.6	S	32.7	S
4	„	56.7	M	61.6	M	23.0	S	23.4	S
5	„	43.2	S	53.8	S	32.0	S	36.4	S
6	„	33.3	M	47.4	M	29.4	A, S	38.1	A, S
8	„	15.2	A	45.5	M	22.6	A, S	58.5	M
10	„	13.9	A	14.0	A	15.4	A	18.0	A
15	„	13.9	A	14.0	A	15.4	A	18.0	A
20	„	24.1	A	24.9	A	17.3	A	18.0	A
30	„	21.2	A	21.7	A	17.4	A	18.7	A
40	„	22.2	A	22.3	A	18.4	A	18.5	A
2	4.3 (Saturated with carbon)	58.0	P, Ce	57.6	P, Ce	52.4	P, Ce	52.6	P, Ce
4	„	28.8	A, G, Ce	48.4	M, G. Ce	25.8	S, G, Ce	28.9	S, G, Ce
6	„	56 6	A, G, Ce	58.4	M, G, Ce	45.8	A, G, Ce	56.4	M, G, Ce
8	„	54.8	A	53.4	A	55.2	A	66.0	A
10	„	52.0	A	52.6	A	52.0	A	56.0	A
15	„	44.0	A	45.0	A	44.8	A	47.4	A

From the above result, we notice that the iron-manganese alloys do not change in hardness on immersion in liquid air (Fig. 7, a). But as shown in Fig. 7, b~c, the iron-carbon-manganese alloys increase in hardness after such immersion. This fact shows that some austenitic manganese steels change into martensitic by being cooled to the temperature of liquid air.

Fig. 7.

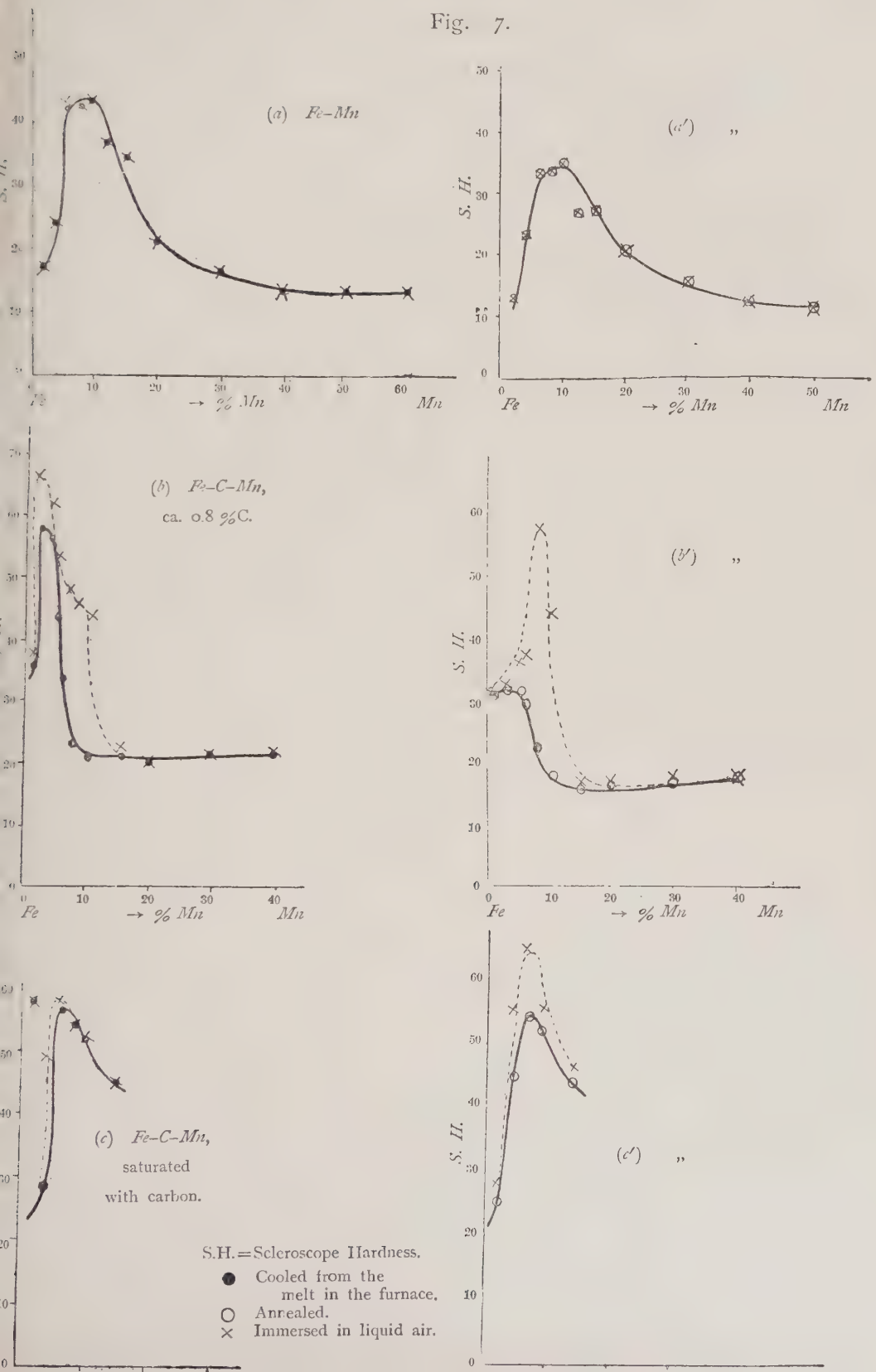
(a) Fe–Mn
(a′) ,,
(b) Fe–C–Mn, ca. 0.8 %C.
(b′) ,,
(c) Fe–C–Mn, saturated with carbon.
(c′) ,,
S. H.
Fe
→ % Mn
Mn
S.H. = Sclerscope Hardness.
Cooled from the melt in the furnace.
Annealed.
Immersed in liquid air.

(*b*) *Magnetic and Dilatometric Analyses.*

The magnetic analysis of manganese steels was made with the results shown in Table V.

TABLE V.

% Mn		% C		Transformation Point (°C)		
Cal.	Anal.	Cal.	Anal.	Ac_1 (Ac_3, Ac_2)	Ar_1 (Ar_3, Ar_2)	Ar_3'.$_2$
2.5		Trace		780 (Ac_2)	730 (Ar_2)	
5.0		„		760 („)	600 („)	110 (Ar_2')
10.0		„		680 („)	280 („)	
15.0		„		625 („)	140 („)	
20.0~30.0		„		—	—	
2.0	1.88	0.30	0.28	740	615	150
4.0	3.57	„	0.30	735	500 (?)	300
8.0	7.65	„	0.27	725	90	
10.0		„		—	—	
1.0	0.91	0.9	0.94	740	615	
5.0	5.02	„	0.89	735	(100)	
8.0~15.0		„		—	—	
2.0		1.2		740	620	145
4.0	3.73	„	1.14	730	620	140
6.0~10.0		„		—	—	—
6.0	5.90	2.0	1.79	725	560	100
8.0	8.15	„	1.50	710	—	—
9.0	9.62	„	1.62	700	—	—
10.0	10.10	„	2.02	660	—	—
13.0	12.73	„	1.41	—	—	—
15.0	14.50	2.0	1.93	—	—	—
1.0	0.86	4.0	3.04	760	680	180
2.0	1.55	„	3.78	755	665	170
4.0	4.02	„	4.10	750	625	125
5.0	4.57	„	3.66	740	200	100

% Mn		% C		Transformation Point (°C)		
Cal.	Anal.	Cal.	Anal.	Ac_1 (Ac_3, Ac_2)	Ar_1 (Ar_3, Ar_2)	$A_{13}'_{,2}$
8.0	7.70	Trace	4.25	(725)	180	(90)
10.0	9.97	,,	4.11	—	—	—
* 6.0		0.3	0.31	755		(200, carbide)
* 8.0	7.65	,,	0.27	750	250	—
* 1.0	0.91	0.90	0.92	740	615	(175, carbide)
* 5.0	5.02	,,	0.89	735	(100)	(50, carbide)
* 8.0	7.98	,,	0.93	720	—	—
* 10.0	10.21	,,	0.91	—	—	—
* 2.0		1.2		740	620	(160, carbide)
* 4.0		,,	1.14	730	620	140
* 6.0		,,	1.23	725	—	—
* 8.0		,,	1.21	725	—	—
* 10.0		,,	1.14	700	—	—
* 15.0		,,		—	—	—
* 5.0	4.57	4.0	3.66	750	200	(200, carbide)
* 8.0	7.70	,,	4.25	730	160	(160, carbide)
* 10.0	9.97	,,	4.11	730	—	—

(* These alloys were immersed in liquid air.)

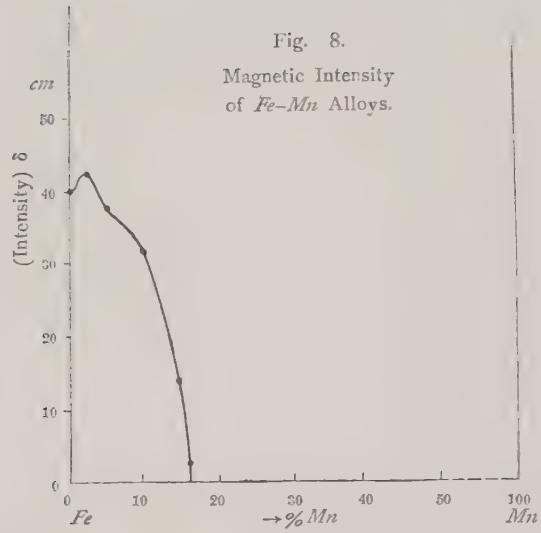

Fig. 8.
Magnetic Intensity
of *Fe–Mn* Alloys.

From the above table, we see that in the case of the iron-manganese system, as the content of manganese increases, not only does the transformation point of iron gradually fall, but also the magnetic intensity, the alloys containing more than 15 per cent manganese being non-magnetic at room temperature. Fig. 8 shows this relation.[1] If the binary alloy contains some carbon, the concentration of manganese at which the ferromagnetism disappears, decreases in proportion to the content of carbon. The alloys containing up to 10 per cent of manganese and some carbon are non-magnetic at room temperature, but become magnetic when immersed in liquid air.

We see also in Table V, that in the case of manganese steels containing 3–4 %C, the Ar_0 point (215° C) of cementite (Fe_3C) decreases gradually as the content of manganese increases, this showing that manganese makes a solid solution with cementite. Further, the transformations which take place below room temperature, were examined dilatometrically during cooling to −190° C. The results are given in Table VI. As an example, some of the curves of the dilatometric and magnetic analyses at low and high temperatures are also given in Figs. 3, (1)~(6), and Fig, 4, (1)~(6), Pl. II.

TABLE VI.

% Mn		% C		Temperature at which anomalous expansion occurs (Ar_3)	$\frac{\delta v}{v}$ (%) at 15° C
Cal.	Anal.	Cal.	Anal.		
4	3·57	Trace	0.30	—	0
6	5·57	,,	0.31	(−31)	0.31
8	7.65	,,	0.27	(− 5)	2.35
2	1.20	0.9	0.93	—	0
4	4.23	,,	1.09	(−15)	0.46
5	4.72	,,	0.97	−20	1.56
6	5·70	,,	0.90	−35	2.08
8	7.98	,,	0.93	−55	4.23
10	10.21	,,	0.91	—	0
1~3		1.2		—	0
4	3·73	,,	1.14	(−30)	0.18
6	5.48	,,	1.23	−10	1.38
8	7·75	,,	1.21	− 2	2.80
10	8.94	,,	1.14	0	1.10
15		,,		—	0
6	5.90	2.0	1.79	−28	1.46
8	8.15	,,	1.50	−17	3.21
4	4.02	,,	4.10	—	0.08
5	4·57	,,	3.66	−15	0.39
8	7.10	,,	4.25	−17	1.31
10	9.02	,,	4.11	−72	0.94

From the above data, the structural diagram of the iron-carbon-manganese system is to be constructed as shown in Fig. 9, and its percentage composition in Fig. 10. Further, it is to be noted that the effect of manganese on the hardness and the lowering of the transformation point is about twice as much as that of nickel.

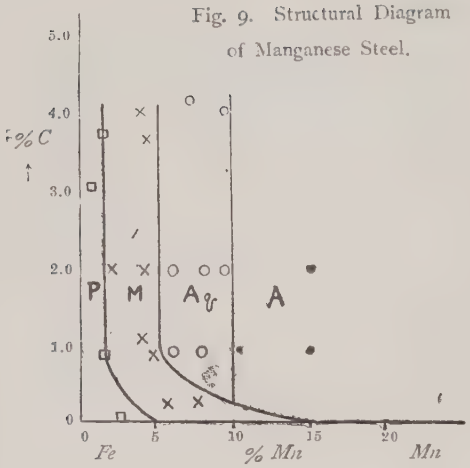

Fig. 9. Structural Diagram of Manganese Steel.

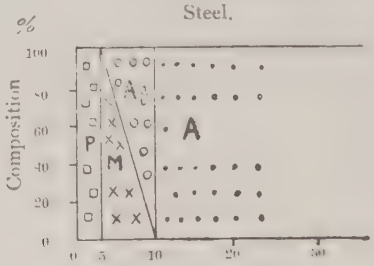

Fig. 10. Percentage Structural Composition of Manganese Steel.

§ 4. CHROMIUM STEEL.

The structural diagram of chromium steel, according to Guillet, is shown in Fig. 11. In this diagram three domains pearlite (P), martensite (M), and austenite (A) and cementite (Ce), (or rather a double carbide of iron, chromium, and carbon), are given. For a more recent investigation of the constitutional diagram of chromium steel, a paper by Professor T. Murakami[1] is referred to.

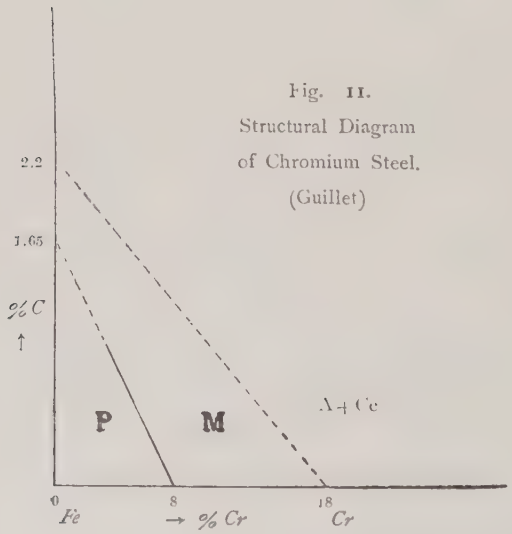

Fig. 11. Structural Diagram of Chromium Steel. (Guillet)

(*a*) *Hardness and Microstructure.*

The relation between the hardness and the microstructure of chromium steels of various composition, after the four modes of heat-treatment mentioned above, is as shown in Table VII and Figs. 12, a~c.

(1) Sci. Rep. **7** (1918), 217.

TABLE VII.

% Cr	% C	Scleroscope Hardness and Microstructures							
		Cooled from melt		Immersed in liquid air		Annealed		Immersed in liquid air	
2	Trace	17.1	S	17.2	S	10.2	S	10.3	S
4	„	17.5	S	17.5	S	11.2	S	11.2	S
6	„	17.0	S	20.2	S	12.2	S	12.4	S
8	„	20.5	S	22.2	S	12.4	S	12.5	S
10	„	34.9	M	35.0	M	11.9	S	11.9	S
12	„	34.8	M	34.8	M	14.2	S	14.1	S
18	„	21.8	S	21.9	S	13.7	S	13.9	S
20	„	23.1	S	23.1	S	13.7	S	13.8	S
30	„	19.7	S	20.1	S	15.7	Cr. F, S	15.7	Cr, F, S
40	„	22.1	S	22.2	S	18.5	Cr. F, S	18.5	Cr, F, S
70	„	23.3	S	23.5	S	20.8	Cr. F, S	20.7	Cr, F, S
2	0.8	45.8	M	45.9	M	23.1	S	23.5	S
4	„	59.4	M	62.0	M	24.4	S	25.1	S
6	„	45.2	M	57.3	M	24.8	S	25.1	S
8	„	37.2	M	54.4	M	23.1	S	24.2	S
10	„	39.9	M	55.1	M	22.4	S	22.9	S
15	„	34.1	M	51.2	M	23.5	S	23.8	S
20	„	33.1	M, S	47.4	M, S	22.6	S	22.7	S
25	„	28.8	Fc,* S	33.4	Fc, S				
30	„	26.2	Fc, S	26.7	Fc, S	22.8	Fc, S	25.6	Fc, S
40	„	27.1	Fc, S	27.4	Fc, S	24.1	Fc	24.5	Fc
2	4.0	55.2	E,** N	55.4	E, N	46.9		48.2	
4	„	66.5	E, N	56.6	E, N	56.6		56.9	
6	„	62.0	E, N	66.8	E, N	47.3		47.4	
8	„	58.0	E, N	64.3	E, N	49.3		50.7	
10	„	59.5	E, N	66.8	E, N	54.6		57.1	
15	„	50.5	E	69.6	E	43.2		43.2	
20	„	46.5	E, H	60.2	E, H	44.2		43.8	
30	„	47.5	E, H	48.1	E, H	41.7		41.6	
40	„	48.8	E, H	49.0	E, H	42.5		42.9	

(* Cr. F=Chromium Ferrite)

(** E=Ternary eutectic, N=Primary needle shaped crystal (α or β double carbide), H=Hexagonal plate shaped crystal (Cr_4C)).

Fig. 12.

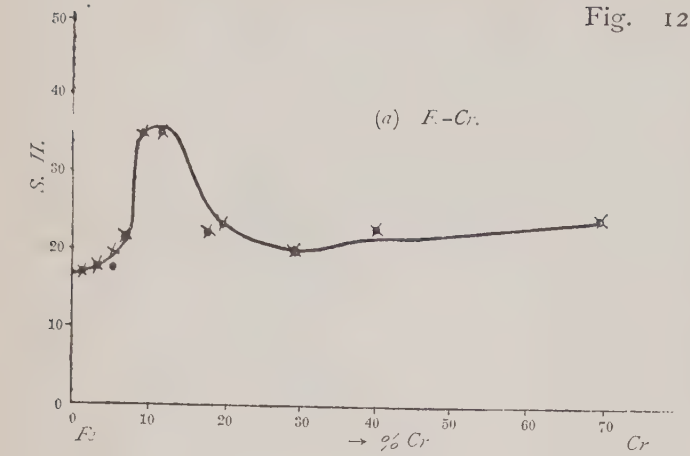

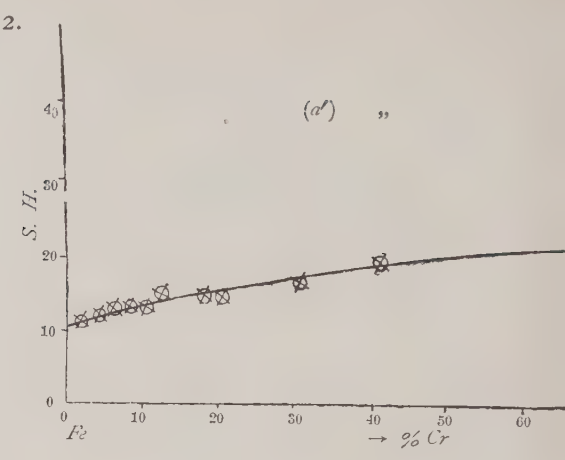

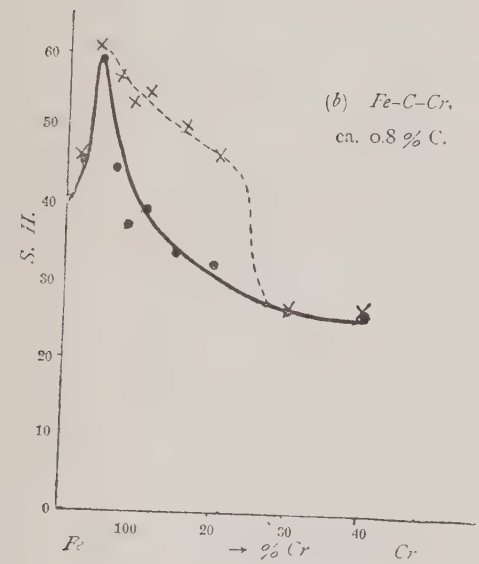

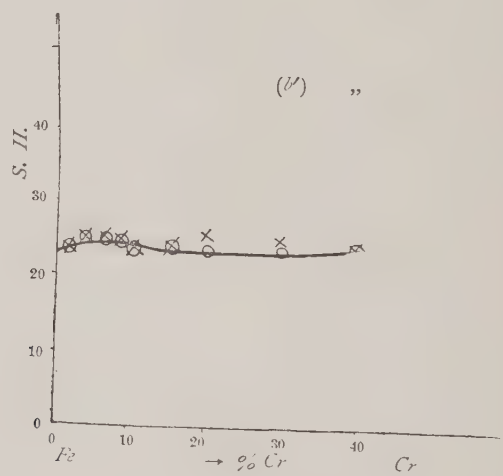

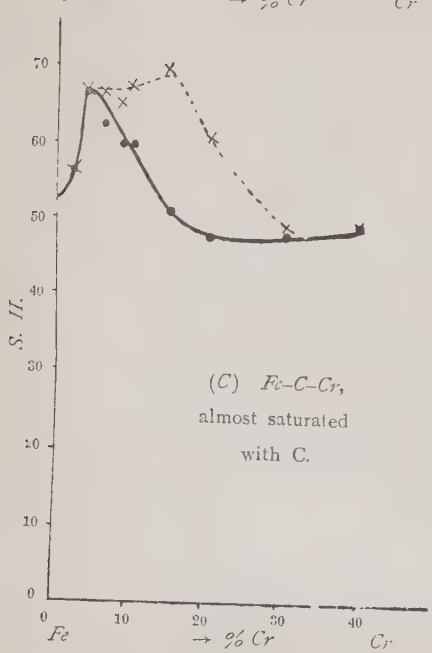

S.H. = Scleroscope Hardness.

● Cooled from the melt in the furnace.

○ Annealed.

× Immersed in liquid air.

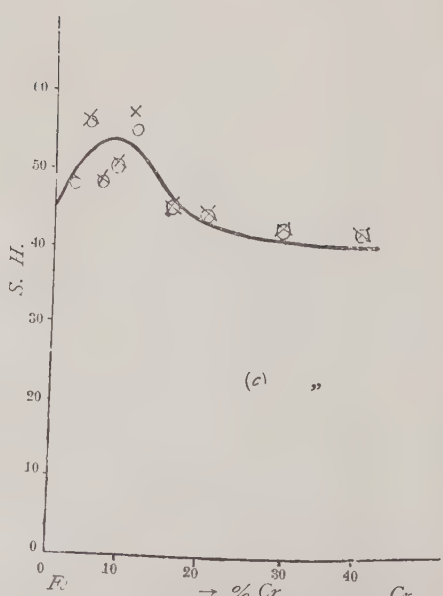

According to the result of the scleroscope hardness test, the iron-chromium alloys, when annealed and slowly cooled, cannot be hardened by being quenched in liquid air ; but the iron-carbon-chromium alloys, when rapidly cooled, do so harden, their structure changing into the martensitic.

(*b*) *Magnetic and Dilatometric Analyses.*

The A_2 transformation of iron-chromium alloys has already been determined by Professor T. Murakami.[1] His result shows a continuous solubility of iron and chromium and also a gradual depression of the A_2 point of iron to a very low temperature by the addition of an increasing content of chromium.

The present writer also made the magnetic analysis of some iron-chromium and iron-carbon-chromium alloys, the results of which are shown in Table VIII. The A_2 points in iron-chromium alloys are shown in Fig. 13, the result perfectly agreeing with that of Professor T. Murakami.

TABLE VIII.

% Cr		% C		Transformation Point (°C)		Stepped transformation Ar_2' (Ar_3') (°C)	Maximum temperature (°C)
Cal.	Anal.	Cal.	Anal.	Ac_2(Ac_3, Ac_1)	Ar_2(Ar_3, Ar_1)		
0		Trace		795(Ac_2)	790(Ar_2)		1000
10		„		795(„)	790(„)	(450)	„
20		„		760(„)	740(„)		„
30		„		650(„)	630(„)		„
40		„		580(„)	560(„)		„
50		„		460(„)	440(„)		„
60		„		320(„)	300(„)		„
70		„		190(„)	135(„)		„
2	2.03	0.8	0.80	765	660		„
4	3.59	„	0.78	770	655		„
6	5.14	„	0.78	780	665		„
8	7.11	„	0.79	790	670		„

(1) loc. cit.

% Cr		% C		Transformation Point (°C)		Stepped transformation Ar_2' (Ar_3') (°C)	Maximum temperature (°C)
Cal.	Anal.	Cal.	Anal.	$Ac_2(Ac_3, Ac_1)$	$Ar_2(Ar_3, Ar_1)$		
10	9.56	Trace	0.76	780	690		1000
15	14.92	„	0.79	760	695	250	„
20	19.15	„	0.74	770	700	200	„
2	2.07	2.00	2.03	790	700	(185, carbide)	1200
6	6.17	„	1.65	790	700		„
6	5.14	0.8	0.78	790	650	100	„
8	7.11	„	0.79	790	625	70	„
20	19.65	„	0.74	770	700	70	„
25	25.22	„	0.75	—	—	—	„
6	6.17	2.00	1.65	780	670		„
8	7.75	„	1.78	790	705		„
10		„		780	670		„
15	14.15	„	1.95	770	660		„

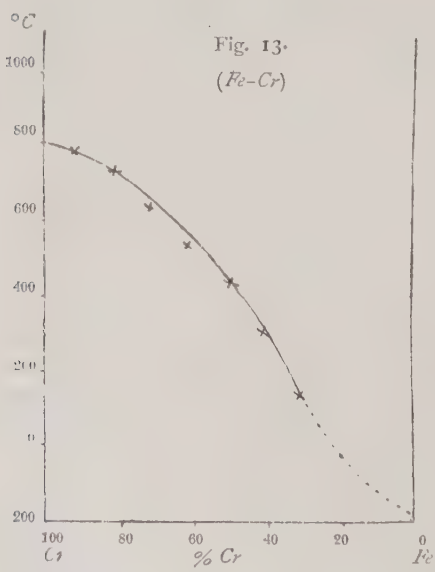

Fig. 13.
(*Fe-Cr*)

Thus, according to the result of magnetic analysis, the $A_{3,2}$ transformation point of iron-chromium alloys gradually falls, the magnetic intensity at the same time becoming weak, and at about an 80 %Cr content, it falls below room temperature. Also, as is well known, in the case of iron-carbon-chromium alloys, the maximum temperature to which the alloy was heated, has a remarkable effect on the lowering of the transformation point. That is, a chromium steel cooled from 1000° C returns to its initial state, but in the case of the same specimen cooled from 1200°C more or less rapidly, its $Ar_{3,\ 2,\ 1}$

point is remarkably lowered, and it does not return to its initial state at room temperature. This shows that the carbide, when once dissolved during heating, cannot separate on rapid cooling. Such chromium steels are expected to be hardened by being immersed in liquid air, as is the case with manganese steels. Also, in the case of chromium steels, as the content of chromium increases, their transformation point decreases and becomes stepped, the upper transformation being gradually weakened. As the maximum temperature becomes higher the lower transformation also decreases.

Some chromium steels after the various kinds of heat-treatment before mentioned were examined dilatometrically to see whether they underwent transformations below room temperature, but only a few alloys, which were quenched in water from 1200° C, showed an abnormal change, as shown in the following table.

TABLE. IX.

% Cr		% C		Temperature at which anomalous expansion occurs (Ar_3)	$\frac{\delta v}{v}$ (%) at 15°C	Heat-treatment
Cal.	Anal.	Cal.	Anal.			
15	14.92	0.8	0.75	—	(weak)	Cooled somewhat rapidly.
20	19.15	„	0.74	—	„	„
10	9.56	„	0.76	−70	0.29	Quenched in water from 12 0°C.
15		„	0.79	−25	2.28	„
20	19.15	„	0.74	0	0.79	„

Examining the expansion-temperature curves of some chromium steels containing about 0.7%C,[1] we observe that the $Ac_{1,3}$ point is gradually raised as the content of chromium added increases up to about 21% of chromium, above which this point becomes imperceptible.

In the case of certain chromium steels, which are chill cast and

(1) T. MURAKAMI :– loc. cit.

annealed at 1000°C for 6 hours, the contraction curves are reversible and show no abnormal expansion during cooling; but the same steels when heated to 1200°C and cooled somewhat rapidly undergo a weak anomalous expansion. Again, these steels, when heated to 1200°C and quenched in water, undergo a large anomalous expansion.

The above mentioned results afford structural diagrams of chromium steel as shown in Figs. 14, a~b. Fig. 14, a is for the alloys cooled from the melt more or less rapidly; and Fig. 14, b, for those annealed and slowly cooled in the furnace. These diagrams are only approximate ones.

Fig. 14 (a)
Structural Diagram of Chromium Steel.
(Cooled from the melt in the furnace)

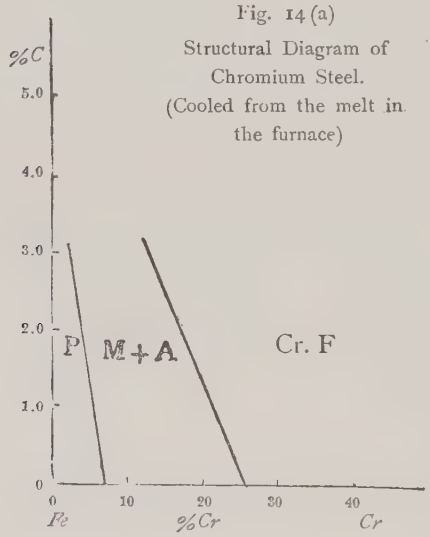

Fig. 14 (b)
Structural Diagram of Chromium Steel.
(Annealed at 900~1000°C)

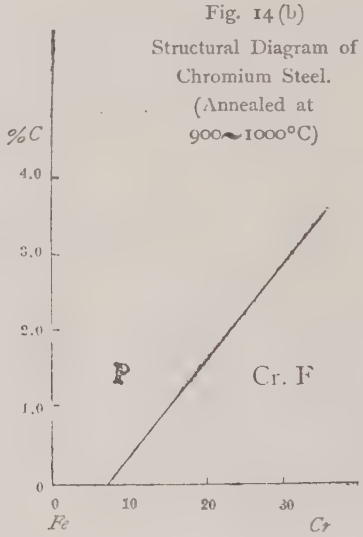

(Cr. F. = chromium ferrite, having an austenitic appearance, but its Ar_1 change is completed, owing to the less solubility of carbon in the high chromium alloys.)

§ 5. MICROSCOPIC INVESTIGATION.

The results so far obtained agree satisfactorily with those of the microscopic observations; some of the micro-photographs are given in Pl. IV.-V.

Photogr. 1. A nickel steel, (ca. 25% Ni, and ca. 0.8%C), chill

cast in an iron mould, annealed at 1000°C for 6 hours. It shows an ordinary polygonal austenitic structure.

2. A nickel steel, (ca. 15% Ni, ca. 0.8%C), treated by the same procedure as that in Photogr. 1. A martensitic structure generated in the ground mass of austenite is seen. If the specimen in Photogr. 1 is immersed in liquid air, it expands strongly, and forms a similar structure.

3. The same specimen as that in Photogr. 2, after being immersed in liquid air, and considerably expanded. The structure is wholly of fine martensite.

4. An iron-manganese alloy, (ca. 6% Mn), cooled from the melt in the furnace. It shows a martensitic structure, and has the greatest hardness in this binary system.

5. An iron-manganese alloy, (ca. 40% Mn), cooled from the melt in the furnace. It shows an austenitic structure, and its hardness is rather less than that in Photogr. 4.

6. A manganese steel, (ca. 2% Mn, ca. 0.8%C), cooled from the melt in the furnace. It shows a martensitic structure, and is very hard.

7. A manganese steel, (ca. 8% Mn, ca. 0.9%C), chill cast in an iron-mould, and annealed at 1000°C for 6 hours. It shows an austenitic structure. (The alloy, containing the same composition as this specimen cooled from the melt in the furnace is on a low degree in hardness.)

8. The same specimen as that in Photogr. 7, immersed in liquid air. It expanded strongly, and assumed a martensitic structure.

9. An iron-chromium alloy, (ca. 10% Cr.), cooled from the melt in the furnace. It shows a martensitic structure, and is comparatively of a high degree of scleroscope hardness.

10. An iron-chromium alloy, (ca. 30% Cr), cooled from the melt in the furnace. It shows an austenitic structure, and is comparatively of a low degree of hardness.

11. A chromium steel, (ca. 4 % Cr. ca. 0.8 %C), cooled from the melt in the furnace. It releases free carbides, and hence its hardness is great.

12. A chromium steel, (ca. 30% Cr, ca. 0.8% C), cooled from the melt in the furnace. It shows an austenitic structure, and is comparatively of a low degree of hardness. Also, it does not increase in hardness even when immersed in liquid air.

13. A chromium steel, (ca. 15% Cr, ca. 0.8% C), cooled from the melt and quenched in water from 1200°C. It shows an austenitic structure.

14. The same specimen as that in Photogr. 13, treated as above, and immersed in liquid air. It expanded strongly, and has a martensitic structure.

SUMMARY.

The present investigation may be summarised as follows:—

1. The present writer has investigated the structural diagrams of nickel, manganese, and chromium steels, by examining their scleroscope hardness, microstructure, and transformations by the magnetic and dilatometric methods, especially at low temperatures.

2. Alloys which have completed the Ar_3 (Ar_1, Ar_2) transformation at room temperature, do not undergo any increase of hardness, change of structure, or abnormal expansion, when cooled down to the temperature of liquid air. Those having an austenitic or austenite-martensitic structure, when immersed in liquid air, may be transformed into martensite and expanded abnormally, the hardness thereby increasing.

3. The alloys which make stepped transformations ($Ar_{3,1}$ $Ar'_{3,1}$,) in magnetic analysis, assume some martensitic structure, in virtue of the lower transformation (below 300°C).

4. The structural diagrams of the three special steels determined as above, are somewhat different from those which are well known and were formerly proposed by Guillet. Namely, in these steels cooled slowly from the melt in the furnace, the structural fields after an addition of a small quantity of carbon are bordered by straight lines almost parallel to the axis of the carbon.

In conclusion, the present writer wishes to express his cordial thanks to Professors K. Honda, T. Murakami, and T. Ishiwara for their kind guidance and useful advice throughout this investigation.

$\frac{\delta l}{l} = 1.67 \times 10^{-4}$

Plate I.

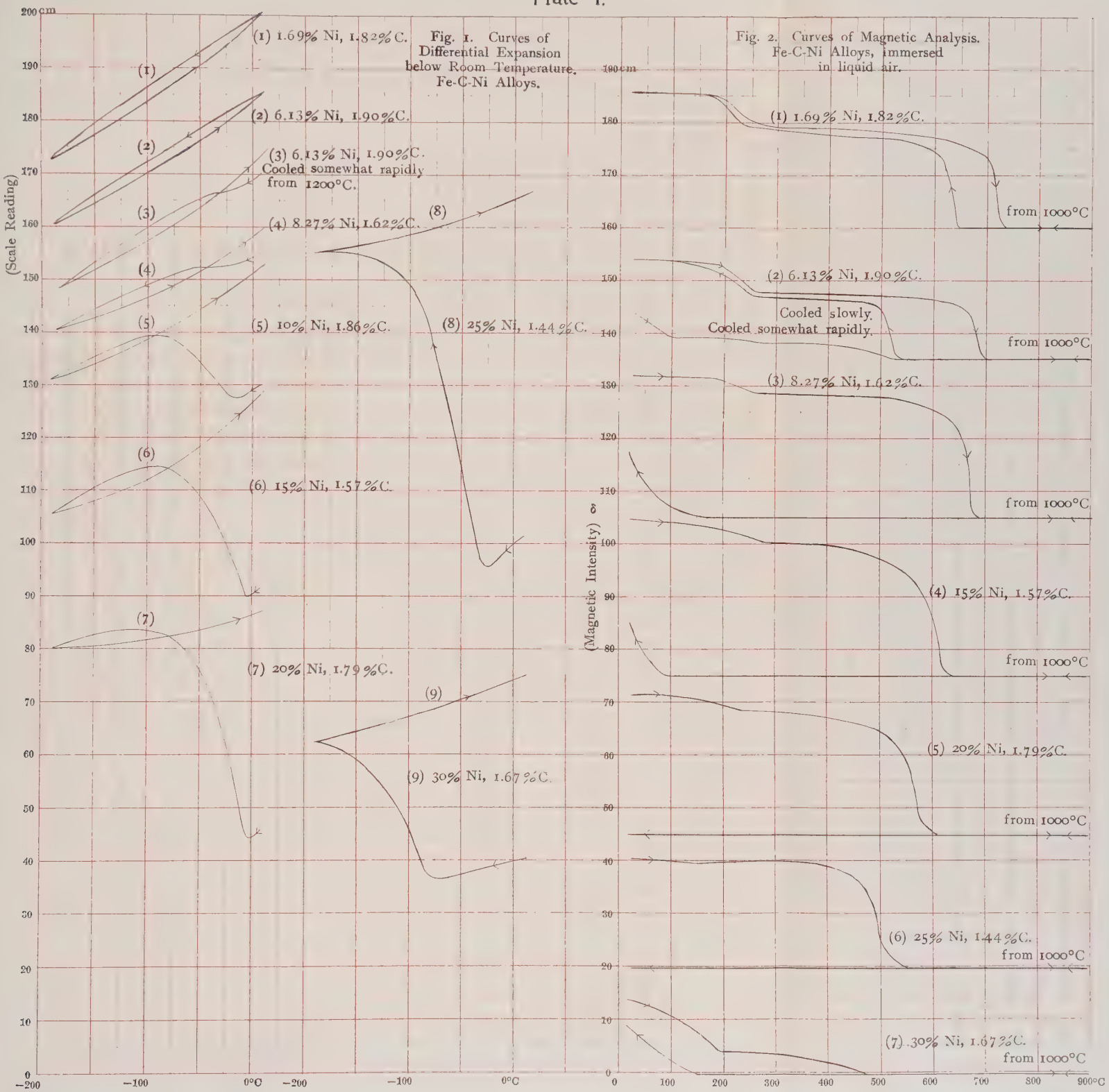

Plate II.

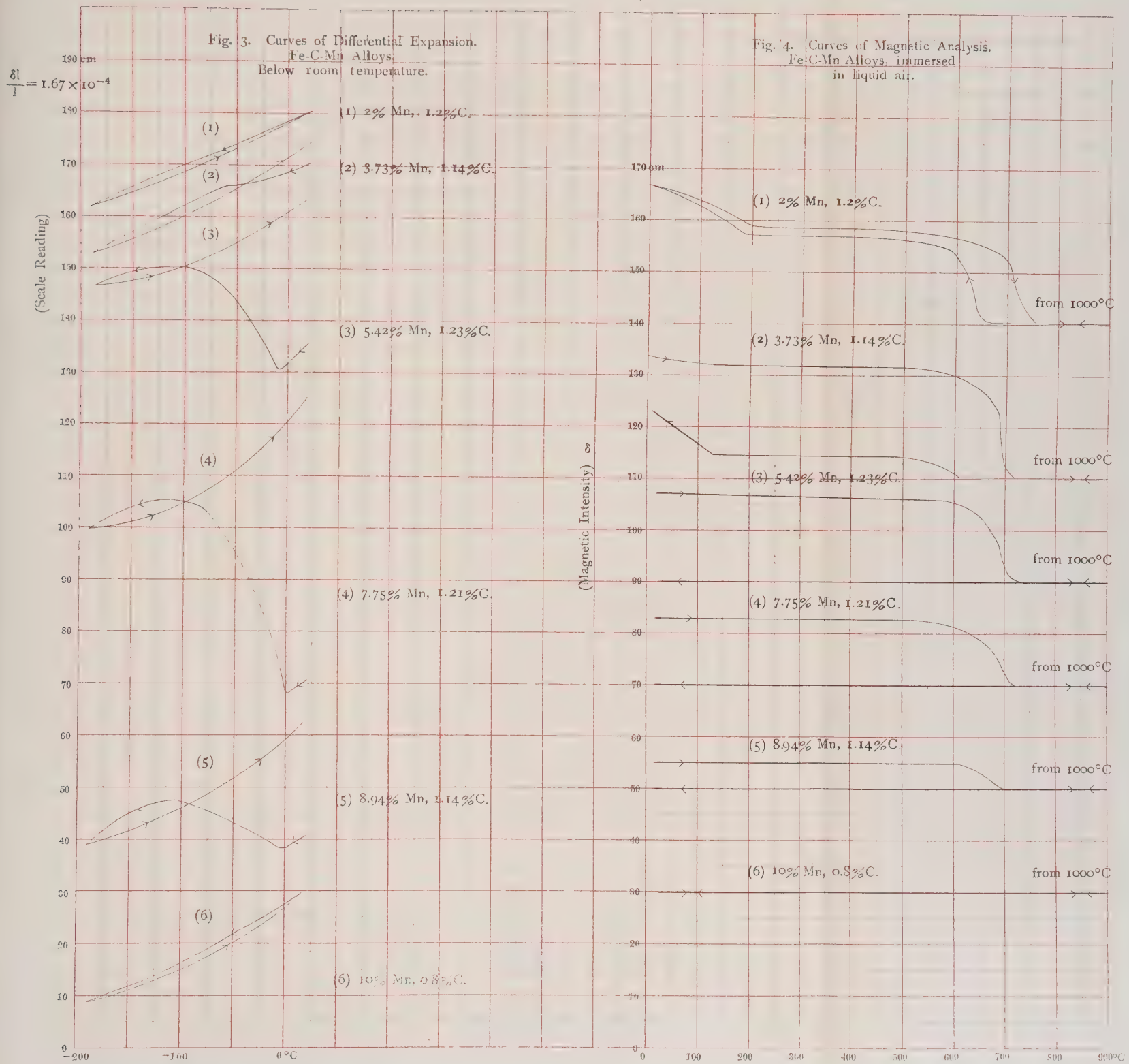
Fig. 3. Curves of Differential Expansion.
Fe-C-Mn Alloys.
Below room temperature.
$\frac{\delta l}{l} = 1.67 \times 10^{-4}$
(Scale Reading)
(1) 2% Mn, 1.2%C.
(2) 3.73% Mn, 1.14%C.
(3) 5.42% Mn, 1.23%C.
(4) 7.75% Mn, 1.21%C.
(5) 8.94% Mn, 1.14%C.
(6) 10% Mn, 0.8%C.
−200
−100
0°C
Fig. 4. Curves of Magnetic Analysis.
Fe-C-Mn Alloys, immersed
in liquid air.
(Magnetic Intensity) δ
(1) 2% Mn, 1.2%C.
from 1000°C
(2) 3.73% Mn, 1.14%C.
from 1000°C
(3) 5.42% Mn, 1.23%C.
from 1000°C
(4) 7.75% Mn, 1.21%C.
from 1000°C
(5) 8.94% Mn, 1.14%C.
from 1000°C
(6) 10% Mn, 0.8%C.
from 1000°C
0
100
200
300
400
500
600
700
800
900°C

$\frac{\delta l}{l} = 1.67 \times 10^{-4}$

Plate III.

Fig. 5. Curves of Differential Expansion Below Room Temperature. Fe-C-Cr Alloys.

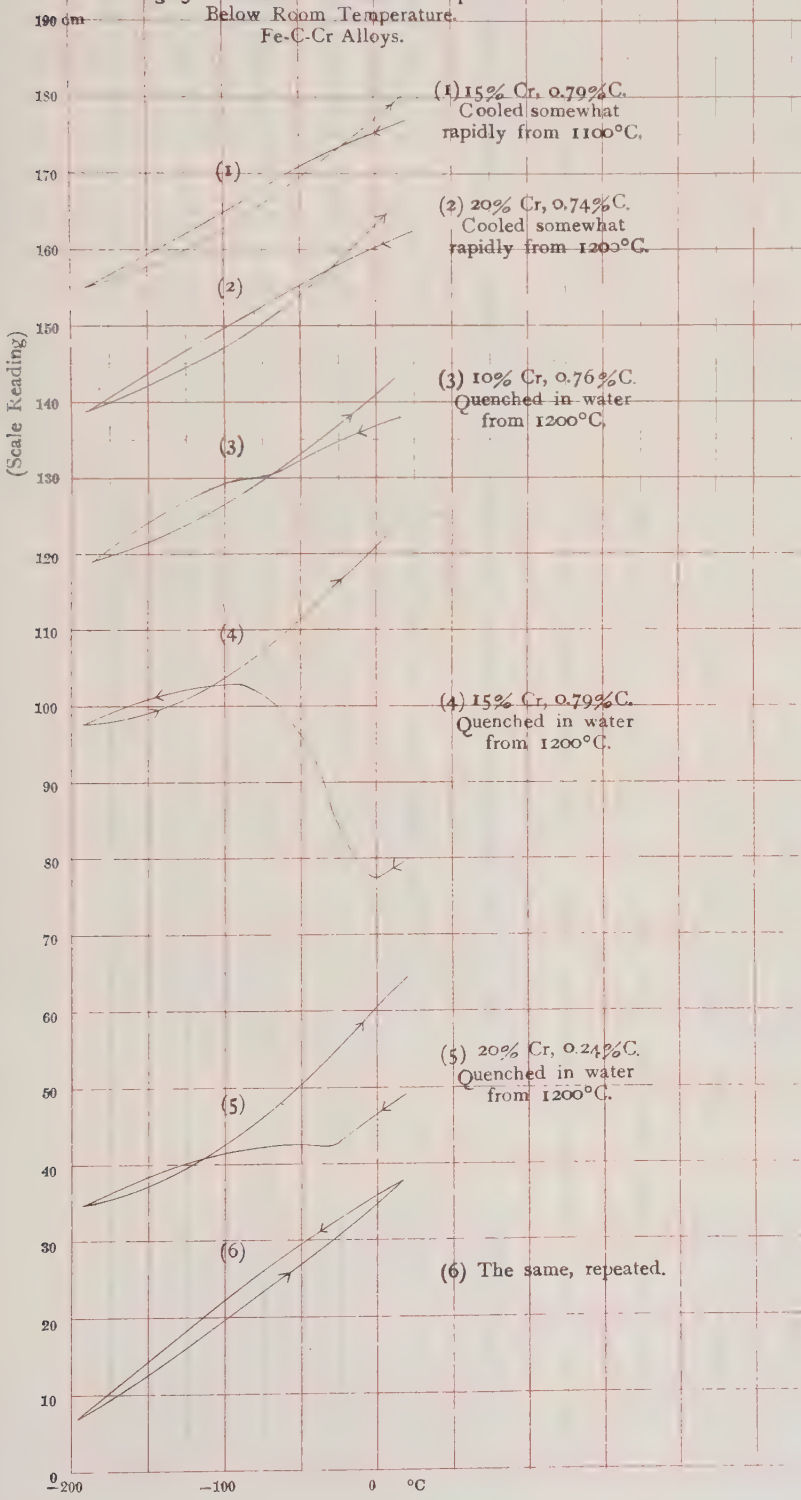

Fig. 6. Curves of Magnetic Analysis. Fe-C-Cr Alloys.

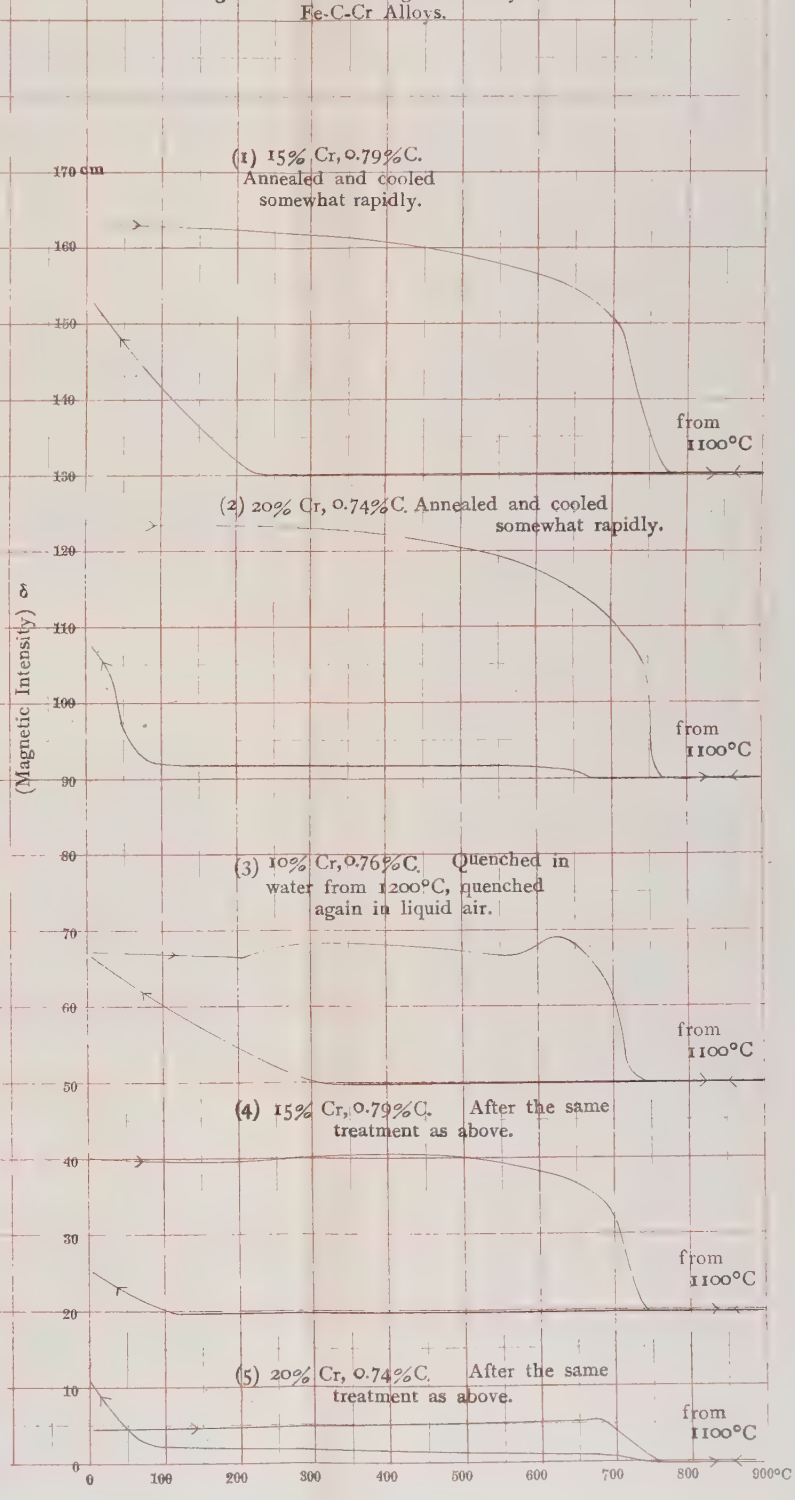

Plate IV.

Photogr. 1. Fe-C-Ni, ca. 25 % Ni, ca. 0.8 % C. Annealed. ×100.

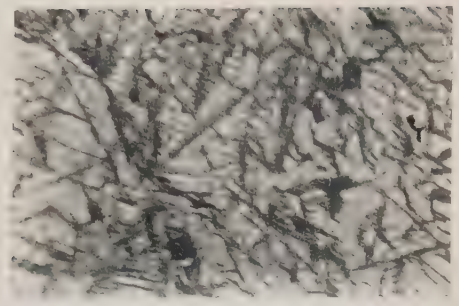

Photogr. 2. Fe-C-Ni, ca. 15 % Ni, ca. 0.8 % C, Annealed. ×100.

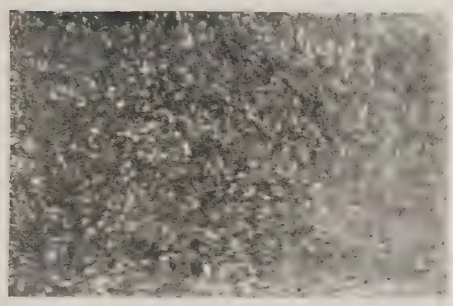

Photogr. 3. The same specimen as Photogr. 2. Immersed in liquid air. ×100.

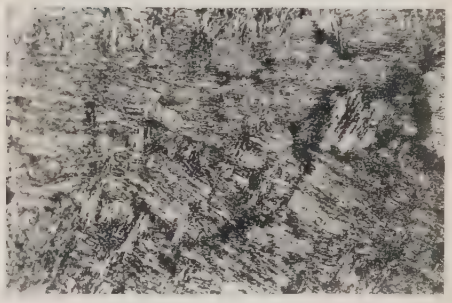

Photogr. 4. Fe-Mn. ca. 6 % Mn, Normally cooled in the furnae. ×100.

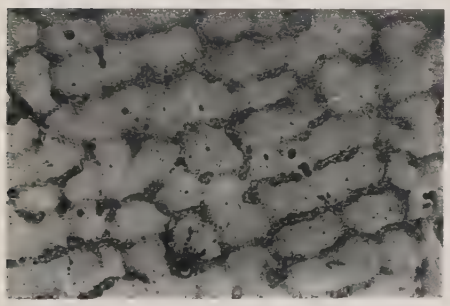

Photogr. 5. Fe-Mn, ca. 40 % Mn. Normally cooled from melt in the furnace. ×100.

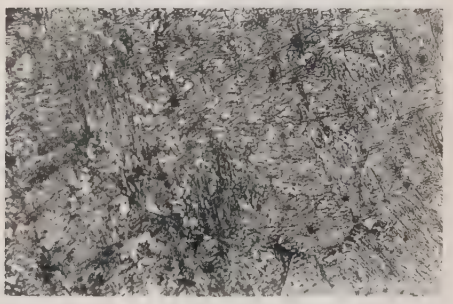

Photogor. 6. Fe-C-Mn, ca. 2 % Mn, ca. 0.8 % C. Normally cooled from melt in the furnace. ×100.

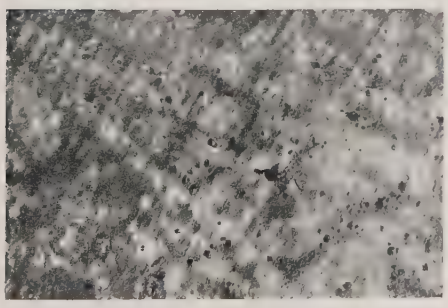

Photogr. 7. Fe-C-Mn, ca. 8 % Mn, ca. 0.9 % C. Annealed. ×100.

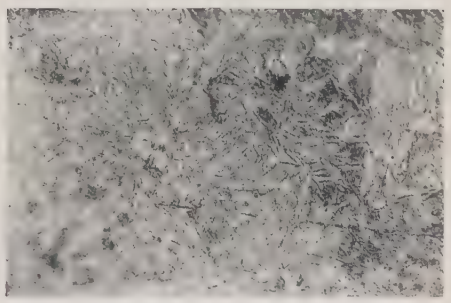

Photogr. 8. The same specimen as Photogr. 7. Immersed in liquid air. ×100.

Plate V.

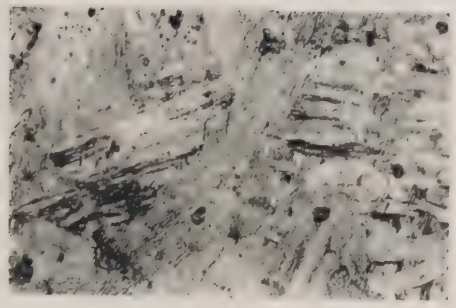

Photogr. 9. Fe-Cr, ca. 10 % Cr. Normally cooled from melt in the furnace. × 100

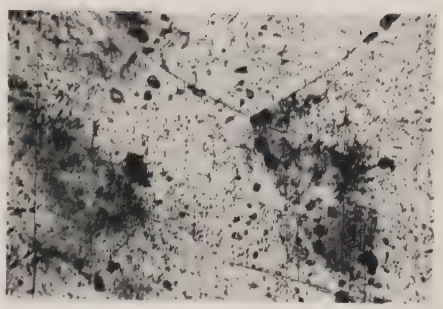

Photogr. 10. Fe-Cr, ca. 30 % Cr. Normally cooled from melt in the furnace. × 100.

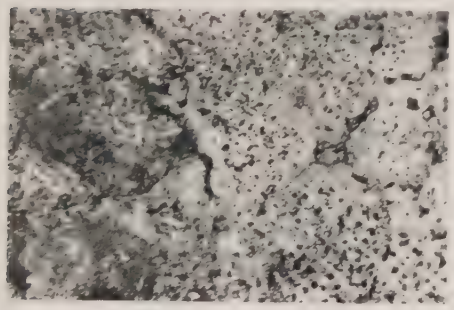

Photogr. 11. Fe-C-Cr, ca. 4 % Cr, ca. 0.8 % C. Normally cooled from melt in the furnace. × 100.

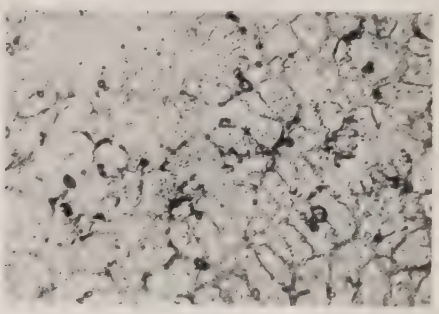

Photogr. 12. Fe-C-Cr, ca. 30 % Cr, ca. 0.8 % C. Normaly cooled from melt in the furnace. × 100.

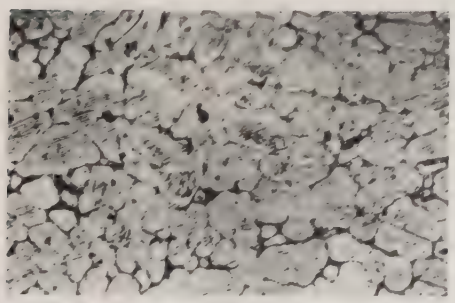

Photogr. 13. Fe-C-Cr, ca. 15 % Cr. ca. 0.8 % C. Quenched in water from 1200°C. × 100.

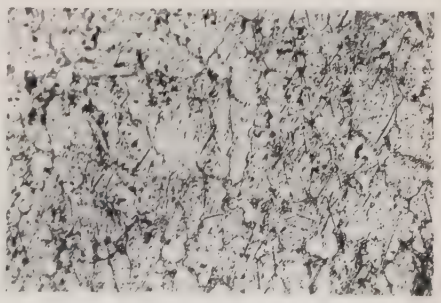

Photogr. 14. The same specimen as Photogr. 13, treated as above, and immersed in liquid air. × 100.

On the Relation between the Equilibrium Diagram and the Magnetic Susceptibility in Binary Alloys.[1]

By

Hikozô Endo.

CONTENTS.

§ 1. Introduction.
§ 2. Method of Measurement and Apparatus.
§ 3. Determination of the Constant of the Apparatus.
§ 4. Measurement of the Magnetic Susceptibilities of following Binary Alloys:—
(1) Copper-Tin.
(2) Zinc-Tin.
(3) Bismuth-Tin and the Equilibrium Diagram of this System.
(4) Copper-Zinc.
(5) Lead-Thallium.
(6) Bismuth-Lead.
(7) Antimony-Tin.
(8) Antimony-Copper.
(9) Bismuth-Zinc.
(10) Antimony-Lead and the Equilibrium Diagram of this System.
(11) Bismuth-Tellurium and the Equilibrium Diagram of this System.
(12) Copper-Manganese.
Summary.

§ 1. INTRODUCTION.

Although a large number of experiments have already been made for the determination of the magnetic susceptibility of chemical elements, of various kinds of compounds, and of the ferromagnetic alloys, yet there have been few investigations to establish the relation between the magnetic susceptibility and the equilibrium diagram in the case of the diamagnetic and paramagnetic alloys.

(1) The one hundred ninth report from the Research Institute for Iron, Steel and other Metals.

The measurement of the magnetic susceptibility of binary alloys has been a subject of inquiry by several investigators among whom are to be mentioned S. C. Laws,[1] O. C. Clifford[2] and C. E. Mendenhall and W. F. Lent.[3] In 1913, Professor K. Honda and Dr. T. Sone[4] investigated the same subject by means of a torsion balance to find the relation for simple binary alloys, such as antimony-bismuth, antimony-aluminium, antimony-zinc, antimony-tellurium etc. and obtained the following important relations :—

In the case of paramagnetic and diamagnetic alloys, (1) A compound has a magnetic susceptibility characteristic of it ; (2) The magnetic susceptibility-concentration curve becomes a straight line in alloys consisting of a heterogeneous mixture of two consituents ; (3) In the case of an alloy forming a solid solution, this is a curve.

In 1917, Professors K. Honda and T. Ishiwara,[5] who studied the same relation for the antimony-manganese system and the effect of temperature on the susceptibility, also arrived at the same result.

The present investigation was undertaken to get further knowledge of the relation between the magnetic susceptibility and the concentration of binary alloys which have more complicated equilibrium diagrams, by means of the Weiss electromagnetic method as improved on by Professor K. Honda.

§ 2. METHOD OF MEASUREMENT AND APPARATUS.

The method of measurement is based on the following principle. If a small quantity of a substance is put in a heterogeneous field of an electromagnet, it will be displaced along the gradient of the field from a weak field to a strong one, if the substance is paramagnetic, and in the opposite direction, if it is diamagnectic. If the force acting on the

(1) Phil. Mag., **6**, (1904), 49.
(2) Phys. Rev., **26**, (1908), 424.
(3) Phys. Rev., **32**, (1911), 406.
(4) Sci. Rep., **2**, (1913), 1.
(5) Sci. Rep., **6**, (1917), 9.

substance be known, the magnetic susceptibility χ of the substance can be calculated by using the following formula :—

$$\chi = \frac{f}{m H \frac{\partial H}{\partial y}}$$

where m is the mass of the substance, H and $\frac{\partial H}{\partial y}$ the strength of the magnetic field and its gradient in the direction of y, respectively.

The apparatus used in the present investigation was nearly the same as that constructed by P. Weiss, with one important improvement to be described below. As shown in Fig. 1, the specimen to be tested

Fig. 1.

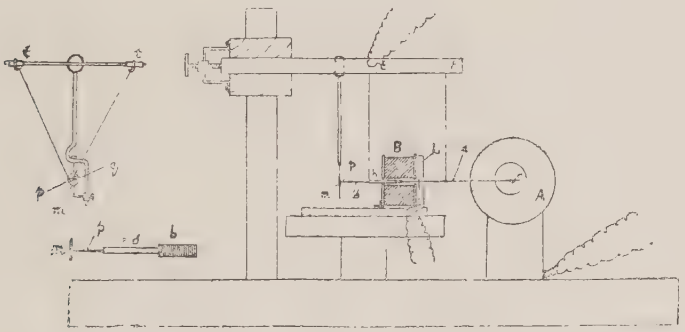

is put in a small glass vessel at one end of a horizontal silica tube suspended by means of two pairs of bifilar systems. The specimen is so placed between the pole-pieces of an electromagnet that it occupies a place where $H\frac{\partial H}{\partial y}$ is a maximum. The silica tube carries a small coil b; concentric with this coil and quite detached from it, there is another fixed coil B. A constant current I is passed through the latter coil, and the electromagnet is excited; then the specimen is slightly displaced from its initial position. This displacement is just compensated for by the mutual action of these two coils by passing a suitable current i through the moving coil b. Then the force acting on the substance is just balanced by the action of the coils, which is proportional to the product Ii, and hence K being a constant,

$$f = K I i,$$

$$\therefore \quad \chi = \frac{f}{m H \frac{\partial H}{\partial y}} = A \frac{i I}{m}; \qquad A = \frac{K}{H \frac{\partial H}{\partial y}}.$$

If the current through the electromagnet be kept constant, A is constant. Hence if we have once determined A, the susceptibility can be known from the currents I, i and the mass of the specimen.

The movable coil b made of a thin insulated copper wire 6 cm long and 3.3 mm thick; it is wound in 360 coils on the silica tube, 3.5 mm thick. The fixed coil B made of an insulated copper wire about 48 mm thick is also 6 cm long and its outer and inner diameters are respectively 2 and 12 cm; it is wound in 740 coils. L is an air-damper made of a mica disc fixed to the silica tube, and serves to prevent any small vibration of the suspended system.

The position of the specimen in the field is found by means of a mirror m fixed to a revolving axis (Fig. 1) and a scale and a telescope being placed in front of the mirror. To the other end of the silica tube carrying the specimen, a magnetized steel needle p is attached and the sharp end of this needle is in contact with a small piece of soft iron attached to the back of the small mirror, this arrangement ensuring a flexible and sure contact between the mirror and the needle. This ingenious device is the invention of Professor K. Honda. When a magnetizing current is passed through the electromagnet, the silica tube together with the specimen is displaced in the direction of its length and causes the rotation of the mirror, the amount of which can be read by means of the scale and the telescope. Then by passing a suitable current through the movable coil b, the mirror is brought to its original position. This current measures the magnitude of the magnetic susceptibility as already explained. In the present experiment, the pole distance of the electromagnet is 1.7 cm and the applied current 10 amperes, this generating a field of 13000 gausses. The whole arrangement is set up on a stone foundation and enclosed in a large carton case to prevent disturbances due to air currents.

In the present investigation the thermal analysis, electric resistance

and microscopic observations were carried out to confirm the results of the magnetic analysis, and the equilibrium diagrams of the bismuth-tin, the antimony-lead and the bismuth-tellurium systems were revised.

The thermal analysis was carried out by the usual method to determine the liquidus and solubility limit of a solid solution, if it exists, i. e. by measuring the time of the solidification interval at a eutectic temperature. The alloys were melted in a small electric furnace of nichrome wire, a melting tube made of porcelain and a carbon powder or carbon dioxide being used, to prevent the oxidation of the specimen. The measurement of temperature was made by means of a platinum-platinum-rhodium thermoelement whose cold junction was always kept at zero.

The electric resistance measurement was carried out to determine the solubility-curve of the solid solution, and the method for this measurement was similar to those used in our laboratory.[1] It consists in measuring the difference in potential between two fixed points in the specimen, which was placed in a range of uniform temperature in the furnace. The current passed through the specimen for the measurement of the potential fall was 1.5 ampéres, and the heating of the specimen was sufficiently slow to obtain an equilibrium state at constant temperature. The alloys to be tested were in the form of rods, 10 cm in length and 6 mm in diameter, these rods being made by casting the alloys in an iron mould and afterwards annealing them just below their solidus lines for a sufficiently long time to obtain a homogeneous structure, if the alloys consist of a solid solution.

§ 3. DETERMINATION OF THE CONSTANT OF THE APPARATUS.

For the determination of the constant of the apparatus, four normal aqueous solutions of nickel sulphate were used. Its magnetic susceptibility has already been determined by Professor T. Ishiwara[2] and found

(1) Sci. Rep., **4**, (1917), 210; **7**, (1918), 167.
(2) Sci. Rep., **3**, (1912), 310.

to be 27.10×10^{-6}. The magnetic susceptibilities of the normal solutions were calculated by using the following formula :—

$$\chi_{m_1} = \frac{p}{100}\chi_m + \left(1 - \frac{p}{100}\right)\chi_{m_0}$$

where $\chi_{m_0} = 0.720 \times 10^{-6}$ and is the magnetic susceptibility of water per unit volume, χ_m = that of nickel sulphate and p = the weight percent of the substance with no crystalline water present.

(i) The Magnetic Susceptibility of a Solution of $\frac{1}{2}$ gram mol. The weight of the solution containing 20.01 c.c. = 21.492 gr. ; the weight of the solution containing 1000 c.c. = 1074.59 gr. ; the molecular weight of nickel sulphate = 154.75.

$$\therefore \quad p = \frac{154.75}{1074.59} \times \frac{1}{2} \times 100 = 7.184.$$

$$\therefore \quad \chi_{m_1} = \frac{7.184}{100} \times 27.10 \times 10^{-6} + \left(1 - \frac{7.184}{100}\right)(-0.720 \times 10^{-6})$$

$$= 1.279 \times 10^{-6}.$$

(ii) The Magnetic Susceptibility of the Solution of 1 gram mol.
$p = 13.465, \qquad \chi_{m_1} = 3.026 \times 10^{-6}.$

(iii) The Magnetic Susceptibility of the Solution of $1\frac{1}{2}$ gram mol.
$p = 19.010, \qquad \chi_{m_1} = 4.569 \times 10^{-6}.$

(iv) The Magnetic Suscepticility of the Solution of 2 gram mol.
$p = 23.975, \qquad \chi_{m_1} = 5.950 \times 10^{-6}.$

The relation between the magnetic susceptibility and the concentration is linear. By the measurement of the susceptibility of the solution by means of compensating currents i and I, the effect of the glass vessel and of air were of course corrected. The weight of the specimen was 0.17~0.20 gram in each measurement, and for each solution four independent observations were made and their mean was taken as the final result. The constant A was calculated using the formula $A = \frac{m\chi_{m_1}}{iI}$. The mean of the four values of the constant A, 21.26, 21.20, 21.18 and 21.24, was 21.22.

As a control, it was thought necessary to test the constant for the well-known cases of water and of the several pure metals. The water used in this experiment was prepared in the following way:—The organic substances contained in the water were oxidized with potassium permanganate; then the water was distilled in the usual way. It was then freed from carbonic acid by passing a current of air free of carbon dioxide through the water. The air was purified by passing it first through a tube containing a layer of calcium chloride, then a layer of soda-lime and lastly a layer of cotton wool. This operation was of course carried out in an atmosphere free from fumes and the air was drawn from out-of-doors. The copper and chromium were electrolically prepared and the other metals from Kahlbaum were extra pure. These metals were tested in an ellipsoidal form weighing about 0.2~0.5 grams, and the surface of these specimens was treated with diluted hydrochloric acid and washed out with water; they were then dried in absolute alcohol and in ether. The results of the experiment are given in the table below and are compared with those found by Professors K. Honda and T. Ishiwara.

TABLE I.

Sul.stance.	Mangnetic suscep. observed $\chi \times 10^6$	Magnetic. suscep. in literature $\chi \times 10^6$
water	−0.719	−0.72
Cu	−0.084	−0.086
Cr	+3.78	+3.75
Zn	−0.126	−0.127
Sn	+0.026	+0.026
Pb	−0.121	−0.120
Tl	−0.215	−0.244
Sb	−0.857	−0.860
Bi	−1.358	−1.380

The agreement between these numbers is very satisfactory. Thus we see that the constant A found in the foregoing experiment can be used with confidence.

For each series of binary alloys, a number of specimens were prepared by alloying pure metals and casting them in an iron mould; they were then annealed at a suitable temperature for ten to twenty hours. This temperature was so chosen that, for eutectic alloys, it is just below the eutectic point, and for a solid solution, it is little below the solidus line.

§4. MEASUREMENT OF THE MAGNETIC SUSCEPTIBILITY OF BINARY ALLOYS.

(1) *Copper-Tin system.*

The most complete equilibrium diagram of this alloy has recently been obtained by Dr. T. Isihara[1] in our laboratory; Fig. 2 is his

Fig. 2.

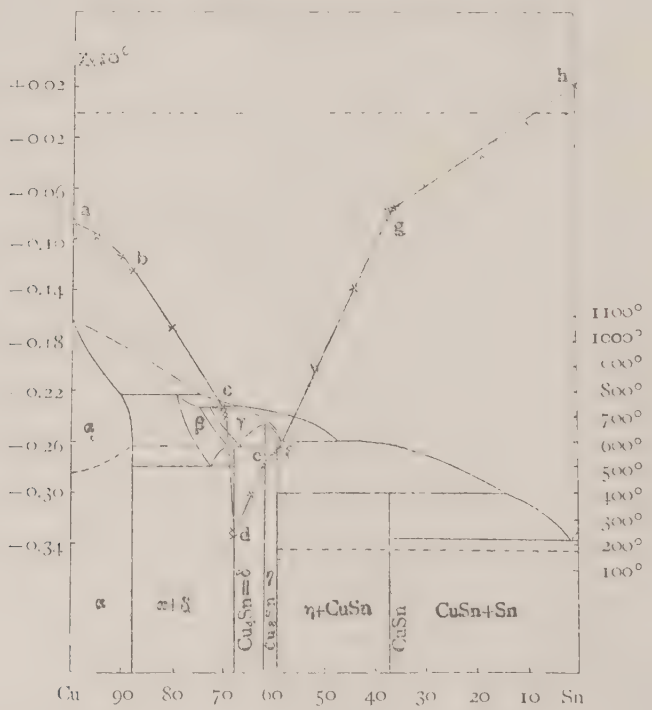

(1) Sci. Rep., **13**, (1924), 75.

diagram. The results of the magnetic measurement together with the analysis for copper and the annealing temperature are given in the following table.

TABLE 2.

Alloys No.	Copper (%)	Annealing temp. (°C)	Annealing time (h)	$\chi \times 10^6$
1	100.00	900	10	−0.084
2	95.35	900	10	−0.101
3	90.40	800	10	−0.115
4	88.00	800	10	−0.127
5	80.08	700	10	−0.171
6	69.80	700	10	−0.234
7	68.02	700	10	−0.331
8	65.00	700	10	−0,305
9	62.17	600	10	−0.276
10	60.50	500	10	−0.271
11	59.58	450	10	−0.268
12	51.80	400	18	−0.201
13	44.20	400	18	−0.141
14	40.00	400	18	−0.094
15	36.90	400	25	−0.081
16	29.99	400	18	−0.054
17	19.40	400	18	−0.037
18	9.95	400	18	−0.009
19	2.00	300	18	−0.016
20	—	180	10	−0.026

The relation between the magnetic susceptibility-concentration curve and the equilibrium diagram is given in Fig. 2. As is to be expected, the portion *ab* of the curve belonging to the range of a homogeneous solid solution α slightly bends downwards, and the portion *bc* which belongs to the range of a mixture of α and Cu_4Sn is straight, and the

alloy of the composition Cu_4Sn has its own magnetic susceptibility, this being of the smallest value. But from the rapid change of magnetic susceptibility along the curve *cd*, we may conclude that at room temperature, the compound Cu_4Sn dissolves about two percent of copper. In the diagram as given by Dr. T. Isihara, this solubility was not observed. The magnetic susceptibility of the alloys between those whose composition is denoted by *d* and *e*, which consist of a mixture of Cu_4Sn and Cu_3Sn, varies along a straight line *de* and that of the alloys between those denoted by *e* and *f*, consisting of a solid solution, varies along a curved line *ef*. Two straight lines *fg* and *gh* intersect at a point *g* which corresponds to the concentration of the compound *Cu Sn*. The alloys lying between the concentrations denoted by *f*~*g* and *f*~*h* are all mechanical mixtures of η and *Cu Sn*, and *Cu Sn* and *Sn* respectively. Thus the above results, as regards the magnetic susceptibility, agree with the equilibrium diagram as given by Dr. T. Isihara, except in the fact that the copper is slightly soluble in the compound Cu_4Sn.

Fig. 3.

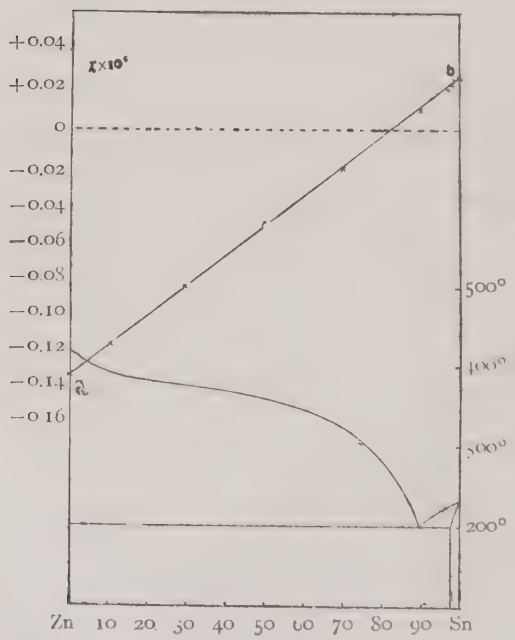

(2) *Zinc-Tin System.*

According to Heycock and Neville,[1] zinc and tin form a simple eutectic mixture, with a small limited solubility on the tin side as shown in Fig. 3. The results of my experiment are given in the following table.

(1) Jour. Chem. Soc., **71**, (1897), 383.

TABLE 3.

Alloys No.	Tin (%)	$\chi \times 10^6$
1	0	−0.125
2	10.8	−0.113
3	29.7	−0.080
4	50.3	−0.047
5	69.7	−0.020
6	80.0	−0.000
7	90.0	−0.010
8	92.4	−0.021
9	100	−0.026

The line *ab* in Fig. 3 shows the relation between the magnetic susceptibility and the concentration. We see that the line is quite straight throughout the whole concentration, and hence it is to be concluded that there is no solid solution on the tin side; this view agrees with the equilibrium diagram constructed by Arnemann and Guertler.[1] Hence the small range of the solid solution on the tin side, as given by Heycock and Nevill, must be rejected.

(3) *Bismuth-Tin Alloy and the Equilibrium Diagram of this System.*

According to Lepkowski,[2] this system has a limited solubility of 5 per cent of bismuth on the tin side and a eutectic at 140° and 58 per cent of bismuth, as shown in dotted lines in Fig. 4. The following table contains the results of observation.

(1) Metall., **7**, (1910), 201.
(2) Zeit. anorg. Chem., **57**, (1908), 287.

TABLE 4.

Bismuth (%)	$\chi \times 10^6$	Bismuth (%)	$\chi \times 10^6$
0	+0.026	69.4	−0.596
2.8	−0.081	73.3	−0.668
5.8	−0.115	87.1	−0.752
8.3	−0.126	90.8	−0.763
17.0	−0.235	96.7	−0.791
25.8	−0.296	99.0	−0.801
37.4	−0.399	99.7	−1.271
47.2	−0.440	100	−1.360
52.6	−0.530		

From Fig. 4, we see that the magnetic susceptibility of tin decreases along curve *ab* in the range of the *α* solid solution and afterwards decreases linearly along the straight line *bc* in the range of the mixture. Close to the bismuth side, an abrupt decrease of the susceptibility from *c* to *d* is observable, showing a small solubility of tin in bismuth. The results obtained in the present experiment nearly agree with the equilibrium diagram as given by Lepkowski; but two points of discrepancy may be noticed. First, in my experiment, the solubility of bismuth in tin is 16 per cent, while, after Lepkowski,

Fig. 4.

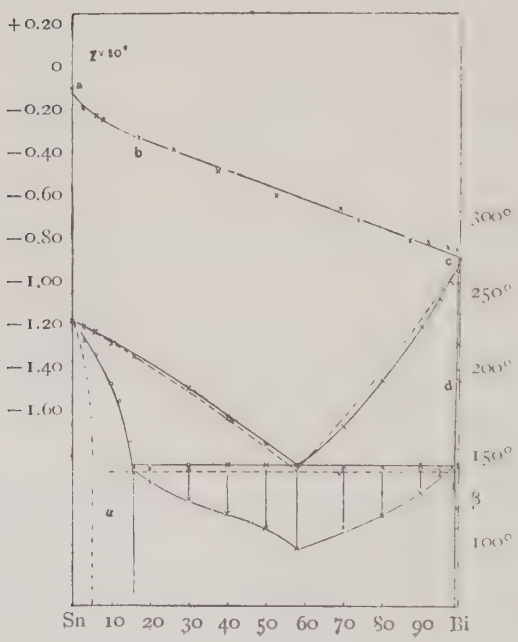

the solubility limit is only 5 per cent. Secondly, in my observation, bismuth has a distinct solubility of 0.9 per cent for tin, but Lepkowski did not observe it. In order to confirm the result of my magnetic analysis, the equilibrium diagram of the system was again studied by means of thermal analysis, electric resistance, specific volume and microscopic observation, as described below.

The cooling curves for thermal analysis were taken at a very slow cooling rate, and arrests on the curves in these alloys are tabulated below :—

TABLE 5.

Alloys No.	Bismuth (%)	Liquidus (°C)	Eutectic (°C)	Eutectic solidifying interval (sec)
1	0	232	—	—
2	3	229	—	—
3	6	226	—	—
4	10	221	—	—
5	16	214	138	5
6	18	211	137	70
7	20	208	138	130
8	30	191	138	330
9	40	170	140	450
10	50	153	140	575
11	58	—	139	750
12	70	164	139	600
13	80	192	138	500
14	90	228	140	250
15	95	246	139	85
16	98	254	138	10
17	99.5	269	—	—
18	100	271	—	—

The first arrest, i. e. the primary crystallization point decreases to the eutectic temperature 139°, as the bismuth content increases up to 58 per cent. As the bismuth content further increases, the temperature of the liquidus increases to the melting point of bismuth. The second arrests in alloys Nos. 2, 3, 4 and 17 did not appear in the cooling curves, this arrest, which occurs at 139° in alloys containing 16 to 99

Fig. 5. a.

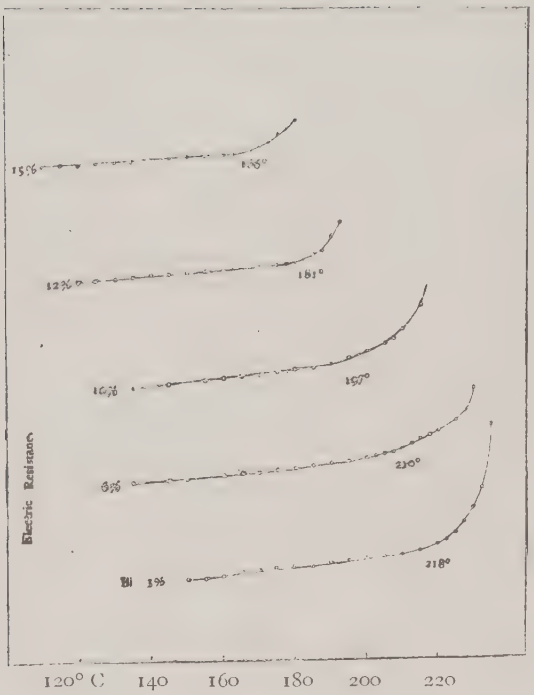

per cent of bismuth, being due to the solidification of a eutectic mixture of the two solid solutions; the eutectic concentration is 58 per cent of bismuth. The fact that the solubility limit of the α solid solution at the eutectic temperature is about 16 per cent of bismuth, was also confirmed, by measuring the solidification interval.

In order to determine the solubility curves of the solid solutions on both sides, the measurement of the electric resistance was carried out. The results of observations are given in the following table and curves in Fig. 5.

Table 6.

Alloys No.	Bismuth (%)	Solidus (°C)	Eutectic (°C)
2	3	218	—
3	6	210	—
4	10	102	—
4′	12	181	—
5	15	166	—
8	30	—	140
11	58	—	138
14	90	—	138
15	99.5	254	—
15′	99.7	265	—

From the curve in Fig. 5, we see that with the rise of temperature, the resistance continuously increases, till a point is reached, where the curve changes its course. This changing point falls to the eutectic temperature, with the increase of bismuth content. The alloy containing 16 per cent of bismuth shows this point at the eutectic temperature, and from these results, it is to be concluded that the solubility limit of bismuth in the α solid solution at 139° is about 16 per cent. The electric resistance-temperature curve of alloys containing 99.5 to 99.8 per cent of bismuth continuously rises with the rise of temperature, but changes its course abruptly at a temperature a little below the melting point of bismuth, and the resistance rapidly falls as the temperature further increases. Hence we can conclude the existence of the β solid solution on the bismuth side, though its range is very small.

Fig. 5. b.

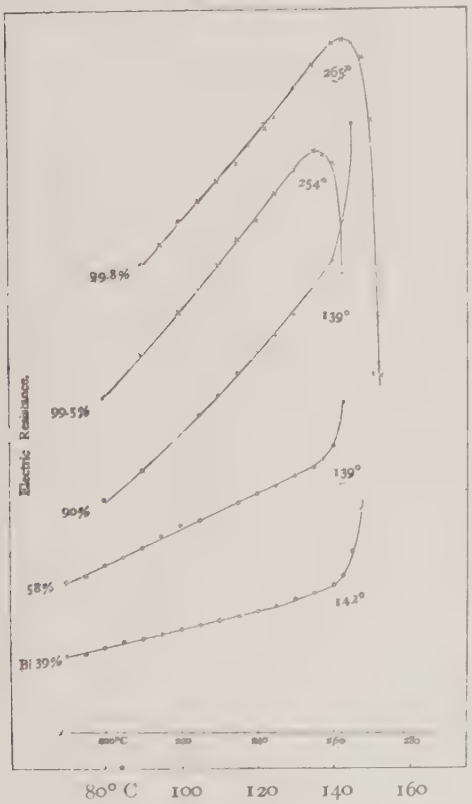

The measurement of the specific volume of the alloys was also carried out. The specimens weighing 23~25 grams, were cooled from their melting point in the furance, and were forged by being hammered to the same condition. The measurement of the density was made in the usual way, and calculated by using the following formula :—

$$\rho = \frac{W_1}{W_1 - W_2}\rho_w + 0.0012\left(1 - \frac{W_1}{W_1 - W_2}\right)$$

where ρ, W_1, W_2, ρ_w and 0.0012 are the density of the specimen, weight

in air, that in water, the density of water and that of air, respectively. The results obtained are given in the following table :—

TABLE 7.

Alloys No.	Tin (%)	Density obs.	Specific volume cal.	Specific volume obs.	$\frac{\Delta v}{v} \times 100$
1	100	7.2820	—	0.1373	—
2	93.9	7.3507	0.1325	0.1360	+0.636
3	90.0	7.4477	0.1331	0.1347	+0.894
4	86.2	7.5008	0.1318	0.1333	+1.168
5	82.8	7.5451	0.1306	0.1325	+1.478
6	79.9	7.6736	0.1296	0.1303	+0.540
7	69.8	7.9092	0.1267	0.1264	−0.205
8	48.9	8.4391	0.1194	0.1186	−0.610
9	41.7	8.5681	0.1168	0.1167	−0.086
10	29.8	8.8827	0.1124	0.1126	−0.160
11	18.2	9.2621	0.1086	0.1080	−0.543
12	7.7	9.5695	0.1049	0.1045	−0.362
13	4.6	9.6501	0.1039	0.1036	−0.250
14	1.8	9.7400	0.1028	0.1027	−0.103
15	0	9.7880	—	0.1022	—

On the other hand, if x and y be the masses of the two constituents, and v_1 and v_2, their specific volumes, then the specific volume of a mixture can be calculated, if the law of mixture be assumed, that is,

$$v = \frac{xv_1 + yv_2}{x+y} = v_1 + (v_2 - v_1)\frac{y}{x+y}$$

In the case of the bismuth-tin alloys, $v_1 = 0.1022$ and $v_2 = 0.1373$ and and hence the above expression may be written in the form :—

$$v = 0.1022 + 0.0003515\ C_{Sn}$$

where $C_{Sn} = \frac{y}{x+y}$ is the concentration of tin.

Fig. 6 shows the relation between the concentration and the specific volume (○) as calculated from the above equation and that (×) obtained by actual determination. In the case of the alloys containing 20 to 100 per cent of bismuth, where they consist of the mechanical mixture of two constituents, these two values of specific volume coincide with each other; but in that of other alloys, a small deviation is observed, indicating a solubility of bismuth in tin.

Fig. 6.

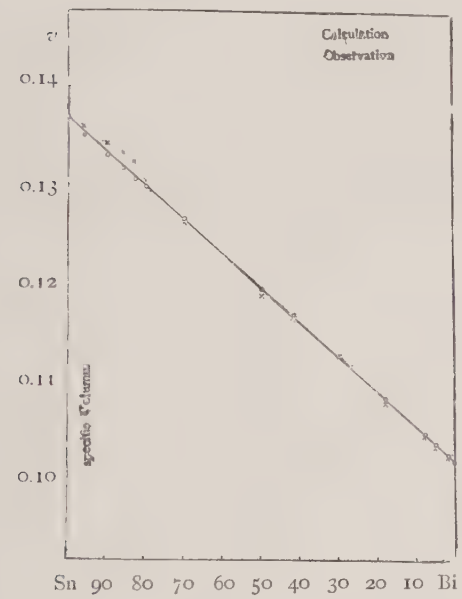

Microscopic observation showed also that the alloys containing less than 16 per cent of bismuth all show a polygonal structure consisting of a solid solution, and that in an alloy containing 99.7 per cent of bismuth, the structure also consists of a solid solution.

From the data so far obtained, the equilibrium diagram of the bismuth-tin system is revised, as shown in full lines in Fig. 4.

(4) *Copper-Zinc System.*

Assist. Professor H. Imai[1] gave recently a complete equilibrium diagram as shown in Fig. 7.

The result of the magnetic investigation also confirms his diagram. The measurements were made at ordinary and high temperatures; the results obtained are given below and also in Fig. 7.

(1) Sci. Rep., **11**, (1922), 213.

TABLE 8.

Alloys No.	Copper (%)	$\chi \times 10^6$	Alloys No.	Copper (%)	$\chi \times 10^6$
1	100	−0.084	10	31	−1.023
2	90	−0.108	11	25	−0.716
3	80	−0.141	12	20	−0.367
4	70	−0.165	13	15	−0.330
5	60	−0.210	14	10	−0.265
6	50	−0.275	15	6	−0.201
7	40	−0.337	16	2	−0.172
8	38	−0.405	17	0	−0.125
9	35	−0.607			

Fig. 7.

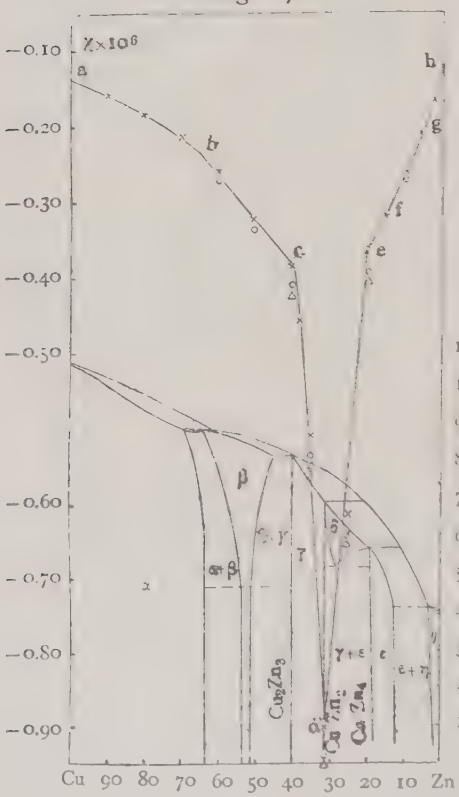

From Fig. 7, we see that the curve *ab* in the range of the *α* solid solution gradually falls to the concentration of the solubility limit of zinc and the curve *bc* is practically a straight line in the range of the mechanical mixture. The break point *c* corresponds to the compound Cu_2Zn_3, and the occurrence of the maximum degree of diamagnetic susceptibility at a concentration of 31 per cent of copper content also confirms the existence of the compound $CuZn_2$. In the range of the solid solution *γ*, the magnetic susceptibility rapidly decreases from *c* to *d*. The increase from *d* to *e* is practically a straight line, this confirming the fact that the alloys between the

concentrations *d* and *e* consist of a mechanical mixture of γ and ε. The break point *e* corresponds to a compound $Cu\,Zn_4$. The curve *eh* can be separated into three portions *ef*, *fg* and *gh*, corresponding to ε, $\varepsilon+\eta$ and η respectively. Thus the results so far obtained agree with the equilibrium diagram as given by Mr. H. Imai.

Measurements of the susceptibility at high temperatures were also made to find the change of magnetic susceptibility in the above specimens; the results obtained at 300° and 500° are tabulated below :—

Table 9.

Alloys No.	$\chi\times10^6$ 500° C	$\chi\times10^6$ 300° C	$\chi\times10^6$ 18° C
5	—	−0.220	−0.210
6	—	−0.285	−0.275
7	−0.370	−0.357	−0.337
9	−0.645	−0.635	−0.607
10	−1.055	−1.040	−1.023
11	−0.750	−0.745	−0.716
12	−0.405	−0.390	−0.367
14	—	−0.273	−0.265

Fig. 8.

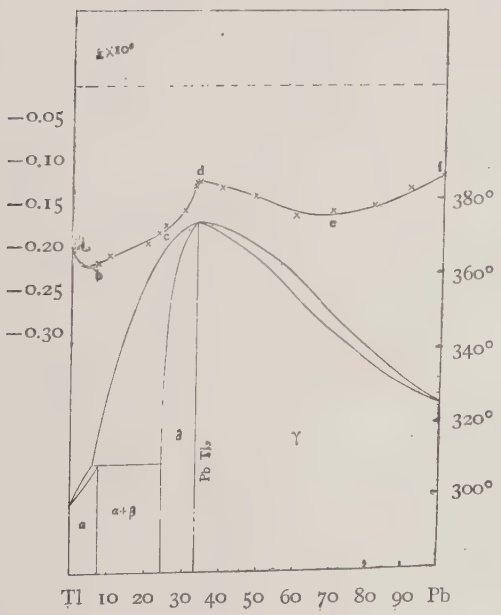

Thus as far as investigated, the change in magnetic susceptibility due to temperature, is very small as is to be expected from the diagram.

(5) *Lead-Thallium System.*

Fig. 8 is the equilibrium diagram of this system obtained by Lewkonja.[1] The chemical analysis, heat treatment and results of magnetic measurement are given below.

(1) Zeit. anorg. Chem., **52**, (1907), 435.

TABLE 10.

Lead (%)	Annealing temp. (°C)	Annealing time (h)	$\chi \times 10^6$
100	300	14	−0.121
90.8	320	14	−0.136
81.0	320	14	−0 160
70.0	340	14	−0.167
60.0	340	14	−0.176
49.2	360	14	−0.148
39.8	360	14	−0.135
33.1	360	20	−0.130
30.0	340	14	−0.164
25.3	310	14	−0.185
23.0	300	20	−0.194
20.3	300	20	−0.211
10.1	300	20	−0.223
7.0	280	20	−0.235
3.0	280	20	−0.236
0	280	14	−0.215

In Fig. 8, the portion *ab* of the susceptibility curve shows its change in the range corresponding to the α solid solution, and the portion *bc* is straight in the range of a mechanical mixture. The alloy containing 34 per cent of lead is a compound $Pb\ Tl_2$ having a maximum susceptibility. The portions *cd* and *dcf* correspond to the solid solutions β and γ respectively. Thus the result of my magnetic investigation confirms the diagram as given by Lewkonja.

(6) *Bismuth-Lead System.*

Fig. 9 is the equilibrium diagram of this system obtained by Barlow.[1]

(1) Jour. Americ. Chem. Soc., **32**, (1910), 1394; Zeit. anorg. Chem., **70**, (1911), 183.

The results obtained in the present experiment are tabulated below and also given in Fig. 9.

TABLE II

Lead (%)	$\chi \times 10^6$	Lead (%)	$\chi \times 10^6$
0.9	−1.335	70	−0.409
1.5	−1.254	82	−0.301
4.0	−1.073	88	−0.260
8.0	−1.024	92	−0.213
21.8	−9.914	95	−0.204
41.5	−0.653	98	−0.188

Fig. 9.

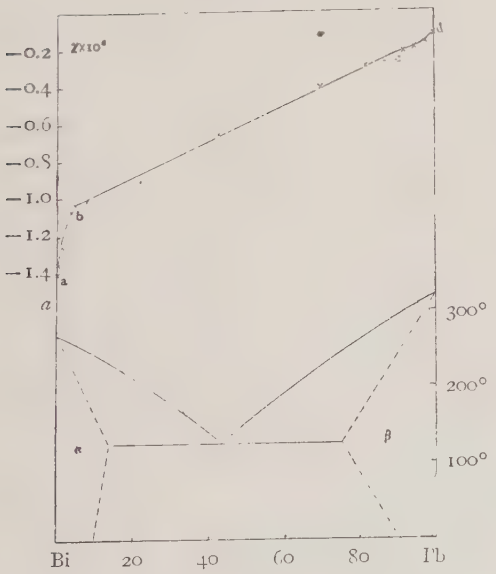

From Fig. 9, we see that the magnetic susceptibility of bismuth rapidly increases on adding lead to a concentration at the solubility limit *b* and afterwards increases linearly along a straight line *bc* in the range of a mixture of two solid solutions α and β, and then, the susceptibility increases from *c* to *d*, but not linearly in the range of the β solid solution. The above results obtained in the present experiment nearly agree with the equilibrium diagram as given by Barlow; but in my result, the solubility limit of lead in bismuth is 4 per cent at room temperature, and this agrees with the result of the hardness test and the electric conductivity as investigated by Herold.[1]

(1) Zeit. anorg. Chem., **112**, (1920), 131.

(7) *Antimony-Tin System.*

Fig. 10 is the equilibrium diagram of this system obtained by Williams.[1] The results obtained are given below and in Fig. 10.

TABLE 12.

Tin (%)	$\chi \times 10^6$	Tin (%)	$\chi \times 10^6$
0	−0.857	40	−0.123
0.2	−0.767	70	−0.091
0.8	−0.679	88	−0.087
2.0	−0.364	93	−0.085
7.5	−0.153	97	−0.051
10.6	−0.132	100	−0.020
20.0	−0.130		

Fig. 10

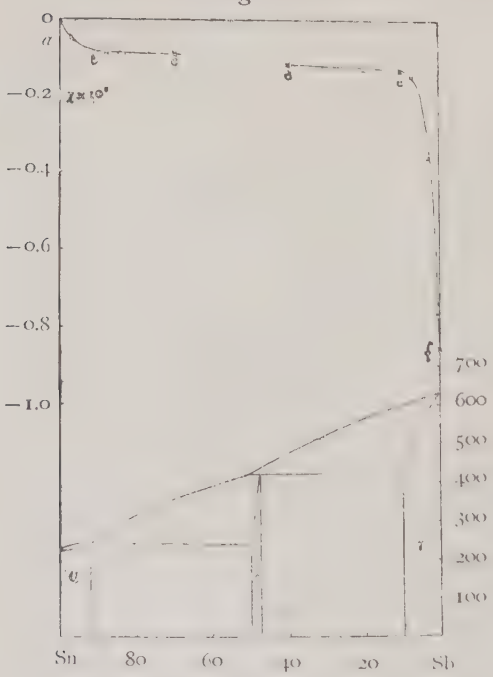

The magnetic susceptibility of tin decreases along curve *ab* on the addition of antimony up to the solubility limit *b*. Similarly the magnetic susceptibility of antimony rapidly increases on adding tin up to its solubility limit, i.e. 10 per cent of tin. In the range of mechanical mixture, the magnetic susceptibility-concentration curves *bc* and *de* are each straight.

(1) Zeit. anorg. Chem., **55**, (1907), 14.

(8) *Antimony-Copper System.*

Fig. 11 is the equilibrium diagram based on the investigation by Reimann.[1] The results obtained are tabulated below and given in Fig. 11.

Fig. 11.

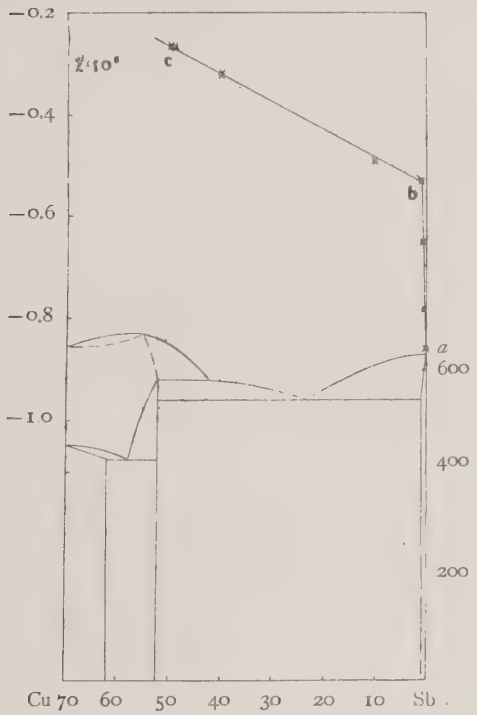

TABLE 13.

copper (%)	$\chi \times 10^6$
0	−0.857
0.5	−0.786
0.8	−0.652
1.4	−0.539
5	−0.494
6	−0.318
7	−0.265

From Fig. 11, we see that close to the antimony side, an abrupt increase in the magnetic susceptibility from *a* to *b* is observable, showing a small solubility of copper in antimony and afterwards the susceptibility increases linearly along a straight line *bc* in the range of the mechanical mixture. From this result, the existence of a solid solution on the antimony side is confirmed and the solubility of copper in antimony is about 1.4 per cent.

(9) *Bismuth-Zinc System.*

Fig. 12 is the equilibrium diagram based on the investigations by

(1) Zeit. Metallkunde, **12**, (1920), 320.

Spring and Romanoff,[1] Arnemann,[2] Heycock and Neville.[3] The results obtained in the present experiment are tabulated below and are also given in Fig. 12.

TABLE 14.

Zinc (%)	$\chi \times 10^6$	Zinc (%)	$\chi \times 10^6$
0	−1.360	28.2	−0.888
0.2	−1.330	47.8	−0.658
1.4	−1.272	68.7	−0.477
2.0	−1.157	91.2	−0.220
10.0	−1.106	99.0	−0.122
14.0	−1.049	99.5	−0.121
19.5	−1.011	100	−0.125

Fig. 12.

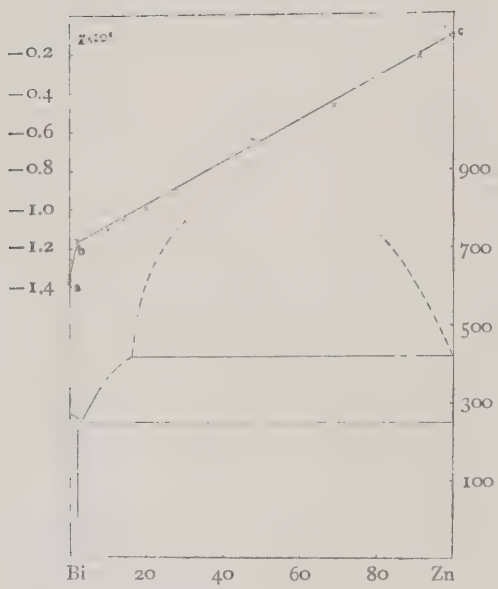

The magnetic susceptibility of bismuth rapidly increases along a curve *ab* to the alloy containing 2 per cent of zinc in the range of solid solution, and then increases along a straight line *bc* in the range of mechanical mixture. The existence of the solid solution *a* on the bismuth side is thus confirmed.

(1) Zeit. anorg. Chem., **13**, (1897), 29.
(2) Metall., **7**, (1910), 201.
(3) Jour. Chem. Soc., **71**, (1897), 394.

(10) *Antimony-Lead Alloy and the Equilibrium Diagram of this System.*

The equilibrium diagram shown in Fig. 13 is due to Stead[1] and Gontermann.[2] The results obtained in the experiment are given in the following table and in Fig. 13.

TABLE 15.

Lead (%)	$\chi \times 10^6$	Lead (%)	$\chi \times 10^6$
0	−0.858	6.5	−0.295
0.5	−0.591	16.0	−0.268
0.8	−0.497	31.2	−0.243
1.5	−0.391	49.5	−0.200
1.9	−0.360	72.0	−0.177
2.4	−0.345	98.0	−0.117
3.1	−0.320	99.6	−0.118
3.2	−0.310	100	−0.121
6.0	−0.290		

Fig. 13.

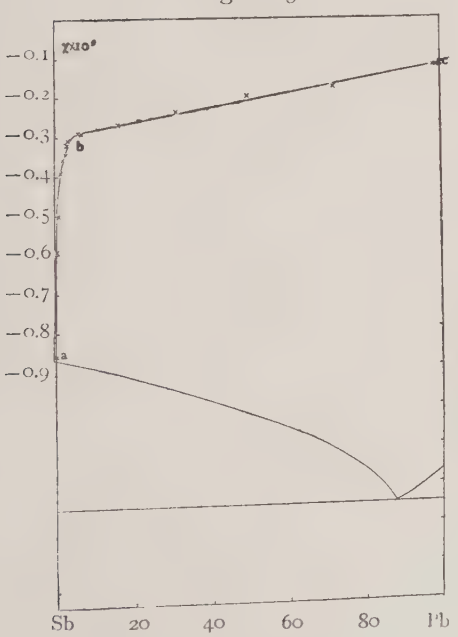

The magnetic susceptibility of antimony rapidly increases along curve *ab* up to 5 per cent of lead and afterwards increases linearly along a straight line *bc*, this indicating the existence of a solid solution on the antimony side. This solid solution had not been previously confirmed. No solid solution on the lead side and no compound have been confirmed at room temperature, notwithstanding the existence of the compound SbPb suggested by Gontermann. In order

(1) Jour. Soc. Chem. Ind., **16**, 200, 505.
(2) Zeit. anorg. Chem., **55**, (1907), 419.

to confirm the above results of the magnetic analysis, the present writer also studied the binary system by means of thermal analysis, electric resistance and microscopic observation as described below.

The thermal analysis for eighteen alloys containing 2 to 99.8 per cent of antimony was carried out in the usual way. The arrests on the cooling curves are tabulated in the following table.

TABLE 16.

Alloys No.	Antimony (%)	Liquidus (°C)	Eutectic temp. (°C)	Eutectic solidifying interval (sec.)
1	2	309	247	3
2	6	288	249	17
3	10	261	251	35
4	13	252	248	56
5	20	306	251	38
6	30	350	249	27
7	40	413	250	23
8	50	462	250	18
9	60	512	251	15
10	70	545	249	10
11	80	582	251	6
12	90	608	251	3
13	94.5	—	250	—
14	95	621	—	—
15	97	—	—	—
16	98	623	—	—
17	98.7	—	—	—
18	99.8	—	—	—

The first arrest decreases to the eutectic temperature 250°, as the antimony content increases up to 12.5 per cent of eutectic concentration. As the antimony content further increases, the temperature of the

liquidus increases to the melting point of antimony. The second arrest in the alloys Nos. 15, 16, 17 and 18 did not appear on the cooling curves, and those occurring at a constant temperature of 250° in alloys containing 2 to 95 per cent of antimony is attributed to the solidification of the eutectic mixture. The time for eutectic solidification decreases rapidly in the case of the alloys containing from 12.5 to 30 per cent of antimony, and in those containing between 30 to 95 per cent, it decreases linearly.

The specimens for measuring the electric resistance, Nos. 14~18, were annealed for 24 hours at the required temperature i.e. 200°~500°. The curves in Fig. 14 are the electric resistance-temperature curves and the results obtained in the present experiment are tablated below.

Fig. 14. a.

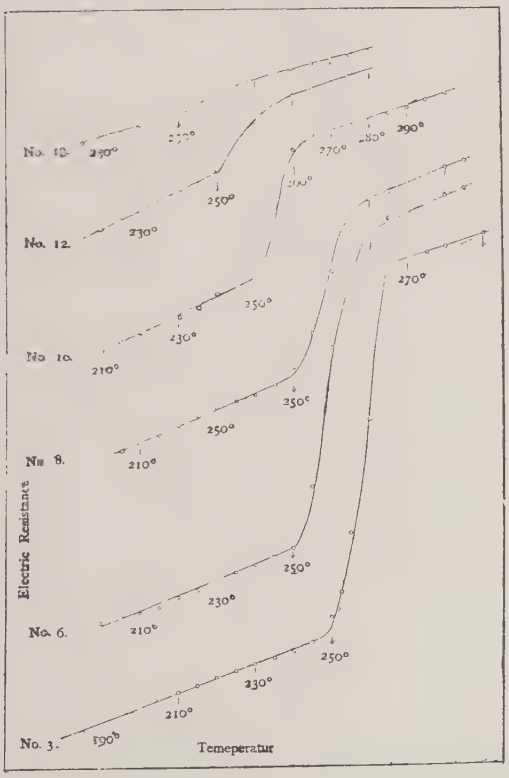

Fig. 14. b.

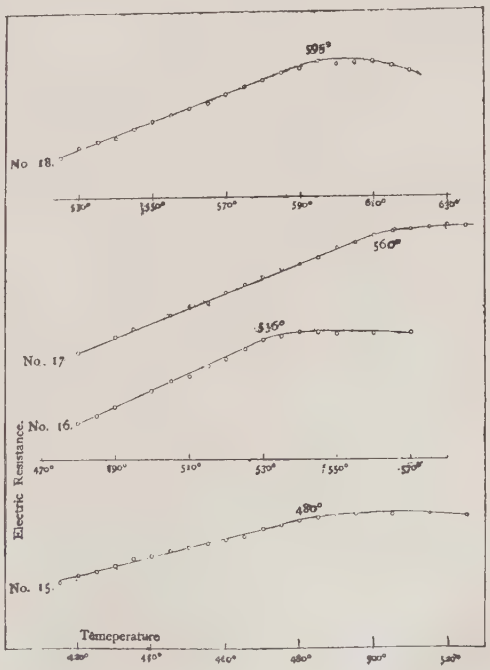

TABLE 17.

Alloys No.	Antimony (%)	Length of specimen (cm)	Solidus (°C)	Eutectic temp. (°C)
1	2	12	—	247
3	10	12	—	250
6	30	12	—	247
8	50	12	—	248
10	70	12	—	250
12	90	12	—	247
13	94.5	8	—	250
15	97	8	480	—
16	98	10	536	—
17	98.7	12	563	—
18	99.8	10	595	—

With the rise of temperature, the resistance continuously increases, till a point is reached, where the curve changes its course. This point falls to the eutectic temperature, with the increase of lead content, and remains afterwards constant. From this fact, we may conclude that the solubility limit of lead in antimony at 250° is 5 per cent. The solubility below 250° was not determined in the present experiment, but it is probably parallel to the temperature axis. On the other hand, the alloys containing more than 90 per cent of lead did not show any break but the eutectic temperature in the electric resistance-temperature curve, this fact indicating no trace of a solid solution on the lead side.

Fig. 15

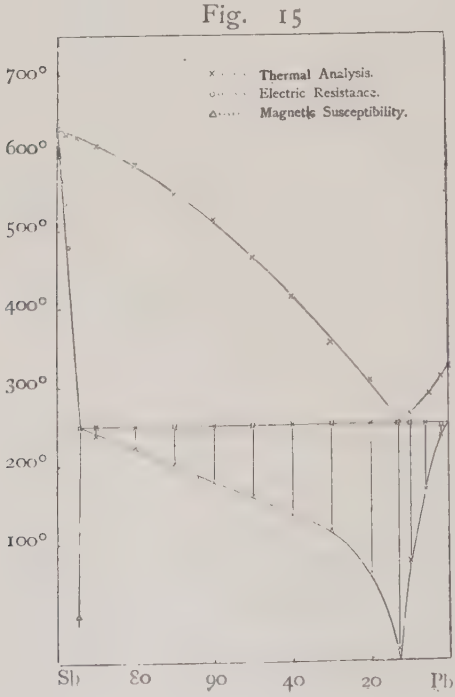

The microscopic investigation also confirms the above results. The alloys containing more than 95 per cent of antimony show a

polygonal structure consisting of a solid solution of lead in antimony, as shown in Photogr. No. 3. The other alloys all consist of a mixture of the saturated solid solution and lead; Photogr. No. 4 is the structure of the eutectic alloy. Fig. 15 is the revised diagram based on these data.

(11) *Bismuth-Tellurium Alloy and the Equilibrium Diagram of this System.*

The equilibrium diagram in Fig. 16, shown in a dotted line, is due to Mönkemeyer.[1] It is very simple showing a maximum at 60 atomic per cent of tellurium corresponding to the compound Bi_2Te_3 and two eutectic points, one at 2 per cent and the other at 93 per cent. The existence of a solid solution on both sides of the compound was afterwards confirmed by Professor K. Honda and Dr. T. Soné.[2] According to the results obtained by the them, which was again confirmed by the present writer, the existence of solid solutions on both sides of the compound Bi_2Te_3 and that of a very narrow range on the bismuth side can be recognized. The results of the magnetic analysis are given in the following table, and graphically in Fig. 16. The equilibrium diagram based on the present investigation is given in Fig. 16 in full lines.

Fig. 16.

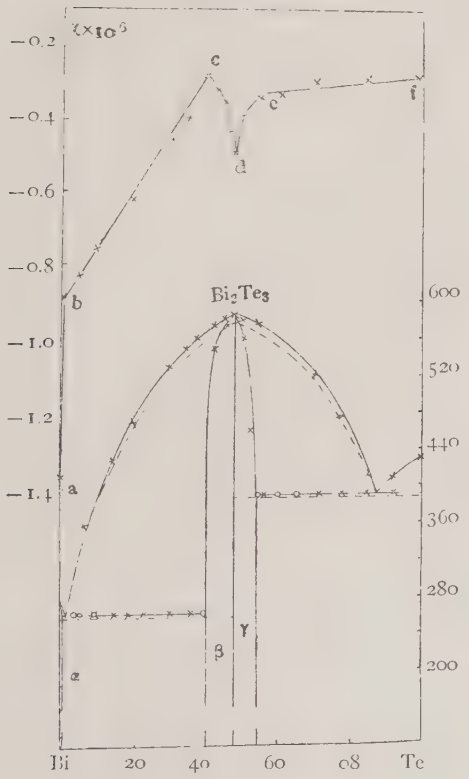

(1) Zeit. anorg. Chem., **46**, (1905), 419.

(2) Sci. Rep., **2**, (1913), 1.

TABLE 18.

Tellurium (%)	$\chi \times 10^6$	Tellurium (%)	$\chi \times 10^6$
0	−1.350	45	−0.349
0.5	−0.956	46.5	−0.429
1	−0.891	47.8	−0.477
5	−0.832	50	−0.388
10	−0.764	56	−0.345
20	−0.638	60	−0.330
30	−0.461	70	−0.310
35	−0.398	86	−0.288
40	−0.286	100	−0.294
43	−0 320		

The magnetic susceptibility-concentration curve is a straight line *bc* in the range of a mixture, that is, 1 to 10 per cent of tellurium, and the curves *cd* and *de* correspond to the ranges of solid solutions; the minimum susceptibility is due to the compound Bi_2Te_3. Another straight portion *ef* corresponds to the range of a mixture of the solid solution and tellurium. The rapid increase of susceptibility very near the bismuth side confirms the existence of a very diluted solid solution of tellurium in bismuth.

In order to confirm the results of the magnetic analysis above referred to, the thermal analysis, the electric resistance method and microscopic observations were also made. The arrests on the thermal cooling curves are tabulated below.

TABLE 19.

Tellurium (%)	Liquidus (°C)	Solidus (°C)	Eutectic temp. (°C)
1	268	—	—
3	302	—	266*
4	—	—	266*
7	368	—	265*
10	385	—	265

Tellurium (%)	Liquidus (°C)	Solidus (°C)	Eutectic temp (°C)
15	433	—	266
20	473	—	265
30	530	—	263
35	552	—	264
38	558	—	263
40	—	—	264
42	572	549*	—
45	581	568	—
48	585	—	—
50	582	560	—
52	—	460*	—
54	—	—	389*
55	576	—	388
60	—	—	389*
65	—	—	388*
70	520	—	388
78	475	—	388
85	410	—	389
92	408	—	389

The alloys containing 1 to 40 per cent of tellurium have two arrests, those between 40 and 53 per cent, one, and those containing more than 53 per cent, two. The first point rises as the tellurium content increases to 48 per cent. As the tellurium content further increases, it decreases to the eutectic temperature 389° at the eutectic concentration of 87 per cent and then increases to the melting point of tellurium. The second arrest in the alloys containing 1 to 40 per cent of tellurium is due to the eutectic point 265°. In alloys containing 40 to 53 per cent, the corresponding point is absent. As the tellurium content increases to more than 53 per cent, the second arrest is due to another eutectic point 389°. The solubility of bismuth and tellurium in the compound $Bi_2 Te_3$ was determined by the electric resistance method. In the above table, the temperatures marked by * were obtained by this method.

Microscopic observations also confirmed the above view. Photogr.

Fig. 17

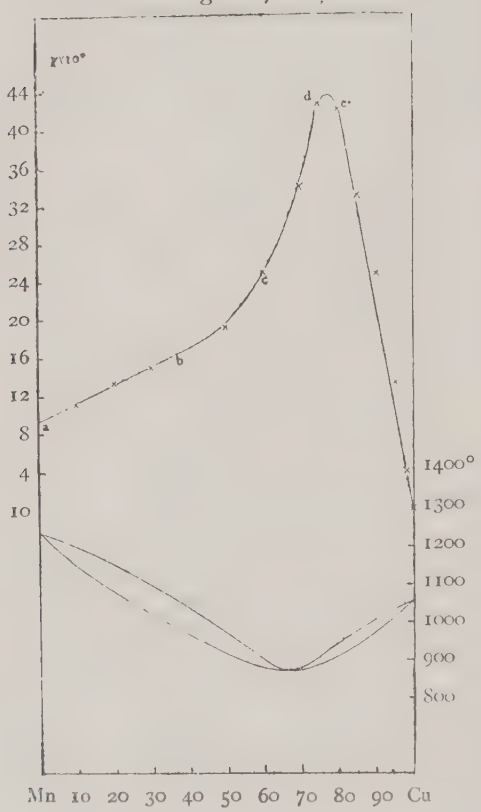

No. 7 shows the microstructure of the alloy in the range of the solid solution of bismuth and tellurium in the compound. Photogr. Nos. 6 and 8 show the eutectic structures and primary solid solution on both sides of the compound.

(12) *Copper-Manganese System.*

According to A. Rykowski[1] and others, copper and manganese form a solid solution in all proportions at room temperature as given in Fig. 17. The results obtained in the present experiment are given in the following table and also in Fig. 17.

Table 20.

Copper (%)	$\chi \times 10^6$	Copper (%)	$\chi \times 10^6$
100	0.084	70	34.38
98	1.93	60	24.96
95	9.43	50	18.96
90	21.34	30	24.97
85	28.93	20	13.45
80	38.18	10	11.22
75	38.40	0	10.60

(1) Zeit. anorg. Chem., **57**, (1908), 256.

The magnetic susceptibility-concentration curve can be divided into three parts; i.e. a straight portion *ab*, a curved portion *bc* and a straight portion *ef*; these portions are not completely confirmed by the equilibrium diagram, as shown in Fig. 17. From these results, it is suggested that the alloy containing 0 to 30 per cent of copper and those containing 80 to 100 per cent, consist of a mechanical mixture of two components. The range of the alloys containing 30 to 80 per cent is to be confirmed by other methods. A more complete investigation is now being made in our laboratory.

SUMMARY.

The results of the present investigation may be summarised as follows:—

1. The present experiment was carried out in order to find the relation between the magnetic susceptibility and the equilibrium diagram in binary alloys, and if necessary, to revise the diagram.

2. The systems of the alloys investigated in the present experiment were (1) Cu-Sn. (2) Cu-Zn, (3) Bi-Sn, (4) Zn-Sn, (5) Pb-Tl, (6) Bi-Pb, (7) Sb-Sn, (8) Sb-Cu, (9) Bi-Zn, (10) Sb-Pb, (11) Bi-Te and (12) Cu-Mn.

The following relations were confirmed.

(a) A compound has a magnetic susceptibility characteristic of it.

(b) The magnetic susceptibility-concentration curve becomes a straight line in the case of alloys consisting of a mechanical mixture of two constituents.

(c) In the case of alloys forming a solid solution, the same curve consists of a curved line. If a small amount of another element is dissolved in a strong diamagnetic element such as bismuth or antimony, the magnetic susceptibility of the latter rapidly increases to the concentration of the solubility limit.

3. The present writer revised the equilibrium diagrams of the bismuth-tin antimony-lead and bismuth-tellurium systems on the basis of the magnetic analysis, combined with other methods of investigation.

In conclusion, the present writer expresses his cordial thanks to

Professor K. Honda under whose direction the present investigations were carried out, and also to Professors T. Murakami and T. Ishiwara for their valuable advice and criticisms during the progress of the work. His thanks are also due to Mr. T. Kato who helped him in the chemical analysis of the alloys.

Photogr. 1. ×150

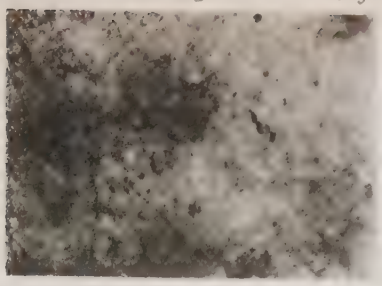

Bi–Sn. 6% Bi.
α solid solution.

Photogr. 2. ×150

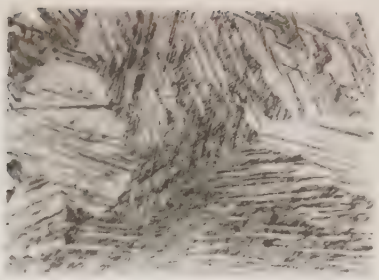

Bi–Sn. 99.7% Bi.
β solid solution.

Photogr. 3. ×150

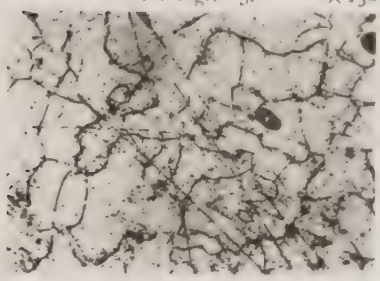

Sb–Pb. 98.5% Sb.
Annealed at 500° for 24 hours.
α solid solution.

Photogr. 4. ×150

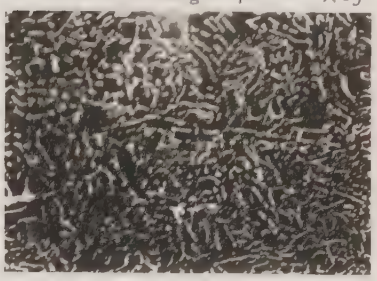

Sb–Pb. 12.5% Sb.
Eutectic structure.

Photogr. 5. ×150

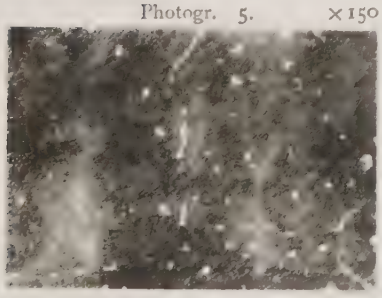

Sb–Pb. 3% Sb.
Annealed at 230° for 24 hours.
Eutectic+lead (dark).

Photogr. 6. ×150

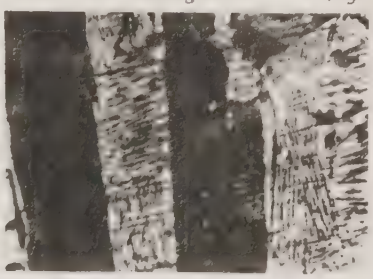

Bi–Te. 75% Te.
β solid solution (dark)+eutectic.

Photogr. 7. ×150

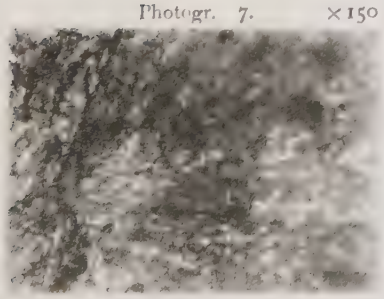

Bi–Te. 48% Te.
β solid solution.

Photogr. 8. ×150

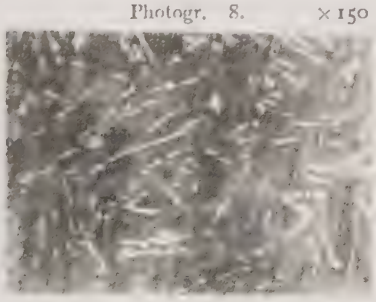

Bi–Te. 3% Te.
Near the eutectic structure.

(Bismuth—Tin alloys etched with solution of ferric chloride with a little hydrochloric acid.
Antimony—Lead and Bismuth—Tellurium alloys etched wich a nitric acid.)

Dilatometric Investigation of the A_3 and A_4 Transformations in Pure Iron.[1]

By

Seikichi Satô

§ 1. INTRODUCTION.

The magnetic investigation of the A_3 and A_4 transformations in iron has already been made by Curie,[2] Weiss, Föex[3] and others.[4] Among them, Prof. T. Ishiwara from the result of his experiment with a torsion balance, showed that during heating, the magnetic susceptibility of pure iron increases discontinuously at the A_4 point and afterwards gradually decreases, and, on cooling, the change is reversed.

From his study of the A_3 and A_4 transformations with regard to the changes in physical properties of pure iron at high temperatures, Prof. K. Honda predicted that by the A_4 transformation, γ-iron will be retransformed to α-iron, that is, δ-iron will be the same as α-iron. A year later, this was actually confirmed by Westgren[5] by X-ray analysis.

The answer to the question, whether during the Ac_4 transformation, iron will expand or contract, is not evident; because this depends on

(1) The one hundred tenth report from the Research Institute for Iron, Steel and Other Metals.

(2) Curie: Oeuvres, 289.

(3) Weiss & Föex: Arch des Sci., Genève, **31**, (1911), 89.

(4) K. Honda & H. Takagi: Sci. Rep. **4**, (1915), 261. T. Ishiwara: Sci. Rep. **6**, (1917), 133–138. E. M. Terry: Phys. Rev. **9**, (1917), 394.

(5) Westgren: Engineering, (1922), 631; Stålets Kristallbygnad, (1921); Journ. Iron & Steel Inst., (1922), I, 240.

the coefficient of expansion of γ-iron. The present investigation was undertaken to decide this point experimentally. Since the A_4 point lies at so high a temperature as 1400°, this investigation is not an easy matter. The writer carried out his investigation with a very pure iron and succeeded in finding a distinct expansion during the Ac_4 trnasformation. In fact the thermal dilatation curve of δ-iron formed the continuation of that of α-iron, showing that both α and δ irons belong to the same phase.

§ 2. ARRANGEMENT AND METHOD OF EXPERIMENT.

The present experiment was commenced with a dilatometer similar to that used by Prof. K. Honda ;[1] the heating was effected by using Rosenhain's carbon ring electric furnace, which is a modified form of that used by Lecturer S. Kaya.[2] The furnace worked in a vacuum and gave a sufficient length of uniform heating at very high temperatures, say a maximum variation of only 2° along the length of 70 mm at 1300°C. The specimens were cylindrical rods, 6 mm in diameter and 70 mm in length, made of armco iron. The linear magnification of the apparatus was 1200, so that at the A_3 point, a sharp discontinuous deflection of scale by about 24 centimetres was observed. But owing to the yielding of the silica tubes used in the apparatus at very high temperatures, this apparatus could not be used beyond 1200°C.

After several fruitless trials, a differential method was adopted, a short description of which will be necessary. The specimen and the neutral were connected to form a differential dilatometric couple, as

Fig. 1.

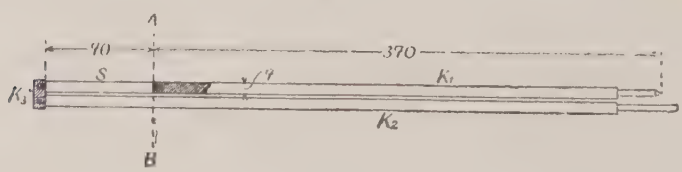

(1) K. Honda: Sci. Rep. **6**, (1917), 204.
(2) S. Kaya: Kinzoku no Kenkyu, **2**, (1925), 45.

shown in Fig. 1. For the neutral, metallic cobalt was chosen, because it has no transformation in the vicinity of 900° and 1400°, and its coefficient of expansion, specific heat and melting point are of nearly the same value as those of pure iron. In the figure, two rods K_1 and K_2 are cobalt neutrals having the same diameter as that of specimen S. S, K_1, K_2 and a piece of cobalt K_3 are tightly screwed together in the form of a hair pin, leaving a clearance of about 1 mm between the two parallel rods. If this pair of connected rods be introduced into the heating furnace so as to heat the left portion of AB sufficiently uniformly and its left end K_3 be lightly supported, the differential elongation between the iron and cobalt rods will cause a relative displacement between the ends of K_1 and K_2 rods. This displacement can be measured, if the right end of K_2 rod be clamped and the same end of K_1 rod be lightly supported and its motion transmitted to a mirror system.

Fig. 2 shows the mirror system. The right end of K_2 rod is clam-

Fig. 2.

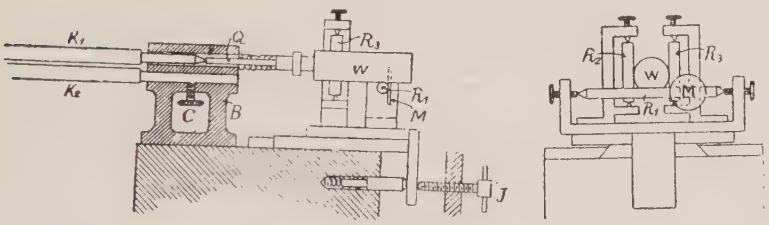

ped to the base B by a screw C, and the coned end of K_1 rod touches the end of a quartz tube Q, which is co-axially fixed to a cylindrical rod W. W rests on a horizontal roller R_1 and is guided by two vertical rollers R_2 and R_3. Hence a displacement of the coned end can be observed as the deflection of a small mirror M attached to R_1. J is a screw for adjusting the mirror to the zero position.

Fig. 3 shows the general arrangement of the apparatus; here the electric furnace, the connected rods, the mirror system, etc, are put into a closed vessel V, equipped with a water cooling device. This vessel is connected with a pump through outlet I, and the heating and

cooling of the specimen can be made in a vacuum. The temperature of the specimen is measured by a Le Chatelier thermocouple H. E is

Fig. 3.

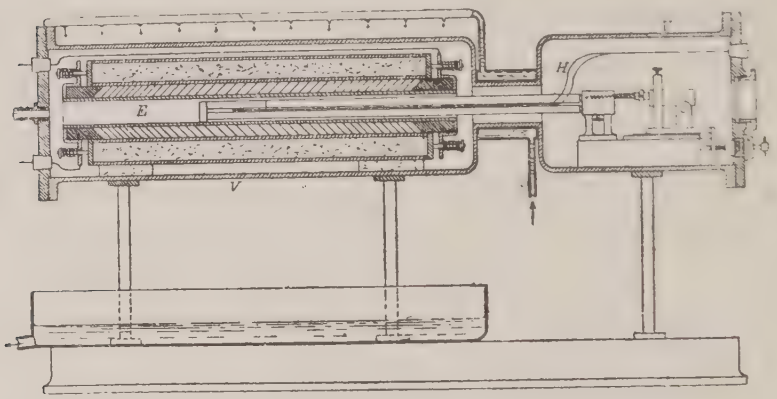

the carbon ring electric furnace as stated above.

If r be the radius of the horizontal roller and D be the scale distance, the relative change of length between the specimen and the neutral, that is, $\delta l - \delta l_0$, is given by

$$\delta l - \delta l_0 = r\vartheta$$

where θ is the deflection angle of the mirror. Further, if n be the scale deflection, we have

$$\tan 2\theta = \frac{n}{D} \fallingdotseq 2\theta$$

$$\therefore \quad \delta l - \delta l_0 = \frac{rn}{2D}$$

In the present case,

$$r = 2.50 \text{ mm}; \qquad D = 1500 \text{ mm},$$

$$\therefore \quad \delta l - \delta l_0 = \frac{n}{1200} \text{ mm}$$

The test specimens were cylindrical rods, 7 mm in diameter and 70 mm in length. They were made from electrolytic iron melted in a vacuum furnace. The result of the chemical analysis is given below:

TABLE I.

C (%)	Si (%)	Mn (%)	S (%)	P (%)	Cu (%)
0.006	no trace	trace	0.006	no trace	no trace

§ 3. RESULTS OF EXPERIMENT.

The change of length during the A_3 transformation was first observed, a typical result of which is given in Fig. 4, and in Table II. In the figure, the ordinate represents the scale deflection and the abscissa the temperature.

Fig. 4. A_3 Transformation.

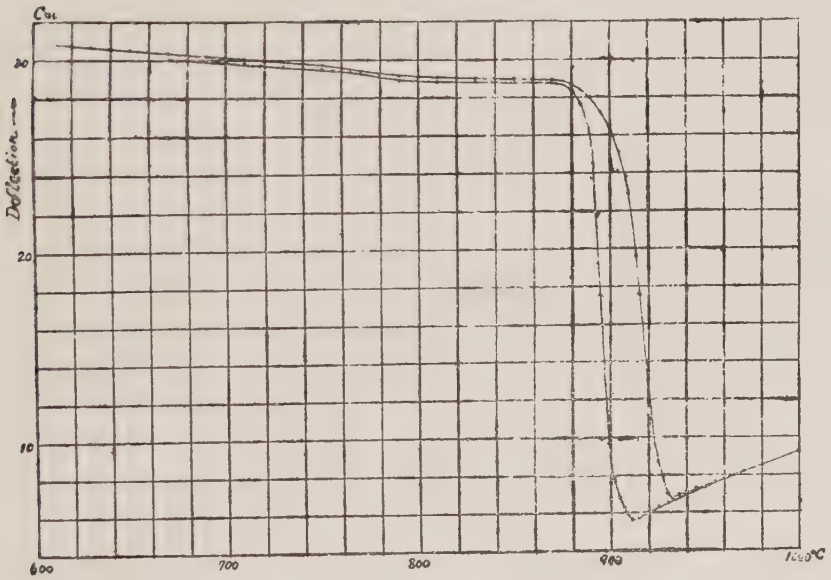

TABLE II.

Temperature in deg. C.	Scale Deflection in cm.	Temperature in deg. C.	Scale Deflection in cm.
(Heating)		630	30.70
610	30.80	640	30.60
620	30.75	650	30.50

TABLE II. *Continued*

Temperature in deg. C.	Scale Deflection in cm.	Temperature in deg. C.	Scale Deflection in cm.
660	30.45	910	22.90
670	30.35	914	19.60
680	30.30	918	16.00
690	30.20	920	11.90
700	30.15	923	9.50
710	30.05	925	8.70
720	30.00	930	7.00
730	29.87	933	6.70
740	29.81	936	6.95
750	29.76	940	7.10
760	29.50	945	7.23
770	29.40	950	7.36
780	29.24	955	7.60
790	29.15	959	7.80
800	29.10	970	8.20
810	29.04	980	8.50
820	29.01	1000	9.20
830	29.00	(Cooling)	
840	29.00	960	7.75
850	29.00	940	6.90
860	29.00	930	6.50
870	28.94	925	6.30
880	28.69	920	6.00
885	28.40	915	5.70
890	28.00	911	5.62
895	27.20	909	5.90
900	26.30	907	6.30
905	25.10	904	6.80
909	23.80	901	7.80

TABLE II. *Continued*

Temperature in deg. C.	Scale Deflection in cm.	Temperature in deg. C.	Scale Deflection in cm.
899	9.70	800	28.80
897	14.00	790	28.85
894	19.20	780	29.06
891	24.50	765	29.36
889	26.40	756	29.40
885	27.60	750	29.41
880	28.40	730	29.60
870	28.80	718	29.70
860	28.80	710	29.80
850	28.80	700	29.83
838	28.80	690	29.90
830	28.80	680	30.00
820	28.80	670	30.05
810	28.80		

From Fig. 4, we take the scale deflection due to the A_3 transformation to be :

$$n = 240 \text{ mm}$$

$$\therefore \quad \delta l - \delta l_0 = \frac{240}{1200} = 0.200 \text{ mm}$$

As the transformation proceeds at a constant temperature, so that

$$\delta l_0 = 0,$$

$$\therefore \quad \delta l = 0.200 \text{ mm}$$

Next, in order to see the effect of the screwed parts (3.5 mm thick, 4 mm long and 1/32 inch pitch) on the value of δl, the following experiment was made :—

Cylindrical specimens of the same length and diameter, i. e. 70×7 mm., and of the same material, but without the screw ends, were

Fig. 5. A_3 Transformation.

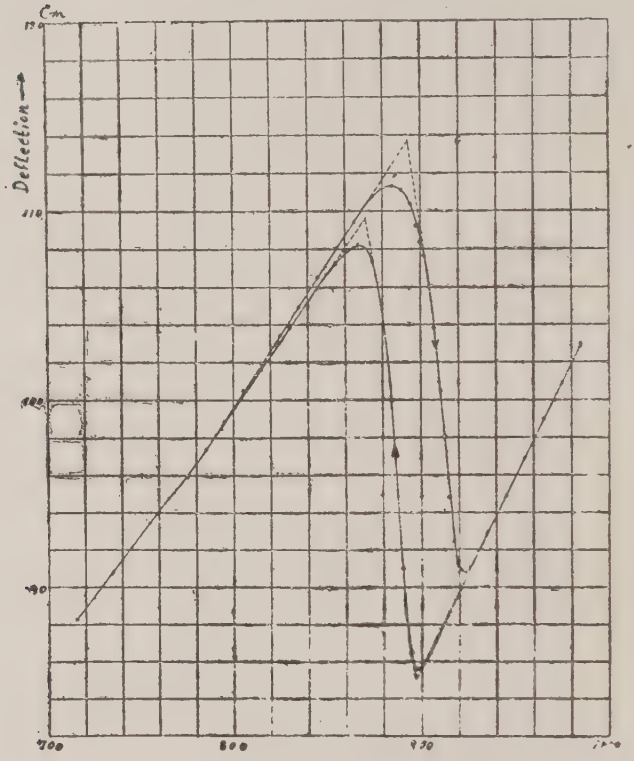

prepared and the change of length due to the A_3 transformation was measured by using the total dilatometer already mentioned. Fig. 5 shows an example of such measurements. Hence we take

$$n \doteqdot 240 \text{ mm.}$$

$$\therefore \quad \delta l \doteqdot 0.200 \text{ mm.}$$

i. e. exactly the same result as before. Hence it is to be concluded, that the effect of the screwed parts on the change of length is not appreciable.

Let l_α be the length of the specimen just below the A_3 point and

" l_γ " " " " above " " " ,

then we have :—

$$l_\alpha = l_\gamma + \delta l,$$

$$l_\alpha / l_\gamma = 1 + \delta l / l_\gamma$$

and l_γ can be deduced from the initial length and the scale deflection at 920° in Fig. 5, thus :—

$$n = 900 \text{ m.m.}$$

$$\therefore \quad l_\gamma = 70.0 + \frac{900}{1200} = 70.75 \text{ m.m.}$$

$$\frac{\delta l}{l_\gamma} = \frac{0.200}{70.75} = 0.00282$$

Fig. 6. A_4 Transformation.

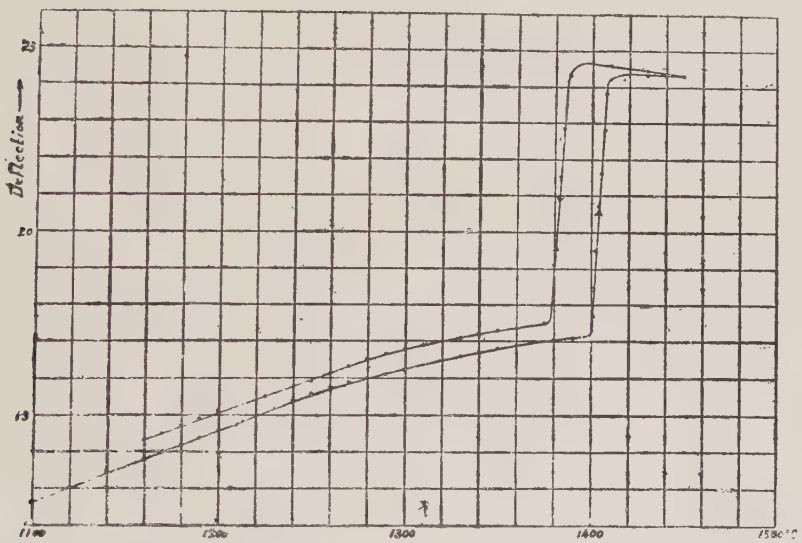

Next the heating was further continued to as high as 1390°C ; but in this range, no abnormal change of length was observed, γ-iron continuously expanding with the rise of temperature, at a rate greater than that of α-iron. As the temperature reaches 1400°, an abrupt increase of length is observed, as shown in Fig. 6 and Table III.

TABLE III.

Temperature in deg. C.	Scale Deflection in cm.	Temperature in deg. C.	Scale Deflection in cm.
(Heating)		1370	17.00
1000	9.25	1380	17.05
1020	10.00	1390	17.10
1040	10.70	1400	17.30
1060	11.40	1401	17.90
1080	12.10	1402	19.50
1100	12.60	1403	20.70
1120	13.00	1405	21.60
1140	13.40	1407	22.80
1160	13.80	1408	23.80
1180	14.20	1410	24.20
1190	14.40	1420	24.35
1200	14.60	1430	24.30
1210	14.71	1440	24.30
1220	15.00	1450	24.30
1230	15.20	(Cooling)	
1240	15.40	1450	24.30
1250	15.54	1440	24.30
1260	15.70	1430	24.45
1270	15.90	1420	24.50
1280	16.00	1410	24.60
1290	16.10	1400	24.70
1300	16.20	1388	24.30
1310	16.35	1385	22.85
1320	——	1383	21.50
1330	16.60	1380	19.10
1340	16.70	1375	17.50
1350	16.80	1360	17.35
1360	16.90	1350	17.30

TABLE III. *Continued*

Temperature in deg. C.	Scale Deflection in cm.	Temperature in deg. C.	Scale Deflection in cm.
1340	17.20	1260	16.10
1330	17.10	1250	15.90
1320	17.00	1225	15.50
1310	16.90	1200	15.10
1300	16.80	1190	14.90
1290	16.65	1180	14.70
1280	16.50	1170	14.50
1270	16.30	1160	14.30

This increase is due to the A_4 transformation. When this discontinuous change has been completed, the rate of expansion becomes less than that in the γ-region and the deflection-temperature curve lies in the prolongation of that in α-iron, as shown in Fig. 7.

Fig. 7. A_3 and A_1 Transformations.

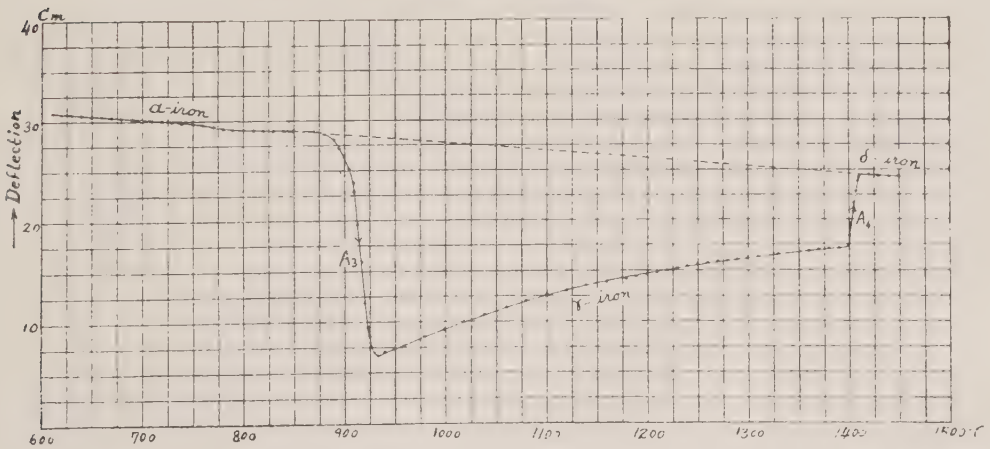

This fact confirms the conclusion that δ-iron is the same phase as α-iron. During cooling, the reversed change takes place at the Ar_4 point, which lies a little below the Ac_4 point, i. e., 20 degrees. lower.

From Fig. 6, the scale deflection during the A_4 transformation is taken to be:

$$n = 73.0 \text{ mm.}$$

and therefore

$$\delta l = \frac{73.0}{1200} = 0.0608 \text{ mm.}$$

Fig. 8 shows an example of the expansion-temperature curve obtained by the total dilatometer. In this case, however, observation beyond 1200° was not possible as stated above; but if the heating curves of both α-and γ-irons be produced to 1400°C, the difference between the ordinates of these curves at this temperature gives an expansion of $73\frac{1}{2}$mm.

Fig. 8.

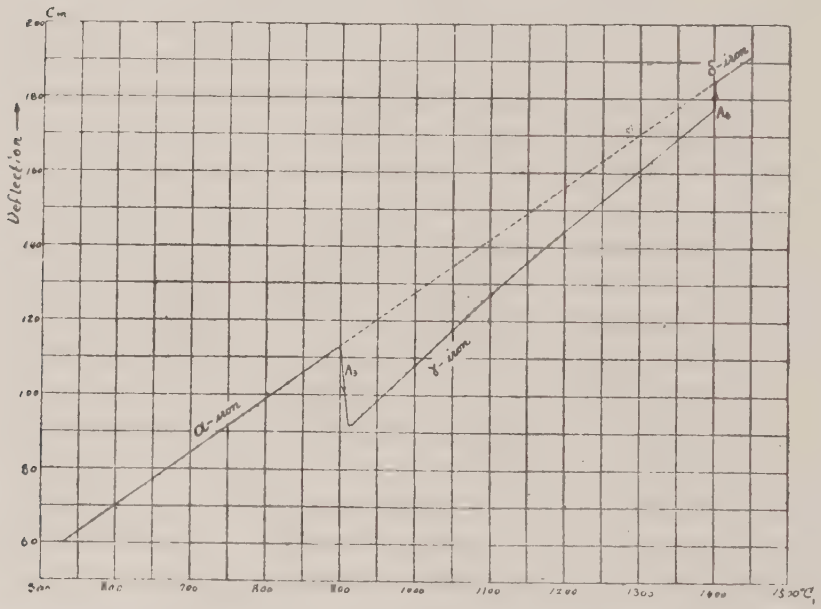

corresponding to the A_4 transformation, which is in satisfactory agreement with the observed value.

If l_γ be the length of specimen just below the Ac_4 point

and l_δ ,, ,, ,, ,, ,, above ,, ,, ,

we have:—

$$l_\delta = l_\gamma + \delta l$$

$$\frac{l_\delta}{l_\gamma} = 1 + \frac{\delta l}{l_\gamma}$$

From the initial length and the scale deflection as given in Fig. 8, we obtain:

$$l_\gamma = 70.0 + \frac{1770}{1200} = 71.47 \text{ mm.}$$

$$\therefore \quad \frac{\delta l}{l_\gamma} = \frac{0.0608}{71.47} = 0.000851$$

§ 4. COMPARISON OF THE RESULTS OF EXPERIMENT WITH THAT OF X-RAY ANALYSIS.

Let a_α be the lattice parameter of α-iron just below the A_3 point,
and a_γ „ „ „ „ γ-iron „ above „ „ ,
then one side of an elementary cube, occupied by one atom of either α or of γ-iron is respectively given by,

$$\frac{a_\alpha}{\sqrt[3]{2}} \quad \text{or} \quad \frac{a_\gamma}{\sqrt[3]{4}},$$

and the difference between these two is evidently the contraction or expansion due to the A_3 transformation.

Similarly, if

a_δ be the lattice parameter of δ-iron just above the A_4 point,
and a_γ „ „ „ γ-iron „ below „ „ ,
then the difference between $\frac{a_\delta}{\sqrt[3]{2}}$ and $\frac{a_\gamma}{\sqrt[3]{4}}$ shows the expansion or contraction due to the A_4 transformation.

According to Westgren, the values of a_α and a_γ are as follows:—

Temperature	a_α (Å)	Temperature	a_γ (Å)
20°C	2.86	1000°C	3.65
800°C	2.89	1100°C	3.66
1450°C	2.93	1425°C	3.68

The lattice parameters just below and above the A_3 and A_4 points are not given in the table, but they can be found from Fig. 9.

Fig. 9.

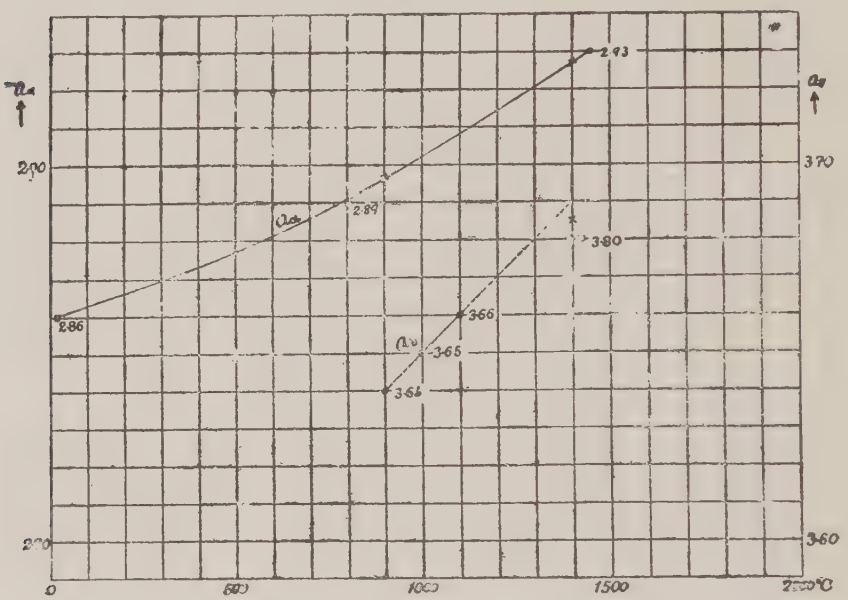

Thus at the A_3 point, we have

$$a_\alpha = 2.897 \ \mathring{A}; \quad a_\gamma = 3.640 \ \mathring{A},$$

$$1 + \frac{\delta l}{l_\gamma} = \frac{2.897}{3.640} \times 1.2599 = 1.00273$$

or

$$\frac{\delta l}{l_\gamma} = 0.00273,$$

which is in close agreement with the observed value

$$\frac{\delta l}{l_\gamma} = 0.00282.$$

Again at the A_4 point, we have

$$a_\alpha = 2.927 \ \mathring{A}; \quad a_\gamma = 3.685 \ \mathring{A},$$

and hence

$$\frac{\delta l}{l_\gamma} = 0.000767,$$

which is again in close agreement with the observed value

$$\frac{\delta l}{l_\gamma} = 0\ 000851$$

SUMMARY.

The present investigation may be summarised as follows :—

(1) In the case of pure iron, during heating, the A_4 transformation is accompanied by an expansion, and the A_3 transformation by a contraction, and during cooling these changes are reversed.

(2) The ratio of the magnitudes of the change of length due to the A_3 and A_4 transformations is about 10 : 3.

(3) The thermal dilatation curve of δ-iron forms the continuation of that of α-iron, showing that δ-iron is of the same phase as α-iron.

The writer wishes to express his cordial thanks to Professor K. Honda under whose kind guidance, the present investigation was carried out, and also to Professors T. Ishiwara and M. Yamada for their valuable advice during the course of the present investigation. He is also much indebted to Lecturer S. Kaya for the construction of the electric furnace.

On the Solidus Line in the Iron-Carbon System.[1]

By

Seiji Kaya.

§ 1. INTRODUCTION.

In the equilibrium diagram of the iron-carbon system, the solidus line has been chiefly determined by thermal analysis[2] and the quenching method.[3] It is, however, very dfficult to determine the line by the former method, as the heat effect on this line is very small. The latter method, used by Gustowsky and Asahara, is the more accurate; but it has also some defect. Thus, the cooling effect of the sample during its fall from the furnace into water can not be konwn, this effect causing an apparent rise in the solidus temperature.

In the present investigation, the author used the electric resistance method and found the solidus line by a break in the resistance-temperature curve. It is, however, to be remarked that we met with several difficulties in constructing a furnace working at a temperature up to 1500° C., and in avoiding decarburisation of the samples during a long period of heating. The solubility line of cementite into austenite was also determined by the same method, and the solubility limit was found at the intersection of the eutectic line with the solubility line of cementite.

(1) The one hundred and eleventh roport from the Research Institute for Iron, Steel and other Metals.

(2) Carpenter and Keeling; Journ. Iron & Steel Inst. No. 1, (1904), 224.

(3) Gustowsky; Metallurgie (1909), 731. Asahara; Scientific papers of the Inst. Phys. & Chem. Research Lab., Tokyo, **2**, No. 4, (1924), 420.

This line has been already determined by Dr. S. Konno[1] and Dr. I. Iitaka[2] in our institute, the former by a differential dilatometric method and the latter by the electric resistance method, but their result are not very accurate, especially for an ally of high carbon content. The present writer repeated the same experiment with steel containing up to 1.7 percent of carbon.

§ 2. APPARATUS.

The heating furnace was the same as that constructed by Rosenhain[3]; it consists of a number of carbon rings placed in contact with each other, so as to form a tube 30 cm. in length and with a radius of 3.5 cm.. The cooling effect on the ends of the furnace is partly eliminated by diminishing the thickness of the rings at those portions, and thus a fairly long portion of uniform temperature is obtained. The carbon rings are made from fine powder of cryptol kneaded with a suitable amount of coal-tar into paste, and are slightly heated to allow the excess of coal-tar to evaporate. After being pressed into the required form (Fig. 1.), they are heated at 800° C for 20 hours. The dimensions of the ring are as follows :—

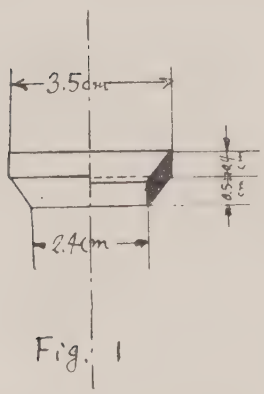

Fig. 1

Outer radius = 3.5 cm.,
inner radius = 2.4 cm.,
their thickness varies from 0.3 cm. to 0.5 cm..

The thicker rings are placed in the central portion and the thinner ones in the outer portions of the furnace. Those carbon rings loosely fitted on an alundum tube are compressed by means of two springs through carbon tubes provided with iron terminals. The pressure of the springs can be adjusted by screws on the ends of a frame supporting the furnace. The outside of the carbon

(1) Science reports **12**, (1923), 127.
(2) „ „ **7**, (1918), 167.
(3) Trans. Faraday Soc. **14**, (1919), 264.

rings are protected by schamotte powder and asbestos paper, as shown in fig. 2. The whole of the furnace is placed in an iron cylinder, which can be evacuated by a pump.

The heating current in the furnace is controlled by an auto-transformer, and for the fine adjustment a water rheostat is inserted in the secondary circuit. If the number of carbon rings is 80 to 90 and the length of the

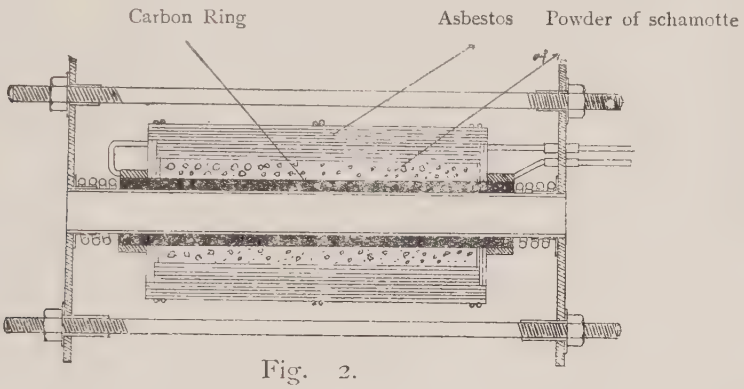

Fig. 2.

heating portion is 28 cm., a current of 35 to 50 amperes is required to obtain a temperature of 1500° C. If the furnace is used in free air, the oxidation of the carbon rings shortens the life of the furnace. Hence in my experiment, the coal gas is passed within the outer cylinder of the furnace from one end of it and evacuated from the other. This prevents the oxidation of carbon rings and the change in the distribution of the temperature. In this way, I can obtain a furnace in which the temperature is uniform over 10 cm. within 5° at 1200°~1300° C.

The length of the specimen was 10 cm. and its diameter 0.5 cm., and the electric resistance at its central portion was determined by passing a constant current through it and measuring the difference of the potentials in the central portion, which is 5 cm. in length. The heating was conducted at first in a vacuum in order to avoid the decarburisation of the specimen; but as this method was found insufficient, coal gas was introduced into the furnace from one end of the iron cylinder, and constantly pumped out from the other end of it, the pressure of the gas being

regulated by a cock in the gas lead tube. It was, however, very difficult to regulate the pressure of the coal gas so as to keep the carbon content in the specimen unaltered; this pressure depends not only on the composition of the coal gas, but also on the temperature and the carbon content of the specimen, and hence it was only possible to adjust the pressure of the gas so as to meet our requirements during a comparatively short period of heating. In our experiments, the pressure was 15~20 cm. of Hg, and the heating was conducted rapidly till the temperature attained 200° C below the required degree, and then very slowly at the rate of about 150° C per hour. In this way, decarburisation was fairly well avoided. Only those experimental data were adopted, in which the micro-structure of the specimen showed no trace of decarburisation. The experiments were always made during heating.

For the measurment of the temperature, thermo-couple platin platin-rhodium and a millivoltmeter were used. The couple was sealed in a quartz tube and inserted in the furnace in contact with the specimen. The calibration of the couple was made by the following standard temperature, and repeated several times during the experiments.

Melting point of electrolytic iron . . . . . 1530° C,
„ „ „ nickel . . . . . 1452° C,
eutectic point of nickel-carbon . . . . . 1331° C,
„ „ „ iron-carbon . . . . . 1130° C,
melting point of silver . . . . . 960.5° C.

For the measurment of the resistance of the specimen, Leeds & Northrup potentiometer was used, the lead wires being of iron. The resistance was measured at an interval of 5°~7° from a temperature of about 200° C below the solidus point. In order to elimnate the disturbing effect of thermo-electricity, the observations were always made for direct and reversal currents passing through the specimen, and their mean was adopted as the final result.

The solubility line of cementite was also determined by the resistance method. Here, as the highest temperature did not exceed 1130° C, the ordinary nichrome furnace was used for the sake of

convenience; this furnace had a uniformity range of 15 cm. within 2°.. To prevent the decarburisation of the specimen, a mixture of alumina and sugar in suitable proportions was used to coat the specimen, the heating being effected in a vacuum. Since in high carbon steels, the cementite decomposes more or less at high temperatures into iron and graphite, the latter being not so easily soluble in iron as cementite, it is not convenient to make the observation during heating. Hence in our experiment, the specimens were at first heated to a temperature sufficiently high for the complete dissolution of carbon or cementite into iron, and then the solubility line was determined during a very slow cooling.

§ 3. RESULTS OF THE EXPERIMENT.

The specimens used for the determination of the solidus line were Swedish steels, the composition of which is given in Table I.

TABLE I.

C (%)	Si (%)	Mn (%)	P (%)	S (%)	Solidus Pt. ° C.
1.60	0.22	0.18	0.026	0.020	1140
1.31	0.31	0.22	0.026	0.022	1171
1.16	0.28	0.22	0.031	0.017	1198
1.01	0.27	0.20	0.027	0.020	1220
0.90	0.34	0.19	0.028	0.016	1242
0.77	0.31	0.21	0.023	0.019	1287
0.60	0.32	0.44	0.025	0.018	1337
0.48	0.27	0.41	0.029	0.020	1377
0.41	0.33	0.43	0.023	0.021	1394
0.36	0.30	0.44	0.013	0.017	1408
0.75	0.00	0.00	0.000	0.006	1289
0.23	0.00	0.00	0.000	0.006	1444

These specimens contain a certain amount of impurity, especially silicon and manganese etc.; the last two specimens in the above table

were made by alloying electrolytic iron and sugar carbon, and used as a contrast experiment for detecting the effect of impurities on the solidus point. The specimens used for the determination of the solubility line of cementite were prepared by alloying Swedish iron, Armoco-iron and Swedish white pig. The composition of these specimens is given in Table 2. These data here tabulated were those for such specimens, which showed no trace of decaburisation.

The results of the determination of the solidus and solubility lines are given in the last columns in tables I aud II, respectively.

TABLE II.

C (%)	Si (%)	Mn (%)	P (%)	S (%)	A cm
1.60	0.22	0.18	0.026	0.020	1100° C
1.57	0.15	0.05	0.001	0.022	1092
1.48	0.09	0.05	0.001	0.023	1048
1.46	0.09	0.05	0.001	0.023	1044
1.26	0.31	0.22	0.026	0.022	945
1.23	0.12	0.05	0.001	0.024	927
1.02	0.27	0.20	0.027	0.020	798

The resistance-temperature curves for different specimens are graphically shown in PL. I and II. The curves in Pl. I show the change of the resistance in the neighbourhood of the solidus point, and those in Pl. II that of the resistance for the solubility point of cementite. The last curve in Pl. I (0.23 % C) shows the solidus point at 1444° C, and also an abrupt change occurring at 1475° C. This change corresponds to the peritictic reaction due to A_4 transformation; its temperature is, however, a little lower than the result found by Ruer and Klesper[1].

The solidus and solubility curves determined by the present experiment are graphically shown in Fig. 3, together with those previously

(1) Ferrum, **11**, (1914), 257.

Fig. 3.

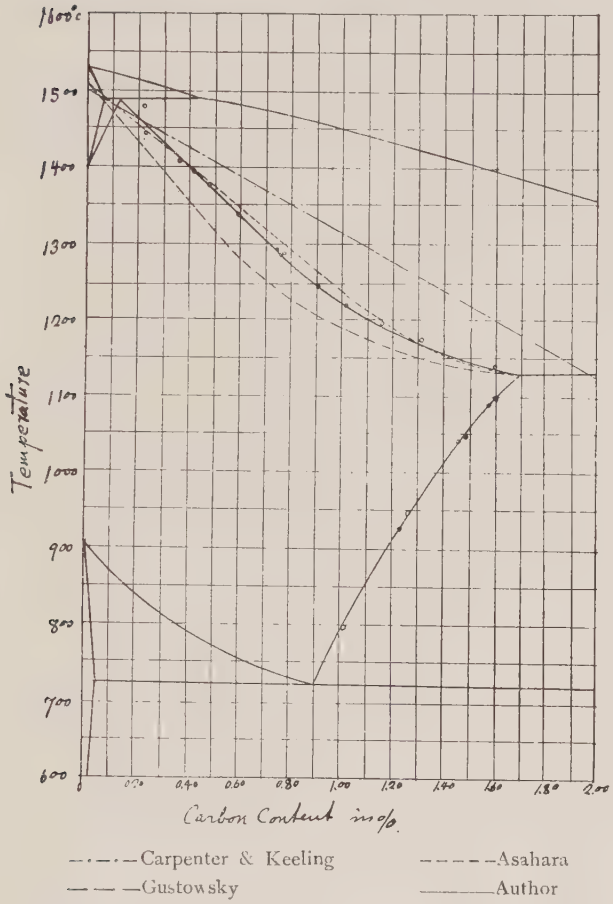

determined. As will be seen from the figure, the solidus line here determined lies between the curve as obtained by Carpenter and Keeling and that of Gustowsky, and slightly below the line obtained by Dr. G. Asahara. The solubility limit of cementite is conveniently determined from the point of intersection of the solubility and the eutectic lines. This limit thus determined is 1.7 percent of carbon in accordance with the previously accepted result.

Though the specimens here used were of a high degree of purity, still they contain a small amount of impurities, such as Si, Mn, P, S, etc.. Their effect on the solidus line may safely be considered quite

small, since the solidus points of the specimens, made by alloying electrolytic iron with sugar carbon, coincided with that of the above specimens.

In conclusion, I wish to express my hearty thanks to Professors K. Honda and T. Ishiwara, under whose direction the present investigation was carried out.

Pl. I.

Heating Curve for Solidus Line

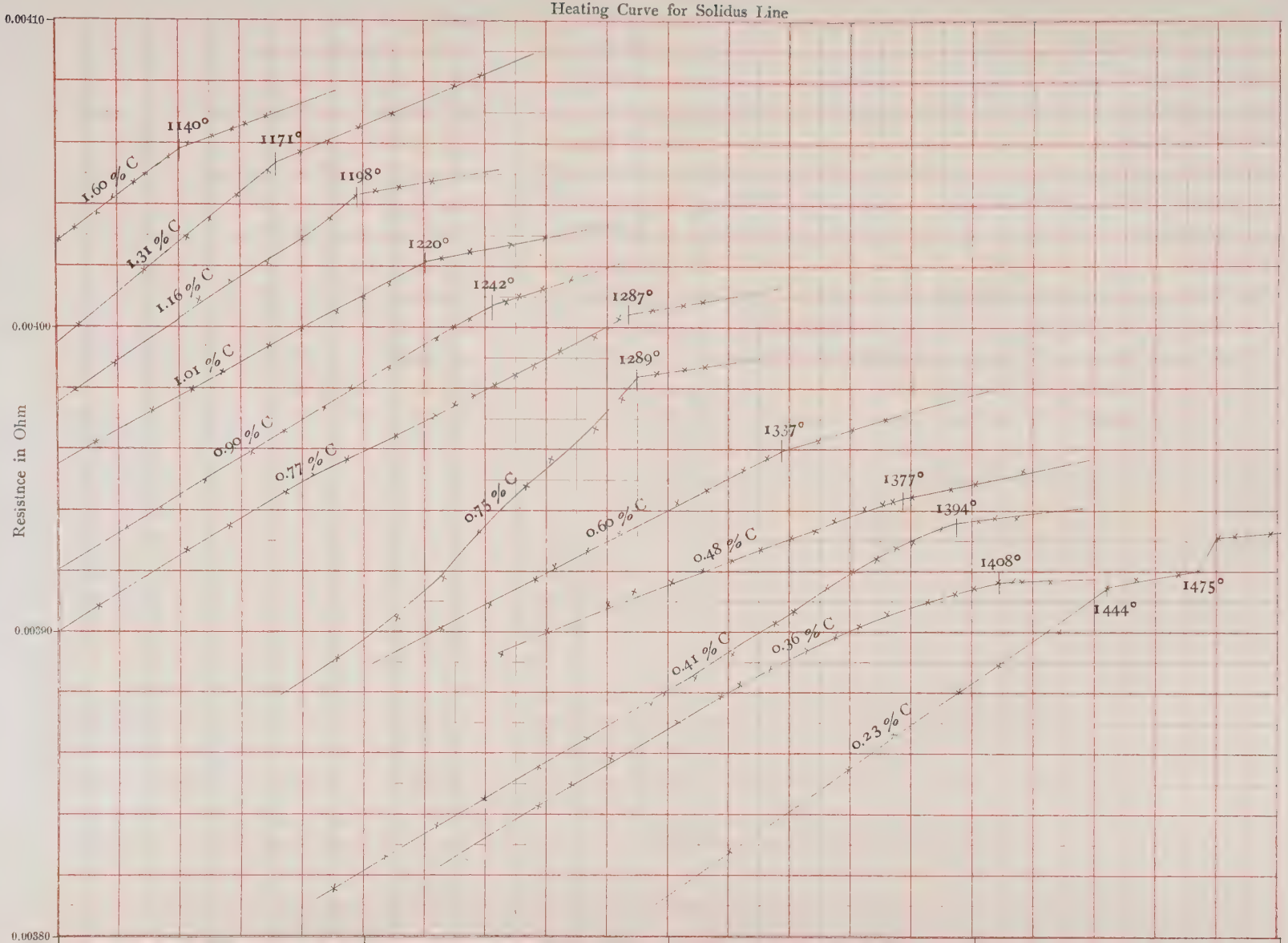

Pl. II.

Cooling Curves for Solubility Line

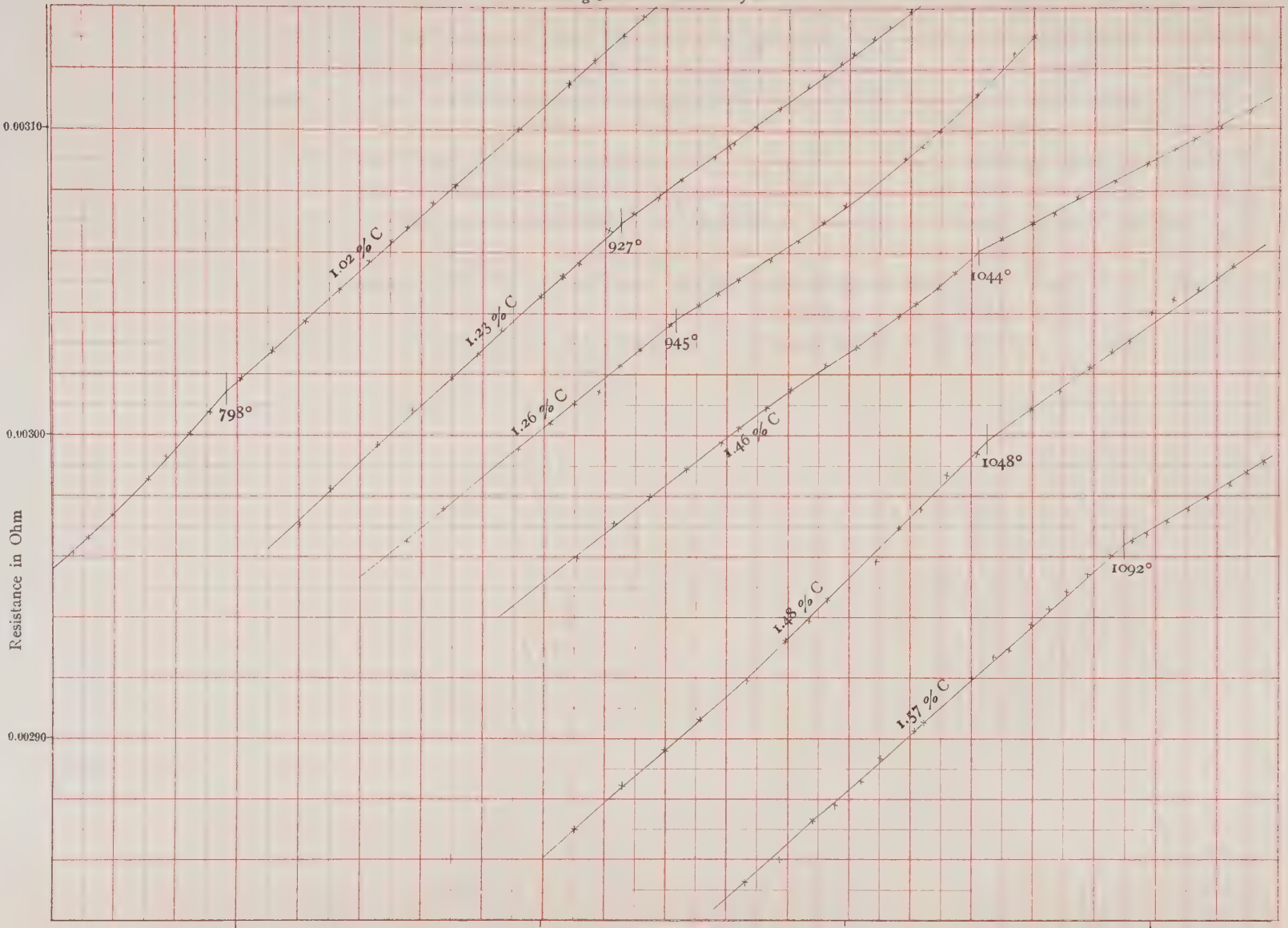

On the Widmannstätten Structure in Iron-Carbon and Iron-Nickel Alloys and in Meteorites.[1]

By

Tutom Kasé.

With 4 Plates.

CONTENTS.

§ 1. Introduction.
§ 2. The Widmannstätten Structure in Iron-Carbon Alloys.
§ 3. The Widmannstätten Structure in Iron-Nickel Alloys and Meteorites.
§ 4. Chemical Composition of Camacite and Taenite.
§ 5. Magnetic Analysis.
§ 6. Thermal Expansion.
§ 7. Hardness of the Camacite and Taenite.
§ 8. The Change of Microstructure of the Meteorite under Various Heat-treatment.
§ 9. The Effect of Impurities on the Widmannstätten Structure.
§ 10. The Effect of Heating to a Very High Temperature.
Summary.

§ 1. INTRODUCTION.

It is not only due to mere curiosity that many investigations have been hitherto made of the meteorites which have fallen from another part of the cosmos to our earth, but also to the mysterious character of the macroscopic Widmannstätten structure. Many investigators have tried to reproduce this characteristic structure with terrestrial iron-nickel alloys, but almost always in vain.

(1) The one hundred and twelveth report from the Research Institute for Iron, Steel and Other Metals.

The microscopic Widmannstätten structure in iron-carbon alloys, however, was obtained by Osmond,[1] Arnold and Mc. William,[2] and by N. Belaiew.[3] Also the occurrence of the characteristic structure in the meteorites or iron-nickel alloys was accounted for by Osmond and Roozeboom[4] by their diagram for iron-nickel alloys. Their conclusion was supported by C. Benedicks,[5] F. Rinne, etc., but disputed by W. Fraenkel and G. Tammann,[6] as the said structure in the meteorite is not a stable form at room temperature.

In a recent paper, Belaiew[7] discussed the same question both experimentally and theoretically, and attributed the origin of the Widmannstätten structure to the octahedral section of the face-centred cubic lattice.

In his recent papers,[8] he also remarked that the Widmannstätten structure belongs to one of a triad of secondary structures, the other two being the structure of the large crystals (dendrite) and the net work structure.

According to Prof. C. Benedicks,[9] the Widmannstätten structure exists in a substance, which crystallizes in the regular (tesseral) system and contains octahedrally orientated enclosures (lamellae); and this structure also occurs, when the enclosures of a regular substance are orientated according to planes other than octahedral; or it occurs in a substance belonging to any crystallographic system, with enclosures uniformly orientated according to crystallographic planes. N. Belaiew

(1) F. Osmond :— Sur la Crystallographie du Fer, Paris, (1900), 24. F. Osmond and G. Cartaud :— Metallographist, **4**, (1901), 119.

(2) J. O. Arnold, and A. Mc William :— Journ. Iron & Steel Inst., (1905), No. II, 35. Also, Nature, **71**, (1904), 32.

(3) N. T. Belaiew :— Thesis, (1909). Also, Rev. de Mét., **7**, (1910), 510.

(4) F. Osmond and G. Cartaud :— Rev. de Mét, **1**, (1904), 69.

(5) Rev. de Mét., **8**, Mé., (1911), 88.

(6) Zeit. anorg. Chem., **60**, (1908), 416.

(7) N. T. Belaiew :— Journ. Inst. Metals., **29**, (1), (1923), 379.

(8) N. T. Belaiew :— Am. Soc. Steel Treating, **5**, (1924), 6.
„ :— Minerallogical Magazine, **20**, (1924), 173–185.

(9) Journ. Inst. Metals, **12**, (2), (1914), 45.

who was drawing attention towards a more detailed investigation of this subject, seems to adopt the last view.

According to C. H. Desch,[1] the Widmannstätten structure, the twin, and martensite are apparently similar; the first, however, is produced by the crystallization of one constituent from the solid solution, the separation taking place by preference along certain planes. The second structure appears, on etching, as light and dark bands, showing differences of level due to orientation, and not difference of chemical composition. The third, the martensitic structure, is in character probably an intermediate form between the other two.

The present investigation is to reproduce the Widmannstätten structure in carbon and nickel steels and to explain the origin of the said structure in meteorites.

§ 2. IRON-CARBON ALLOYS.

According to Belaiew, the mechanism of the formation of the Widmannstätten structure in iron-carbon alloys is as follows:— Referring to Fig. 1, if an iron-carbon alloy containing less than 1.7 per cent of carbon is cooled from the melt, the primary crystallization begins along the curve *AB* and ends on the curve *AE*, forming γ-iron; on the curves *FG* and *GE*, the secondary crystallization begins to take place. If the cooling be slow, ferrite or cementite is forced to separate on the octahedral planes of the γ-iron, and to diffuse towards the grain boundaries resulting in an ordinary

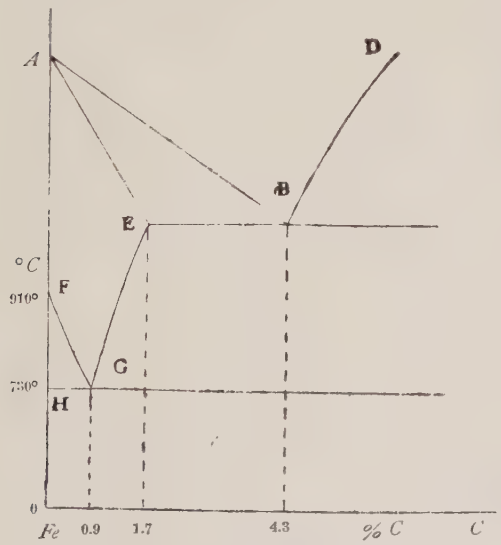

Fig. 1. Equilibrium Diagram of Iron-Carbon System.

(1) Journ. Inst. Metals, **12**, (2), (1914), 45.

network structure. If, however, the cooling be rapid, the ferrite or cementite is unable to reach the boundary surface, thus resulting in a Widmannstätten structure. The hypo-eutectoid steel gives the said structure with bands of ferrite, and the hyper-eutectoid steel the same structure with those of cementite.

The present writer tried to obtain the said structure with various steels by cooling under various conditions. The specimens were blocks about 8 mm^2 wide and 4 cm long, cut from forged Swedish carbon steel. The number of experiments was 45 ; the results are summarised below :—

(i) The hypo-eutectoid steel gives the Widmannstätten structure on annealing at a high temperature above 1000°C or on heating it to a partial melting and cooling in the air from a temperature above the Ar_3 point (see Photogr. 1). For the hyper-eutectoid steel the air cooling is to be made from a temperature above the A_{cm} point.

(ii) Quenching is not an effective method for obtaining the said structure in the carbon steel, as it gives the martensitic structure ; but in iron containing the least impurities, the same structure is obtained by quenching the specimen in water at a high temperature (above Ar_3).

(iii) By slow cooling through the A_1 transformation point, the characteristic structure is destroyed.

(iv) After chill casting, the Widmannstätten structure of free ferrite cannot be seen, but that of free cementite can clearly be observed (see Photogr. 2).

§ 3. THE WIDMANNSTÄTTEN STRUCTURE IN IRON-NICKEL ALLOYS AND METEORITES.

According to Osmond-Roozeboom's theory,[1] the formation of the Widmannstätten structures in meteorites is explained as follows :—

Meteorites are divided into two principal groups ; that is,

(1) C. Benedicks :— Rev. de Mét., Mé., (1911), 88. Also, F. Osmond and G. Cartaud :— Rev. de Mét., 1 Mé., (1904), 69.

1. Meteorites consisting of cubic iron, principally composed of camacite, its content of nickel being less than 6–7 per cent;

2. Meteorites consisting of octahedral iron, composed of camacite, taenite, and their conglomerate –plessite; its content of nickel being more than 6–7 per cent.

The nature of these constituents is explained by referring to Osmond-Roozeboom's equilibrium diagram, Fig. 2, and even now such a type of diagram is supported by certain scientists. In this diagram, the so-called camacite, taenite and plessite correspond to the composition of *E*, *F* and *B* respectively, though the line *FF'* is displaced to about 33 per cent content of nickel by Hansons.[1] It is, however, to be remarked that the curve *AB*, being the depression curve of the A_3 point due to nickel, does not actually terminate at the point *B*, but falls below room temperature, and curve *BCD* represents the magnetic transformation point, which is not really due to the change of phase, and consequently, should not be included in the equilibrium diagram, as in the case of the A_2 line in carbon steel. Hence the diagram as shown in Fig. 2, is certainly untenable.

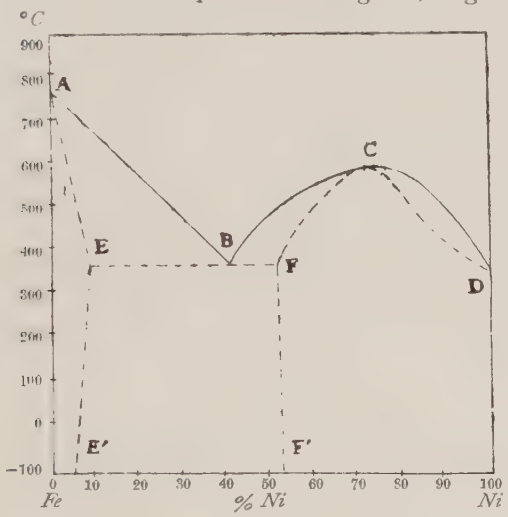

Fig. 2.

At any rate, Prof. C. Benedicks[2] obtained the Widmannstätten structure with an iron-nickel alloy containing about 12 per cent of nickel, by the thermit process and slow cooling. According to the view of the present writer, he might have obtained a better form of the said structure, if it had been quenched from a temperature above the Ar_3 point.

(1) D. Hanson and H. Hanson:— Journ. Iron & Steel Inst., (1920), No. II, 39.
(2) Rev. de Mét., 8, Mé, (1911), 85.

The view that the formation of this structure is due to the presence of two kinds of crystals in iron, was proposed by Guillet-Laumont,[1] in 1813. Afterwards, the investigation of meteorites by Sorby, Osmond, and others attracted the attention of many scientists and finally the origin of the structure was explained by Belaiew, as stated above.

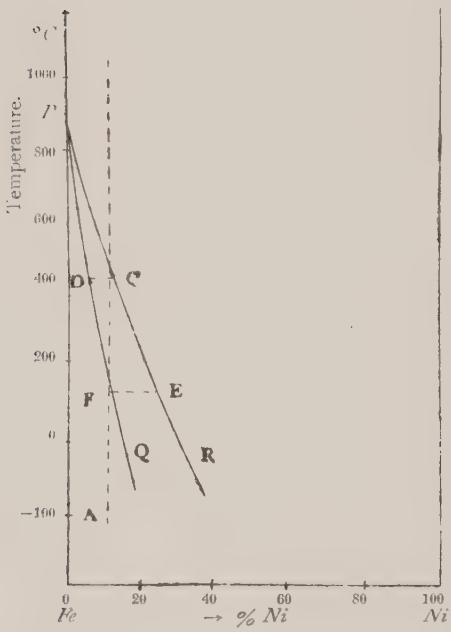

Fig. 3. Equilibrium Diagram of *Fe–Ni* System.

The present writer found that the Widmannstätten structure is obtained in iron-nickel alloys by a long annealing above the Ac_3 point and then quenching in water. Also, according to his investigation,[2] iron and nickel form a continuous series of solid solution, as shown in Fig. 3, and the formation of the Widmannstätten structure is accounted for as follows:—

In Fig. 3,[3] the line *PR* represents the beginning of the Ar_3 transformation, and *PQ*, its ending. When an alloy of a composition *A*, after being completely solidified, undergoes somewhat rapid cooling across the line *PR*, ferrite containing nickel precipitates from the austenitic cleavages, just as in the case of carbon steels across the Ar_3 line. Then the γ-solid solution *C* and the corresponding α-solid solution *D* coexist, both changing their compositions from *C* and *D* to *E* and *F* respectively. Thus the resulting alloy shows the Widmannstätten structure consisting of camacite and taenite, or of

(1) Cohen:— Meteoritenkunde, **1**, (1894), 41.

(2) Sci. Rep., **14**, (1925), 175.

(3) Recently R. Vogel (Zs. anorg. allg. Chem. 142, (1925) 193.) explained the mechanism of the formation of the meteoric structure as having a wider type of δ transformation range, the peritectic reaction being considdred to be continued to an alloy containing about 35 per cent of nickel. But such results do not agree with that of our repeated experiments.

α-and γ-solid solutions, the latter probably changing into the α-modification by further cooling. In most meteorites, however, which have various impurities, this relation may be somewhat modified. The most effective factor may be phosphorus, which will be discussed later.

The present writer investigated the occurrence of the structure in meteorites with a given specimen (Sacramento iron) and artificial iron-nickel alloys for reference. The chemical analysis, magnetic analysis, thermal expansion, and test of the microstructure after various kinds of heat-treatment were made, and they shed some light on the subject.

§ 4. CHEMICAL COMPOSITION OF THE CAMACITE AND TAENITE.

According to previous investigators,[1] the contents of elements in the camacite in certain meteorites are as shown in Table I.

TABLE I.

Contained Elements (%)	Meteorites			
	Bendegó	Cañon Diablo	Beacorsfield	Magura
Undissolved residue, Iron-nickel-phosphide.	0.33	0.35	0.4	0.58
Fe	93.01	94.09	92.62	93.01
Ni	6.22	5.51	6.81	6.25
Co	0.77		0.57	0.74
Cu	trace	0.05		
C		0.34		0.00
Total	100.00	100.00	100.00	100.00

For the analysis of taenite, the numerical data are as shown in Table II.

(1) Cohen :— Meteoritenkunde, Stuttgart, **2**, (1894), 214–220.

TABLE II.

Contained Elements (%)	Meteorites						
	Cañon Diablo	—	Bischtübe	Penkarring Rock	Beacons-field	Casas grandes	Kenton Co
Undissolved residue, iron-nickel-phosphide.	3.60	2.34	5.95–16.15	4.18	3.73	0.60	
Fe	68.13	63.55	61.89	61.87	50.73	83.28	80.3
Ni	30.85	34.65	36.95	} 38.13	47.80	} 16.68	} 19.6
Co	0.69	1.01	0.36		0.63		
Cu	0.33	0.30		trace	0.37	6.04	
C		0.49	0.80		0.47		
Total	100.00	100.00	100.00	100.00	100.00	100.00	99.9

From the above results, we see that taenite contains much more phosphide than camacite does. The apparent difference between the micro- and macro-structures of taenite and camaite may be due to the difference in chemical compostion. In the above results, it is doubtful whether there is any phosphorus dissolved in the camacite and taenite or not. It is suspected that the phosphorus in the camacite and taenite may have been lost in the course of the analysis.

The fact that the difference of nickel content in camacite and taenite is large, as we see in the above table, may also be explained by the Osmond-Roozeboom's diagram, Fig. 2; it is, however, very difficult to explain by the same diagram why there is so much discrepancy between the nickel contents in taenites, for the taenite must have a certain definite composition, provided the phase is one of the constituents in a eutectoid, such as cementite is in the pearlite of a carbon steel. Moreover a high percentage of nickel for taenite may probably be attributed to the action of phosphorus as taenite containing much nickel also contains high phosphorus. As is well known, nearly all meteorites contain

some phosphorus, existing as a compound (?) of iron, nickel and phosphorus, that is, schreibersite or rhabdite.[1] According to previous investigators, the compositions of the schreibersite and rhabdite are as follows :—[2]

TABLE III.

(a) Analysis of Schreibersite.

Meteorites	Contained elements in schreibersite.					
	P	Fe	Ni	Co	Total	Schreibersite (%) in Meteorites.
Zacatecas	16.10	72.62	10.72	0.56	100.00	3.06
Cranbourne	16.04	69.55	14.41		100.00	—
S. julião de Moreira	15.74	69.54	13.81	1.31	100.40	—
Kendal Co	15.70	62.00	21.92	0.38	100.00	—
Glorieta Mountain	15.49	63.36	19.63	1.23	99.71	4.70
Bischtübe	15.47	65.75	18.35	0.43	100.00	2.02
Toluca *	15.38	63.97	19.15	1.68	100.18	1.73
Hraschina	15.31	57.46	25.78	1.32	99.87	0.43
Toluca *	15.01	57.11	28.35	trace	100.47	1.23
Knoxville	14.86	56.53	28.02	0.28	99.69	—
Bohumilitz	14.76	69.45	15.79		100.00	1.29
Cambria	14.25	55.13	30.62		100.00	—
Elbogen	14.17	68.11	17.72		100.00	2.21
Cranbourne	13.51	56.12	29.18		98.81	0.93
Magura	13.23	50.95	34.05	0.59	98.82	2.09

(* By the different analysts.)

(1) Cohen :— Meteoritenkunde, **1**, l. c., 124.

The iron-nickel-phosphide in meteorites occurs in manifold form :— in crystals; in somewhat irregularly bordered tinsels, plates and grains; in large plate-shaped parts; in leaflets; in fine needles. In the latter form it is usually described as rhabdite or schreibersite.

(2) Cohen :— Meteoritenkunde, Stuttgart, **1**, l. c., 132–133.

(b) Analysis of Rhabdite.

Meteorites	Contained elements in Rhabdite.					
	P	Fe	Ni	Co	Total	Schreibersite (%) in Meteorites.
Santa Rosa, Coahuila	16.35	48.85	33.15	1.65	100.00	1.26
Lime Creek	15.49	51.10	32.99	0.42	100.00	1.19
Hex River Mounts	15.46	56.71	27.36	0.47	100.00	—
Sancha Estate Coahuila.	15.32	55.30	28.76	0.60	100.00	1.27
Bolson de Mapimi	15.03	52.54	31.71	0.72	100.00	1.26
Seelăsgen	13.61	49.76	36.17	0.46	100.00	0.44
Cranbourne	12.95	49.33	38.24		100.52	—

From the above table, we can easily deduce the empirical formula of rhabdite as Fe_2NiP, the content of cobalt being negligible. We see also that the content of iron in schreibersite is greater than that in rhabdite. At any rate the content of iron in rhabdite is about twice as much as that of nickel. Hence the nickel contents in taenites might have been dispersed by the agency of phosphorus, notwithstanding that they are either solid solutions or compounds. In fact we see in Table II that in the taenites containing much residual rhabdite, the content of nickel is high, while in those containing less undissolved residue, the nickel is very low, as seen in the two last columns. Further, Davison[1] gives the composition of the camacite and taenite from the Welland iron, found in Canada, as follows :—

Constituents	Camacite	Taenite
Fe (%)	93.09	74.78
Ni (%)	6.69	24.32
Co (%)	0.25	0.33
C (%)	0.02	0.50
Total	100.05	99.93

(1) Handbook and Descriptive Catalogue of the Meteorite Collections in the United States National Museum :— Washington, (1916), 9.

Thus the content of nickel in taenite is comparatively low as compared with the result of old analysis. The large difference in nickel content in taenite, however, are reasonably recognized by the equilibrium diagram proposed by the present writer;[1] according to the diagram the nickel content in taenite is probably 27 per cent at room temperature.

The composition of the meteorite[2] examined by the present writer was as follows:— 7.8 % *Ni*, 0.10 % *P*, 0.04 % *C*, a trace of silicium, a little of cobalt and none of manganese. We did not intend to make an exact chemical analysis, as the taenite bands in our specimen were very fine, and the whole mass was not large enough for a total analysis.

The contents of nickel in the various bands in the meteorite were examined. That is, the one face of the meteorite was etched with a 4 per cent nitric acid alcoholic solution, and the bands as shown in Photogr. 3 were shaved layer by layer. The samples thus prepared were analysed. The results show that for one coloured flake (camacite containing taenite), the content of nickel is 7.80 %, and for another coloured flake (another camacite without (?) taenite), 7.53 %. And for other two parts, we found, corresponding to the above two constituents, 7.82 and 7.46 % respectively. From this result alone we cannot find the conspicuous difference in the contents of nickel in camacite and taenite, though our sampling and chemical analysis were not very accurate.

---

(1) loc. cit.

(2) This sample is told as a fragment of the meteorite found at Sacramento Mountains, Eddy County, New Mexico. According to the Handbook of the Meteorite Collections (loc. cit.), the following data are already known:—

Weight of original mass, 237 kilograms.
Date of fall uncertain, perhaps 1876.
Analysis by J. E. Whitfield yielded:

	%
Iron (Fe)	91.39
Nickel (Ni)	7.86
Cobalt (Co).....	0.52
	99.77

§ 5. MAGNETIC ANALYSIS.

The present writer also made a magnetic analysis with a meteorite specimen of proper length (some fragments jointed together) to see whether it was composed of two phases differing greatly in the concentration of nickel. The curves are shown in Fig. 1 (a)–(b), Pl. I. Curve (a) is for the meteorits as received, and curve (b), for the same one annealed for a short time. In Fig. 1 (a), we see two distinct transformation points corresponcing to those of camacite and taenite, containing ca. 7 and 25 per cent of nickel respectively. The microstructure of the specimen once heated above 1000°C in the magnetic analysis became more homogeneous and granular than in its original state, but the taenite lamellae were not much affected by the heating.

Further, the iron-nickel alloy containing about 8 per cent of nickel, being annealed for many hours and quenched in water above the Ac_3 point, shows the Widmannstätten structure and its curve for magnetic analysis is as shown in Fig. 2 (a), Pl. I, and the repeated one in Fig. 2 (b), Pl. I.

In order to check the transformation points of the meteorite by means of the magnetic analysis, the present writer prepared the following specimens, being 5 mm. thick in total and each 7 cm. long ;

(i) a specimen consisting of two pieces of the alloys containing about 6 % and 30 % of Ni respectively, which were jointed together side by side. The latter corresponds to the supposed taenite, being about 10 per cent in weight f the total alloy (the average content of nickel being 7.8 %).

(ii) a specimen consisting of 7 % Ni and 25 % Ni alloys, the latter being about 4.5 per cent in weight of the total alloy (the average nickel content being 7.8 %).

The magnetic curves for these two specimens are shown in Fig. 3 (a), (b), Pl. I. Curve (a) does not resemble to that of the meteorite as seen in Fig. 1, Pl. I, while curve (b) is quite similar. The small changes

in the magnetic intensity at about 550°C and 90°C in curve (b) correspond to the $Ac_{3,2}$ and $Ar_{3,2}$ changes of an about 25 % Ni alloy.

Mr. S. Iguchi[1] considers that the Widmannstätten structure of a meteorite may be due to the separation of phosphide along the octahedral faces of the iron-nickel alloys. If this be true, the Widmannstätten structure of our specimen would show some symptom of the transformation of phosphide in magnetic analysis. Hence some iron-nickel alloys, containing about 8 per cent of nickel and 0.2–3.0 % of phosphorus were examined by magnetic analysis. From this experiment we found that the effect of a small quantity of phosphorus is not conspicuous, but the transformation of phosphide is clearly seen between 300° and 400°C, as shown in Fig. 4 (a), Pl. I, for an iron-nickel-phosphorus alloy containing 1.21 per cent of phosphorus. This curve is not similar to that of the meteorite. Also some iron-nickel alloys containing 25 per cent of nickel and 0.2–3.0 per cent of phosphorus were examined magnetically, but the effect of phosphorus was not clear in a low phosphorus alloy, as shown in Fig. 4 (b), Pl. I. Hence the phosphorus in the meteorite may have been contained as a solid solution, or as a compound too small in quantity to be detected by the magnetic analysis.

§6. THERMAL EXPANSION.

The present writer prepared from the meteorite a specimen, about 5 mm. thick and 3.3 cm. long, and examined its thermal expansion with a dilatometer,[2] from room temperature down to the temperature of liquid air, −190°C. The curve in Fig. 5, Pl. I, shows no abnormality, which is to be expected in iron-nickel alloys containing about 30 per cent of nickel. That is, if the taenite in our meteorite contains about 30 per cent of nickel, an abnormal expansion should be observable at a temperature below room temperature; but this was not the case.

Also the iron-nickel-phosphorus alloys containing about 8 per cent

(1) Suiyōkaishi, **4**, (1923), 558.
(2) T. Kasé:— Sci. Rep. **14**, (1925), 185.

of nickel and a varied content of phosporus were examined dilatometrically for the transformation of phosphide at 350°C. which is observable in the magnetic analysis. But there was no appreciable break in the corresponding temperature of the dilatometric curves. Hence the transformation at about 350°C is the magnetic change of the phosphide, not being a change of phase like the A_2 transformation in iron.

§7. HARDNESS OF CAMACITE AND TAENITE.

The given fragment of the meteorite was polished, and its scleroscope hardness was determined; afterwards the microstructures of the hammered points were also examined. The results are shown in Table IV.

TABLE IV.

Microstructure.	Scleroscope Hardness.	Mean Hardness (10 measurements)
Camacite.	18–33	24.6
Taenite.	20–33	22.9
Boundary of the Camacite and Taenite	26–32	28.4

According to the result, the hardness numbers are very irregular, owing to the heterogeneity of the alloy. But the mean values of hardness for the camacite and taenite are nearly equal; this is attributed to the fact that they are alloys containing about 7 per cent and 25 per cent of nickel respectively, as shown in the hardness-composition diagram of iron-nickel alloys, Fig. 4.

Fig. 4. Scleroscope Hardness Curve of *Fe–Ni* Alloys.

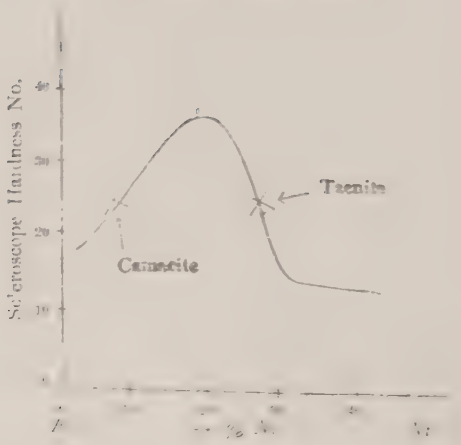

§ 8. THE CHANGE OF MICROSTRUCTURE IN THE METEORITE UNDER VARIOUS HEAT-TREATMENTS.

The present writer examined the microstructures in Sacramento meteorite under various heat-treatment. The results are shown in Table V.

TABLE V.

Number of experiments and heat-treatments.	Microstructure.(1)
No. 1. A fragment of the meteorite, as received.	The macrostructure is shown in Photogr. 3. Neumann bands are clearly visible in this specimen. (Photogr. 4). Some Neumann bands are broken at a grain boundary. (Photogr. 5).
No. 2. A small fragment. Annealed at 1000°C for 20 minutes, and cooled in the furnace.	Nearly all the Neumann bands have disappeared. (Photogr. 6).
No. 3. A small fragment. Annealed at 1050°–1100°C for 33 hours, and cooled in air.	The original structure was partially changed, becoming granular. (Photogr. 7).
No. 4. A small fragment. Annealed at 1000°–1100°C for 90 hours, and cooled in air.	The whole mass consists of large grains, being an almost homogeneous solid solution. (Photogr. 8).
No. 5. A small fragment. Annealed at 1000°–1100°C for 108 hours, and quenched in water.	The camacite lamellae or the incomplete Widmannstätten structure will developed. (Photogr. 9).
No. 6. A small fragment. Annealed at 550°–560°C for 46 hours, and cooled in air.	Some Neumann bands disappeared, and new grain boundaries have been produced. The Neumann bands seem to be in coincidence with the cleavages of the crystals.
No. 7. The same specimen, after above treatment, further annealed at 550°–560°C for 92 hours in total.	The Neumann bands have been spoiled, and have become more granular. (Photogr. 10).
No. 8. Further annealed at 550°–560°C for 110 hours in total, and cooled in air.	The Neumann bands have further decreased in number, and become more granular. (Photogr. 11).
No. 9. Further annealed at 550°–560°C for 191 hours in total, and cooled in air.	The structure is wholly granular. (Photogr. 12). The shape of the grains is somewhat different from that of Photogr. 8, suggesting that the former shows the ferrite grains, and the latter austenitic grains.

(1) 4% nitric acid alcoholic solution was used for the etching reagent.

Number of experiments and heat-treatments.	Microstructure.
No. 10. A fragment of the original meteorite. Immersed in liquid air.	No change in the structure, especially in the lamellae of the taenite, is observable.
No. 11. A polished fragment. Heated once to 900°C in a vacuum and cooled in the furnace.	The camacite is coloured blue to purple, while the taenite remains white as before. The macrostructure is similar to that in Photogr. 3.
No. 12. A small fragment. Heated to 1100°C, kept at that temperature for a moment, and then quenched in water.	The area of the taenite and plessite is shown in Photogr. 13. The broad boundaries of the taenite suggest its slight oxidation. Plessite has become homogeneous by diffusion.
No. 13. A small fragment. Heated to 1200°C kept at that temperature for 3 minutes, and then quenched in water.	Granulation proceeds in the camacite, and the taenite is dispersed by diffusion into the surrounding mass. (Photogr. 14).
No. 14. A small fragment. Heated to 1300°C, kept for 4 minutes, and quenched in water.	The areas of the taenite and plessite are remarkably decreased by diffusion, the surrounding mass being martensitic. (Photogr. 15).
No. 15. A small fragment. Heated to 1400°C, kept for 2 minutes, and quenched in water.	The grains have become very large, and the areas of the taenite and plessite have almost disappeared by diffusion. (Photogr. 16).
No. 16. A small fragment. Melted and cooled in the furnace.	A fine martensitic structure is observable, some impurities (?) being concentrated at the grain boundaries (Photogr. 17).

From the above experiments, the following conclusions may be drawn :—

(i) The annealing of the meteorite (7.8 percent of nickel) at high temperature and subsequent slow cooling give a homogeneous solid solution. Hence the Osmond-Roozeboom's theory with regard to the origin of the Widmannstätten structure, depending on the equilibrium diagrm as shown in Fig. 2, is untenable.

(ii) The Widmannstätten structure of the meteorite can be obtained by a rapid cooling after long annealing at a temperature above the Ac_3 point.

(iii) The Neumann bands are spoiled by annealing at 550°–560°C (below Ar_3), and mostly change into grain boundaries.

§9. THE EFFECT OF IMPURITIES ON THE WIDMANNSTÄTTEN STRUCTURE.

The present writer also investigated the effect of various elements on the said structure in iron-nickel alloys.

(i) Iron-nickel alloys containing about 8 per cent of nickel and various percentages of other elements, were annealed at 1000°C for 24 hours and quenched in water. The microstructure of these alloys and their composition are shown in Table VI. Here sign + means a well developed Widmannstätten structure and sign — its absence.

TABLE VI.

Alloys	Elements added (%) and Microstructures.									
Fe—Ni—Co	0.20	+	0.50	+	1.00	+	2.42	+	2.88	+
Fe—Fi—Cu	0.21	+	0.52	+	1.02	+	1.89	+	2.95	—
Fe—Ni—C	0.1	(+)	0.18	—	1.00	—	2.00	—	3.00	—
Fe—Ni—Mn	0.18	+	0.30	+	0.65	+	1.13	+	1.56	—
Fe—Ni—Cr	0.66	+	0.58	+	1.00	—	1.60	—	2.50	—
Fe—Ni—P	0.28	+	0.52	(+)	1.21	—	3.35	—	4.93	—
Fe—Ni—S	0.18	+	0.34	+	0.63	+	1.16	—	1.54	—

(ii) Iron-nickel alloys, containing ca. 25 per cent of nickel and various percentages of other elements, were treated as in the above case. The results are shown in Table VII.

TABLE VII.

Alloys	Elements added (%) and Microstructures.							
Fe—Ni—Co	0.87	+	1.11	+	2.56	(+)	3.61	(+)
Fe—Ni—Cu	0.60	+	1.00	+	2.27	(+)	3.78	(+)
Fe—Ni—C	0.45	—	0.57	—	2.00	—	3.00	—
Fe—Ni—Mn	0.28	+	0.72	+	1.00	+	2.41	—
Fe—Ni—Cr	0.50	+	1.00	+	1.33	+	3.82	—
Fe—Ni—P	0.26	+	0.59	+	2.34	—	4.80	—
Fe—Ni—S	0.32	+	0.66	—	1.69	—	4.12	—

(iii) Iron-nickel alloys, containing about 8 per cent of nickel, and

various percentages of other elements were annealed at 1000°C for 20 hours, and cooled in the furnace. The results are shown in Table VIII.

TABLE VIII.

Alloys	Elements added (%) and Microstructures.									
Fe–Ni–Co	0.20	–	0.50	–	1.00	–	2.42	–	2.88	–
Fe–Ni–Cu	0.21	–	0.52	–	1.02	–	1.89	–	2.95	–
Fe–Ni–C	0.10	–	0.18	–	1.00	–	2.00	–	3.00	–
Fe–Ni–Mn	0.18	–	0.30	–	0.65	–	1.13	–	1.56	–
Fe–Ni–Cr	0.58	–	0.66	–	1.00	–	1.60	–	2.50	–
Fe–Ni–P	0.28	–	0.52	–	1.21	–	3.35	–	4.93	–
Fe–Ni–S	0.18	–	0.34	–	0.63	–	1.16	–	1.54	–

(iv) Iron-nickel alloys containing ca. 25 per cent of nickel and various percentages of other elements were treated as in the last case. The results are shown in Table IX.

TABLE IX.

Alloys	Elements added (%) and Microstructures.							
Fe–Ni–Co	0.87	+	1.11	+	2.56	+	3.61	+
Fe–Ni–Cu	0.60	+	1.00	+	2.27	+	3.78	+
Fe–Ni–C	0.45	(+)	0.57	(+)	2.00	–	3.00	–
Fe–Ni–Mn	0.28	+	0.72	+	1.00	+	2.41	–
Fe–Ni–Cr	0.50	+	1.00	(+)	1.33	–	3.82	–
Fe–Ni–P	0.26	+	0.59	(+)	2.34	–	4.80	–
Fe–Ni–S	0.32	+	0.66	+	1.09	–	4.12	–

Thus from the above data, we conclude that the effect of these elements on the formation of the Widmannstätten structure is no adverse or at least unfavorable.

Next, the effect of carbon and phosphorus on the said structure

will be specially considered. Meteorites contain some carbon, sometimes in the form of diamonds. A small quantity of carbon in iron-nickel alloys gives a martensitic structure, but a large quantity of it gives the Widmannstätten structure by the separation of cementite along the cleavage planes of octahedral austenitic crystals. Photogr. 18 shows the structure of an alloy containing about 2.5 % Ni, and 2.34 %C; and Photogr. 19, that of one containing about 6 % Ni and 2.88 % C; both cooled from the melt in the furnace. The Widmannstätten or martensitic structure is observable. The cementite showing the appearance of the Widmannstätten structure is completely separated by the Acm line, but independent of the A_1 transformation. Of course, the cementite has little relation to the structure of the meteorite familiar to us.

The effect of phosphorus on the structure of the meteorite seems to be equal to that of carbon. Iron and phosphorus form a compound Fe_3P, which makes a eutectic with the saturated solid solution of iron and phosphorus, as shown in Fig. 5.(1) Also nickel and phosqhorus form a phosphide Ni_3P by a peritectic reaction and this has little solubility in nickel as shown in Fig. 6.(2)

Fig. 5.

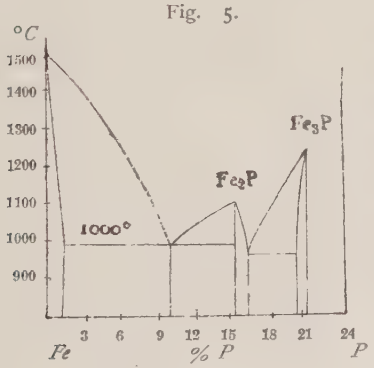

Fig. 6.

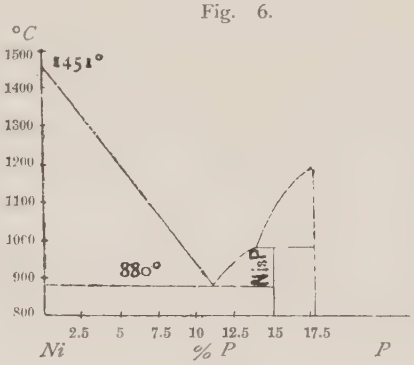

The meteorite contains iron, nickel and phosphorus. The former two form a solid solution, while phosphorus combines with the two elements, probably forming a double phosphide (?), and this compound

(1) E. Gercke :— Metall. **5**, (1908), 604.

(2) N. Konstantinow :— ZS. anorg. Chem., **60**, (1908), 410.

may form a eutectic with the solid solution. Also there is an expectation that the peritectic reaction in the ternary system will produce a structure similar to the plessite, for instance, as seen in the case of the Cu-Sn-Zn system.[1]

For reference, the present writer prepared an iron-phosphorus alloy, containing ca. 2 % P, and examined its microstructure; Photogr. 20 shows the structure of the alloy etched with Stead's reagent. The grain boundaries consist of phosphide. Photogr. 21 shows the microstructure of an iron-nickel-phosphorus alloy containing ca. 8 % Ni, and ca. 0.6 % P, cooled from the melt in the furnace, polished and etched with a 4 % nitric acid alcoholic solution. We see the phosphide separated in an irregular form in the martensitic matrix.

From Figs. 5 and 6, we can infer that the solubility of phosphorus in iron-nickel alloys gradually decreases with increasing nickel and decreasing temperature, the relation being similar to that of A_{cm} line in the iron-carbon alloy. It was not, however, a favourable factor, as to be expected, for obtaining the Widmannstätten structure in our experiments.

As remarked by J. S. Vanick[2] some meteorites contain well developed taenite while others do not. Also the camacite, taenite, and plessite in a certain meteorite, show almost no symptoms of the presence of phosphorus. A weak colouration by the boiling picrate solution was suspected to reveal the presence of cementite in the patches of plessite in the Casus Grandes meteorite. These results well coincide with that obtained by the present writer above referred to, that is, phosphorus and carbon are not necessarily favourable elements for obtaining the Widmannstätten structure.

§ 10. THE EFFECT OF HEATING TO A VERY HIGH TEMPERATURE.

(1) Hoyt:— Journ. Inst. Met., **1**, (1913), 235.
(2) Trans. Am. Soc. Steel Treat. **7**, (1925), 171.

Lastly the effect of exposing the alloys at very high temperature will be considered.

10 specimens of iron and nickel alloys containing various percentages of nickel (8–25 %) were melted (500 grs. each) and subjected to various treatments at high temperatures (solidifying range), such as made by R. Vogel, but the results were negative. These results do not support the recent theory put forward by R. Vogel.[1]

An alloy containing about 21.0 per cent of nickel was prepared by chill casting in an iron mould, 1 cm. thick and 20 cm. long. After being annealed for an interval of time, the alloy was placed in the alumina tube in the Tammann furnace, and heated gradually up to the melting point. When the lower part of the alloy was melted, the specimen ws taken out of the furnace, and cooled in the air. The microstructure of the part partially melted is shown in Photogr. 22. We see well developed thick bands showing the appearance of the Widmannstätten structure.

When an iron-nickel alloy containing 25 per cent of nickel is annealed at 1000°–1100°C for 24 hours and quenched in water, or slowly cooled in the furnace, a beautiful Widmannstätten structure is developed as shown in Photogr. 23.

About 500 grs. of an alloy having the same composition as Coopertown meteorites,[2] namely,

89.59 % Fe, 9.12 % Ni, 0.35 % Co, 0.04 % P, trace of Cu

was melted and kept at a temperature between the liquidus and solidus for about 2.5 hours, slowly cooled to about 1400°C, and quenched in water. Its macrostructure is shown in Photogr. 24, and its microstructure in Photogr. 25. The Widmannstätten structure is clearly seen in the latter, while in the former the structure is not observable. The microstructure is very similar to the macrostructure of certain meteorites.

---

(1) loc. cit.

(2) Handbook and Descriptive Catalogue of the Meteorite Collections in the United States National Museum. Washington, (1916), 58.

On the whole, a long exposure to a very high temperature, as well as a moderate rapid cooling, is quite effective in obtaining the well developed Widmannstätten structure, usually observable in meteorites.

SUMMARY.

The present investigation may be summarised as follows:—

1. The conditions for developing the Widmannstätten structure in iron-carbon alloys were determined. Moderate rapid cooling from high temperature (above A_3 or Acm) gives the said structure, but slow cooling does not.

2. Some experiments were also made with a fragment of a meteorite (Sacramento iron), and it was found that annealing at a temperature above the Ac_3 point effaces the said structure. The Neumann bands are spoiled by a long annealing at a temperature even below the Ar_3 point (550°–560°C).

3. The formation of the said structure in meteorites may be probably due to a long exposure to a very high temperature and subsequent rapid cooling.

In conclusion, the present writer wishes to express his cordial thanks for the kind guidance of Professor K. Honda, and for the useful advice of Professors T. Murakami and T. Ishiwara.

Plate I.

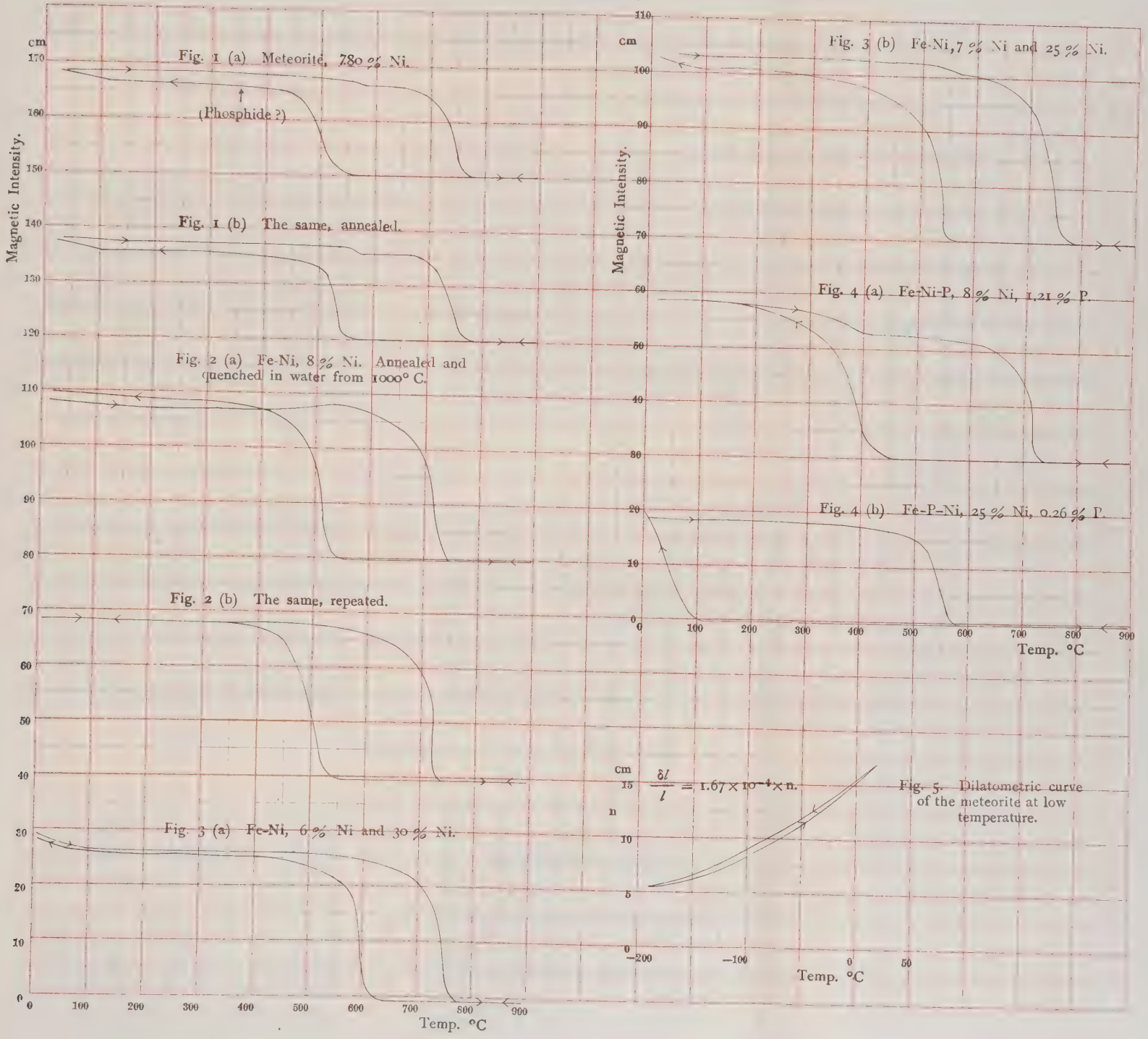
Fig. 1 (a) Meteorite, 7.80 % Ni.
(Phosphide ?)
Fig. 1 (b) The same, annealed.
Fig. 2 (a) Fe-Ni, 8 % Ni. Annealed and quenched in water from 1000° C.
Fig. 2 (b) The same, repeated.
Fig. 3 (a) Fe-Ni, 6 % Ni and 30 % Ni.
Fig. 3 (b) Fe-Ni, 7 % Ni and 25 % Ni.
Fig. 4 (a) Fe-Ni-P, 8 % Ni, 1.21 % P.
Fig. 4 (b) Fe-P-Ni, 25 % Ni, 0.26 % P.
Magnetic Intensity.
cm
Temp. °C
$\frac{\delta l}{l} = 1.67 \times 10^{-4} \times n.$
n
Fig. 5. Dilatometric curve of the meteorite at low temperature.

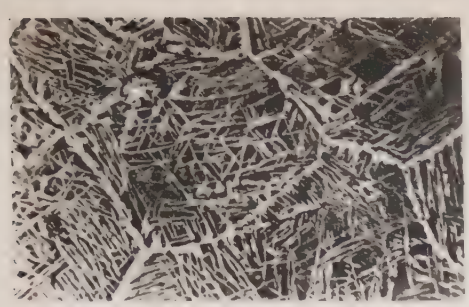

Photogr. 1. Fe–C, 0.5%C, overheated and cooled in the air. ×40.

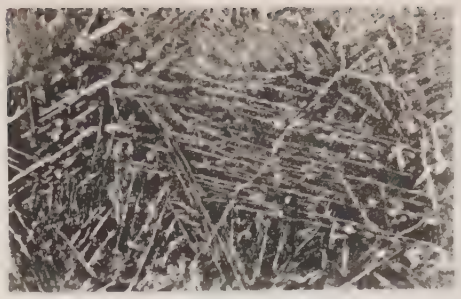

Photogr. 2. Fe–C, 1.08%C, chill cast- ×100.

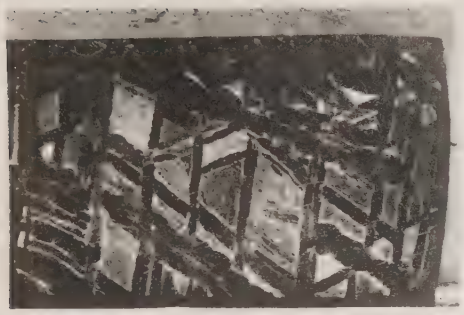

Photogr. 3. The macrostructure of the etched slice of the meteorite. ×1.6

Photogr. 4. Microstructure of the meteorite. ×100

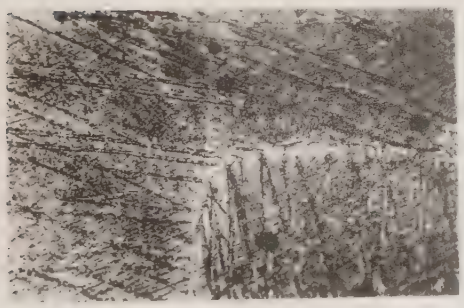

Photogr. 5. Another part of the meteorite. ×100

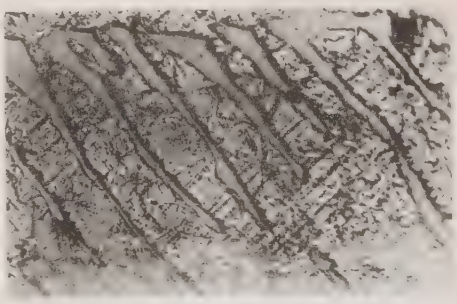

Photogr. 6. The meteorite, annealed at 1000°C, for 20 minutes. ×100

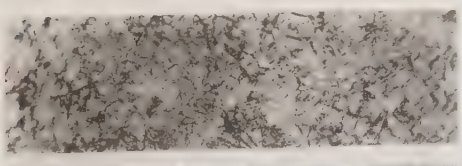

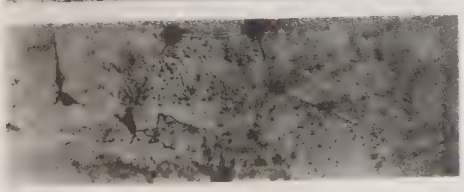

Photogr. 7. The meteorite, annealed at 1050°–1100°C for 33 hours. ×100.

Photogr. 8. The meteorite, annealed at 1000°–110.°C for 99 hours, and cooled in

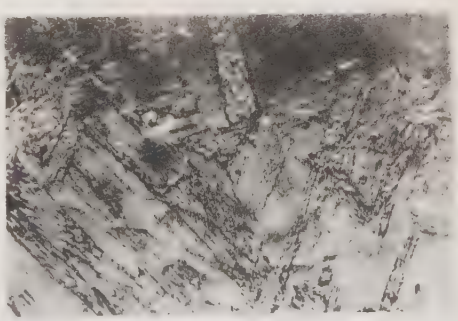

Photogr. 9. The meteorite, annealed at 1000°–110.°C for 108 hours, and quenched in water. ×100

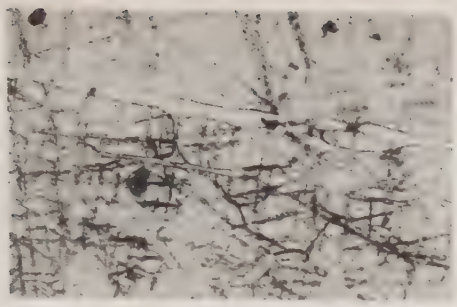

Photogr. 10. The meteorite, annealed at 550°–560°C for 92 hours. ×100

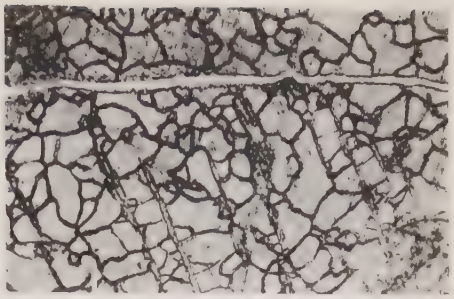

Photogr. 11. The meteorite, annealed at 550°–560°C for 110 hours. ×100

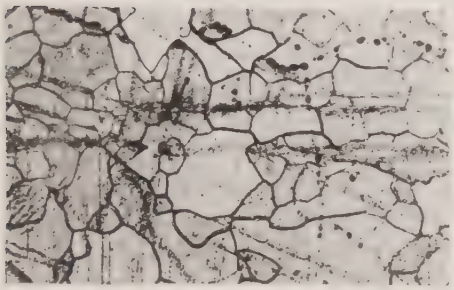

Photogr. 12. The meteorite, annealed at 550°–560°C for 191 hours. ×100

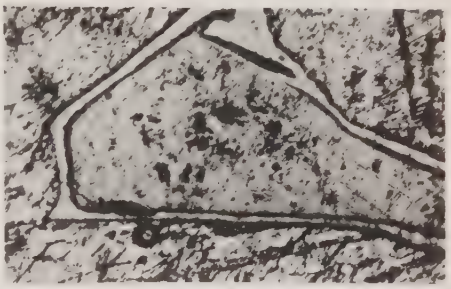

Photogr. 13. The meteorite, heated at 1100°C for a moment, and quenched in water ×100

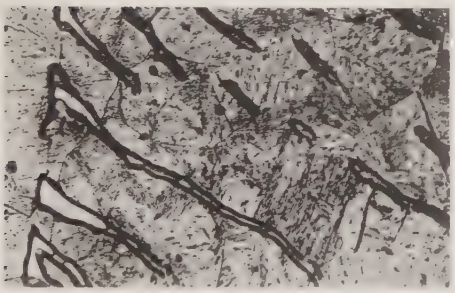

Photogr. 14. The meteorite, heated at 1200°C for 3 minutes, and quenched in water. ×100

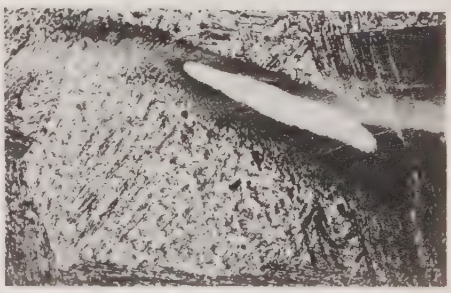

Photogr. 15. The meteorite, heated at 1300°C for 4 minutes, and quenched in water. ×100

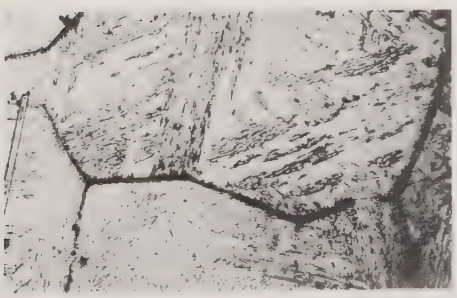

Photogr. 16. The meteorite, heated at 1400°C for 2 minutes, and quenched in water. ×100

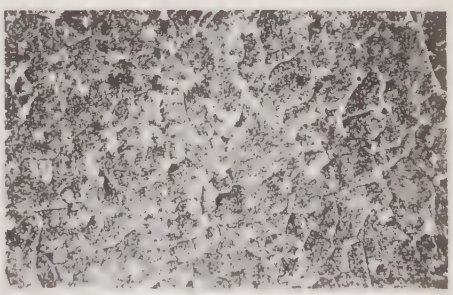

Photogr. 17. The meteorite, melted and cooled in the furnace. ×100

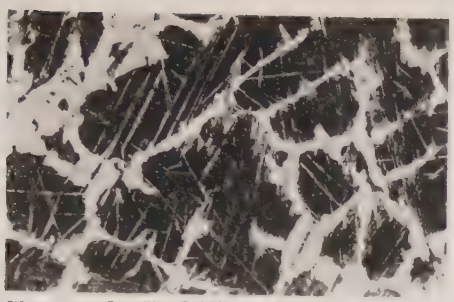

Photogr. 18. Fe–C–Ni, 2.5% Ni, 2.34%C, cooled from the melt in the furnace. ×100

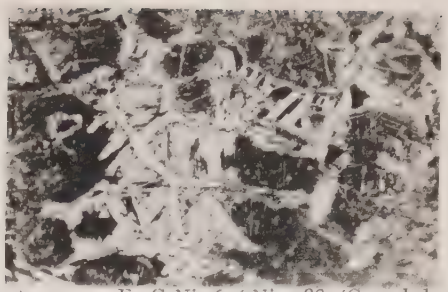

Photogr. 19. Fe–C–Ni, 6% Ni, 2.88%C, cooled from the melt in the furnace. ×100

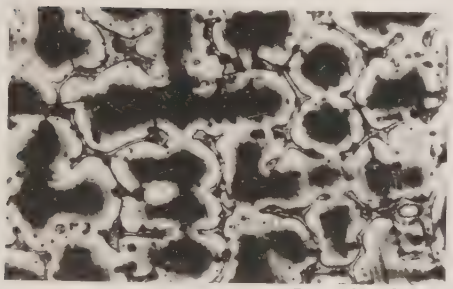

Photogr. 20. Fe–P, ca. 2% P, cooled from the melt in the furnace. ×100

Photogr. 21. Fe–Ni–P, 8% Ni, ca. 0.6% P, cooled from the melt in the furnace. ×100

Photogr. 22. Fe–Ni, 21.0% Ni, overheated. ×100

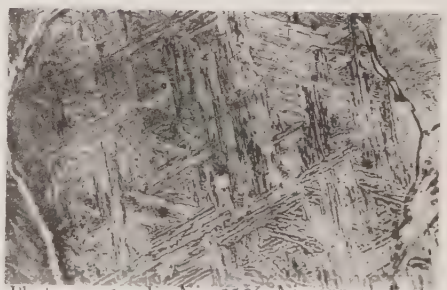

Photogr. 23. Fe–Ni, 25% Ni, annealed at 1000°C for 24 hours. ×100

Photogr. 24. Similar alloy as Coopertown Meteorite, cooled from the melt and quenched in water from 1400°. ×2

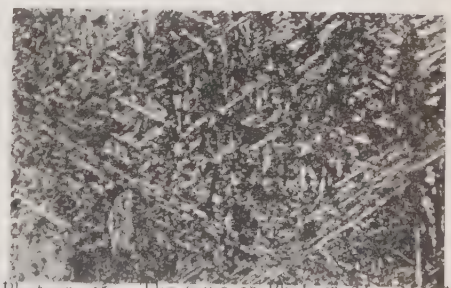

Photogr. 25. The same as Photogr. 24. ×100

On the Determination of the Heat of Precipitation of Cementite from α and β Martensites.[1]

By

Masuo Kawakami.

With two plates.

§ 1. INTRODUCTION.

According to the theory of quenching put forward by Prof. K. Honda,[2] the Ar_1 transformation in carbon steel is a stepped transformation, that is,

Austenite → martensite → pearlite (troostite, sorbite).

Above the A_1 point, a steel is in an austenite state, being then a solid solution of carbon in γ iron. During a slow cooling, at the Ar_1 point, iron atoms in γ iron first take a configuration of α iron, the carbon being still present as a solid solution, that is, austenite changes into martensite; at the next moment, the carbon is precipitated from the α solid solution as cementite, the martensite thus changing into troostite (the same substance as pearlite), i.e. a mixture of cementite and α iron. The result in this case is the same as the change: austenite → pearlite. If, however, the austenitic steel be cooled very rapidly, as it does on being quenched in water, the first change from austenite to martensite is

(1) The One hundred and thirteenth report from the Research Institute for Iron, Steel and Other Metals.

(2) Sci. Rep., **8**, (1919), 181.

so far retarded that it begins to take place at about 300° and when this change is completed, the specimen is nearly at room temperature; then the next change, that is, the precipitation of carbide from the martensite cannot progress; because, at room temperature, the viscosity is too great for the occurrence of this change. Consequently, by quenching the martensitic steel is obtained at room temperature. It is a metastable phase changing extremely slowly into pearlite (troostite) even at room temperature. The precipitation of carbide from the martensite takes place more rapidly, as the temperature rises.

This decomposition of the martensite is indicated by the change in physical properties, such as, the decrease of the electric resistance, the evolution of heat, the diminution of volume, the increase of magnetic property, etc. Consequently by following the change in these physical properties due to a gradual heatig, we can find the temperature of decomposition, the velocity of decomposition or its amount. For example, if a quenched steel is slowly heated and its change in length is measured by means of a dilatometer[1] such as is constantly used in our laboratory, curves, as shown in Fig. 1a, Pl. 1, are obtained. In these curves we observe two contractions taking place at about 170° and 340°. Experimetally it is confirmed that there is the following relation between the specific volumes of austenite, martensite and pearlite,

$$v_{aust.} < v_{pearl.} < v_{mart.}$$

Hence these contractions must correspond to the precipitation of cementite at the two temperatures.

As this precipitation takes place at two different temperatures, it is necessary to distinguish two kinds of martensite, α and β. α martensite is etched more easily than β martensite, and the separation of cementite from the former is easier than that from the latter. Some metallurgists[2] attribute the second contraction to the decomposition of austenite, but this view is not correct; for, the change of austenite into pearlite must

(1) Sci. Rep., 8, (1919), 182.

(2) B. D. Enland, Jour. of Iron and steel inst., No. 1, (1925), etc.

be accompanied by an increase of volume ($v_{aust} < v_{pearl}$), but, actually, there is in this case a decrease in volume. In the case of high carbon steels, a small abnormal expansion is observable from 200° to 300°. This is probably due to the change of the arrested austenite into martensite, which above 300° is in turn readily changed into pearlite.

The precipitation of cementite from the martensite is accompanied by the evolution of heat, that is, of the latent heat of precipitation or dissolution. Mr. N. Yamada[1] measured the total heat of precipitation of cementite from both α and β martensites, by letting martensitic steels fall into a high temperature calorimeter at about 400°, and found that the latent heat is proportional to the content of carbon, being 6.57 cal. per one gram of eutectoid steel.

The object of the present investigation was to measure the heats of precipitation of α and β martensites separately.

§ 2. APPARATUS.

The apparatus used in the present investigation is almost the same as that of Mr. Yamada;[2] the heat quantity is calorimetrically measured by the method of mixture. Fig. 1 shows an arrangement of the calorimetry. The calorimeter is a cylindrical vessel A made of silver. The thermostat is a large cylindrical vessel B, within which a small vessel C made of a sheet iron is placed. The calorimeter is contained in this vessel with a space of one cm between the walls of the vessel and the container. The space is kept from varying in extent by a mica ring D on the side-wall of the calorimeter, and by a quartz cone E on the bottom of it, so as to minimize the loss of heat by conduction.

As we see from the curves in Fig. 1, Pl. 1, α martensite is tempered at below 200°, and β martensite at above 300°, these temperatures depending more or less on the rate of heating. Hence in order to measure the heat of precipitation of α martensite alone, a much lower

(1) Sci. Rep., **10**, (1922), 455.
(2) Sci. Rep., **10**, (1922), 453.

temperature of the calorimeter-bath, say 200°, is required than that used by Mr. Yamada, and therefore about 100 grams of a eutectic mixture of potassium, sodium and lithium nitrates were used as a calorimeter liquid, its melting point being 128°.

Fig. 1.

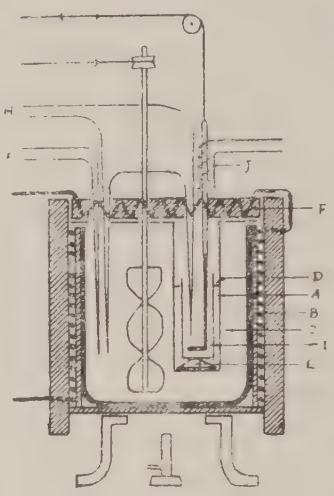

The side-wall of the thermostat is wound round with a nichrome wire and the cover *F* also contains a nichrom wire spiral, both heated by an electric current; the bottom is also heated by a Bunsen burner. A mixture of the above nitrates was used as the thermostat liquid, which melts at 180°. The liquid in these vessels is constantly stirred to maintain a uniform temperature throughout them. The temperature of the thermostat was measured by a couple *G* of copper-constantan, and maintained at a constant temperature between 210° and 250°, by regulating the electric current and the Bunsen burner. The temperature of the calorimeter was measured by a differential thermocouple of copper-constantan *H*, two junctions of which are placed between the calorimeter and the thermostat, and by a mirror-galvanometer placed in the circuit of the differential thermocouple. The galvanometer was calibrated, and a deflection of one cm of the reflection of the scale corresponded to 0.0225°. In Mr. Yamada's experiment the stirrer in the calorimeter was made of glass, but in my case,—glass being affected by lithium nitrate and becoming brittle,—it was replaced by one made of copper *I*, but in order to minimize the loss of heat through the stirrer-rod, its upper portion was connected with a porcelein tube *J*. When the stirrer moved up and down, cold air took part in the motion, entering into the calorimeter, and moreover, the liqnid in the calorimeter adhering to the stirrer was solidified, and such an accident may cause an error in the measurement of the heat of dissolution. In order to avoid these accidents, the upper part of the stirrer lying outside the

calorimeter liquid was heated by a suitable electric current through a nichrome coil wound round the supporting rod, so as to keep the temperature of the rod the same as that of the calorimeter.

§ 3. METHOD OF MEASUREMENT.

Specimens in the form of cylinder, 7 cm long and 0.5 cm thick, containing various amounts of carbon were subjected to experiments. Before quenching these specimens, a turbid solution of silicate "tonoko" was painted on their surface and dried; they were then dipped in molten lead and held at a hardening temperature for over twenty minutes and then quenched in cold water. If the tonoko was not used, small lead grains were often found, after quenching, adhering to the surface of the specimens; these portions had a troostic, but not a martensitic structure. The tonoko, however, prevented the adhering of lead grains to the surface of the specimens, thus resulting in the martensitic structure without any trace of troostite.

The measurement was conducted as follows. When the thermostat was kept at a constant temperature and the deflection of the mirror-galvanometer became stationary for a sufficiently long time, a quenched specimen was let fall into the calorimeter and the reading of the scale observed every thirty seconds for about ten minutes. Then the same process was repeated with a tempered specimen of exactly the same dimentions and made of the same material. During the observation, the stirrers were constantly working. An example of such a measurement is given in Figs. 2 a, b; the first curve shows the temperature-time curve for the quenched specimen, and the second that of the annealed specimen. If the strait portion of the curves is produced backwards, it cuts the axis of temperature at a point which corresponds to the temperature of the calorimeter raised, when there is no loss of heat outwards. We see that the first curve for the quenched specimen, after reaching a minimum, rapidly rise for about two minutes and then continues almost linearly. The first rapid rise of temperature is due to the latent heat of precipitation of cementite from α martensite. Hence this

phenomenon is not observable in the case of the tempered specimen.

It was necessary to confirm the supposition that during the tempering in the calorimeter-bath, α martensite was all decomposed, but β martensite not at all. For this purpose, the dilatometric method was made use of; that is, a quenched specimen was kept at 200° for various intervals of time and then after cooling, examined dilatometrically. The specimen heated for 0.5 and 1.5 minutes showed the presence of a little α martensite, but that heated for 2.5 minutes showed no trace of α martensite, as seen in Fig. 2, Pl. 1. The presence of β martensite could be seen with the magnitude unaltered as before tempering. Hence for the precipitation of cementite from martensite, 2 minutes were sufficient. The tempering at 400° for a few minutes causes the decomposition of both α and β martensites.

The analysis of the specimens is given in table. 1.

TABLE 1.

Specimen No.	C (%)	Si (%)	Mn (%)	P (%)	S (%)
1	0.30	0.30	0.43	0.021	0.021
2	0.39	0.32	0.30	0.026	0.021
3	0.50	0.31	0.20	0.029	0.022
4	0.72	0.27	0.20	0.028	0.017
5	0.95	0.27	0.19	0.027	0.017
6	1.03	0.08	0.21	0.027	0.020
7	1.12	0.28	0.19	0.031	0.017
8	1.32	0.24	0.18	0.026	0.020

The water equivalent of the calorimeter was determined by using pure copper and silver having the same form as the specimen. At 200°, the water equivalent was found respectively to be 47.4 and 46.3 grams for copper and silver, their mean value being 46.85 grams. At 400°, it was 49.2 and 47.9 grams for copper and silver respectively, the mean being 48.55 grams.

§ 4. RESULTS OF EXPERIMENT.

The calcuration of the heat of precipitation from the observed data is as follows:—

m = mass of a specimen,

w = water equivalent of the calorimeter,

$q_{t_1-t_2}$ = heat required to raise one gram of the specimen from t_2 to t_1,

$c_{t_1-t_2}$ = mean specific heat of pearlite (troostite, sorbite) between t_1 and t_2,

dt = fall of temperature in the calorimeter,

then we have

$$mq_{t_1-t_2} = wdt, \text{ or } q_{t_1-t_2} = \frac{w}{m}dt;$$

but as $q_{t_1-10} = q_{t_1-t_2} + q_{t_2-10} = q_{t_1-t_2} + c_{10}\ (t_2-10)$,

$$\therefore\quad q_{t_1-10} = \frac{wdt}{m} + c_{10}\ (t_2-10),$$

and finally we get

$$c_{t_1-10} = \frac{wdt}{m(t_1-10)} + c_{10}\frac{t_2-10}{t_1-10}.$$

The last term is very small, so that c_{10} may be assumed to be 0.12 for all specimens without introducing any sensible error. The results of the measurements are given in the following tables; the results at 200°, i.e. those for α martensite, are found in table 2, and the results at 400°, i.e. those for α and β martensites, in table 3. From these results, the relations of $q_{t_1\ t_2}$ to t_1 for quenched and tempered steels are obtained and given, pair by pair, in Figs. 4 and 5, Pl. II, from which the difference in heat, Q, per gram of the specimen in each case, is obtained and given in the same tables. If the observed points for one set of experiments happen to lie close togather, or if there is only a single observed point, the direction of the lines is indeterminate; in such cases, the lines are drawn parallel to those of the other sets of experiments.

The relation of this difference in heat to carbon content is given in Fig. 2. The curves in Fig. 2 show that the heat of precipitation of cementite from α martensite is proportional to the carbon content and about one-half as large as that of cementite from β martensite. This

TABLE 2.

Specimen No.	Quenched specimen			Tempered specimen			Diff. of calories Q.
	Quenched temp.	t_1	q_{t_1-10}	t_1	q_{t_1-10}	c_{t_1-10}	
No. 1. (0.30%C)	1250°C	211.1	22.40	219.4	24.83	0.1203	1.5
	1250°C	221.8	23.97	212.3	24.00	0.1192	
No. 2. (0.39%C)	980°C	234.8	24.37	232.0	26.11	0.1187	2.2
	980°C	232.0	24.20	230.0	26.00	0.1182	
No. 3. (0.50%C)	950°C	244.5	24.89	243.8	28.03	0.1219	2.6
	950°C	242.8	25.33	242.8	27.40	0.1196	
	960°C	243.1	25.11	243.1	27.55	0.1207	
	960°C	241.8	24.36	240.4	26.91	0.1173	
No. 4. (0.72%C)	860°C	235.7	23.28	235.4	26.20	0.1162	3.0
	875°C	225.2	22.00	227.3	24.82	0.1142	
	860°C	233.7	22.78	235.4	25.92	0.1163	
No. 5. (0.95%C)	860°C	238.7	23.97	238.7	27.54	0.1192	3.4
	850°C	239.1	23.23	239.1	27.31	0.1182	
	850°C	238.7	23.67	239.1	27.32	0.1179	
	900°C	226.0	22.32	222.8	25.03	0.1192	
	900°C	226.6	22.11	238.8	27.70	0.1204	
	900°C	238.4	23.85	239.4	27.76	0.1210	
No. 6. (1.03%C)	860°C	241.8	23.87	241.4	27.67	0.1215	4.4
	860°C	238.7	22.74	238.7	27.50	0.1220	
	900°C	226.3	21.24	238.3	27.06	0.1203	
	900°C	232.1	21.26	226.3	25.57	0.1196	
No. 7. (1.12%C)	1000°C	238.7	23.14	237.0	27.10	0.1209	4.4
	1000°C	242.8	23.79	244.4	28.79	0.1220	
	1020°C	242.4	24.09	241.1	27.81	0.1217	
	1020°C	234.8	22.20	234.8	26.75	0.1221	
No. 8. (1.32%C)	1110°C	251.8	24.02	252.1	29.20	0.1226	5.0
	1110°C	250.5	23.88	251.8	29.24	0.1230	
	1110°C	249.8	23.90	248.8	28.77	0.1218	

TABLE 3.

Specimen No.	Quenched specimen			Tempered specimen			Diff. of calories Q.
	Quenched temp.	t_1	q_{t_1-10}	t_1	q_{t_1-10}	c_{t_1-10}	
No. 4. (0.72%C)	860°C	402.5	39.76	395.4	47.88	0.1247	9.4
No. 5. (0.95%C)	900°C	414.2	41.01	399.8	49.61	0.1267	10.5
	900°C	398.5	38.78	391.5	47.56	0.1261	
No. 6. (1.03%C)	930°C	409.2	39.84	397.2	49.81	0.1306	11.1
	930°C	400.8	39.22	388.2	49.07	0.1280	
No. 7. (1.12%C)	1020°C	388.1	36.54	387.1	48.61	0.1295	12.2
No. 8. (1.32%C)	1110°C	405.5	36.88	401.1	52.13	0.1341	15.0
	1110°C	399.1	37.32	390.1	50.11	0.1330	

Fig. 2.

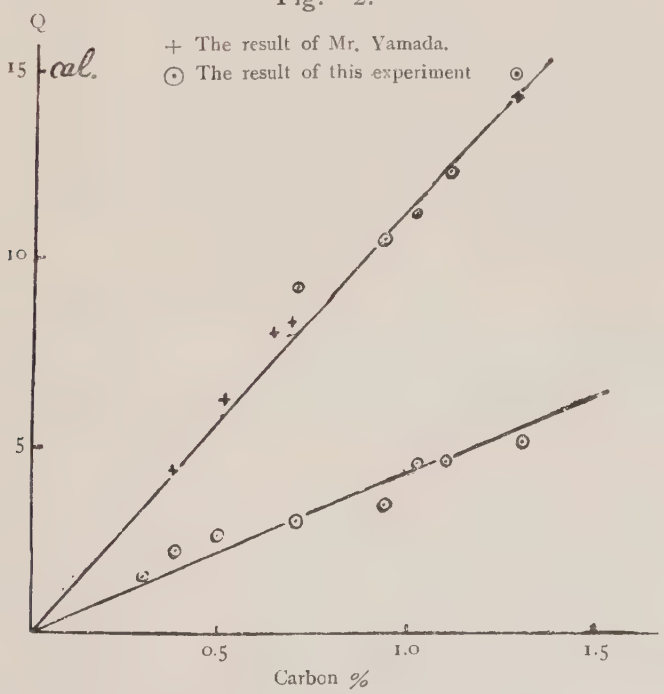

agrees with the fact that α martensite is more unstable than β martensite. The result for the sum of the heats of precipitation of α and β martensites almost coinsides with that as found by Mr. Yamada.

It was also confirmed dilatometrically that during the tempering of the specimen at about 230° in the calorimeter for several minutes, α martensite is completely decomposed, but β martensite not at all. Fig. 1b, Pl. 1, shows the dilatation curve for a specimen for which the heat of precipitation of cementite from α martensite has been measured. It does not show any contraction at 170° corresponding to the decomposition of α martensite.

From the present experiment, we may conclude that both α and β martensites are definite phases, though they are not quite stable, but not an indefinite substance consisting of a mixture of pearlite and cementite, as is often believed by some metallurgists.

CONCLUSION:

1. The heat of precipitation of cementite from α martensite was measured for eight kinds of carbon steel, whose carbon contents vary from 0.30 to 1.32%. The heat increases proportionally to the content of carbon; the heat for eutectoid steel is 3.7 calories per gram.

2. The heat of precipitation of cementite from both α and β martensites was also measured for five kinds of carbon steel, the result of which almost coincides with that of Mr. Yamada.

3. The heat of precipitation of cementite from α martensite is about half as large as that from β martensite.

In conclusion, I wish to express my cordial thanks to Professor K. Honda, under whose direction the present investigation was carried out.

Pl. I.

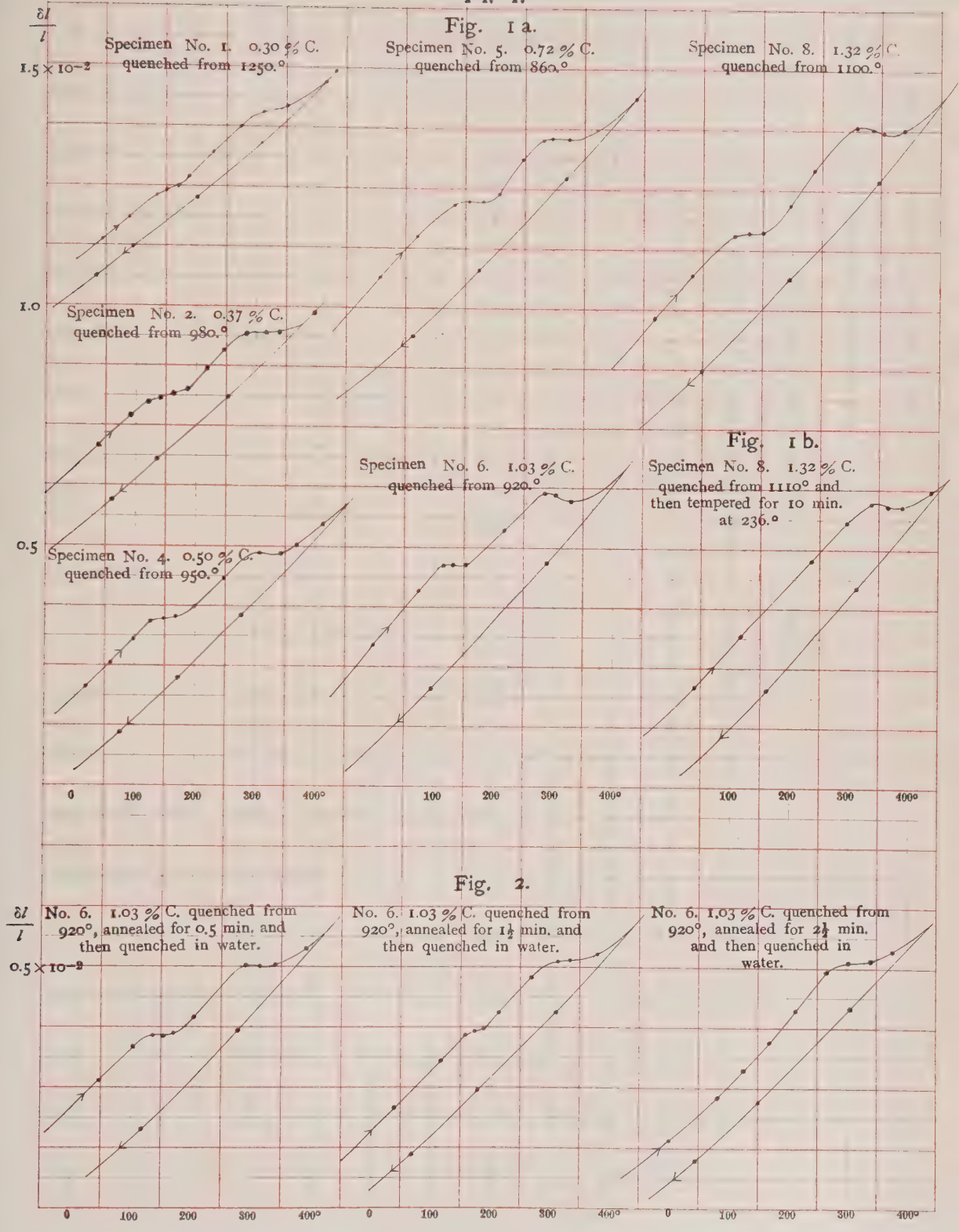
Fig. 1 a.
δl/l
1.5 × 10⁻²
1.0
0.5
Specimen No. 1. 0.30 % C. quenched from 1250.°
Specimen No. 2. 0.37 % C. quenched from 980.°
Specimen No. 4. 0.50 % C. quenched from 950.°
Specimen No. 5. 0.72 % C. quenched from 860.°
Specimen No. 6. 1.03 % C. quenched from 920.°
Specimen No. 8. 1.32 % C. quenched from 1100.°
Fig. 1 b.
Specimen No. 8. 1.32 % C. quenched from 1110° and then tempered for 10 min. at 236.°
0
100
200
300
400°

Fig. 2.
δl/l
0.5 × 10⁻²
No. 6. 1.03 % C. quenched from 920°, annealed for 0.5 min. and then quenched in water.
No. 6. 1.03 % C. quenched from 920°, annealed for 1½ min. and then quenched in water.
No. 6. 1.03 % C. quenched from 920°, annealed for 2½ min. and then quenched in water.
0
100
200
300
400°

Pl. II.

Fig. 3 a.

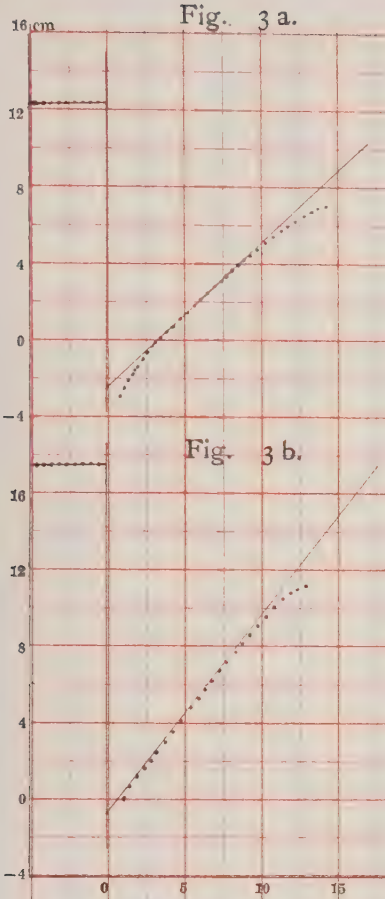

Fig. 3 b.

Fig. 4.

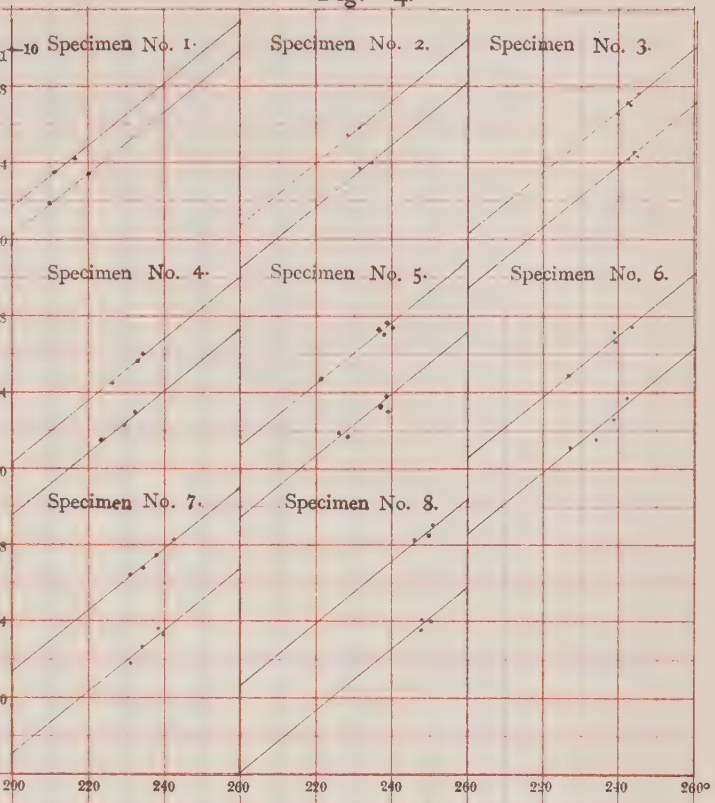

Fig. 5.

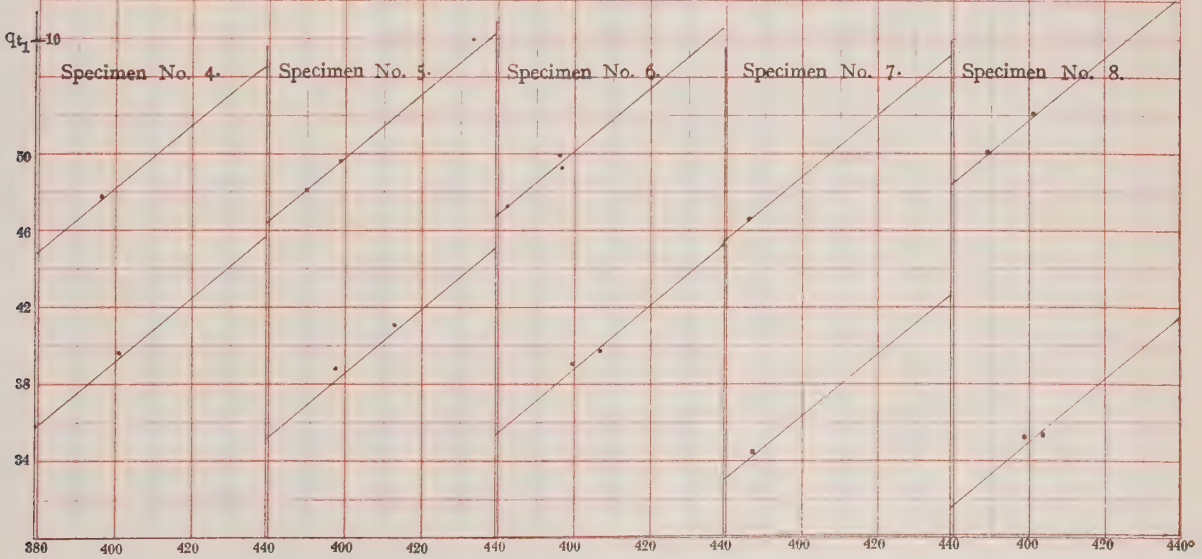

The Use of Liquid Amalgams in Volumetric Analysis, Part III. Determination of Phosphoric Acid by Using Lead Amalgam.[1]

By

Kinichi Someya.

INTRODUCTION.

The molybdate-permanganate method is one of the most important ones for the determination of phosphorus in iron and steel. While as to the composition of the ammoniumphosphomolybdate, precipitated under various conditions ordinarily prescribed for the determination of phosphorus in iron and its ores, it has been shown by the very careful work of Blair and Whitefield[2] that it is of the definite composition expressed by $24\,MoO_3.\,P_2O_5.\,3\,(NH_4)_2\,O.2\,H_2O$, the stage of oxidation to which the various methods of reduction carry differs considerably according as the methods are different, and in many cases complete reduction to the tervalent codition is a matter of considerable difficulty.

Jones,[3] who first determined molybdenum by his reductor method, considered that the reduction goes to the condition represented by the formula $Mo_{12}\,O_{19}$, the same degree of reduction that Wernke[4] obtained with zinc and sulphuric acid in a closed flask. Doolittle and Eavenson[5]

(1) The one hundred and fourteenth report from the Research Institube for Iron, Steel and Other Metals.

(2) Journ. Amer. Chem. Soc., **17**, (1895), 747.

(3) Amer. Inst. Min. Eng., **18**, (1889), 705.

(4) Zeitschr. analyt. Chem.. **14**, (1875), 1.

(5) Journ. Amer. Chem. Soc., **16**, (1894), 234.

found that, by varying the strength of the acid and the speed at which the molybdenum was passed through, different degrees of reduction might be obtained, but none were lower than that represented by the formula $Mo_{12}O_{19}$. Blair and Whitefield[1] were unable to press the reduction below the condition represented by the symbol $Mo_{24}O_{37}$. Miller and Frank[2] in repeating the experiments of Blair and Whiefield obtained in general the same results, though by taking extraordinary precautions they were able to get a reduction to a little below the midway point between the conditions represented by the symbols $Mo_{24}O_{37}$ and Mo_2O_3. W. A. Noyes and Frohman,[3] by taking pains to replace the air in the reductor flask by carbon dioxide, were able to obtain a reduction to the form of Mo_2O_3. Rundall[4] obtained the same result by receiving the reduced solution in a ferric alum solution.

The widely extended use of this method, however, is probably due to the fact that, despite some uncertainty as to the nature of the oxide produced by reduction, this possibly being different for different workers, by working always in exactly the same way, the reduction is uniform, and hence the titration is a reliable method for estimating the yellow precipitate and indirectly the amount of phosphorus. But it would scarcely need mention that it would be best and safest if we could find a method which ensures us an easy and complete reduction to the tervalent condition.

Before we go into the description of a new method for the phosphorus determination, it would be desirable to give a brief remark on the method of amalgam reduction. The general advantages of the amalgam method can hardly be a matter of dispute. Nakazono[4] showed in his zinc amalgam reduction of the molybdic anhydride that for complete reduction of 0.2 g. of the oxide with 200 g. of amalgam, only a few

(1) l. c.

(2) Journ. Amer. Chem. Soc. **25**, (1903), 919.

(3) Ibid., **16**, (1894), 553.

(3) Amer. Journ. Sc. **24**, [4], (1907), 313.

(4) Journ. Jap. Chem. Soc., **42**, (1921), 526. For apparatus and methods the reader may also be referred to the first communication, Sc. Rep. **14**, (1925), 47.

minutes' vigorous shaking was necessary. In reality, far less time would be required to attain this stage of oxidation, but the trace of oxygen which may be present in the amalgam apparatus, oxidizes back the lower oxide, and the above time of shaking seemed to have been necessary even to eliminate this trace of oxygen. After this elimination of the oxygen, there is absolutely no chance of air accidentally entering the reduction flask, and hence the titration could be carried out with the greatest ease. The advantage of his amalgam apparatus was even more apparent in the case of the reduction of vanadium oxide.[1] While Gooch and Gilbert[2] found it very difficult to keep the divalent vanadium solution as such, and had to have recourse to the registration of the reduction by a ferric alum solution or to the oxidation of the salt to its tetravalent stage by means of silver sulphate, in this case, it was found that the reduction to the divalent stage occurred after 3 minutes' shaking, and moreover the reduced divalent solution kept well as such and could be directly titrated by permanganate with the greatest ease.

Knowing the great advantages of the method of amalgam reduction, it seems but natural that one should try to apply this also to the molybdate method for phosphorus. When first zinc or cadmium amalgam was chosen as the reducing agent, an unexpected difficulty presented itself in the reduction of the phosphomolybdate precipitate, which was later found to be attributable to the presence of a phosphate ion by a few qualitative experiments. Since in his second communication[3] the writer has described some applications of lead amalgam, and showed in it that in a strongly hydrochloric acid solution the amalgam reduces an ammonium molybdate solution to its tervalent condition with great ease, he tried to see whether the use of this amalgam in the present case could remove the disturbing influence of phosphate ion. Experiments showed this to be the case, and under suitable and easily realized conditions the reduction goes also with the greatest ease and rapidity. Consequently

(1) Journ. Jap. Chem. Soc., **42,** (1921), 761; Sc. Rep. **14,** (1925), 109.
(2) Zeitschr. anorg. Chem., **35,** (1903), 420.
(3) Sc. Rep., **14,** (1925), Vol. 3., 235; Zeitschr. anorg. Chem., **145,** (1925), 168.

the use of lead amalgam led us to the working out of an accurate and useful method for the determination of phosphoric acid.

EXPERIMENTAL PART.

To confirm the result obtained by Nakazono,[1] the writer heated pure ammonium molybdate in a platinum dish to convert it into the anhydride, which was now spread over in a porcelain boat and introduced into a porcelain tube and electrically heated to 900° C. The glistening sublimed needles which attached to the mouths of the tube were collected, a definite portion of which substance was taken and dissolved in ammonia or purest sodium carbonate, acidified with 10–25 cc. of sulphuric acid (1 : 1) for 100 cc. of the total volume, reduced with zinc amalgam, and was titrated with decinormal potassium permanganate. The titrating solution was standardized against purest dry sodium oxalate. The results are seen in the following table. They show that Nakazono's result was fully confirmed, i. e., that they stand in good agreement with the weighed molybdenum trioxide when we assume that it is reduced completely to the tervalent condition.

TABLE I.

No.	MoO_3 weighed, g.	$KMnO_4$ req., cc.	MoO_3 found, g.	MoO_3 error, g.
1.	0.1500	31.31	0.1501	0.0001
2.	0.1500	31.32	0.1501	0.0001
3.	0.2000	41.76	0.2002	0.0002
4.	0.2000	41.69	0.1999	0.0001
5.	0.2000	41.74	0.2001	0.0001
6.	0.2000	41.70	0.1999	0.0001
7.	0.1000	20.87	0.1000	0.0000
8.	0.1000	20.86	0.1000	0.0000
9.	0.1000	20.87	0.1000	0.0000

Normality of $KMNnO_4$, 0.09987 *n*.

(1) Journ. Jap. Chem. Soc., **42**, (1921), 526.

Further, the same molybdenum trioxide was now dissolved in pure sodium carbonate or ammonia, and the resulting solution was evaporated to a small volume, to which was added a large quantity (ca. 100 cc.) of conc. hydrochloric acid, and was reduced with lead amalgam. The reduction of this phosphate-free salt solution went also very smoothly in a short time. The titration was done in the presence of conc. manganous sulphate and 5 cc. of conc. phosphoric acid. The result is shown in Table II, which convinces us of the same thing as in case of zinc amalgam.

TABLE II.

Nr.	MoO_3 weighed, g.	$KMnO_4$ req., cc.	MoO_3 found, g.	MoO_3 error, g.
1.	0.2000	41.67	0.2002	0.0002
2.	0.2000	41.66	0.2002	0.0002
3.	0.2000	41.62	0.2000	0.0000
4.	0.2000	41.59	0.1998	0.0002
5.	0.2000	41,60	0.1999	0.0001
6.	0.2000	41.64	0.2001	0.0001
7.	0.2000	41.64	0.2001	0.0001
8.	0.1000	20.79	0.0999	0.0001
9.	0.1000	20.82	0.1000	0.0000
10.	0.1000	20.80	0.0999	0.0001

Normality of $KMnO_4$, 0.1001 *n*.

As material for phosphorus determination, disodium hydrogen phosphate from Merck (c. p.) was used. 5 or 10 cc. of 0.2 % solution was used in each determination. The determination of the phosphorus content was made by the method due to Woy,[1] in which the precipitate obtained according to his procedure was filtered in a Munroe crucible, washed with an ammonium nitrate solution and ignited gently to a homogeneous dark green colour.

(1) Chem. Ztg., **21**, (1897), 442.

In the volumetric process, the ammoniumphosphomolybdate obtained in this way was washed twice with acid ammonium sulphate (which was made by adding 25 cc. of conc. sulphuric acid and 15 cc. of conc. ammonia to a suitable quantity of water, which was then diluted to 1 litre.), filtered also in a Munroe crucible, and then was dissolved in a small quantity of ammonia. The resulting solution was transferred to a concial beaker and was evaporated to a small volume. Then it was washed into the amalgam reductor and was, adding 50 cc. of conc. hydrochloric acid, reduced with lead amalgam. The reduction was in every case very rapid and smooth, only about half a minute's vigorous shaking being sufficient for the completion of the reduction. The beautiful reddish brown solution which resulted was titrated in just the same way as above. The following table contains the analytical data.

TABLE III.

No.	P_2O_5 taken, g.	P_2O_5 found, g.	P_2O_5 error, g.
1.	0.011907	0.011894	0.000013
2.	0.011907	0.011897	0.000010
3.	0.011907	0.011900	0.000007
4.	0.005954	0.005954	0.000007
5.	0.005954	0.005951	0.000003
6.	0.005954	0.005946	0.000008
7.	0.005954	0.005937	0.000017

In the table, the "P_2O_5 found" was calculated on the assumption that for every 1 molecule of P_2O_5 there are always 24 molecules of MoO_3, and moreover, that the molybdenum is completely reduced to the tervalent condition. The result is very satisfactory.

An important point to be noticed in this connection is the question whether the manganous sulphate can completely prevent the action of permanganate on hydrochloric acid. In the above experiments the sodium oxalate and the molybdenum trioxide employed were purest

possible stuffs and the experiment was made immediately after the standardization of the titrating solution. The carbonic acid gas for filling the reductor flask was generated from Kahlbaum's purest sodium carbonate and pure hydrochloric acid. Unfortunately, in the case of the permanganate titration of a concentrated hydrochloric acid solution, the end point is not so sharp as in the case of the sulphuric acid solution. However, very near the calculated end point the green colour due to molybdenum fades and the solution becomes a little brownish, and with one excess drop of permanganate, the brown colour becomes much more intense. This phenomenon takes place always without any retardation, so that the writer is convinced that at least with a decinormal standard solution, no appreciable error of this kind is introduced. In the case of the phosphomolybdate reduction the end coloration can be recognized without any such difficulty.

For trial a standard sample from the U. S. Bureau of Standards was analysed for phosphorus by applying this method. The phosphoric acid was thrown down as in the ordinary way as ammoniumphosphomolybdate, and after careful washing with acid ammonium sulphate, was estimated as above. The result is also quite satisfactory.

TABLE IV.

"No. 34. Acid open hearth".	Certificate value, 0.095 % P.	
Analysed by the writer:		
Found	1.	0.0947 % P
	2.	0.0962
	3.	0.0952
Mean		0.0954

SUMMARY.

The method of lead amalgam reduction applied to the ammonium-phasphomolybdate precipitate led us to a new accurate method for the estimation of phosphoric acid.

In conclusion the writer wishes to express his heartfelt thanks to Prof. Honda who showed a great interest in and gave constant encouragement to his work; to Prof. Kobayashi for his useful suggestions, and also to Mr. T. Kato for his enthusiastic help during the course of his work.

June, 1925.

Ein Verfahren zur Bestimmung von Vanadium in Ferrovanadium.[1]

Von

Kinichi Someya.

I. EINLEITUNG.

Mit der Entwicklung der Industrie der Sonderstähle hat das Problem der Bestimmung von Vanadium in Ferrovanadium und verschiedenen Sonderstählen bei den analytischen Chemikern viel Aufmerksamkeit erregt, und eine beträchtliche Zahl von Berichten über diese Aufgabe ist erschienen, und dementsprechend sind die Analysemethoden auch sehr mannigfaltig. Alle diese Methoden untereinander zu vergleichen, zu prüfen und zu beurteilen ist für den Verfasser geradezu unmöglich. Glücklicherweise hat J. R. Cain[2] am U. S. Bureau of Standards gemeinsam mit seinen Mitarbeitern diese Methoden nachgeprüft und gezeigt, dass sie alle mehr oder weniger fehlerhaft sind. Er arbeitete schliesslich eine Ersatzmethode aus, durch welche, wie er meinte, alle vorherigen Nachteile überwunden seien. Auch Verfasser richtete auf dieses Problem seine Aufmerksamkeit und prüfte einige bisher gebräuchliche Methoden. Jedoch fand er, gewisse Schwierigkeiten, überreinstimmende Werte zu erlangen, und hoffte, irgendeine Metdode zu finden, welche einfacher und leichter ausführbar ist. Bei der oben erwähnten Cain'schen Methode ist es nötig, den grösseren Teil von Vanadium und Chrom vom

(1) The one hundred and fifteenth report from the Research Institute for Iron, Steel and Other Metals.

(2) Journ. Ind. Eng. Chem., **3**, (1911), 476.

Eisen unter Verwendung von Kadmiumkarbonat zu trennen, und ferner durch Elektrolyse die zurückgebliebene kleine Menge von Eisen und alles Chrom vollkommen vom Vanadium zu trennen. Der Verfasser begann seine Untersuchung in der Hoffnung, wenn möglich, auch auf diese Trennung vom Vanadium verzichten zu können, und führte seine Versuche erst in beschränkter Umfang nur mit einem Gemisch von Eisen und Vanadium aus.

Da die Erfahrungen des Verfassers, wenigstens bezüglich der Analyse von Ferrovanadium, die von Cain gezeigten Nachteile aller im allgemeinen gebrauchten Methoden bestätigen, so scheint es wünschenswert, jene Kritik, sofern sie mit des Verfassers Problem verknüpft ist, aus Cains Abhandlung zu zitieren, um dadurch klar zu stellen, in welchem Verhältnis die vom Verfasser vorgeschlagene Methode zu den bisherigen steht, und auch, welche Schwierigkeiten durch sie überwunden werden und welche nicht. Cain teilt diese Methoden in drei Klassen und zeigt sowohl die allgemeinen als auch die jene einzelnen Klasse anhaftenden Fehlern.

"I. Klasse A. Die meisten Teile von Eisen werden durch Aether aus der salzsauren Lösung der Probe extrahiert, während das Vanadium in der wässrigen Schicht zurückbleibt. Der letztere Teil wird mehrmals mit Salzsäure eingedampft, um ihn zur vierwertigen Stufe zu reduzieren. Schliesslich wird die Lösung mit Schwefelsäure zu starkem Rauch eingedampft und die resultierende Lösung mit Kaliumpermanganat titriert.

Bei diesem Verfahren, (1) bei der Aetherextraktion, wird fast stets eine kleine Menge Eisen zum Ferrozustand reduziert. Dies wird nicht stets bei der vor der Titration nötigen Operation wiederoxydiert, sondern bleibt in der wässrigen Schicht von Vanadium zurück; und wenn diese Tatsache nicht in Erwägung gezogen wird, so tritt es auch als Vanadium bei der Berechnung auf. (2) Der Aether oder die in ihm enthaltenen Verunreinigungen reagieren beim Eindampfen der Lösung mit Schwefelsäure und bilden eine Kaliumpermanganat angreifende Substanz. Oftmals wird die Bildung von solchen Stoffen beobachtet, welche Kohlenstoff

enthalten oder nach Schwefligesäure riechen. (3) Es muss vermieden werden, Schwefelsäure vor vollstädiger Reduktion durch mehrmaliges Eindampfen mit Salzsäure hinzufügen, denn die Reduktion wird dadurch leicht unvollkommen gemacht; (4) Aber auch zu langes Eindampfen mit starker Schwefelsäure oder seine Ausführung bei zu hoher Temperatur muss vermieden werden, denn im Gegensatz zum vorigen Falle, findet auch Oxydation des vierwertigen Vanadiums ins fünfwertige statt.[1]

Klasse B. Vanadium wird durch direktes Titrieren mittelst Ferrosulfat oder Zurücktitrieren seines Ueberschusses mit Kaliumbichromat bestimmt. In diesem Falle kommt Kaliumfericyanid als äusserer oder innerer Indikator in Anwendung.

Dieses Verfahren, welches die Anwendung von Ferricyanid als Indikator für Ferrosalze bedingt, muss notwendigerweise sehr unsichere Ergebnisse liefern, doch liegt dies in den Verhältnissen, unter denen die Bestimmung auszuführen ist. Der Grund hierfür ist sehr einleuchtend, wenn man sich daran errinnert, dass Ferricyanid in saurer Lösung vierwertiges Vanadium schnell in die fünfwertige Form überfuhrt, wobei gleichzeitig Ferrocyanid gebildet wird. Dies reagiert sofort mit Ferrieisen, so dass in den Tropfen des Indikators eine Blaufärbung vorhanden ist, sobald eine merkliche Menge von Vanadium reduziert ist, und lange bevor die durch einen Ueberschuss der Titerlösung bedingte Farbe auftritt. Dementsprechend müssen solche Verfahren, wenn sie überhaupt anwendbar sind, Ergebnisse liefern, die von dem Arbeitenden abhängen, und willkürliche und unsichere Korrektionsfaktoren bedingen. Man findet bei Ermittelung von Vanadium in reiner Vanadiumsalzlösung bei dieser Methode schon grosse Schwierigkeiten, und diese Tatsache ist auch schon von anderen Autoren[2] als Cain beschrieben worden.

Klasse C. Der grössere Teil von Eisen wird wie bei Klasse A mit Aether extrahiert, die Salzsäure durch Salpetersäure ersetzt und das Vanadium von Chrom und Eisen etc. getrennt durch Eingiessen in

(1) Koppel & Behrend, Zeitschr. anorg. Chem., **35**, (1903), 156.

(2) Campagne, Ber., **36**, (1903) 3164; Brearly & Ibotson, Analysis of Steel Works Materials, p. 89.

siedende Aetznatronlösung. Das Vanadium geht ins Filtrat, welches man mit Merkuronitrat oder Bleinitrat fällt, während man letzte Bestimmung entweder volumetrisch oder gravimetrisch ausführt.

Bei dieser Methode wird mehr oder weniger Vanadium beim Eingiessen der Lösung in Aetznatron durch den Ferrieisen- oder Chromniederschlag weggenommen. Deshalb ist es nötig, um alles Vanadium in der alkalischen Lösung zu gewinnen, zwei- oder dreimal die Fällung wiederholen. Diese Schwierigkeit ist, scheint's, dem anwesenden Mangan zuzuschreiben, weil es bei seiner Abwesenheit möglich war, diese Trennung durch nur einmalige Fällung auszuführen. In der Tat wird das Mangan mittelst Aetherverfahren nicht getrennt, und es gibt keine einfache Methode zur Trennung von Mangan ohne Herbeiführung anderer Verwicklungen.

Auch wenn man das Vanadium durch Schliessen mit Alkalien von Oxyden, welche durch Eindampfen und Verbrennen der Nitratlösung der Metalle erhalten wird, zu trennen versucht, so bietet das doch ähnliche Schwierigkeiten, und wenn die Vanadiummenge beträchtlich kleiner ist, so ist die Anwendung dieser Methode kaum möglich.

Aus obigen Gründen ist es klar, dass die allgemein gebrauchten Methoden bedeutende Fehler besitzen, so dass eine zuverlässige Analyse sich nicht erwarten lässt, wenn der Arbeiter bei Ausführung seiner Analyse nicht ausserordentlich vorsichtig ist, wozu eine für eine gewöhnliche Analyse unzulässig lange Zeit erforderlich ist, oder wenn er nicht geschickt genug ist, solche Tatsachen wie die oben erwähnten zu erkennen und Unerwünschtes sofort zu korrigieren." Der Verfasser konnte, durch Beseitigung der in Klasse B beschriebenen Nachteile betreffs des Indikators, eine Methode ausarbeiten, welche s. E. nicht allgemein befriedigend, doch sehr einfach und ziemlich zuverlässig für eine Probe ist, welche verhältnismässig viel Vanadium enthält.

Ganz neuerdings veröffentlichte J. Knop[1] eine sehr bemerkenswerte Arbeit über die Bichromattitration des Eisens, in welcher er zeigte, dass Diphenylamin ein geeigneter innerer Indikator und ein guter Ersatz für

(1) Journ. Amer. Chem. Soc., **46**, (1924), 263.

die äusseren bei der Penny'schen Methode sei. Er erwähnt dass "..... einige Reaktionen beobachtet wurden, die sich von den bekannten Reaktionen des Diphenylamins unterschieden. Eine verdünnte wässrige Lösung von Diphenylamin, welche mit Chlorwasserstoff- oder Schwefelsäure angesäuert ist und Ferrisalze enthält, gibt die bekannte blaue Farbe erst nach einiger Zeit (Einfluss von Luft oder Sauerstoff?), es tritt aber sofort eine intensive blaue Farbe auf, wenn ein Tropfen einer 0,1 n-Kaliumbichromatlösung zugesetzt wird. Wenn auch Ferrisalze vorhanden sind, so zeigt sich keine Färbung, bis diese zu Ferrisalzen oxydiert sind, dann aber bewirkt der erste überschüssige Tropfen der Bichromatlösung eine intensive violettblaue Färbung, die die Farbe des bei der Titration gebildeten Chromisalzes völlig verdeckt. Bei Zusatz einer Ferrosulfatlösung wird die Flüssigkeit farblos, so dass Rücktitration möglich ist. In Abwesenheit von Eisensalzen wird durch Bichromat keine Färbung hervorgerufen, wodurch sich diese Reaktion von jener unterscheidet, die in Gegenwart von konzentrierter Schwefelsäure stattfindet.

Die angeführten Reaktionen lassen sich erklären auf Grund einer Arbeit von Kehrmann und Miciewicz,[1] wonach sich bei der Oxydation von Diphenylamin durch Ferrisalz ein grünes semichinoides Salz von Diphenylbenzidin bildet, das durch Chromsäure in das dunkelblaue chinoide Salz übergeführt wird."

Da man das Vanadium auch als Eisen leicht, z. B. mit Kaliumpermanganat, in den Vanadinsäure- bzw. Ferrizustand oxydieren und, wenn Kaliumpermanganat verwendet wird, den Ueberschuss des Oxydationsmittels leicht ohne Störung der erreichten Zustände zerstören kann, so wäre es der denkbar beste Weg zur Ermittelung von Vanadium ohne Trennung vom Eisen, das auf diesem Wege oxydierte Gemisch aus beiden Elementen mittelst Ferrosulfat zu titrieren. Es ist eine wohlbekannte Tatsache, dass sich diese Vanadinsäure dabei in das vierwertige Vanadylsalz quantitativ überführen lässt, ein Verhalten auf das sich ja

(1) Ber., **46**, (1912), 2641.

auch viele Methoden (Klasse B in der Cain'schen Klassifikation) stützen. Zum Erkennen des Titrationsendpunktes aber stehen nur wenige Wege offen. Dass die Anwendung vom Ferricyanidsalzen als äusserem oder innerem Indikator mit Schwierigkeiten verbunden ist, wurde schon am Beginn dieser Abhandlung erwähnt. Bei der Methode von Etheridge[1] wird Diphenylcarbazid als innerer Indikator verwendet. Obgleich dieses Reagens bei weitem besser als Ferricyanid zu sein scheint, so ist die vorgeschlagene Methode doch ziemlich verwickelt. Kelley nnd Conant[2] wenden eine elektrometrische Methode mit gewöhnlichem Elektrodensystem an. Auch hier ist der Endpunkt schwer zu finden, und man muss nach Zufügen eines kleinen Ueberschusses von Ferrosulfat vorsichtig mit Kaliumbichromat zurücktitrieren. H. H. Willard & F. Fenwick[3] haben eine Methode ausgearbeitet, bei welcher sie das von ihnen herrührende bimetallische Elektrodensystem anwenden und die Lösung direkt mit Ferrosulfat titrieren. Da es jedoch unbestreitbar ist, dass die Elektrometrie einen verwickelteren Apparat als die gewöhnliche Indikatormethode erfordert, so wurde ein geeignetes Indikatorreagens zu finden versucht, um diese Schwierigkeit zu überwinden.

Zu diesem Zweck versuchte er die Zinkamalgamreduktion[4] des Vanadium-Eisen-Gemisches und das Titrieren mit einer für Eisen indifferenten Flüssigkeit. Alle Versuche dieser Art aber misslangen.

Inzwischen wurde aber die obenerwähnte Knop'sche Abhandlung veröffentlicht. Nach ihrer Stellung in der periodischen Tabelle und in manchen chemischen Eigenschaften stehen Chrom und Vanadium in sehr naher Beziehung zueinander. Deshalb hoffte Verfasser die oben erwähnte Reaktion des Chroms auch beim Vanadium zu finden. Einige qualitative

(1) Analyst, **48**, (1920), 588.

(2) Journ. Amer. Chem. Soc., **38**, (1916), 341; Journ. Ind. Eng. Chem., **8**, (1916), 719.

(3) Journ Amer. Chem. Soc., **45**, (1923), 83.

(4) Nakazono, Journ. Jap. Chem. Soc., **42**, (1921), 526; Someya, Zeitschr. anorg. Chem., **138**, (1924), 291; Sc. Rep., **14**, (1925), 47.

(5) Die Blaufärbung von Diphenylamin durch Vanadinsäure ist bereits von V. L. Meaurio bemerkt worden (Anal. Soc. quim. Argentina, **5**, (1717), 185, durch Chem. Abstr., **12**, (1918), 1221.

Versuche verliefen, wie erwartet. Es wurde beobachtet, dass Ferrieisen und Vanadinsäure Diphenylamin auch in einen tiefblauen Stoff verwandeln, welcher auch mit Ferrosulfat entfärbt wird.

Solche Erscheinungen sind leicht verständlich, wenn wir uns der Tatsache errinnern, dass diese tiefblaue Färbung durch manche Oxydationsmittel hervorgerufen wird, und ausserdem, dass Chrom und Vanadium in ihren Eigenschaften mehrfach bemerkenswerte Aehnlichkeit besitzen.

Beim Versuche, diese Reaktion auf die Bestimmung von Vanadium in Gegenwart von Eisen anzuwenden, wurde das Vanadium mit Kaliumpermanganat oxydiert und mit Ferrosulfat titriert, wobei man Diphenylamin als Indikator benutzte. Man fand aber, dass die Reaktion des Diphenylamins in diesem Falle weit empfindlicher gegen den Säuergrad und andere Versuchsbedingungen war als bei der Bestimmung von Chrom; auch dass der Farbenumschlag meist unscharf und das erhaltene Resultat nicht sehr gut war. In kalter und in schwachschwefelsaurer Lösung verschwand die violette Farbe von Diphenylamin, bevor der berechnete Endpunkt erreicht war; bei höherem Säuregrad aber musste ein beträchtlicher Ueberschuss von Ferrosulfat zugesetzt werden, bevor die Farbe vollständig verblasste. Wenn in heisser Lösung titriert, wurden solche Schwankungen beträchtlich kleiner, aber es fand ein Zersetzung der Farbstoffe statt. Mit Salzsäure ist der Konzentrationseinfluss viel kleiner. Aber hier ging auch vollkommene Entfärbung vor sich, um einige ccm verzögert, wenn die berechnete Menge ca. 15 ccm war. Die Möglichkeit des Titrierens einer heissen Lösung war hier wegen der Zersetzung von Amin gänzlich ausgeschlossen.

Es lag num sehr nahe, zu versuchen, ob sich der Endpunkt der Kelley-Conant'schen elektrometrischen Titration nicht finden liesse unter Verwendung von Diphenylamin als innerem Indikator. Einige Versuche zeigten, dass die Titration sehr viel empfindlicher gegen die Versuchsbedingungen ist als bei der Bestimmung von Chrom; sie lässt sich aber durchführen durch geeignete Regelung des Säuregrades, weil das gebildete Vanadylsalz von Kaliumbichromat nicht angegriffen wird.

VERSUCHSTEIL.

Die Versuche sind auf ganz ähnlichem Wege durchgeführt worden, wie ihn J. Knop bei der Titration von Ferrosulfat mit Kaliumbichromat beschritt.

1. Die für die Titration erforderlichen Lösungen.

(a) Ein Gemisch von Schwefelsäure und Phosphorsäure (Phosphorsäuregemisch). Dies wird folgendermassen hergestellt: 150 ccm Schwefelsäure ($d = 1{,}84$) werden mit 150 ccm Phosphorsäure ($d = 1{,}7$) gemischt, worauf man diese Mischung mit Wasser auf 1000 ccm verdünnt und 15 ccm davon bei der Titration verwendet.

(b) Diphenylaminlösung, bestehend aus 1 g Diphenylamin, gelöst in 100 ccm konzentrierter Schwefelsäure. Die Lösung wird nach einiger Zeit braun, ohne jedoch dadurch ihre Gebrauchsfähigkeit einzubüssen.

(c) Ferrosulfatlösung. 1/10 Mol Ferrosulfat wird in Wasser unter Zusatz von 40 ccm konzentrierter Schwefelsäure gelöst, worauf man das Gemisch auf 1000 ccm verdünnt. Der Gehalt der Lösung wird festgestellt an dem Tag, an welchem man sie zur Titration verwendet, durch Titration mit einer 1/10 Kaliumpermanganatlösung, deren Gehalt wiederun mit reiner Oxalsäure festgestellt wird.

2. Rücktitration mit Kaliumbichromat.

Materialien. Vanadiumpentoxydlösung. Reines Vanadiumpentoxyd (Kahlbaum) wurde in verdünnter Schwefelsäure gelöst. Ein Liter der Lösung enthielt 40 ccm konzentrierte Schwefelsäure ($d = 1{,}84$). Ihren Gehalt bestimmte man nach dem Verfahren von Nakazono,[1] indem man 20 ccm der Lösung mit flüssigem Zinkamalgam reduzierte und mit Kaliumpermanganat, dessen Titer gegen reine Oxalsäure eingestellt war, titriert.

Ferrosulfatlösung. Es wurde ganz dieselbe Lösung wie die Titerlösung verwendet.

Da die meisten analytischen Arbeiten über Vanadium sich auf

(1) Journ. Jap. Chem. Soc., **42**, (1921), 526; Ibidem, 761; Sc. Rep. **14**, (1925), 109.

Sonderstähle und ähnliche Legierungen beziehen, wurden die Versuchsbedingungen so gewählt, dass sie einer schwefelsauren Lösung eines Legierungsstahls müglichst ähnlich waren. Eisen wurde benutzt als Lösung von Ferrosulfat und Vanadium als schwefelsaure Lösung von Vanadinsäure. Nach dem Mischen wurde die Flüssigkeit auf 60–70° erwärmt, mit Kalinmpermanganat (12 g in Liter) auf ein schwach bleibende Rot oxydiert, mit Zapfenwasser auf Zimmertemperatur abgekühlt und der Ueberschuss des Permanganats mit 1 oder 2 Tropfen einer Ferrosulfatlösung zerstörte. Dann setzte man 15 ccm Phosphorsäuregemisch und 3 Tropfen der Indikatorlösung zu und verdünnte die Flüssigkeit mit Wasser auf 120–200 ccm. Darauf setzte man den Ueberschuss von Ferrosulfat hinzu, welcher nun mit Kaliumbichromat zurücktitriert wurde. Beim Zusatz der Bichromatlösung vertiefte sich die grüne Farbe der Flüssigkeit zn blaugrün oder in Gegenwart von grossen Eisenmengen fast zu graublau in der Nähe des Endpunktes. In diesem Stadium der Titration liess man die Lösung in Tropfen zufliessen. Als Ende der Titration nahm man den Punkt an, bei dem eine stark violette Färbung (bei Anwendung von Schwefelsäure war die Farbe heller und bläulicher) eintrat. Durch geeignete Regelung der Konzentration von Säure und Materialien ist eine zuverlässige Titration leicht ausführbar. Der Kürze wegen sind hier die experimentellen Daten ausgelassen und nur ihre Resultate im Folgenden erwähnt.

(a) Finfluss der Säurekonzentration. Im Falle, wo nur Schwefel- oder Phosphorsäure enthalten ist, zeigt kein Farbenumschlag des Indikators an, wenn die Säurekonzentration zu klein (2 ccm konz. Schwerelsäure in 200 ccm) ist. Wenn die Säuremenge zunimmt, macht sich der Farbwechsel beim Endpunkt schärfer bemerkbar. Aber wenn die Schwefelsäure zu viel wird, findet der Farbwechsel zu schnell statt. Wenn 10–40 ccm Schwefelsäure (1 : 1) in 200 ccm enthalten sind, kann man die Endfarbe leidlich scharf erkennen. Im allgemeinen wurde der schärfste Endpunkt erhalten, wenn die Lösung 15–30 ccm Schwefelsäure (1 : 1) und 15 ccm des Phosphorsäuregemisches enthielt. Bei mehr als 40 ccm Schwefelsäure war die Endfarbe nicht sehr scharf. Wenn man Chlorwasserstoff-

säure benutzte, so konnte der Säuregrad sehr weitgehend erhöht werden, ohne dass man den Endpunkt zu früh erhielt. Bei mehr als 50 ccm Chlorwasserstoffsäure (1 : 1) in 200 ccm Lösung, verdunkelte aber die gelbe durch das Ferrisalz und die Säure hervorgerufene Farbe die Blaufärbung beträchtlich, wodurch es schwieriger wurde, den wahren Endpunkt zu unterscheiden. Den schärfsten Endpunkt erhielt man, wenn die Lösung 15–30 ccm Chlorwasserstoffsäure (1 : 1) und 15 ccm des Phosphorsäuregemisches enthielt. Die durch Diphenylamin hervorgerufene blaue Farbe war etwas stärker mit Chlorwasserstoffsäure als mit Schwefelsäure. Die folgende Tabelle zeigt ein Beispiel der Versuche, welche unter den oben beschriebene besten Bedingungen ausgeführt wurden.

Tabelle I.

Titriertes Gemisch		$K_2Cr_2O_7$—0,05 ccm	$K_2Cr_2O_7$ Theorie, ccm
V, g	Fe, g		
0.0678	0.000	6.12	6.12
0.0678	0.000	6.13	6.12
0.0678	0.056	6.12	6.12
0.0678	0.056	6.14	6.12
0.0678	0.112	6.11	6.12
0.0678	0.112	6.15	6.12
0.0678	0.224	6.10	6.12

(b) Einfluss der Konzentration des Probesalzes. Wenn nur Vanadium genommen wird, so ist der Endpunkt scharf erkennbar auch wenn die Probemenge ziemlich gross ist. Die Farbe des gebildeten Chromisulfats, wenn es konzentriert ist, ist der von Diphenylamin stammenden ähnlich, und wenn die Eisenmenge verhältnissmässig grösser ist als Vanadium, dann wird das Erkennen des Endpunktes sehr erschwert. Aber wenn Eisen und Vanandium als Metalle 0,5 g, das Vanadium mehr als wenige Prozent beträgt, so ist der Endpunkt gut erkennbar.

4. Zusatz des Ueberschusses von Kaliumbichromat und seine Rücktitration mittelst Ferrosulfat.

Die oben beschriebene Titriermethode ist selbstverständlich ähnlich

der Bestimmung von Chrom in Gegenwart von Eisen, und das hierbei gebildete vierwertige Vanadylsalz entspricht dem dreiwertigen Chromsalze. Aber die Farbe des gebildeten Vanadylsalzes ist viel bläulicher als die des Chromsalzes, so dass im allgemeinen dieser Farbenumschlag von blau in tief dunkelblau nicht so scharf wie im Falle des Chroms ist. Nach einigen Versuchen, diesen Punkt zu verbessern, wurde es so gemacht, dass man anstatt das überschüssige Ferrosulfat mittelst Kaliumbichromat zu titrieren, eine Menge von Kaliumbichromat, welche grösser ist als das Aequivalent für den Ferrosulfatüberschuss, hinzusetzen und mit Ferrosulfat zurückzutitrieren mit Diphenylamin als Indikator. Es wurde beobachtet, dass der Farbwechsel beim Endpunkt in diesem Falle so scharf wie erwünscht war.

Auch sind in diesem Falle der Einfluss des Säuregrades und die Konzentration des Salzes ganz ähnlich wie im vorigen Falle. Die folgende Tabelle zeigt die Versuchsergebnisse, welche unter ähnlich guten Bedingungen ausgeführt worden sind.

TABELLE II.

Titriertes Gemisch		$FeSO_4$, (n_1) ccm	$K_2Cr_2O_7$, (n_3) ccm	$FeSO_4$, (n_2) ccm	V gef., g	V, Fehler, g
V, g	Fe, g					
0.0685	0.000	20	20	13.82	0.0684	0.0001
0.0685	0.056	20	20	13.82	0.0684	0.0001
0.0685	0.112	20	20	13.85	0.0686	0.0001
0.0685	0.112	20	20	13.80	0.0684	0.0001
0.0685	0.224	20	20	13.82	0.0684	0.0001
0.0685	0.224	20	20	13.85	0.0686	0.0001
0.0685	0.224	20	20	13.79	0.0680	0.0005
0.0685	0.224	20	40	24.12a	0.0686	0.0001
0.0685	0.224	20	40	34.13a	0.0686	0.0001
0.0685	0.280	20	20	13.85a	0.0686	0.0001
0.0685	0.560	20	20	13.87a	0.0687	0.0002

Normalität von $FeSO_4$ Lösung: 0,09867; die Zeichen n_1, n_2 und n_3 haben dieselbe Bedeutung, wie in der "Berechnung" (s. S. 589) gezeigt wurde.

a. Der Endpunkt war nicht gut, weil die Eisenmenge zu gross war.

(c) Einfluss von Fremdsalzen. In den obenerwähnten zwei Fällen ist der Einfluss von Fremdsalzen kurz untersucht worden. Alkalien, Chrom, Aluminium, Cobalt, Mangan, Nickel, Zink, kleine Mengen von Molybdän oder Wolfram liessen keine Wirkung auf die Ergebnisse der Titration erkennen, wenngleich grosse Mengen von Manganosalzen die Blaufärbung verdunkelten. In Gegenwart von grossen Mengen von Molybdän oder Wolfram wurde das Auftreten der blauen Endfarbe sehr gehindert und unsicher. Diese Erscheinung ist aller Wahrscheinlichkeit nach mit der Bildung von Vanadiumphosphomolybdat- oder Vanadiumphosphowolframat-Komplexen verknüpft.[1]

5. Ausarbeitung einer neuen Methode.

Auf Grunde der oben beschriebenen Experimente wurde folgende Methode zur Bestimmung von Vanadium in Ferrovanadium ausgearbeitet:

Verfahren. Ca. 0,5 g von der Probe wird in eine Kasserolle getan und mit 20 ccm Salpetersäure (1 : 1) aufgelöst. Wenn nötig, kann mehr Säure verwendet werden. Wenn ausser einer kleinen Menge von Rückstand alles aufgelöst wurde, wird 5 ccm Schwefelsäure hinzuggesetzt und auf einem Wasserbad zum Trocknen, dann auf einem Drahtnetz erhitzt, bis weisser Nebel von Schwefelsäure aufzusteigen beginnt; dann wird der Rückstand mit 50 ccm Wasser, und wenn nötig, ein wenig Schwefelsäure aufgenommen. Die Kieselsäure wird abfiltriert und die Waschflüssigkeit und das Filtrat in einen konischen Becher aufgefangen. Es ist bequem, das Gesamtvolum unter 100 ccm zu halten. Die Lösung wird auf einem Drahtnetz auf 60–70° erhitzt und mit Kaliumpermanganat zu einem schwach bleibenden Rot oxydiert. Der Permanganatüberschuss wird durch einige Tropfen von Ferrosulfat zerstört. Wenn zu viel Ferrosulfat hinzugesetzt und ein Teil des Vanadiums reduziert wurde, muss obiges Verfahren wiederholt werden. Die Lösung zeigt nun die Anwesenheit von Vanadium durch eine schön gelbe Farbe an. Man nimmt sie nun

(1) Im Falle des Wolframs wurde eine ähnliche Meinung von H. H. Willard & F. Fenwick (l. c.) geäussert.

von dem Drahtnetz herunter und neutralisiert die überschüssige Schwefelsäure durch Hinzusetzen kleiner Mengen konz. Ammoniak. Die Ammoniakmenge darf nur so gross sein, dass wenn die Lösung abgekühlt wird, keine durch Eisen hervorgerufene Rotfärbung auftritt. Man kühlt die Lösung mit Zapfenwasser auf Zimmertemperatur. Die Lösung wird auf 100–120 ccm verdünnt. Sie ist nun für die Titration bereit.

Titration. Man setzt 3 Tropfen von Diphenylamin und den Ueberschuss von Ferrosulfat hinzu. Dann setzt man ein solche Menge von Kaliumbichromat hinzu, dass sie grösser ist als die äquivalente Menge des Ferrosulfatüberschusses. Die Lösung ist nun mit Diphenylamin tiefblau gefärbt. Nach Zusatz von 10 ccm konz. Salzsäure und 15 ccm Phosphorsäuregemisch wird die Lösung mit Ferrosulfat zurücktitriert, indem man als Ende der Titration den Punkt nimmt, bei welchem die tiefblaue Farbe verschwindet und plötzlich in blau umschlägt.

Berechnung. Wenn S g von der Probe zur Titration n_1 ccm (erstes Zusatz) und n_2 ccm (bei der Rücktitration) f_{FeSO_4} normalen Ferrosulfats, und wenn man n_3 ccm $f_{K_2Cr_2O_7}$ normales Kaliumbichromat verwendet, so ist

$$\% V = \frac{\left[(n_1 + n_2 + 0{,}05) f_{FeSO_4} - n_3 f_{K_2Cr_2O_7}\right] \times 5.10}{S}.$$

Anmerkungen. 1. Ferrovanadium reagiert auf Salpetersäure heftig und wird dadurch leicht aufgelöst, es bleibt aber meistens ein Rückstand ausser der Kieselsäure zurück, welcher in Salpetersäure schwer löslich ist. Wenn man aber die Behandlung mit Salpetersäure einige Mal vorsichtig wiederholt, wird der Rückstand schliesslich so klein, dass er keinen merkbaren Einfluss mehr auf das Resultat ausübt. Wenn grössere Genauigkeit erforderlich ist, ist es besser, auch diesen Teil mit Alkalien aufzuschliessen und mit Schwefelsäure aufzunehmen.

2. Der Hauptfehler dieser Diphenylaminmethode besteht darin, dass der Endpunkt sich schwer erkennen lässt, wenn die Gesamtmenge beträchtlich gross ist. In manchen Fällen zeigt sich, dass wenngleich die Endpunktserkennung bei 1 g der Probe schwer ist, sie leichter wird, wenn die Probe halbiert wird. Daher empfiehlt es sich, wenn man die

Probe nicht sonderlich schätzt, dass man z. B. 2 g von der Probe nimmt und die resultierende Lösung in einen Messkolben bringt, auf 200–250 ccm verdünnt, und 50–100 ccm davon für die Bestimmung verwendet.

3. Um einen scharfen Farbenumschlag von Diphenylamin zu erzielen, ist genügende Zerstörung der Salpetersäure nötig. Wenn man in der darauffolgenden Behandlung viel Schwefelsäure hinzufügt und die Lösung erhitzt, lässt sich der Rückstand schneller auflösen. Aber dabei wird ein Teil der Vanadinsäure reduziert und färbt die Lösung etwas bläulich. Diesen Zustand kann man aber mittelst Kaliumpermanganat und Ferrosulfat leicht zum fünfwertigen oxydieren und die Schwefelsäure auch mit Ammoniak neutralisieren. Die Anwesenheit von viel Ammoniumsalzen übt keinen störenden Einfluss auf die Titrationsergebnisse aus. Es ist bereits im Versuchsteil besprochen worden, dass viel freie Schwefelsäure schädlich wirkt und dass sich mit Salzsäure der Endpunkt schärfer erkennen lässt.

4. Salzsäure von einer Konzentration, wie in dem Bestimmungsverfahren angegeben, hat in der Kälte keine reduzierende Wirkung auf die Vanadinsäure.

5. Bei der Titration wird durch 5 oder 6 Tropfen vor dem Endpunkt die blaue Farbe heller und geht in stahlgrau über. Nach diesem Punkt lässt man die Lösung in Tropfen zufliessen und nimmt als Titrationsende den Punkt, wo die Blaufärbung völlig verschwindet und die Lösung plötzlich hell bläulichgrün gefärbt wird. Wenn die Probemenge gross und die Vanadinmenge klein ist, ist dies Umschlag nicht scharf erkennbar.

6. Ein Ueberschuss von 10 ccm des Phosphorsäuregemisches order 3 oder 4 Tropfen der Indikatorlösung üben keinen grossen Einfluss auf das Endresultat aus.

Analyse von Normalproben. Zur Kontrolle wurden zwei Ferrovanadiumproben aus U. S. Bureau of Standards analysiert unter Anwendung der oben erwähnten Methode.

(a) B. S. Standard sample, No. 60, "Low carbon".

Angegebene Gesamtanalyse:

$V = 33{,}55\%$; $C = 0{,}24\%$; $Mn = 3{,}38\%$; $P = 0{,}055\%$;
$S = 0{,}105\%$; $Si = 1{,}30\%$; $Al = 12{,}5\%$; $Mo = 0{,}90\%$;
$Fe = 47{,}1\%$.

Analysiert vom Verfasser:

$V = 33{,}54$; $33{,}57$; $33{,}54$; $33{,}40$; $33{,}65\%$; Mittel $33{,}54\%$.

(b) B. S. Standard sample, No. 61, "High carbon".

Angegebene Gesamtanalyse:

$V = 31{,}15\%$; $C = 1{,}16\%$; $Mn = 3{,}55\%$; $P = 0{,}243\%$;
$S = 0{,}003\%$; $Si = 7{,}75\%$; $Al = 0{,}02\%$; $Fe = 52{,}84\%$.

Analysiert vom Verfasser:

$V = 31{,}14$; $31{,}13$; $31{,}13\%$; Mittel $31{,}13\%$.

Die Resultate darf man zuverlässig nennen. No. 60 enthält ca. 1% Molybdän, das Resultat aber ist sehr gut (vgl. Versuchtsteil).

Viele Ferrovanadiumproben wurden mit dieser Methode in unserer Anstalt analysiert, und das Resultat war stets als zufriedenstellend zu betrachten.

III. SCHLUSS.

Eine neue, einfache und zuverlässige Methode zur Ermittelung von Vanadium in Eisen wurde ausgearbeitet, indem man eine Vanadiumprobe in ihre schwefelsaure Lösung verwandelt und nach dem Oxydieren die Lösung mittelst Kaliumbichromat und Ferrosulfat titriert, mit Diphenylamin als Indikator.

Diese Methode kann man hauptsächlich auf Ferrovanadium oder verhältnismässig vanadiumreiche Legierungen (mindestens 1%) anwenden, aber wenn die Menge davon zu klein ist, oder die Legierung Chrom, Wolfram etc. enthält, lässt sich diese Methode nicht direkt gebrauchen.

Zum Schluss möchte der Verfasser Herrn Prof. K. Honda und Herrn Prof. Murakami, der diese Untersuchung viel Interesse entgegengebracht hat, und Herrn T. Kato für seine ausgezeichnete Unterstützung bei diesen Versuchen seinen herzlichsten Dank aussprechen.

Index to Vol. XIV.

AUTHORS. PAGE.

Aoyama, S. :—On the Reaction Products of Ruthenium Tetroxide and Hydrochloric Acid. 1

Endô, H. :—On the Relation between the Equilibrium Diagram and the Magnetic Susceptibility in Binary Alloys. 479

Honda, K. and Yamada, R. :—Some Experiments on the Abrasion of Metals. 63

——— :—On the Formation of Martensite in Carbon Steels.... ... 165

——— and Ishigaki, T. :—On the law of Depression of Freezing Points in Metallic Alloys... 219

Ichikawa, J. :—The Condensation of Vanillin with Methyl Ethyl Ketone... 127

Isihara, T. :—On the Influence of some Elements on the Spheroidization of Carbides in Steels. 377

Kanô, N. :—On the Determination of Cyanides and the use of Benzene as an Indicator in Iodimetry. 101

Kase, T. :—On the Equilibrium Diagram on the Iron-Carbon Nickel System... 173

——— :—On the Stractual Diagrams of some Special steels... ... 453

——— :—On the Widmannstätten Structure in Iron-Carbon and Iron-Nickel Alloys and in Meteorites. 537

Kaya, S. :—On the Solidus Line in the Iron-Carbon System... ... 529

Kubota, T. :—Uber die Konvex geschlossenen Mannigfaltigkeiten im n=dimensionalen Raume. 85

——— :—Uber die (2, 2) deutigen quadratischen Verwandtschaften V.... 155

——— :—Uber die Doppelsechs. 391

——— :—Uber die Eibereiche im n-dimensionalen Raume. 399

AUTHORS. PAGE.

Kawakami, M. :—On the Determination of the Heat of Precipitation of Cementite from α and β Martensites. 559

Matsuda, T. :—The Effect of Cold-Working and Annealing on some Physical Properties of Copper, Aluminium and their Alloys. 343

Matsuike, Y. :—Dielectric Constants of Liquids. Part 1. On the Method of Measuring Dielectric Constants of Liquids. ... 445

Murai, J. :—Synthesis of a Homologue of Zingerone, 4-hydroxy-3 methoxyphenylethyl Ketone. 145

——— :—Synthesis of m-Hydroxyphenylethyl Methyl Ketone and 3-Hydroxy-4-methoxyphenylethyl Methyl Ketone (Isozingerone). 149

Mitsukuri, S. and Rokkaku, T. and Watase, T. :—The Vapor Pressures of Hydrogen Chloride on Aqueous solutions. Part. 1. ... 251

Nakazono, T. :—Application of Liquid Amalgams to Volumetric Analysis. Part 1. Estimation of Molybdenum, Titanium and Iron. 109

Nomura, H. and Hotta, S :—Relation between the Chemical Constitution and the Pungency. Synthesis of the Reduction Products of Zingerone and Di-4-hydroxy-3-methoxyphenylethyl Ketone. 119

——— and Hotta S. :—Synthesis of the Homologues of Zingerone. 131

——— :—Preparation of Zingerone, 4-Hydroxy-3-methoxyphenylethyl methyl Ketone... 143

Ôsawa, A. :—The X-ray Examination of Inner Structure of Various Calcium Carbonates. 33

——— :—On the Atomic Structure of Palladium and Platin Black which absorb Gases. 43

Saegusa, H. :—On the Variation of Residual Charge and the Ratio of Electrical Conductivity to Capacity due to Temperature. 319

——— :—Further Studies on the Variation of Residual Charge and the Ratio of Electrical Conductivity to Capacity due to Temperature. 335

Authors.	Page.
Satô, M. :—Some experiments on the Contact Electric Layers. ...	313
——— :—A Kinetic Theory of the Viscosity of Liquids.	403
Satô, S. :—Dilatometric Investigation of the A_3 and A_4 Transformations in Pure Iron.	513
Someya, K. :—The Use of Liquid Amalgam in Volumetric Analysis. Part I. Application of Zinc and Bismuth Amalgams. ...	47
——— :—The Use of Liquid Amalgams in Volumetric Analysis. Part II. Oxidimetric Estimation of Tungsten, etc. by Using Lead and Bismuth Amalgams.	235
——— :—The Use of Liquid Amalgams in Volumetric Analysis. Part III. Determination of Phosphoric Acid by Using Lead Amalgam.	568
——— :—Ein Verfahren zur Bestimmung von Vanadium in Ferro-vanadium.	577
Tamaru, K. :—On the Equilibrium Diagram of the System Iron-Carbon-Titanium.	25
Takasu, T. :—Bemerkungen zu den geodätischen Linien auf Böschungflächen.	259
——— :—On the Relation between the Intrinsic Equations of Analytic Functions under Linear Transformations and Curves under Inversions...	263
——— :—Geometry of Doubly Oriented Spheres in Non-Euclidean Space.	279
Utida, Y. and Saito, M. :—The Influence of Metallic Elements on the Corrosion of Iron and Steel.	295